UNIVERSITY
of
GLASGOW

Department of Civil Engineering

Behaviour of Steel Fibre Reinforced High Performance Concrete under Biaxial Loading Conditions

Thesis submitted to the University of Glasgow
in candidacy for the degree of
Doctor of Philosophy

By

Boris Kölle

GLASGOW
THE UNITED KINGDOM

September 2006

Declaration

I declare that this thesis is a record of the original work carried out solely by myself in the Department of Civil Engineering at the University of Glasgow, United Kingdom, during the period of October 2000 to September 2006. The copyright of this thesis therefore belongs to the author under the terms of the United Kingdom Copyright acts. Due acknowledgement must always be made of the use of any material contained in, or derived from, this thesis. The thesis has not been presented elsewhere in consideration for a higher degree.

Boris Kölle

September 2006

Abstract

With increased compressive strength, concrete has also become more brittle. Therefore steel fibres are often added to the mix of high performance concrete (HPC) to combine the advantages of both materials. With the application of such a new material in the construction industry, the understanding of its behaviour under multiaxial loading is essential for reliable analysis and safe designs. This thesis includes an experimental investigation of the behaviour of steel fibre reinforced high performance concrete (SFRHPC) under biaxial loading conditions. Also included are constitutive models to enable numerical predictions of the strength behaviour of such a material.

Within the experimental stage a large biaxial test machine was designed and manufactured. The load capacity of each axis was 2000 kN. Special thought was given to the load platen system because of the friction which occurs between the platen system and the concrete specimen. Brush bearing platens and solid steel blocks with and without Teflon friction reducing pads were tried. Because the brush platen and the Teflon pads were constantly damaged during testing, solid steel block platens were finally used. For tests where tension loads were involved, experiments were carried out with dog-bone shaped specimens and specimens glued onto the platens. Finally the tension loads where transferred through threaded rods cast into the specimens and connected to the machine platens with screws.

Modern control schemes and high speed data acquisition systems were used to monitor the material response and to collect experimental stress and strain results. The principal deformations were monitored and the crack patterns and failure modes examined. Failure envelopes were developed based on the strength data for each fibre variable. The load capacity of SFRHPC under biaxial load conditions was found to be larger than for plain HPC for all fibre types and volume fractions. The stress-strain recordings indicated a linear

behaviour almost up to failure. The examined failure mode between plain and steel fibre HPC was similar and all specimens failed very suddenly with a splitting failure type.

The test variables included four different types of hooked ended steel fibres with different fibre volume fractions from plain to 2 % in 0.5 % steps. The specimens were tested under the entire range of stress combinations including uniaxial compression and tension and biaxial compression-compression and compression-tension. As a result the specimen still failed in an explosive manner but the pieces were still connected together by fibres after failure. The biaxial strength compared to the uniaxial strength increased more, as observed with normal strength concrete. With the addition of fibres the biaxial strength behaviour of HPC was almost the same as for plain normal strength concrete. The deformation characteristics of plain and SFRHPC showed a linear behaviour up to a higher stress than normal strength concrete. In fact the linear limit was almost as high as the failure load.

The examined strength data was used to model the biaxial strength envelopes of HPC and SFRHPC using different methods. These included the Ottosen failure criterion and the Willam and Warnke failure criterion. To model the presence of steel fibres under biaxial loading a confinement stress in the third direction was introduced depending on the fibre variables. Other approaches involved the development of data fitting processes including a regression analysis which basically is a second order polynomial and a distorted and stretched ellipse. These envelopes can be implemented into a finite element analyses.

Acknowledgements

I would like to express my sincere gratitude to several people who made this research and completion of this thesis possible.

Firstly, I would like to thank my supervisor, Dr. David V. Phillips who gave me the chance of this challenge and who made the completion of this thesis possible throughout his guidance and supervision.

Further thanks to Prof. Simon J. Wheeler, Prof. Nenad Bicanic, Dr. Ben Zhang, Dr. Chris J. Pearce, Dr. Bill Sloan, Dr P. Bhatt and Dr. Peter Grassl for their useful discussions and ideas given for this project. Also mentioned is the Faculty of Engineering which research scholarship helped me to survive throughout this period of time.

Many thanks go to the Technical staff in the Heavy Structures Lab of the Department of Civil Engineering at the University of Glasgow. Alan A. Burnett and Stuart McLean for their technical supervision, Ian Gardner and Robert Boyd for their help in producing the entire concrete specimen needed for this project, William Thomson, Cliff Loader, Tim Montgomery and Wilson MacDougall for performing all the cutting, milling, welding and assembling of the test facility, Robert McCaskie for preparing the concrete specimens with strain gauges and Alan Yuill for his help with the electronic side of the test-set up and the preparation of so many tests. For all his assistance and help with the computing facilities I wish to thank Kenneth McColl. Also a very warm thank you to Mary McGoldrick for providing me with fresh café at the tearoom.

Also acknowledged is Bekaert for providing free steel fibres for this project and EPSRC who contributed a grant towards the cost of some equipment such as strain gauges and machine parts as well as the material costs of the concrete specimens.

My sincerest thanks to Dimitrios Kourepinis my office mate for the first few years who helped me with all kinds of problems not only work related. Many thanks to Anne Reungoat my other office mate and to all my colleagues and friends in the Department of Civil Engineering, Colin Davie, Gerrit Klemm, Chris Sterling, Dave Watson, Lindsay Beevers, William Algaart, Kevin McGinty, Xu Jiandong, Jan von Thun, Marti Que Quer, Kourosh Babaeyan-Koopaei, Tomek Koziara, Konrad Kukla, Laurent Glasson, Stephen Woodcock, Joseph Xu Zhou, Arunasalam Raveendiraraj, Lukasz Kaczmaczyk, Alasdair Andersen, Ronald Wallis Maclachlan Dempster and Nigel Atkins which I spent so many nice hours also outside of the Rankine building. Many of these friends were regular members of our Departmental Basketball Team which I always enjoyed to play with. Thanks to all my friends, sport buddies and flatmates I lived and laughed together and who helped me to think of something else at the right times.

Included here are all the friends I met in various University Sport Clubs I enjoyed during my stay in Glasgow. Especially the friends from the University Boat Club who I spend so much time together in all this lovely training sessions in the boathouse and the Gym and weekend outings in rowing boats on the river Clyde.

In this context my special gratitude to Barry Passion Crane and his family who showed me the way of living in Glasgow and with whom I went to football matches and night clubs afterwards.

I would like to take this chance to express my profound gratitude to my parents, grandparent, sister and all members of my family and friends back home for encouragement and support throughout all the years of my study.

The most special, deepest and warmest thanks are due to my girlfriend Klaudia. Never ending encouragement and understanding with all the assistance and sacrifices she made has made a huge contribution to me to complete this thesis.

Table of Contents

Notation

Throughout this thesis SI units are used. Important symbols which are used are listed in the following. Furthermore most of the symbols are described in the text when they occur.

Abbreviations

BS	British standards
C-C	Compression-compression
C-T	Compression-tension
FRC	Fibre reinforced concrete
HSC	High strength concrete
HPC	High performance concrete
HPSFRC	High performance steel fibre reinforced concrete
kN	Kilo Newton
LVDT	Linear voltage displacement transducer
m	Metre
mm	Millimetre
NSC	Normal strength concrete
OPC	Ordinary Portland cement
PP	Polypropylene fibres
RILEM	Reunion Internationale des Laboratoires d'Essais et de Recherches sur les Materiaux et les Constructions
SFRC	Steel fibre reinforced concrete
SFRHPC	Steel fibre reinforced high performance concrete
SIFCON	Slurry infiltrated fibre concrete
t	Ton
T-T	Tension-tension
UHPC	Ultra high performance concrete

Roman letters

E_c	Modulus of Elasticity of concrete in N/mm^2
f_c	Uniaxial compressive strength in N/mm^2
f_c'	Cylinder compressive strength in N/mm^2
f_{cb}	Equal biaxial compressive strength in N/mm^2
f_{cp}	Uniaxial plate compressive strength in N/mm^2
f_{cu}	Cube compressive strength in N/mm^2
f_{ci}	Early age strength in N/mm^2
f_t	Direct tensile strength in N/mm^2
f_t'	Cylinder splitting strength in N/mm^2
f_{tb}	Equal biaxial tensile strength in N/mm^2
l	fibre length
l_c	critical fibre length
d	fibre diameter
l/d	aspect ratio of steel fibres (fibre length / fibre diameter)
V_f	Fibre volume fraction/content in % by weight
r	ratio of the cross-sectional area to the circumference of the fibre
h	thickness of specimen
b	width of specimen
I_1	Invariant of the stress tensor
J_2	Invariant of the stress deviator tensor
J_3	Invariant of the stress deviator tensor

Greek letters

Δ_1	principal direction
Δ_2	principal direction
Δ_3	principal direction
ε_1	Principal strain
ε_2	Principal strain
ε_3	Principal strain
σ_1	Principal stress in N/mm^2
σ_2	Principal stress in N/mm^2
σ_3	Principal stress in N/mm^2
σ_{co}	Uniaxial compression plate stress of plain concrete in N/mm^2
σ_{tu}	Post cracking tensile strength of SFRC
ν	Poisson ratio
ν_f	Poisson ratio of steel fibre reinforced concrete
ν_p	Poisson ratio of plain concrete
μ	Micro
ξ,	Projection of OP on the hydrostatic axis in the Haigh-Westergaard coordinate system
ρ	Polar coordinates on the deviatoric plane normal to the hydrostatic axis
θ	Polar coordinates on the deviatoric plane normal to the hydrostatic axis
ρ_t	tensile meridian
ρ_c	compression meridian
η_0	fibre orientation factor
η_l	fibre length efficiency factor
τ_u	ultimate fibre bond strength
$\overline{\theta}$	angle between fibre and the XY plane
$\overline{\rho}$	angle between the projection of the fibre on the XY plane and the direction of σ_1

Definitions

The following definitions are used throughout the description of the failure envelope models:

Stress order $\sigma_1 \geq \sigma_2 \geq \sigma_3$ **(0.1)**

Hydrostatic axis: $\sigma_1 = \sigma_2 = \sigma_3$ **(0.2)**

Compression meridian: $\sigma_1 > \sigma_2 = \sigma_3$ **(0.3)**

Tension meridian: $\sigma_1 = \sigma_2 > \sigma_3$ **(0.4)**

Octahedral normal stress: $\sigma_{oct} = \frac{\sigma_1 + \sigma_2 + \sigma_3}{3}$ **(0.5)**

Octahedral shear stress: $\tau_{oct} = \frac{1}{3}\sqrt{(\sigma_1 - \sigma_2)^2 + (\sigma_2 - \sigma_3)^2 + (\sigma_3 - \sigma_1)^2}$ **(0.6)**

Hydrostatic length: $\xi = \left|\overline{ON}\right| = \frac{I_1}{\sqrt{3}}$ **(0.7)**

Deviatoric length: $\rho = \left|\overline{NP}\right| = \sqrt{2J_2}$ **(0.8)**

Θ is the angle of similarity with: $\cos 3\Theta = \frac{3\sqrt{3}}{2}\frac{J_3}{J_2^{3/2}}$ **(0.9)**

First invariant of stress tensor: $I_1 = \sigma_1 + \sigma_2 + \sigma_3 = \sigma_{ii}$ **(0.10)**

Second invariant of stress deviator tensor: $J_2 = \frac{1}{2}\left(s_1^2 + s_2^2 + s_3^2\right) = \frac{1}{2}s_{ij}s_{ij}$ **(0.11)**

Third invariant of stress deviator: $J_3 = \frac{1}{3}\left(s_1^3 + s_2^3 + s_3^3\right) = \frac{1}{3}s_{ij}s_{jk}s_{ki}$ **(0.12)**

Deviator stress: $s_{ij} = \sigma_{ij} - \left(\frac{1}{3}\right)\delta_{ij}\sigma_{kk}$ **(0.13)**

Expressed in principal stresses: $J_2 = \frac{1}{6}\left[(\sigma_1 - \sigma_2)^2 + (\sigma_2 - \sigma_3)^2 + (\sigma_3 - \sigma_1)^2\right]$ **(0.14)**

Expressed in principal stresses:

$$J_3 = \frac{1}{27}\left[2\sigma_1^3 + 2\sigma_2^3 + 2\sigma_3^3 - 3\sigma_1^2\sigma_2 - 3\sigma_1^2\sigma_3 - 3\sigma_2^2\sigma_1 - 3\sigma_2^2\sigma_3 - 3\sigma_3^2\sigma_1 - 3\sigma_3^2\sigma_2 + 12\sigma_1\sigma_2\sigma_3\right]$$ **(0.15)**

List of Figures

List of Tables

1. Introduction

1.1. Overview

In recent years the use of chemical admixtures and silica fumes as a partial replacement for cement, in combination with improved design methods and mixing techniques, has led to concrete strengths well above 100 N/mm^2. The advantages of such high performance concrete (HPC), however, are not only the increased compressive strength. Also its low permeability which results in better behaviour against chemical and salt attack, better freeze-thaw resistance and lower creep deformation resulting in a reduction of loss of prestressed force, are well recognised features of this fairly new material. Consequently the use of HPC has increased dramatically over the last years within the concrete industry for structures such as high rise buildings, bridges and even offshore platforms.

The disadvantage of higher strength concrete is its brittle and explosive failure. This loss of ductility is unfortunate because structures could fail suddenly without developing an appropriate collapse mechanism. Mixing fibres into the concrete matrix can increase the ductility and fracture toughness compared to plain concrete. Different types of fibres have been used, amongst them fibres made of steel, glass, carbon or polypropylene.

When concrete materials start to fail under loading, deformations occur by forming micro cracks. Fibres mixed into the concrete matrix act as crack arresters. For ductile behaviour it is important that the bond between the fibres and the concrete matrix allow fibre pull out rather than fibre breaking. The objectives for the addition of fibres are to improve the tensile strength, flexural strength and toughness, to change the mode of failure and to control cracks. Most of the previous research was focusing on uniaxial load applications. This is due to the fact that these tests can be done very easily with not much effort

spent on expensive test equipment. Because uniaxial tests provide only limited scope, biaxial and triaxial concrete tests are needed to cover more possible combinations and types of stresses and to provide the designer with information about multiaxial stress states which exist in most real situations.

Steel fibres are widely used in industry, for example in industrial floors, tunnel linings or prefabricated structures such as facade panels, monobloc garages or pipes. The behaviour of SFRC has been studied extensively in uniaxial tests and bending tests. However, for a better fundamental understanding of the macroscopic properties of this material, records of the deformation and strength characteristics under multiaxial stress states are essential.

For steel fibres mixed into normal strength concrete it has been shown that the uniaxial and the biaxial compressive strength increase with increasing fibre volume. The material becomes more ductile but still performs a splitting failure with the specimen pieces held together by the fibres after the failure point was reached. The strength and ductility also increase significantly under compression-tension stress states.

For normal strength plain and fibre concrete and high strength plain concrete a reasonable amount of biaxial experimental data is available. Very few experiments have been carried out on the behaviour of steel fibres in high strength concrete under biaxial states of stress. Therefore, this extensive experimental program was initiated to investigate the behaviour of this material and to provide meaningful test results for the use in computational investigations such as the finite element method.

1.2. Research Objectives and Scope

The current study was carried out to examine the behaviour of steel fibres in high performance concrete when subjected to biaxial states of stress. The objectives and scope of the research program can be summarised as follows:

1. To examine the available methods used in biaxial concrete testing of normal strength concrete and to identify a suitable method that can be used for SFRHPC.

2. Design, build and modify a suitable biaxial test facility which allows testing HPC and SFRHPC under a combination of compression and tension load ratios. This includes an appropriate platen system and measurement devices which will produce reliable test data.

3. Collect and analyse strength data, load deformation behaviour and strain measurements of plain and steel fibre HPC under biaxial loading conditions. This includes obtaining fundamental failure surfaces and deformational responses for different types of steel fibres.

4. To examine the failure modes and crack patterns for different stress ratios.

5. To compare plain HPC with SFRHPC with different fibre volumes and fibre types.

6. To adopt constitutive models suitable for finite element analyses and use the experimental test results to verify them. The main aim was to develop mathematical models to represent the observed failure surfaces.

1.3. Thesis Outline

Chapter 2 is divided into six parts. The first part of the literature review gives a historical overview of concrete in the past centuries. The second part introduces the ingredients which are needed in addition to normal strength concrete to create SFRHPC. Part three reviews the different methods of load application used in testing concrete under compression and tension loads used for biaxial testing. The fourth part reviews previous research conducted on concrete under biaxial state of stress. This part is divided into biaxial testing of NSC, HPC and SFRC. Followed by a review of the influence of the load path, Chapter 2 closes with a brief review of constitutive models with different methods for developing failure envelopes in a mathematical matter.

Chapter 3 describes the experimental investigation. Details of the experimental facilities, instrumentations, test specimens, mix preparation and test procedure are presented.

Chapter 4 presents the test results in respect of strength measurement and the influence of steel fibres. In the first section of this chapter the standard uniaxial tests are presented which are important as reference tests. The second part presents the biaxial test results as strength envelopes also focusing on the difference of the two load platen systems, the brush platen system and the solid steel block system.

Chapter 5 and 6 are organised similarly to Chapter 4 but focus on strain measurements and failure types respectively. The Chapters are again divided with respect to plain HPC and SFRHPC.

Chapter 7 presents the analytical and mathematical description of the failure envelopes.

Finally, a summary of the current investigation and the conclusions reached are given in Chapter 8.

2. Literature Review

This chapter contains a short literature review covering the issues of biaxial concrete tests. It will start with a brief historical overview of concrete within the last centuries before it focuses on the materials used in this study. Different ingredients are introduced which are of particular interest for this project such as silica fume, Superplasticizer and steel fibres. A short review is given on load application systems. Special attention is given to the point in the system where the load is transferred from the machine platen into the concrete specimen. It shall be shown that different testing methods constrain the test specimens differently and therefore influence the observed material response. Various methods established by other researchers are introduced for compression and tension application systems. The use of a lubricant, friction reducing pads consisting of aluminium sheets, Teflon sheets or plastic foil, steel brushes and solid dry platens or a combination of different methods is well known and discussed for compression loads. The variety of tension load application systems ranges from glued to dog bone shaped specimens and is also discussed.

The biaxial behaviour of concrete was being researched as early as the end of the 19th century, but it was Kupfer et al. (1969) who produced the first full set of reliable test results for the entire biaxial compression and tension strength envelope for concrete plates with compression strength up to 57 N/mm^2. Other researchers explored the issue of biaxial concrete testing with more variables from normal strength concrete (NSC) to high strength concrete (HSC) and to fibre reinforced concrete (FRC). This will lead to a combination of HPC with FRC under biaxial stress states which is the focus of this study.

Furthermore the influence of different load paths, proportional and sequential loading, on biaxial concrete behaviour is discussed. Finally different methods to

generate biaxial failure envelops as mathematical expressions in respect of a constitutive model are introduced and examined.

2.1. A historical review of concrete

The first use of lime mortar as a binding agent was approximately 8,000 years BC in buildings in the region of modern day Turkey. The Egyptians built the Pyramids using similar materials around 2000 years BC whereas the Mycenae and Tiryns used it for foundations about 1000 years BC. The Romans used cementitious materials called 'Opus Caementitium' 2000 years ago to build structures like aqueducts and the Pantheon. The main components of the early concrete was quicklime, water, sand and coarse aggregates. Quicklime was limestone which was burned at 900 °C. During the centuries many improvements were made to concrete materials.

It was in 1824 when Portland cement was introduced by J. Aspdin as a binding agent between aggregates. Other ingredients such as fly ash, silica fume and chemical admixtures like Superplasticizer were introduced during the last 50 years to improve the material properties and workability of the material. Different manufacturing processes ensured that materials such as concrete for pumping, shotcrete concrete, under water concrete, transport concrete and self compacting concrete were made possible.

The compressive strength of concrete f_c has increased constantly, and now exceeds 600 N/mm^2. Concrete with a compressive strength over 100 N/mm^2 can be easily produced commercially within a standardised industrial environment using conventional methods and materials. Therefore the cross-section area of compression members can be reduced compared to NSC which led to less self weight, resulting at least for buildings in more space available per walled room (floor space), lighter members and smaller, more economical foundations. These advantages will over the years compensate for the increase

in cost emerging from the use of high performance concrete (HPC). Also the resistance against abrasion is increased because the higher density of the material, as well as a lower permeability will better resist freeze-thaw attack, chemical attack, salt attack or reinforcement corrosion. (Naaman and Reinhard, 1995)

One of the most important improvements were made by introducing **reinforcement** into the cementitious material. It was now possible to use concrete in structural members where tension or bending forces are occurring. Before concrete could only cope with compression forces. Starting with the introduction of iron wires and steel bars into concrete by J. Monier in 1867, prestressed concrete was developed in the 1920's by Freyssinet. These developments made concrete one of the most used materials in the world, with which almost every new structure is built.

It was during the Egyptian and Babylonian civilisations that **fibres** were first used to reinforce brittle material. Sun baked bricks were reinforced with straw and horsehair. (Nawy, 1996) From the early 1920's fibre reinforced concretes were introduced using many different kinds of fibres, from the well known steel fibres to organic fibres, with parallel developments in glass fibres and textiles. Gani (1997) records one of the earliest patents, held by Alfsen in 1918 on the use of fibres such as iron or wood to improve the tensile strength of concrete. This was followed by Martin in 1926 who suggested steel wires and Constantinesco in 1943 who described the use of steel fibre similar to the ones which are in use today. Asbestos fibres were abandoned when it was realised that they are a risk to human health.

The latest improvement in the material properties of fibre reinforced concrete was achieved with a combination of different fibre types, a fibre cocktail called hybrid fibre concrete. This includes two or more different fibre types of the same or different material or shape which make complementary and additive contributions to the performance of a concrete mix. Numerous publications on this topic are available, for example within the proceedings of recent

conferences such as BEFIB 2004 in Varenna, Italy (Prisco et al., 2004). Micro fibres made out of steel or PVA (polyvinyl alcohol) are combined with steel macro fibres. Strength and toughness of this concrete are increased because the micro fibres delay the formation of macro cracks and the different fibres influence the crack growth at different stages of the failure process, each fibre adding its own qualities to the combination.

Even after recent developments, continuous research on concrete and cementitious material still continues. Because of the huge amount of concrete being used today even small improvements in the material properties will produce an economically more efficient material and therefore result in a financial benefit. Modern materials will have their role in tackling problems developing with an increasing population in towns and the need for functional and aesthetic buildings in the future.

2.2. Ingredients used in HPSFRC

In order to achieve higher strengths, the mix design has to be optimised. Optimisations include not only better quality of the concrete content like higher strength aggregates and better cement control mechanisms but also the arrival of new chemical admixtures made the development possible. The key point of the production of HPC is the reduction of the water/cement ratio. The addition of water reducing admixtures such as Superplasticizer is essential and its use is very common these days.

Most **Superplasticizers** are made from organic sulfonates or sulfonic acid esters and carbohydrate esters (Nawy, 1996). The use of 1 to 2 % by weight of the cement is advisable. For higher Superplasticizer percentages the cement content has to be increased as well in order not to reduce the compressive strength. The Superplasticizer works by decreasing the surface tension of water and by directing the cement particle charges into one direction. Together with

the addition of silica fume the concrete achieves a reduction in the water/cementitious material ratio and therefore a higher strength without losing its workability.

Silica fume is a highly reactive pozzolan and a by-product from the electric arc furnace in the production of silicon metal and ferrosilicon alloys. The size of silica fume particles is about 0.1 µm compared to 10 µm in Portland cement and fly ash. The fine spherical particles of silica fume makes it an ideal cement replacement which also increases the concrete strength. As well as replacing cement, the density of the mixture is also increased as the silica fume acts as micro filler of the pores filled with mix water in normal strength concrete. Normally the proportion of silica fume within high strength concrete varies between 5 and 30 % by weight of the cement content. Because of the water demand with increasing proportions of silica fume a high range water reducing Superplasticizer is needed to keep the workability and the water/cement ratio of the mix. The strength development of concrete using silica fume is more rapid within the first few days, with a further relatively small increase in strength after one month (Nawy, 1996).

The chemical reaction of silica fume is called a pozzolanic reaction and happens only if hydration is also taking place. Therefore the use of silica fume makes sense only during the combination with cement and water.

Overall the major improvement achieved by the use of silica fume is increased concrete strength and improved resistance against permeability resulting in better freeze-thaw and chemical attack resistance because of the more dense and compact matrix of the hardened concrete.

Different types of fibres made from steel, glass, polypropylene, graphite, asbestos, Kevlar and textiles can be used in FRC. In this review, special attention is drawn to **steel fibres** as they are widely used and also the focus of this project.

Steel fibres are available in lengths between 6 and 80 mm and with a cross section area between 0.1 and 1.5 mm^2. This is equal to a diameter between 0.15 and 1.2 mm. The tensile strength is normally in a range between 300 and 2400 N/mm^2 (VDS Merkblatt, 2005, Bekaert Dramix datasheet, 2005) with a specific gravity at appropriately 7800 kg/m^3. They are of circular or rectangular cross-sectional shape and are produced by cutting or chopping steel wires or by shearing sheets of flattened metal sheets and steel bars. The fibres are usually crimped or deformed with either a hook at each fibre end or a small head in order to improve the bond between fibre and concrete matrix. An overview of different fibre types from different producers is given in Table 1 below.

Fibre Form	Manufacturing process	Company	Brand name
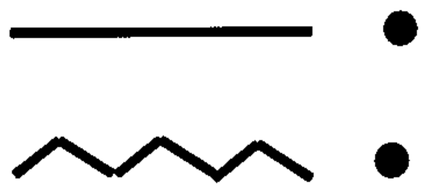	Drawing	Trefil ARBRED	Wirex Eurosteel
	Cutting Slitting	Australin Wire	Fibresteel
	Drawing	Bekaert	Dramix
	Drawing	National- Standard	Duoform
	Meltextraction	National- Standard	Meltextracted
	Milling Filling	Harex Stahlfasertechnik	Harex
	Drawing	Stax	-
	Drawing	Thibo	-
	Cutting Slitting	US-Steel	Steel sheet fibres

Table 1 Overview of different fibre forms (Maidl, 1995)

The formation of end anchorage or hooked ends on the fibres is of particular importance as they take effect as soon as the pullout process begins and can greatly increase the pullout forces and the toughness. Hooked end steel fibres generate flexural strength and energy absorption capacity which are higher than those of straight fibres. (Soroushian and Bayasi, 1991)

However, the workability and the formation of fibre balling with some types of fibres with deformed surfaces can be a problem. A successful method of solving this problem involves the use of fibre bundles together with water-soluble glue where the fibres separate during mixing when they come in contact with the mixing water. Such a fibre bundle produced by Bekaert, which was also used for some fibre types in this study, is shown in Figure 2.1.

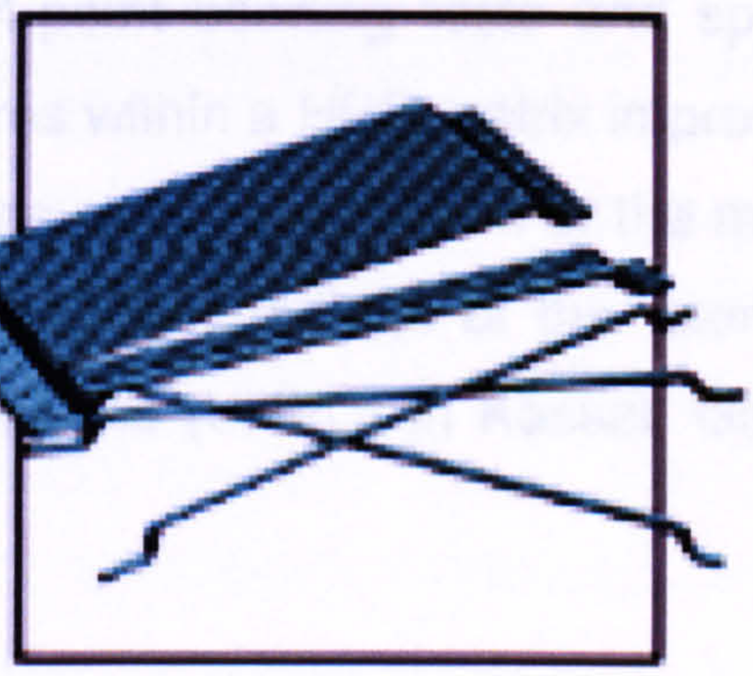

Figure 2.1 Fibre bundle (Bekaert, 2005)

The fibre volume content V_f can vary up to 2 % by volume in normal mixed concrete. For higher volume contents the mix tends to fibre balling during the mixing process and workability can not be easily achieved. The placing of SFRC becomes also critical with higher fibre contents as the material properties of the hardened concrete might result in irregularities within the same structural member because of de-mixing.

Fibre concentration of up to 25 % fibre content are achieved in special mixing procedures such as slurry infiltrated fibre concrete (SIFCON) or shotcrete

concrete. For the use of SIFCON the fibres are distributed in the moulds and infiltrated with the cement past. Using shotcrete concrete the fibres are shot together with the cement paste in place, for example in tunnel lining.

Fibres improve the mechanical properties of concrete not as a replacement of the continuous reinforcement bars but in addition to them. The reinforcement bars cannot stop the development of micro cracks, but the randomly distributed fibres can prevent the micro cracks from propagating or widening and help to control the cracks. The fibres also improve the ductility of the material due to their energy absorption capacity, and stiffen it. When used in concrete steel fibres have the advantage of being resistant against corrosion and chemical attack and behave better than other fibres at high temperatures, for example in the event of fire.

Beams under 3-point or 4-point bending tests and specimens under uniaxial tension show that steel fibres within a HPC matrix improved ductility and tension capacity which therefore prevents brittle failure of the material. This was shown in several publications in the proceedings of the international symposium on ultra high performance concrete (UHPC) in Kassel, Germany (Schmidt, et al., 2004).

Therefore one of the major applications is in industrial floors where properties such as crack control, resistance against punching forces, and low permeability are needed, and the static requirements are of secondary interest. Because of the low permeability produced by controlling the cracking, fibre reinforced concrete is also widely used in silo buildings and basement floors and walls. SFRC is also used today for fibre concrete pipes, industrial floors, highway and airport runways, overlays in bridge decks or temporary structures in tunnelling. (Bakaert data sheets, 2005)

2.3. Different load application systems

When testing concrete special thought has to be given to the load application system and the interaction between test machine and specimen. Overall the concrete specimen is to be tested, not the machine. Different load application systems have been developed over the last few decades in order to test concrete under a multiaxial stress state. The aim of all methods is to reduce the influence of the loading system caused by the constraining effects between the load bearing system and the specimen. These different constraining effects can influence the concrete strength, the deformational behaviour and also the type of failure. In order to reduce friction between load platen system and concrete specimen different loading systems were developed.

2.3.1. Mechanisms for applying compression loads

For compression loads, the constraining effects are caused by friction between the load platen system and the concrete specimen as a result of the difference in lateral expansion between the two. Shear stresses might occur at the specimens' surface leading to a stress distribution which is not uniform. This non-uniformity is very hard to monitor and therefore to interpret. It is preferable therefore to remove sources of friction and any other kind of boundary influence.

The different load application systems used for compression load studies can be classified into two main groups. One group attempts to reduce the friction between machine platen and concrete specimen by transferring the compression loads through for example friction reducing pads whereas the other group uses flexible loading platens such as brush bearings and fluid cushion systems.

Hussein (1998) discussed tests carried out by Sheppard (1967). He used a **lubricant** between the loading platen and the test specimen. This test assembly is one of the easiest ways to reduce friction. However the lateral extrusion of the lubricant will induce lateral tensile stresses and a non-uniform stress distribution in the specimen's surface resulting in a reduction of its apparent strength. Similar results were observed when friction reducing pads were used combining two layers of plastic film and a layer of grease between.

Friction reducing pads usually consist of some kind of lubricant or grease, aluminium sheets, plastic film, Teflon sheets or a combination of these and were used by Hughes and Bahramian (1965). Tests were conducted on 4 in. (ca.100 mm) cubes with initially two layers of polytetrafluoroethylene (PTFE). They found that the coefficient of friction was not low enough and experimented further until they found a combination of Melinex polyester film, Molyslip grease and a hardened aluminium sheet with 0.76 mm thickness which they called a MGA friction reducing pad. The strength results for the cube tests decreased compared to tests conducted without friction reducing devices and become very close to the strength results obtained from prisms of the same concrete and the same square shape surface but twice as long. Cracking of the failed cubes changed from the cup-cone failure to a vertical plane failure within the direction of loading.

For biaxial loading conditions Vile (1965), Mills and Zimmerman (1970) and Lee et al. (2004) were also experimenting with friction reducing pads and obtained similar strength results as with the use of a brush loading system.

Another test method for concrete under compression is the **oil cushion support system** developed by Andenaes et al. (1977) at the University of Colorado. The specimen is loaded by means of flexible membranes under hydraulic pressure within a closed pressure chamber. This chamber was designed so that prescribed uniform compressive principal stress states could be applied to the material without displacement boundary constraints. The scatter of the failure points was larger in the oil cushion series than in the steel

platen series which was carried out for comparison reasons. Failure occurred in different splitting types with even some specimens' intrusion of the membrane into a pinhole on the surface leading to premature failure because of tensile stress concentration. It was concluded that the stress-strain relation appears unaffected by the boundary conditions of the specimen for all stress levels below failure. Constrained boundary displacements (steel platen) of the loaded specimen surface increase the uniaxial compressive strength and give also relatively higher biaxial strength values.

Brush bearing load application systems consist of individual steel filaments with a cross section of around 5 x 5 mm each and a length between 100 and 140 mm, as in the study of Kupfer et al. (1969). The length of the brush depends on the tested concrete strength as the bristles are likely to buckle for higher strength concrete and therefore have to be reduced in length. Uniaxial tests provided sufficient proof that the end restrain of concrete cubes or plates can be eliminated by the use of brush bearing platens. They provided similar results as a tested prism with a height to side length ratio of more than 4, where also no restraining effects are assumed to influence the concrete strength. Similar results are obtained by the use of a **comb** like load bearing system (Buyukozturk et al. (1970), Liu et al. (1972) and Tasuji (1978)).

The simplest way to test concrete is the use of **solid dry steel platens**. They don't need special preparation and are simple to use. Iyengar et al. (1965) were using such loading platens which produced overestimated biaxial compression strength because the confinement effect caused by friction and the resulting constraints.

An extensive study on the interaction between specimen and platen system is given by Newman, 1979. He distinguishes between

a) loading directly through rigid platens
b) rigid platen loading through soft intermediate materials

c) rigid platen loading through materials with a low E value, i.e. cardboard
d) loading through platens of the same material as specimen
e) loading through non-rigid platens, i.e. brush or hydraulic platens.

For rigid platens, lateral restraint stresses are induced which increase from the axis towards the periphery. They tend to reduce the lateral deformation of the specimen and initiate failure within the central zone. The failure load decreases when the ratio of specimen height to width increases, up to a ratio of H/W = 2.5 after which it remains constant.

Using soft intermediate materials tensile lateral restraint stresses are induced at the interface due to extrusion of the insert material. The restraint tensile stresses increase with the thickness of the insert material and reduce with increasing H/W ratio. Failure starts within the end zones and progresses towards the centre.

Using material such as cardboard reduces the strain concentration within the specimen, particularly where the loading surfaces are not plane. Since their lateral movement under load is very small they do not induce any significant tensile or compressive restraint stresses in the specimen.

Loading through platen of the same material would produce the best result as the specimen and the platens react as one monolithic specimen. However, for testing concrete this method is not practical as each test would destroy the platen systems.

Brush loading platens apply the loads as a series of concentrated loads which may affect the behaviour of the heterogeneous materials. It was shown that higher lateral deformations are induced in specimens than by rigid steel platens. The W/H ratio has less influence on the strength results for brush platen tested specimen as shown by van Mier, 1986.

In order to generate information about the influence of different test methods a joint test program was carried out between seven research institutions which had been active in multiaxial concrete testing in the past: Bundesanstalt für Materialprüfung, Berlin, Germany; Ente Nazionale per l'Energia Elettrica, Milan, Italy; Imperial College of Science and Technology, London, England; Institut für Massivbau, Technische Universität, München, Germany; New Mexico State University, Las Cruces, New Mexico, USA; University of California, Davis, California, USA; and University of Colorado, Boulder, Colorado, USA.

Identical materials were used and the production of specimens took place in the laboratory at the University of Colorado in Boulder, USA and specimens were then shipped under controlled conditions to the other partner Institutions in Germany, Great Britain and Italy. The cylinder concrete strength f_c' varied around 33 N/mm^2. They were tested at identical ages and it can be assumed that the variation in material is minimised by this procedure. The test variables which remained were the different sizes of test specimen and the different methods of testing which included fluid cushions, brush bearing platens, flexible loading platens or loading stamps, steel platens with different kind of friction reducing pads and lubrication and solid dry steel platens. An overview of the different loading systems is shown as schematic drawings in Figure 2.2.

The use of an appropriate test method is therefore essential and the effect of surface constraints on the specimen needs to be considered very carefully. On one side there are rigid steel platens which causing uniform normal displacements but variable normal stress as a result of friction, on the other side there are fluid cushions which perform uniform normal stresses but variable normal displacements because of local surface failure. The results of this investigation are published in Gerstle et al. (1979) and Gerstle et al. (1980) and are summarised in the following paragraphs.

The variation between the various laboratories in biaxial strength within the compression-compression region is much greater than the range observed for uniaxial strengths. However a distinction has to be made between load systems

with high constraint like dry steel platen and systems with lesser constraints such as lubricated platens, brushes or fluid cushions which, were of a remarkably narrow band for the equal biaxial strength. The shape of the strength envelopes is also influenced by the different brush systems and specimen shapes.

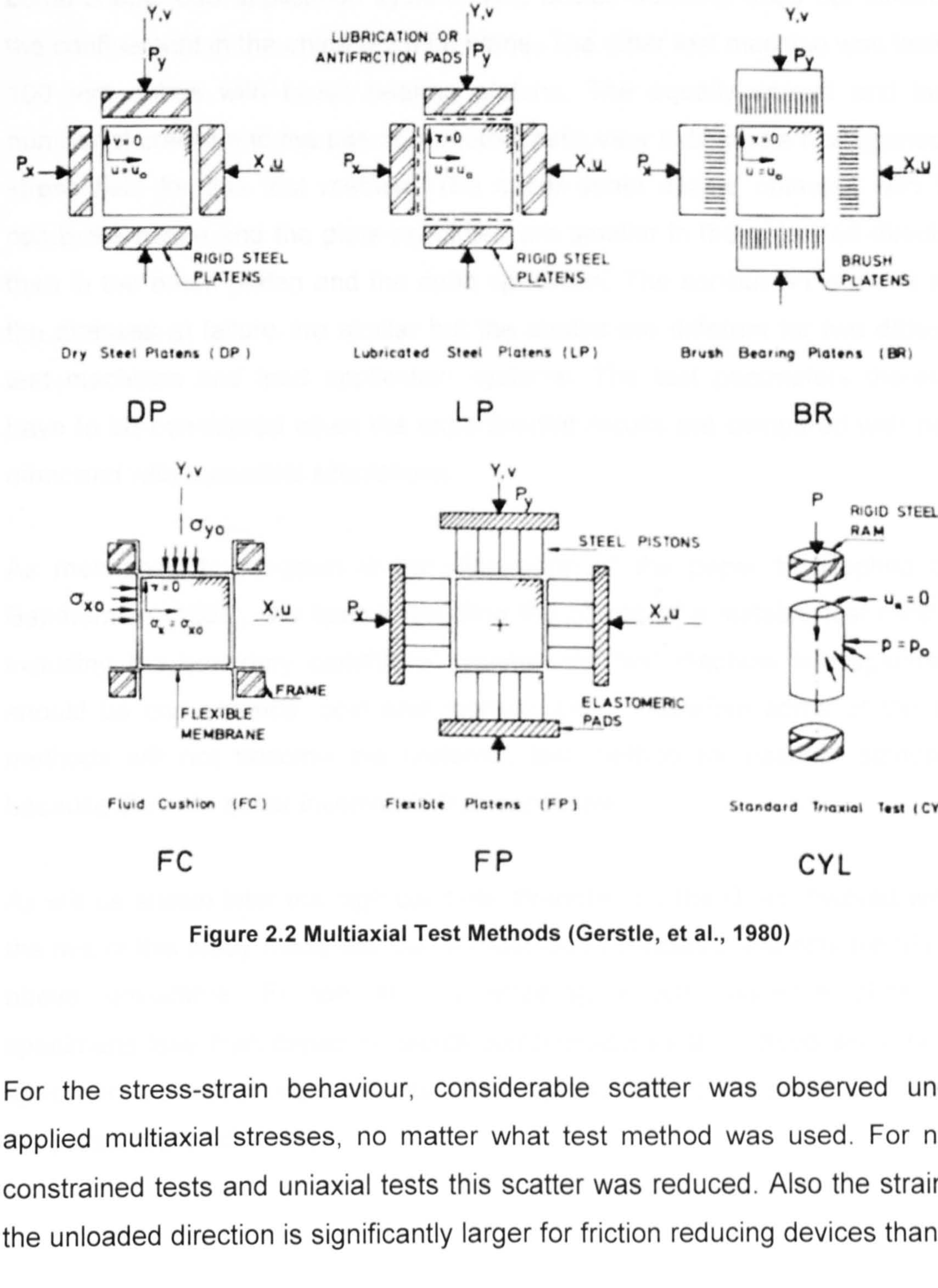

Figure 2.2 Multiaxial Test Methods (Gerstle, et al., 1980)

For the stress-strain behaviour, considerable scatter was observed under applied multiaxial stresses, no matter what test method was used. For non-constrained tests and uniaxial tests this scatter was reduced. Also the strain in the unloaded direction is significantly larger for friction reducing devices than for

dry steel platens. Within the direction of loading the difference becomes smaller. No strain data was obtained near or past failure because of the brittle failure of the tested concrete.

Similar comparisons between two biaxial test machines were carried out by Torrenti et al. (1991). One machine was testing 160 x 160 x 30 mm slabs with a comb shape load application system. This device however does not eliminate the confinement in the unloaded third plane. The other test machine was testing 100 mm cubes with brush bearing platens. The equally spread and large number of cracks and the use of a photo-elastic view indicated a homogeneous stress field for this test method. The stress-strain curves obtained with the comb-like platen and the plate specimen are smaller in the unloaded direction than in the brush platen and the cube specimen. The conclusion is made that the stresses at failure are similar but the strains are different for two different test machines and load application systems. The test parameters therefore have to be considered when the experimental results are compared with each other and with numerical simulations.

As mentioned by Lingram in the discussion of the paper by Hughes and Baharamian (1966), the factors affecting the choice of a suitable test method, including the boundary conditions between the test machine and specimen, should be convenience, cost and reproducibility. Therefore some of the test methods will not become the preferred test method for national standards because they are either inconvenient or expensive.

As will be shown later the high concrete strength and the fibres involved within the mix of this study made the use of most load application systems mentioned above unsuitable. Friction and constraining effects influence plate like specimens less than cubes in biaxial compression as the loaded sides of the specimen are restraining each other anyway and the out of plane dimension of the plates are much smaller.

2.3.2. Mechanisms for applying tension loads

Popovics (1998) stated that almost any kind of fracture that occurs in concrete through cracking is caused by tensile stresses. This means that concrete fracture is essentially a tensile failure regardless of whether the failure is caused by compression or other factors.

However to capture the tensile load capacity of concrete in a direct tension load test is particularly difficult. Different approaches have been made over the years starting at the beginning of the last century with dog bone shaped specimens, specimens with a notch in the middle section, glued specimens or specimens with metal bars or rods cast into them.

The difficulties with this form of direct tensile testing is that it is burdened with misalignment and clamping stresses. Thus the stress concentrations, bending and torsion created during testing produces reductions of unknown magnitude in the measured strength and making the reliability of these strength results highly questionable. Because of the stresses introduced due to gripping, there is a tendency for the specimen to break near the ends. This problem is often overcome by reducing the section of the central portion of the specimen (dog bone specimen).

The method in which metal pulling pieces are glued with epoxy to the end of the specimen eliminates stresses caused by gripping. However the eccentricity problem still exists. Similar problems occur when metal bars are cast into the tension specimen. An overview of different tensile test methods is schematically shown in Figure 2.3.

The introduction of a compressive load in the second direction brings even more difficulties with it in terms of eccentricity and makes precise alignment of the test equipment necessary.

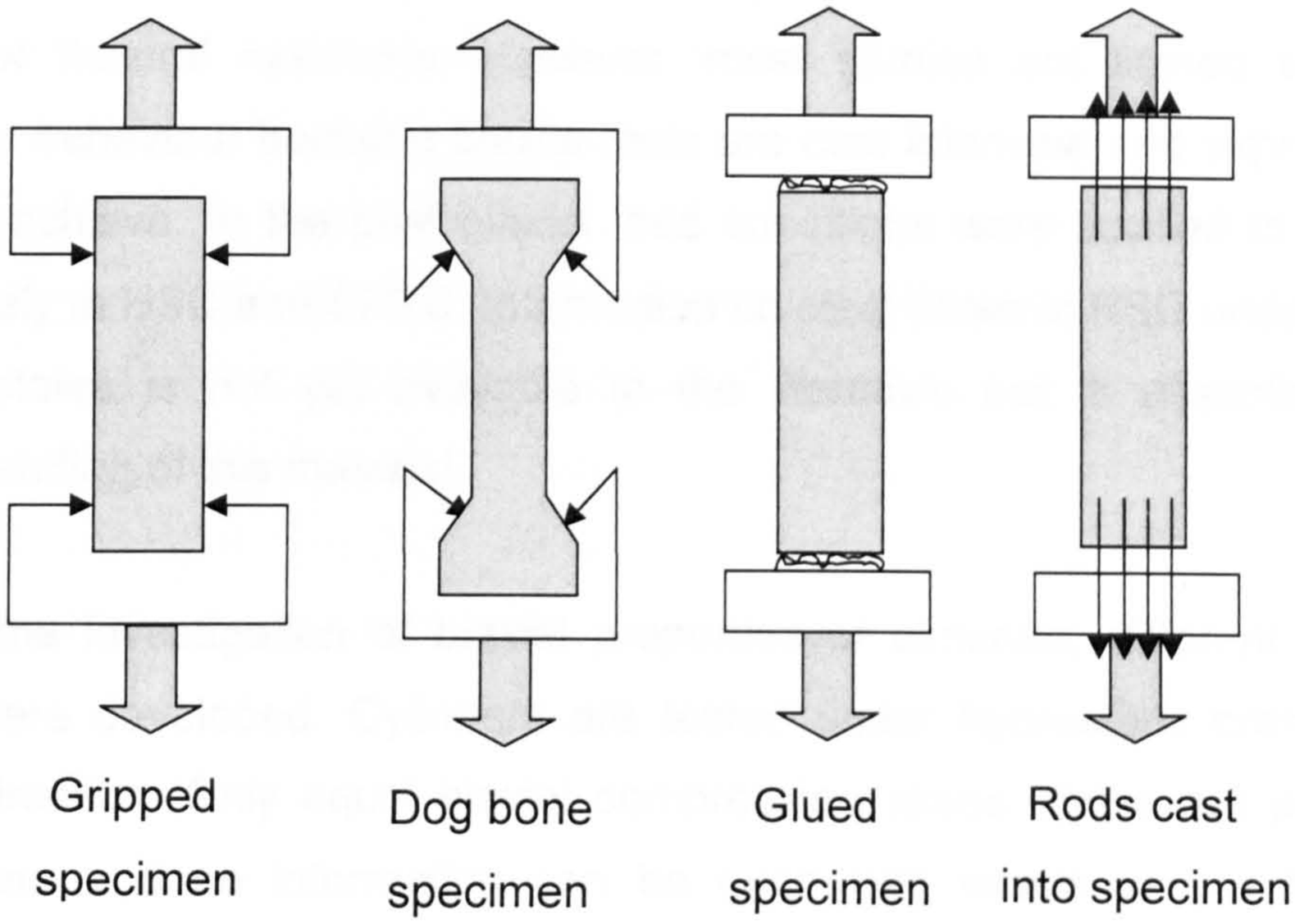

Figure 2.3 Tension applying systems

2.4. Biaxial concrete testing

Studies about the behaviour of concrete not only under uniaxial but also under biaxial stress states are essential to develop a failure criterion for different concretes. To do so a good understanding of the failure strength envelope is needed. Hannant (1974) summarised several test results in strength envelopes and Nomograms in order to generate one single failure surface for concrete. Therefore he collected most available data on the strength of concrete under multiaxial stress states to provide information for engineers in such a manner that he indicated a safe minimum envelope which could be adopted. Within his attempt it became obvious that the scatter of test points is too large depending on many variables such as the test method, specimen type or concrete strength.

Many structural deformations are caused by a biaxial stress state like in slabs, shells or flexural members. However, most studies are limited to uniaxial concrete behaviour because biaxial tests are cost intensive and experimentally hard to achieve. In the past biaxial load conditions were applied to NSC and very rarely to HSC and SFRC. Information on steel fibres in HSC under different stress states is not yet available in the literature but is essential for the understanding of this material.

During the investigation of biaxial properties of concrete, different specimen types were developed. Cylinders are tested under hydrostatic pressure in a radial direction. Only equal biaxial compression stress states are possible to investigate and no information can be generated where tensile forces are involved. The hydraulic fluid may penetrate the specimen, generating local tensile stresses, which can be avoided by the use of a membrane. The only observation which could be drawn from this kind of test was that concrete is at least as strong in biaxial as in uniaxial compression.

Similar problems exist for hollow cylinders. McHenry and Karni (1958) applied a combination of internal hydrostatic pressure and axial compression load and generated good agreement in the compression-tension region of the biaxial strength envelope of concrete, which is represented by an S-shape curve.

Bresler and Pister (1958) applied torsion and axial compression to create information about the combination of shear and compression stresses, then Bellamy (1961) tested hollow cylinders under external hydrostatic load and axial compression. His result shows an increase in the biaxial compressive strength of 250 % compared to its uniaxial compressive strength and therefore is greatly overestimated.

Rosenthal and Glucklich (1970) combined inner and outer hydrostatic pressure with axial compression and tension forces. Their results were also overestimated in the compression branch within the biaxial strength envelope.

In all these tests the thickness of the hollow cylinder may influence the results significantly and therefore lead to incorrect conclusions.

Cube or plate type specimens were used in the past by various researchers which are reviewed below. They allow a simpler method of strain measurement and observation of the deformational characteristics, crack propagation and the failure mechanism. It is also easier to apply any principal stress ratio with hydraulic actuators. The problem with this type of specimen is the confining effects between the machine platen and the loaded concrete surfaces due to friction. Friction reducing load application systems were developed and were discussed earlier in this literature review.

In the following section different publications are reviewed in respect of plate like specimens under biaxial loading for NSC, HSC and SFRC respectively.

2.4.1. Normal strength concrete

Sundara Raja Iyengar et al. (1965) tested 150 and 100 mm cubes with a concrete strength of up to 48 N/mm^2 through rigid platens. No difference was observed in the results of sequence and proportional type of loading and also for different types of curing and capping conditions. Both this finding and that of an increase of 350 % in the biaxial compressive strength compared to its uniaxial strength, was questioned by researchers in the discussion part of the publication (Fumagalli, et al., 1965). Reason for the overestimation might be the use of solid rigid steel platen and the sequential loading.

Within the study by Vile (1965), 256 x 256 x 103 mm plates were tested in compression-compression, and dog-bone shaped specimens in compression-tension and tension load cases. Solid platens were used to apply compression loads, with the addition of friction reducing pads for the compression-tension specimens. A distinction was made between discontinuity level and ultimate

load for the biaxial strength envelopes. Discontinuity was defined as a critical point during loading when there is a marked change in the mechanical properties of the material and a more severe cracking take place. Again, no significant differences were obtained for proportional or sequential loading, however most tests were loaded with a fixed ratio between the two stresses.

Robinson (1967) tested specimens of the same dimension as Vile under biaxial compression. He used a special concrete curing compound which partially soaked into the concrete and therefore provided a layer to permit relative displacement between the solid steel platen and the concrete specimen. His conclusions are that a lateral compressive load increases the ultimate compressive strength and also the load at which major microcracks develop. The failure of concrete is caused by tensile cracking, and the elastic parameters as Poisson's ratio and Modulus of Elasticity are not constant in states of biaxial compression.

Kupfer et al. (1969) was one of the first publications with a full set of experimental test data for NSC up to 56 N/mm^2 under biaxial loading within each of the three regions, C-C, C-T and T-T. Many researchers refer to these fundamental results and use it for their research. The biaxial stress envelopes are shown in Figure 2.4.

The tests were carried out with brush platens on 200 x 200 x 50 mm plates. Under equal biaxial compression f_{cb} (σ_2/σ_1 = 1) a strength increase of approximately 16 % was achieved whereas at a stress ratio of σ_2/σ_1 = 0.5 the maximum strength increase was 27 % higher than the uniaxial strength. Within the compression-tension region the compressive stress at failure decreases almost linearly when the tensile stress is increased. In biaxial tension the strength is approximately equal to the uniaxial tensile strength. Similar results were obtained by Stegbauer and Linse (1972) who carried out their biaxial tests in the same machine in Munich not only on normal strength concrete but also on lightweight concrete, cement paste and gypsum.

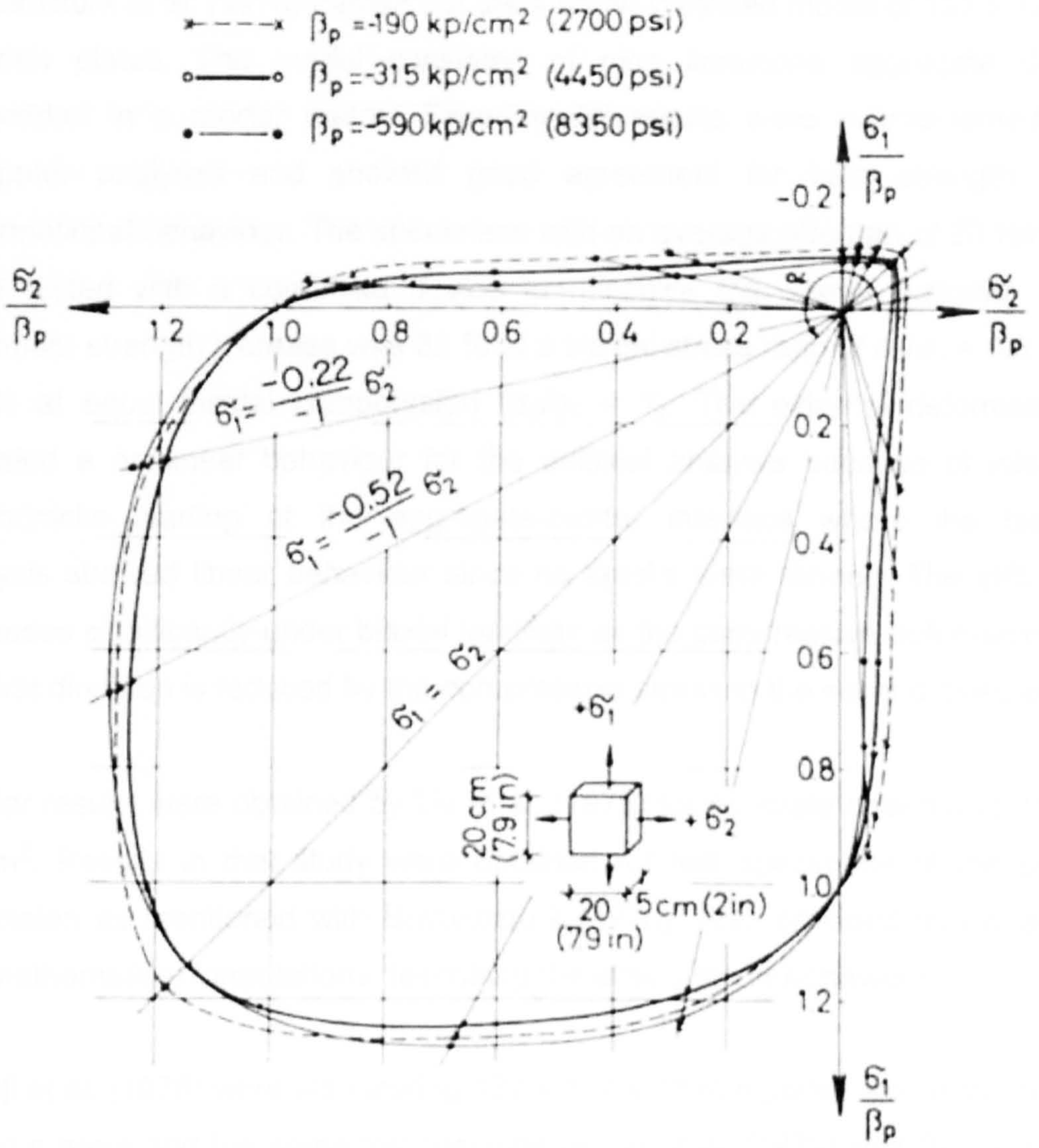

Figure 2.4 Biaxial strength of concrete; results of expeimental investigation (Kupfer et al., 1969)

Mills and Zimmerman (1970) tested relatively small cubes of 57 mm in a 27 ton capacity triaxial test machine. Concrete strength was recorded around 30 N/mm^2. Special attention was given to friction reducing pads which consisted of a combination of grease and Teflon, aluminium or polyester. The cracks at the tested specimen indicated splitting in the direction of the smallest principal stress and the biaxial tests ended with explosive failure.

Buyukozturk et al. (1970) carried out tests on an idealised model of 127 x 127 x 13 mm plates. The model consisted of nine limestone aggregate discs embedded in a mortar matrix. Experimental results were supplemented by computer analyses and showed good agreement for both strength and deformational behaviour. The specimens with an average strength of 20 N/mm^2 were tested with a comb-like device to minimise the lateral restraint. The maximum strength increase was 32 % at a biaxial stress ratio of $\sigma_2/\sigma_1 = 0.5$ and 24 % at equal biaxial compression ($\sigma_2/\sigma_1 = 1$). The external deformations revealed a nonlinear behaviour for the uniaxial analysis because of internal microcracks starting at the aggregate-mortar interface where the biaxial analysis showed linear behaviour since no cracks were formed. The stiffness increases significantly under biaxial loadings as the compressive deformation in the first direction is reduced by the compressive stress in the second direction.

Similar results were obtained by Liu et al. (1972) for concrete strength up to 35 N/mm^2. Results in that study were obtained for test specimens of the same dimension as mentioned with Buyukozturk (1970). Also provided by Liu et al. are mathematical formulations describing the stress-strain behaviour.

Tasuji et al. (1978) were also testing 127 x 127 x 13 mm plates with a comb-like platen system and the same test machine as Liu et al. (1972) and Buyukozturk et al. (1970). Therefore they came to similar conclusions as those described previously. A 22 % strength increase for a stress ratio of $\sigma_2/\sigma_1 = 0.5$ was achieved. The maximum strain under uniaxial and biaxial compression at maximum load was about -2500 microstrains and for uniaxial and biaxial tension tests +150 microstrains for a concrete strength of about 33 N/mm^2.

The primary types of failure for all combination of biaxial stresses are summarised by Nelissen (1972) and shown in Figure 2.5. The failure types are shown for 177 x 177 x 126 mm plate specimens tested with a brush like platen system and with solid platens. Plain concrete fails under biaxial compression by tensile splitting with cracks parallel to the unloaded surface for higher ratios of σ_2/σ_3. For lower ratios of σ_2/σ_3 cracks appear perpendicular to both the σ_2 and

σ_3 direction. For stress ratios with tensile forces, cracks form in the direction of the tensile load. Under uniaxial tension only one major crack was observed. It was mentioned that the use of different platen systems influences the failure mode. With the solid platens there existed less splitting failure cracks and the failure happened more to the end of the specimen towards the loaded surfaces, leaving the middle part undamaged.

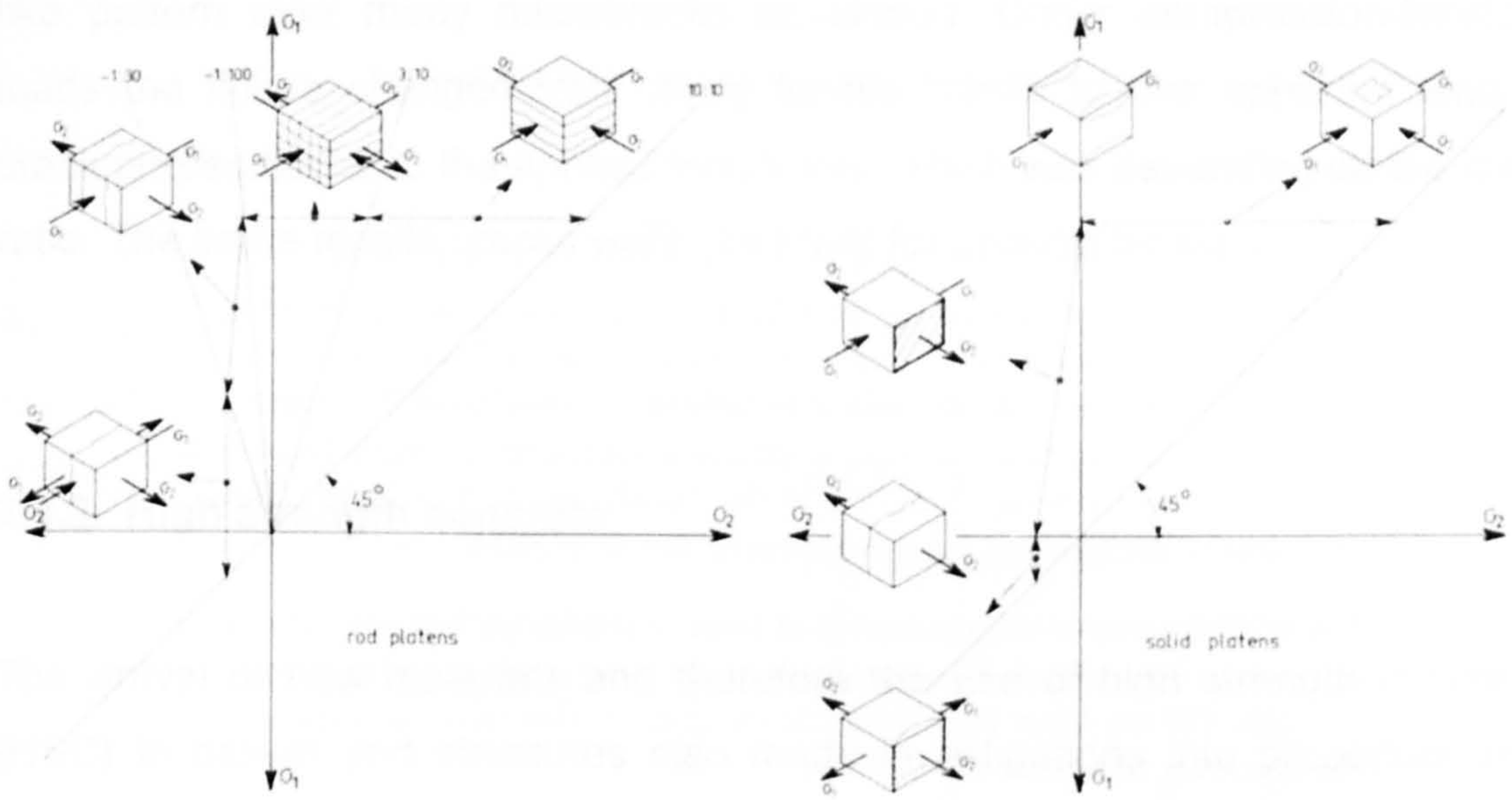

Figure 2.5 Failure mode of biaxial loaded concrete (Nelissen, 1972)

Another series of tests was carried out by Wang et al. (1987). 100 mm cubes with a concrete strength around 40 N/mm^2 were tested in two different test devices under biaxial and triaxial compressive load conditions. Dry steel platens as well as several friction reducing pads were used. However the strength result of the dry steel platens generated higher biaxial strength, all biaxial tests showed a wide scatter. The overall biaxial strength followed the trend which was established and discussed previously.

A recent study on NSC used in Korean nuclear containment buildings was completed by Lee et al. (2004). Concrete plates of dimension 200 x 200 x 60 mm and a concrete strength of 30 and 39 N/mm^2 were tested under biaxial

loads covering all three regions on the strength envelope, C-C, C-T and T-T. The loads were applied with solid steel platens through the use of Teflon pads to avoid confinement effects due to friction. The equal biaxial compression strength f_{cb} was 17% higher than f_c and the biaxial tension strength f_{tb} was almost similar to f_t. Stress-strain response, crack patterns and failure mode were similar to those obtained by other researchers. Under biaxial compression loading, failure was reported with an explosive failure and the formation of H-like pattern after many microcracks developed. Under compression-tension loads the failure changed from many tensile cracks to one apparent tensile crack perpendicular to the applied tensile load which was depending on the load ratio. The same tensile cracks were observed for uniaxial tension.

2.4.2. High strength concrete

The arrival of new materials and therefore the use of high strength concrete (HSC) in design and structures also made investigations into properties and behaviour of this material under biaxial stress conditions necessary. The basic information gained by different investigations follows the trend which was known from normal strength concrete, where test data is more widely available. However, for HSC the aspects of ultimate load, cracking and deformation is only covered by a limited number of investigations.

As Reinhardt (2000) stated, HSC becomes stiffer and more brittle than normal strength concrete (NSC) due to several factors. The mortar matrix stiffness is higher and approaches the stiffness of the aggregates. Therefore HSC is more homogeneous than NSC and the crack arresting effect between aggregates and matrix is limited. In fact, the cracks run through the aggregate grains which also lead to brittle failure. The bond between matrix and aggregates becomes higher as well as the matrix tensile strength. Therefore internal cracking is reduced in number and size up to a higher stress where they will extend at once leading to almost immediate brittle failure.

The biaxial compression strength in HSC is, as in NSC, higher than the uniaxial strength. The maximum biaxial strength occurs at a biaxial stress ratio of 0.2 to 0.5. However the increase in biaxial compressive strength f_{cb} compared to the uniaxial compressive strength f_c become less at higher concrete strengths. This was already stated by Kupfer et al. (1969) and Tasuji et al. (1987). Also mentioned in the previous sources is the decrease in uniaxial tensile strength of HSC when compared to the uniaxial compressive strength. Plain HSC seems to be more influenced by tensile strengths in the biaxial compression-tension region than NSC.

As Chen et al. (1985) stated the ultimate strength in biaxial compression is significantly higher than the uniaxial strength and occurs between a biaxial stress ratio σ_2/σ_1 = 0.2 to 0.5. The addition of a minor principal stress increases the stiffness of the specimen in the major principal stress direction. As the biaxial stress ratio increases the stress-strain curve becomes linear up to a higher stress. The HSC behave elastically up to a higher stress than NSC.

The discontinuity point and the proportional limit also occur at a higher stress for HSC than for NSC. Within the publication the discontinuity point was described as the point where concrete indicates the onset of an unstable, self-propagating, progressive crack growth mechanism where the Poisson's ratio begins to increase significantly under monotonic loading. The proportional limit is defined as the point at which the stress-strain curves deviates by 3 % from the initial tangent line. Chen et al. carried out their tests on concrete plate models similar to those used by Buyukozturk (1971) and Liu (1972) with a brush bearing load system under displacement control and with concrete strength up to 50 N/mm^2 under biaxial compression.

Nawy et al. (2003) tested 100 mm cubes with concrete strength of 82 N/mm^2 under biaxial compression using a concrete mix without silica fume. Half of the test groups were tested with solid dry steel platens facing the surface of the specimen. The other half use Teflon pads in order to reduce or eliminate any

friction. Loads were applied incrementally via a manual control panel. Stiffness and ultimate strength were increased within the specimen tested without Teflon pads. A maximum biaxial compression strength increase of 30 % over the uniaxial strength was recorded for a stress ratio of σ_2/σ_1 = 0.5 for dry steel platen. This increase was only 15 % when friction reducing pads were used. For the equal biaxial load case the increase was 20 % and 1 % respectively.

The stress-strain relationship for biaxial tested specimens was almost linear until the ultimate load with a higher proportional limit than in the uniaxial tested cubes. Confinement through the introduction of a minor principal compressive stress prevents and delays the internal microcracks from being created resulting in a stiffer and more linear stress-strain response. The HSC specimens under uniaxial loading perform a splitting type of failure inclined cracks at about 20 -30 degrees to the minor principal axis. Under biaxial conditions cracks occur in the loading directions. The cracks developed through the aggregate as well as the mortar. This shows that for higher strength concrete stronger aggregates are needed.

Calixto (2002) used the same biaxial test machine as Chen et al. (1985) to gain information about discontinuity and ultimate stress levels in the compression-tension region. He used 125 mm square by 12.5 mm thick plates with a cylinder compressive strength f_c' of around 74 N/mm^2. The plate compressive strength f_{cp} was reported as 60 N/mm^2. The difference between the two values can be attributed to the confinement effect with the cylinders and the solid platen test machine. The tensile strength was 7 % of the compressive strength and therefore less than in NSC. The introduction of a principal tensile stress reduces the ultimate compressive strength in HPC more rapidly than in NSC. Therefore the shape of the biaxial compression-tension strength envelope for HPC is more linear than for NSC.

This strength was achieved only by adequate mixture proportion, careful placement and proper curing, using quality controlled cement and aggregates. Superplasticizer was used for a better slump result but no silica fume. The

specimens were glued with epoxy adhesive to an aluminium comb platen in the tension direction while the compressive loads were applied through a steel brush platen. For uniaxial compression the stress-strain curve deviated from linearity at high levels of straining where for all other stress combinations the curves are almost linear until failure. Modulus of elasticity in both tension and compression were reported as almost identical at around 46 kN/mm^2 whereas the Poisson' ratio was slightly higher in uniaxial compression (ν = 0.20) than in tension (ν = 0.19). The failure mode was observed as tensile splitting in a plane perpendicular to the direction of the principal tensile strain with a more brittle failure than for NSC.

The results of 150 x 150 x 40 mm HSC plates with a concrete strength up to 96 N/mm^2 under the full range of biaxial load combinations, C-C, C-T and T-T, is published in Hussein (1998), and Hussein & Marzouk (2000). Comparison is made between NSC, HSC and lightweight HSC. The HSC used, in addition to the normal concrete materials, silica fume, Superplasticizer and a water-reducing agent. The specimens were tested with brush loading platens manufactured from one steel block by cutting the 75 mm long filaments using the electronic discharge wire cutting technique. The first axis was under displacement control while the second axis was receiving the control signal from the output of the first actuator and was therefore in a load control closed loop.

Similar results were obtained as mentioned previously in the work of other researchers. The biaxial compression strength is up to 35 % higher than under uniaxial compression for a stress ratio of σ_2/σ_3 = 0.5. In equal biaxial compression σ_2/σ_3 = 1, the relative strength increase becomes smaller (around 9 %) as the concrete strength is increased. This means that the confining stress of the second axis is less effective for HSC. The ratio between compressions to tension strength also decreases for higher concrete strengths. Tension strength for HSC was only 5 % of its compression capacity (compared to 8 to 10 % for NSC). Again the compression capacity in the biaxial compression-tension region decreased more radically by introducing a small amount of tension. The HSC specimens showed linear stress-strain behaviour up to a higher stress

than NSC, leading also to a higher discontinuity limit. The failure mode was reported with no fundamental difference between HSC and NSC.

Within the work of Curbach et al. (2000) 100 mm cubes were tested with a brush loading platen system under biaxial compression. The concrete strength varied up to 94 N/mm^2. It is important to note that with increasing concrete strength the relation between uniaxial and biaxial compressive strength decreases.

2.4.3. Steel fibre reinforced concrete

One of the first publications on steel fibres in concrete under biaxial loading was by Tailor et al. (1975). A fibre volume fraction V_f = 2 % was mixed into a mortar matrix with a strength of around 30 N/mm^2. The round, straight fibres were 13 mm long with an aspect ratio of l/d = 85. The difference between brush platens to solid steel platens was investigated as well as comparing the effect of sequential loading to proportional loading and load control to displacement control for plain and fibre mortar.

The biaxial compression-compression strength for the solid platen was almost double the strength of that for the steel brush as reported before by Kupfer et al. (1969). Also higher biaxial strength was observed for the proportional load application especially for higher load ratios close to σ_2/σ_3 = 1. Specimens tested with solid steel blocks showed almost no change caused by the chosen control system where the brush platen tests showed higher biaxial strength for load control. The difference between plain and fibre concrete was reported in the limiting curve whereas the maximum strength value was at a stress ratio of σ_2/σ_3 = 0.8 for SFC in contrast to 0.5 for plain NSC. The test also showed that SFRC has a much larger biaxial envelope than NSC. This was explained with the enhanced tensile capacity of SFRC which works against the splitting failure in the plane perpendicular to the load. Finally it was concluded that biaxial

compression and fibre reinforcement can transform brittle mortar into an essentially elasto-plastic material.

Yin et al. (1989) tested 152 x 152 x 38 mm plates of plain and SFRC with brush loading platens under uniaxial and biaxial compression. The concrete strength of the plain concrete was reported as 38 N/mm^2 for the plate specimens and 42 N/mm^2 for cylinders. The fibre volume fraction V_f of the straight steel fibres was up to 2 % with steel fibres lengths l of 19 and 25 mm.

There was only a minor strength increase observed with the addition of steel fibres for the uniaxial load case. In contrast the biaxial strength of fibre concrete was significantly greater than that of plain concrete. The biaxial strength increases with increasing fibre length whereas the increase of V_f from 1 % to 2 % had little effect. The failure type changes from splitting failure in plain concrete to a failure type which was by the authors named as a shear based faulting failure. The addition of steel fibres increased the stiffness and the ductility under biaxial conditions but not under uniaxial loads. Therefore it was concluded that the addition of steel fibres has a similar effect in biaxial stress condition as the application of a small confining pressure in the unloaded direction.

Within the discussion of the above paper (Yin (1990)) it became evident that the strength increase of SFRC depends of many factors such as fibre type, shape, fibre volume, aspect ratio, aggregate size, mix design, specimen shape and size, specimen age and testing equipment and that ongoing research is necessary to make this material more practical and economical when used in structures under uniaxial or biaxial loading conditions.

For that reason Traina and Mansour (1991) tested 76 mm cubes with a concrete strength of 40 N/mm^2 using friction reducing pads and with different fibre variables. The hooked ended, smooth drawn fibres were 30 mm long with an aspect ratio l/d = 60. Another fibre type used was a carbon steel fibre with a

half-round cross section, a length of 25 mm and an aspect ratio l/d = 33. Both fibre types were tested for different fibre volumes up to V_f = 1.5 %.

Under uniaxial stress SFRC does not show a clear trend. Some mixes generated higher strength than plain concrete others were weaker depending on the fibre variables. For biaxial compression SFRC had a higher compressive strength over plain NSC. Again a change in the failure mode was reported from a tensile failure in plain NSC to a shear type failure for SFRC. Passive confinement was used as term for the effectiveness of fibres for confinement of plain concrete. As mentioned previously for plain HPC, the increase of the uniaxial strength of a concrete mix decreases the gain in biaxial strength significantly.

Within the study of Torrenti and Djebri (1995), two metal fibre concretes were tested under biaxial compression. One contained amorphous iron fibres with a length of 30 mm and V_f = 0.5 %. The other 60 mm long hooked ended steel fibres with V_f = 1 %. Tests were carried out on 100 mm cubes by using brush platens.

The strains within SFRC were greater than those reported in plain concrete as well as exhibiting a gain in biaxial strength. The failure was reported with fibre pull out. Within the amorphous iron fibre specimen, the failure type was similar to plain specimens with the fibres breaking at the end of the test. In general it was stated that the addition of fibres makes the material more ductile and the direction of casting and therefore the fibre orientation has an influence on the biaxial strength.

SFRC under biaxial tension-compression was tested by Demeke and Tegos (1994). 30 mm long hooked ended steel fibres with an aspect ratio l/d = 60 were used in a concrete matrix with f_c = 30 N/mm^2. The specimens were 100 mm square and 300 mm long with metal rods on each side to apply the tension force. The central region where the compression load was applied through friction reducing Teflon pads was 60 mm wide. The compression load was

applied first with a simple uniaxial compression machine followed by the tensile load of two oil jacks applied through fine metal bars cast into the specimen.

The results show that when steel fibres are mixed into plain concrete a significant increase in uniaxial tensile strength f_t is achieved. The increase of f_t depends on the fibre volume V_f, with almost double the plain tensile strength for a SFRC mix with V_f = 1.5 %. In the biaxial compression-tension region the strength increased also by adding fibres to plain concrete. For higher V_f, the biaxial strength becomes equal to the uniaxial tensile strength for almost the entire region and smoothes the shape of the biaxial stress curve. The effect of steel fibres on plain concrete, even in high concentration, shows little change in the uniaxial compression strength. Fracture for SFRC occurred by a pullout process of the fibres accompanied by a more or less extensive cracked region. In plain concrete, fracture occurred in an explosive way with one crack appearing abrupt and dividing the specimen into two parts.

A full set of test data in all three regions of the strength envelope for SFRC is provided by Abdull-Ahad and Abbas (1989). 300 mm square plates with a thickness of 75 mm were tested by using a sequential solid bearing loading system. The tension specimens were enlarged in dog bone shapes on two sides in order to apply the tension forces. The fibre volume fraction was up to 1.5 % for fibres with aspect ratios of 60 and 100.

Within the biaxial strength envelope, large scatter was observed for the individual test points of each test series. Therefore, a clear trend could only be stated that FRC achieves higher strengths than plain concrete. For example a decrease in biaxial strength was observed for V_f = 1.5 %. The maximum strength increase in compression was 38 % at sequential stress ratio of σ_2/σ_1 = 0.5 for V_f = 1 %. Plain concrete increased by 24 % in comparison for the same stress ratio. Within the biaxial tension region a strength increase was observed compared to uniaxial tension. In general SFRC became more ductile than plain concrete.

In general, the strength of SFRC increases compared to plain NSC in all regions of the strength envelope. The steel fibres also influence the brittle failure mode of NSC from splitting failure with cracks parallel to the applied load to a more ductile material with inclining shear cracks.

2.4.4. High strength and steel fibre reinforced concrete

Steel fibres within HPC under biaxial loading conditions were not investigated by many research programs. This was one reason why this study was initiated to combine the advantages of both materials, SFRC and HPC. It is of great interest because any change and positive influence within the material properties will also lead to financial benefit in the long term. As stated before, because of the sheer amount of concrete used at present, even the smallest improvements will result in major economical benefits and make research necessary.

One research group which combined HPC and fibres was at the Technische Universität Dresden, Germany, lead by Curbach. (Curbach and Speck, 2002). They have extensive knowledge of testing plain HPC concrete under biaxial load conditions (Curbach et al., 2000) and combined their high strength concrete material with a fibre cocktail consisting of a variety of Polypropylene (PP) fibres and steel fibres. Therefore the advantages of two fibre types were combined. The Polypropylene fibres are active in the pre-peak state of the failure process where they initiate and lock microcracks. This lead to a more ductile behaviour where the energy at failure is not suddenly released anymore. This provides the steel fibres the possibility to develop enough interlock bonds between fibre and concrete matrix to bridge the cracks. Therefore the steel fibres develop and contribute a positive effect in the post-peak region.

The concrete strength in this study ranged between 55 and 90 N/mm^2. These two values were chosen because 55 N/mm^2 indicates the highest possible

strength by using normal concrete mix designs existing of cement, water, coarse aggregates and fine aggregates. The higher value of 90 N/mm^2 indicates the strength which is possible to achieve with normal strength aggregates and the addition of silica fume and superplasticizer. Therefore the entire range of today's use of industrial concrete is covered. The specimens were 100 mm cubes tested with steel brushes under uniaxial and biaxial compression. Materials included cement, micro silica, retarder and plasticizer.

With the use of the fibre cocktail the increase for biaxial compression ($\sigma_2/\sigma_3 = 1$) was recorded to be around 17 % compared to uniaxial compression and therefore higher than for plain HPC and in the region of NSC. Under uniaxial compression the fibre cocktail HPC behaved also more ductile and the explosive failure could be prevented.

The use of PP fibres only did not increase the strength. Steel fibres increase the strength but best results were gained with the fibre cocktail as a combination of both fibre types. Best results were gained when the fibre volume was adjusted to the concrete strength and the material used. Lower strength concrete does not need as much PP fibres as crack initiators, as enough weak links are already present to activate the steel fibres. The increase from 120 kg/m^3 to 160 kg/m^3 (equivalent to an increase from V_f = 1.5 % to 2 %) steel fibre content did not gain better strength results for HPC.

2.5. Loading path dependency

Two different types of load paths are possible for biaxial testing. One is called sequential loading where the load or displacement in one axis is applied first and held constant, followed by the other load or displacement until failure. This can be made in several small load steps or in two steps. The other method is called proportional loading where both axes apply the load at the same time and

the ratio between both stresses is fixed and remains in constant proportionality until failure. The two load paths are schematically shown in Figure 2.6

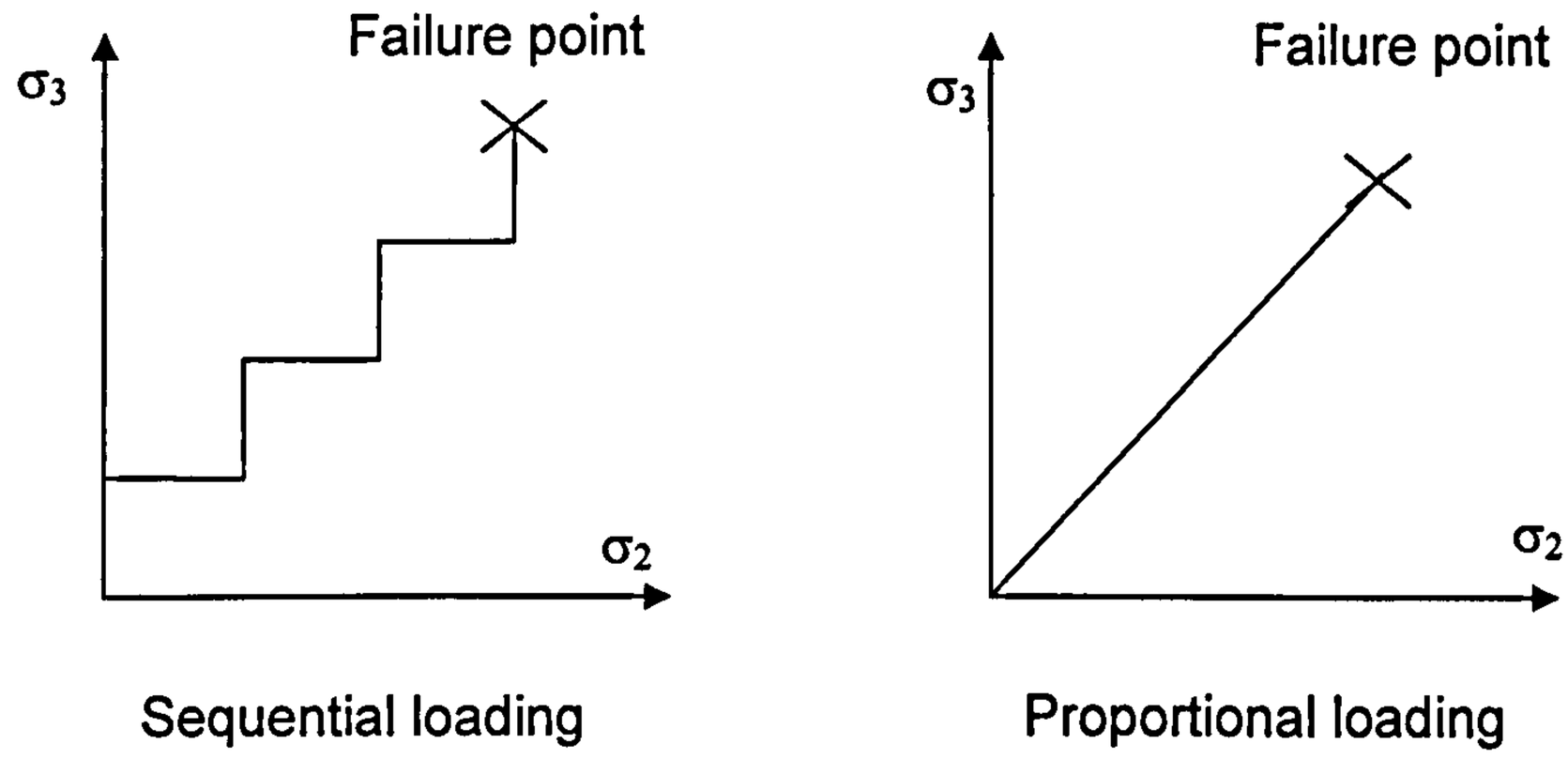

Figure 2.6 Different types of load paths

Different opinions and test results are available on the influence of the stress path to the biaxial strength envelope. Some researchers found a decrease for the sequential loading path compared to the proportional; others found an increase or no difference at all like Nelissen (1972).

Vile (1965) reported no significant difference in the values of discontinuity and ultimate stress for proportional or sequential loading in the compression-compression and compression-tension region of NSC and mortar. For the C-T region the compressive stress was applied first followed by the tensile stress.

For dry specimens Taylor and Patel (1974) found that two step sequential loaded specimen gives stronger strength envelopes than proportional loading. When the specimens were saturated the two step sequential loading produced either no difference or a small decrease in strength. Wet specimens in general provide higher biaxial strength than dry specimen from the same batch.

This is in contrast to his previous observations on dry lightweight concrete, Taylor et al. (1972), where the results were reversed. The strength envelope

decreased for two steps loading. With increasing concrete strength and solid steel bearing systems, the differences became smaller.

The specimens Taylor worked with were 50 mm cubes loaded with a brush type loading platen and compressive strengths up to 34 N/mm^2. Only the compression-compression region is covered, with a large scatter in the results and an overestimation in general for the biaxial strength envelopes. Other conclusions obtained were that surface friction generates a great difference in shape and magnitude in the biaxial strength envelopes as discussed earlier.

Lan and Guo (1997) also investigated the influence of the stress path in the compression-compression region. They tested four different sequential and a proportional loading path. No difference was found neither for the biaxial strength envelops, nor for the splitting failure type. Therefore they concluded that the compressive strength depends only on the final stress ratio and appear independent of the loading path. Tests were carried out on 100 mm and 70 mm cubes with a solid load bearings and three layers of aluminium foil friction reducing pads.

Pandit (1970) mentioned in the discussion of the paper by Kupfer et al. (1969) that several stress ratios in biaxial strength envelopes cannot be reached with the sequential testing method. He claimed that if one stress is kept constant and the other stress is increased until failure the constant stress can't exceed the uniaxial strength. This has to be considered in design when two different loads are applied asynchronously. In such a case the first load should not be greater than the uniaxial strength capacity of the element. Even so, the biaxial strength envelope would allow higher strengths for the final stress ratio.

The overall conclusion from the preceding investigations must be that the loading path might influence the biaxial strength envelope. However other factors such as friction between the loading platen and the specimen, or misalignment of the machine and therefore uneven loading, influences the test result to a much greater extent. This was also stated by Torrenti et al. (1993)

who showed strain results influenced by different loading paths. But this influence is less important than other differences e.g. to the bearing devices.

Moreover, careful judgment is necessary for the interpretation of the loading path results. In most applications a proportional loading might not occur and therefore the strengths of the biaxial envelopes are overestimated when they are gained from proportional loading tests. When using the biaxial strength envelopes other factors should be taken into consideration such as the concrete strength, the weight of aggregates or if the results were gained with wet or dry specimens. Most important in this respect is, what kind of loading technique was used to develop the test results as discussed earlier.

2.6. Approximation of the failure envelopes with mathematical formulations

The use and development of computers and with it for example the finite element method in analysis and design of concrete structures makes it necessary to establish constitutive relations and strength criteria for concrete. The failure envelope plays a key role and has been investigated experimentally over the last few decades. Therefore concrete strength and deformation under multiaxial stress states was investigated and put into mathematical formulations which can be used to build into constitutive relations which by themselves can be built into commercial software packages. Several attempts have been made to express the biaxial failure envelope empirically to provide meaningful engineering tools. Such formulae were presented by several researchers in various forms.

2.6.1. Constitutive modelling of concrete

Within a constitutive model the aim is to reproduce the stress-strain relations mathematically on the macroscopic level for different loading conditions. The microscopic mechanisms are therefore overlooked. Constitutive relations are used for example in plasticity models. The ultimate strength condition expressed for example as failure envelopes are essential. Other basic assumptions are the initial yield surface, the hardening rule and the flow rule.

The yield surface defines the stress level at which plastic or at least inelastic deformation begins. In HPC the yield surface is almost identical with the failure surface as the material is more homogeneous than NSC. The hardening rule defines the change of the yield surface and the change of the material properties during plastic deformation. The flow rule describes the direction of the plastic strain increment.

Knowing that a proper constitutive model for analysing a concrete structure requires a complete description of the behaviour of the material in the pre-failure (hardening) and post-failure (softening) range, this study concentrates on the failure criteria as the basis of almost all concrete constitutive models (Chen and Han, 1988).

2.6.2. Characteristics of failure surfaces

The general form of a failure surface can be expressed using the octahedral stresses σ_{oct} and τ_{oct} together with the angle of similarity θ

$$f(\sigma_{oct}, \tau_{oct}, \theta) = 0 \tag{2.1}$$

or in the Haigh-Westergaard coordinate system

$$f(\xi,\rho,\theta)=0 \tag{2.2}$$

with $\cos 3\theta = \frac{3\sqrt{3}}{2}\frac{J_3}{J_2^{3/2}}$

or by using the stress invariants I_1, J_2 and J_3

$$f(I_1,J_2,J_3)=0 \tag{2.3}$$

Concrete is a hydrostatic pressure dependent material and has curved meridians. The tensile meridian ρ_t and the compressive meridian ρ_c correspond to $\theta = 0°$ and $\theta = 60°$ respectively. The ratio between ρ_t / ρ_c increases from about 0.5 to about 0.8 with increasing hydrostatic pressure. Because of isotropy the deviatoric planes have symmetry of 60°. They are convex and a function of θ. The failure surfaces used for concrete material look all similar and are displayed in the next paragraphs for the associated failure criteria (Figure 2.10, Figure 2.11, Figure 2.7). The number of parameters can vary between one for the more simple ones (von Mises and Tresca for ductile metals) up to five parameters. The four parameter model by Ottosen and the five parameter model by Willam and Warnke both have parabolic meridians and are θ dependent.

2.6.3. Ottosen failure criterion

Ottosen (1977) defined a four-parameter failure criterion containing all three stress invariants. It is demonstrated to be valid for short-term monotonic loading. It corresponds to a smooth convex failure surface with quadratic parabolic curved meridians, which open in the negative direction of the hydrostatic axis. The trace in the deviatoric plane changes from nearly

triangular for small stresses to more circular shape with increasing hydrostatic pressure.

The state of stress as represented by a point in the Haigh-Westergaard system is described by the coordinates ξ, ρ and θ, where ξ is the projection of OP on the unit vector e = (1,1,1)/$\sqrt{3}$ on the hydrostatic axis and ρ and θ are the polar coordinates on the deviatoric plane normal to the hydrostatic axis as shown in Figure 2.7. The values of ξ, ρ and θ can be expressed in terms of the stress invariants I_1, J_2 and J_3 as defined earlier.

The failure criterion for plain concrete under the state of stress (σ_1, σ_2, σ_3) is expressed in terms of the stress invariants as:

$$f(I_1,J_2,\cos 3\theta) = A\frac{J_2}{f_{cp}^2} + \lambda\frac{\sqrt{J_2}}{f_{cp}} + B\frac{I_1}{f_{cp}} - 1 = 0 \qquad \textbf{(2.4)}$$

where f_{cp} = the uniaxial compressive strength of plain concrete and

λ = a function of cos3θ expressed as:

$$\lambda = K_1\cos\left[\tfrac{1}{3}\cos^{-1}(K_2\cos 3\theta)\right] \qquad \textbf{for } \cos 3\theta \geq 0 \qquad \textbf{(2.5)}$$

and

$$\lambda = K_1\cos\left[\tfrac{\pi}{3} - \tfrac{1}{3}\cos^{-1}(-K_2\cos 3\theta)\right] \qquad \textbf{for } \cos 3\theta < 0 \qquad \textbf{(2.6)}$$

The value of $f(I_1,J_2,\cos 3\theta) < 0$ corresponds to stress states inside the failure surface. The parameters A, B, K_1 and K_2 depend on the ratio of the uniaxial tensile to uniaxial compressive strength f_t/f_{cp}. For this study the values were taken as

A = 1.8076

B = 4.0962

K_1 = 14.4863 and

$K_2 = 0.9914$

as these values were recommended by Ottosen (1977) for a ratio of $f_t/f_{cp} = 0.08$, which is appropriately the value of the concrete used in this study..

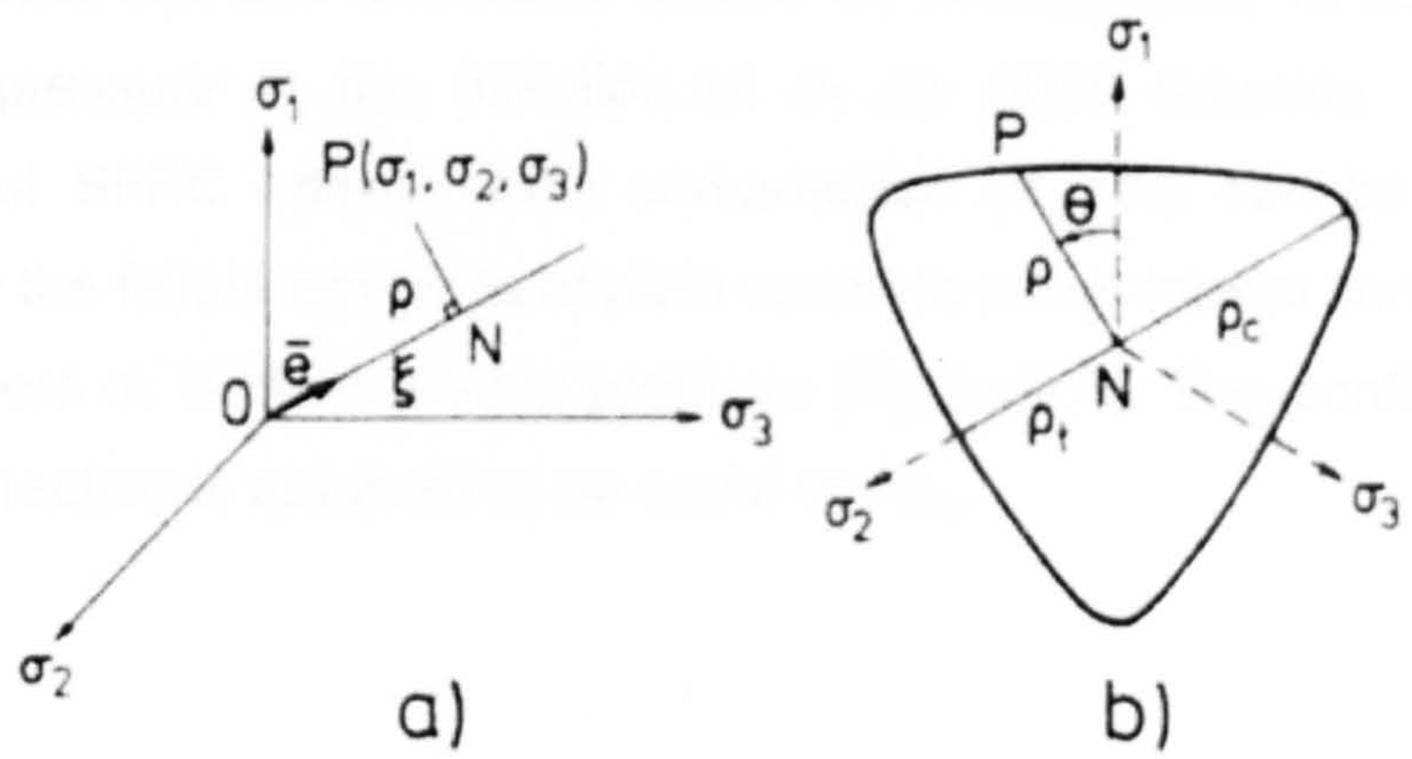

Figure 2.7 a) Haigh-Westergaard Coordinate System; b) Deviatoric Plane by Ottosen (1977)

2.6.4. SFRC failure model

The failure envelopes for plain concrete are generally arrived at from constitutive modelling and curve-fitting experimental data. To overcome the need of enormous amount of experimental data for each fibre type under biaxial load conditions, Murugappan, et al. (1993) and Tan, et al. (1994) derived the failure envelope for fibre concrete in terms of the post-cracking tensile strength σ_{tu}. This can be obtained for a given mix proportion and fibre type and content from direct tensile tests.

As shown earlier plain concrete under biaxial compression fails by tensile splitting with cracks parallel to the unloaded surface. The addition of steel fibres does not significantly change the stress-strain behaviour of plain concrete before cracking. Thereafter the fibres reduce the strains in the tensile direction and apply a confining pressure as mentioned by Yin, et al. (1989). Therefore the

behaviour of SFRC under biaxial compression is similar to plain concrete under a triaxial state of stress.

The presence of steel fibres was treated by Murugappan, et al. (1993) as a confining pressure in the direction of σ_1 on plain concrete. The strength envelope of SFRC under biaxial compression (σ_2, σ_3) can be regarded as identical to the failure envelope of plain concrete under triaxial compression (σ_1, σ_2, σ_3), where σ_1 is the confining pressure (Figure 2.8). This confining pressure in the σ_1 direction is assumed to be equal to - σ_{tu}.

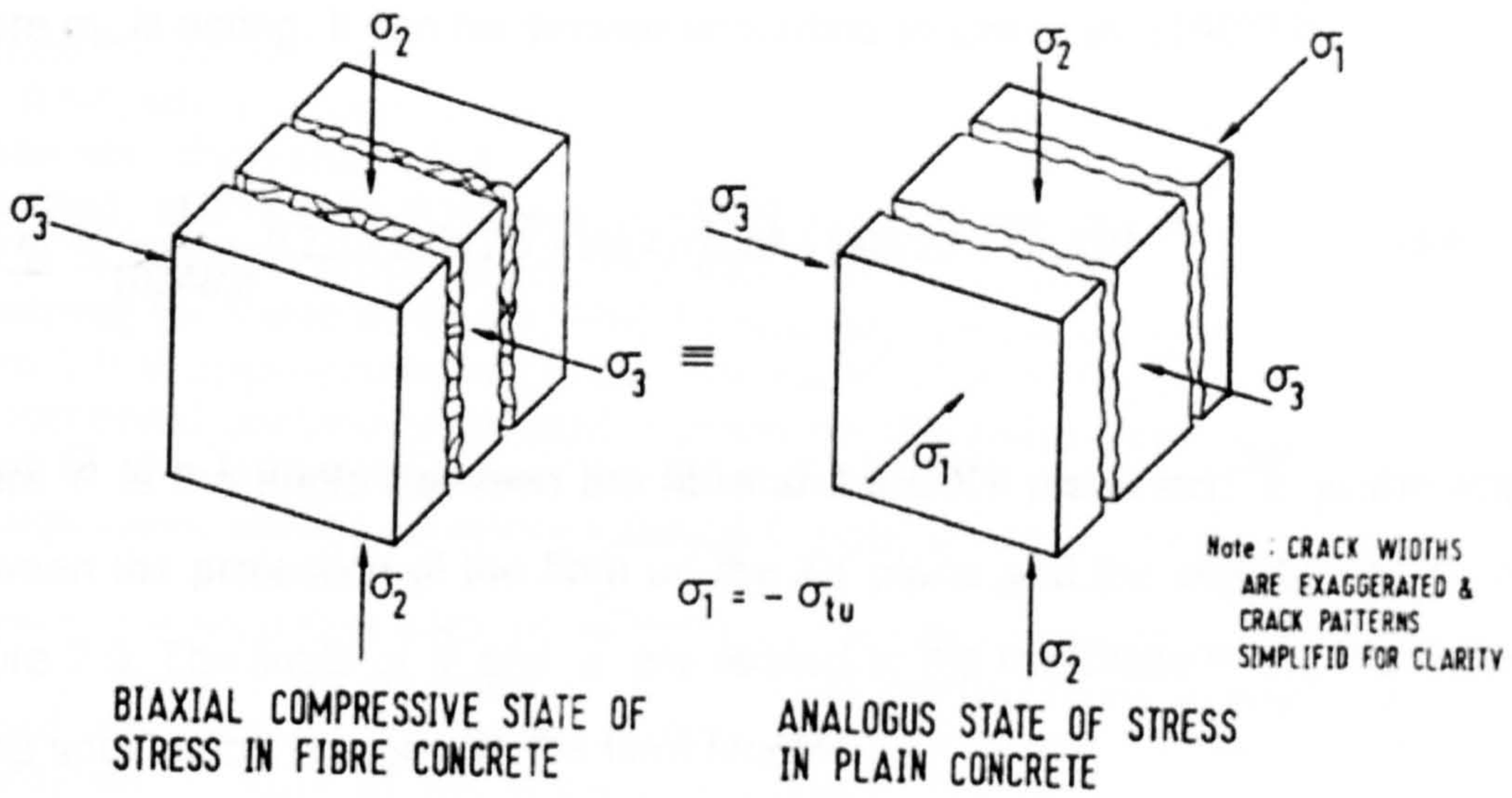

Figure 2.8 Confining stress model of SFRC for biaxial compression by Murugappan et al. (1993)

According to Lim et al. (1987) the post-cracking tensile strength σ_{tu} depends on the volume fraction V_f, the orientation factor η_0, the length efficient factor η_l, the aspect ratio l/d and the ultimate bond strength τ_u of the fibre as

$$\sigma_{tu} = \frac{\eta_l \eta_0 V_f l \tau_u}{2r} \qquad (2.7)$$

where r = the ratio of the cross-section area to the circumference of the fibre. The value for η_0 and η_l can be obtained according to Lim et al. (1987).

The value of η_l can vary between 0.5 and 1 depending on the critical fibre length l_c which is the length required to develop the ultimate fibre stress.

$$\eta_l = \begin{Bmatrix} 0.5 \\ 1 - l_c/2l \end{Bmatrix} \quad \text{for} \quad \begin{matrix} l \le l_c \\ l > l_c \end{matrix} \tag{2.8}$$

η_0 should be determined according to the σ_1 direction as that is the direction where σ_{tu} is acting. It can be derived according to Lim et al. (1987) by

$$\eta_0 = \frac{1}{1024\bar{\theta}\bar{\rho}}\left(12\bar{\rho} + 8\sin 2\bar{\rho} + \sin 4\bar{\rho}\right)\left(12\bar{\theta} + 8\sin 2\bar{\theta} + \sin 4\bar{\theta}\right) \tag{2.9}$$

where $\bar{\theta}$ is the angle between the fibre and the XY plane and $\bar{\rho}$ is the angle between the projection of the fibre on the XY plane and the direction of σ_1, see Figure 2.9. The limits of $\bar{\theta}$ and $\bar{\rho}$ are related to the thickness h and the width b of the specimen in respect to the fibre length:

$$\bar{\theta} = \sin^{-1}\left(\frac{h}{l}\right) \le \frac{\pi}{2} \tag{2.10}$$

$$\bar{\rho} = \sin^{-1}\left(\frac{b}{l}\right) \le \frac{\pi}{2} \tag{2.11}$$

If the fibres are randomly orientated in a three dimensional manner the two dimensions h and b should be greater or equal to the fibre length l. Hence $\bar{\theta}$ and $\bar{\rho}$ are equal to $\frac{\pi}{2}$ and the value obtained in Equation 2.9 above leads to η_0 = 0.14. For the case that the dimensions of the specimen h and b are smaller

than the fibre length l the value leads to $\eta_0 = 1$ which would be complete constraint.

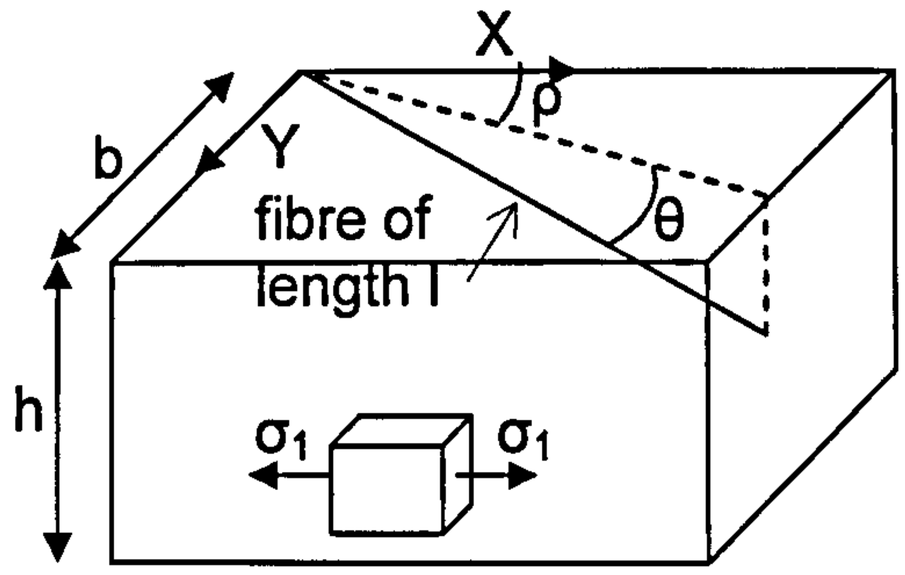

Figure 2.9 Fibre orientation

As $\sigma_1 = -\sigma_{tu}$ is constant throughout the loading history the stress state is not a proportional loading. This however as shown before does not influence the result significantly and can be neglected.

The above SFRC model proposed by Murugappan, et al. (1993) was used in combination with Ottosen's four-parameter failure criterion for plain concrete under triaxial conditions with the confining pressure $\sigma_1 = -\sigma_{tu}$.

2.6.5. Willam and Warnke failure criterion

Three parameter model

Because of symmetry of an isotropic material like concrete only a sextant of the principal stress space has to be considered. The failure surface of the Willam-Warnke model (1974) is represented by a hydrostatic and a deviatoric section. The hydrostatic section contains the equisetic $\sigma_1 = \sigma_2 = \sigma_3$ as an axis of revolution where the deviatoric section lies in a plane normal to the equisetic and being described by the polar coordinates ρ and θ. The failure envelope for

concrete material has a conical surface with curved meridians and a non-circular base section.

The failure curves of Willam and Warnke use elliptic curves to describe the deviatoric sections. Therefore they are convex and smooth everywhere. Due to the symmetry it is only necessary to consider the part between $0° < \theta < 60°$. The equation of the elliptic trace $\rho_{(\theta)}$ can be expressed in polar coordinates (ρ and θ) in terms of the parameters ρ_t and ρ_c:

$$\rho_{(\theta)} = \frac{2\rho_c\left(\rho_c^2 - \rho_t^2\right)\cos\theta + \rho_c(2\rho_t - \rho_c)\sqrt{4\left(\rho_c^2 - \rho_t^2\right)\cos^2\theta + 5\rho_t^2 - 4\rho_t\rho_c}}{4\left(\rho_c^2 - \rho_t^2\right)\cos^2\theta + (\rho_c - 2\rho_t)^2} \quad \textbf{(2.12)}$$

with the angle of similarity θ:

$$\cos\theta = \frac{\sigma_1 + \sigma_2 + \sigma_3}{\sqrt{2}\sqrt{(\sigma_1 - \sigma_2)^2 + (\sigma_2 - \sigma_3)^2 + (\sigma_3 - \sigma_1)^2}} \quad \textbf{(2.13)}$$

A linear variation with hydrostatic stress generates a cone with straight line meridians. In this case the failure surface is defined in principal stress space by the stress components σ_{oct}, τ_{oct} and the angle of similarity θ:

$$f_{(\sigma_{oct},\tau_{oct},\theta)} = \frac{1}{z}\frac{\sigma_{oct}}{f_{cu}} + \frac{1}{\rho_{(\theta)}}\frac{\tau_{oct}}{f_{cu}} - 1 = 0 \quad \textbf{(2.14)}$$

σ_{oct} and τ_{oct} are stress components representing the mean normal and shear stress. These values are normalised by the uniaxial compressive strength f_{cu}.

The three parameters z, ρ_t and ρ_c are defined by typical concrete test data such as uniaxial tensile strength f_t, uniaxial compression strength f_{cu} and biaxial compression strength f_{cb}, introducing the strength ratios α_z and α_u:

$$\alpha_z = f_t / f_{cu}$$
$$\alpha_u = f_{cb} / f_{cu} \qquad (2.15)$$

$$z = \frac{\alpha_u \alpha_z}{\alpha_u - \alpha_z} \qquad (2.16)$$

$$\rho_t = \sqrt{\frac{6}{5}} \frac{\alpha_u \alpha_z}{2\alpha_u + \alpha_z} \qquad (2.17)$$

$$\rho_c = \sqrt{\frac{6}{5}} \frac{\alpha_u \alpha_z}{3\alpha_u \alpha_z + \alpha_u - \alpha_z} \qquad (2.18)$$

The proposed three parameter model by Willam and Warnke (1974) is illustrated in Figure 2.10. The hydrostatic and the deviatoric section indicate the convexity and smoothness of the failure envelope.

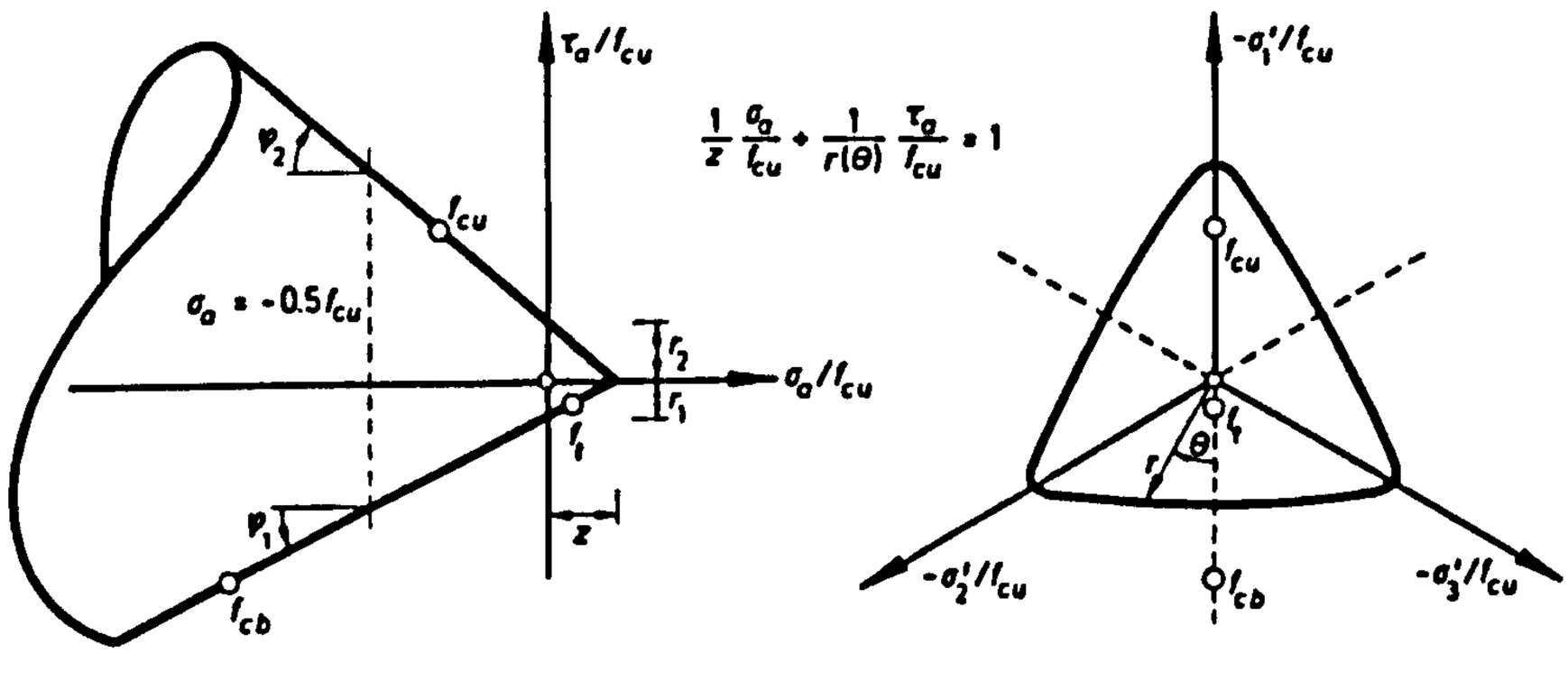

Figure 2.10 Three Parameter Model by Willam and Warnke (1974)

The three parameter model shows close agreement with low strength concrete test data. In the high compression regime the compression branch disagrees with the experiments. Therefore two more parameters were introduced. This five parameter model has second order parabolic curved meridians along the tension meridian (θ=0°) and the compression meridian (θ=60°) and is introduced in the next paragraph.

Five parameter model

The five parameter model of Willam and Warnke (1974) was one of the first failure criterions which involves curved meridians and a smooth convex trace in the deviatoric plane for all values of ρ_t/ρ_C between $½ < \rho_t/\rho_C < 1$ as shown in Figure 2.11. The curved tensile and compressive meridians at θ=0° and θ=60° were quadratic parabolas second order of the form:

$$\rho_{t(\sigma_m)} = a_0 + a_1 \frac{\sigma_m}{f_{cp}} + a_2 \frac{\sigma_m^2}{f_{cp}^2} \tag{2.19}$$

$$\rho_{c(\sigma_m)} = b_0 + b_1 \frac{\sigma_m}{f_{cu}} + b_2 \frac{\sigma_m^2}{f_{cu}^2} \tag{2.20}$$

where $\sigma_m = I_1/3$ is the mean stress and ρ_t and ρ_c are the stress components perpendicular to the hydrostatic axis at θ = 0° and θ = 60° connected by an ellipsoidal surface. a_0, a_1, a_2, b_0, b_1 and b_2 are material constants and can be derived from typical test points such as uniaxial compression, uniaxial tension and biaxial compression tests. $a_0 = b_0$ since the two meridians intersect the hydrostatic axis at the same point. The formula for the elliptic trace $\rho_{(\theta)}$ stays the same as described in the paragraph before. A typical set of values for the parameters for normal strength concrete are from the literature:

$a_0 = b_0 = 0.1025$

$a_1 = -0.8403$

$a_2 = -0.0910$

$b_1 = -0.4507$

$b_2 = -0.1018$

These values will change to take experimental data into account. The formulation to derive the parameters is described in the literature (Willam and Warnke, 1974).

The failure condition from equation 2.14 changes to the more general case:

$$f_{(\sigma_{oct},\tau_{oct},\theta)} = \frac{1}{\rho_{(\sigma_{oct},\theta)}}\frac{\tau_{oct}}{f_{cu}} - 1 = 0 \qquad \textbf{(2.21)}$$

Note that τ_{oct} now depends on σ_{oct} instead of being the product of two functions. The model features a smooth and convex surface. Close agreement with experiments can be observed for the hydrostatic and for the deviatoric sections as was shown by Willam and Warnke (1974), Figure 2.11.

The ratio between compressive and tensile meridian increases with increasing strength which develop a more circular shape of the deviatoric section. However the tensile strength is always smaller than the compression strength in the same deviatoric plane.

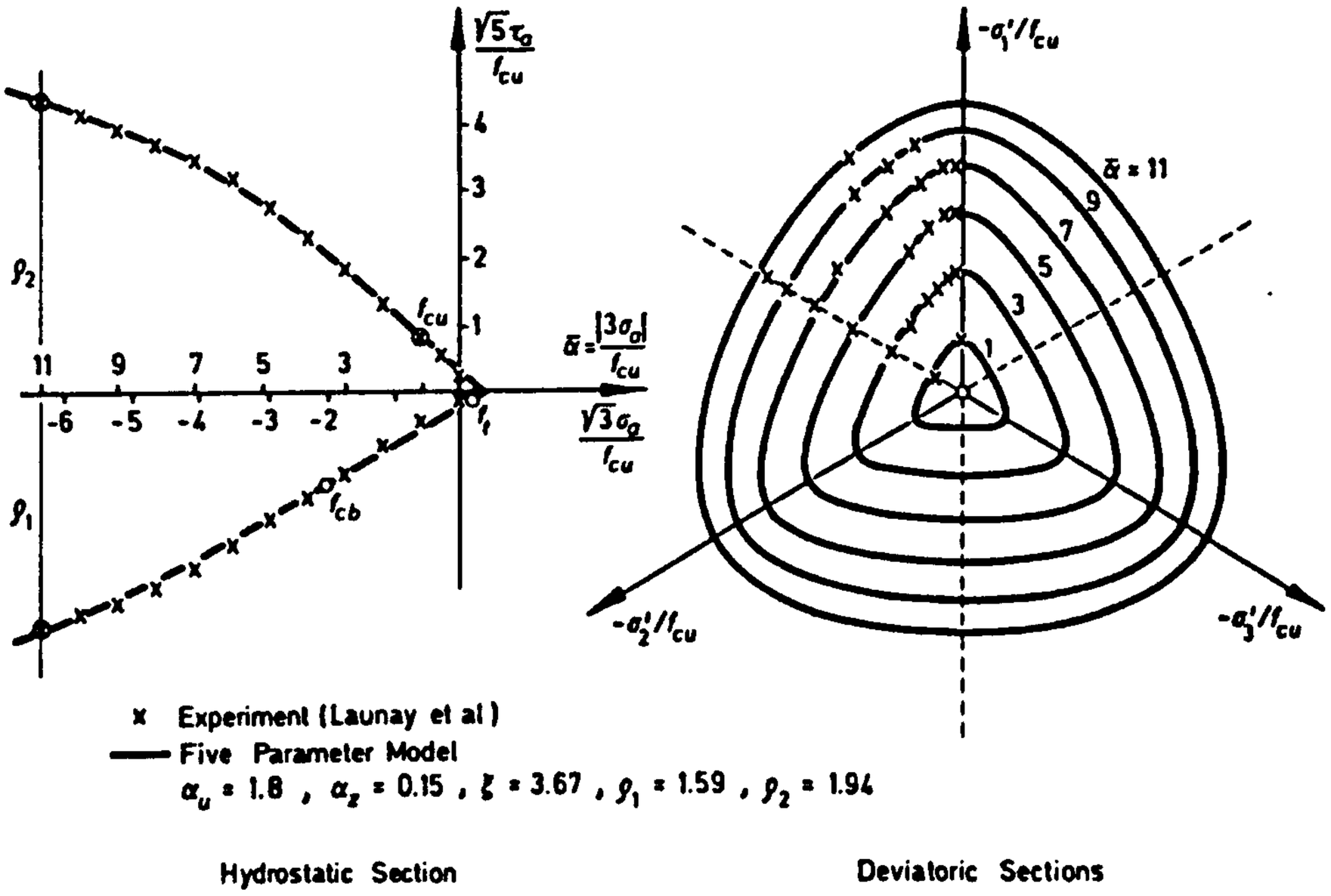

Figure 2.11 Five Parameter Model by Willam and Warnke (1974)

Seow and Swaddiwudhipong (2005) introduced a method to take fibre reinforcement in the Willam-Warnke failure surface model into account. As fibres help to bridge microcracks and carry the load across, the benefits of adding fibres is more obvious when concrete fails in tension rather than compression. Therefore fibres influence the tensile meridian ρ_t more than the compression meridian ρ_c and a coefficient k is introduced to reflect the influence of fibres on the tensile meridian. This coefficient accounts for the increase in the strength at failure due to the confining effect of different amounts of fibres. As the failure surface is determined by interpolating between the tensile and the compression meridian an increase in ρ_t will also result in an increase in other load ratios. The formula in equation 2.19 will therefore change to

$$\rho_{t(\sigma_m)} = a_0 + a_1 \frac{k\sigma_m}{f_{cp}} + a_2 \frac{k\sigma_m^2}{f_{cp}^2} \qquad (2.22)$$

By knowing a control point on the tensile meridian ρ_t (biaxial compression) the constant *k* can be determined with following formula:

$$k = \frac{-a_0 - \sqrt{a_1^2 - 4a_2\left[a_0 + \frac{2}{\sqrt{3}}\left(\frac{f_{cb}}{f_{cu}}\right)\right]}}{a_2\sqrt{\frac{8}{3}}\left(\frac{f_{cb}}{f_{cu}}\right)} \quad \textbf{(2.23)}$$

For plain concrete k=1. When the value of biaxial compression f_{cb} is not known by experiments the same method to predict f_{cb} for SFRC is used as described earlier. Internal confinement was assumed in the out of plane direction σ_1. This confinement pressure was taken as the post cracking tensile strength of SFRC σ_{tu} and can be calculated as described in equation 2.7. Again the biaxial stress state of SFRC is equal to a triaxial stress state of plain concrete with σ_{tu} acting in the third direction as confinement stress.

2.6.6. Simple formula for plain concrete failure envelope

The failure envelope can also be expressed in respect to the stress ratio using regression analysis, as mentioned by Shang, H.S. and Song, Y.P. (2006) in a study about the influence of freezing and thawing cycles on the strength and deformation behaviour of plain concrete under biaxial compressive loading. The formula was given in respect to the freezing and thawing cycles N.

$$\frac{\sigma_3}{f_c} = \frac{f_1(N) + f_2(N) * \alpha}{(1+\alpha)^2} \quad \textbf{(2.24)}$$

where α is the stress ratio in the biaxial compression range ($\alpha = \sigma_2/\sigma_3$). N is the number of freezing and thawing cycles and f_c is the uniaxial compression strength of plain concrete. $f_1(N)$ and $f_2(N)$ are functions of N.

$$f_1(N) = -0.0050544 * N + 1.02214 \quad \textbf{(2.25)}$$

$$f_2(N) = -0.0087264 * N + 3.75944 \quad \textbf{(2.26)}$$

For the use in this study one cycles was assumed (N =1) and therefore

$$\frac{\sigma_3}{f_c} = -\left(\frac{1.0171 + 3.7507 * \alpha}{(1+\alpha)^2}\right) \quad \textbf{(2.27)}$$

Formulations like this are commonly used for the description of the biaxial failure envelope and to present test points in a mathematical way. They can be easily modified to fit experimental data.

2.6.7. Inclined, stretched and distorted ellipse model

Within the work of Hu, et al. (2003) the biaxial failure envelope of SFRC is described by an inclined, stretched and distorted ellipse as a single failure curve in all stress states. The ellipse was multiplied by a power curve producing a single, smooth, closed curve that can define the biaxial failure condition of plain and SFRC in all stress regions and therefore verify experimental data, see Figure 2.12. Through transformation, the formulation can be expressed in terms of the principal stresses σ_1 and σ_2 in a biaxial stress state with the third stress $\sigma_3 = 0$.

$$F_{(\sigma 1,\sigma 2)} = \kappa_1 - 2\sigma_1\sigma_2 + \kappa_2(\sigma_1+\sigma_2) + \kappa_3(\sigma_1+\sigma_2)^2 + \kappa_4(\sigma_1+\sigma_2)^3 + \kappa_5(\sigma_1+\sigma_2)^4 + \kappa_6(\sigma_1+\sigma_2)^5 = 0 \quad \textbf{(2.28)}$$

Including the stress invariants:

$$I_1 = \sigma_1 + \sigma_2$$
$$I_2 = \sigma_1 \sigma_2 \qquad (2.29)$$

the equation above becomes

$$F_{(I1,I2)} = \kappa_1 - 2I_2 + \kappa_2 I_1 + \kappa_3 I_1^2 + \kappa_4 I_1^3 + \kappa_5 I_1^4 + \kappa_6 I_1^5 \qquad (2.30)$$

The six parameters κ_1 to κ_6 can be calculated by solving six linear equations obtained from six experimental data points. Therefore the obtained curves fit the experimental data very closely. Amongst the experimental data points are the values for uniaxial and biaxial compression and tension.

The main advantage of these curves is the continuous smoothness in all biaxial stress regions. As Hu, et al. (2003) demonstrated the numerical difficulties associated with the singularities arising from corner effects disappear. They concluded that this formulation could be more consistent and effective in elastic-plastic formulation and numerical implementation compared to other failure models such as Willam-Warnke (1974) or Ottosen (1977). Not only the ellipse generates curves which are fitting the experimental test points more closely but also the formulations and algorithms for the analysis are simplified.

The need of experimental test points for the biaxial load case to create the failure envelope is limiting this method on the other hand. Biaxial tests are needed for each fibre type and content to verify meaningful failure curves.

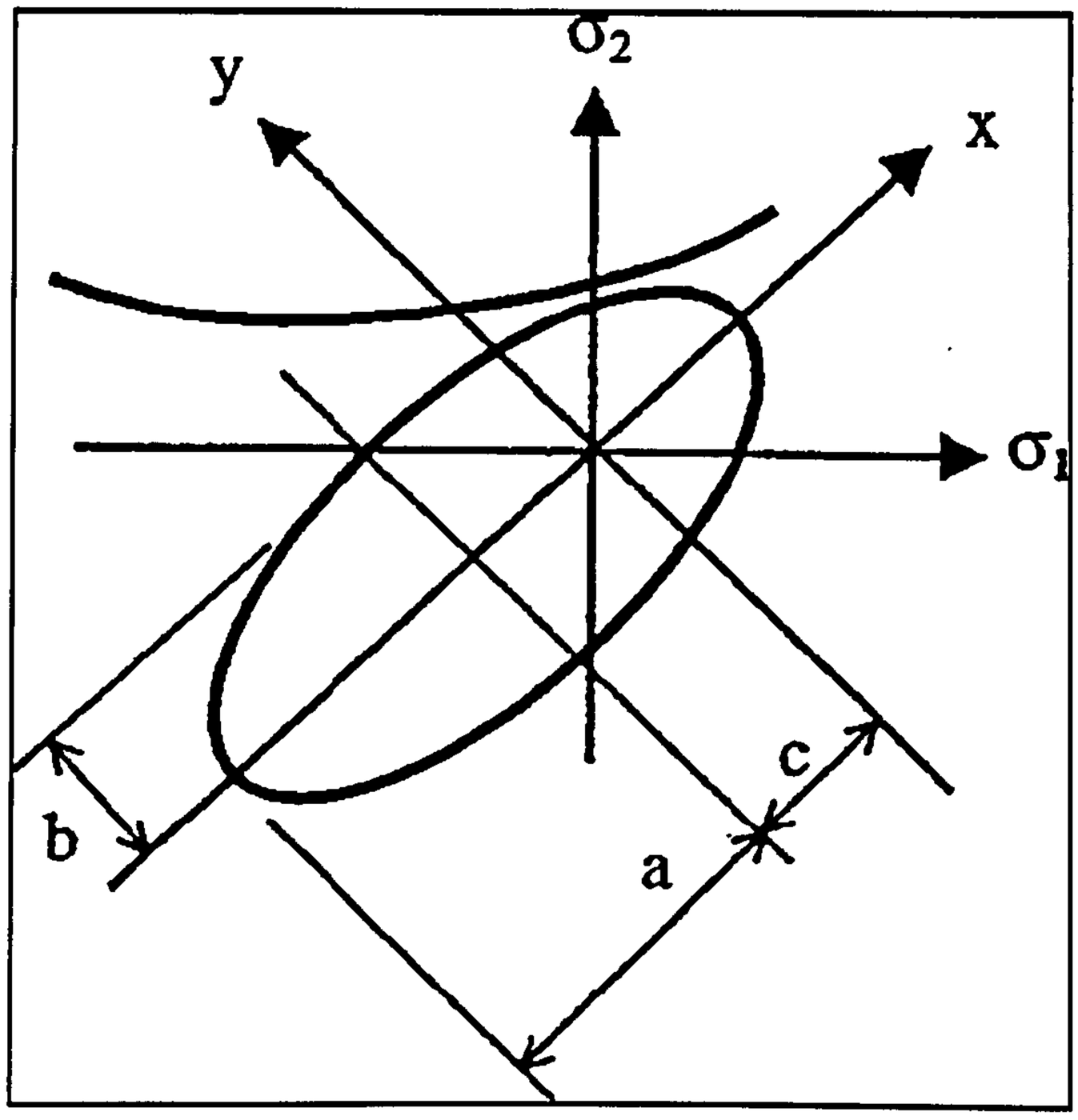

Figure 2.12 Deformation of an ellipse by Hu et al. (2003)

2.7. Summary

Concrete is an ancient material used already thousands of years ago by other civilisations like the Egyptians, the Romans and the civilisations in today's Greece and Turkey. And still it is a modern material used in almost every new structure built these days. Over the years the properties of concrete have improved in many aspects. For example concrete strengths up to 100 N/mm^2 can now be reached for industrial use in mass production.

The ingredients changed and expanded to make these improvements possible. The arrival of steel reinforcement secured the wide range of concrete usage these days and new types of structures can be built by the use of for example prestressed concrete members. Further improvements in the material behaviour are expected with the use of fibres, mixed into the concrete matrix. Within the

wide range of fibres available already, steel fibres are used most. And still, more research is needed to understand the effectiveness and interaction between concrete matrix and steel fibres.

The main ingredient in the mix which was used in this study includes cement, fine aggregates, coarse aggregates and water. In order to optimise the mix design and to achieve HPC, Superplasticizer and silica fume was used. The used steel fibres were hooked ended which increase the bond between fibres and concrete matrix.

In order to reduce friction between the test machine platen system and the concrete test specimen different methods were explored in the past. Lubrication, friction reducing pads, oil cushion systems and brush platens were used to transfer compression loads onto the specimen. Tension loads were applied through clamps and by using dog bone shaped specimens. Gluing the specimen onto the platen system is also widely used as well as metal rods cast into the specimen. Problems with all load application systems are unequal load distribution on the specimen surface arising by small eccentricity introduced by the system.

Because biaxial tests are more cost intensive and experimentally harder to achieve than uniaxial tests, information about the biaxial concrete behaviour is limited, especially for HPC and FRC. In the past cylinders and hollow cylinders were tested under hydrostatic pressure and combinations of torsion, tension and compression loads. Information gained from these experiments is limited. The biaxial strength was mostly over estimated and strain information is difficult to interpret.

Plate like specimens made from NSC show a strength increase of approximately 16 % under equal compression ($\sigma_2/\sigma_3 = 1$) and a maximum increase of 27 % for a stress ratio of $\sigma_2/\sigma_3 = 0.5$. Within the compression-tension region the compressive stress at failure decreases linearly with

increasing tensile stress. In biaxial tension the strength is appropriately equal to the uniaxial tensile strength at about 10 % of the uniaxial compressive strength.

Explosive failure was reported for tests with compressive stresses involved and almost all biaxial tests showed splitting failure in the unloaded direction. Within almost all studies a wide scatter of test points was reported for ultimate stress and strain readings. The maximum strain under uniaxial and biaxial compression was about -2500 microstrain and for tension +150 microstrain. The stiffness of the specimens increases with biaxial loadings.

Splitting failure is the dominant failure mode under biaxial stresses and depends mainly on the stress ratio σ_2/σ_3. For higher ratios splitting failure occurs parallel to the unloaded surface where for lower ratios cracks appear perpendicular to both loading direction. When tensile forces are present only one crack is formed perpendicular to the applied tensile load.

HSC becomes stiffer than NSC. The material is more homogeneous with a higher bond between the aggregates and the concrete paste. Cracks develop through the aggregates as well as the mortar. Internal cracking is reduced in number and size up to a higher stress where they will extend at once leading to a more brittle failure.

With HSC the increase in biaxial strength compared to uniaxial strength is less than for NSC. This means that the confining stress of the second axis is less effective for HSC. Also the uniaxial tensile strength becomes less when compared to the uniaxial compression strength. Therefore plain HSC seem to be more influenced by tensile strength than NSC. Using friction reducing pads the increase in biaxial strength compared to uniaxial strength is less than for dry steel platen tested specimens.

HSC behaves elastically up to a higher stress as the concrete strength is increased. Therefore the discontinuity point and the proportional limit occur at a

higher stress. As the biaxial stress ratio increases the stress-strain curve becomes linear up to a higher stress.

The steel fibre content which is of interest in the reviewed studies and in this study varies between 0.5 % and 2 %. This was due to limitations during the mixing procedure, called fibre balling.

SFRC was reported to have a larger biaxial strength envelope in the compression-compression region as well as the compression-tension region compared to plain concrete. The maximum strength value was at a stress ratio of $\sigma_2/\sigma_3 = 0.8$ for SFRC compared to 0.5 for plain concrete. This was explained by the enhanced tensile capacity of SFRC which works against the splitting failure in the plane perpendicular to the load which has similar effect as the application of a small confining pressure in the unloaded direction. It was concluded that biaxial compression and fibre reinforcement can prevent NSC from brittle failure and change the failure mode from splitting failure into a more shear based faulting failure.

While the increase in uniaxial compression can be neglected by adding fibres to a plain concrete mix it will increase the tensile capacity. The improvements depend on fibre variables, concrete mix design, specimen shapes and test methods. Within the compression-tension region the largest expansion of the biaxial envelope was reported compared to the other regions.

As in plain concrete the scatter for biaxial tests was already reported to be large and it increases even more with SFRC specimen. The conclusion in some studies was that fibres increase the biaxial strength for higher volume fractions although sometimes the opposite occurred, for example when the fibre length was longer than the specimen height.

Two loading paths are possible for biaxial loading. One is called sequential loading, the other proportional loading. The difference on the biaxial test results is diverse. In some publication a difference was observed in others not.

Sometimes the proportional loading path develops higher strength. Sometimes it was the other way around. It turned out that the difference become smaller as better the friction reducing platen system was. In general the used platen system and the test method are of more importance for meaningful results than the loading path.

The Ottosen (1977) four-parameter failure criterion defines a smooth convex failure surface with quadratic parabolic curved meridians, which open in the negative direction of the hydrostatic axis. It is demonstrated to be valid for short-term monotonic loading. The trace in the deviatoric plane changes from nearly triangular for small stresses to more circular shape with increasing hydrostatic pressure.

The proposed three parameter model by Willam and Warnke (1974) consists of a conical shape with straight meridians and non-circular base sections in the deviatoric plane. To agree better with experimental data for higher compression further two parameters were introduced by the same authors. The proposed five parameter model consists also of a conical shape but with curved meridians and non-circular base sections in the deviatoric plane.

In order to model fibre reinforcement and to overcome the enormous amount of experimental data for each fibre type under biaxial load conditions a failure envelope for fibre concrete in terms of the post-cracking tensile strength σ_{tu} was introduced by Murugappan, et al. (1993) and Tan, et al. (1994). The fibres reduce the strains in the tensile direction and apply a confining pressure. Therefore the behaviour of SFRC under biaxial compression is similar to plain concrete under a triaxial state of stress. The strength envelope of SFRC under biaxial compression (σ_2, σ_3) can be regarded as identical to the failure envelope of plain concrete under triaxial compression (σ_1, σ_2, σ_3), where σ_1 is the confining pressure.

2.8. References

Abdull-Ahad, Ramzi B. and Abbas, Jassim M., 1989, ' Behaviour of steel fibre reinforced concrete under biaxial stresses', in Swamy, R.N. and Barr, B., *Fibre Reinforced Cements and Concretes – Recent Developments,* Elsevier Applied Science, London, pp. 126 – 135.

Andenaes Einar, Gerstle Kurt and Ko Hon-Yim, 1977, 'Response of Mortar and Concrete to Biaxial Compression', *Journal of the Engineering Mechanical Division ASCE*, Vol. 103, No. EM4, pp. 515 – 526.

Bakaert product data sheets, retrieved 09. December 2005, <http://ww.bekaert.com/building/>

Bellamy, C.J., 1961, 'Strength of Concrete Under Combined Stress', *Journal of the American Concrete Institute*, *Proceedings* vol. 58, no. 4, October 1961, pp. 367 - 382.

Bresler, B. and Pister, K.S., 1958, 'Strength of Concrete Under Combined Stresses', *Journal of the American Concrete Institute*, *Proceedings* vol. 55, no. 3, September 1958, pp. 321 - 346.

Buyukozturk, Oral, Nilson, Arthur H. and Slate, Floyd O., 1970, 'Stress-Strain Response and Fracture of a Concrete Model in Biaxial Loading', *American Concrete Institute Journal, Proceedings*, vol. 68, no. 8, August 1971, pp. 590 – 599.

Calixto, José M., 2002, 'Behavior of High-Performance Concrete Subjected to Biaxial Tension-Compression Stresses', in Malhotra, V.M. *High-performance concrete: performance and quality of concrete structures, Proceeding of the third International conference, Recife, Brazil, 2002,* American Concrete Institute, ACI Special Publication 207-1, pp. 1 – 14.

Chen, Robert C., Carrasquillo, Ramon L. and Fowler, David W., 1985, 'Behavior of High-Strength Concrete under Uniaxial and Biaxial Compression', *American Concrete Institute, ACI Special Publication 87-14*, pp. 251 – 273.

Chen, W.F. and Han, D.J., 1988, *Plasticity for Structural Engineers*, Springer-Verlag, New York.

Curbach, Manfred, Hampel, Torsten, Speck, Kerstin and Scheerer, Silke, 2000, 'Versuchstechnische Ermittlung und mathematische Beschreibung der mehraxialen Festigkeit von Hochleistungsbeton bei zwei- und dreiaxialer Druckbeanspruchung', Abschlussbericht, Deutsche Forschungsgemeinschaft, Förderkennzeichen: Cu 37/1-2, Dresden, pp. 318.

Curbach, Manfred und Speck, Silke, 2002, 'Mehraxiale Festigkeit von duktilem Hochleistungsbeton', Deutscher Ausschuss für Stahlbeton, Heft 524, Beuth Verlag GmbH, Berlin, pp. 219.

Demeke, Ayele and Tegos, I.A., 1994, 'Steel Fibre Reinforced Concrete in Biaxial Stress Tension-Compression Conditions', *American Concrete Institute Structural Journal, Proceedings*, vol. 91, no. 5, pp. 579 – 584.

Fumagalli, Emanuele, Gunasekaran, Muthian, Linger, D.A., Gillespie, H.A., Vile, G.W.D. and Sigvaldason, O.T., 1965, Discussion of the paper by Sundara Raja Iyengar, K.T., Chandrashekhara K. and Krishnaswamy, K.T., 1965, 'Strength of Concrete Under Biaxial Compression', *Journal of the American Concrete Institute*, *Proceedings* vol. 62, no. 2, February 1965, pp. 239 – 250, *Journal of the American Concrete Institute*, *Proceedings* vol. 62, no. 9, September 1965, pp. 1187 - 1198.

Gani, M.S.J., 1997, *Cement and Concrete*, Chapman & Hall, London.

Gerstle, Kurt H., Linse, Diethelm L., Bertacchi, Paolo, Kotosovos, M.D., Ko, Hon-Yim, Newman, John B., Rossi, Pio, Schickert, Gerald, Taylor, Michael A., Traina, Leonard A., Zimmerman, Roger M. and Bellotti Roberto, 1978, 'Strength of Concrete under Multiaxial Stress States', Proceedings of the *Douglas McHenry International Symposium on Concrete and Concrete Structures*, held at Mexico City, Mexico, in October 1976, American Concrete Institution, Detroit, Michigan, Special Publication 55, pp. 103 – 131.

Gerstle, Kurt H., Aschl, Helmut, Bellotti, Roberto, Bertacchi, Paolo, Kotsovos, Michael D., Ko, Hon-Yim, Linse, Diethelm, Newman, John B., Rossi, Pio, Schickert, Gerald, Taylor, Michael A., Traina, Leonard A., Winkler Helmut and Zimmerman, Roger M., 1980, 'Behavior of Concrete under Multiaxial Stress States', *Journal of the Engineering Mechanics Division, Proceedings*, vol. 106, EM 6, December 1980, pp. 1383 – 1403.

Hannant, D.J. (1974), 'Nomograms for the failure of plain concrete subjected to short-term multiaxial stresses', *The Structural Engineer*, vol. 52, no.5, pp. 151 – 165.

Hu, Xiao Dong, Day, Robert and Dux, Peter, 2003, 'Biaxial Failure Model for Fibre Reinforced Concrete', Journal of Materials in Civil Engineering, vol. 15, no.6, December 2003, pp. 609 – 615.

Hughes B.P. and Bahramian B., 1965, 'Cube tests and the uniaxial compressive strength of concrete', *Magazine of Concrete,* vol. 17, no. 53, pp. 177 – 182.

Hughes B.P. and Bahramian B., 1966, Discussion on the article: 'Cube tests and the uniaxial compressive strength of concrete', *Magazine of Concrete,* vol. 18, no. 56, pp. 161 – 164.

Hussein, Amgad Ahmed, 1998, *Behaviour of High-Strength Concrete under Biaxial Loading Conditions*, PhD thesis, Memorial University of Newfoundland, St. John's, Newfoundland, Canada, April 1998, 245 pp..

Hussein, A. and Marzouk, H., 2000, 'Behavior of High-Strength Concrete under Biaxial Stresses', *American Concrete Institute Materials Journal, Proceedings*, vol. 97, no. 1, pp. 27 – 36.

Klausen, Dietmar Prof. Dr.-Ing., Handout für *Betontechnologie – Concrete technology* 1999, Fachhochschule Karlsruhe – Hochschule für Technik, Fachbereich Bauingenieurwesen.

Kupfer H., Hilsdorf H.K. and Rusch H., 1969, 'Behavior of Concrete Under Biaxial Stresses', *American Concrete Institute Journal, Proceedings*, vol. 66, No. 8, pp. 656 – 666.

Lan Shengrui and Guo Zhenhai, 1997, 'Experimental Investigation of Multiaxial Compressive Stregnth of Concrete under Different Stress Paths', *American Concrete Institute Materials Journal, Proceedings*, vol. 94, no. 5, pp. 427 – 434.

Lee Sang-Keun, Song Young-Chul and Han Sang-Hoon, 2004, 'Biaxial behaviour of plain concrete of nuclear containment building', *Nuclear Engineering and Design, Proceeding*, vol. 227, pp. 143 – 153.

Lim, T.Y., Paramasivam, P. and Lee, S.L., 1987, 'Analytical Model for Tensile Behavior of Steel-Fibre Concrete', *American Concrete Institute Materials Journal, Proceedings*, vol. 84, no. 4, pp. 286 – 298.

Liu, Tony C.Y., Nilson, Arthur H. and Slate, Floyd O., 1972, 'Stress-Strain Response and Fracture of Concrete in Uniaxial and Biaxial Compression', *American Concrete Institute Journal, Proceedings*, vol. 69, no. 31, pp. 291 – 295.

Maidl, Bernhard R., 1995, *Steel Fibre Reinforced Concrete*, Ernst & Sohn, Berlin, Germany.

McHenry, D. and Karni, J., 1958, 'Strength of Concrete Under Combined Tensile and Compressive Stress', *Journal of the American Concrete Institute, Proceedings* vol. 54, no. 10, April 1958, pp. 829 - 840.

Merkblatt des VDS (Verband deutscher Stahlfaserhersteller e.V.), Veröffentlichungen, *Stahlfaserbeton – Stahlfasertypen*, retrieved 09. December 2005, <http;//www.vdsev.de/>.

Mills, Laddie L. and Zimmerman, Roger M., 1970, 'Compressive Strength of Plain Concrete Under Multiaxial Loading Conditions', *American Concrete Institute Journal, Proceedings*, vol. 67, no. 10, October 1970, pp. 802 – 807.

Murugappan, K., Paramasivam, P. and Tan, K.H., 1993, 'Failure Envelope for Steel-Fibre Concrete under Biaxial Compression', *Journal of Materials in Civil Engineering*, vol. 5, no. 4, November 1993, pp.436 – 446.

Naaman, A.E. and Reinhardt, H.W., 1996 'Characterization of high performance fibre reinforced cement composites – HPFRCC' in *High Performance Fibre Reinforced Cement Composite 2 (HPFRCC 2), Proceedings of the Second International RILEM Workshop*, Ann Arbor, USA, 11-14 June 1995 , RILEM Proceedings 31, p. 2, E & FN Spon.

Nawy, Edward G., 1996, *Fundamentals of high strength high performance concrete*, Longman group limited, Harlow, Essex, England.

Nawy, Edward G., Lim, Dong Hwan and McPherson, Kristi L., 2003, 'Compressive Behavior of High-Strength High-Performance Concrete Under Biaxial Loading', in Furlong, R.W. and Mirza, S.A. *The art and*

science of structural concrete design, Proceeding of a Symposium, Detroit, MI, USA, April 2002, American Concrete Institute, ACI Special Publication 213-3, pp. 43 – 60.

Nelissen, L.J.M., 1972, *Biaxial testing of normal concrete,* Heron, vol. 18, no. 1, 90 pp, Technological University, Delft, Netherlands.

Newman, J.B., 1979, 'Concrete under complex stress', in F.D. Lydon (ed.), *Developments in Concrete Technology – 1*, Applied Science Publishers LTD, London, pp. 151 – 220.

Ottosen, N.S., 1977, 'A failure criterion for concrete', *Journal of the Engineering Mechanics Division, Proceedings*, vol. 103, EM 4, pp. 527 – 535.

Pandit, G.S., 1970, Discussion of the paper by Kupfer H., Hilsdorf H.K. and Rusch H., 1969, 'Behavior of Concrete Under Biaxial Stresses', *American Concrete Institute Journal, Proceedings*, vol. 66, No. 8, pp. 656 – 666, *American Concrete Institute Journal, Proceedings*, vol. 67, No. 2, pp. 194 – 197.

Popovics Sándor, 1998, Strength and related properties of concrete – a quantitative approach, John Wiley & Sons. Inc., New York.

Prisco di M., Felicetti R. and Plizzari G.A., *BEFIB 2004: Fibre-Reinforced Concretes, Proceedings of the sixth International RILEM Symposium, Varenna, Italy, 20-22 September 2004,* RILEM Publication, Bagneux, France, Volume 1 and 2.

Reinhardt, Hans W., 2000, 'Structural Behaviour of High Performance Concrete, Annual Journal on Research and Testing Materials', *Otto-Graf-Journal, Materialprüfanstalt Universität Stuttgart*, MPL Stuttgart, Otto-Graf-Institut, vol. 11, pp. 9 – 17. Retrieved January 25, 2006 from <http://www.mpl.uni-stuttgart.de/publicationen/otto_graf_journal.html>.

Robinson, George S., 1967, 'Behavior of concrete in biaxial compression', *Journal of the structural division, Proceeding of the American Society of Civil Engineering*, vol. 93, no. ST1, pp. 71 - 86.

Rosenthal, Israel and Glucklich, Joseph, 1970, 'Strength of Plain Concrete Under Biaxial Stress', *Journal of the American Concrete Institute, Proceedings* vol. 67, no. 11, November 1970, pp. 903 - 914.

Schmidt M., Fehling, E. and Geisenhanslüke, C., 2004, *Ultra High Performance Concrete (UHPC), Proceeding of the International Symposium on Ultra High Performance Concrete, Kassel, Germany, 13-15 September 2004,* kassel university press GmbH, 2004, Schriftenreihe Baustoffe und Massivebau, Structural Materials and Engineering Series, Heft 3, no.3.

Seow, Puay, Eng and Swaddiwudhipong, Somsak, 2005, 'Failure Surface for Concrete under Multiaxial Load – a Unified Approach', *Journal of Materials in Civil Engineering, ASCE*, vol. 17, no.2, pp. 219 – 228.

Shang, H.S. and Song, Y.P., 2006, 'Experimental study of Strength and deformation of plain concrete under biaxial compression after freezing and thawing cycles', *Cement and Concrete Research*, 2006.

Sheppard P.G., 1967, A Study of the Strength of Concrete Under Biaxial Compressive Stresses, M.S. thesis, New Mexico State University sited in Hussein A.A. 1998, Behaviour of high-strength concrete under biaxial loading condition, PhD thesis, Memorial University of Newfoundland, St. John's, Newfoundland, Canada, April 1998, 245 pp..

Soroushian, Parviz and Bayasi, Ziad, 1991, 'Fibre-Type Effect on the performance of Steel Fibre Reinforced Concrete', *American Concrete Institute Materials Journal, Proceedings*, vol. 88, no. 2, March-April 1991, pp. 129 – 134.

Stegbauer, Alfred and Linse, Diethelm, 1972, 'Comparison of stress-strain behaviour of concrete and other materials under biaxial loading', in *RILEM International Symposium*, Cannes, France, 1972, vol. 1, pp. 229 – 243.

Sundara Raja Iyengar, K.T., Chandrashekhara K. and Krishnaswamy, K.T., 1965, 'Strength of Concrete Under Biaxial Compression', *Journal of the American Concrete Institute*, *Proceedings* vol. 62, no. 2, February 1965, pp. 239 - 250.

Swaddiwudhipong, Somsak and Seow, Puay, Eng, Constance, 2006, 'Modelling of steel fibre-reinforced concrete under multi-axial loads', *Cement and Concrete Research*, vol. 36, pp. 1354 – 1361.

Tan, K.H., Murugappan, K. and Paramasivam, P., 1994, 'Constitutive Relation for Steel Fibre Concrete Under Biaxial Compression', *Cement & Concrete Composites*, vol. 16, pp. 9 -14.

Tasuji, Ebrahim M., Slate, Floyd O. and Nilson, Arthur H., 1978, 'Stress-Strain Response and Fracture of Concrete in Biaxial Loading', *American Concrete Institute Journal, Proceedings*, vol. 75, no. 7, pp. 306 – 312.

Taylor, Michael A., Jain, Arun K. and Ramey, Melvin R., 1972, 'Path Dependent Biaxial Compressive Testing of All-Lightweight Aggregate Concrete', *American Concrete Institute Journal, Proceedings*, vol. 69, no. 12, pp. 758 – 764.

Taylor, Michael A. and Patel, B.K., 1974, 'The Influence of Path Dependency and Moisture Conditions on the Biaxial Compression Envelope for Normal Weight Concrete', *American Concrete Institute Journal, Proceedings*, vol. 71, no. 12, pp. 627 – 633.

Taylor, Michael A., Tai, M.K. and Ramey, Melvin R., 1975, 'Biaxial Compressive Behavior of Fibre Reinforced Mortar', *American Concrete Institute Journal, Proceedings*, vol. 72, no. 9, pp. 496 – 501.

Tho, K.K., Seow, P.E.C and Swaddiwudhudhipong, S., 2003, 'Numerical method for analysis of concrete under multi-axial loads', *Magazine of Concrete Research*, vol. 55, no. 6, pp. 537 – 547.

Torrenti, J.M., Djebri, B., Bascoul, A. and Granju, J.L., 1991, 'Comparative study of two biaxial presses for concrete', *53-MTC final report in Materials and Structures / Matériaux et Constructions, Proceedings,* vol. 24, pp.52 – 60.

Torrenti, J.M., Djebri, B. and Bascoul, A., 1993, 'Biaxial compression of concrete – Influence of the stress path on concrete strains', *Materials and Structure, RILEM Proceedings*, vol. 26, pp. 181 – 184.

Torrenti, J.M., Djebri, B., 1995, 'Behaviour of Steel-Fibre-Reinforced Concrete Under Biaxial Compression Loads', *Cement & Concrete Composites, Proceedings, Elsevier Science Limited, Great Britain*, vol. 17, pp. 261 – 266.

Traina, Leonard A. and Mansour, Shahin A., 1991, 'Biaxial Strength and Deformational Behavior of Plain and Steel Fibre Concrete', *American Concrete Institute Materials Journal, Proceedings*, vol. 88, no. 4, pp. 354 – 362.

Van Mier, J.G.M., 1986, ‚Fracture of concrete under complex stress', Heron, vol. 31, no. 3, 90 pp, Technological University, Delft, Netherlands.

Vile, Gerald W.D., 1965, 'The strength of concrete under short-term static biaxial stress' in Anthony E. Brooks and Kenneth Newman: *The Structure of Concrete and its behaviour under load, Proceedings of an International*

Conference, London, September 1965, Cement and Concrete Association, London, UK, 1968, pp. 275 – 288.

Wang, Chuan-zhi, Guo, Zhen-hai and Zhang, Xiu-qin, 1987, 'Experimental Investigation of Biaxial and Triaxial Compressive Concrete Strength', *American Concrete Institute Materials Journal, Proceedings*, vol. 84, no. 2, pp. 92 – 100.

Willam, K.J. and Warnke, E.P., 1974, 'Constitutive models for the triaxial behavior of concrete', *International Association of the Bridge and Structural Engineers, Proceeding of the Seminar on Concrete Structures Subjected to Triaxial Stresses, ISMES*, Bergamo, Italy, Paper no. III-I.

Yin, W.S., Su, Eric C.M., Mansur, M.A. and Hsu, Thomas T.C., 1989, 'Biaxial Tests of Plain and Fibre Concrete', *American Concrete Institute Materials Journal, Proceedings*, vol. 86, no. 3, pp. 236 – 243.

Yin, W.S., Su, Eric C.M., Mansur, M.A. and Hsu, Thomas T.C., 1990, Discussion of 'Biaxial Tests of Plain and Fibre Concrete', by Traina, Leonard A. and Mansour, Shahin A., *American Concrete Institute Materials Journal, Proceedings*, vol. 87, no. 2, pp. 179 – 180.

3. Experimental Program

This chapter describes the test set up for the biaxial testing machine including the procedure for machine alignment, the platen system used and the control scheme and data compilation system which was fed by the measurement devices. It also contains details of the formwork for both compression-compression and compression-tension specimens, about the production of the specimens including the materials used in the concrete mix, the mix preparation, casting and curing as well as details of the steel fibres used. The complex test procedures for the different specimen types are also presented.

3.1. Biaxial Testing Machine

3.1.1. Loading Frame

Tests were conducted in the biaxial test facility developed and built at Glasgow University. The loading frame together with the control panel and the data compilation system were located in the heavy structures laboratory on a 410 mm thick heavily reinforced concrete floor. Figure 3.1 shows a photograph of the biaxial test facility. The length of the top and bottom beams are 5.5 m and therefore the overall dimension of the machine is 5.5 m x 5.5 m with a total height of 0.95 m.

Two 2 MN actuators in each axis were arranged as an opposing pair and were perpendicular to the other axis. Both axes were in a horizontal plane. The actuators in one axis were working against each other simultaneously in terms of displacement or load, depending on the control system that was chosen. The actuators were placed between massive 152 mm thick steel anchor blocks with

140 mm diameter carbon chromium steel bearings at the ends of the reaction frame. The anchor blocks were welded to 73 mm thick top and bottom steel plates, which were connected by bolts to heavy steel bars with a rectangular cross-section of 155 x 73 mm. Figure 3.2 shows a photograph of the end anchor block assembly. There were four bars for each axis carrying the load applied to the specimens. In front of every actuator a steel frame was based to adjust the level and the alignment of every actuator independently. These actuator frames that were based on the bottom steel plates with bolts were also connected with a channel steel section and bolts to the top steel bars which gave the machine an additional stiffness. This can be seen in Figure 3.3. Diagonal bracings, also made of channel steel sections, were bolted to the top and bottom steel plates to ensure the perpendicular alignment of the two axes. The whole machine was bolted to the concrete floor by six M 36 threaded rods going through the structural floor and was anchored in the tunnels underneath.

Oil pumps with a capacity of 20 l/min hydraulic power produce a continuous system pressure of 200 bars. The air blast cooler where the oil is circulated through a heat exchanger and is forced cooled by a fan which does 24 revolutions per seconds were placed together with the oil pumps underneath the structural floor, in the same tunnels as the machine was anchored, for noise emission reasons.

The inner part including the front pin and the specimen were shielded by a Plexiglas shield to prevent concrete splinters flying through the laboratory caused by the explosive failure of the specimens. A picture of the Plexiglas shield can also be seen in Figure 3.3.

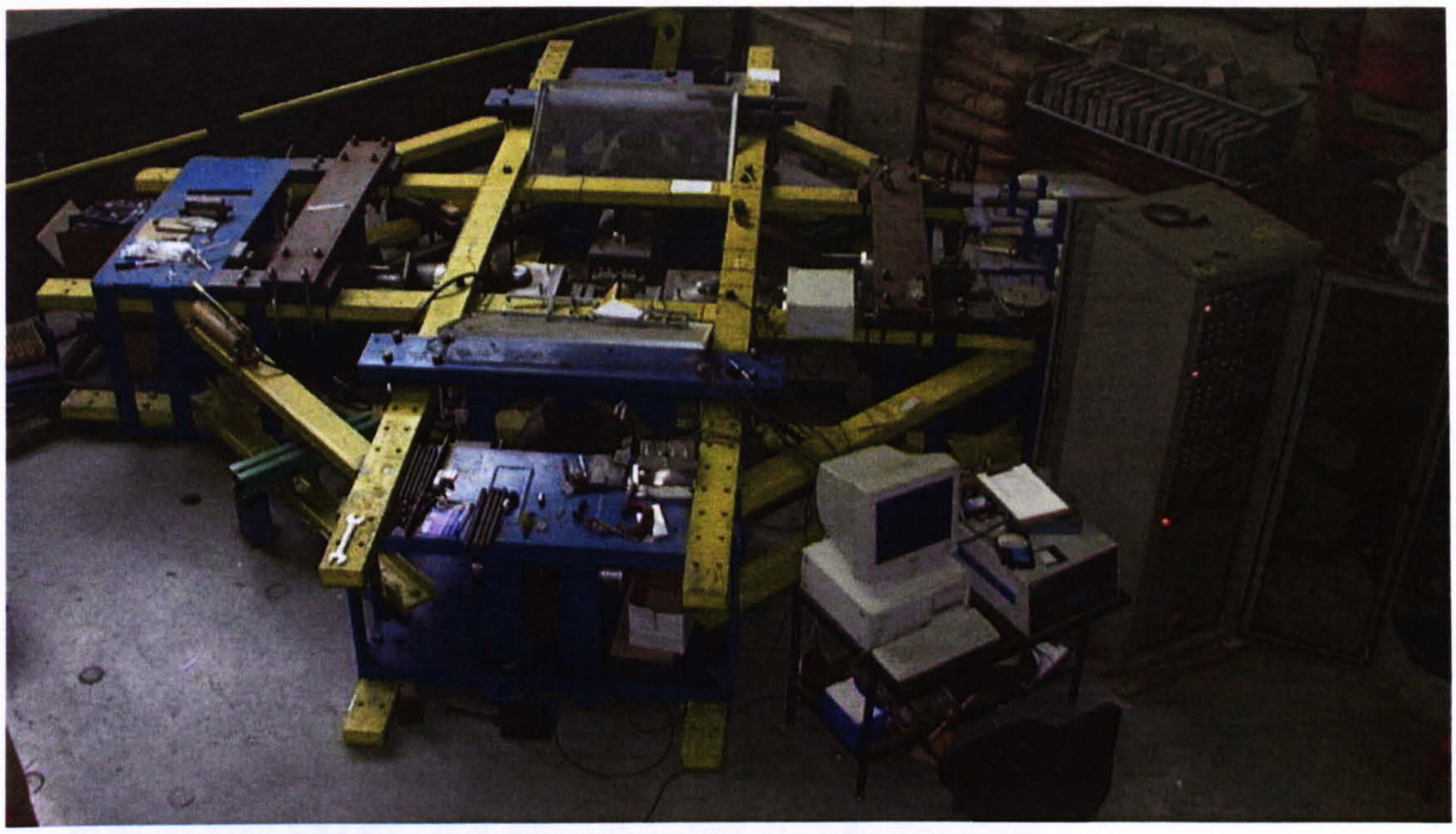

Figure 3.1 Biaxial test facility

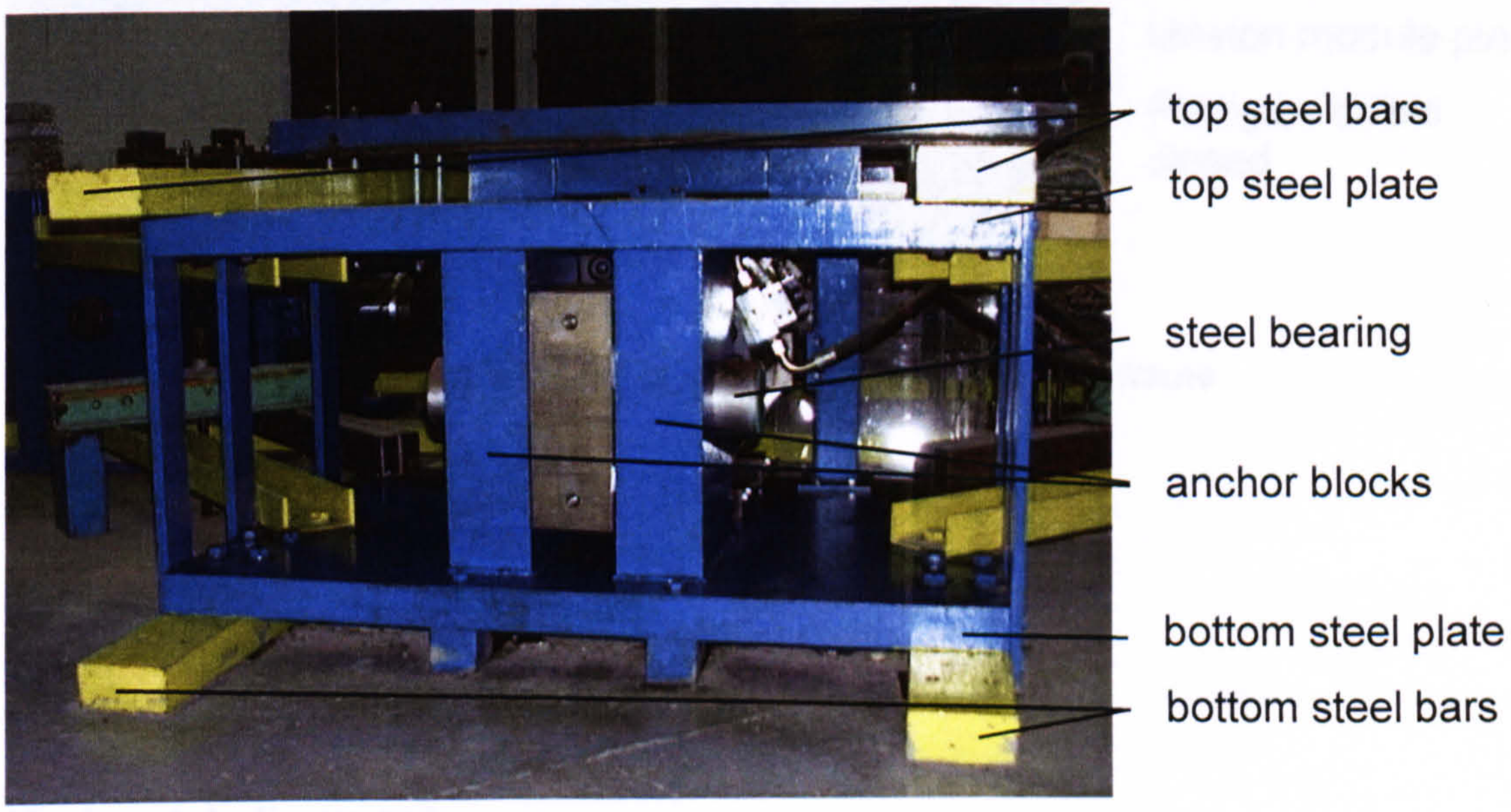

Figure 3.2 Anchor blocks assembly

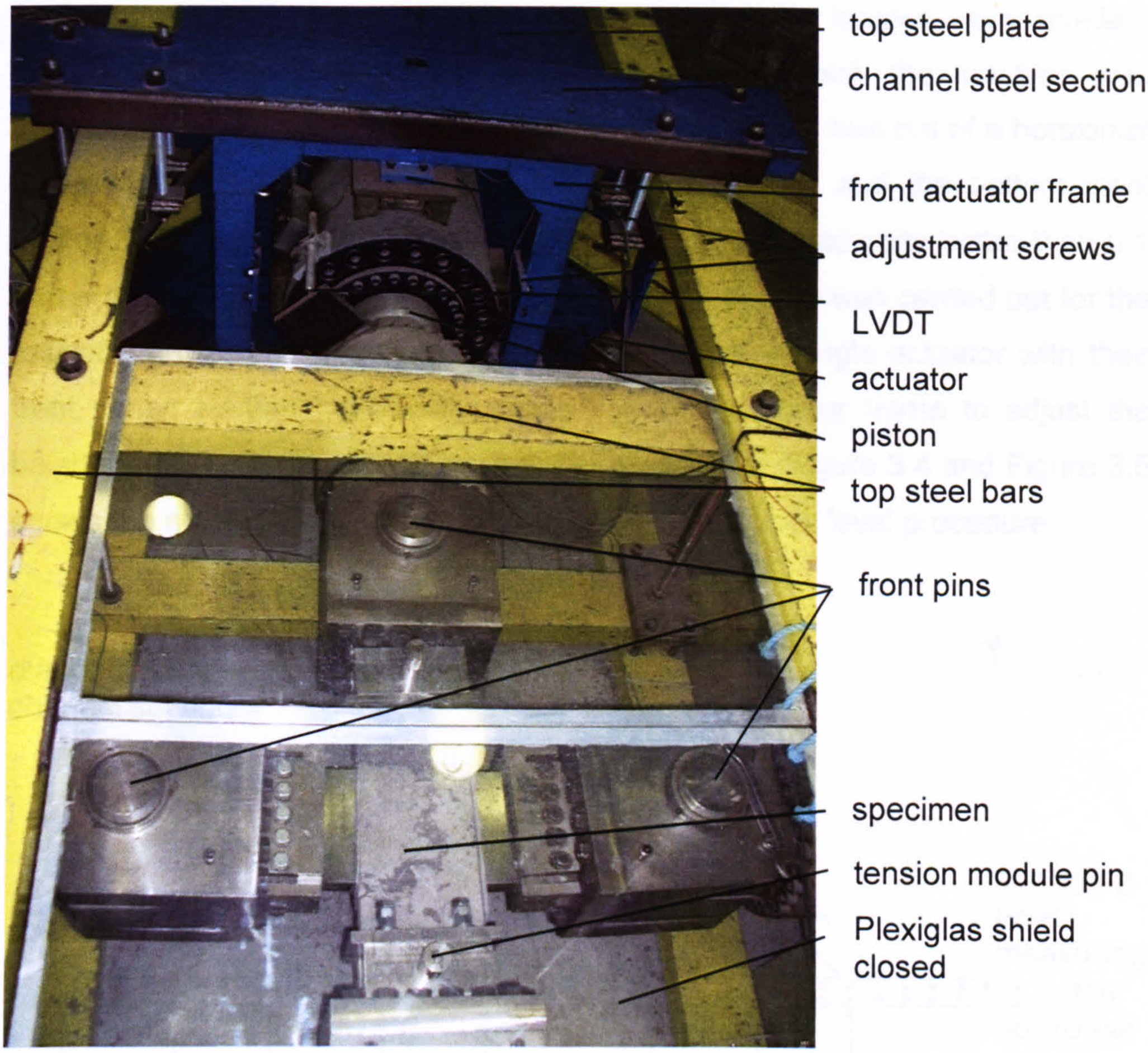

Figure 3.3 Plexiglas shield and front actuator frame

3.1.2. Machine alignment

Horizontal alignment

By using a surveying level the biaxial test facility was levelled in a horizontal plane. This was achieved by lifting up the corners of the machine one at a time using oil jacks and small steel washers of different thickness were put under the machine. After the four 140 mm anchor block pins were levelled into one horizontal plane the bottom steel beams as well as front corners of the 73 mm

thick bottom steel plates on which the actuators were located were levelled. After tightening the six M 36 threaded rods with which the machine was connected to the floor it had a maximum deviation of 0.2 mm out of a horizontal plane at any point of the bottom actuator steel plate and the bottom steel beams. The four actuator pins were on one level with accuracy better than 0.1 mm. From this basic requirement the levelling procedure was carried out for the rest of the machine by adjusting the height of every single actuator with their front platen system individually, using the front actuator frame to adjust the heights until the front platens were at the same level. Figure 3.4 and Figure 3.5 shows the measurement arrangements for the horizontal level procedure.

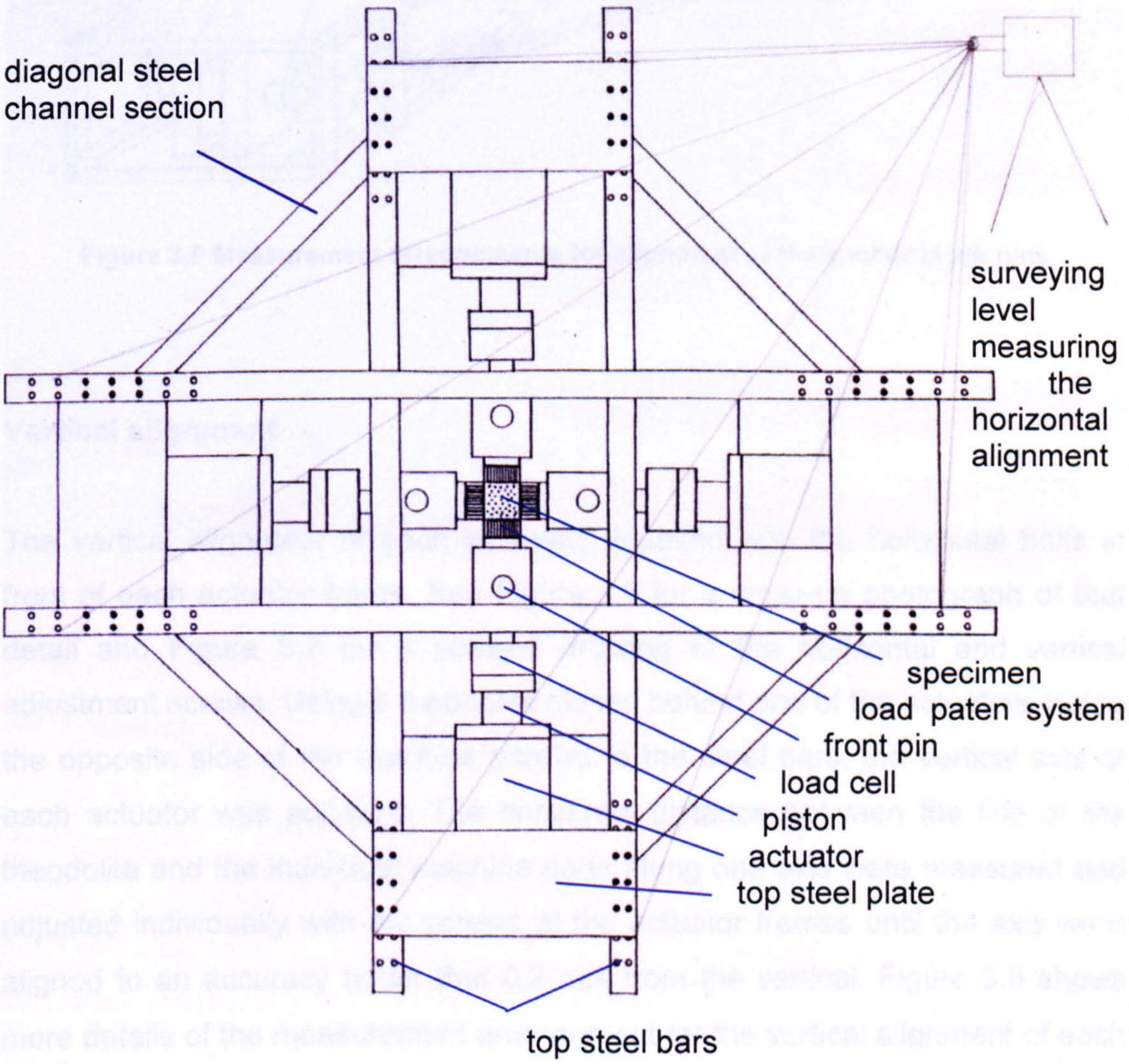

Figure 3.4 Measurement arrangement for alignment of the machine corners

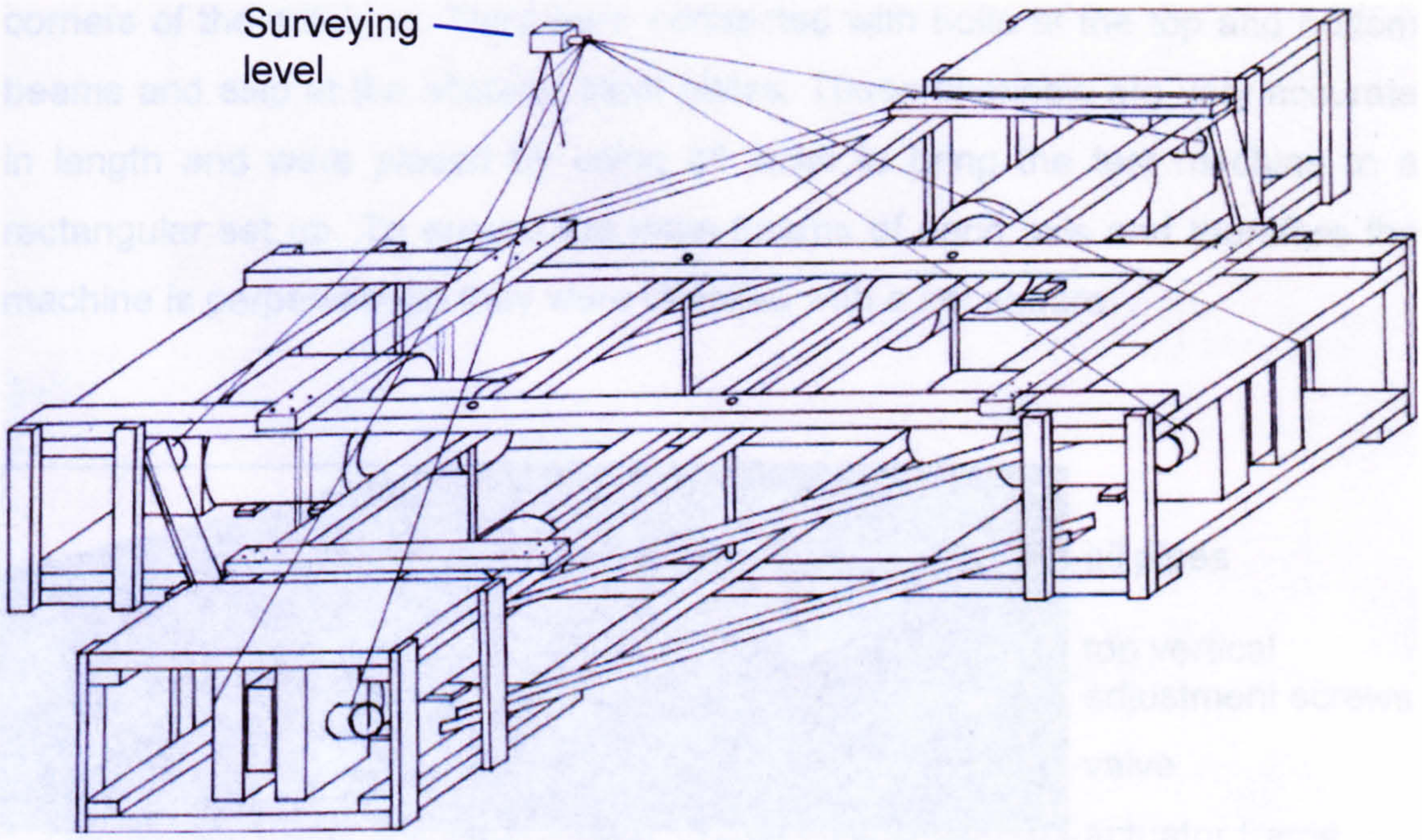

Figure 3.5 Measurement arrangements for alignment of the anchor block pins

Vertical alignment

The vertical alignment of each axis was adjusted with the horizontal bolts in front of each actuator frame. See Figure 3.6 for a close-up photograph of that detail and Figure 3.7 for a detailed drawing of the horizontal and vertical adjustment screws. Using a theodolite placed behind one of the actuators facing the opposite side of the machine parallel to the steel bars, the vertical axis of each actuator was adjusted. The horizontal distance between the line of the theodolite and the individual machine parts along one axis were measured and adjusted individually with the screws at the actuator frames until the axis were aligned to an accuracy better that 0.2 mm from the vertical. Figure 3.8 shows more details of the measurement arrangement for the vertical alignment of each axis.

To ensure that the two axes were rectangular to each other, steel channel sections with the same length were connected diagonally between the end corners of the machine. They were connected with bolts at the top and bottom beams and also at the actuator steel plates. These channels are very accurate in length and were placed by using oil jacks to bring the test machine to a rectangular set up. To ensure the main beams of each axis and therefore the machine is perpendicular they were checked with a set square.

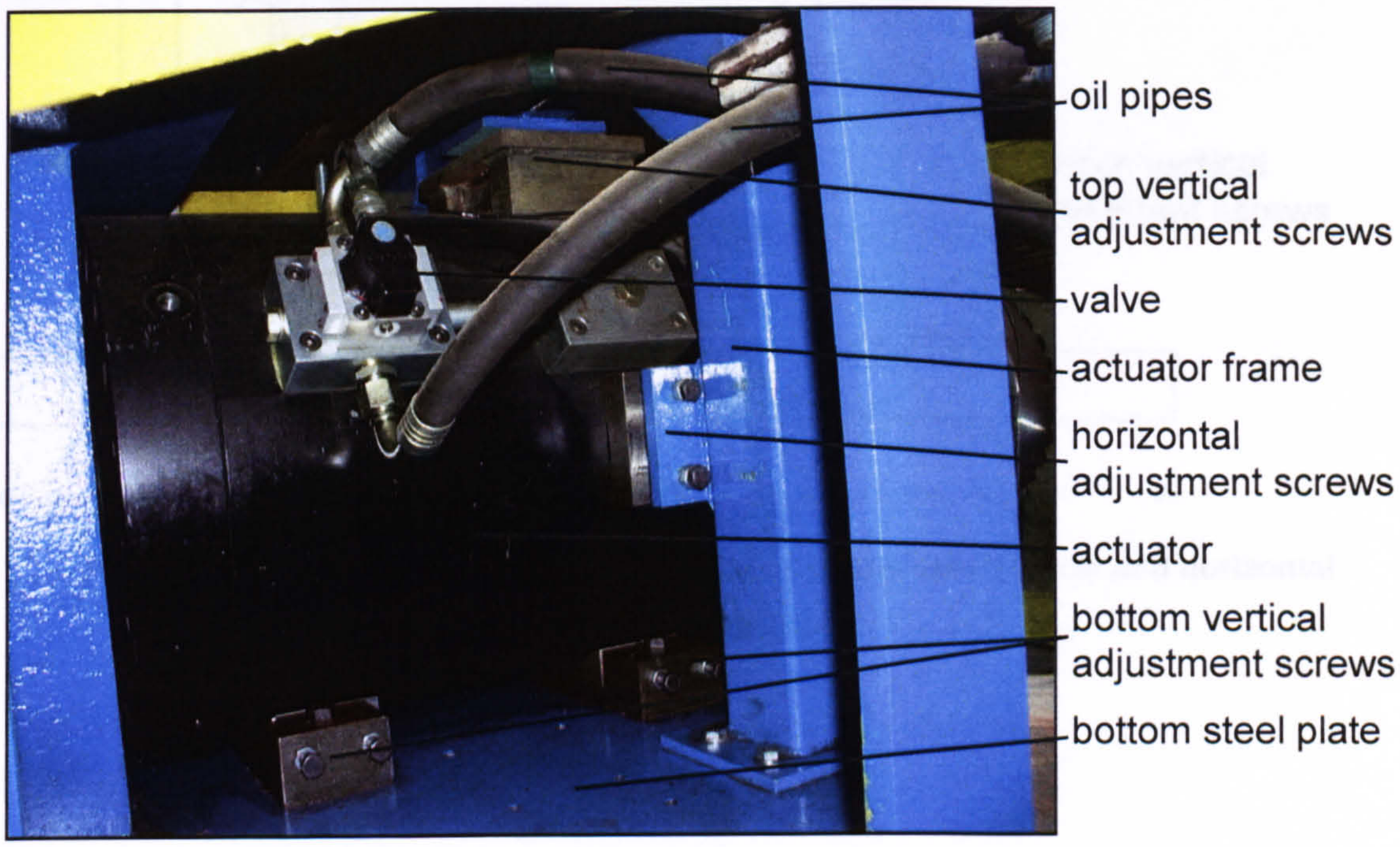

Figure 3.6 Horizontal and vertical adjustment bolts at actuator front

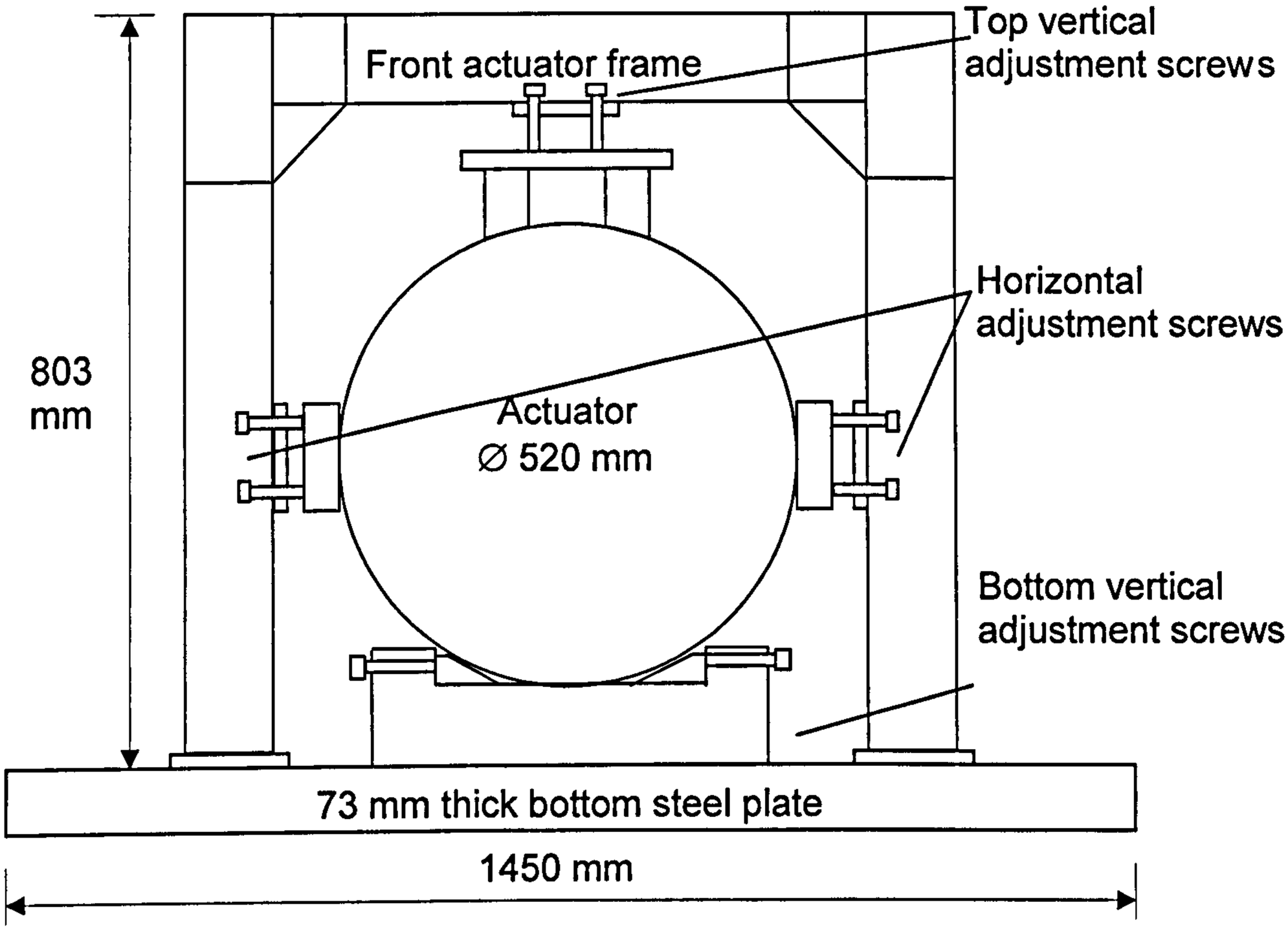

Figure 3.7 Front elevation trough actuator front frame and vertical and horizontal adjustment screws

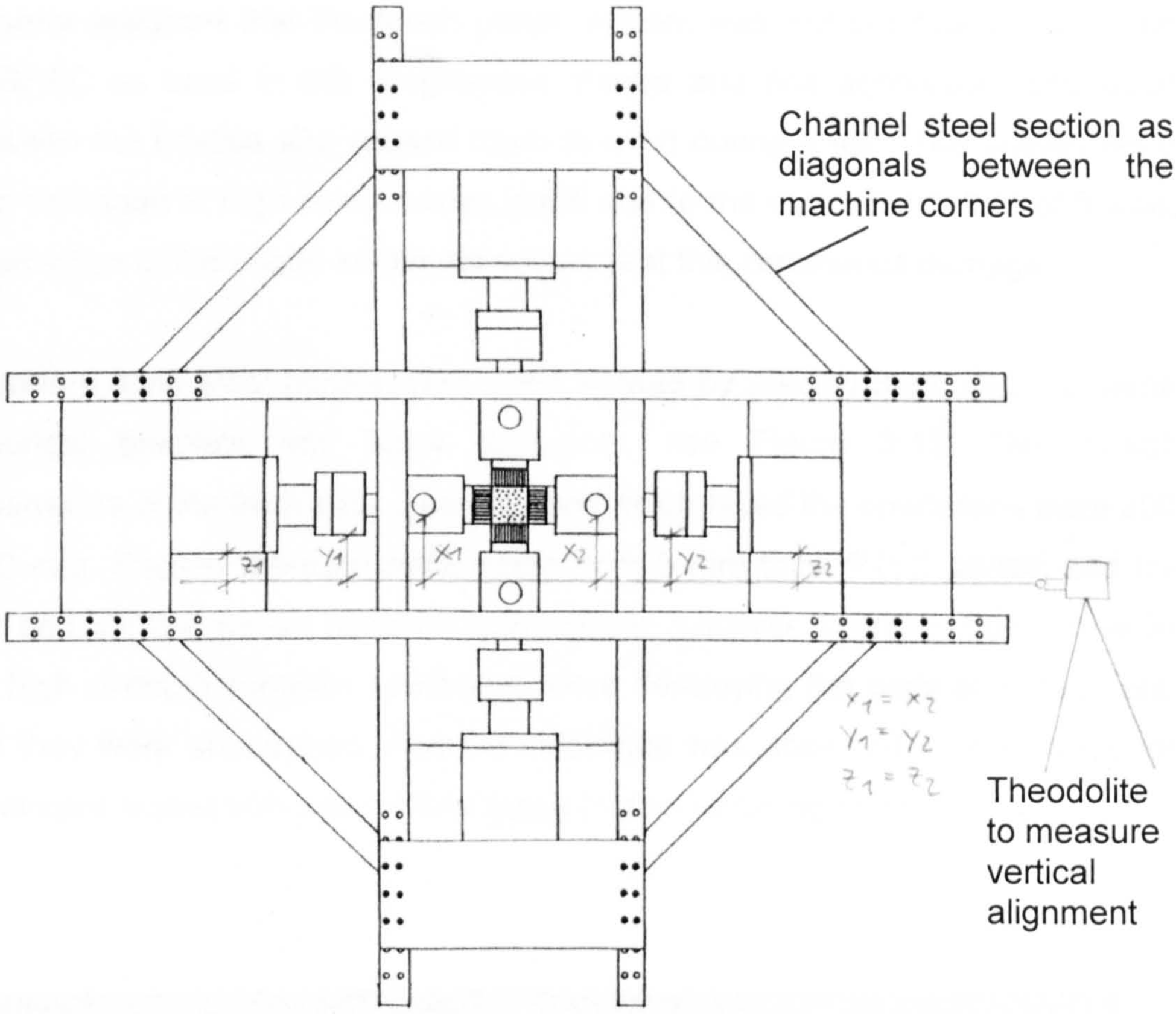

Figure 3.8 Measurement arrangement for vertical alignment

3.1.3. Platen system

Compression

Brush loading platens were used for the first two compression-compression test series before they were replaced by solid steel blocks. Each brush platen contained 400 steel bristles, each 5 mm square and 100 mm long as shown in Figure 3.9. These were machined at both ends to ensure flat bearing surfaces and clamped together within a bracket and block assembly, shown in Figure 3.10. This assembly was bolted to a linkage system containing a spherical bearing, which in turn was bolted to the actuator heads as could be seen in the elevation through the centre-line in Figure 3.11. After the first few specimens it

became apparent that the brush platen system was not practical for use with HPSFRC as used in this programme. Fibres and fine aggregates squeezed between the bristles and caused them to bend during a test. The bristles were also damaged at high compressive loads due to the explosive nature of failure. A reduction of the bristle length did not prevent this continuous damage.

Therefore solid steel blocks were used instead by placing them into the same spherical brackets and block assembly, see Figure 3.12. The overall dimensions of the front steel block surface which faced the specimens were 200 x 50 mm. Friction reducing pads made from 3 mm thick PTFE sheets and foil with and without grease between were tried to minimise lateral friction. However the high strength concrete specimens were destroying the pads after each test and they were abandoned. Also no difference was observed in the results for specimens tested with and without these friction reducing pads.

Figure 3.9 Steel brush platen

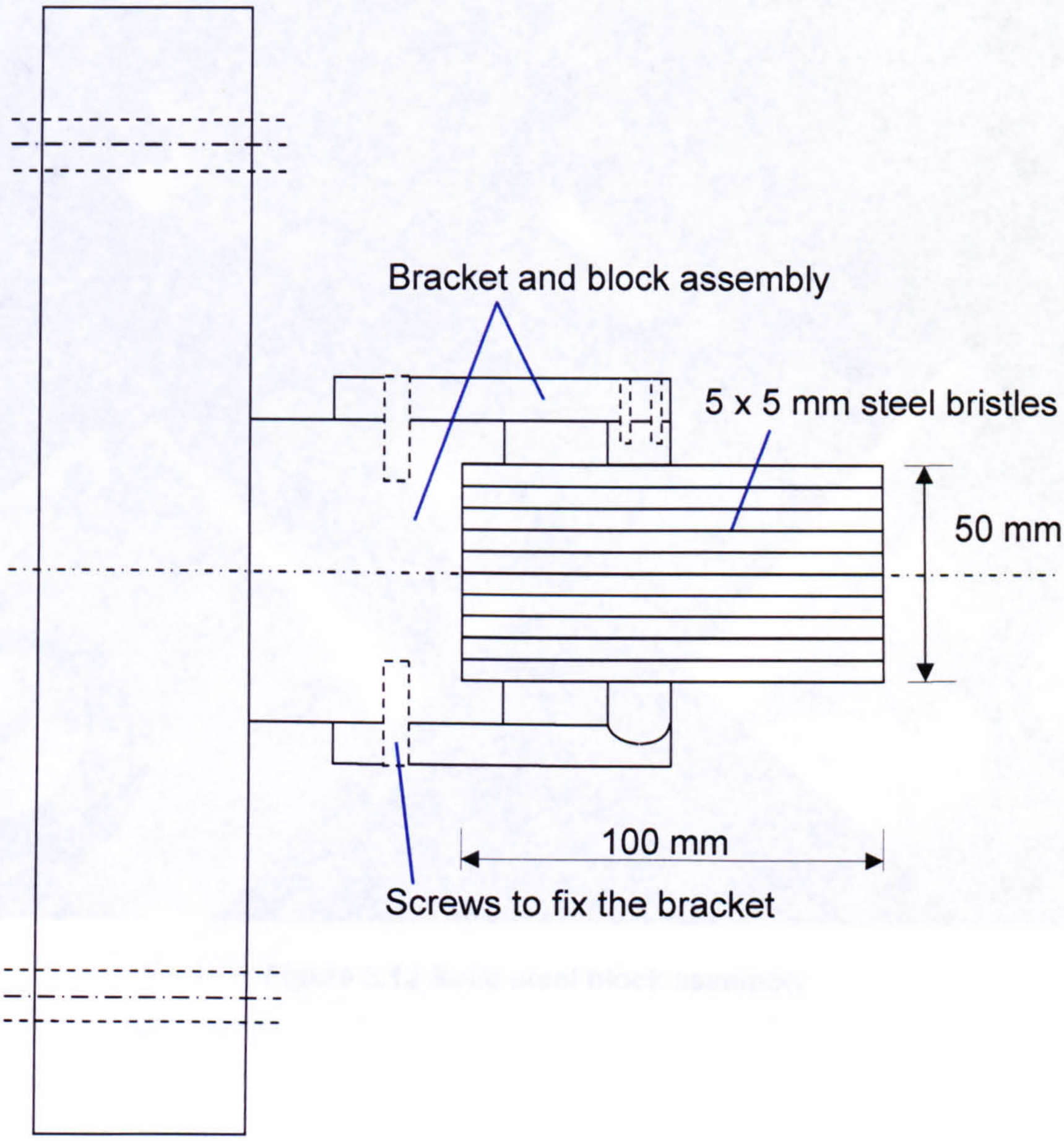

Figure 3.10 Steel brush brackets and block assembly

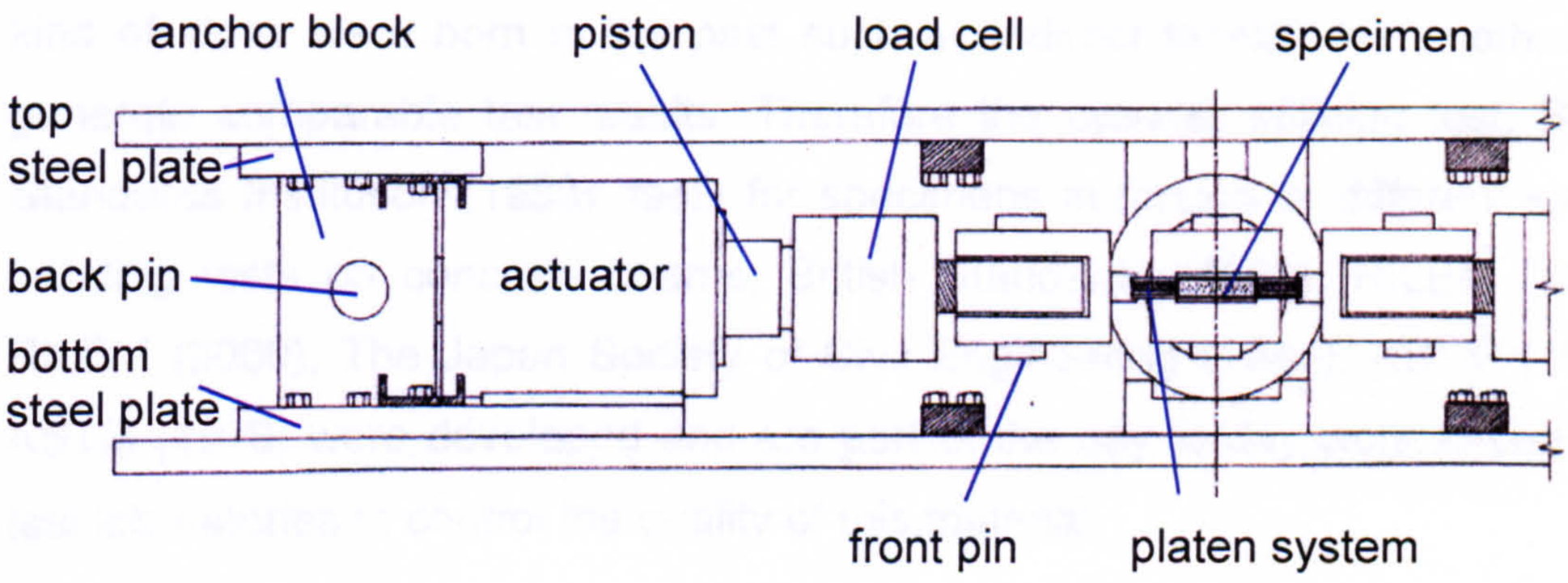

Figure 3.11 Elevation through centre-line of biaxial test facility

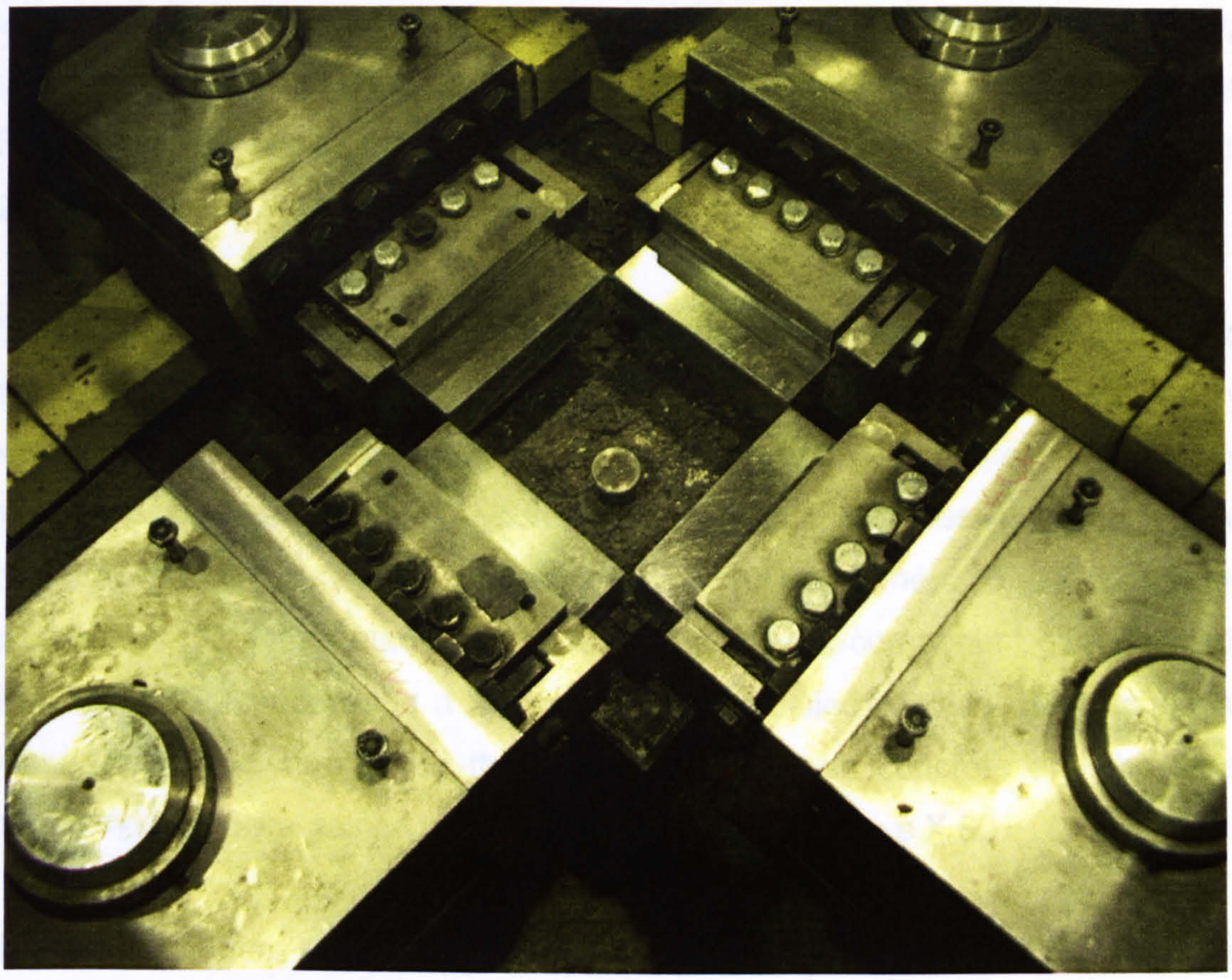

Figure 3.12 Solid steel block assembly

Tension

Tests on concrete under tension load have always been very difficult to do. All kind of ideas were born in the past such as indirect tension test methods to generate comparable test results. Therefore the cylinder splitting test, British Standards Institution (1983), tests for specimens in torsion or different kind of bending tests on concrete beams, British Standards (1983), RILEM (1985), RILEM (2000), The Japan Society of Civil Engineering (1984), ASTM (1984), ASTM (1979) were developed and are part of the day to day work in concrete test laboratories to control the quality of this material.

However, direct tension tests are still a challenge for every laboratory. Great attention has to be given to the connection between test machine and specimen which is more complicated to design than for compressive tests. The tension

load has to be transferred to the specimen without introducing any bending moment caused by unequal loading. This unequal loading could cause a bending failure within the specimen and would no longer present the direct tension stress of that material. Several methods were tried in this study.

One attempt to transfer tension loads into a concrete specimen is by gluing the specimen onto the test machine platen system. Very strong glue is necessary which can glue concrete together with metal, in most cases steel. In this study several glues were tried. A 2-component fast curing adhesive named X 60 made by the company HBM consisting of a liquid component (B) and a powder component (A). Other glues that were tried are the 2-component glue Terokal-221 made by Teroson and a 2-component glue called Araldite. Best results in terms of highest strength in the connection between concrete and the steel platen system were gained with the 2-component adhesive X 60.

The test procedure and the price of the glue turned out to be impractical and too expensive. The specimens needed to be cut, ground and polished very accurately at the surfaces to be glued. This was necessary to get a contact surface within the concrete matrix of the specimen and not only the cement paste on the specimen surface. The machines for doing these preparations were not available in the laboratory and the time required for the preparation of one specimen was too much overall compared with the solution that was finally chosen. Also the problem of small misalignments of the machine platens and the not always perpendicular and flat specimen surfaces made this test method impractical.

With pre-tests a peeling-off mechanism between the machine platens and the specimen surface was observed. The glue turned out to be strong enough to hold on the first layer of concrete matrix to the metal plate of the platen system. But the alignment of the machine platen and the specimen was not good enough and a major crack occurred close to the steel platen and the glued surface. Figure 3.13 shows specimens glued on steel platen and tested in a uniaxial test machine. One of the steel plates of each specimen peeled off close

to the specimen surface. This happened to almost every specimen whether they were notched in the middle like the two on the right or not. Therefore this method was discontinued.

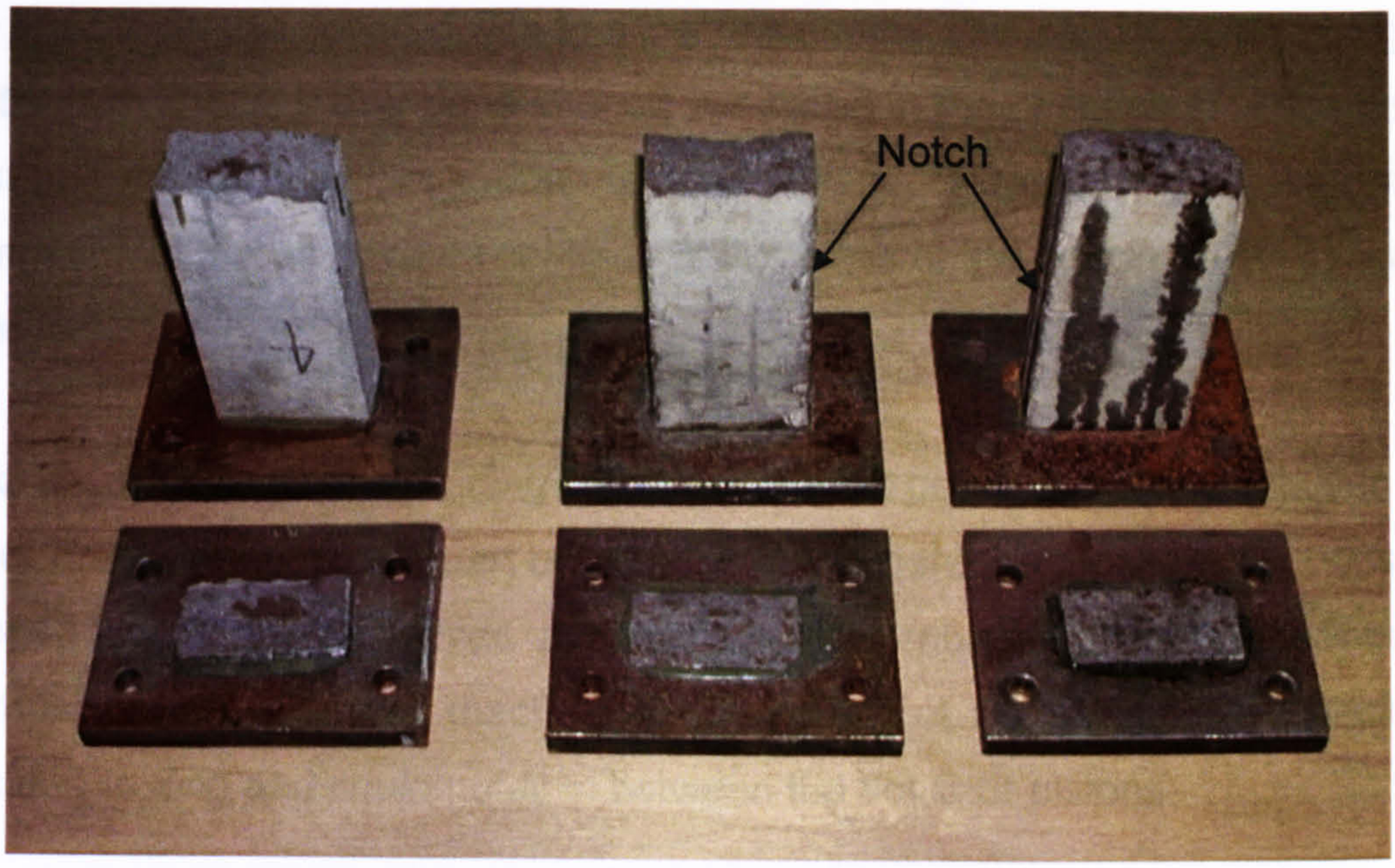

Figure 3.13 Tension specimens glued on steel platen (the two specimen on the right have a notch in the middle)

Another solution of transferring tension loads into concrete was to use dog-bone shaped specimens clamped in front of the actuator heads. With this method the area where the specimen is going to be connected to the machine is widened to allow the clamps a grip onto the specimen and also to resist cracks in that end area because of the increased cross-sectional area.

Figure 3.14 shows two kinds of dog bone shaped specimens. The one with the rectangular cross section was cast vertically to the compression testing direction. The flat specimen was cast in the same direction as the compression-compression specimens before. This would be the preferred type of compression-tension specimen for comparison reasons as the dimensions of

the middle area and the casting direction would be the same as for the compression-compression ones.

However it was impossible to reduce the air pockets on the top surface which arise on the vibrating table between the concrete and the mould surface which the specimen was covered with to allow this shape. This can be seen on Figure 3.15 which shows a dog-bone shaped specimen in the direction in which it was cast and the large air pockets on the top surface. Because of the rather large elongation of the air pockets continuous thickness of the specimen could not be guaranteed.

Also the difficult part of finding an adequate shape of the curve between the wider part and the middle part of the specimen where the crack was suppose to happen could not be solved sufficiently. The problem of building adequate clamps within the limited machine space could not be solved. The specimen became to long and could not fit in between the actuator pistons.

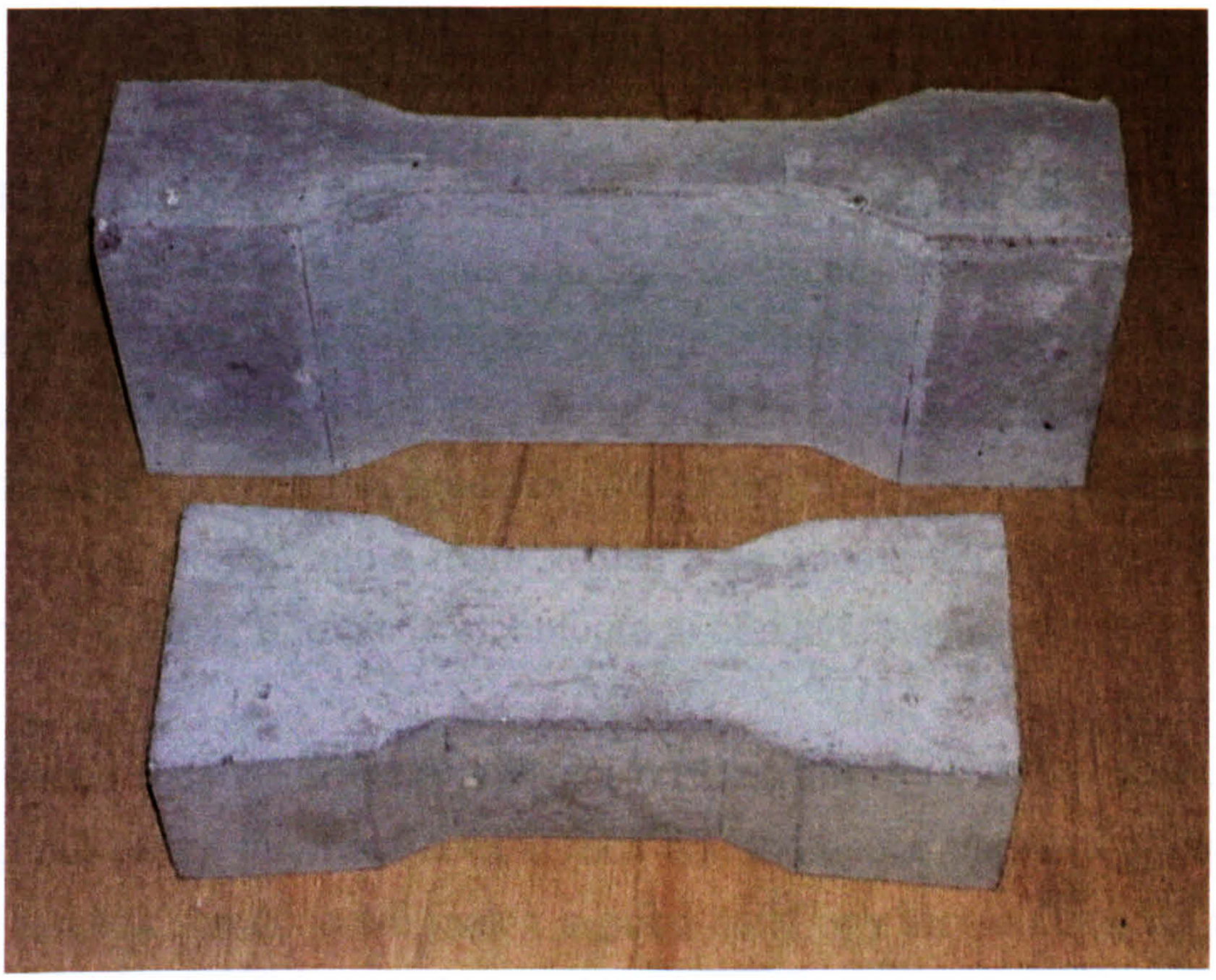

Figure 3.14 Specimens in dog-bone shape

Therefore this method was discontinued because of difficulties of casting and the production of moulds which would reduce the air pockets on the top specimen surface during casting and the problem of finding an adequate curve shape within the limited space of the testing rig.

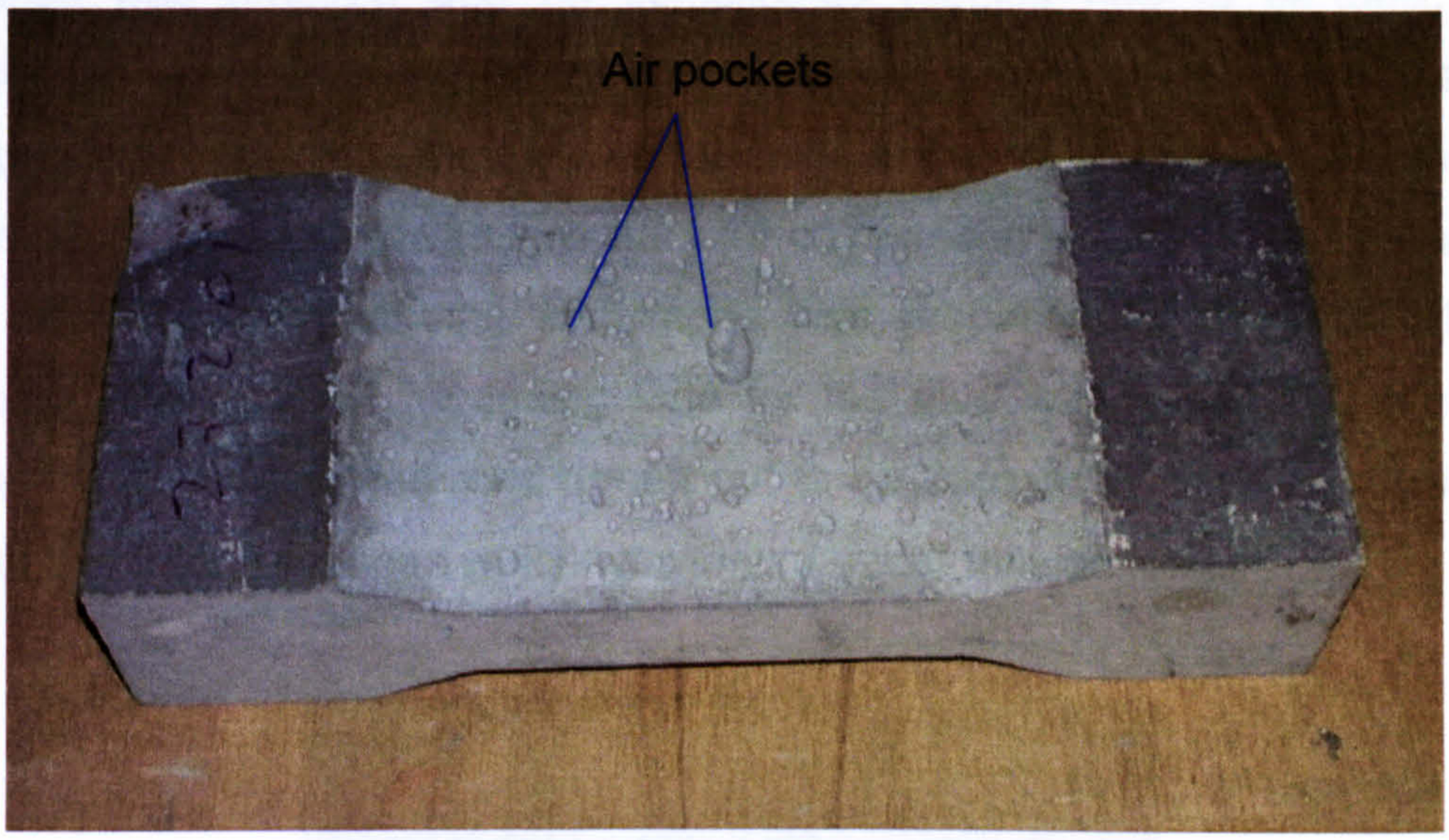

Figure 3.15 Dog-bone shaped specimen in casting direction with large air pockets on top surface

The solution which was finally adopted was to cast fourteen M8 threaded rods into each specimen on both sides and connect them with bolts to the machine platen system. Details of the moulds and the connection system are described with more drawings in section 3.2.2 about the Compression-Tension Specimen. The rods were cast into the specimen with different length to allow the tension force to be transmitted into a more diffuse area within the specimen. This can be seen in Figure 3.16 which is a photograph of a cut through this detail.

The threaded rods will transfer the tension load directly into the specimen by resisting pull out. If the length of the rods and the space between them is well chosen to allow the concrete matrix a good bond any tension load on the rod will be transferred to the central area of the concrete specimen.

The advantages for this kind of connection are the low price of the rods and the easy and simple way for casting and connecting the specimen with the machine. The number of rods per specimen was cheaper than the glue which would be used for one specimen. For casting and test preparation no extra skills and machines were necessary. The rods were cut from 3 m long bars in the technical workshop with a simple band saw. No special grinder for preparing the surfaces was required and no complicated moulds had to be built. The specimens were cast in the same horizontal plane as the compression-compression specimens before and the middle area of the specimens had the same dimensions. That was important for comparison reasons. The time which was used for changing the specimens was probably the same in all test methods. However no hardening time for the glue was needed. Overall the method with the screwed rods turned out to be successful. Figure 3.17 shows one of the failed specimen which was tested under tension loads.

Figure 3.16 Cut through a plane where the threaded rods had been cast into a specimen

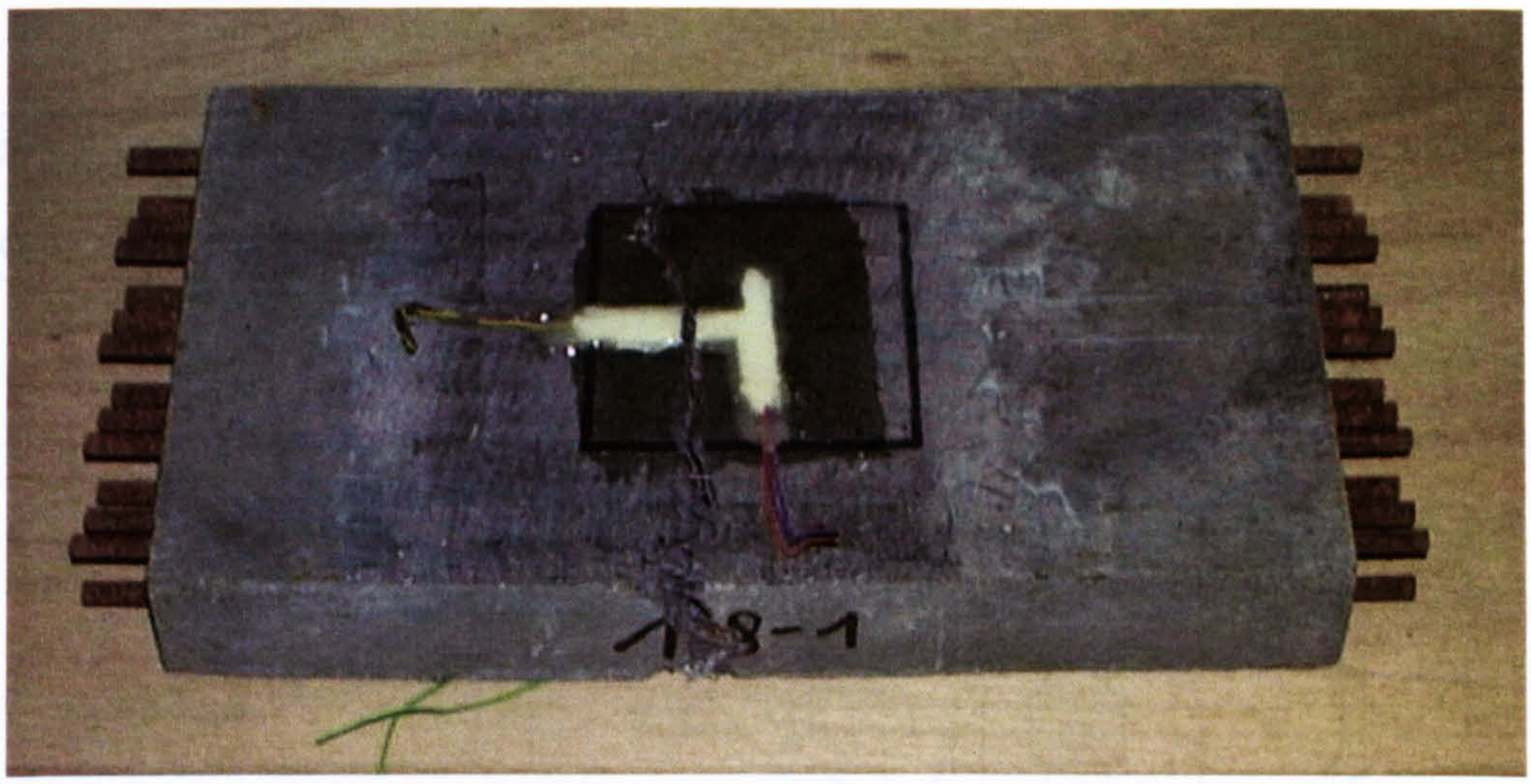

Figure 3.17 Failed specimen after tension test with threaded rods cast into

3.1.4. Control scheme and data compilation system

One actuator on each axis was under control from either a load cell or a displacement transducer using a dual channel controller, selected according to test circumstances. The other was a reactive actuator under high gain control that responded in proportion to the active actuator. This arrangement ensured that actuator pairs moved together so that the centre-line of specimens did not translate.

For the compression-compression specimens both axes were position controlled which means that the actuator travelling speed was controlled individually. This results in σ_2/σ_3 ratios for the ultimate stress ratios not always being constant. The block diagram in Figure 3.18 shows how the actuators were controlled for the compression-compression tests. The control panel of each axes was sending the signals to the two actuator in this axes independently to the other axes (red and blue lines). The displacements together with the applied load information were then recorded through the data logger and stored on a PC.

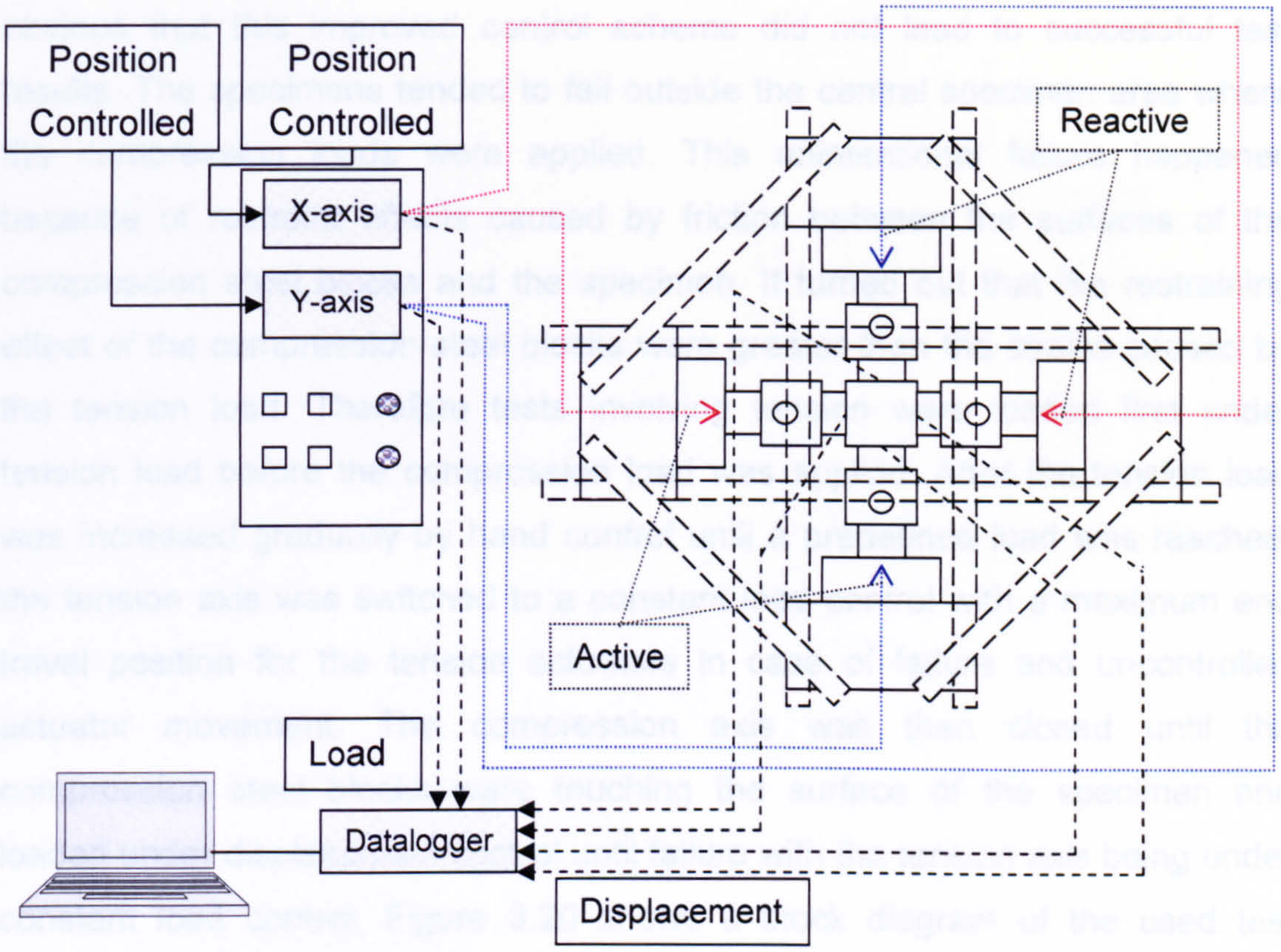

Figure 3.18 Block diagram of the closed-loop test scheme for the compression-compression tests

This was improved for the compression-tension specimens so that it was possible to control the second axis through an amplifier which converted the load output of the major axis into an input signal to the minor axis under a constant load ratio. The major axis was under displacement closed loop control and the minor axis therefore under load control. A block diagram of this closed-loop test scheme for compression-tension tests is shown in Figure 3.19. The tension axis was specified as the major loading direction, as this axis gave the smaller load readings and therefore needed to be controlled very accurately by displacement control. The compression axis followed with multiple load increments and inverse readings as compression loads were negative.

However after a few tests with specimens from the pre-test series it became obvious that this improved control scheme did not lead to successful test results. The specimens tended to fail outside the central specimen area where the compression loads were applied. This unintentional failure happened because of restraint effects caused by friction between the surfaces of the compression steel blocks and the specimen. It turned out that the restraining effect of the compression steel blocks were greater than the strains caused by the tension load. Therefore tests involving tension were loaded first under tension load before the compression load was applied. After the tension load was increased gradually by hand control until a predefined load was reached, the tension axis was switched to a constant load control with a maximum end travel position for the tension actuators in case of failure and uncontrolled actuator movement. The compression axis was then closed until the compression steel blocks were touching the surface of the specimen and loaded under displacement control until failure with the tension axis being under constant load control. Figure 3.20 shows a block diagram of the used test scheme which is also explained in more detail in section 3.6.2 about the test procedure for compression-tension tests.

Data was captured in intervals of one second during a loading sequence. These were automatically recorded through an Orion data logger and transferred to the computer control system and the software packages *win wedge* and *Excel*. All data were stored on the hard disk of a PC after every test, followed by additional investigations. During each test, load-displacement plots of the two axes were displayed with the actual load ratio σ_2/σ_3 and the actuator travelling history. For the compression-compression specimens it was possible to adjust the actuator travelling speed with this control scheme when it was foreseen that the σ_2/σ_3 ratio would go too far beyond the accepted limits. For the compression-tension specimens this adjustment was not necessary because the tension axis was under load control and adjusted itself for a given tension load while the compression axis was under displacement control and continued loading until the specimen failed or one actuator reached its displacement limit which was chosen and set before.

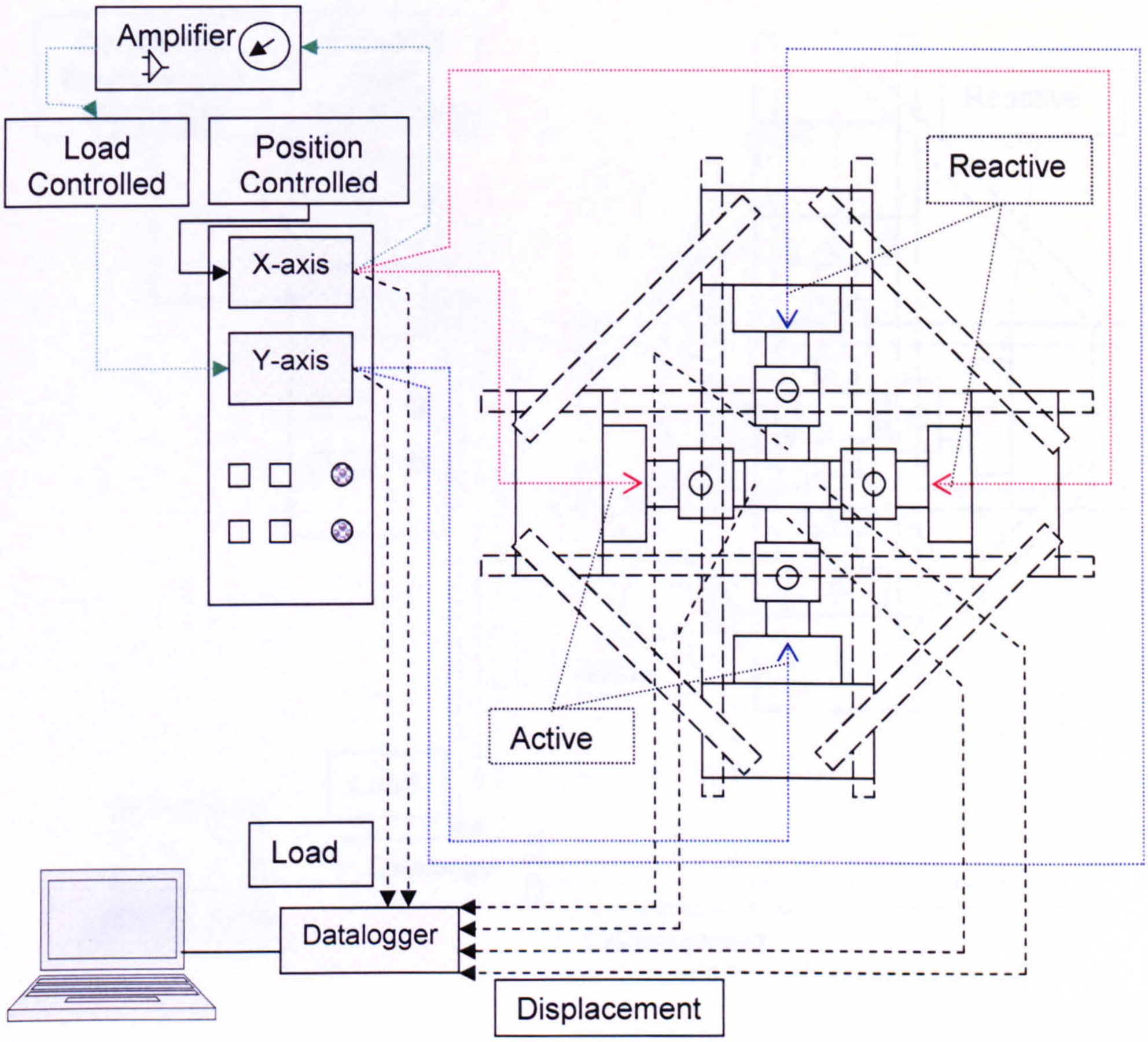

Figure 3.19 Block diagram of the closed-loop test scheme of the first pre-test compression-tension tests (not used for test series)

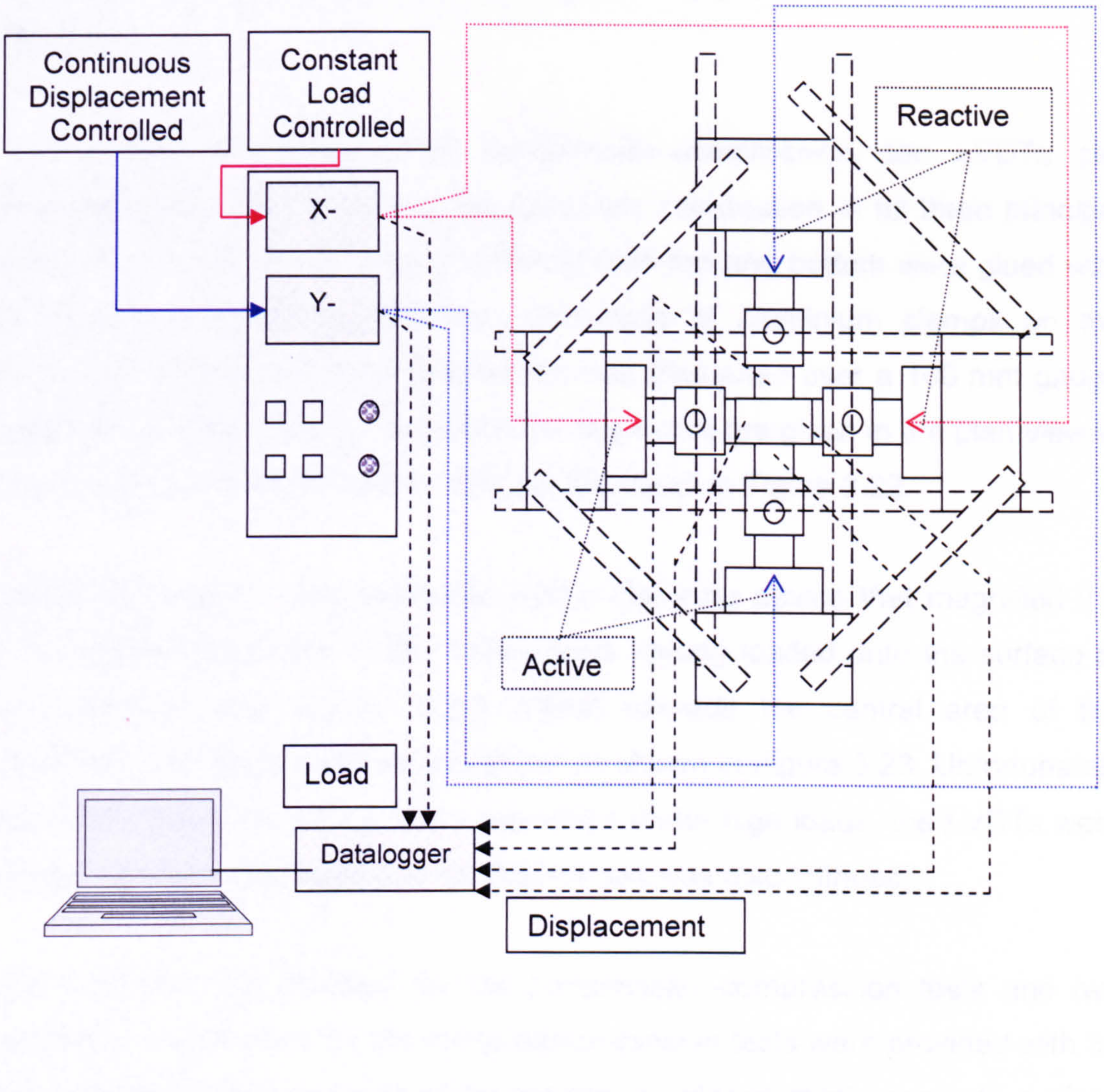

Figure 3.20 Block diagram of the closed-loop test scheme for compression-tension tests

3.1.5. Measurement Devices

Loads were measured by two load cells, one for each axis which was placed with the active actuator. The output voltage (0 to 10 V) from the controller was fed into the input channel of the data acquisition system.

The actuator displacements were measured with one linear voltage displacement transducer (LVDT) on each actuator. They were placed on top of the actuator and measured the piston displacement against the actuator casing.

This AC LVDT signal was the input signal for the closed-loop control of the actuators.

For the first few tests under compression-compression, ten LVDTs per specimen were used to record the specimen deformation in all three principal directions, Δ_1, Δ_2 and Δ_3. Four LVDTs on both top and bottom were glued with epoxy and a special arrangement consisting of aluminium clamps on the surface of a specimen. The deformation was measured over a 100 mm gauge length. More details of the measurement alignment are given in the plan view in Figure 3.21 and in the elevation through this detail in Figure 3.22.

Lateral deformation was measured with a clamping device that magnified the displacement using one LVDT. These were sprung loaded onto the surface of the specimen, the probes being placed towards the central area of the specimen. Two were used per specimen as shown in Figure 3.23. Unfortunately due to the explosive failure of the specimen under high loads, the LVDTs were being irreparably damaged and so this method was discontinued.

One specimen out of three for the compression-compression tests and two specimens out of three for the compression-tension tests were provided with 30 mm long electrical resistance strain gauges in order to obtain concrete surface strain directly for every stress ratio and every fibre variable. Four gauges were placed in the middle of the specimens in a T shape, two on top and two at the bottom, in the direction of the principal loading directions σ_2 and σ_3. Those have a resistance of 120.2 Ω ± 0.2 Ω and a gauge factor of 2.11 ± 1 %. The position of the strain gauges can also be seen in Figure 3.21 in the plan view of the displacement measurement devices. In addition Figure 3.24 shows a photograph of a test specimen with two strain gauges mounted at the centre of the top surface together with the lateral deformation measurement device.

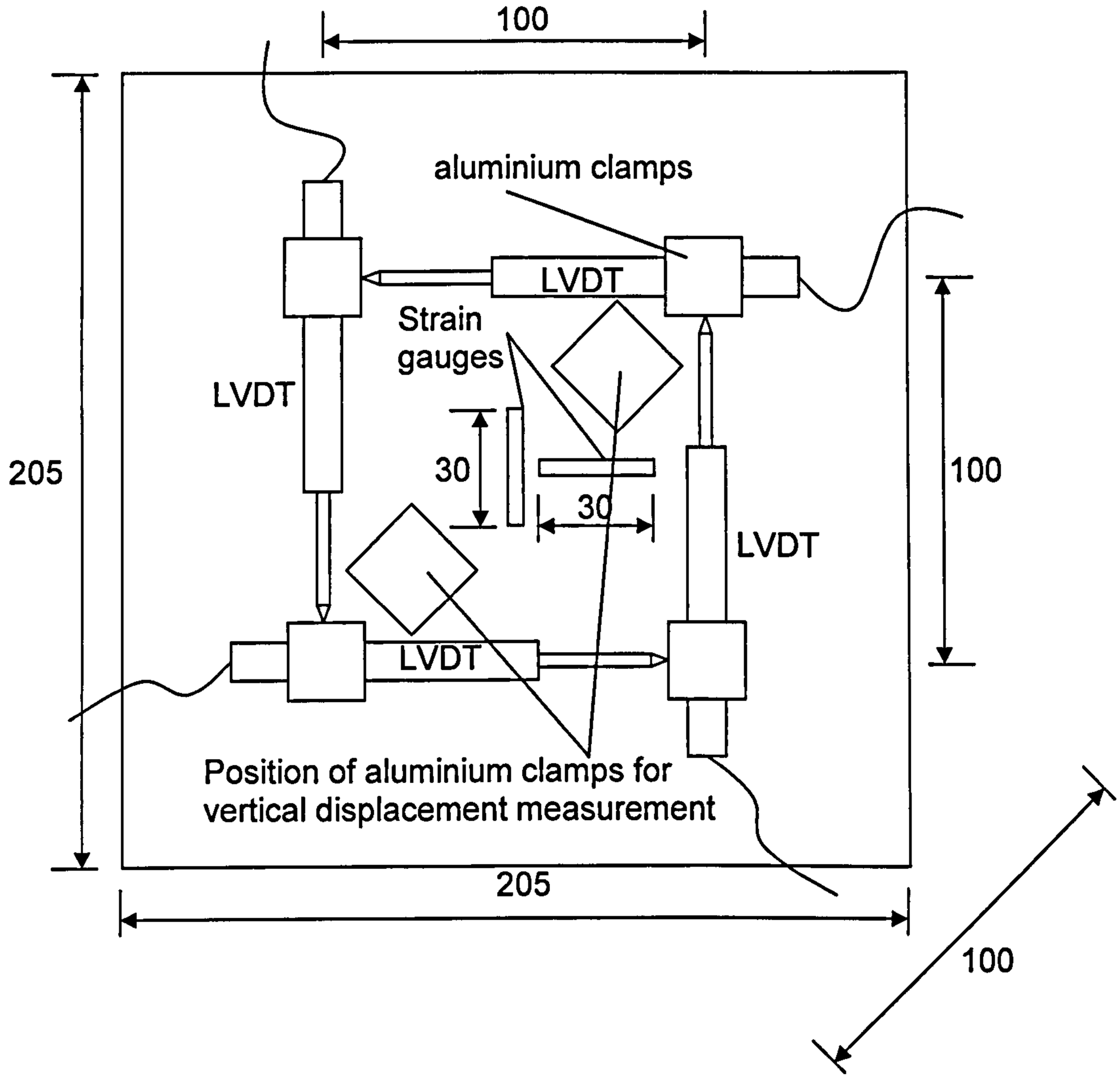

Figure 3.21 Plan view of the positions for the displacement measurement devices

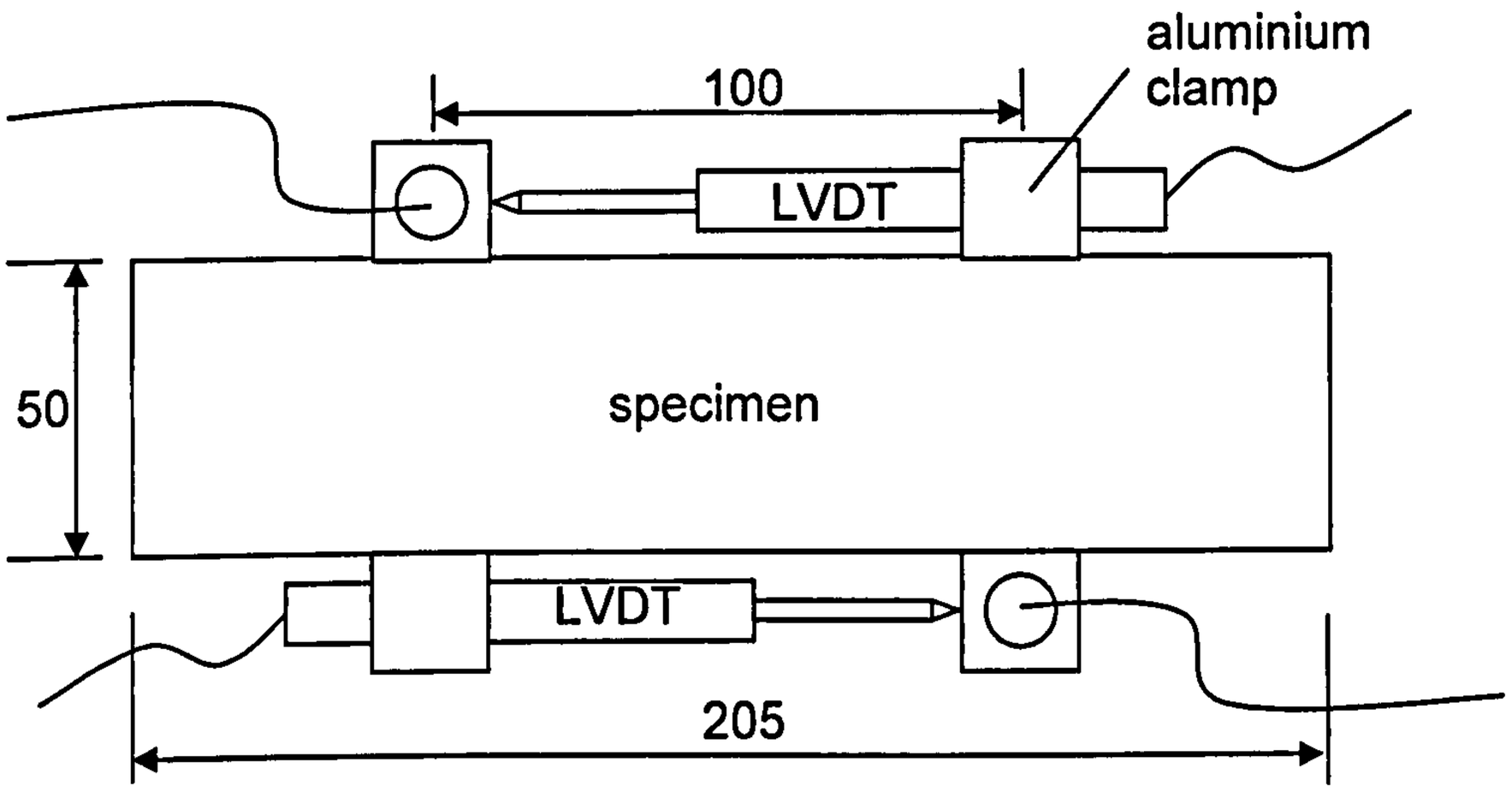

Figure 3.22 Elevation through the positions for the measurement devices

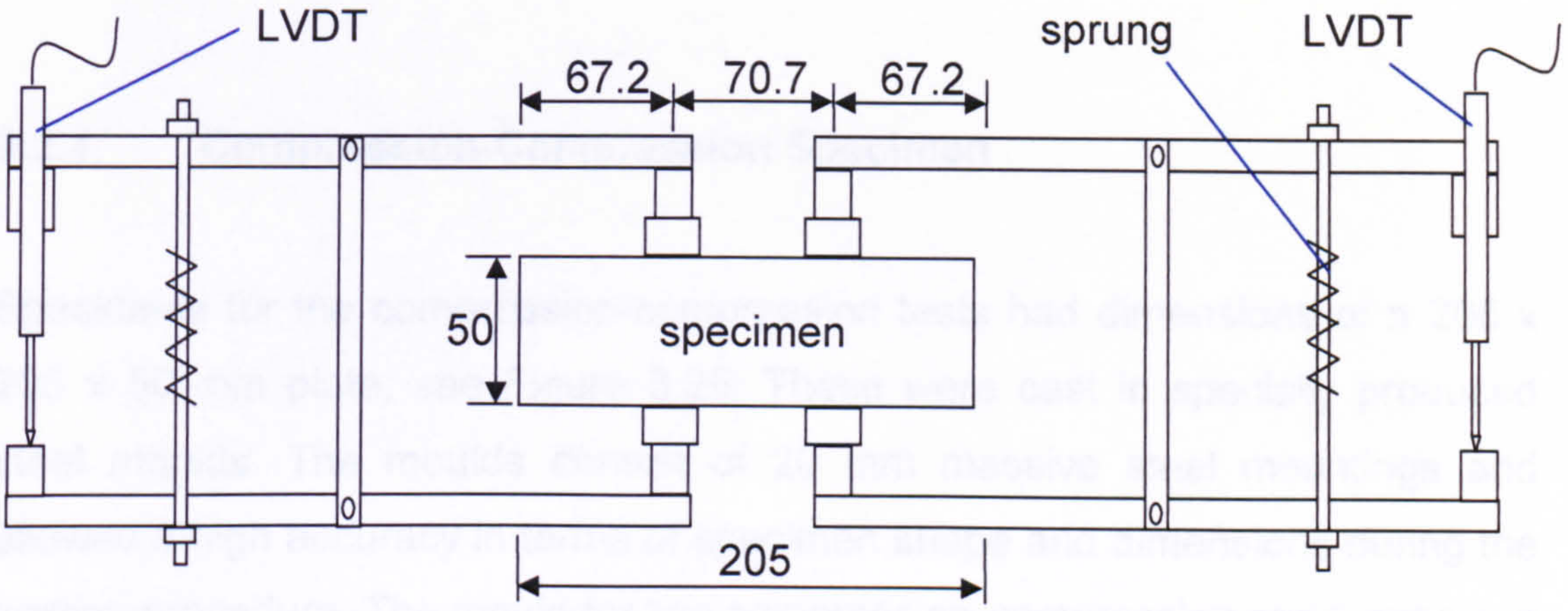

Figure 3.23 Elevation through the position of the sprung loaded clamping device measuring the vertical displacement

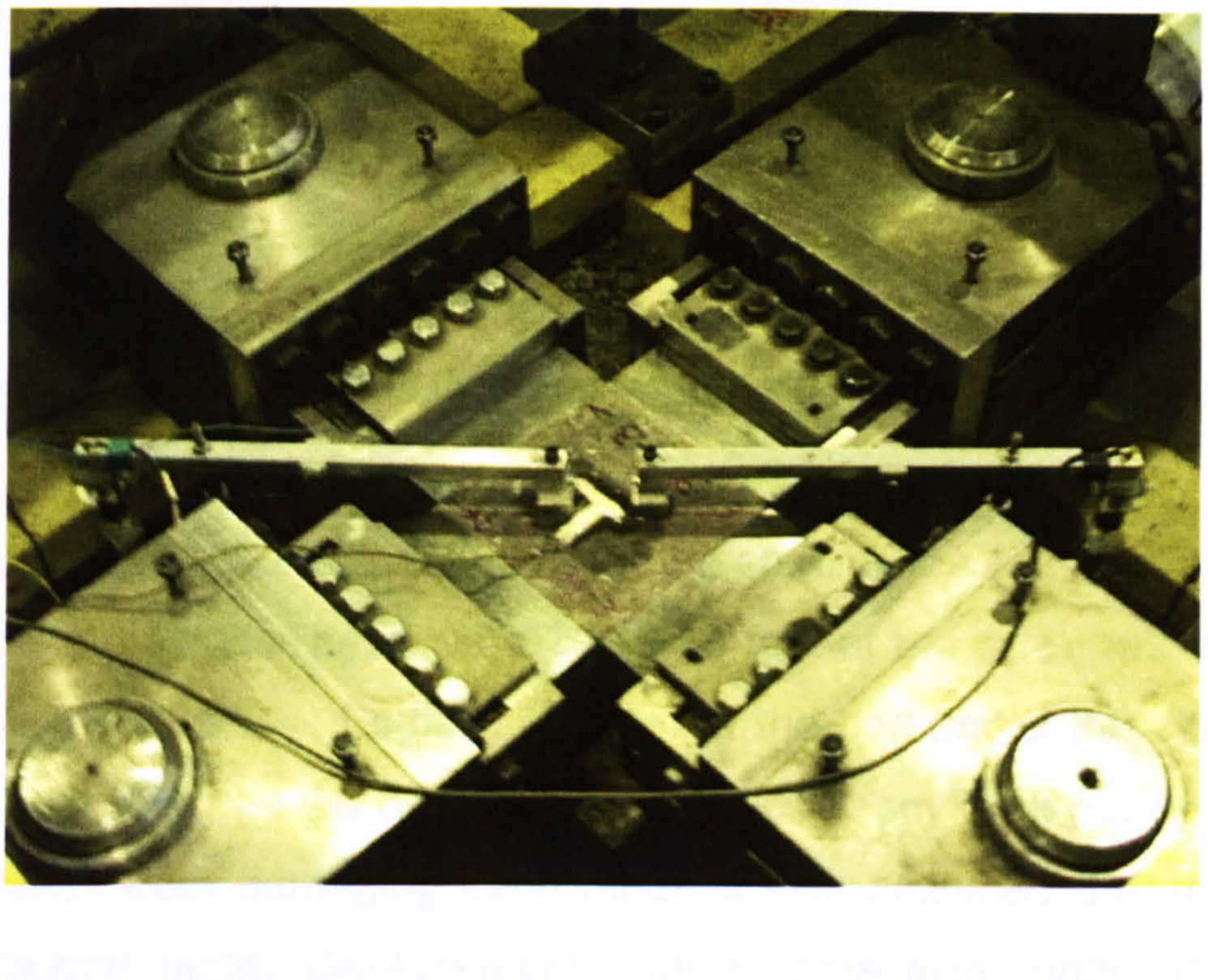

Figure 3.24 Compression-compression specimen with two strain gauges mounted on the top centre surface together with the lateral deformation measurement (discontinued after the first couple of tests)

3.2. Test Specimens

3.2.1. Compression-Compression Specimen

Specimens for the compression-compression tests had dimensions of a 205 x 205 x 50 mm plate, see Figure 3.25. These were cast in specially produced steel moulds. The moulds consist of 20 mm massive steel mountings and allowed a high accuracy in terms of specimen shape and dimensions during the casting procedure. The mould for two compression-compression specimens can be seen in Figure 3.26.

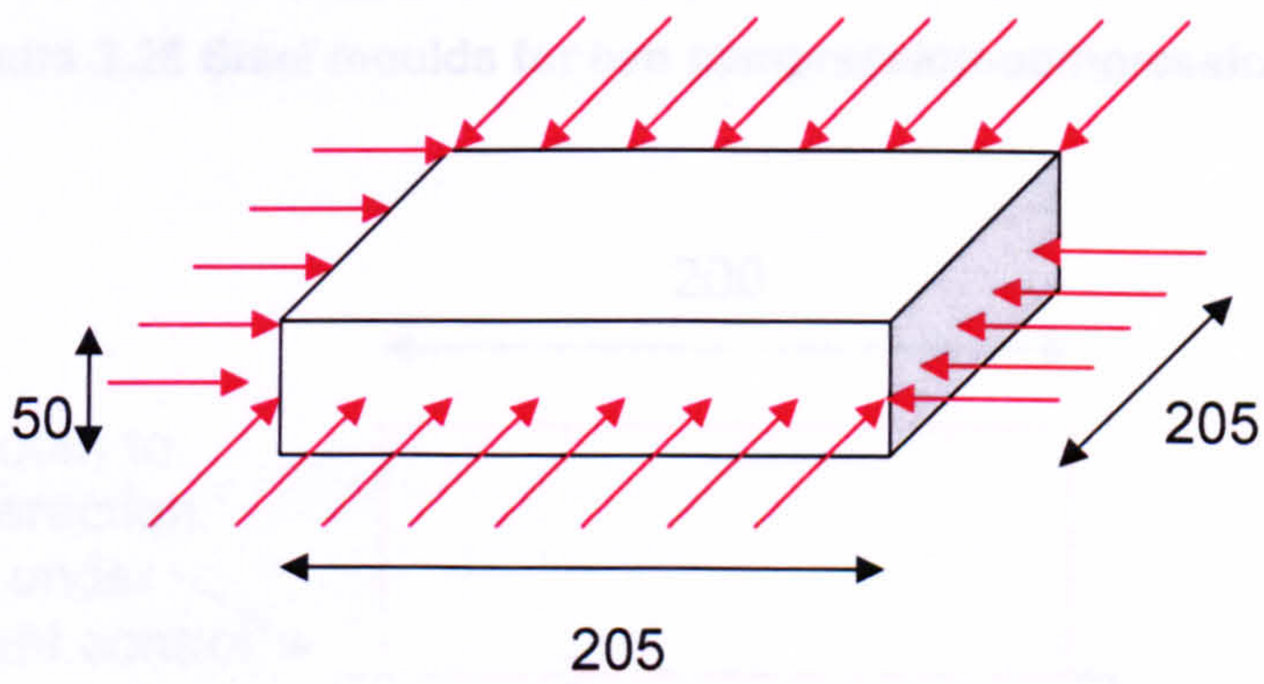

Figure 3.25 Dimension of the Compression – Compression specimens

The dimensions of 205 x 205 x 50 mm for the specimen were chosen in relation to the machine platens. These were 200 x 50 mm at the sides where they face the specimen. This allowed sufficient room at the corners of the steel platens, which ensured that they did not come in contact at any time during a test and prevented them from damaging each other. It was assumed that the machine actuators moved under displacement control; otherwise, under load control there would be a great risk that the machine platens ran into each other at the corner when the specimen failed. Figure 3.27 shows the dimensions. A compression-compression specimen ready for testing can also be seen in Figure 3.24.

Figure 3.26 Steel moulds for two compression-compression specimens

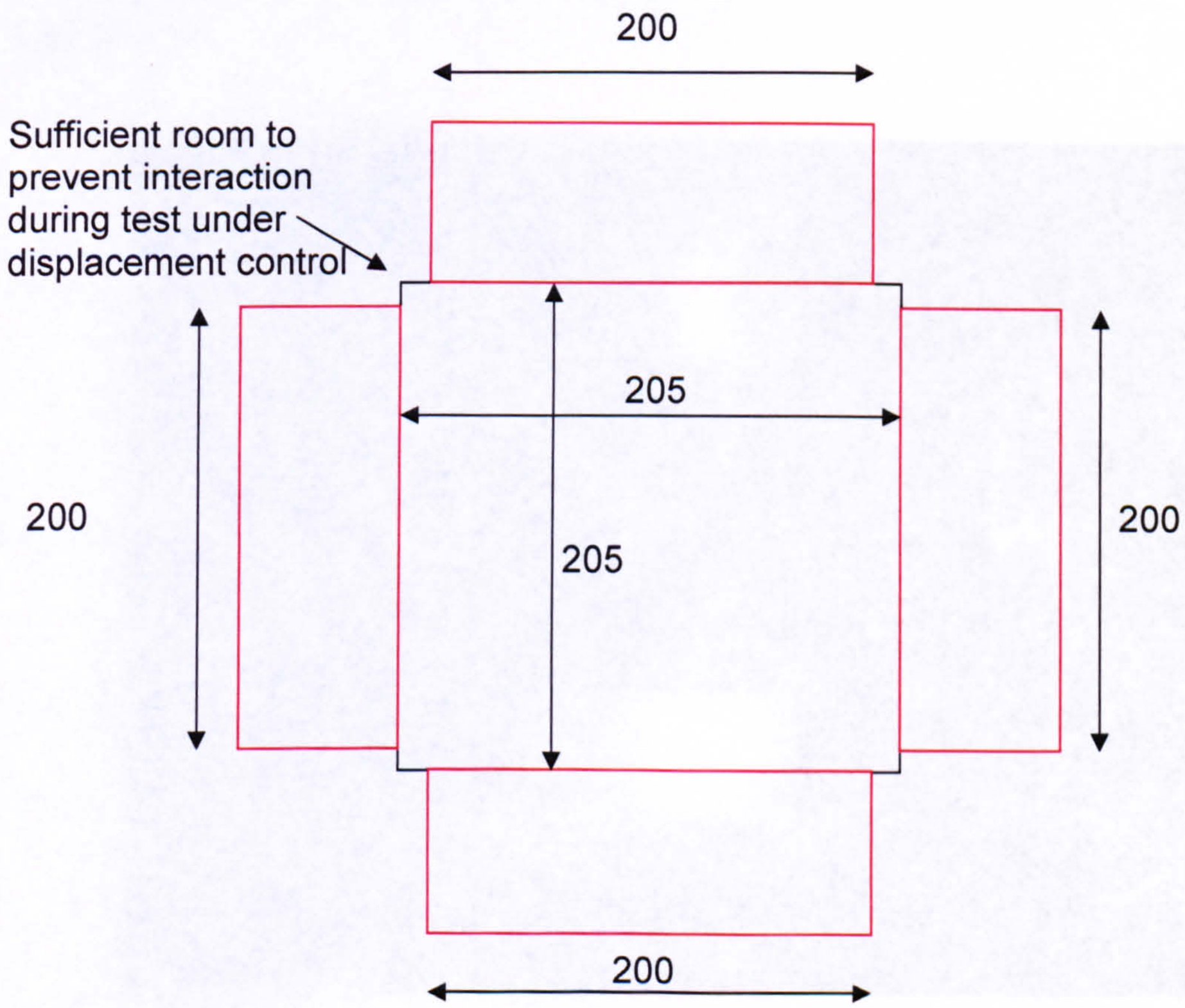

Figure 3.27 Dimension of compression-compression specimen and steel platen

3.2.2. Compression-Tension Specimen

The specimens for the compression-tension tests look similar to the compression-compression ones. However one dimension was extended by 80 mm on each side to allow the tension force to transmit to the middle section of the specimen through threaded rods cast into the specimen. Fourteen M8 threaded rods on each side were connected with bolts to an anchor plate which was connected to the machine with a pin. A compression-tension specimen in the machine during testing is shown in Figure 3.28. The loaded area on the specimen was as large as for the compression-compression specimens. This allows direct comparison of the results of both specimen types, compression-compression and compression-tension, and present them in one diagram because no size effect need to be considered. Figure 3.29 shows the compression-tension specimen dimensions. The alignment of the threaded rods on each of the specimen tension sides is shown in Figure 3.30 and the compression-tension mould with threaded rods before casting is shown in Figure 3.31.

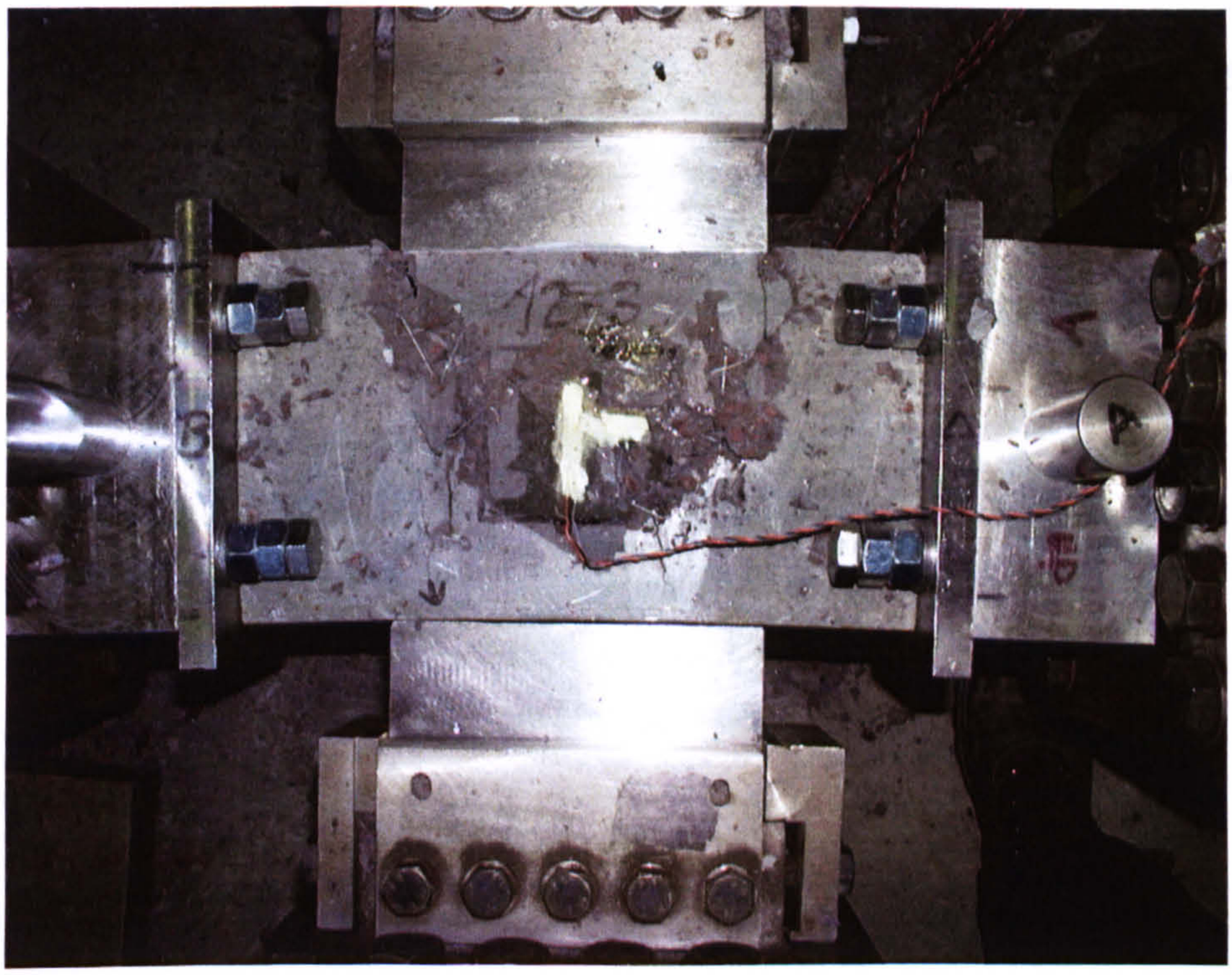

Figure 3.28 Picture of a compression-tension specimen in the machine during testing

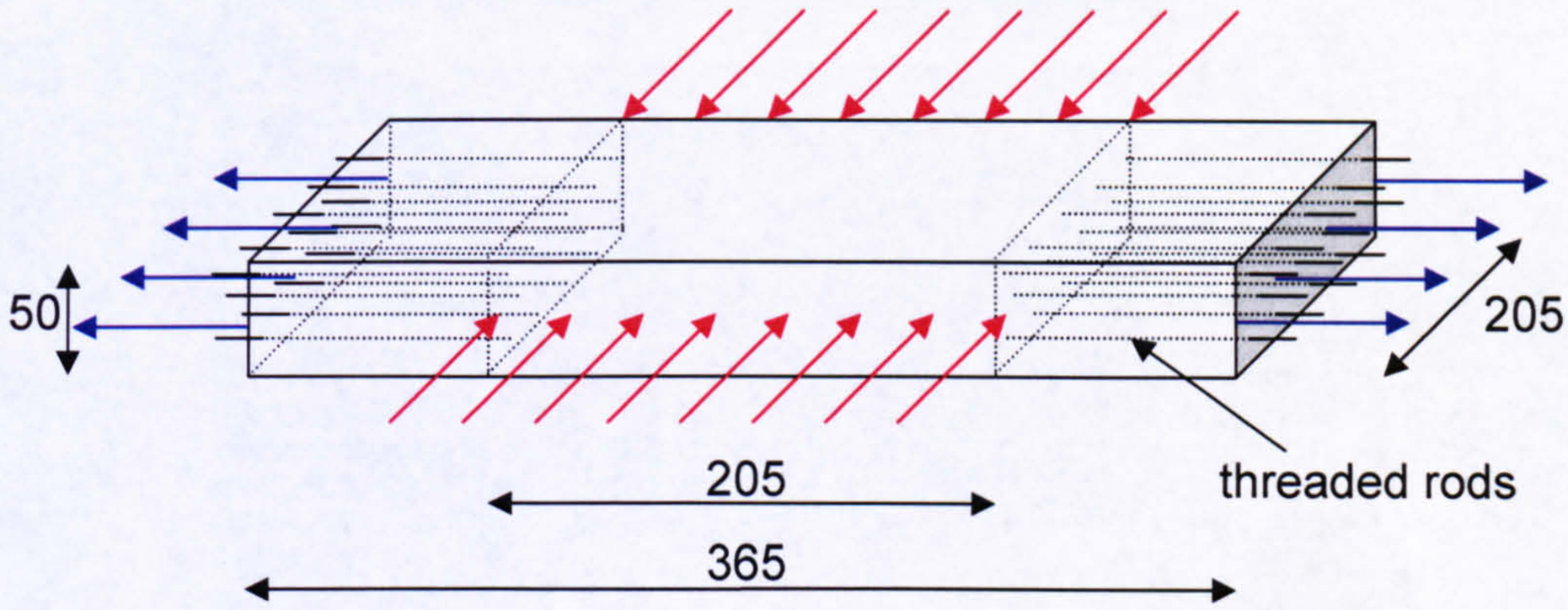

Figure 3.29 Dimension of the compression-tension specimens

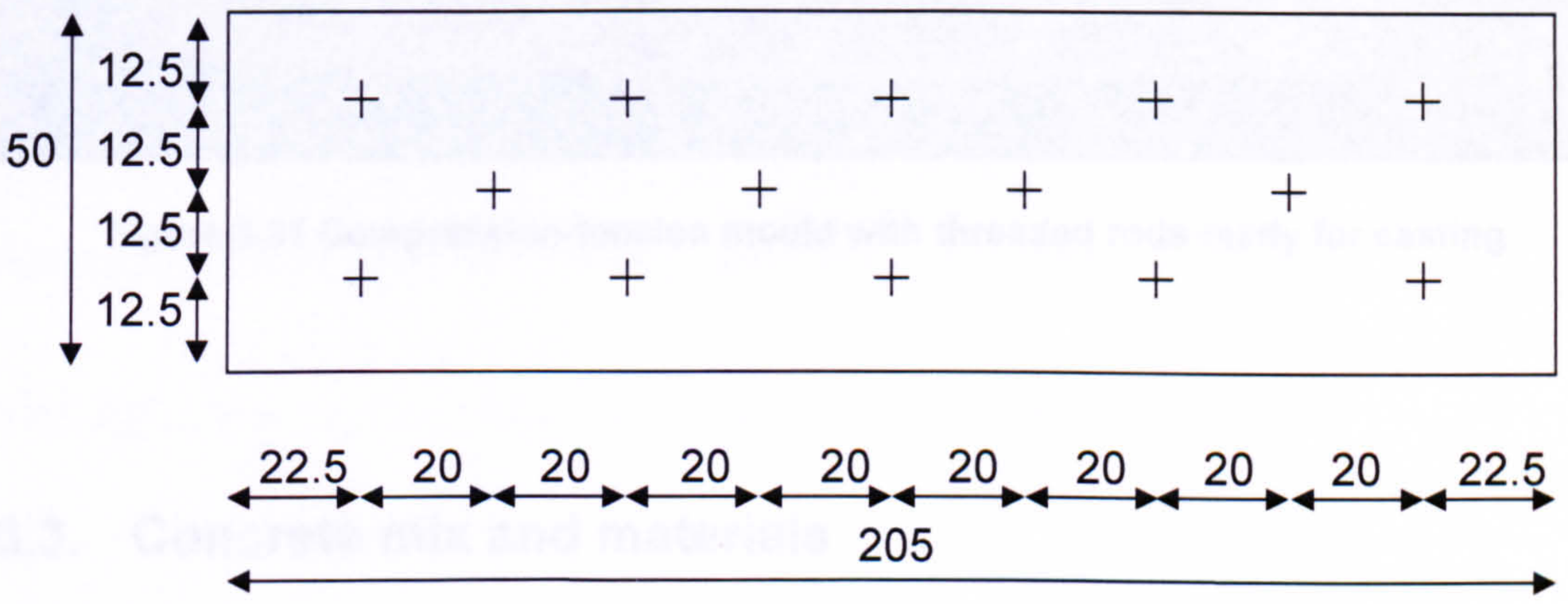

Figure 3.30 Alignment of the threaded rods within the concrete compression-tension specimen

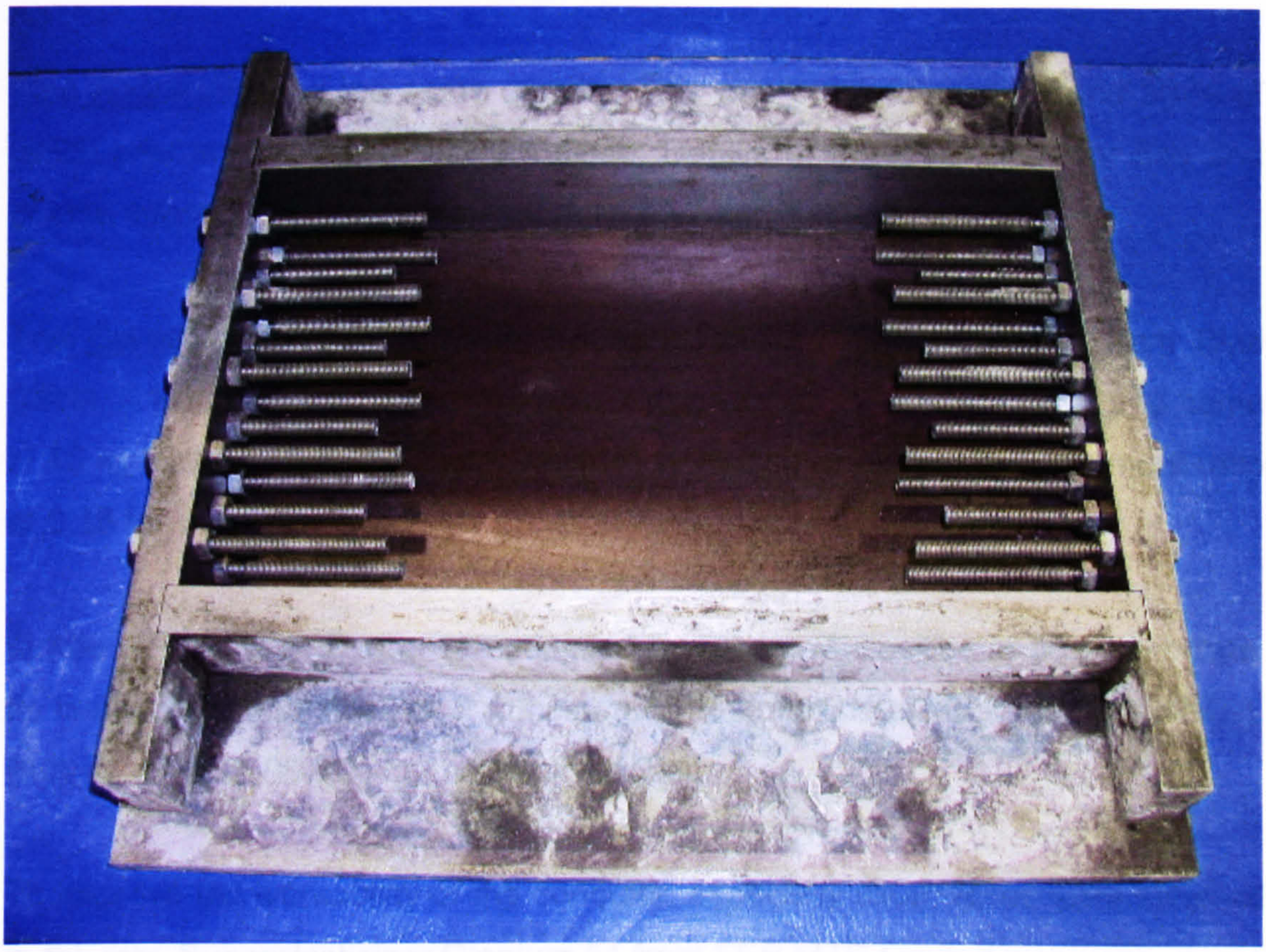

Figure 3.31 Compression-tension mould with threaded rods ready for casting

3.3. Concrete mix and materials

The plain concrete mix was designed for a target 28-day 100 mm cube compressive strength f_{cu} = 100 N/mm^2. To obtain this strength and sufficient workability, silica fume and Superplasticizer were used. Table 2 shows the ingredients of the concrete mix for 1 m^3 of material in order of weighing. It should be noted that the used cementitious material (cement and silica fume) in this study is more than the maximum recommended amount by the British Standards. In the recommendations the maximum limit for cementitious material is at 550 kg/m^3 compared to 577 kg/m^3 in this study.

Coarse Aggregate was 10 mm graded crushed granite with a density of 2610 kg/m^3.

Fine Aggregate had the same density. This was crushed granite sand 30 % of which passed through a 600 μm sieve. Details of the sieve lines for fine and coarse aggregates are shown in Figure 3.32 and Table 3.

The Cement type was Scottish Ordinary Portland Cement (OPC) from Blue Circle. It was Class 42.5 N CEM 1 cement according to BS EN 197-1 and came in 25 kg batches. The cement content was 525 kg/m^3 with a water/cement ratio of 0.33 for that mix.

Grade 920-D Silica Fume was supplied by Elkem Microsilica in 20 kg batches. Its chemical composition is of minimum 85 % amorphous silicon dioxide (SiO_2). Bulk density is 600-700 kg/m ^{3} when packed.

To improve the workability of the concrete, especially when fibres were involved in the mix, Superplasticizer Glenium 51 from FEB MTB Limited was used. It was added to the mix after two thirds of the water had been added.

The water was Scottish water from the mains supply.

	Mass ratio	kg per m^3
Fine Aggregate	1.53	805
Cement	1	525
Silica Fume	0.1	52
Coarse Aggregate	1.8	945
Water	0.33	175
Superplasticizer	0.007	3675 ml
Steel Fibres (not for plain concrete mix)	0.15	83 for 1% volume content

Table 2 Concrete mix proportions

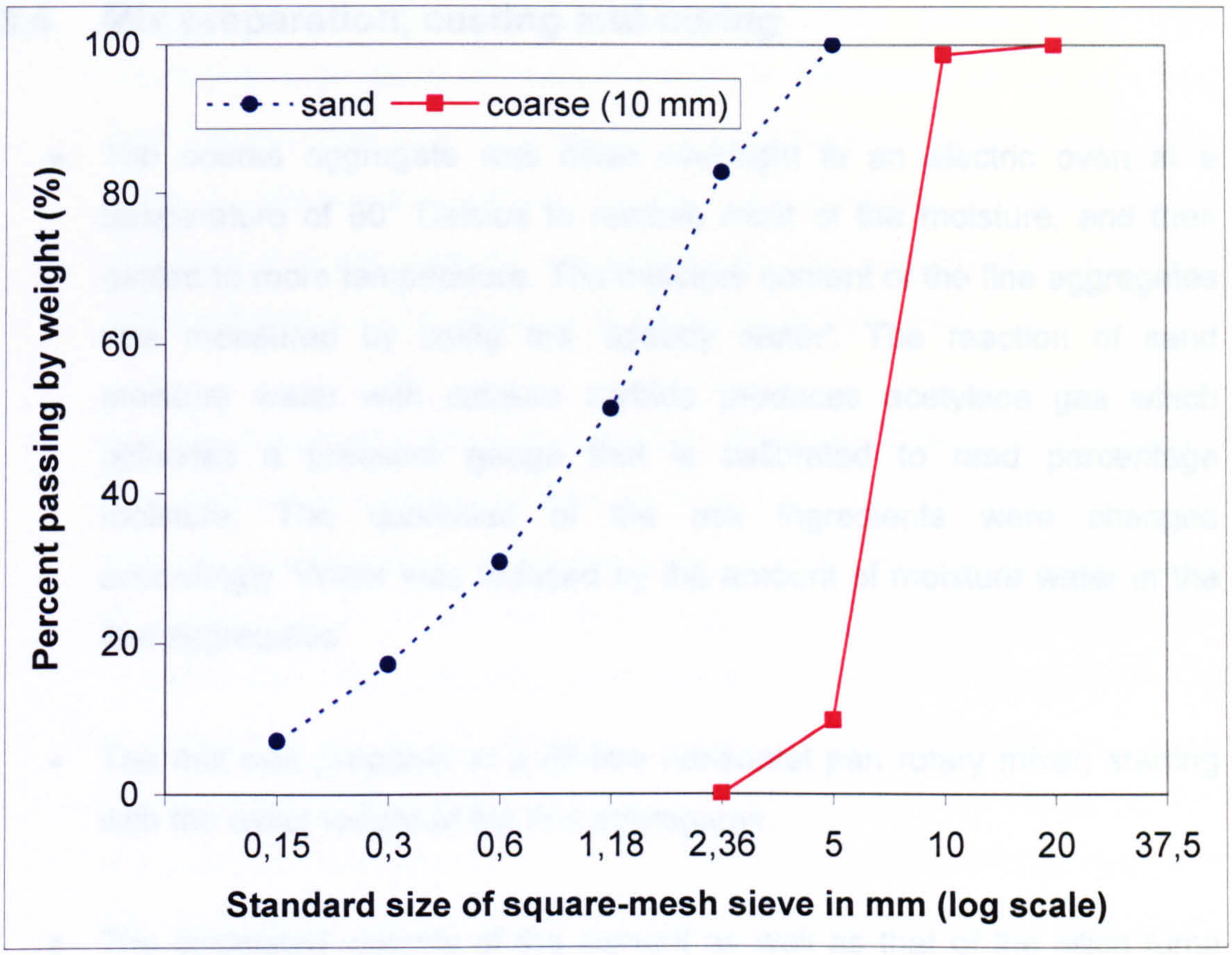

Figure 3.32 Grading of aggregates

Sieve size	Cumulative percentage retained	
	Fine aggregates	Coarse aggregates
37.5 mm		0
20		0
10		1.4
5	0	90.2
2.36	17.2	100
1.18	48.8	
0.6	69.2	
0.3	82.8	
0.15	92.9	

Table 3 Grading of aggregates

3.4. Mix preparation, casting and curing

- The coarse aggregate was dried overnight in an electric oven at a temperature of 80° Celsius to remove most of the moisture, and then cooled to room temperature. The moisture content of the fine aggregates was measured by using the 'speedy tester'. The reaction of sand moisture water with calcium carbide produces acetylene gas which activates a pressure gauge that is calibrated to read percentage moisture. The quantities of the mix ingredients were changed accordingly. Water was reduced by the amount of moisture water in the fine aggregates.

- The mix was prepared in a 60-litre horizontal pan rotary mixer, starting with the exact weight of the fine aggregates.

- The calculated weights of the cement as well as that of the silica fume were added, followed by the coarse aggregates.

- The dry ingredients were mixed for about one minute before two thirds of the water was added.

- Superplasticizer was added before the remaining water followed.

- After three minutes of mixing a slump test was carried out to assess the workability.

- From this concrete a reference group of three 100 mm concrete cubes were cast for every batch of the compression-compression series and the compression-tension series.

- The mix was designed for a slump of 120 mm. The slump test was conducted on the plain concrete before adding the fibres. This was

because the nature of fibre reinforced concrete makes slump tests impractical and would no longer reflect the workability of the concrete. Also the intention was to compare the influence of different steel fibre types in different fibre volumes to the same concrete. Therefore it was important that the concrete ingredients and the properties of the fresh and hardened plain concrete were as similar as possible.

- After the reference cubes were cast, the calculated amount of steel fibres was added to the fresh concrete to produce 0.5 %, 1 %, 1.5 % or 2 % of steel fibre reinforced concrete by volume. The components were mixed for another three minutes before casting. This procedure was necessary to gain information about the plain concrete strength of every batch. By comparing the plain concrete strength it was possible to make adjustments of the strength recordings of fibre specimens. Assuming that the plain concrete strength of a mix deviate a certain percentage from the design strength, the remaining strength recordings of the fibre specimens would have been corrected by the same percentage. This procedure allows a statement of the strength of fibre concrete compared to a fixed design strength which is the same for every mix.

- One of the four fibre types were glued together in bundles. They were separated in a bucket of water and dried before being added to the concrete. This was to ensure that the fibre bundles did not require any water from the mix for their process of separating.

- From this mix eight compression-compression test specimens with the reference cubes and cylinders were cast. For each fibre type in each fibre content two batches were necessary to cover the amount of concrete. Nine cubes and six cylinders were cast as reference specimens with fibre concrete for every odd batch number. Three of the six cylinders were tested with the splitting test and the other three were used for the compressive cylinder test both at the day when the plates of the compression-compression specimens were tested. The fibre cubes

were tested at 7, 28 and also at the plate testing day. For every even batch number only six fibre cubes were cast as reference compressive test points at 28 and plate testing day.

- For the compression-tension tests six test specimens were cast with nine reference cubes tested at 7, 28 and plate testing day. Also six cylinders were cast to be tested at the plate testing day. Three cylinders were tested with the compression cylinder test and three with the cylinder splitting test. As further reference tests six cubes were cast before fibres were added to compare cube compressive strength of each plain mix at 28 and the testing day. Again for each fibre type in each fibre content two batches were necessary. A summary of the number of specimens and reference cubes and cylinders are shown in Table 4 and Table 5.

- All specimens were properly compacted through vibration on the vibration table in the concrete laboratory.

- After the specimens had been cast their surfaces were finished with a float and covered with plastic to prevent the moisture from evaporating.

- The specimens were stripped 24 hours later and stored under water for 28 days.

- They were taken out of the water tank and cured in a curing room with a temperature of 20 ± 2 °C and a relative humidity of 90 % until they were tested.

batch	fibre type	fibre volume	number of test specimen	plain cubes tested at plate test day	fibre cubes tested at 7, 28 and plate test day	com. cylinder	splitting cylinder
1	65-35	1 %	8	3	9	3	3
2	65-35	1 %	8	3	6		
3	45-35	1 %	8	3	9	3	3
4	45-35	1 %	8	3	6		
5	45-50	1 %	8	3	9	3	3
6	45-50	1 %	8	3	6		
7	45-50	2 %	8	3	9	3	3
8	45-50	2 %	8	3	6		
9	plain	0 %	8	9	-	3	3
10	plain	0 %	8	9	-		
11	65-50	1 %	8	3	9	3	3
12	65-50	1 %	8	3	6		
13	65-50	2 %	8	3	9	3	3
14	65-50	2%	8	3	6		
15	45-35	2%	8	3	9	3	3
16	45-35	2%	8	3	6		
17	65-35	2%	8	3	9	3	3
18	65-35	2%	8	3	6		
19	65-35	0.5 %	8	3	9	3	3
20	65-35	0.5 %	8	3	6		
21	45-50	0.5 %	8	3	9	3	3
22	45-50	0.5 %	8	3	6		
23	45-35	0.5 %	8	3	9	3	3
24	45-35	0.5 %	8	3	6		
25	45-50	1.5 %	8	3	9	3	3
26	45-50	1.5 %	8	3	6		
27	65-50	0.5 %	8	3	9	3	3

batch	fibre type	fibre volume	number of test specimen	plain cubes tested at plate test day	fibre cubes tested at 7, 28 and plate test day	com. cylinder	splitting cylinder
28	65-50	0.5 %	8	3	6		
29	65-50	1.5 %	8	3	9	3	3
30	65-50	1.5 %	8	3	6		
31	45-35	1.5 %	8	3	9	3	3
32	45-35	1.5 %	8	3	6		
33	65-35	1.5 %	8	3	9	3	3
34	65-35	1.5 %	8	3	6		

Table 4 Number of specimens and the related reference cubes and cylinders for compression-compression test series

batch	fibre type	fibre volume	number of test specimen	plain cubes tested at 28 and plate test day	fibre cubes tested at 7, 28 and plate test day	com. cylinder	splitting cylinder
1	45-35	1 %	6	6	9	3	3
2	45-35	1 %	6	6	9	3	3
3	45-35	1 %	6	6	9	3	3
4	Plain	0 %	6	9	-	3	3
5	Plain	0 %	6	9	-	3	3
6	Plain	0 %	6	9	-	3	3
7	45-50	1 %	6	6	9	3	3
8	45-50	1 %	6	6	9	3	3
9	65-35	1 %	6	6	9	3	3
10	65-35	1 %	6	6	9	3	3

batch	fibre type	fibre volume	number of test specimen	plain cubes tested at 28 and plate test day	fibre cubes tested at 7, 28 and plate test day	com. cylinder	splitting cylinder
11	65-60	1 %	6	6	9	3	3
12	65-60	1 %	6	6	9	3	3
13	45-35	2 %	6	6	9	3	3
14	45-35	2 %	6	6	9	3	3
15	45-50	2 %	6	6	9	3	3
16	45-50	2 %	6	6	9	3	3
17	65-35	2 %	6	6	9	3	3
18	65-35	2 %	6	6	9	3	3
19	65-60	2 %	6	6	9	3	3
20	65-60	2 %	6	6	9	3	3

Table 5 Number of specimens and the related reference cubes and cylinders for compression-tension test series

3.5. Steel fibres

Hook-ended round steel fibres DRAMIX from the Belgium producer N.V. Bekaert S.T. were used. These came in 20 kg bags and were randomly added to the mix design after having been weighed in accordance with the volume percentage of the fibre concrete. A diagram of the used fibre can be seen in the Literature Review in Figure 2.1.

Four fibre types were tested in this study, named 45-35, 65-35, 45-50 and 65-50(60). The first number indicates the aspect ratio, the fibre length divided by the fibre diameter. The second number represents the fibre length. The fibre length of the fibre type 65-50 changed for the compression-tension tests from

50 to 60 mm because the fibre producer changed their product line whilst this test program was going on. The fibres were cold drawn and made of bright low carbon steel with a minimum tensile strength of 1100 N/mm^2.

The fibre volume content of each mix was calculated using the density of steel and is expressed as a percentage. The density of steel fibres was established to be 8255 kg/m^3. This means that 82.55 kg fibres are needed to produce 1 m^3 of steel fibre reinforced concrete with a fibre volume content V_f = 1%.

3.6. Test procedure

Before the specimens were tested in the biaxial test machine they were prepared as follows. First the edges of each specimen were smoothed with an electrical grinder and furthermore with a grindstone by hand to cut off the ridge and to ensure a plane surface between the concrete of the specimens and the steel surface of the machine platen system. The specimens were weighed and the thicknesses were measured with a mechanical sliding calliper.

For the compression-compression test series five out of every second batch of eight specimens were chosen and from the compression-tension series four out of every batch of six specimens were chosen. The surfaces of these specimens were specially prepared for attaching electrical strain gauges on top and bottom. Therefore the middle area of the specimens were first ground and then polished with the same electrical grinder as used before for smoothening the edges. The surfaces were cleaned, neutralised and dried before they were coated with super glue to make them smooth and usable for gluing the strain gauges on. After the strain gauges were attached together with their strain gauge base and the wires were soldered they were sealed with Araldite to prevent water and dust damaging the gauges and the wire connection.

3.6.1. Compression-Compression specimens

Before a compression-compression specimen was lifted into the machine by hand the four front actuator heads with the solid steel block platens were levelled with the front actuator head screws by using a level instrument. While one person held the specimen in the right position between the loading platen another person controlled the actuator movement from the control panel by position control. The person holding the specimen had to make sure that the height of the specimen was exactly in the centre between the loading platens. It was essential that the top and bottom of the specimen was equally loaded and the loading platens was plane to the surface of the specimen.

When one axis was touching the specimen with a load less than 5 kN the specimen was held between the loading platens by friction and the movements of the first axis were switched to hold. Then the other axis was brought inwards until this axis was touching the specimen on both sides. The first axis was opened again to allow adjustments and to find the new centre line again. This procedure of closing and opening the two axes in turn was repeated until the specimen was both centred and all loading platens were just touching the surface of the specimen with a small load.

Both control panels were switched to constant position control of a ramp generator and the travelling speed of the actuator were set. The test was started and after the specimen was loaded with more than 10 kN in one axis all front actuator head screws were loosened to allow the actuator heads a two dimensional freedom to apply the load onto the specimen in both axis. The Plexiglas shield was closed and the specimen was loaded until it failed.

3.6.2. Compression-Tension specimens

The six specimens of each test series were numbered beginning from the heaviest and thickest of the four gauged specimens with number 1 to number 4. Specimen number 5 was the heavier of the remaining two specimens with no gauges. The small variation in thickness and therefore in weight happened because of the production process. It was not possible to assure the same thickness with the tools provided and the problems in workability caused by the fibres. This variation in thickness had a maximum difference within one test series which was less than 3 mm.

This numbering system was chosen in respect of the test order. The heaviest of all specimens was suppose to resist the highest applied loads and was therefore tested under pure tension to generate a reference point for this test series. In respect of this tension load which was reached by the first specimen of each test series the rest of the test program was set. This means that the other specimens in this series were tested with predefined tension load applied before the compression load was applied.

Before tests could start the front actuator heads of both the tension and the compression actuators were aligned. The horizontal level of the front actuator heads were checked with a level instrument and adjusted accordingly with the front actuator head adjustment screws.

Both steel plates together with the bottom pin plates were screwed on with bolts to 14 M8 threaded rods sticking out of the two tension sides of the specimen. The bottom pin plates were already connected with two M20 screws each to the steel plates with the 14 M8 holes. This specimen assembly was lifted into the biaxial test rig by using an over head crane provided. The two top pin plates were attached with a further two M20 screws each to the steel plates after the specimen was in place within the machine. This procedure was necessary because the limited space within the machine rig and the limited travel distance of the actuator pistons.

The rough surface of the specimens caused by the casting direction was up side down for all tests. This was necessary to have the smooth and plane surface of the specimen now as top surface to put on the level instrument and to adjust the height and the position of the specimen. To find the exact position of the specimen within the test machine it also helped to find some orientation at the gaps between the back of the pin plates and the front of the tension actuator heads as an adjustment in the vertical axis. If necessary the actuator heads were moved and aligned into one axis.

To adjust the horizontal axis the front adjustment screws at the actuator heads were used to bring the specimen into a horizontal position which was checked with the level instrument. Figure 3.33 shows details of the tension module and the different parts of the connection mechanism between specimen and machine.

The specimens with electrical strain gauges were initialised and set to zero. The tension pistons were moved together until they were close enough to put in the pins of the tension module on both sides. The specimen was then connected to the machine and all actuator movements if any had to be watched very carefully because the smallest movements with the actuators in tension would cause damage to the specimen.

The alignment and the horizontal level of the specimen was checked again and adjusted accordingly with the front actuator head screws before a tension load of 20 kN was applied. This preload was necessary to control the electrical strain gauge readings. In case they were uneven for their top and bottom readings adjustments were necessary with the front actuator head screws and the M20 screws connecting the front steel plates and the top and bottom pin plates. With the readings of the electrical strain gauges it was possible to eliminate any moments and uneven stress distribution within the specimen caused by uneven connection forces between top and bottom and misalignment of the specimen. For specimens without electrical strain gauges the procedure described above

was not possible. For such cases equally good results were observed with the experience gained from the tests before.

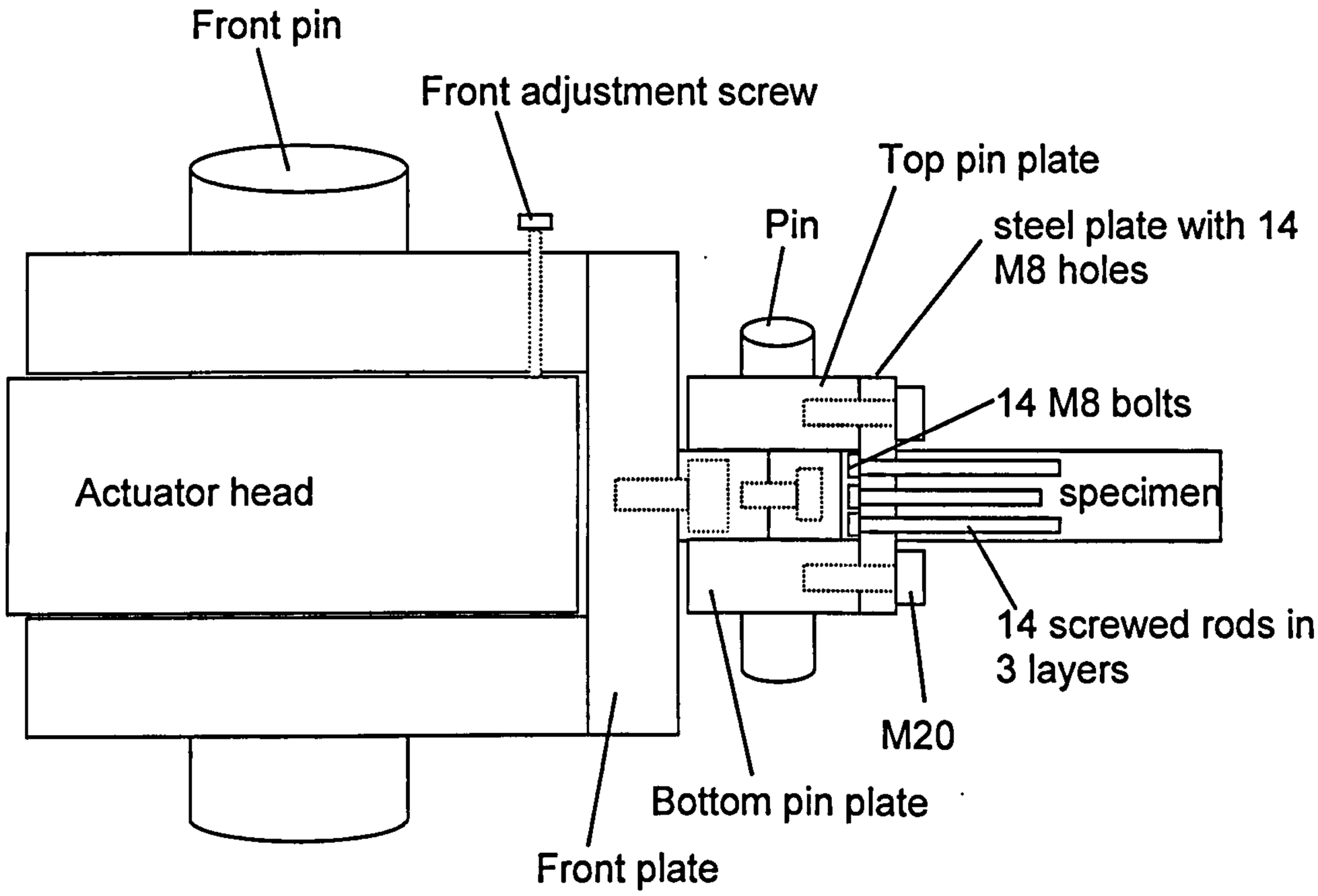

Figure 3.33 Connection between concrete specimen and machine when tension load is involved (tension module)

For the case of uniaxial tension tests without the compression force the tension load of 20 kN was reduced back to zero before the test was started and recorded under displacement control of the tension actuators.

For compression-tension tests the compression actuators were moved inwards. First they were moved together until one of the steel block platens almost touched the specimen. Then they were individually controlled starting with the actuator with the load cell attached to the piston. When a small load was observed and the steel block platen touched the surface of the specimen, the actuator movement was stopped.

A sheet of paper was used to check if the steel block was continuously aligned over the specimen plane. The paper was put between the steel block and the

specimen. For the case where the paper was able to be put in partly the actuator had to be moved backwards and the specimen and actuator head had to be aligned accordingly. The same procedure was carried out until the alignment was sufficient and the paper could not be put between the specimen and the machine platens anymore.

The same procedure was carried out with the other compression actuator until both compression steel blocks were touching the specimen plane under a very small load of less than 1 kN. This procedure was carried out very carefully because any higher load by one of the two actuators in the compression axis would result in the failure of the specimen due to bending moment effects caused by the unequal loading.

Both compression actuators were opened together for about one mm after their centre line was found by the procedure described before. The specimen was then loaded under pure tension load to the value which was defined before as a fraction of the pure tension test of the same test series. Therefore it was possible to find different stress ratios which can be compared between the different test series with the different fibre variables. The tension load was increased either by hand control at the control panel under load control or it was increased by using the ramp generator.

The ramp generator was used in such cases when the failure point of the compression-tension biaxial test was expected to be close to the failure point of the uniaxial tension failure point. By using the ramp generator it was possible to be more accurate in increasing the load.

When the intended tension load was reached the displacement limit of the actuator was set to a value where the machine would not damage itself and would stop moving the specimen apart when it failed. The tension axis was then switched to constant load control. The machine was now holding this tension load by moving the two tension actuator apart from each other if necessary until the actuators reached their displacement limits which were set before.

At the start, the compression actuators were moved together with a constant speed of $1.25x10^{-3}$ $^{mm}/_{sec}$. The gap between the specimen and the compression steel block platen was constantly watched and controlled with a sheet of paper.

When the compression load reached a load of 10 kN, the front actuator head screws on all four actuators were loosened. This ensures for every actuator head a two dimensional freedom to apply the load onto the specimen.

The test was carried out until the specimen failed. Most of the specimens failed under an explosive compression failure even with a high tension load close to the maximum tension capacity of the specimen. This indicates the dominant effect of the compression axis.

Note that one of the original motivation for this project of including steel fibres into HPC was to improve ductility and hence to examine post-peak behaviour. With the used test equipment this was not possible when high compression loads were involved. The reason for that is that the closed loop acquisition system was not quick enough to adjust the applied load to the new circumstances after the peak strength of the material was reached. Even though the specimens were tested under displacement control the load was applied by the oil pressure controlled actuators and therefore the actuators were under load control. In the situation where the peak load is reached the oil pressure would have to be reduced in the very same moment to adjust for the new pressure which is required for the next incremental displacement. To overcome the problem of the required response time of the oil pressure system the whole load application system could be changed to a system where the load is applied through threaded rods. In such a case it would be possible to test the specimens under real displacement control.

Another concern which was discovered during the use of the test machine was that the energy which is stored in the main steel members during a test is being released at the moment when the peak strength of the material was reached.

Therefore it would make sense to increase the stiffness of the test rig by increasing the size of the main steel members.

3.7. References

ASTM, 1979, 'Standard Test Method for Flexural Strength of Concrete (Using Simple Beam with Center-Point Loading)', ASTM Designation C 78-79

ASTM, 1984, 'Standard Test Method for Flexural Strength of Concrete (Using Simple Beam with Third-Point Loading)', ASTM Designation C 78-84

British Standards Institution, 1983, 'Testing concrete - Method for determination of tensile splitting strength', BS 1881, Part 117, 1983, London, BSI.

British Standards Institution, 1983, 'Testing concrete - Method for determination of flexural strength', BS 1881, Part 118, 1983, London, BSI.

RILEM, 1985, 'RILEM Draft Recommendation, 50-FMC Committee Fracture Mechanics of Concrete, Determination of the fracture energy of mortar and concrete by means of three-point bend tests on notched beams'.

RILEM, 2000, 'RILEM Recommendations for TC 162-TDF: Test and design methods for steel fibre reinforced concrete, Bending Test.

The Japan Society of Civil Engineering, 1984, 'JSCE-SF 4: Methods of tests for flexural strength and flexural toughness of steel fibre reinforced concrete'.

4. Strength Data - Test Results and Discussion

All experimental strength results and observations from the biaxial tests and their relevant control tests are reported and analysed in this chapter. Strength data and biaxial envelopes for the different fibre types and fibre volumes are presented. Standard test methods were carried out for additional information about the influence of the test parameters and are included here. These include cube strength, cylinder compressive strength, Poisson's ratio using cylinders and cylinder splitting tests.

4.1. Uniaxial strength

4.1.1. Cube tests

The concrete mix was designed for a cube strength f_{cu} of 100 N/mm^2 after 28 days. The plain concrete cubes from each test series are used as a control group to compare the ultimate strength of each mix with the different fibre and mix variables.

For the compression-compression series f_{cu} of the plain test series was 92 N/mm^2, 119 N/mm^2 and 140 N/mm^2 in average after 7, 28 and 330 days respectively. For the compressive-tension series the values are 97 N/mm^2, 115 N/mm^2 and 128 N/mm^2 after 7, 28 and 256 days. The values at 330 and 256 days represent the day when the biaxial test specimens of this series were tested.

The cubes were made and tested in accordance with the British Standards, Part 108 and 116 (1983). They were tested in a Dension Mayes 7229 3000 kN

compression test machine which complies with the British Standards, Part 115 (1986) and which is located in the same laboratory as the biaxial test machine. The cubes and cylinders were stored in the same way as the appropriate biaxial test specimens according to British Standards, Part 111 (1983). A set of three plain and three fibre cubes of each mix were tested the same day as the biaxial tests.

In addition fibre cubes were also tested at 7 and 28 days for the compression-compression and the compression-tension test series. For the compression-tension series, another set of three plain cubes were also tested at 28 days to generate information about the strength development over time. Table 6 provides the uniaxial compressive cube strength data for different ages of the compression-compression test series for the plain and fibre cubes of each mix. The corresponding values for the compression-tension series is shown in Table 7. Each value represents the average of three tested cubes.

The statistical details of the tested cubes for each batch indicate a small standard deviation for plain and fibre cubes. The full details can be seen in Table 20 and Table 21 in the Appendix where all tested cubes are listed together with the standard deviation and the relative error in %. The numbers in red indicate a higher standard deviation where the relative error is higher than 5 %. This percentage was chosen as a sensible value below which it can be assumed to be a reliable test result to testify the strength of this test series.

All plain cubes exhibited a dramatic failure. Even those tested at 7 days behaved in a similar manner because of the early high strength of the mix. Cracks developed through the concrete matrix as well as the crushed aggregates and performed a double cone shape failure.

The fibre cubes achieved in most cases a marginal higher strength than the plain control cubes of the same batch and after the maximum strength were still recognisable as cubes because the fibres were holding them together. However they were no longer able to take higher load.

Figure 4.1 summarises the values of Table 6 and shows f_{cu} over time of each batch for the compression-compression test series. The uniaxial plain and fibre cube strengths of the compression-tension test series which are given in Table 7 are presented in Figure 4.2. This shows the large variation between the test series in terms of f_{cu} for a standardised test method. Even the plain cubes of different batches vary a lot, for example between 92.9 N/mm^2 and 124.8 N/mm^2 for the 28 day strength. Therefore for further analyses the results obtained for each test was adjusted to the corresponding f_{cu} of the plain cubes of each batch in relation to the plain test series. This procedure will generate information about the influence of the different fibre variables such as fibre type and fibre volume and would not take the compressive concrete strength into account which would be a further variable. The difference in each individual concrete mix and the associated strength variation can be caused by unpredictable small changes of the mixes depending on the day to day performance of the technician, the influence of weather or the small variations in the material quality or storing conditions.

It should be noted that the graphs in Figure 4.1 and Figure 4.2 are developed from only two or three test points depending which batch was observed and how many cubs were cast and available for testing. Therefore the development of strength over time is only to be taken as a rough trend. The graphs indicate after the first few days an almost linear strength increase over time which is normally not the case. Normally the graph would indicate a maximum strength which could be reached after a certain amount of time and thereafter no increase in strength anymore. However the limited amount of test data of only two or three points over time creates these graphs and they should be seen only to indicate a trend and to show the difference between each batch.

Fibre Volume and Type	Batch No	Compressive cube strength f_{cu} fibre			plain	Test day
		7 days	28 days	test day	test day	
		N/mm^2	N/mm^2	N/mm^2	N/mm^2	days
Plain	9	92.3	117.0	140.1		325
	10	91.3	120.9	139.6		324
0.5% 45-30	23	82.2	103.7	121.9	122.9	248
	24		105.6	122.6	125.9	321
0.5% 45-50	21	86.2	108.7	127.0	131.6	262
	22		111.9	130.5	126.3	330
0.5% 65-35	19	87.9	114.8	138.0	132.0	269
	20		114.3	133.7	131.6	337
0.5% 65-60	27	78.6	106.5	123.5	129.6	233
	28		99.2	120.0	120.1	306
1% 45-35	3	93.8	118.7	133.9	136.4	194
	4	97.1		138.9	132.6	190
1% 45-50	5	90.6	118.9	135.9	128.7	318
	6		114.7	133.7	128.8	316
1% 65-35	1	96.0	125.3	138.6	133.9	183
	2		120.3	134.4	140.3	182
1% 65-60	11	97.5	123.7	138.1	130.6	281
	12		115.9	130.8	129.5	280
1.5% 45-30	31	89.2	111.8	127.1	123.9	220
	32		102.0	119.4	114.0	293
1.5% 45-50	25	85.5	105.2	121.6	123.7	241
	26		109.0	125.7	127.7	314
1.5% 65-35	33	81.4	105.1	117.5	116.7	213
	34		102.3	115.6	116.7	285
1.5% 65-60	29	81.5	106.6	122.4	119.0	227
	30		99.1	115.2	118.2	300
2% 45-30	15	93.5	122.9	146.5	136.2	268
	16		116.4	136.7	126.5	267
2% 45-50	7	96.6	112.3	135.1	131.6	315
	8		115.4	132.8	131.4	314
2% 65-35	17	90.2	118.8	142.9	131.9	261
	18		115.8	138.7	125.4	260
2% 65-60	13	99.3	122.2	141.1	135.0	274
	14		112.1	123.9	125.1	273

Table 6 Uniaxial compressive strength f_{cu} for different batches of the compression-compression test series at different ages for 100 mm plain and fibre cubes

Fibre Volume and Type	Batch No	Compressive cube strength f_{cu} fibre			plain		Test day
		7 days	28 days	test day	28 days	test day	
		N/mm^2	N/mm^2	N/mm^2	N/mm^2	N/mm^2	days
Plain	4	98.2	113.8	128.0			255
	5	95.0	113.6	128.8			263
	6	97.6	117.3	127.2			252
1% 45-35	1	97.2	113.1	128.1	103.3	122.6	265
	2	87.8	106.3	125.4	99.5	111.1	258
	3	81.5	100.9	112.2	92.9	117.6	260
1% 45-50	7	104.0	121.9	139.8	101.4	136.6	281
	8	108.1	126.8	141.1	124.8	138.8	285
1% 65-35	9	94.1	119.5	132.3	122.3	127.9	285
	10	101.3	123.7	135.0	119.8	130.2	288
1% 65-60	11	86.7	108.4	120.1	110.3	124.0	307
	12	103.5	123.8	137.5	119.2	132.7	303
2% 45-35	13	106.7	124.6	139.8	112.9	131.9	306
	14	105.2	127.0	135.7	115.5	130.8	288
2% 45-50	15	99.87	122.3	135.8	115.2	123.3	287
	16	100.0	119.7	134.3	112.1	123.5	286
2% 65-35	17	106.9	131.7	146.1	111.7	134.5	281
	18	107.3	132.2	147.1	121.2	139.1	280
2% 65-60	19	102.3	127.6	135.3	113.0	124.2	275
	20	94.4	115.1	127.9	105.4	117.1	273

Table 7 Uniaxial compressive strength f_{cu} for different batches of the compression-tension test series at different ages for 100 mm plain and fibre cubes

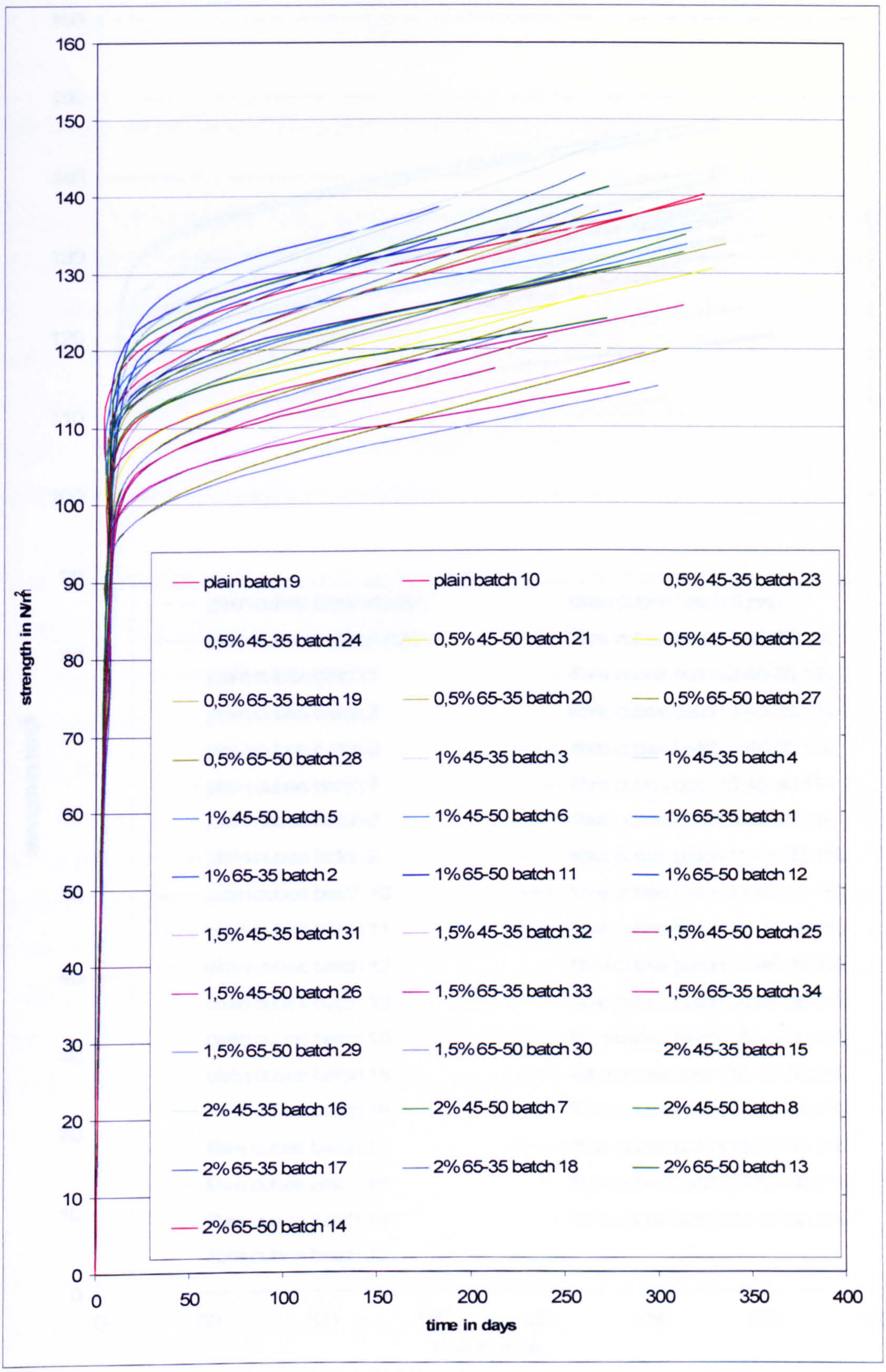

Figure 4.1 Strength development of fibre cubes over time for the compression-compression test series

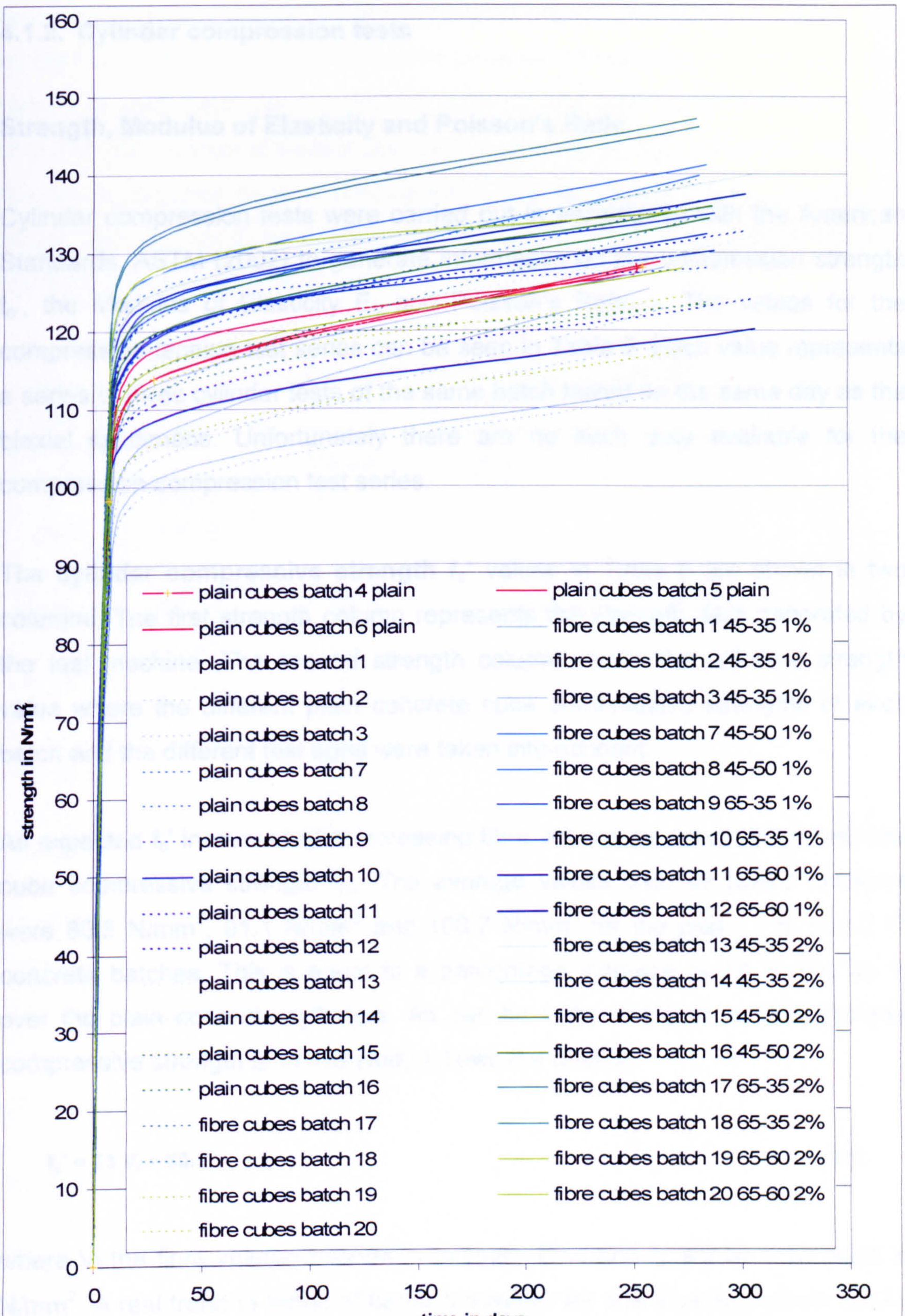

Figure 4.2 Strength development of plain and fibre cubes over time for the compression-tension test series

4.1.2. Cylinder compression tests

Strength, Modulus of Elasticity and Poisson's Ratio

Cylinder compression tests were carried out in accordance with the American Standards, ASTM (2002) to generate information on the compression strength f_c', the Modulus of Elasticity E_c and Poisson's Ratio ν. The values for the compression-tension test series can be seen in Table 8. Each value represents a series of three cylinder tests of the same batch tested on the same day as the biaxial specimens. Unfortunately there are no such data available for the compression-compression test series.

The **cylinder compressive strength f_c'** values in Table 8 are shown in two columns. The first strength column represents the strength data generated by the test machine. The second strength column shows the adjusted strength value where the different plain concrete cube compressive strengths of each batch and the different test ages were taken into account.

As expected f_c' increases with increasing fibre volume as noted before with the cube compressive strength f_{cu}. The average values over all tested cylinders were 80.5 N/mm^2, 91.1 N/mm^2 and 106.7 N/mm^2 for the plain, 1 % and 2 % concrete batches. This is equal to a percentage increase of 13 % and 33 % over the plain concrete cylinders. As can be seen in Figure 4.3 the cylinder compressive strength f_c' in this study follows the relation

$$f_c' = 13\ V_f + 80.5 \qquad (4.1)$$

where V_f the fibre volume fraction in % represents and f_c' will be expressed in N/mm^2. A real trend in terms of better behaviour for one fibre type could not be observed within the different fibre volumes.

Note that the trend shown above only expresses the mathematical relation of a straight line as best fit over all tested cylinders for different V_f. The statistical details of each batch can be seen in Table 22 and Table 23 in the Appendix 2 and indicate a higher standard deviation in average as the cube tests. Some of the tested batches have a relative error between 5 and 10 %. Therefore a health warning has to be expressed towards the use of these results and also the further investigation of E_c and ν.

Fibre volume and type	Batch No	Cylinder compressive strength f_c' in N/mm² actual Value	Cylinder compressive strength f_c' in N/mm² normalised to plain cubes	Modulus of Elasticity E_c in N/mm²	Poisson's Ratio ν
plain	4 C-T	83.6	83.6	41347	0.24
	5 C-T	77.7	77.7	38823	0.25
	6 C-T	80.4	80.4	45777	0.27
average	**Plain**	**= 80.5**	**= 80.5**	**= 41982**	**= 0.25**
1% 45-35	1 C-T	76.0	79.3	41560	0.24
	2 C-T	88.2	101.6	39189	0.26
	3 C-T	80.1	87.2	37059	0.22
1% 45-50	7 C-T	98.2	92.0	36301	0.21
	8 C-T	89.0	82.1	33481	0.19
1% 65-35	9 C-T	101.3	101.4	35147	0.24
	10 C-T	92.1	90.6	35071	0.22
1% 65-60	11 C-T	88.6	91.5	38845	0.27
	12 C-T	98.1	94.6	42744	0.24
average	**1 %**	**= 90.2**	**= 91.1**	**= 37711**	**= 0.22**
2% 45-35	13 C-T	104.8	101.7	42748	0.18
	14 C-T	107.0	104.7	45723	0.22
2% 45-50	15 C-T	103.8	107.8	43922	0.22
	16 C-T	104.7	108.4	43949	0.23
2% 65-35	17 C-T	111.2	105.8	43990	0.20
	18 C-T	119.7	110.2	46514	0.20
2% 65-60	19 C-T	105.4	108.6	44174	0.22
	20 C-T	99.3	108.6	42533	0.26
average	**2 %**	**= 107.0**	**= 106.7**	**= 44194**	**= 0.21**

Table 8 Strength, Modulus of Elasticity and Poisson's Ratio determined from cylinder compression tests for compression-tension test series

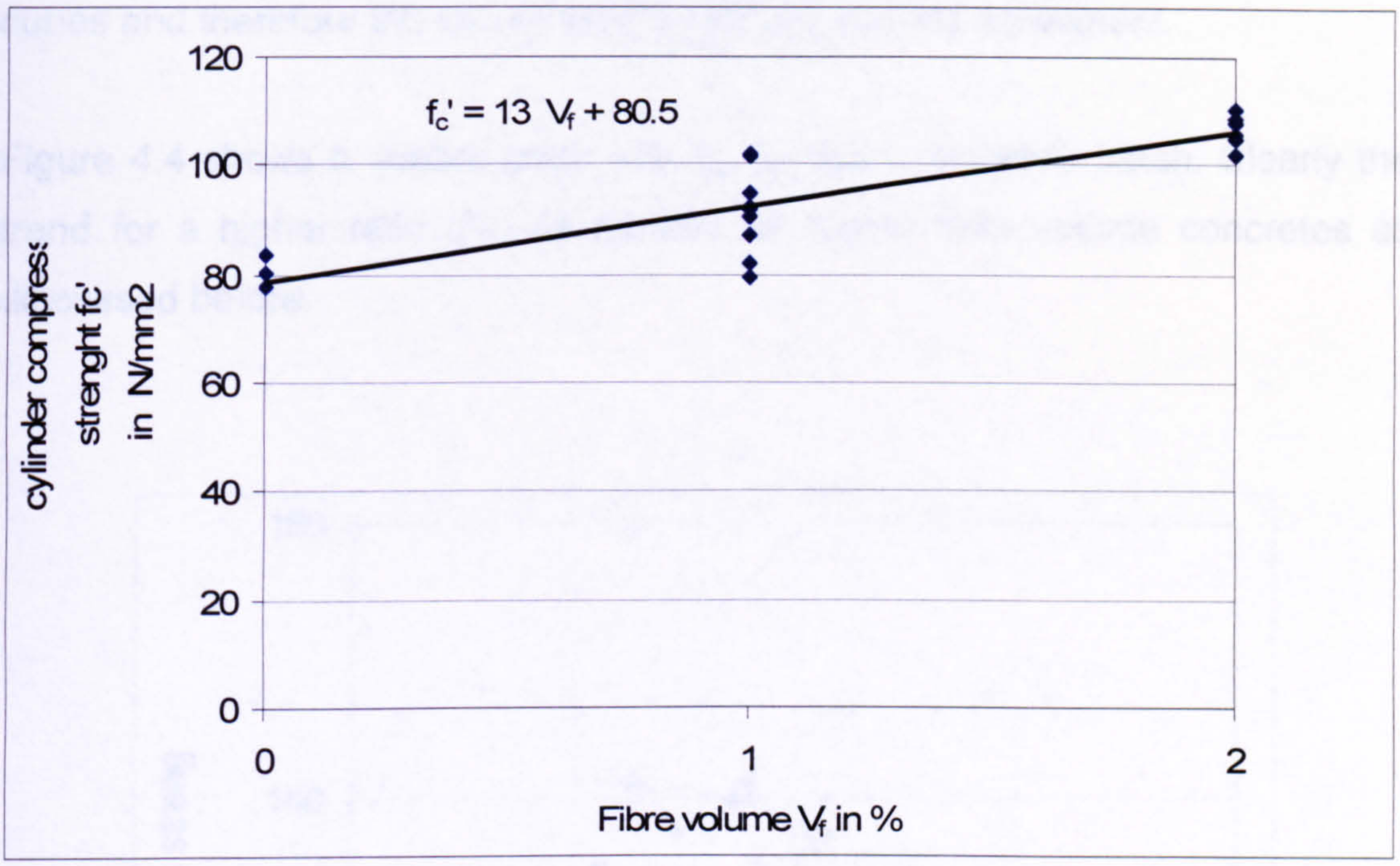

Figure 4.3 Relation between the cylinder compressive strength f_c' and the fibre volume fraction V_f

The cylinder compressive strength f_c' is lower than the uniaxial cube compressive strength f_{cu}. The ratio between them increases from 0.63 for the plain series to 0.70 for the 1 % and 0.78 for the 2 % fibre volume series. This increase is justified with the stronger increase of f_c' than f_{cu} for higher fibre volume fractions. f_{cu} increases only about 2 % and 8 % on average for the 1 % and 2 % fibre volume batches compared to the plain concrete; f_c' increases for 13 % and 33 % respectively as discussed before.

A typical f_c' / f_{cu} ratio for normal strength concrete given in the literature (British Standards, 1983) is 0.8 and 0.78 (lecture notes). Within a study of Hughes and Bahramia, (1965) it became obvious that the ratio between prisms and cubes may vary between 0.59 and 0.99. They found that the ratio depends on aggregate size, material type and mix proportion and therefore concrete strength and also on the restraining effect of the test machine platen on the specimen. Even so this results show the difference between prism and cube

strengths the results are also valid for the relationship between cylinders and cubes and therefore the value in this study are in good agreement.

Figure 4.4 shows a scatter gram with f_{cu} versus f_c' for each batch. Clearly the trend for a higher ratio can be noticed for higher fibre volume concretes as discussed before.

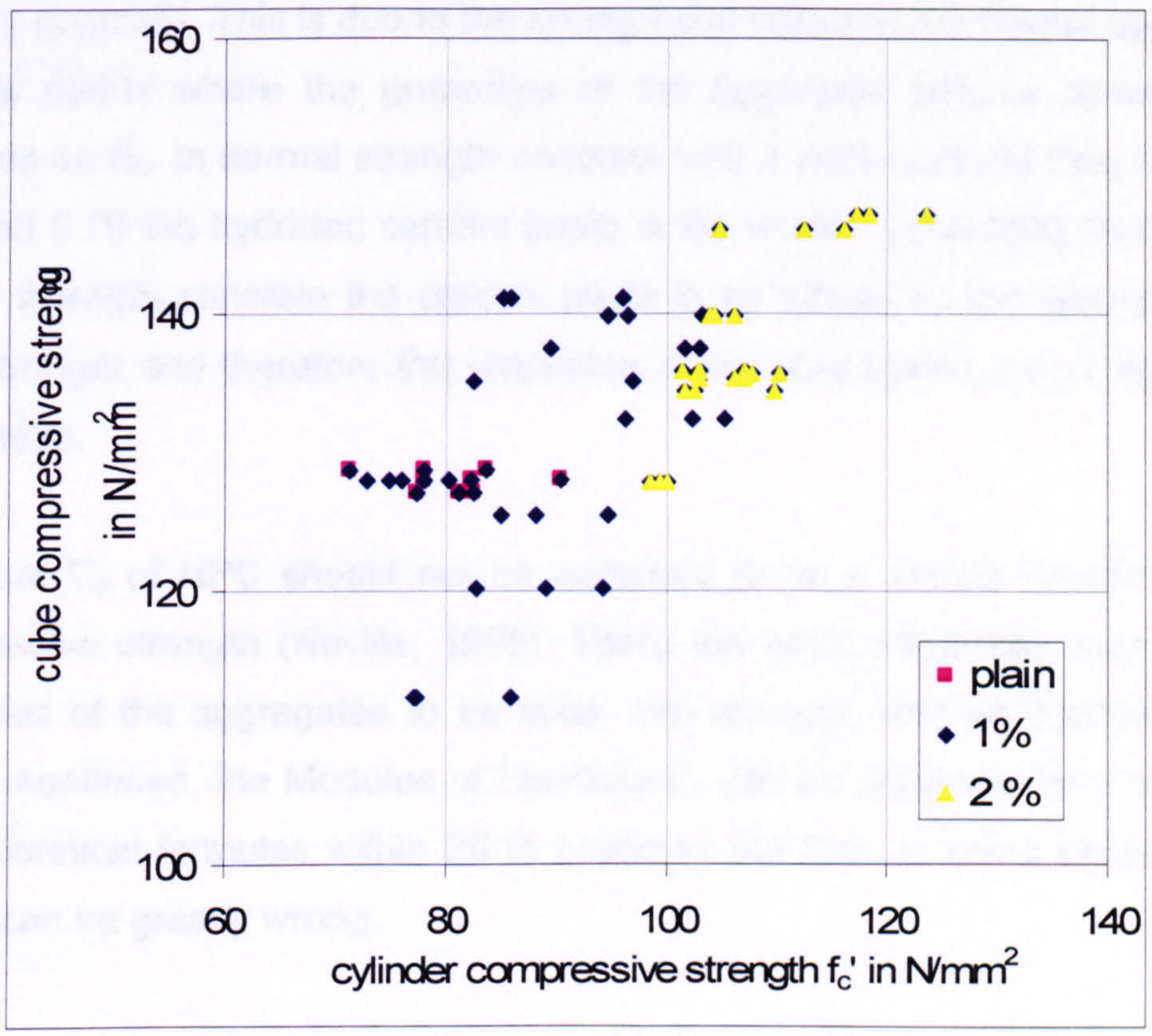

Figure 4.4 Relationship between cube compressive strength f_{cu} and cylinder compressive strength f_c'

The **Modulus of Elasticity E_c** shows a decrease in the average of plain to 1 % fibre cylinders and an increase in the 2 % batches with a variation from 33.5 kN/mm^2 to 46.5 kN/mm^2. Each test point expresses the average from three individual tests. Figure 4.5 shows the general trend for increasing E_c with increasing fibre volume fraction V_f. The large scatter and the increased standard

deviation of the cylinder compression tests where the Modulus of Elasticity was reported from makes it difficult to derive any general trend. A clear trend for any fibre type behaving different than the others in all fibre volumes can not be observed. The scatter for one fibre type within the same fibre volume was up to 17 % within two different batches.

According to Baalbaki et al. (1992) the relationship between the Modulus of Elasticity E_c and its compressive strength f_c' of HPC is less consistent than in ordinary concrete. This is due to the strong bond between the coarse aggregate and the matrix where the properties of the aggregate have a considerable influence on E_c. In normal strength concrete with a water/cement ratio between 0.40 and 0.70 the hydrated cement paste is the weaker controlling factor while in high strength concrete the cement paste is as strong as the aggregates or even stronger and therefore the properties of the aggregates are of significant importance.

Therefore E_c of HPC should not be assumed to be a simple function of the compressive strength (Neville, 1995). There are other influences such as the properties of the aggregates to be taken into account. And as Baalbaki et al. (1992) mentioned, the Modulus of Elasticity E_c can be predicted from empirical and theoretical formulas within 20 % precision but that, in some cases, these values can be greatly wrong.

This can be seen when E_c is plotted against f_c' over all tested specimens. The same scatter as above can be observed as shown in Figure 4.6. Because of the large scatter it is very difficult to make any statement of the relationship and to produce a mathematical expression of the two values to each other.

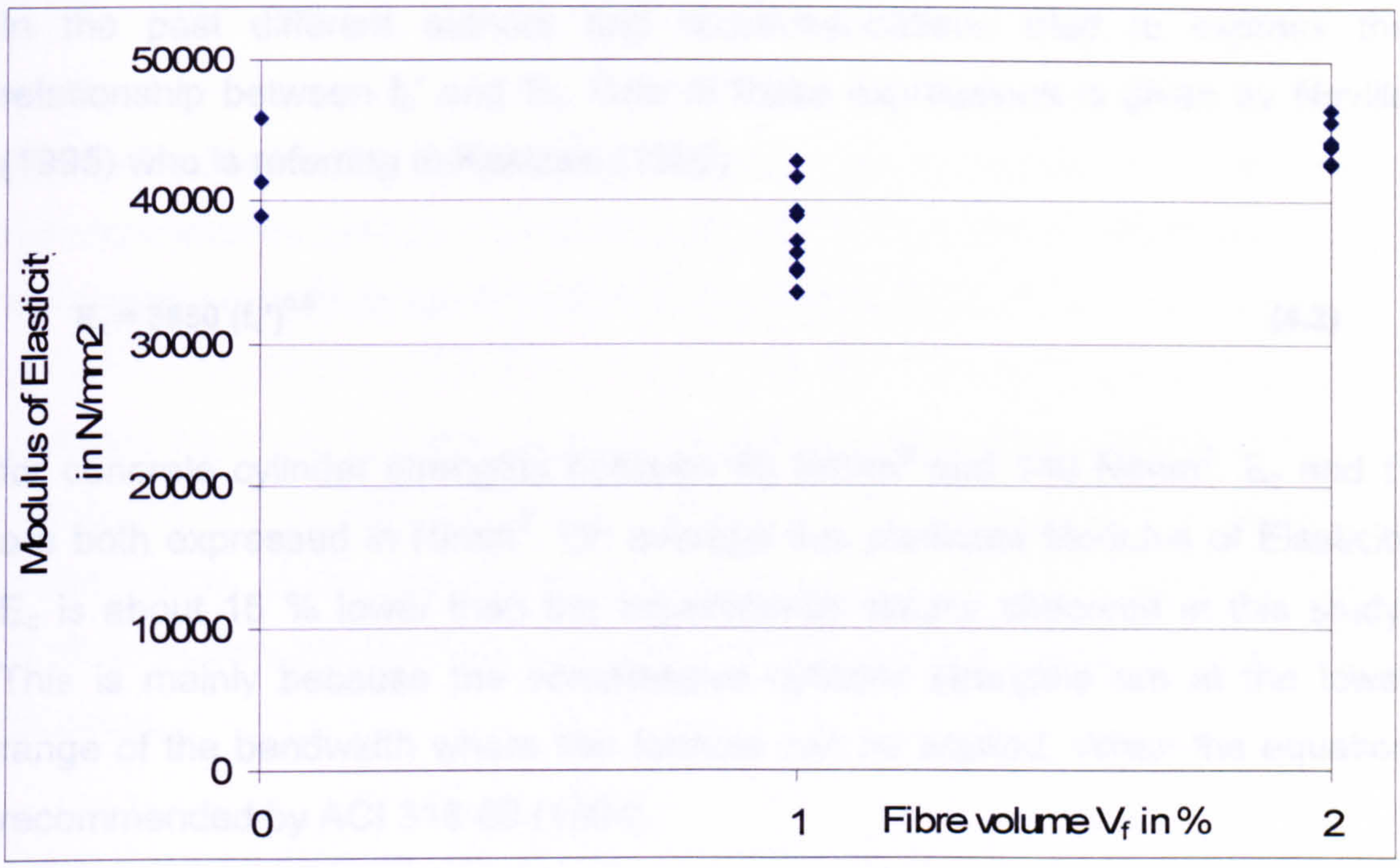

Figure 4.5 Modulus of Elasticity E_c versus fibre volume fraction V_f

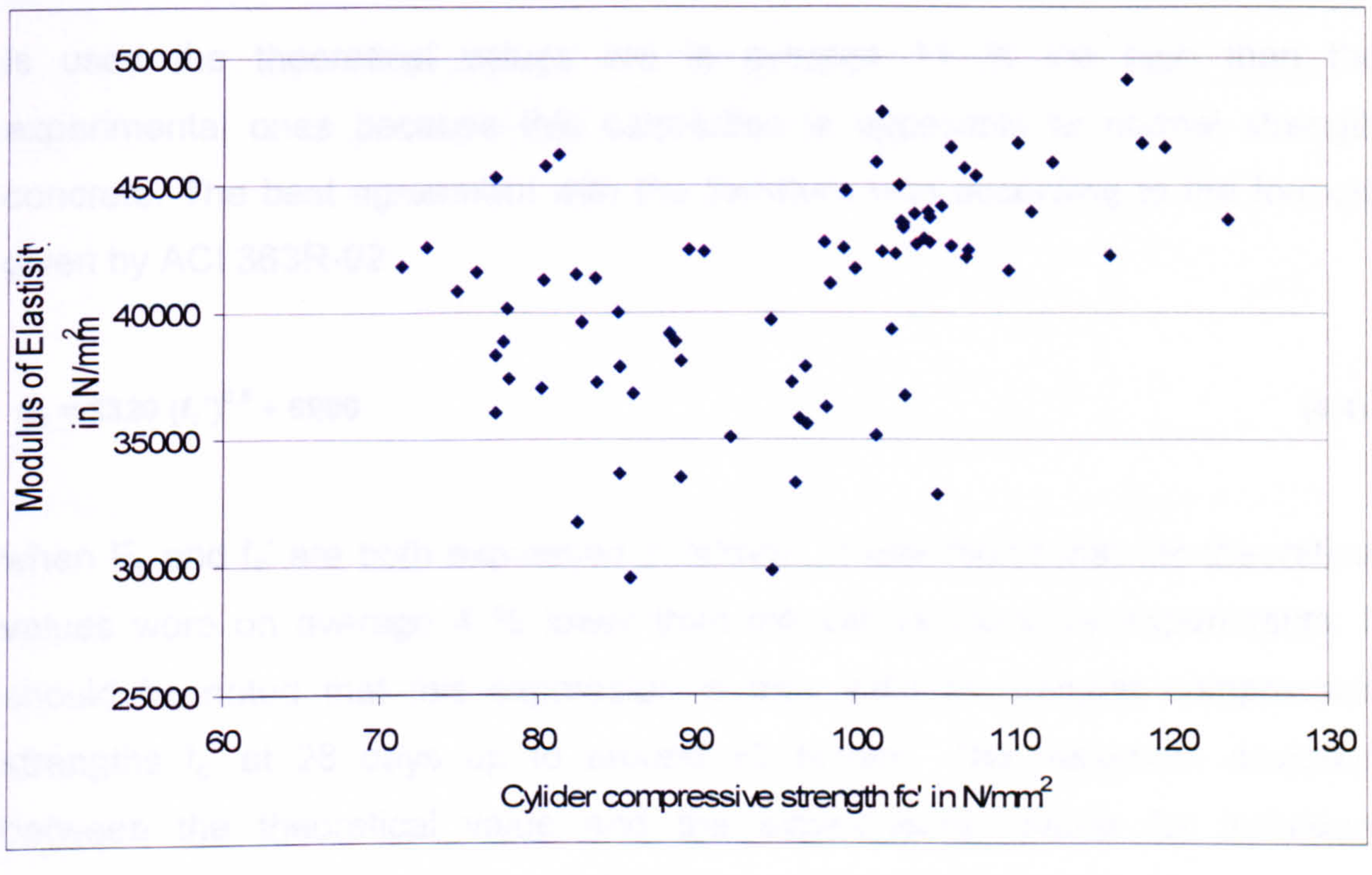

Figure 4.6 Modulus of Elasticity E_c versus cylinder compressive strength f_c'

In the past different authors and recommendations tried to express the relationship between f_c' and E_c. One of these expressions is given by Neville (1995) who is referring to Kakizaki (1992)

$$E_c = 3650\ (f_c')^{0.5} \qquad (4.2)$$

for concrete cylinder strengths between 80 N/mm^2 and 140 N/mm^2. E_c and f_c' are both expressed in N/mm^2. On average this predicted Modulus of Elasticity E_c is about 15 % lower than the experimental results observed in this study. This is mainly because the compressive cylinder strengths are at the lower range of the bandwidth where this formula can be applied. When the equation recommended by ACI 318-89 (1994)

$$E_c = 4730\ (f_c')^{0.5} \qquad (4.3)$$

is used the theoretical values are in average 11 % too high than the experimental ones because this calculation is applicable to normal strength concrete. The best agreement with the literature was according to the formula given by ACI 363R-92

$$E_c = 3320\ (f_c')^{0.5} + 6900. \qquad (4.4)$$

when E_c and f_c' are both expressed in N/mm^2. It was found that the theoretical values were on average 4 % lower than the values found by experiments. It should be noted that this expression is only valid for cylinder compressive strengths f_c' at 28 days up to around 80 N/mm^2. The maximum deviation between the theoretical value and the experimental results for individual cylinder tests were up to about 20 % higher or lower than the average.

Similar results can be observed when using the formula provided by the Euro code 2

$$E_c = 9500\,(f_c' + 8)^{1/3}. \qquad (4.5)$$

The theoretical values found by this equation are in average 7 % higher than the experimental values. The maximum difference between the predicted and the experimental Modulus of Elasticity E_c are also about 20 %.

It should be noted that the values of E_c and ν have a large scatter even within one batch and therefore it is very difficult to draw any general conclusion or interpretation. In general observed Modulus of Elasticity Ec is lower compared to other studies and the Poisson's ratio ν is higher which will be discussed in the following.

Table 8 shows also the data for the **Poisson's ratio** ν for each test series. The average Poisson's ratio decreases with increasing fibre volume from 0.25 to 0.22 and 0.21 for the plain, 1 % and 2 % fibre volume batches. This general trend was also reported by Gao et al. (1997) for steel fibre reinforced high strength, lightweight concrete. For this study the relationship between Poisson's ratio ν and fibre volume fraction V_f follows the equation

$$\nu_f = \nu_p\,(1 - 0.1\ V_f) \qquad (4.6)$$

where ν_f = Poisson's ratio of steel fibre reinforced high strength concrete, ν_p = Poisson's ratio of plain high strength concrete and V_f = fibre volume fraction in %. In this study ν_p was found to be on average 0.25. By using the above equation Poisson's ratio ν_f for SFHSC becomes 0.22 and 0.20 for 1 % and 2 % fibre volume concrete. This complies approximately with the experimental data shown as a red line in Figure 4.7 where the relation between f_c' and Poisson's ratio ν is shown. A similar graph is show in Figure 4.8 where the Poisson's ratio is plotted against V_f. This graph is represented by an equation of the form

$$\nu = -0.02\,V_f + 0.25. \qquad (4.7)$$

This equation also follows the trend found by Gao et al. (1997) that with increasing V_f the Poisson's ratio ν decreases.

There is no clear trend for any fibre type performing different than others in all fibre volume fractions. However the average over all fibre volume fractions for all fibre types shows that Poisson's ratio tend to decrease for increasing V_f.

As it is not easy to generate adequately accurate values with only a few tests there is only limited data available for normal strength concrete and even less for high-strength concrete. To generate a meaningful value there should be a fair amount of tests been carried out to produce information about the standard deviation of this value and to eliminate outliers.

In general it could be said that the data in this investigation complies with the literature of Aïtcin (1998) who is referring to Poisson's ratio values found by Ahmad and Shah (1985) between 0.18 and 0.24 and Kaplan (1959) between 0.23 and 0.32 for high strength concrete.

Similar values are reported by Rashid et al. (2002) who combined 153 data points collected from various existing literature. Based on these available data, Poisson's ratio of higher-strength concrete seems to be comparable to the expected range of values for lower strength concrete. Poisson's ratios found by the researchers mentioned in the above study vary between 0.15 and 0.25 with an average value of 0.2. The concrete strength ranged between $f_c' = 20$ to 120 N/mm^2 for the studies considered.

When the values for the Poisson's ratio found in this investigation are coupled with the graph produced by Rashid et al. (2002) it can be seen that they fit into the overall picture. This is shown in Figure 4.7. Together with Figure 4.8 it can be observed that there exists a huge scatter even within one batch with the same concrete mix and the same fibre variables. This scatter was already reported by Williamson G.R., 1974. This shows again how difficult it is to

generate a meaningful value of this kind of investigation and it is only possible to give a bandwidth for the Poisson's ratio results.

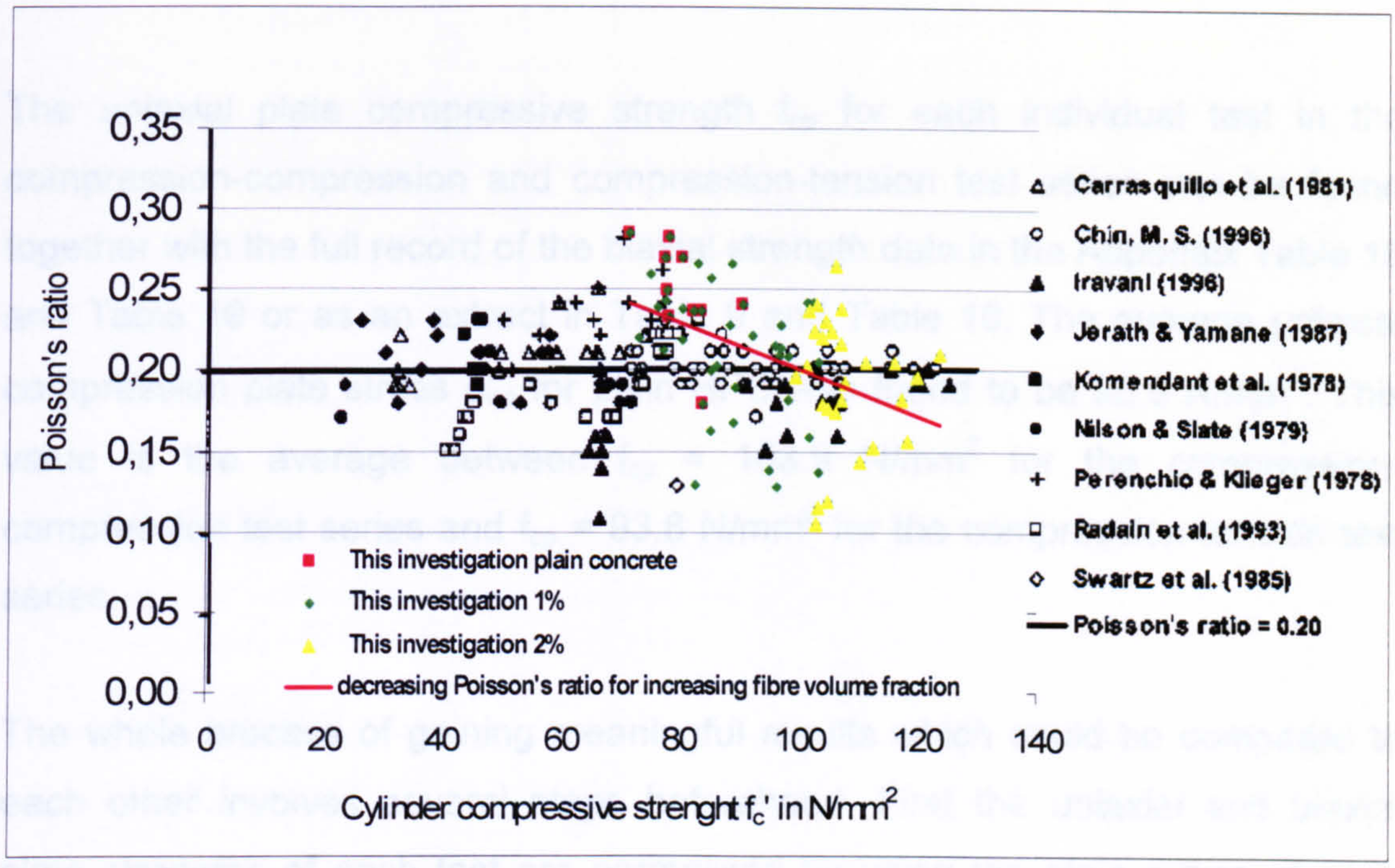

Figure 4.7 Poisson's ratio ν over cylinder compressive strength f_c' (Rashid et al., 2002 combined with own data from this study)

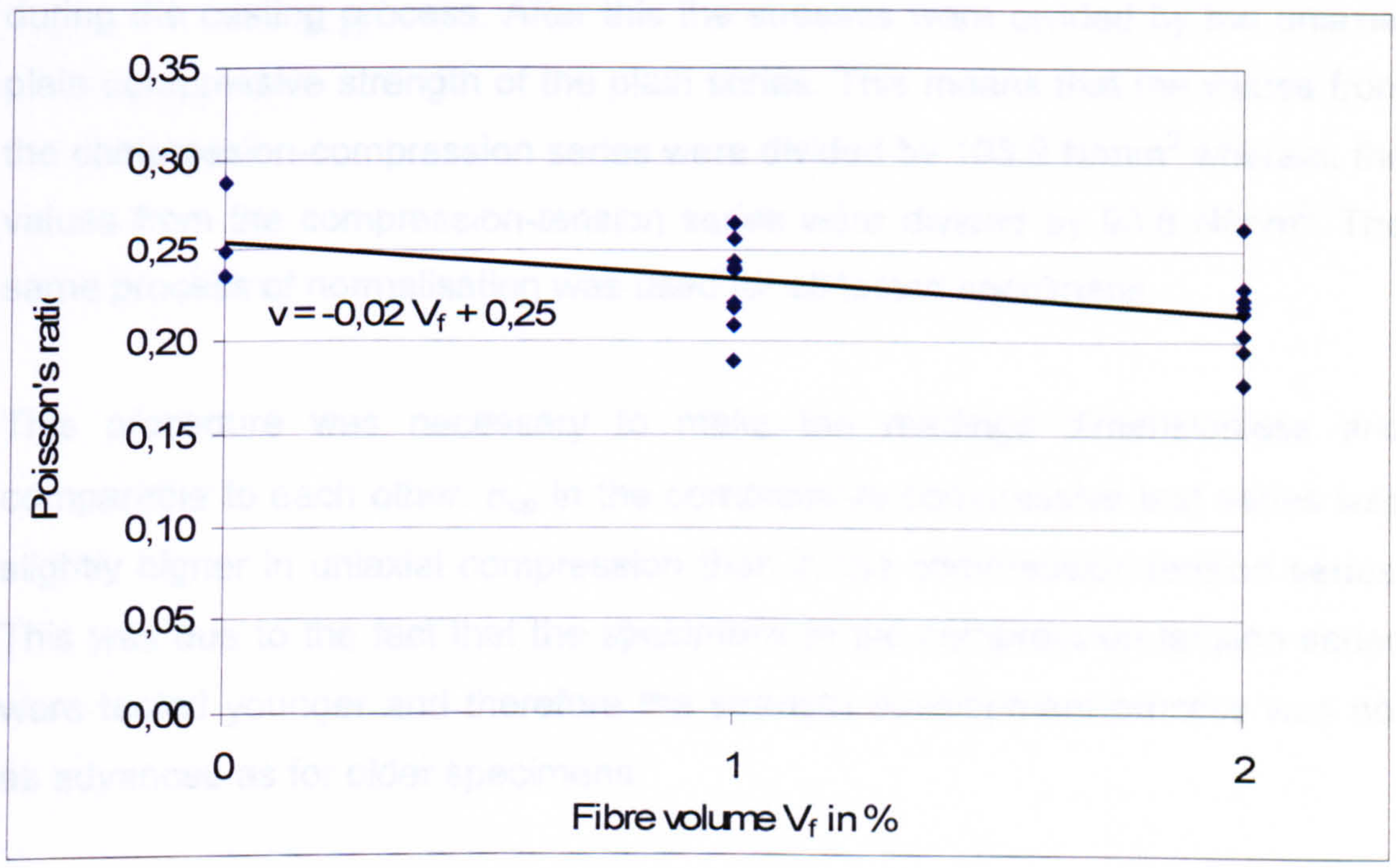

Figure 4.8 Poisson's ratio ν over the fibre volume fraction V_f

4.1.3. Uniaxial plate compressive strength

The uniaxial plate compressive strength f_{cp} for each individual test in the compression-compression and compression-tension test series can be found together with the full record of the biaxial strength data in the Appendix Table 18 and Table 19 or as an extract in Table 9 and Table 10. The average uniaxial compression plate stress σ_{cp} for plain HPC was found to be 98.9 N/mm^2. This value is the average between f_{cp} = 103.9 N/mm^2 for the compression-compression test series and f_{cp} = 93.8 N/mm^2 for the compression-tension test series.

The whole process of gaining meaningful results which could be compared to each other involves several steps beforehand. First the uniaxial and biaxial plate strengths of each test are normalised by using the plain cubes of each batch as explained earlier. Thereafter the recorded and normalised forces were divided by the width and the individual height of each specimen. This was necessary to take the difference in the thickness into account which occurred during the casting process. After this the stresses were divided by the uniaxial plain compressive strength of the plain series. This means that the values from the compression-compression series were divided by 103.9 N/mm^2 whereas the values from the compression-tension series were divided by 93.8 N/mm^2. The same process of normalisation was used for all tested specimens.

This procedure was necessary to make the readings dimensionless and comparable to each other. σ_{cp} in the compressive-compressive test series was slightly higher in uniaxial compression than in the compression-tension series. This was due to the fact that the specimens in the compression-tension series were tested younger and therefore the strength development process was not as advanced as for older specimens.

Fibre volume and type	Batch No	σ_2 N/mm^2	σ_3 N/mm^2	σ_2/σ_3	σ_2/σ_{fcp}	σ_3/σ_{fcp}
plain	9	0	-114,67	0	0	-1,104
	9	0	-80,19	0	0	-0,772
	10	0	-108,12	0	0	-1,041
	10	0	-99,75	0	0	-0,960
0.5% 45-35	23	0	-120,81	0	0	-1,163
	23	0	-120,87	0	0	-1,163
	24	0	-116,95	0	0	-1,126
	24	0	-118,19	0	0	-1,138
0.5% 45-50	21	0	-97,28	0	0	-0,936
	21	0	-96,60	0	0	-0,930
	22	0	-102,31	0	0	-0,985
	22	0	-97,03	0	0	-0,934
0.5% 65-35	19	0	-114,04	0	0	-1,098
	19	0	-122,62	0	0	-1,180
	20	0	-123,15	0	0	-1,185
	20	0	-117,38	0	0	-1,130
0.5% 65-60	27	0	-120,99	0	0	-1,164
	27	0	-103,02	0	0	-0,992
	28	0	-123,19	0	0	-1,186
	28	0	-115,09	0	0	-1,108
1% 45-35	3	0	-95,06	0	0	-0,915
	3	0	-73,94	0	0	-0,712
	4	0	-116,76	0	0	-1,124
	4	0	-103,82	0	0	-0,999
1% 45-50	5	0	-119,02	0	0	-1,146
	6	0	-111,65	0	0	-1,075
	6	0	-111,22	0	0	-1,070
1% 65-35	1	0	-101,62	0	0	-0,978
	1	0	-124,08	0	0	-1,194
	2	0	-108,55	0	0	-1,045
	2	0	-107,77	0	0	-1,037
1% 65-60	11	0	-121,27	0	0	-1,167
	11	0	-113,69	0	0	-1,094
	12	0	-119,86	0	0	-1,154
	12	0	-119,16	0	0	-1,147
1.5% 45-35	31	0	-112,14	0	0	-1,079
	31	0	-114,80	0	0	-1,105
	32	0	-117,00	0	0	-1,126
	32	0	-109,37	0	0	-1,053
1.5% 45-50	25	0	-94,67	0	0	-0,911
	25	0	-117,35	0	0	-1,129
	26	0	-117,00	0	0	-1,126
	26	0	-95,72	0	0	-0,921
1.5% 65-35	33	0	-120,02	0	0	-1,155
	33	0	-116,29	0	0	-1,119

Fibre volume and type	Batch No	σ_2 N/mm^2	σ_3 N/mm^2	σ_2/σ_3	σ_2/σ_{fcp}	σ_3/σ_{fcp}
	34	0	-116,49	0	0	-1,121
	34	0	-117,59	0	0	-1,132
1.5% 65-60	29	0	-113,36	0	0	-1,091
	29	0	-117,96	0	0	-1,135
	30	0	-105,85	0	0	-1,019
	30	0	-120,68	0	0	-1,162
2% 45-35	15	0	-117,56	0	0	-1,132
	15	0	-119,82	0	0	-1,153
	16	0	-138,52	0	0	-1,333
	16	0	-102,18	0	0	-0,983
2% 45-50	7	0	-105,78	0	0	-1,018
	7	0	-120,34	0	0	-1,158
	8	0	-114,42	0	0	-1,101
	8	0	-109,75	0	0	-1,056
2% 65-35	17	0	-123,23	0	0	-1,186
	17	0	-133,93	0	0	-1,289
	18	0	-125,96	0	0	-1,212
	18	0	-134,12	0	0	-1,291
2% 65-60	13	0	-106,89	0	0	-1,029
	13	0	-125,27	0	0	-1,206
	14	0	-118,54	0	0	-1,141
	14	0	-114,63	0	0	-1,103

Table 9 Uniaxial plate compressive strength f_{cp} of the compression-compression test series

Fibre volume and type	Batch No	σ_1 N/mm^2	σ_3 N/mm^2	σ_1/σ_3	σ_1/σ_{fcp}	σ_3/σ_{fcp}
plain	4	0	-93,11	0	0	-0,992
	5	0	-87,81	0	0	-0,936
	5	0	-100,35	0	0	-1,069
	6	0	-94,07	0	0	-1,003
1% 45-35	1	0	-104,98	0	0	-1,119
	2	0	-113,25	0	0	-1,207
	3	0	-104,44	0	0	-1,113
1% 45-50	7	0	-99,58	0	0	-1,061
	8	0	-96,53	0	0	-1,029
1% 65-35	9	0	-99,28	0	0	-1,058
	10	0	-102,03	0	0	-1,087
1% 65-60	11	0	-95,52	0	0	-1,018
	12	0	-106,80	0	0	-1,138
2% 45-35	13	0	-111,16	0	0	-1,185
	14	0	-123,12	0	0	-1,312

Fibre volume and type	Batch No	σ_1 N/mm^2	σ_3 N/mm^2	σ_1/σ_3	σ_1/σ_{fcp}	σ_3/σ_{fcp}
2% 45-50	15	0	-116,43	0	0	-1,241
	16	0	-124,12	0	0	-1,323
2% 65-35	17	0	-106,00	0	0	-1,130
	18	0	-103,76	0	0	-1,106
2% 65-60	19	0	-92,64	0	0	-0,987
	20	0	-105,82	0	0	-1,128

Table 10 Uniaxial plate compressive strength f_{cp} of the compression-tension test series

Comparing f_{cp} with the 100 mm cube strength f_{cu} and the cylinder strength f_c' it can be seen that

$$f_c' < f_{cp} < f_{cu(100)} \qquad (4.8)$$

with a ratio of 1 : 1.2 : 1.6 for plain HPC in the compression-tension series. This has to do with the apparent strength increase for shorter specimens when solid dry steel platens are used. The restraining effect has more influence on shorter specimens than on longer specimens. The length of the cylinders, plates and cubes are 300, 200 and 100 mm respectively.

The size influence is also expressed by a convention factor between $f_{cu(100)}$ and $f_{cu(200)}$ of 0.85 in the German standards. Therefore the relationship between f_c' and $f_{cu(200)}$ will change to 1 : 1.3 for cubes with 200 mm side length.

Van Mier (1986) stated that this size effect could be eliminated by using a brush type testing device. But such loading platens cannot be used in either the standard testing codes or in this study. In the standard codes it would raise the costs significantly and in this study it turned out not workable and practical enough.

In conclusion Figure 4.9 shows the relationship between all different uniaxial compressive strength measured with cubes f_{cu}, cylinders f_c' and plates f_{cp} for both test series over the increasing fibre volume. All specimens have increasing strength with increasing fibre volume fraction, with the compression-compression test series developing higher strength because of their older age.

Table 11 to Table 13 contain the full Modulus of Elasticity E_c and Poisson's' ratio ν results for the plate specimens in both test series. Compared with the results of the cylinder compressive tests it was found that the plates generated higher E_c and ν. Due to the different shape of the plate like specimens compared to the standardised cylinder specimens this values need to be considered very carefully when used for further investigations.

Comparing E_c and ν of uniaxial tension and uniaxial compression tested within the same batches of the compression-tension series it was recognised that the values for both material properties are slightly higher in uniaxial tension as can be seen in Table 13. This is in good agreement with Hussein, 1998.

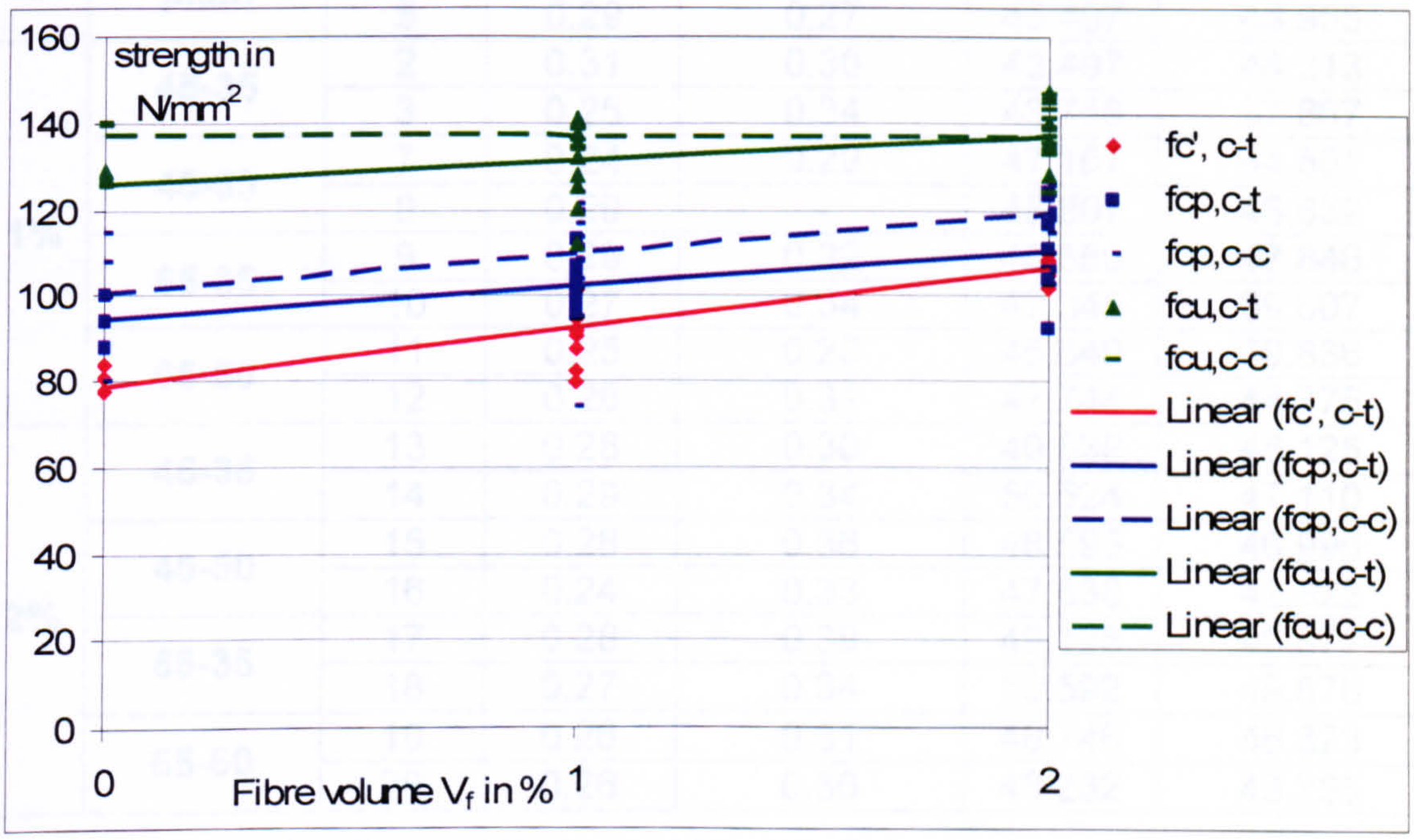

Figure 4.9 Strength development over increasing fibre volume fraction V_f for uniaxial compressive strength of cylinders f_c', plate specimen f_{cp} and 100 mm cubes f_{cu} in both series, compression-compression and compression-tension

kN/mm²	0.5 %	1%	1.5 %	2%
45-35	43.755	44.200	42.283	42.979
45-50	45.237	45.444	42.784	46.313
65-35	40.614	45.592	43.166	43.873
65-60	43.118	43.156	45.124	44.731
plain	45.836			

Table 11 Modulus of Elasticity E_c for SFRHPC and plain HPC specimens of the compression-compression test series under uniaxial compression

	0.5 %	1%	1.5 %	2%
45-35	0.28	0.31	0.33	0.25
45-50	0.27	0.29	0.28	0.23
65-35	0.34	0.25/ 0.28	0.27	0.31
65-60	0.23	0.26	0.27	0.23
plain	0.25			

Table 12 Poisson's ratio ν for SFRHPC and plain HPC specimens of the compression-compression test series under uniaxial compression

			Poisson's ratio ν		Modulus of Elasticity E_c in N/mm²	
V_f	Fibre type	batch	tension	compression	tension	compression
-	plain	4	0.28	0.32	47.292	44.419
		5	0.29	0.27	45.407	43.955
1%	45-35	2	0.31	0.30	43.497	44.213
		3	0.25	0.34	43.758	37.867
	45-50	7	0.24	0.29	47.167	44.501
		8	0.29	-	48.807	43.632
	65-35	9	0.29	0.32	45.550	47.846
		10	0.27	0.34	47.345	39.607
	65-60	11	0.25	0.23	45.640	39.836
		12	0.28	0.31	47.744	44.775
2%	45-35	13	0.28	0.30	49.639	48.125
		14	0.29	0.34	50.524	47.110
	45-50	15	0.28	0.36	48.595	46.996
		16	0.24	0.33	47.838	42.322
	65-35	17	0.28	0.39	49.128	46.577
		18	0.27	0.34	50.592	49.578
	65-60	19	0.26	0.31	48.746	46.323
		20	0.26	0.36	48.232	43.285

Table 13 Poisson's ratio ν and Modulus of Elasticity E_c for the compression-tension test series in both uniaxial tension and uniaxial compression

4.1.4. Cylinder splitting tests

The cylinder splitting tests were carried out in accordance with the British Standards for testing concrete (1983). The tests were undertaken in the same compression machine that was used for the compression cube tests.

Table 14 shows the tensile splitting strength f_t' of all tested batches for both test series. Each value is an average of three cylinder splitting tests of the same batch. They were all tested between 182 and 337 days on the same day as the biaxial test plates. The first strength column shows the actual value reported from the test machine. The second strength column represents an adjusted value which takes the strength difference of each plain mix into account before the fibres were added and also normalises the variation within the testing age.

From the values in Table 14 it can be seen that f_t' increases with higher fibre volumes. This can also be seen in Figure 4.10. A real trend in terms of one of the fibre types compared to the others could not be obtained. The general trend of increasing f_t' with increasing V_f can be expressed with the following equation

$$f_t' = 3.7\, V_f + 6.2 \qquad (4.9)$$

where f_t' is expressed in N/mm^2 and V_f in %. The data for the compression-tension batch number 19 was lost because of a mistake within the testing procedure.

Fibre volume and type	Batch No	Cylinder splitting strength f_t' in N/mm^2	
		actual value	normalised to plain cube
plain	9 C-C	5.4	5.4
	4 C-T	6.0	6.0
	5 C-T	5.8	5.8
	6 C-T	5.9	5.9
0.5% 45-35	23 C-C	7.0	7.9
0.5% 45-50	21 C-C	7.6	8.1
0.5% 65-35	19 C-C	7.3	7.8
0.5% 65-50	27 C-C	8.0	8.7
1% 45-35	3 C-C	9.3	9.6
	1 C-T	10.1	10.5
	2 C-T	9.5	10.9
	3 C-T	8.9	9.7
1% 45-50	5 C-C	10.2	11.1
	7 C-T	10.3	9.6
	8 C-T	10.6	9.8
1% 65-35	1 C-C	10.4	10.9
	9 C-T	10.1	10.1
	10 C-T	9.8	9.6
1% 65-50	11 C-C	9.9	10.6
	11 C-T	9.1	9.4
	12 C-T	9.4	9.1
1.5% 45-35	31 C-C	10.8	12.2
1.5% 45-50	25 C-C	10.1	11.5
1.5% 65-35	33 C-C	11.5	13.8
1.5% 65-50	29 C-C	11.0	13.0
2% 45-35	15 C-C	12.1	12.4
	13 C-T	12.4	12.0
	14 C-T	13.8	13.5
2% 45-50	7 C-C	12.3	13.1
	15 C-T	12.9	13.4
	16 C-T	11.7	12.1
2% 65-35	17 C-C	14.1	14.9
	17 C-T	15.6	14.9
	18 C-T	14.6	13.5
2% 65-50	13 C-C	12.7	13.2
	19 C-T	no data	no data
	20 C-T	12.8	14.0

Table 14 Splitting tensile strength f_t' for different batches of the compression-compression and compression-tension test series

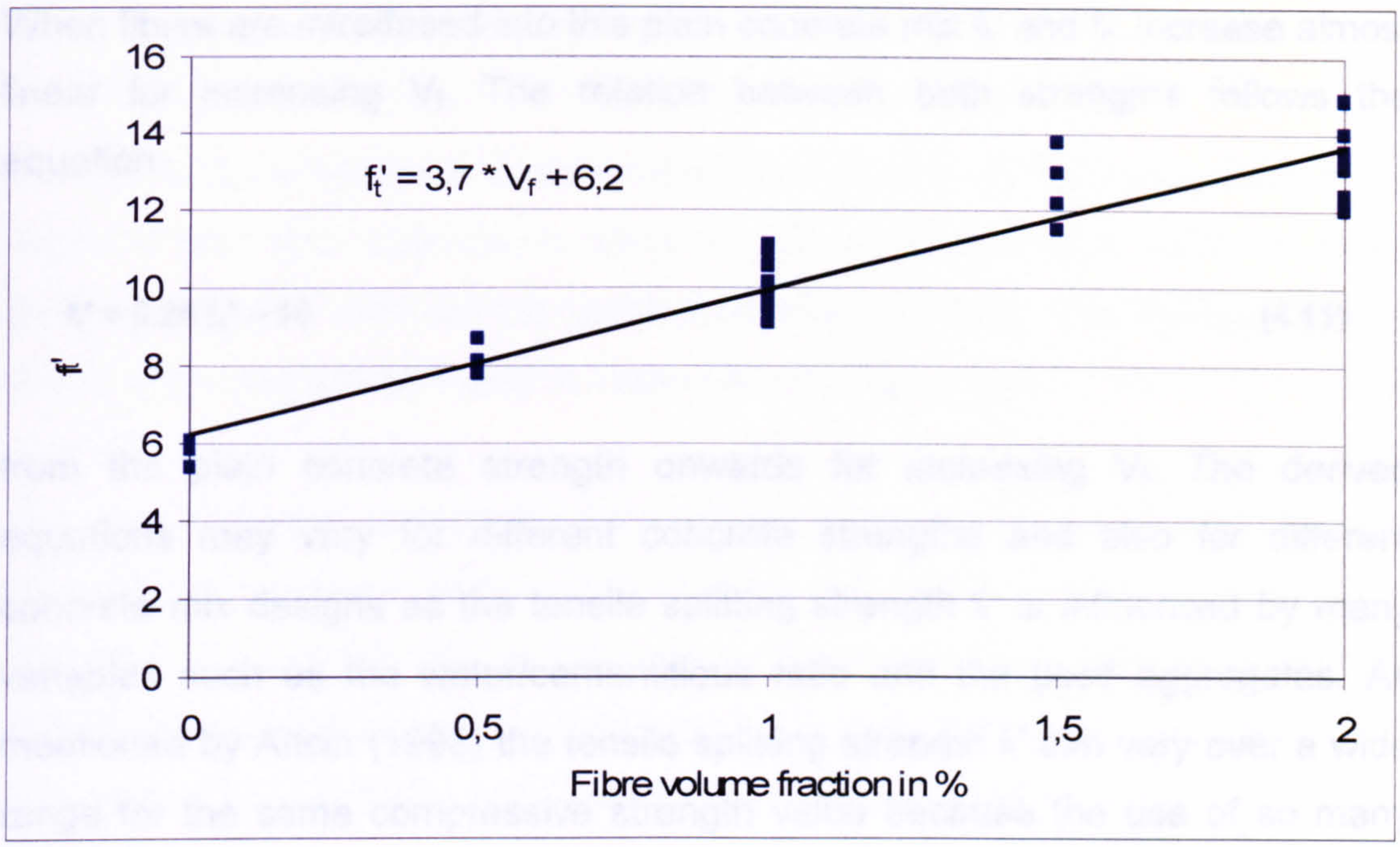

Figure 4.10 Cylinder splitting strength f_t' over fibre volume fraction V_f

The relationship between the normalised values for the cylinder splitting strength f_t' from Table 14 and the normalised cylinder compressive strength f_c' presented in Table 8 is shown in Figure 4.11 for the compression-tension test series.

Clearly it can be seen that for increasing V_f both f_c' and f_t' increase in a fairly linear manner. The relationship between f_t' and f_c' for the plain test series of high strength concrete is in good agreement with the expression quoted by Neville (1995) and the DIN 1045

$$f_t' = 0.3\,(f_c')^{2/3}. \qquad (4.10)$$

The test points for the plain concrete tests are almost on the line described by the above formula and which is expressed in Figure 4.11 by the blue curved line.

When fibres are introduced into this plain concrete mix f_t' and f_c' increase almost linear for increasing V_f. The relation between both strengths follows the equation

$$f_t' = 0.28\, f_c' - 16 \qquad (4.11)$$

from the plain concrete strength onwards for increasing V_f. The derived equations may vary for different concrete strengths and also for different concrete mix designs as the tensile splitting strength f_t' is influenced by many variables such as the water/cementitious ratio and the used aggregates. As mentioned by Aïtcin (1998) the tensile splitting strength f_t' can vary over a wide range for the same compressive strength value because the use of so many different cementitious compositions and mix designs.

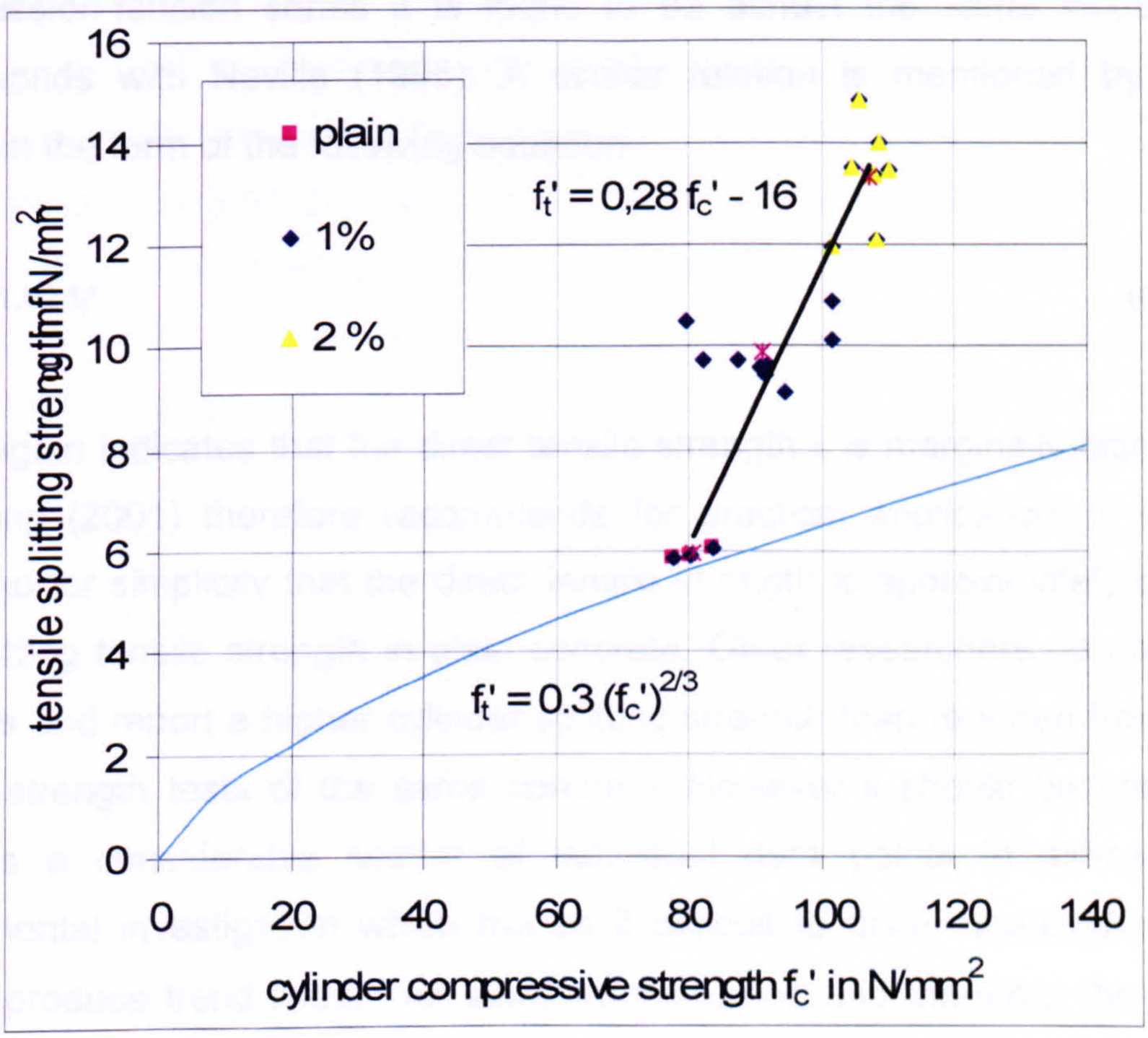

Figure 4.11 Relation between cylinder splitting tensile strength f_t' and cylinder compressive strength f_c'

4.1.5. Uniaxial direct tensile strength

In order to generate a complete strength envelope in the compression-tension region it was also essential to carry out direct tension tests with the same specimen type as used for the compression-tension tests. The full record of all tested specimen can be found in Table 19 in the Appendix.

The uniaxial tensile strength for plain HPC plate specimens was found to be f_t = 5.7 N/mm^2 on average and therefore 6.2 % of f_{cp} = 93.8 N/mm^2, 7.6 % of f_c' = 80.5 N/mm^2 and 4.7 % of f_{cu} = 128 N/mm^2. These values are in good agreement with other researchers such as Ansari and Li (1998), Marzouk and Chen (1995), Phillips and Zhang (1993) and Reinhardt and Rinder (1998).

Comparing f_t = 6.1 N/mm^2 with f_t' = 5.9 N/mm^2 for plain HPC of the compression-tension series it is found to be almost the same value which corresponds with Neville (1995). A similar relation is mentioned by Zheng (2001) in the form of the following equation

$$f_t = 1.02\, f_t' \qquad (4.12)$$

which again indicates that the direct tensile strength f_t is marginally higher than f_t'. Zheng (2001) therefore recommends for practical applications it may be assumed for simplicity that the direct tensile strength is approximately equal to the splitting tensile strength in plain concrete. Other researchers do not agree with this and report a higher cylinder splitting strength than reported from direct tensile strength tests of the same concrete. However it should be noted that there is a considerable scatter of individual data points in almost every experimental investigation which makes it difficult to draw meaningful results and to produce trend lines. The standard derivation and therefore the relative error of the three tested splitting cylinders of each batch varies up to 15 % in this study as can be seen in Table 25. The increased standard deviation for a standardised test underlines the difficulties to gain meaningful experimental test results about this material property.

The two tensile strength values can be put into relation to create a ratio of $f_t/f_t' = 0.97$ which corresponds with a value found by Phillips and Zhang (1993). They found a value of 0.95 for plain concrete with different w/c ratios and therefore different concrete strengths. This difference is well known and is attributable to the different stress distributions developed within the two types of specimen and the different loading rates.

Overall as Popovics (1998) summarised the splitting strength is usually greater than the direct tensile strength of the same concrete although the opposite has also been reported. A great range was realised within the values he collected from various researches for the value of f_t/f_t' which varied between 0.52 and 1.28.

Several reasons were mentioned which could lead to some untrue values for both strengths. The measured direct tensile strength might be reduced by loading eccentricity or stress peaks where the splitting strength might be increased by the preset failure area of the specimen in or near the central vertical plane. This reduces the number of weak links in the zone of maximum strength where for the direct tensile specimen the entire length of the specimen is exposed to the tensile stress.

Also friction between the splitting specimen and the machine platens may increase the apparent value of f_t'. Moreover, and maybe more important in this matter, is the type and the strength of the used aggregates. An increase in the maximum size of the aggregate reduces f_t' less than f_t. Therefore with crushed aggregates with a small maximum particle size used in this project, f_t is expected to be higher than f_t'.

Curbach and Speck (2002) mentioned another variable which might have an influence on the tensile strength. The casting direction might be of crucial interest taking into account that pore water and air pockets might form underneath the aggregates during casting. This would be the preferred place

where cracks would develop. In a specimen tested in the same direction as it was cast the negative effect of the flat air pockets would sum up.

Overall, like with every value concerning concrete tests, they are tested under certain conditions and have to be handled with great care when they are extrapolated into general material behaviour laws. Certain variables have to be taken into account and mentioned, before final conclusions can be determined.

For SFRHPC f_t increases with higher V_f as can be seen in Figure 4.12. The same observation was made by Sato et al. (2000) who found that the tensile strength greatly increase as V_f increases and Li et al. (1998) who reported an increase of the tensile strength which is around 10 % compared to plain concrete for V_f = 2 %. The maximum strength increase of f_t in this study was 7.5 % for fibre type 45-50 and V_f = 2 %.

A similar trend was observed for f_t' as mentioned before. The strength increase was however greater with f_t' than for f_t for increasing fibre volume fractions. Almost the same tensile strength was observed for plain HPC in both test methods. A 52 % increase for f_t' was observed in average for the 1 % fibre volume batches and even 94 % increase for the 2 % fibre volume batches. The value for the ratio f_t/f_t' decrease for increasing fibre content in average from 0.97 to 0.65 and 0.51 for the plain, 1 % and 2 % SFRHPC respectively. This decrease of the f_t/f_t' value was mainly because the higher increase in f_t' for increasing V_f and is shown in Figure 4.13.

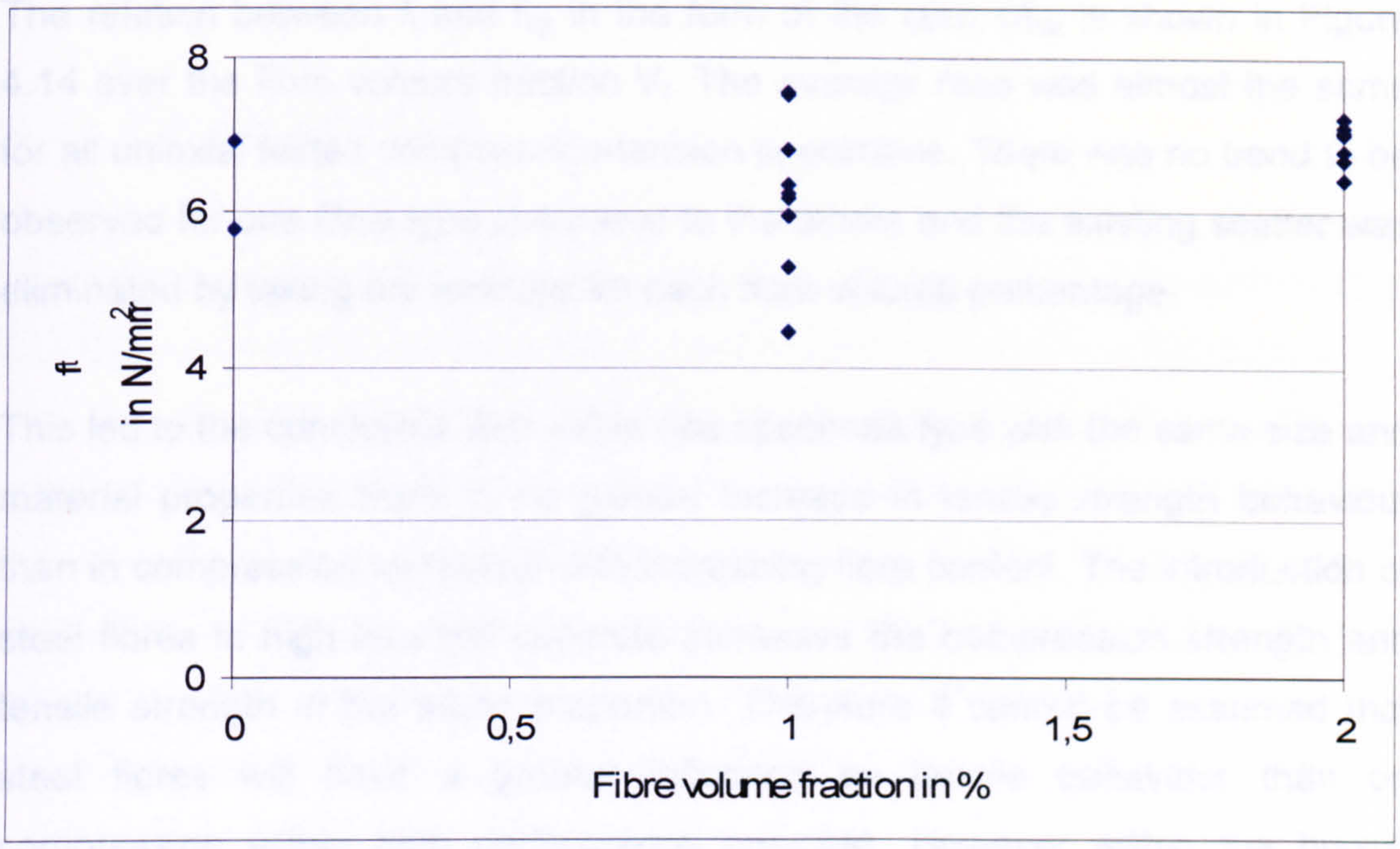

Figure 4.12 Uniaxial direct tensile strength f_t versus fibre volume fraction V_f

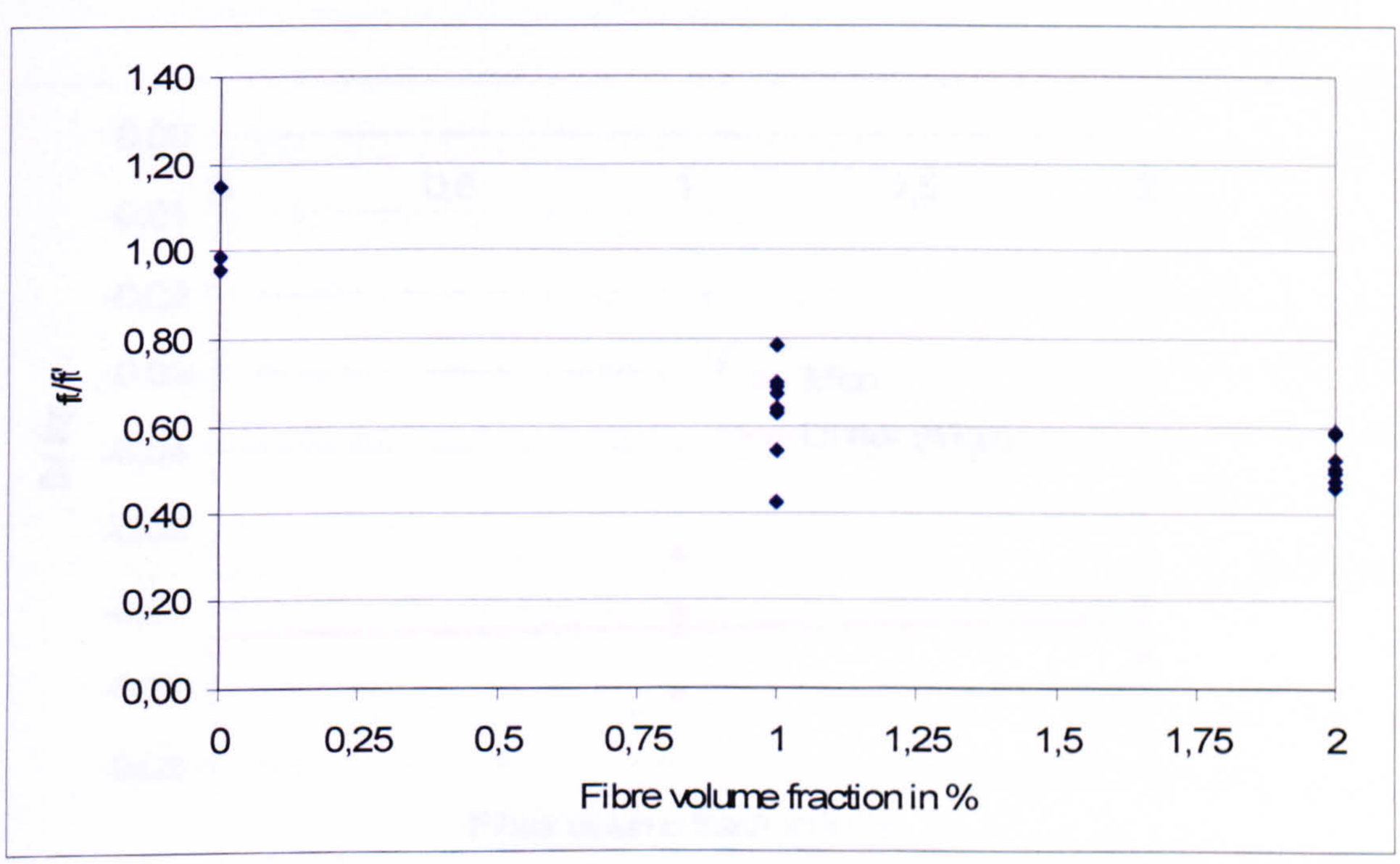

Figure 4.13 Ratio f_t/f_t' versus fibre volume fraction V_f

The relation between f_t and f_{cp} in the form of the ratio f_t/f_{cp} is shown in Figure 4.14 over the fibre volume fraction V_f. The average ratio was almost the same for all uniaxial tested compression-tension specimens. There was no trend to be observed for one fibre type compared to the others and the existing scatter was eliminated by taking the average for each fibre volume percentage.

This led to the conclusion that within one specimen type with the same size and material properties there is no greater increase in tensile strength behaviour than in compression behaviour with increasing fibre content. The introduction of steel fibres in high strength concrete increases the compression strength and tensile strength in the same proportion. Therefore it cannot be assumed that steel fibres will have a greater influence on tensile behaviour than on compression within high performance concrete. However within the biaxial compression-tension region the addition of steel fibres gives a larger load capacity. This will be shown within the next paragraph.

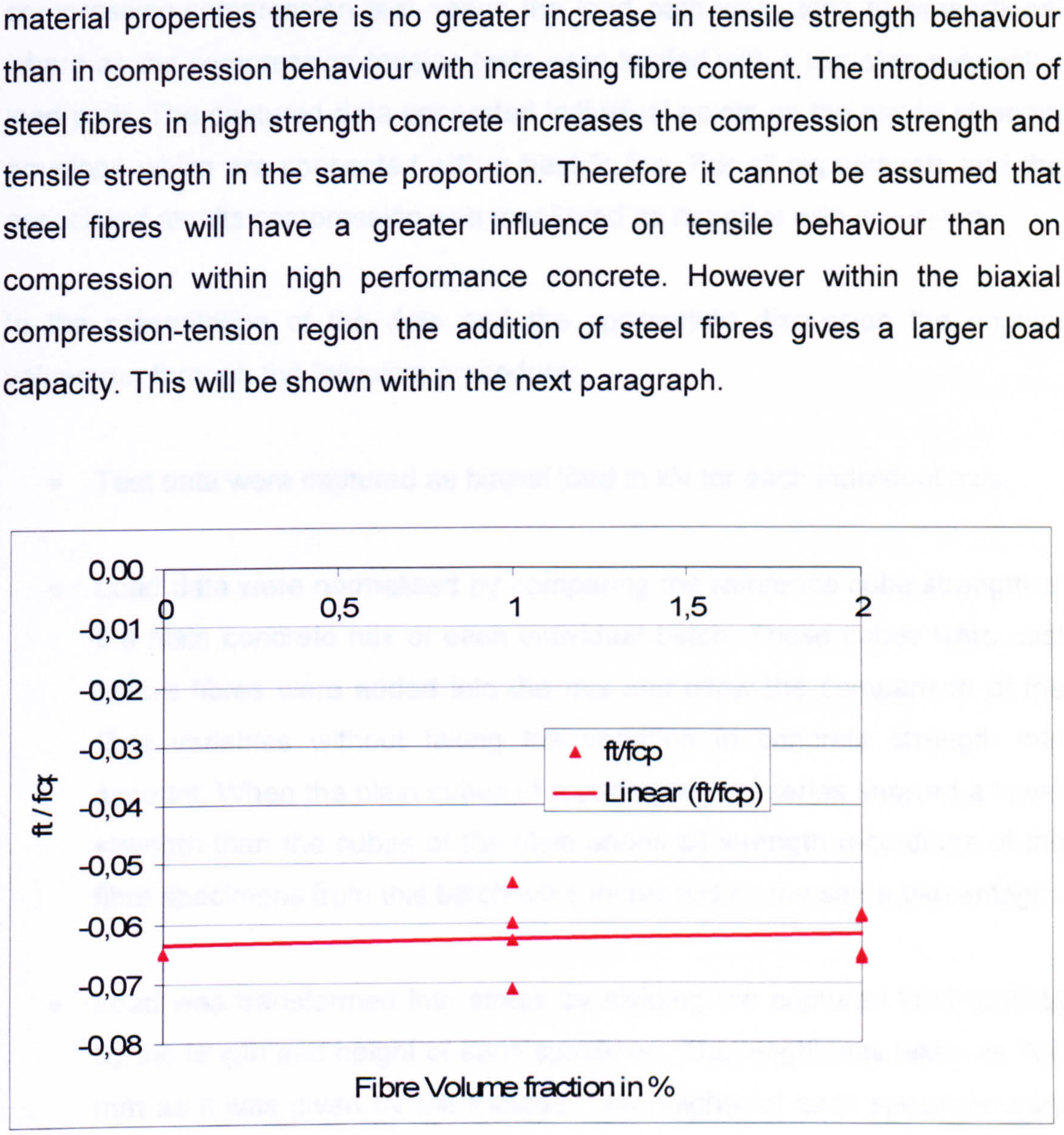

Figure 4.14 Ratio between uniaxial tensile strength and uniaxial plate compressive strength f_t/f_{cp} over the fibre volume fraction V_f

4.2. Biaxial strength

The plate specimens were tested under different combinations of biaxial loading and data were captured as mentioned before. With the test procedure chosen it was not possible to perform the tests under constant stress-ratios. For the compression-compression test series the load path was close to proportional where as the compression-tension tests were loaded with a two step sequential load path. The captured data generated individual points on the biaxial strength envelope which are connected with a best fit line. For all experiments and the associated results compression was monitored as negative with $\sigma_1 > \sigma_2 > \sigma_3$.

In the presentation of the data and the appropriate discussion the original values run through the following procedure:

- Test data were captured as biaxial load in kN for each individual axis.
- Load data were normalised by comparing the reference cube strength of the plain concrete mix of each individual batch. These cubes were cast before fibres were added into the mix and allow the comparison of the fibre variables without taking the variation in concrete strength into account. When the plain cubes of a particular test series showed a lower strength than the cubes of the plain series all strength recordings of the fibre specimens from this batch were increased by the same percentage.
- Load was transformed into stress by dividing the captured load reading by the length and height of each specimen. The length was taken as 205 mm as it was given by the moulds. The heights of each specimen vary because of small individual casting finishes and were taken into account by measuring them before testing. These stress values can be seen in columns 3 and 4 in Table 18 in Appendix 1 for the compression-

compression (σ_2 and σ_3) test series and Table 19 for the compression-tension (σ_1 and σ_3) test series respectively.

- For presentation purposes the stress data were divided by the uniaxial compressive plate strength f_{cp} of the plain concrete series. This means that the strength recordings from the compression-compression test series were divided by 103.9 N/mm^2 and from the compression-tension series by 93.8 N/mm^2. These values are presented in column 6 and 7 in Table 18 and Table 19 in Appendix 1 and are graphically presented in graphs.

The data from Table 18 and Table 19 are presented in Figure 4.15 below. This graph shows the overall picture of all experimental strength data for the biaxial tests in both compression-compression and compression-tension test series. It combines the biaxial strength envelopes for plain, 1 % and 2 % fibre volume concrete in the compression-compression and compression-tension region and for the 0.5 % and 1.5 % fibre volume series in the compression-compression region only. The biaxial strength envelopes for each individual test series on their own can be seen together with the test points in Appendix 1. Figure 4.16 gives a more detailed view for the compression-tension branch as the tension axis σ_1/f_{cp} is enlarged.

The envelopes represent a best-fit line through all individual testing points of each fibre type. Test points which deviated substantially from the best-fit line were discarded. Each envelope represents two concrete batches with eight specimens each in the compression-compression branch. The plain, 1% and 2% series had also two concrete batches with six specimens each in the compression-tension branch with only the plain series and the 1% 45-35 fibre type which had three batches tested for the compression-tension branch. In total there were 392 individual tested specimens which generated the test points represented by the best fit lines of the biaxial strength envelopes.

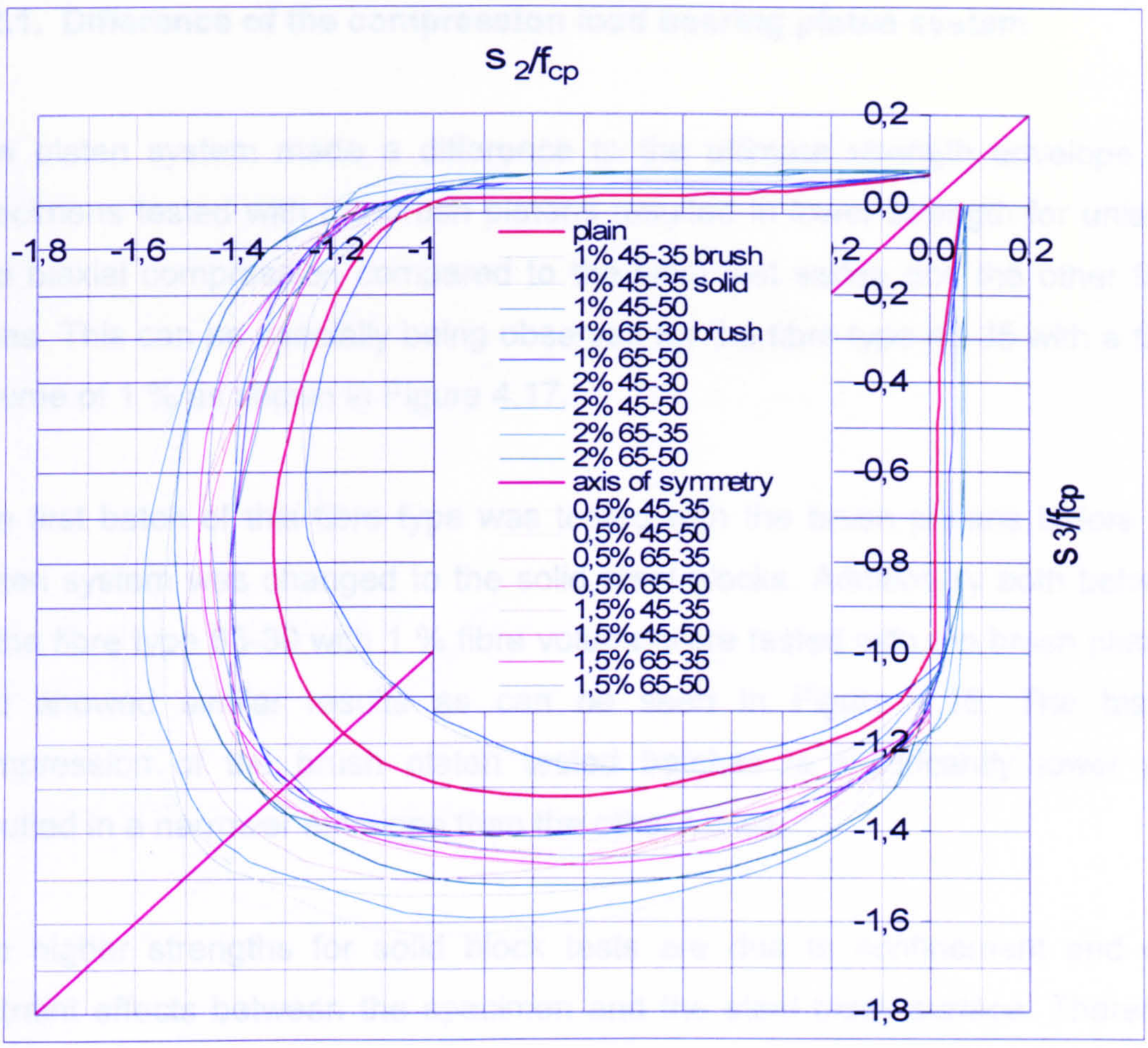

Figure 4.15 Biaxial strength envelopes in the compression- compression and compression-tension region

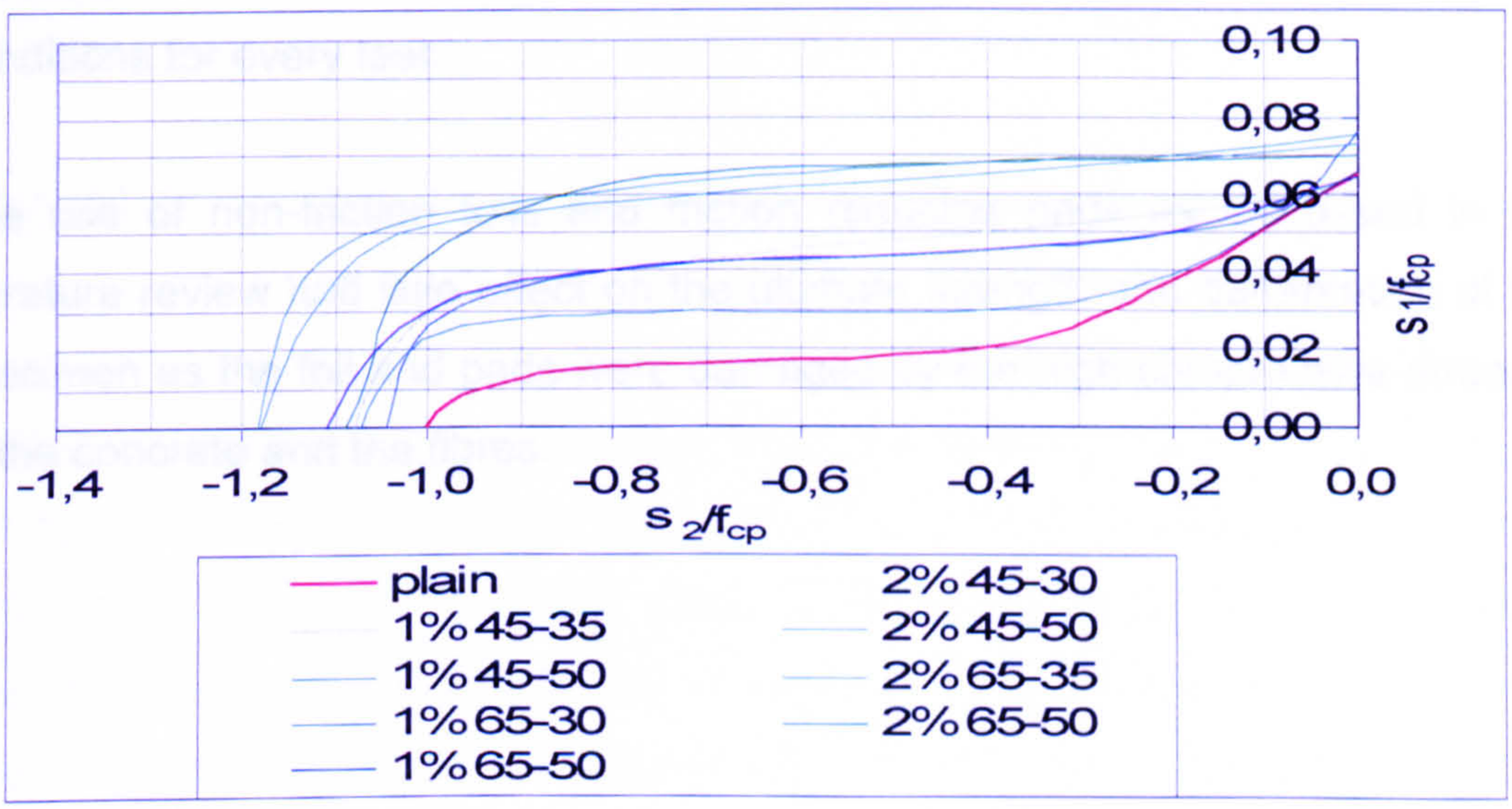

Figure 4.16 Biaxial strength envelopes in the compression-tension region for plain, 1 % and 2 % fibre concrete

4.2.1. Difference of the compression load bearing platen system

The platen system made a difference to the ultimate strength envelope. All specimens tested with the brush platens resulted in lower strength for uniaxial and biaxial compression compared to the plain test series and the other fibre types. This can be specially being observed for the fibre type 45-35 with a fibre volume of 1 % as shown in Figure 4.17.

The first batch of this fibre type was tested with the brush platens before the platen system was changed to the solid steel blocks. Additionaly both batches of the fibre type 65-30 with 1 % fibre volume were tested with the brush platens and showed similar results as can be seen in Figure 4.15. The biaxial compression of the brush platen tested batches is significantly lower and resulted in a narrower envelope than the other series.

The higher strengths for solid block tests are due to confinement and end restraint effects between the specimen and the steel block surface. Therefore the uniaxial and biaxial strengths are probably overestimated compared to concrete behaviour under ideal testing conditions. Although normally brush platens ought to give results closer to the actual strength, here the results were unreliable because the continuous damage to the bristles caused different conditions for every test.

The use of non-friction foils and friction reducing pads as discussed in the literature review had little effect on the ultimate strength and deformation of the specimen as the foil and pads were damaged by the high compressive strength of the concrete and the fibres.

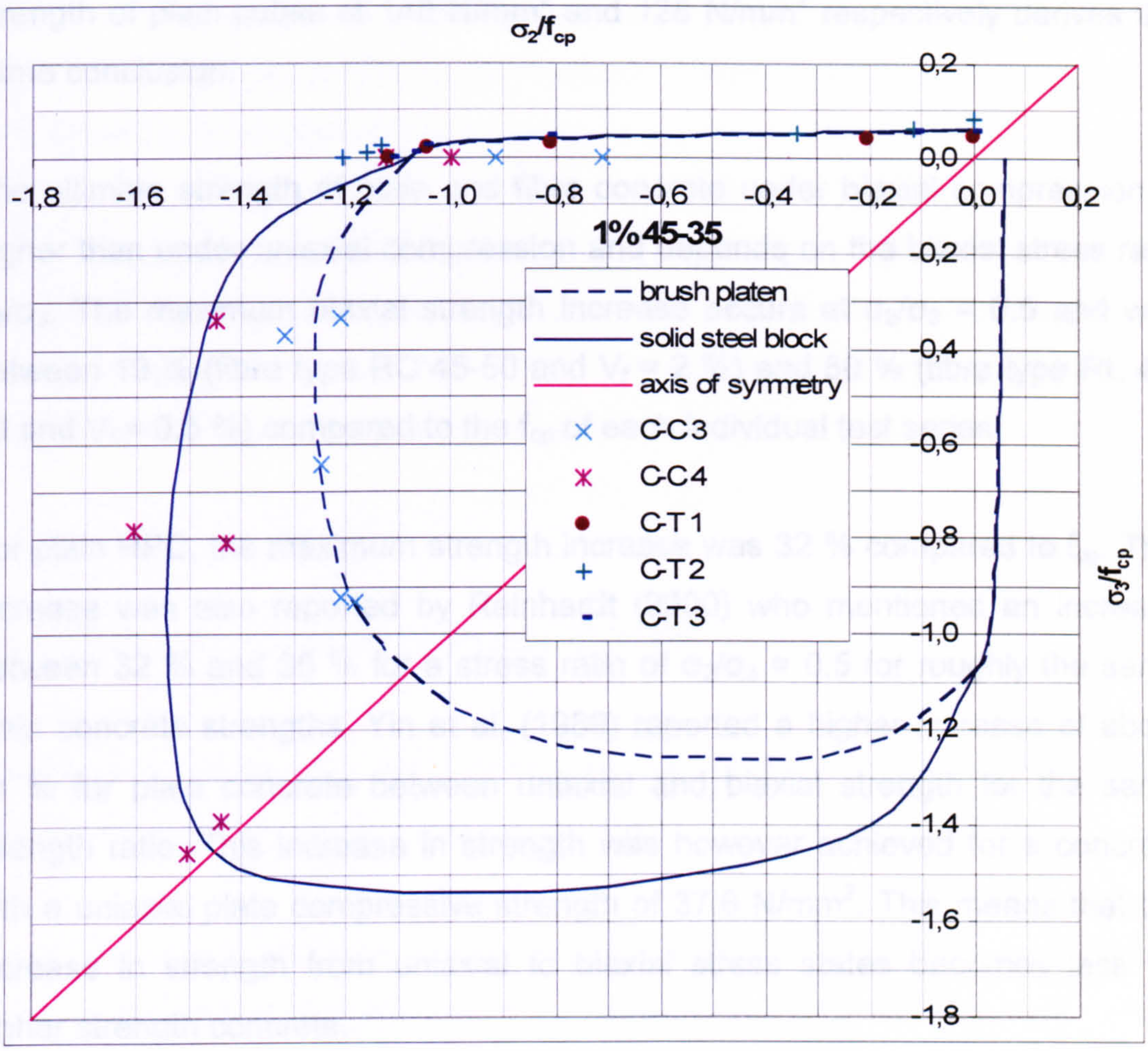

Figure 4.17 Difference of the load bearing platen system for the biaxial strength envelopes within one fibre type

4.2.2. Difference between uniaxial and biaxial strength

In this study the average uniaxial compressive plate strength of plain HPC is f_{cp} = 98.9 N/mm^2. This value derived from the average of the compression-compression test series (f_{cp} = 103.9 N/mm^2) and the compression-tension test series (f_{cp} = 93.8 N/mm^2). These almost equal values for both test series show that the different shape, in terms of specimen length, does not have much influence on the results. The higher value for the compression-compression series was caused by the older age of the specimen at testing (325 days compared to 255 days). Comparing the corresponding uniaxial compressive

strength of plain cubes of 140 N/mm^2 and 128 N/mm^2 respectively derives the same conclusion.

The ultimate strength of plain and fibre concrete under biaxial compression is higher than under uniaxial compression and depends on the biaxial stress ratio σ_2/σ_3. The maximum biaxial strength increase occurs at σ_2/σ_3 = 0.5 and was between 19 % (fibre type RC 45-50 and V_f = 2 %) and 50 % (fibre type RL 45-50 and V_f = 0.5 %) compared to the f_{cp} of each individual test series.

For plain HPC, the maximum strength increase was 32 % compared to f_{cp}. This increase was also reported by Reinhardt (2000) who mentioned an increase between 32 % and 35 % for a stress ratio of σ_2/σ_3 = 0.5 for roughly the same plain concrete strengths. Yin et al. (1989) reported a higher increase of about 44 % for plain concrete between uniaxial and biaxial strength for the same strength ratio. This increase in strength was however achieved for a concrete with a uniaxial plate compressive strength of 37.6 N/mm^2. This means that the increase in strength from uniaxial to biaxial stress states becomes less for higher strength concrete.

At equal biaxial compression (σ_2/σ_3 = 1) the strength increase becomes smaller than for the stress ratio mentioned before but still higher than for uniaxial compression. The strength increase is between 11 % (fibre type RL 65-50 and V_f = 0.5 %) and 40 % (fibre type RL 45-50 and V_f = 0.5 %) compared to f_{cp} of each series. The increase for plain HPC at σ_2/σ_3 = 1 is 18 % compared to f_{cp}.

Again Yin et al. (1989) produced similar results. Their maximum increase for σ_2/σ_3 = 1 for fibre concrete was about 70 % over the uniaxial plain compressive strength. As mentioned before the strength increase for biaxial strength also depends on the concrete strength itself with less increase for higher strength concrete. Therefore these results are in good agreement with the ones in this study as Yin's et al. compressive strength was only 37.6 N/mm^2 compared to 98.9 N/mm^2 in this study, almost three times higher.

In general it could be said that the increase in the biaxial strength compared to the uniaxial strength is due to confinement effects under biaxial compression and depends on the σ_2/σ_3 ratio.

In the biaxial compression-tension region shown in Figure 4.16 it was noted that the introduction of a tensile load rapidly decreases the compression load capacity. This is well known and can be seen within all research publications in this area as stated in the literature review.

4.2.3. Difference between plain and SFRHPC

Adding steel fibres into HPC increases the uniaxial compression, uniaxial tension, biaxial compression and biaxial compression-tension strength.

- The maximum increase in uniaxial compressive strength f_{cp} for HPSFRC compared to plain HPC is 20 % and occurred for the fibre type RL 45-35 with V_f = 2 %.

- The maximum increase in uniaxial tension strength f_t is 16 % for the fibre type 45-50 and V_f = 2 % compared to the plain HPC.

- In biaxial compression (σ_2/σ_3 = 1) the increase in strength for fibre concrete over plain HPC is 22 % again for the fibre type RL 45-35 with a V_f = 2 %.

- For the biaxial compression ratio σ_2/σ_3 = 0.5 (strength ratio with the largest strength increase for all concrete types) the increase of HPSFRC over HPC is between 6 % (fibre type 65-50 and V_f = 1 %) and 23 % (fibre type 45-35 and V_f = 2 %; again same fibre type than before).

- Compared to f_{cp} of plain HPC the maximum strength increase is 58 % for the fibre type RL 65-35, V_f = 2 % and for σ_2/σ_3 = 0.5.

- At equal compression (σ_2/σ_3 = 1) the maximum strength increase for HPSFRC compared to uniaxial plain HPC strength is 44 % for the fibre type RL 45-35 and V_f = 2 %.

- In the compression-tension region the strength envelopes are wider and indicate a higher load capacity for all fibre types for higher fibre volume concretes as shown in Figure 4.16.

- The increase of the fibre volume fraction does not always result in higher strengths in the compression-compression region. However trends can be observed for fibre types RL 45-35 and RC 65-35 where higher fibre volume fractions results in higher uniaxial and biaxial strengths as seen in Figure 4.18 and Figure 4.19. The 1 % fibre content envelopes of this fibre type cannot be compared to the other envelopes because of the different loading conditions (brush and solid platens).

- The fibre types RL 45-50 and RC 65-50 tend to have the same biaxial strength behaviour for all four different V_f as can be seen in Figure 4.20 and Figure 4.21. Therefore V_f seems to make a difference in biaxial strength for fibres with the fibre length of l = 35 mm but not for fibre length l = 50 mm where the biaxial strength does not increase with higher fibre volume content V_f. Similar results were found by Yin et al. (1989) who reported little effect on the biaxial compressive strength by increasing the fibre volume percentage from 1 % to 2 %. This was observed for 1 inch (25.4 mm) long fibres.

- The lack of definite trends for fibre length l = 50 mm with increasing fibre volume fraction V_f could be caused by the reduced workability of the fresh concrete and the resulting problem in mixing and compacting this long fibre concrete. Furthermore the 50 mm thickness of the specimen

was perhaps too small for that fibre length to ensure a total random fibre distribution within the specimen. Therefore any beneficial fibre effect in the lateral direction which might prevent splitting failure would be diminished because the long fibres tend to be more horizontally distributed. The same apply to the result of Yin et al. (1989) and verify the findings from above. His specimens were of the dimension of 152 x 152 x 38 mm and therefore only slightly thicker than the tested fibre length.

The increase of uniaxial and biaxial strength in HPSFRC compared to plain HPC for all fibre types in all fibre volume fractions V_f indicate a confining stress caused by the steel fibres. This has been noted before by Yin et al., (1989). Their maximum strength increase for steel fibre concrete over plain concrete was about 70 % at the biaxial stress ratio $\sigma_2/\sigma_3 = 1.0$ for a concrete with $f_c' = 42$ N/mm^2 compared to 44 % in this study.

However as mentioned before the increase in strength depends on the concrete strength itself with higher strength increase between uniaxial and biaxial stress conditions for lower strength concrete. This observation can be made for plain and fibre concrete. The significant increase of biaxial strength due to the addition of fibres was explained by van Mier (1986) as it is similar to the addition of a small amount of confinement pressure.

Van Mier tested plain concrete in triaxial compression, σ_2 and σ_3, with a small confining stress in the out-of-plane direction σ_1. The confining stress σ_1 varies from 0, 0.05 to 0.10 σ_3. To gain the same increase of 22 % in biaxial strength than for the fibre type RL 45-35 with $V_f = 2$ % compared to the plain HPC a small out-of-plain stress of around 0.01 % of the major stress σ_3 would be necessary to achieve the same result. This means that the fibres provide a small amount of passive confining stress.

Within the compression-tension region a dip is recognised in the strength envelope for plain HPC for stress ratios σ_1/σ_2 close to uniaxial tension. See the

red line in Figure 4.16 which is in agreement with the test result from Curbach and Hampel (1998 and 1999). High strength concrete in comparison to normal strength concrete behaves much more sensitive to tensile stresses. After an initial crack forms the specimen fails instantly. There is no tensile stress transfer over an existing crack.

But this is different with steel fibres. The fibres behave like crack arrestors and the load capacity of SFRHPC becomes more with higher fibre volume factors V_f which can also be seen in Figure 4.16.

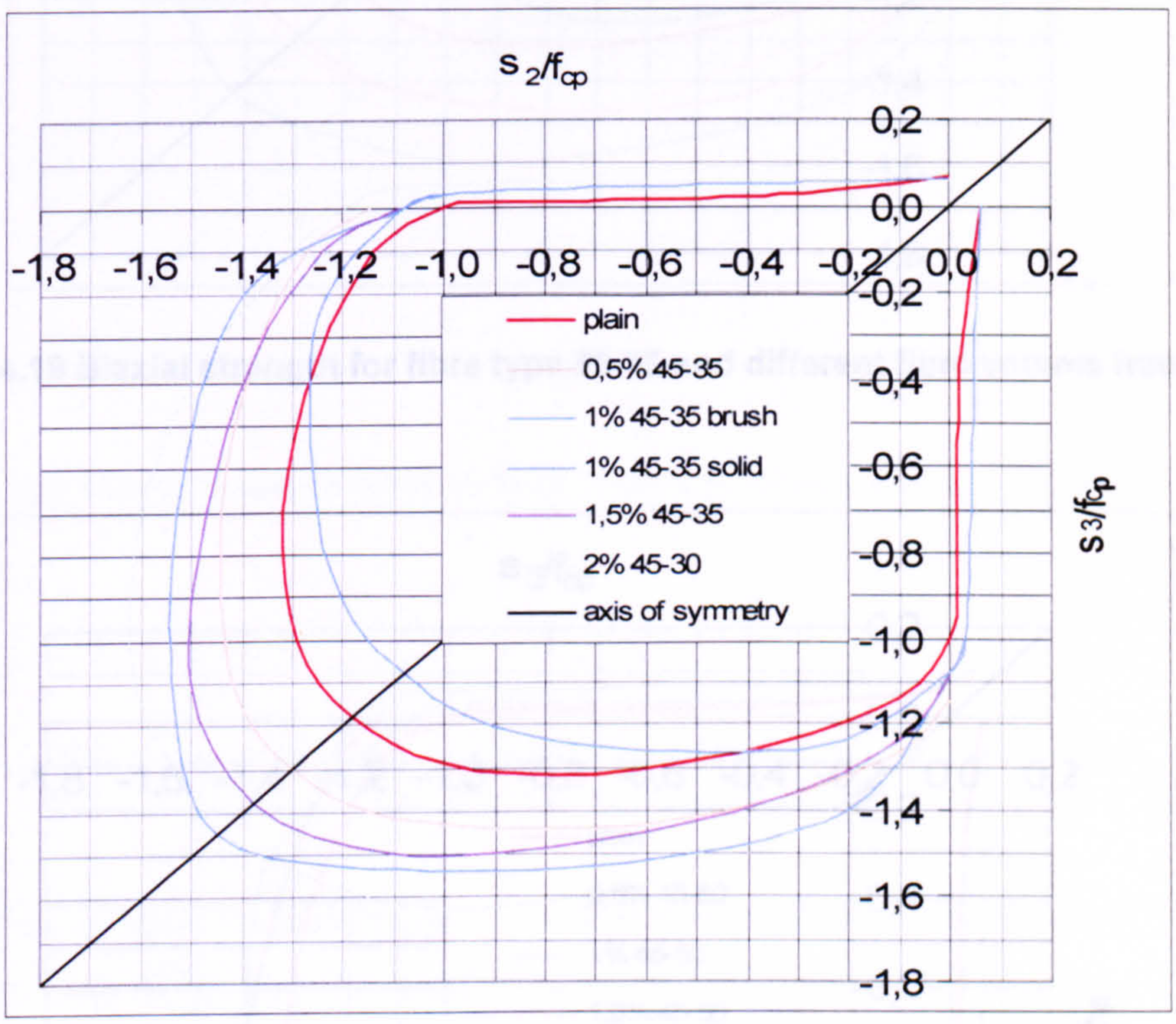

Figure 4.18 Biaxial strength for fibre type 45-35 and different fibre volume fractions V_f

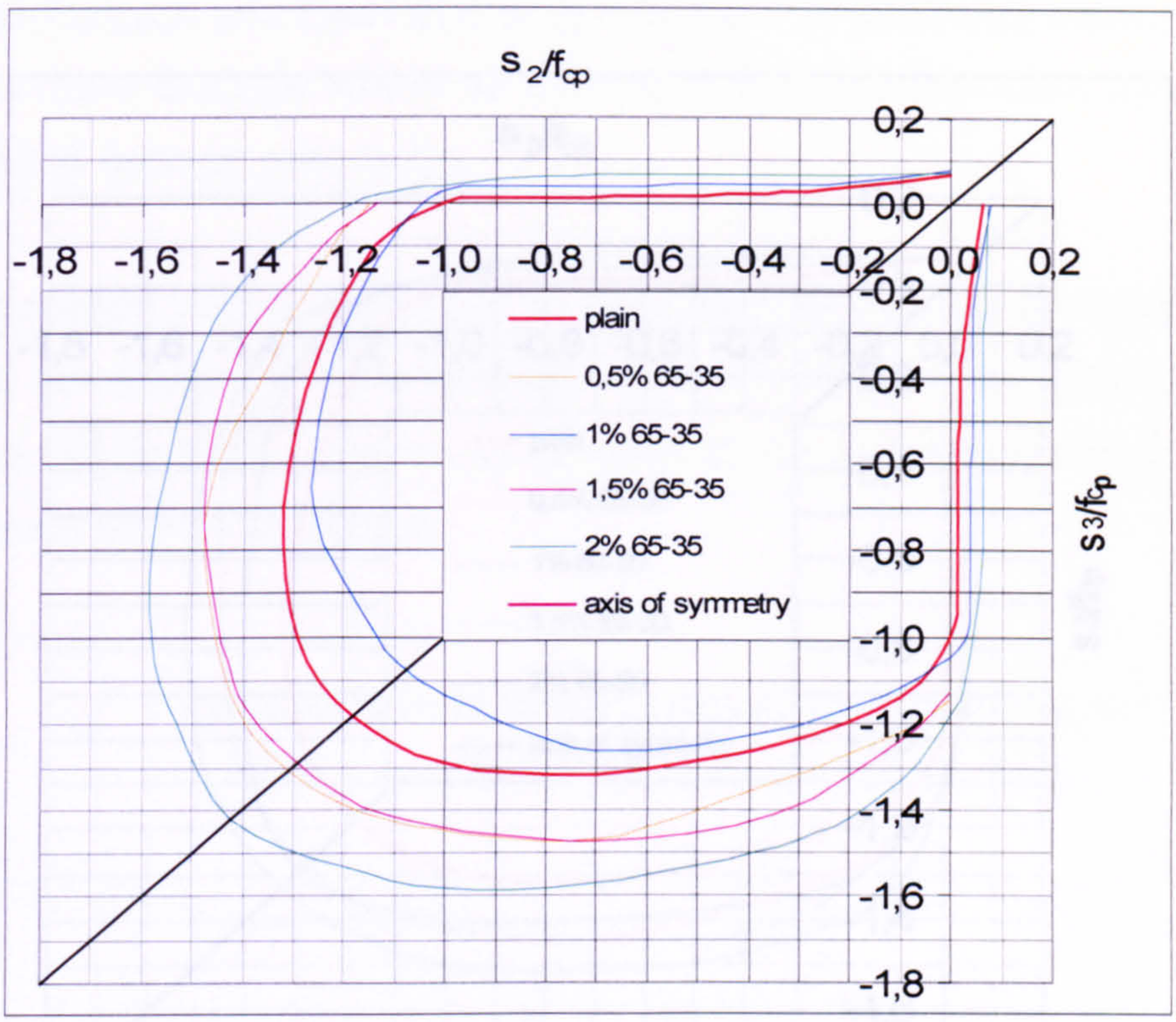

Figure 4.19 Biaxial strength for fibre type 65-35 and different fibre volume fractions V_f

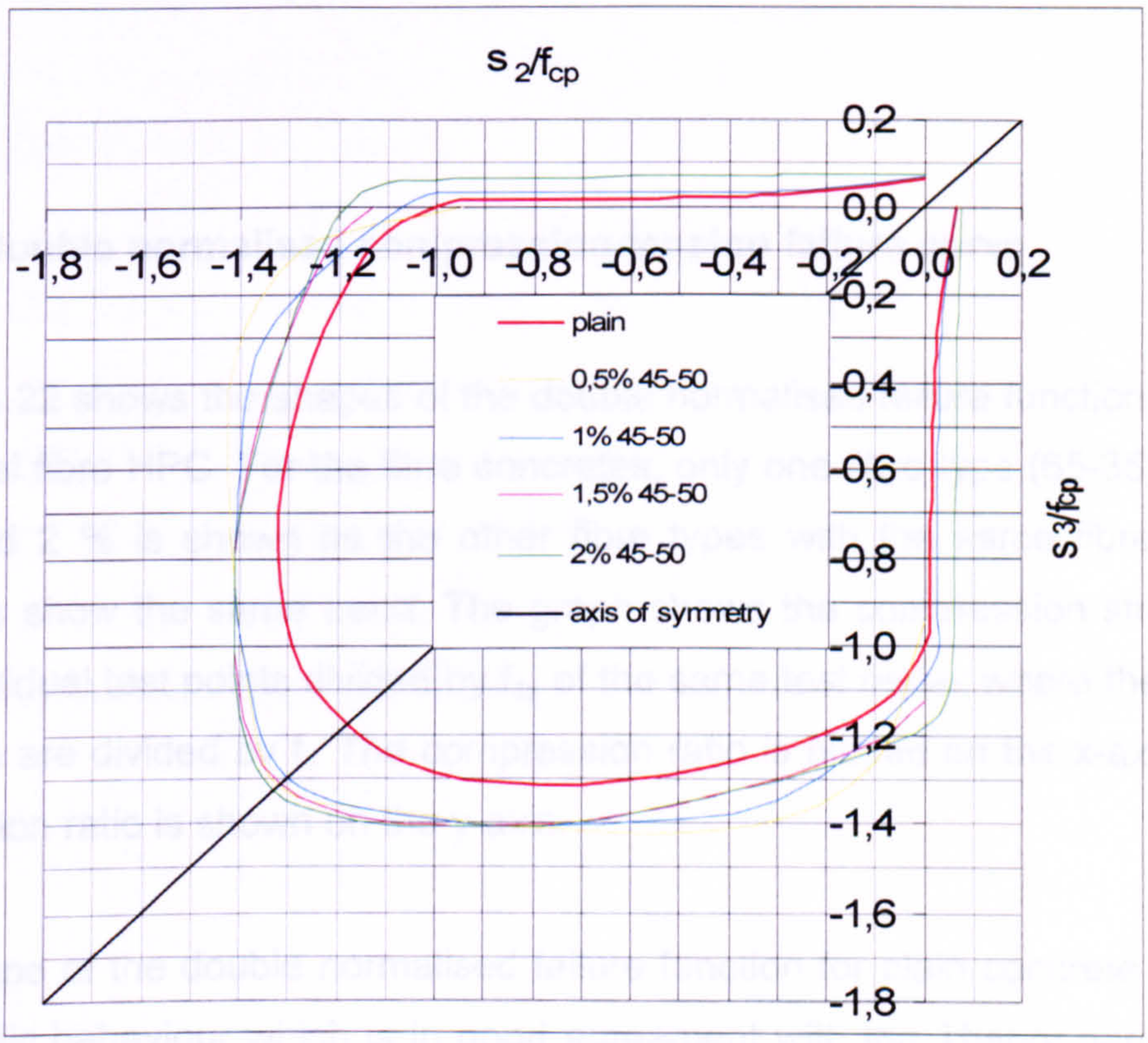

Figure 4.20 Biaxial strength for fibre type 45-50 and different fibre volume fractions V_f

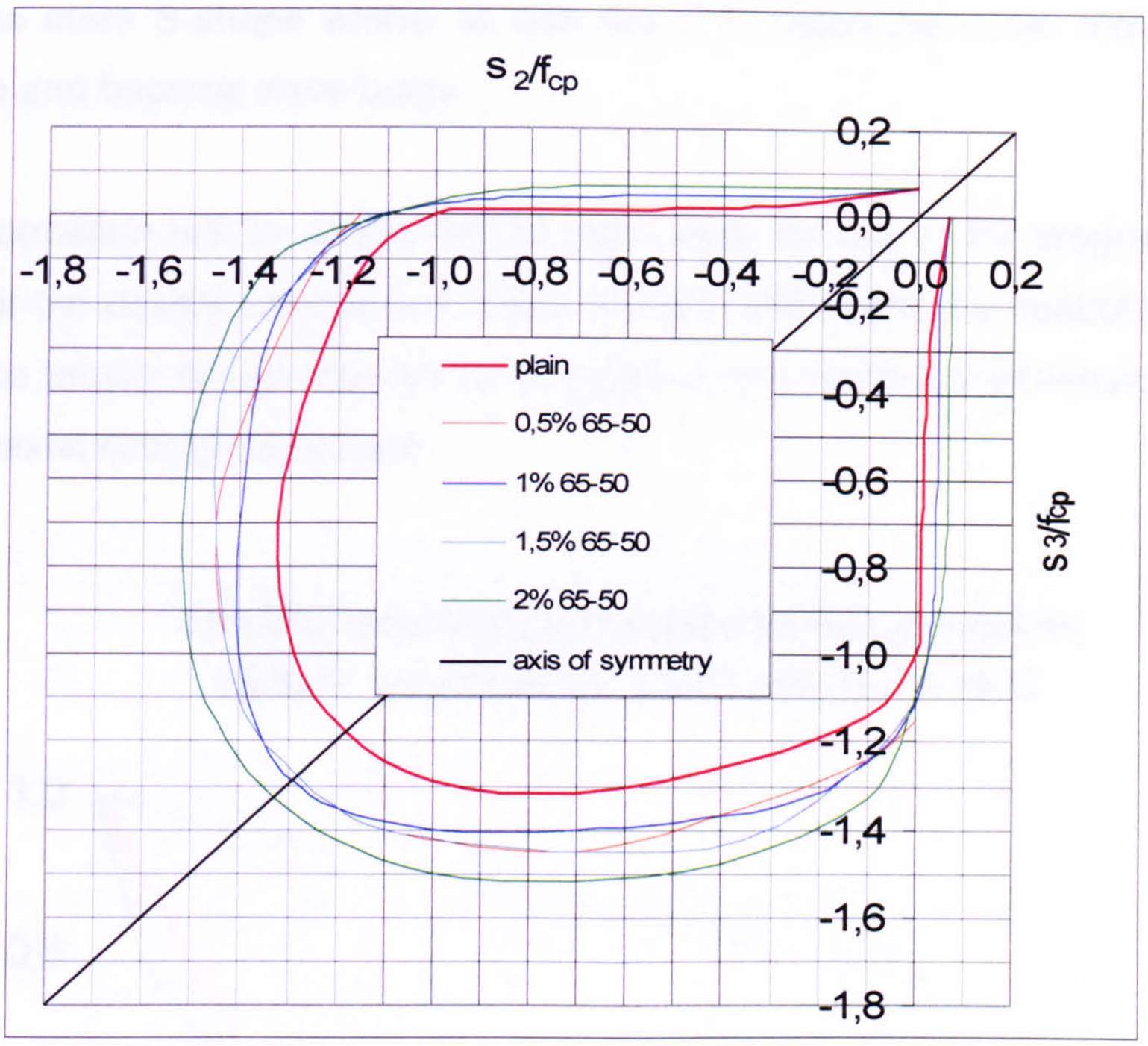

Figure 4.21 Biaxial strength for fibre type 65-50 and different fibre volume fractions V_f

4.2.4. Double normalised compression-tension failure curve

Figure 4.22 shows the shapes of the double normalised failure function for plain and steel fibre HPC. For the fibre concretes, only one fibre type (65-35) for V_f = 1 % and 2 % is shown as the other fibre types with the same fibre volume contents show the same trend. The graph shows the compression stresses of the individual test points divided by f_{cp} of the same test series where the tension stresses are divided by f_t. The compression ratio is plotted on the x-axis where the tension ratio is shown on the y-axis.

The shape of the double normalised failure function for plain concrete shows a hyperbolic behaviour which is in good agreement with the Theory handbook of the ATENA FE program (2003) for high strength concrete and also with the

results of Curbach and Hampel (1999). For the 1 % SFRHPC batch the curve becomes more S-shape where as with the 2 % batch the curve moves even more up and become more bulgy.

This information will be of interest as input data for use in FE programs. The shape of the double normalised failure function will define the reduction factor within the tensile failure criterion for concrete in the compression-tension region of the biaxial strength envelope.

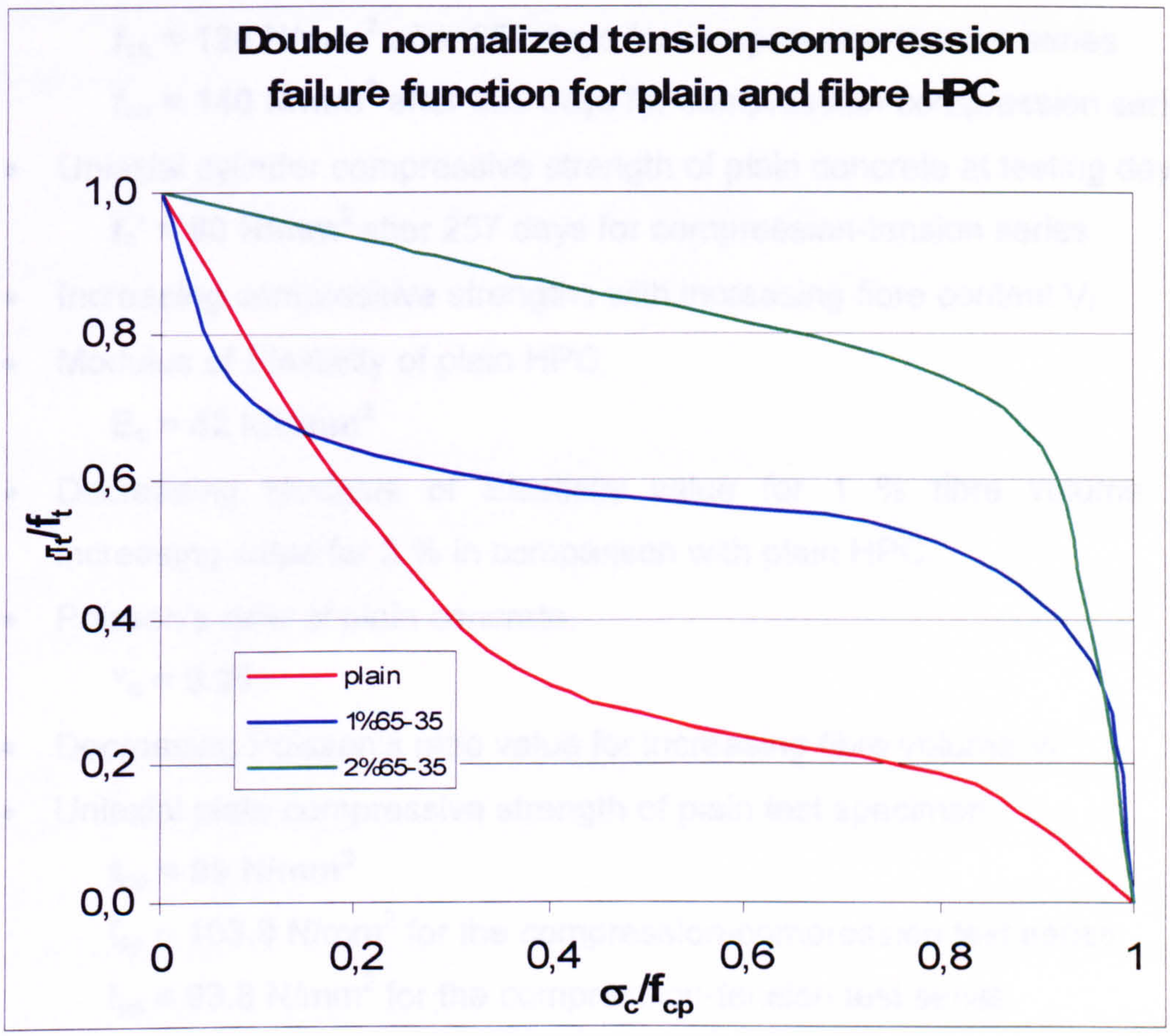

Figure 4.22 Double normalised compression-tension failure function for plain and steel fibre HPC

4.3. Summary

In conclusion the standard concrete properties in this study are:

- Uniaxial cube compressive strength of plain concrete after 7 days,
  $f_{cu,7}$ = **95 N/mm²**
- Uniaxial cube compressive strength of plain concrete after 28 days,
  $f_{cu,28}$ = **117 N/mm²**
- Uniaxial cube compressive strength of plain concrete at testing day,
  f_{cu} = **128 N/mm²** after 257 days for compression-tension series
  f_{cu} = **140 N/mm²** after 325 days for compression-compression series
- Uniaxial cylinder compressive strength of plain concrete at testing day,
  f_c' = **80 N/mm²** after 257 days for compression-tension series
- Increasing compressive strengths with increasing fibre content V_f
- Modulus of Elasticity of plain HPC,
  E_c = **42 kN/mm²**
- Decreasing Modulus of Elasticity value for 1 % fibre volume and increasing value for 2 % in comparison with plain HPC.
- Poisson's ratio of plain concrete,
  ν_c = **0.25**
- Decreasing Poisson's ratio value for increasing fibre volume V_f.
- Uniaxial plate compressive strength of plain test specimen,
  f_{cp} = **99 N/mm²**
  f_{cp} = 103.9 N/mm² for the compression-compression test series
  f_{cp} = 93.8 N/mm² for the compression-tension test series
- Cylinder splitting strength of plain concrete,
  f_t' = **5.9 N/mm²**
- Increasing cylinder splitting strength for increasing fibre volume V_f
- Uniaxial tensile strength of plain concrete,
  f_t = **6.1 N/mm²**
- Increasing tensile strength for increasing fibre volume V_f
- Biaxial compressive strength of plain concrete for stress ratio of $\sigma_2/\sigma_3 = 1$

$f_{bc} = 118$ N/mm^2

- Increasing biaxial compressive strength f_{bc} for increasing fibre volume V_f

The used platen system has an influence on the strength recordings. The brush loading platen results in less strength increase under biaxial compression than the solid dry steel platens.

A uniaxial strength increase for higher fibre volume content can be observed for both compression and tension loads. The value for the ratio between both uniaxial strengths stays the same for all tested fibre volume contents for high strength concrete.

The biaxial strength of plain HPC increases under biaxial compression compared to the uniaxial compression strength. However the increase is not as big as for NSC.

In the biaxial compression-tension region the test set-up had to be dealt with special attention towards the application of the tension load and the alignment of the axis. The introduction of a tension load decreases the compression capacity significantly.

No trend existed for any tested fibre type to behave better than the others in any test and in all tested fibre volume contents. Therefore no forecast can be given for an improvement of the steel fibre concrete behaviour for a single fibre type. The improvement of properties simply depends on the fibre volume content which improves the steel fibre concrete behaviour for the uniaxial compression and tensile strength and the biaxial strength. The increase is more significant in the compression-tension region than in the compression-compression region.

It became apparent during the evaluation of the test results that the thickness of the specimen was not sufficient enough for the longer fibres. Therefore the results have to be considered with a warning. The plate like specimens were only 50 mm thick with the longer fibres also being 50 mm long. Therefore it

could be assumed that almost no fibres were orientated in that direction. On top of this the casting direction was perpendicular to the applied loads which resulted also in an in plane alignment of the fibres. The beneficial behaviour of the fibres is therefore reduced in the out of plane direction. This became obvious by exploring the biaxial strength envelops for every fibre type with almost no biaxial strength increase for the longer fibres for higher fibre volume fractions V_f.

It should be noted that a significant scatter was observed for most of the tests. Even for standardised test procedures, such as the cylinder compressive test or the cylinder splitting test, the standard deviation reached 15 % within one batch.

4.4. References

ACI 318-89 (Revised 1992) Building code requirements for reinforced concrete, *ACI Manuel of Concrete Practice Part 3: Use of Concrete in Buildings – Design, Specifications and Related Topics*, pp. 345, Detroit, Michigan, 1994 in AM Neville 1995, *Properties of concrete*, 4th edn, Longman Group Limited, Essex, England, p. 418.

ACI 363-92 State-of-the-art report on high-strength concrete, *ACI Manuel of Concrete Practice Part 1: Materials and General Properties of Concrete*, pp. 55, Detroit, Michigan, 1994 in AM Neville 1995, *Properties of concrete*, 4th edn, Longman Group Limited, Essex, England, p. 418.

Ahmad, S.H. and Shah, S.P. 1985, 'Structural Properties of high strength concrete and its implications for precast prestressed concrete', *PCI Journal*, vol. 30, no. 6, November-December, pp. 91-119 in Aïtcin, P-C, 1998, *High-performance concrete*, E&FN Spon, London, England, p 442.

Aïtcin, P-C, 1998, *High-performance concrete*, E&FN Spon, London, England, p 442.

Ansari, Farhad and Li, Qingbin 1998, 'High-Strength Concrete Subjected to Triaxial Compression', *ACI Materials Journal*, vol. 95, no. 6, November-December, pp. 747-755.

ASTM 2002, Standard Test Method for Static Modulus of Elasticity and Poisson's Ratio of Concrete in Compression, Designation: C 469-02.

Baalbaki, W, Aitkin, PC and Ballivy, G 1992, 'On Predicting Modulus of Elasticity in High-Strength Concrete', *ACI Materials Journal,* vol. 89, no. 5, pp. 517-520.

British Standards Institution 1983, *Methods of making test cubes from fresh concrete*, BS 1881: Part 108: 1983, London, BSI.

British Standards Institution 1983, *Method of normal curing of test specimens (20°C method)*, BS 1881: Part 111, 1983, London, BSI.

British Standards Institution 1986, *Spec. for compression testing machines for concrete*, BS 1881: Part 115, 1986, London, BSI.

British Standards Institution 1983, *Methods for determination of compressive strength of concrete cubes*, BS 1881: Part 116, 1983, London, BSI.

British Standards Institution 1983, *Method for determination of tensile splitting strength*, BS 1881: Part 117, 1983, London, BSI.

British Standards Institution 1983, Testing Concrete. Method for determination of the compressive strength of concrete cores, BS 1881: Part 120, 1983, London, BSI.

Červenka Vladimír, Jendele Libor and Červenka Jan, 2003, 'ATENA Program documentation, Part 1, Theory', Prague, 4. October, p. 27.

Curbach, Manfred and Hampel, Torsten 1998, 'Festigkeit von Hochleistungsbeton unter mehraxialer Beanspruchung', in *Tagungsband zum 7. Leipziger Massivbauseminar, Erfahrungen mit Hochleistungsbeton, 15. and 16. Oktober 1998*, Leipzig.

Curbach, Manfred and Hampel, Torsten 1999, 'Verhalten von Hochleistungsbeton unter zweiaxialer Druck-Zug-Beanspruchung - Zusammenfassung', Arbeitsgemeinschaft industrieller Forschungsvereinigungen, "Otto von Guericke" e.V. – AiF and Deutscher BetonVereine.V. – DBV, Förderkennzeichen: AiF: 11011 B, DBV: 198, 25.02.1999, Dresden.

Curbach, Manfred und Speck, Silke, 2002, 'Mehraxiale Festigkeit von duktilem Hochleistungsbeton', Deutscher Ausschuss für Stahlbeton, Heft 524, Beuth Verlag GmbH, Berlin, pp. 219.

Deutsche Industrie Norm DIN 1045, Beton- und Stahlbetonbau, Eigenschaften des Festbetons.

European Committee for Standardization, 'Eurocode 2: Design of Concrete Structures, Part 1: General Rules for Buildings (ENV 206)' in Schneider, K-J 1994, '*5A Stahlbeton und Spannbeton nach EC 2*' in *Bautabellen für Ingenieure*, 11th edn, Werner Verlag GmbH, Düsseldorf, Germany, p. 5.23.

Gao Jianming, Sun, Wei and Morino, Keiji 1997, 'Mechanical Properties of Steel Fibre-reinforced High-strength, Lightweight Concrete', *Cement and Concrete Composites*, vol. 19, no. 4, pp. 307-313.

Hughes, B.P. and Bahramian, B. 1965, *Cube tests and the Uniaxial compressive strength of concrete*, Magazine of Concrete Research, Vol. 17, No. 53, pp. 177 – 182.

Hussein, A.A. 1998, *Behaviour of High-Strength Concrete under Biaxial Loading Condition,* PhD thesis, p. 120, Faculty of Engineering and Applied Science, Memorial University of Newfoundland, St. John's, Canada.

Hussein, A. and Marzouk, H. 2000, 'Behavior of High-Strength Concrete under Biaxial Stresses', *ACI Material Journal*, vol. 97, no. 1, January-February, pp. 27-36.

Kakizaki, M. et al. 1992, *Effect of Mixing Method on Mechanical Properties and Pore Structures of Ultra-Strength Concrete*, Katri Report, no. 90, pp. 90, Kajima Corporation, Tokyo, (and also in ACI SP-132, CANMET / ACI) in A.M. Neville 1995, *Properties of concrete*, 4th edition, Longman Group Limited, Essex, England, p. 418.

Kaplan, M.F. 1959, 'Ultrasonic pulse velocity, dynamic modulus of elasticity, Poisson's ratio, and the strength of concrete made with thirteen different coarse aggregates', *RILEM Bulletin*, Paris, New Series, no. 1, March, pp. 58-73 in Aïtcin, P-C, 1998, *High-performance concrete*, E&FN Spon, London, England, p 442.

Lecture notes for M.Sc. in Structural Engineering and Mechanics – Structural Concrete, University of Glasgow, 2004.

Li, Zongjin, Li Faming, Chang Tse-Yung Paul and Mai Yiu-Wing 1998, 'Uniaxial Tensile Behavior of Concrete Reinforced with Randomly Distributed Short Fibres', *ACI Materials Journal,* vol. 95, no. 5, September-October, pp. 564-574.

Marzouk, H. and Chen, Z.W. 1995, 'Fracture Energy and Tension Properties of High-Strength Concrete', *Journal of Materials in Civil Engineering,* ASCE, vol. 7, no. 2, pp. 108-116.

Neville, AM 1995, *Properties of concrete*, 4th edition, Longman Group Limited, Essex, England.

Phillips, DV and Zhang Binsheng 1993, 'Direct tension tests on notched and un-notched plain concrete specimens', *Magazine of Concrete Research*, vol. 45, no. 162, March, pp. 25-35.

Popovics, Sándor 1998, *Strength and related properties of concrete – a quantitative approach*, John Wiley & Sons, Inc., New York.

Rashid, M.A., Mansur, M. and Paramasivam, P. 2002, 'Correlation between Mechanical Properties of High-Strength Concrete', *Journal of Materials in Civil Engineering,* vol.14, no. 3, May-June, pp. 230-238.

Reinhard, Hans-Wolf and Rinder, Tassilo 1998, 'High strength concrete under sustained tensile loading', *Otto-Graf-Journal*, Materialprüfungsanstalt Universität Stuttgart, vol. 9, pp. 123-134.

Reinhard, Hans-Wolf 2000, 'Structural Behaviour of High Performance Concrete', *Otto-Graf-Journal*, Materialprüfungsanstalt Universität Stuttgart, vol. 11, pp. 9-18.

Sato Yasuhiko, van Mier, Jan GM and Walravn, Joost C 2000, 'Mechanical characteristics of multi-modal fibre reinforced cement based composites', in *RILEM Publications: Proceedings of the fifth RILEM Symposium on Fibre-Reinforced Concrete (FRC)*, Lyon, France, 13-15 September 2000, edited by P Rossi and G Chanvillard, pp. 791-800.

Van Mier, J.G.M., 1986, *Fracture of concrete under complex stress*, Heron (Delft), vol. 31, no. 3.

Williamson, Gilbert R., 1974, 'The effect of steel fibres on the compressive strength of concrete', Proceedings of an international Symposium on

'Fibre Reinforced Concrete', Publication SP-44, American Concrete Institute, Detroit, pp. 195 – 208.

Yin, W.S., Su, E.C.M., Mansur, M.A. and Hsu, T.T.C. 1989, 'Biaxial Tests of Plain and Fibre Concrete', *ACI Material Journal*, vol. 86, no. 3, May-June, pp. 236-243.

Zheng, W, Kwan, AKM and Lee, PKK 2001, 'Direct Tension Test of Concrete', *ACI Materials Journal'*, vol. 98, no. 1, January-February, pp. 63-71.

5. Deformational Behaviour - Test Results and Discussion

The stress-strain curves presented here show the relationship of normalised stress to actual strain. The uniaxial compression plate strength of plain HPC used for normalising all other stresses was taken as σ_{cp} = 99 N/mm^2. Strains are expressed in microstrain with $\varepsilon_1 > \varepsilon_2 > \varepsilon_3$ and tensile strength is positive. Because of the explosive failure of the HPC specimens the stress-strain curves are reported up to the peak of the load which also was the failure point. Unfortunately this meant it was impossible to capture post peak behaviour.

5.1. Different strain measurement methods

As explained in chapter 3 different strain measurement methods were used from the start of the experiments. However due to the explosive failure of the specimens some measurement methods had to be abandoned because of constant damage to the measurement devices, mostly the LVDTs. However strain gauges on the unconfined surface of the specimens gave very good results which can be compared with the LVDT measurements. Figure 5.1 shows the measurements for all methods for one uniaxial compression test on a plate specimen with 1 % fibre content of fibre type 65-35. Each green line represents the average of four LVDTs, two from the top and two from the bottom. The blue lines are the average of the top and bottom strain gauges. The averages are produced by all LVDT or strain gauge readings which were monitoring the appropriate deformation in one direction. The exact layout of the measurement devices are presented in Chapter 3. It can be seen that the measurement devices in both methods in x and y directions are in close agreement with each other.

The LVDT strain value in the z direction however shows less strain than the measurement in the x direction which also is unconfined and a free surface with no loading platen attached in this test. This difference can be a result of the fact that the dimensions of the specimens are different in this direction and the fibres are mostly aligned horizontally and therefore the material becomes non-homogeneous in the third dimension. For the two main dimensions however the strain gauge measurements can be used instead of the LVDT measurement to obtain a good prediction of the surface strains.

However they can only express results for one tested specimen at a time and not for an average of more specimens. Unlike reusable test methods such as the LVDT assembly, the used strain gauges are demolished after each test. Because of the large amount which would be necessary to cover every specimen with strain gauges and the excessive costs for them only one specimen for each fibre type and fibre content in each stress ratio is equipped with strain gauges. In total 165 specimens were strain gauged from a total of 392, about 40 % of the total number of specimens and lead to a total of 660 used strain gauges.

It could be concluded that strain measurement systems, strain gauges and LVDTs, are working identically and result in the same graphs. However due to constant damage by the explosive failure of the specimens the LVDT measurements had to be abandoned.

The brown line in Figure 5.1 expresses the strain generated between the actuator movements recorded by the two LVDTs which are also controlling the input signal for the close-loop control scheme for the tests which are under displacement control. This measurement also takes into account the deformation of the actuator pistons with the pin assembly and the steel parts of the loading platens system. Therefore this reading cannot be taken for strain measurements of the concrete surface and gives only an idea of the stress-

strain behaviour of the whole loading system together with the concrete specimen.

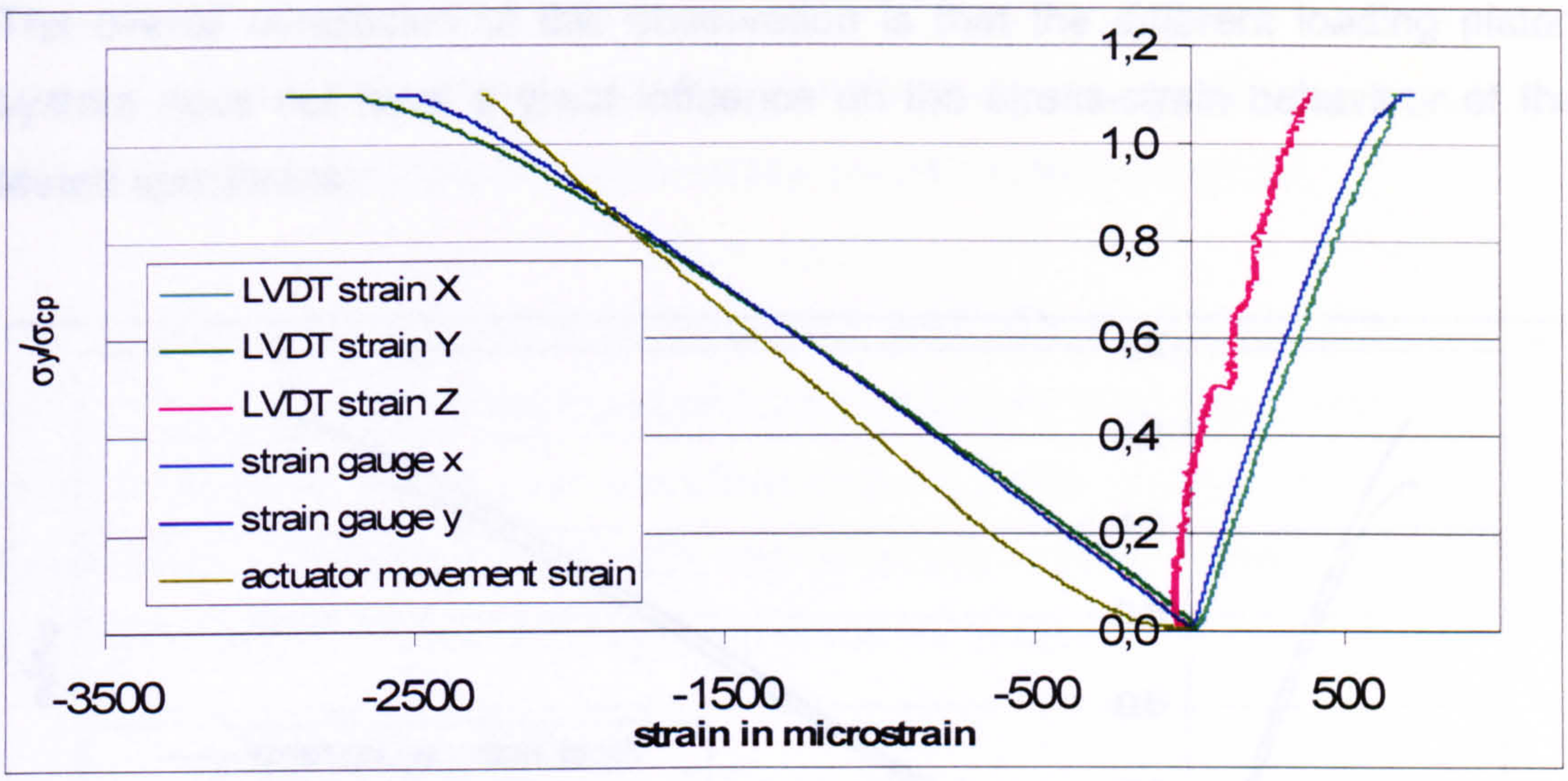

Figure 5.1 Stress-strain diagram for different measurement devices (LVDTs and strain gauges) for a specimen tested in uniaxial compression (fibre type 65-35, V_f = 1 %)

5.2. Influence of different loading platen systems

Comparing the strain measurements of the two used loading platen systems, the steel brush platen and the solid steel block platen, it become obvious that there is almost no influence on the stress strain behaviour generated by the strain gauges mounted on the free surface of two specimens with the same fibre variables (65-35) and 1% fibre content tested under uniaxial compression. This can be seen in Figure 5.2 where the blue lines represent the specimen tested with the steel block loading system and the green lines represent the brush platen system.

One of the most obvious differences is that the strength for the steel block tested specimen becomes higher. However the specimen was almost twice as old (330 days to 185 days) and therefore had a higher original strength. Also observed is the more linear behaviour of the steel block tested specimen up to

the failure point where the brush platen tested specimens diverge from linearity before failure.

The overall conclusion of this observation is that the different loading platen system does not have a great influence on the stress-strain behaviour of the tested specimens.

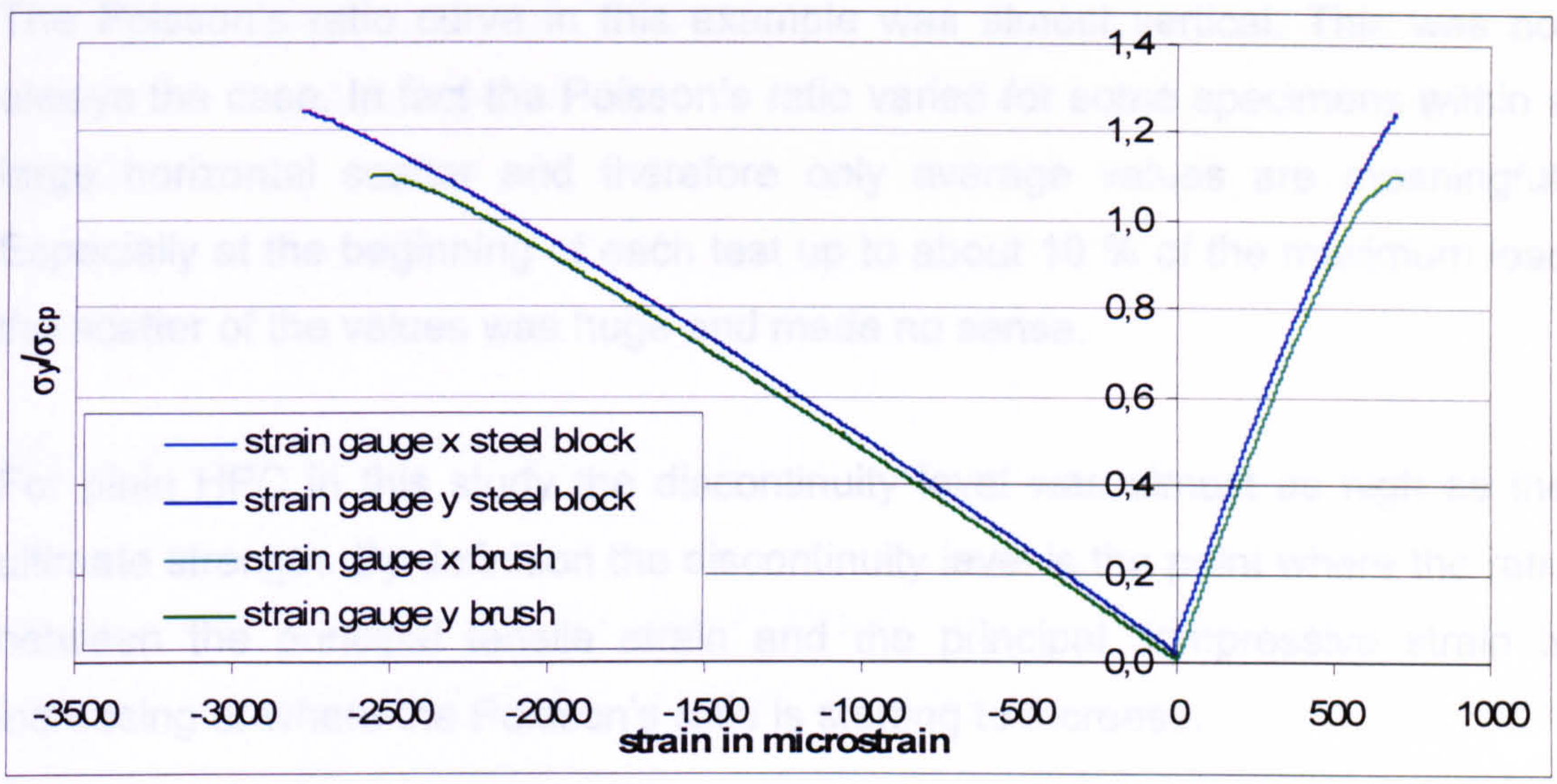

Figure 5.2 Stress-strain diagram for different loading platen systems for two specimens of the same fibre type 65-35 and the same V_f = 1 % in uniaxial compression

5.3. Stress-strain curves for plain HPC

5.3.1. Uniaxial compression

Figure 5.3 shows stress-strain curves for plain HPC tested under different compressive load combinations. Both were measured in plane as mentioned before. The maximum strain was measured at ultimate stress which was also the failure point for the specimen.

With the final strain readings the Poisson's ratio can be calculated to be 0.28 at failure for plain HPC. This corresponds with the value which was earlier mentioned with the investigation of the Poisson's ratio for cylinders in the compression-tension test series for concrete with the same compressive strength. For the full Poisson's ratio development with increasing stress see Figure 5.5. The average of this curve can be calculated to be 0.25.

The Poisson's ratio curve in this example was almost vertical. This was not always the case. In fact the Poisson's ratio varied for some specimens within a large horizontal scatter and therefore only average values are meaningful. Especially at the beginning of each test up to about 10 % of the maximum load the scatter of the values was huge and made no sense.

For plain HPC in this study the discontinuity level was almost as high as the ultimate strength. By definition the discontinuity level is the point where the ratio between the principal tensile strain and the principal compressive strain is increasing or where the Poisson's ratio is starting to increase.

The Modulus of Elasticity for this specimen tested under uniaxial compression was found to be 45.8 kN/mm^2. This value corresponds with the value generated with standard tests on cylinders of the plain HPC batches of the compression-tension tests. The values were calculated as the tangent between stress and strain between 5 % and 40 % of the ultimate load. These limits were also recommended by ASTM, 'Standard Test Method for Static Modulus of Elasticity and Poisson's Ratio of Concrete in Compression', Designation: C 469-02 (2002), and indicate that the tangent between these limits should be fairly linear. Beneath the 5 % limit all kind of interferences at the start of a test could influence a proper value and above the 40 % limit the concrete specimen might become plastic and start failing.

Figure 5.4 shows the relationship between the sums of in-plane stress ($\sigma_2+\sigma_3$) to in-plane strains ($\varepsilon_2+\varepsilon_3$) recorded for plain HPC. The relationship is the sum of the stress and strain readings of the two in plane axis for each individual

specimen. Note that information is mostly available from the two in plane axis in the direction of the load. The third, out of plane, axis was only recorded for the first four tested batches of specimens by using LVDTs.

From those readings the conclusion can be drawn that the third axis behaves in terms of strain and deformational behaviour as the unloaded second axis in a uniaxial test. See therefore the stress-strain diagrams of the first four batches (1 % 65-35 in batch 1 and 2 and 1 % 45-30 in batch 3 and 4) in the next paragraph where LVDT measurements were used to monitor the deformation in the third direction.

5.3.2. Biaxial compression

As discussed in Chapter 3, the load proportion of the two axes was not always constant throughout the biaxial compression tests and therefore the final stress ratio at failure point varies around the target values of 0.25, 0.50, 0.75 and 1.00 for the biaxial compression tests.

The introduction of a second principal stress σ_2 affects the strain readings in the direction of the major principal stress σ_3 considerably. While the ratio between σ_2/σ_3 increases from 0 (uniaxial compression) to 1.00 (biaxial compression) the strain reading in the major principal direction decrease for a given stress level, see Figure 5.3.

The maximum ultimate strength is reached at a stress ratio between σ_2/σ_3 = 0.25 and 0.75. In Figure 5.3 the maximum ultimate strength was reached for a stress ratio σ_2/σ_3 = 0.75. It should be noted that these stress-strain graphs express the readings of individual tests and that for an overall picture the average of several tests is important. Therefore the previous findings of a maximum ultimate strength at σ_2/σ_3 = 0.5 are correct.

The relationship of the sum of in-plane stress to in-plane strain for all tested plain HPC specimens shows a fairly linear behaviour from the start of the tests until failure point. This and the almost linear stress-strain recordings until failure point indicate a high proportional limit. It can be concluded that the material behaves fairly homogeneous with a constant Modulus of Elasticity E_c and Poisson's ratio ν. This can be observed in Figure 5.4 where the sum of the in-plane stress is plotted above the sum of the in-plane strain. The graphs are linear until failure and close together which indicates the same Modulus of Elasticity E_c and Poisson's ratio ν for all tested specimens for different stress ratios σ_2/σ_3. Therefore the beginning of unstable crack propagation with microcracks increasing through the matrix could not be observed.

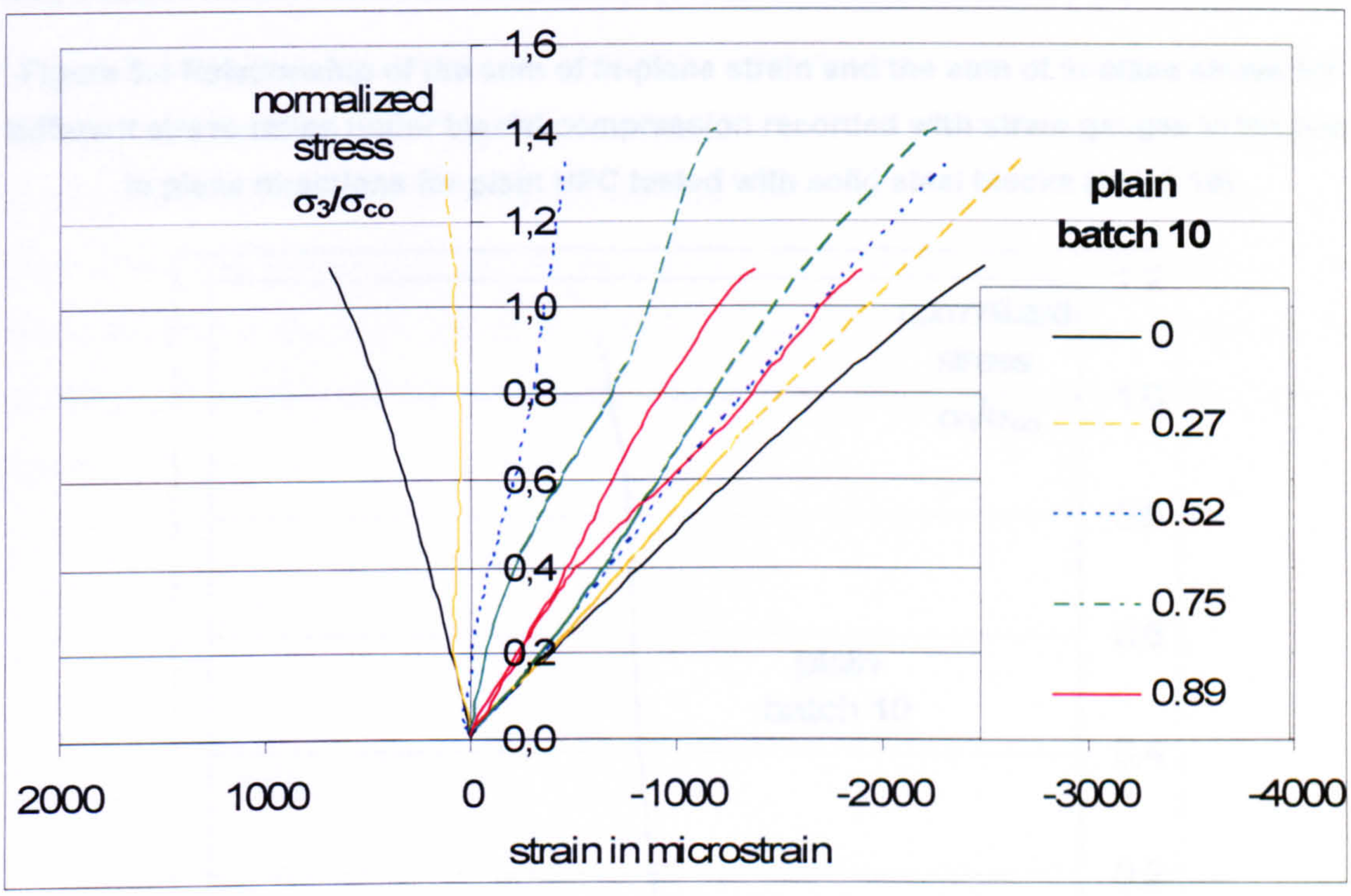

Figure 5.3 Stress-strain relationship for different stress ratios under biaxial compression recorded with strain gauges for plain HPC tested with solid steel blocks (batch 10)

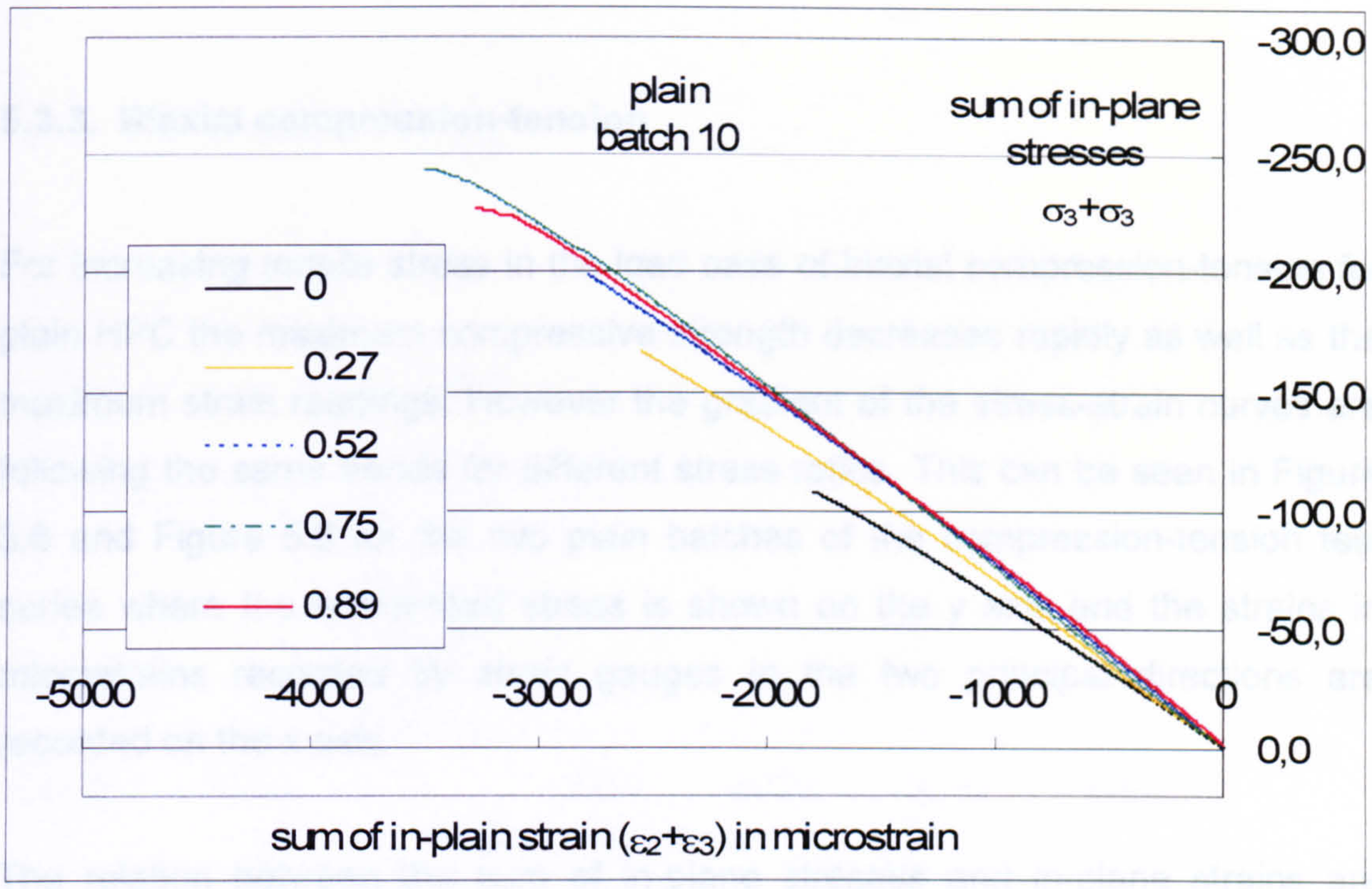

Figure 5.4 Relationship of the sum of in-plane strain and the sum of in-plane stress for different stress ratios under biaxial compression recorded with strain gauges in the two in plane directions for plain HPC tested with solid steel blocks (batch 10)

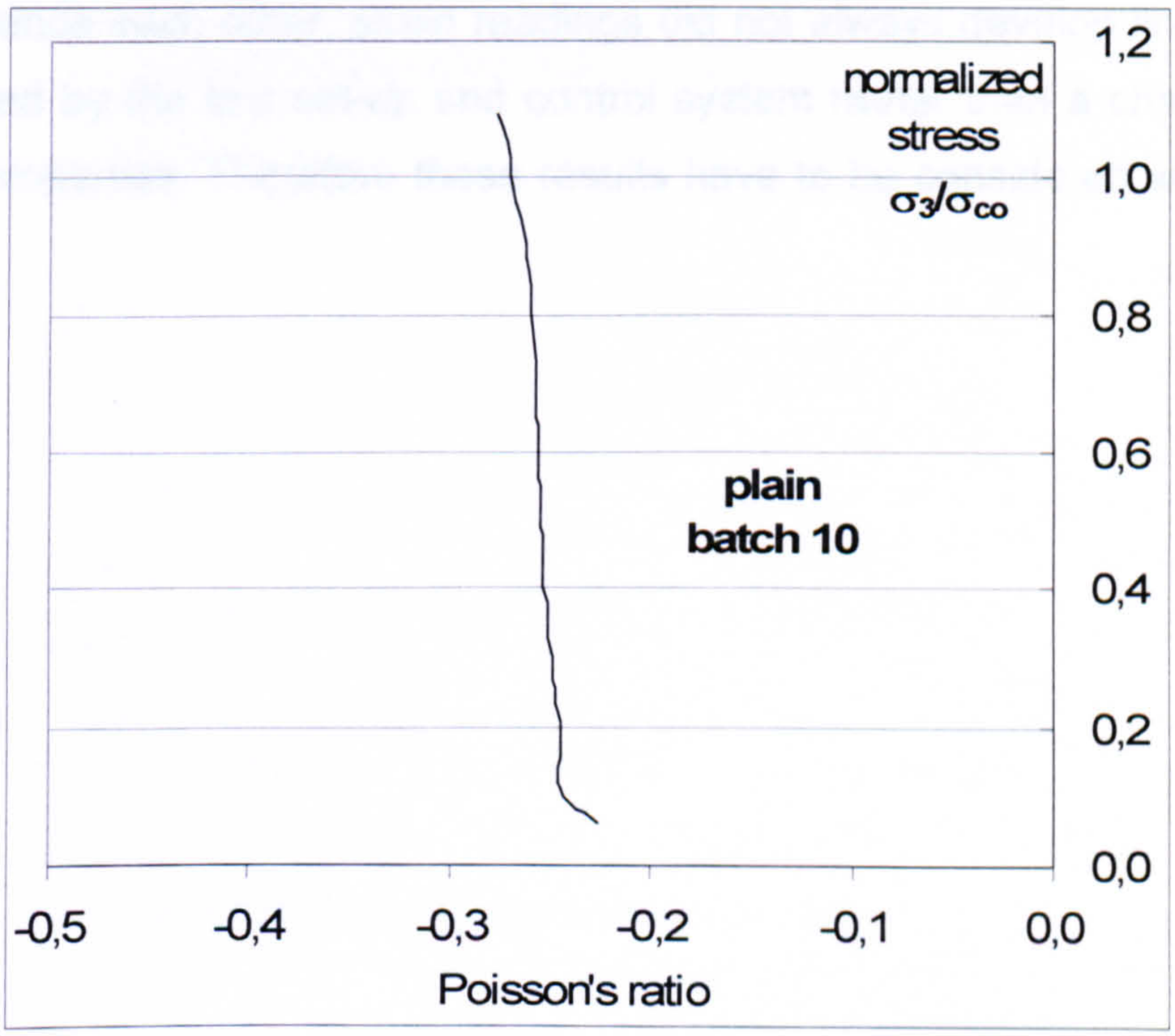

Figure 5.5 Poisson's ratio versus normalised stress in uniaxial compression recorded with strain gauges in the two in plane directions for plain HPC tested with solid steel blocks (batch 10)

5.3.3. Biaxial compression-tension

For increasing tensile stress in the load case of biaxial compression-tension for plain HPC the maximum compressive strength decreases rapidly as well as the maximum strain readings. However the gradient of the stress-strain curves are following the same trends for different stress ratios. This can be seen in Figure 5.6 and Figure 5.8 for the two plain batches of the compression-tension test series where the normalised stress is shown on the y axis and the strains in microstrains recorded by strain gauges in the two principal directions are recorded on the x axis.

The relation between the sum of in-plane stresses and in-plane strains are shown in Figure 5.7 for one of the plain concrete batches in the compression-tension test series. The tangent of all graphs is fairly the same at the beginning of each test for different compression-tension stress ratios. Because the two axes influence each other, strain readings did not always develop linearly. This was caused by the test set-up and control system rather than a change in the material properties. Therefore these results have to be considered with a great warning.

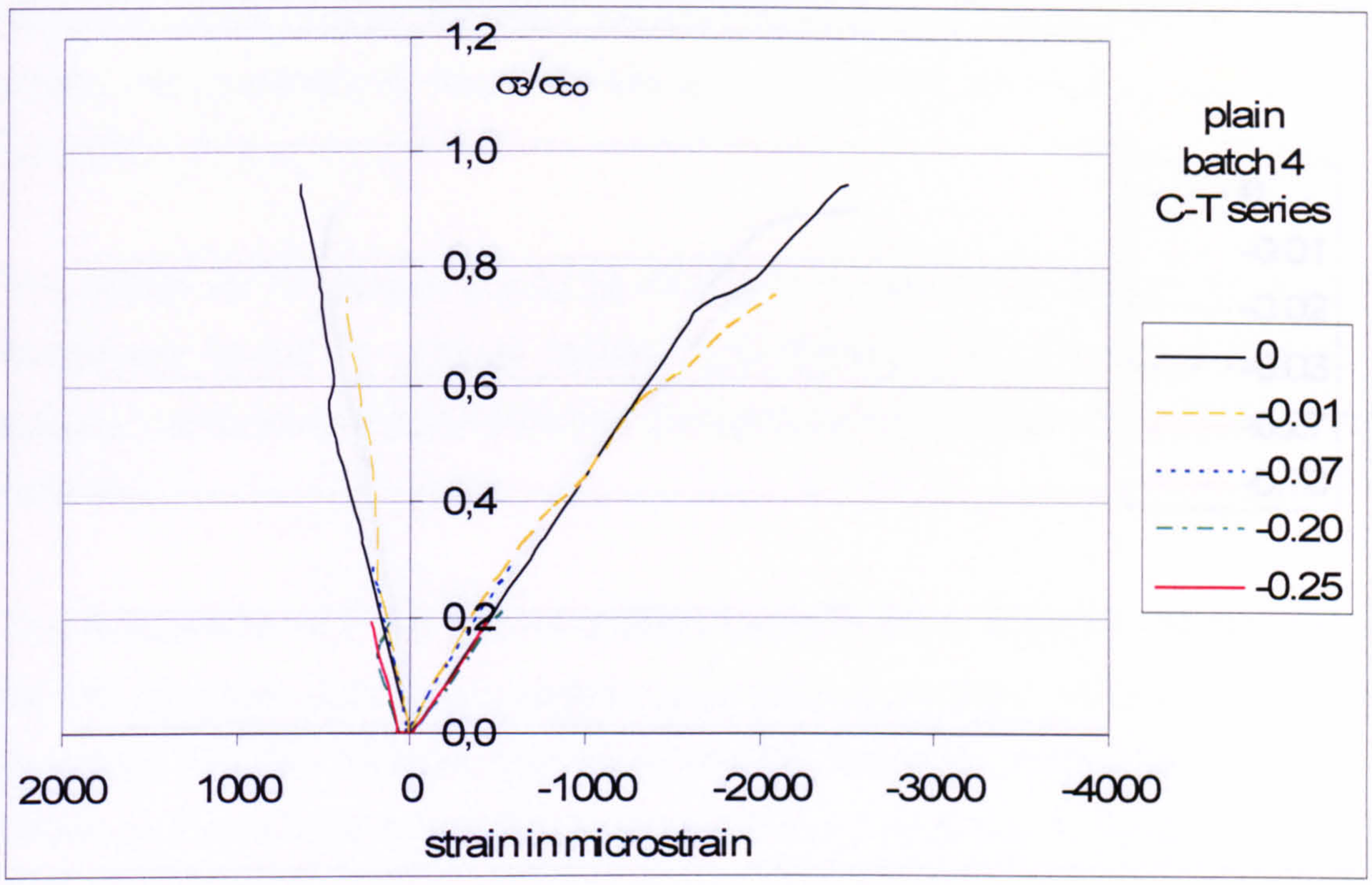

Figure 5.6 Stress-strain relationship for different stress ratios under biaxial compression-tension recorded with strain gauges for plain HPC tested with solid steel blocks (batch 4)

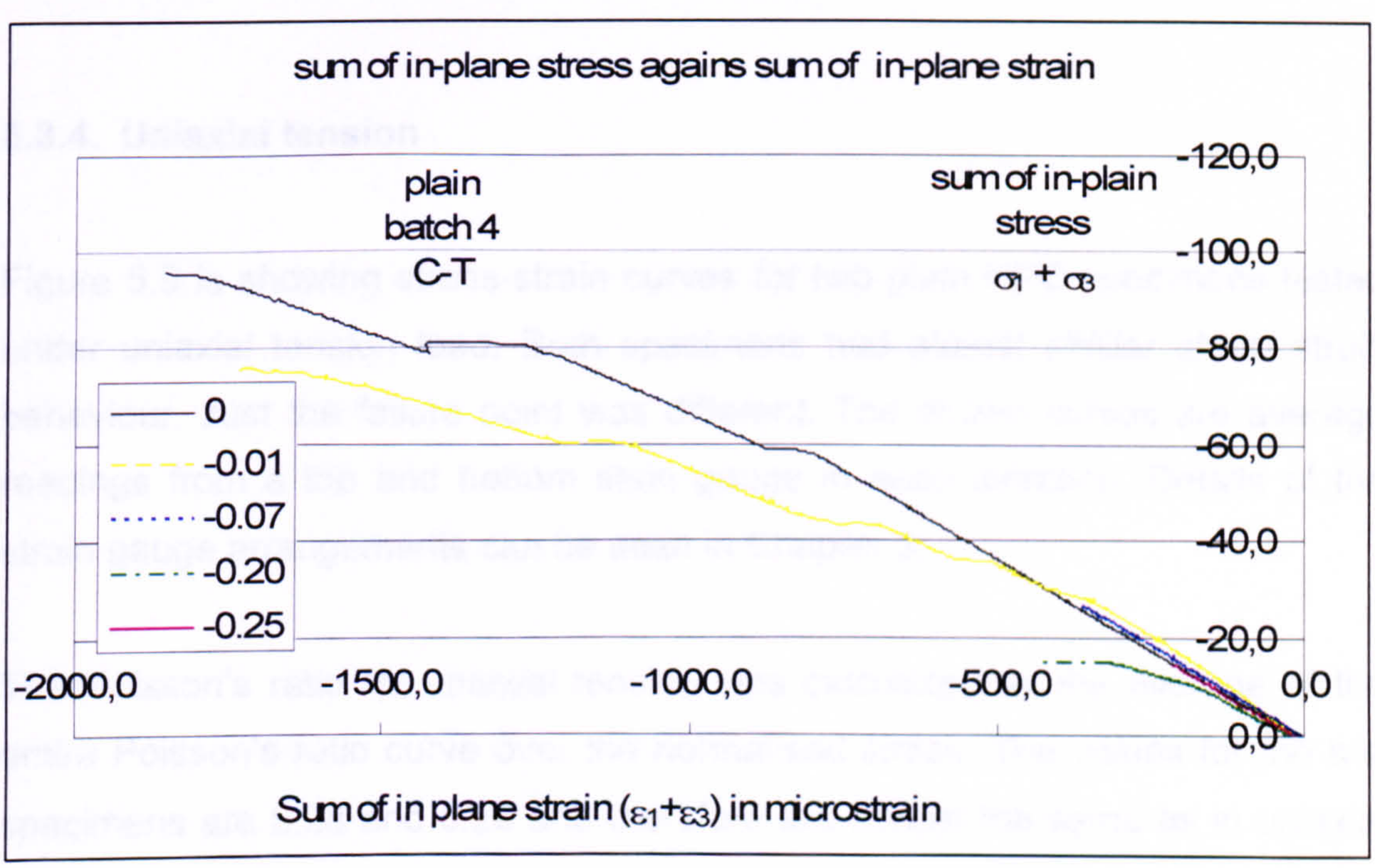

Figure 5.7 Relationship between the sums of in-plane stress and in-plane strain for different stress ratios under biaxial compression-tension recorded with strain gauges in the two in plane directions for plain HPC tested with solid steel blocks (batch 4)

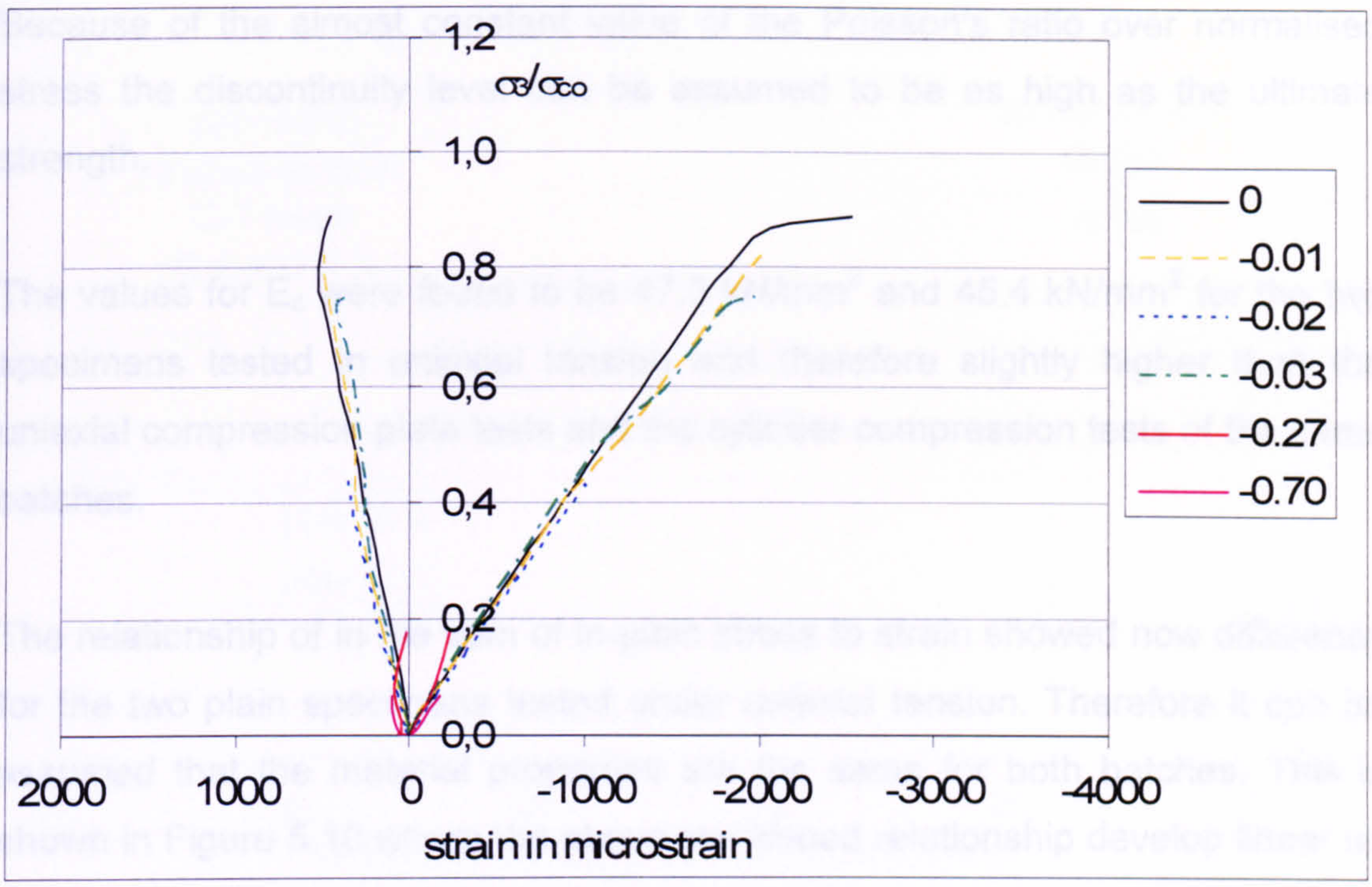

Figure 5.8 Stress-strain relationship for different stress ratios under biaxial compression-tension recorded with strain gauges for plain HPC tested with solid steel blocks (batch 5)

5.3.4. Uniaxial tension

Figure 5.9 is showing stress-strain curves for two plain HPC specimens tested under uniaxial tension load. Both specimens had almost similar stress-strain behaviour. Just the failure point was different. The shown curves are average readings from a top and bottom stain gauge in each direction. Details of the strain gauge arrangements can be seen in Chapter 3.

The Poisson's ratio for uniaxial tension was calculated as the average of the entire Poisson's ratio curve over the normalised stress. The values for the two specimens are 0.28 and 0.29 and therefore are almost the same as in uniaxial compression. The curves are shown in Figure 5.11 where they almost developed simultaneously.

Because of the almost constant value of the Poisson's ratio over normalised stress the discontinuity level can be assumed to be as high as the ultimate strength.

The values for E_c were found to be 47.3 kN/mm^2 and 45.4 kN/mm^2 for the two specimens tested in uniaxial tension and therefore slightly higher than the uniaxial compression plate tests and the cylinder compression tests of the same batches.

The relationship of in the sum of in-plain stress to strain showed now difference for the two plain specimens tested under uniaxial tension. Therefore it can be assumed that the material properties are the same for both batches. This is shown in Figure 5.10 where the above mentioned relationship develop linear up to the failure point.

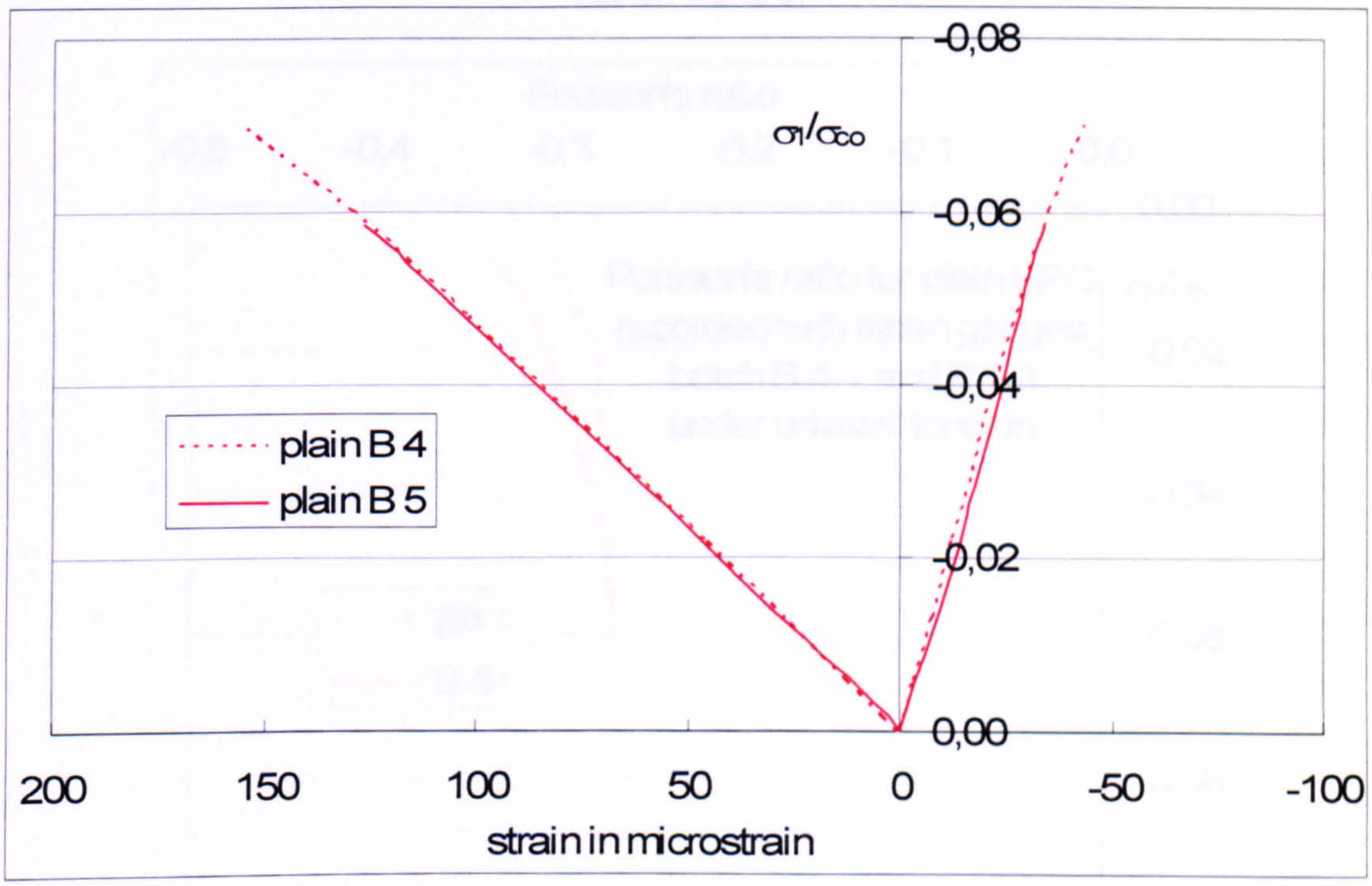

Figure 5.9 Stress-strain relationship for uniaxial tension recorded with strain gauges for plain HPC (batch 4 and 5)

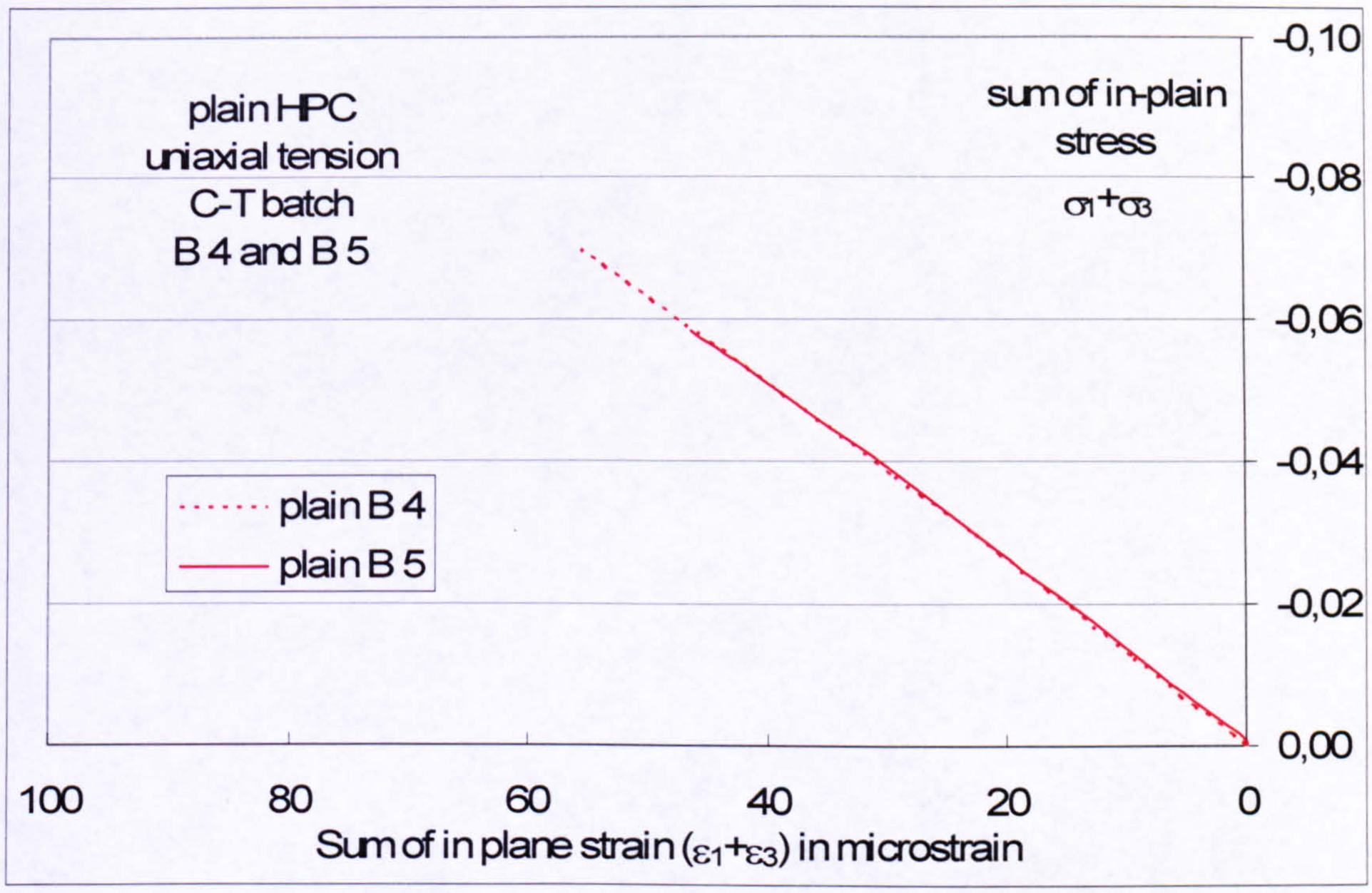

Figure 5.10 Relationship of the sum of in-plane stress to the sum of in-plain strain for uniaxial tension recorded with strain gauges in the two in plane directions for plain HPC (batch 4 and 5)

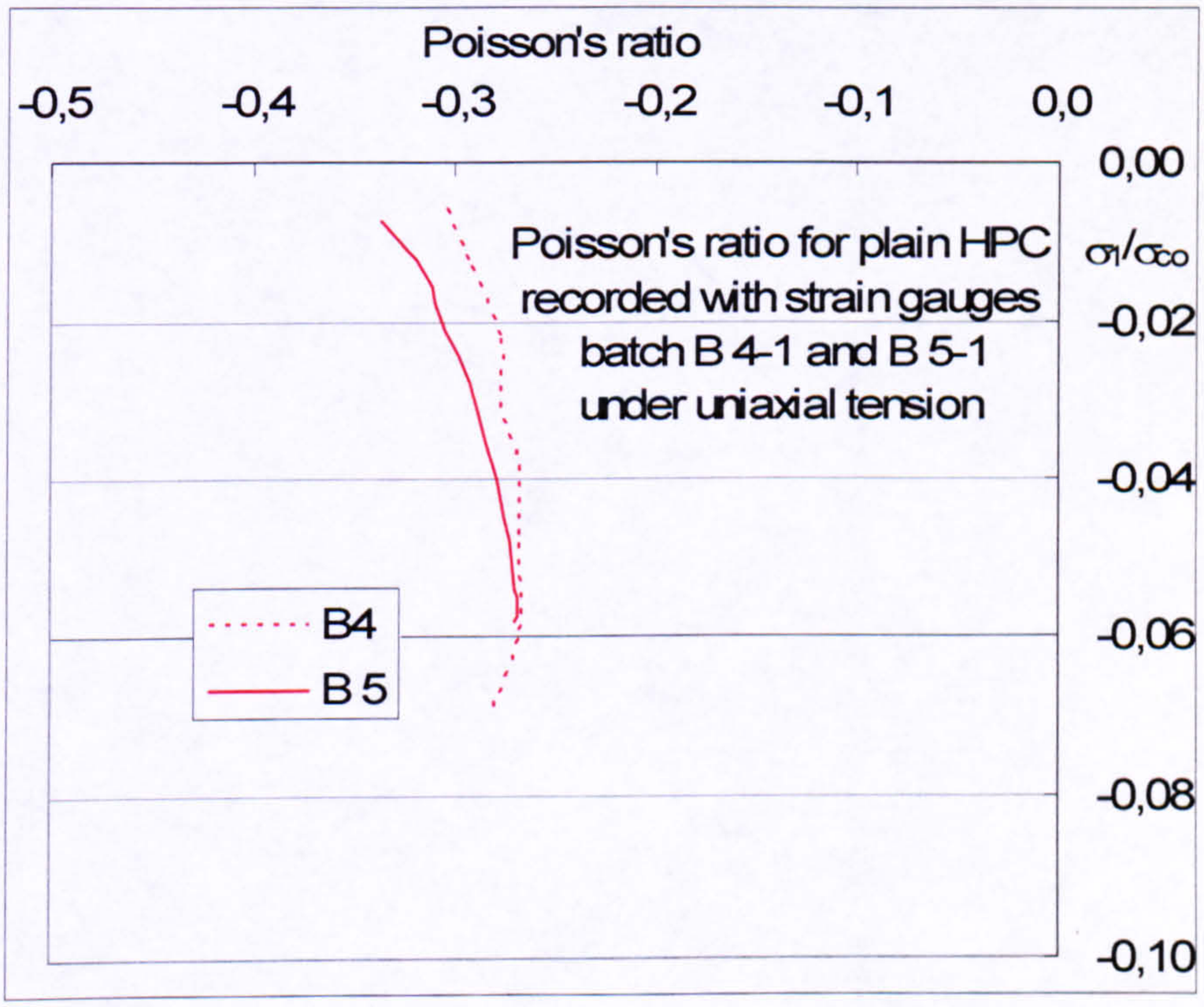

Figure 5.11 Poisson's ratio versus normalised stress in uniaxial tension recorded with strain gauges in the two in plane directions for plain HPC (batch 4 and 5)

5.4. Stress-strain curves for SFRHPC

A full record of stress-strain relationships, Poisson's ratio and most of the the relationships between the sum of in-plain stress to strain for the different fibre types and fibre volume fractions for all stress ratios σ_2/σ_3 can be found in Appendix 1 of this thesis.

5.4.1. Uniaxial compression

Under uniaxial compression all tested specimens with all different fibre types and volume fractions V_f create similar stress-strain curves. This can be examined in Figure 5.12 to Figure 5.15 for the compression-compression test series where the fibre specimens for each V_f are compared independently to the plain specimen (red lines in all four graphs).

The same result can be seen in Figure 5.20 for the compression-tension test series where all tested fibre types in the two fibre volume fraction V_f = 1 % and 2 % and plain HPC are expressed together in one graph. On the y-axis is the normalised compressive stress shown where on the x-axis are strains in microstrain recorded. The lines are close together indicating similar behaviour.

Only for the compression-tension test series the stress strain readings varies a bit more which is caused by the specimen shape. The extent beyond the loaded area between the compression steel blocks in the unloaded direction affects the results slightly and lead to greater scatter in the readings. Another reason for the observed scatter can be the strain gauges which might not be properly attached to the specimens' surface or one of the strain gauges might be glued on the specimen with a fibre or a coarse aggregate near the surface influencing the reading.

The maximum strain readings are between -2150 and -3500 microstrain in the direction of loading and 600 and 1500 microstrain in the unloaded direction. These values are also depending on the ultimate strength of the tested specimen and the behaviour close to failure point. Some specimens showed a more ductile behaviour than others. Even some specimens perform a more ductile behaviour close to failure the overall performance is more linear until failure. Therefore the proportional limit is also high.

Another value to compare the different fibre concretes with the plain HPC is E_c. These values give an idea of the actual gradient of the stress-strain graphs in the direction of loading between 5 % and 40 % of the ultimate strength of each individual specimen tested in uniaxial compression. As expected from the stress strain investigation the values are close together with a maximum of 46.3 kN/mm^2 and a minimum of 40.6 kN/mm^2. The value for plain HPC is 45.8 kN/mm^2 which is close to the higher range. These values are fully listed in paragraph 4.1.3.

Closely related to the above topic is the Poisson's ratio. The value varies between 0.23 and 0.34 with no trend obvious for any fibre type or fibre volume fraction. These values are the average of the complete Poisson's ratio versus stress graph which are presented in the Appendix. The overall list with all values for different fibre types can be found together with E_c in paragraph 4.1.3.

A summary of all Poisson's' ratio developments over normalised strains can be seen in Figure 5.22 for uniaxial compression specimens in the compression-tension test series. The overall average between the different fibre types and fibre volume fractions is 0.28. That is slightly higher than the value found by the cylinder investigation which had an overall average of 0.23. Note that the concrete strength for the cylinder tests was lower with less restraining effects involved. Moreover the different size and the ratio between length and height of the cylinders and plates seem to have an influence.

As shown in Figure 5.16 to Figure 5.19 the relationship between the sum of the in-plain strains to the neutralised uniaxial stress does not change significantly between plain and steel fibre HPC in all tested volume fraction. This indicates similar Modulus of Elasticity E_c and Poisson's ratio ν. Figure 5.21 is showing similar trends for the compression-tension series whereas the previous mentioned graphs are showing the results for the compression-compression test series. Each of these graphs contains the sum of in-plane strain recordings over normalised stress for one fibre type in different fibre volume fractions for the compression-compression test series and all measured in-plane strain readings in one graph for the compression-tensions series. The in-plane strain was calculated as the average from the two strain gauge measurements in each of the principal directions. The red line indicates the plain specimen in all five graphs.

It can be observed that the lines are linear until almost the failure point and that no obvious trend can be found for all the used fibre types. Moreover it should be stated that all tested fibre type concretes behave similarly to the plain specimen under uniaxial compression. For the compression-tension test series there might be some boundary effect involved caused by the extended specimen beyond the loading surface of the compression steel block.

As with plain HPC the discontinuity level is about 90 % of the maximum load capacity of most of the fibre specimens. However this value, like ν is not always meaningful and has to be handled with great care. Only overall observation can be made with no obvious trend occurring.

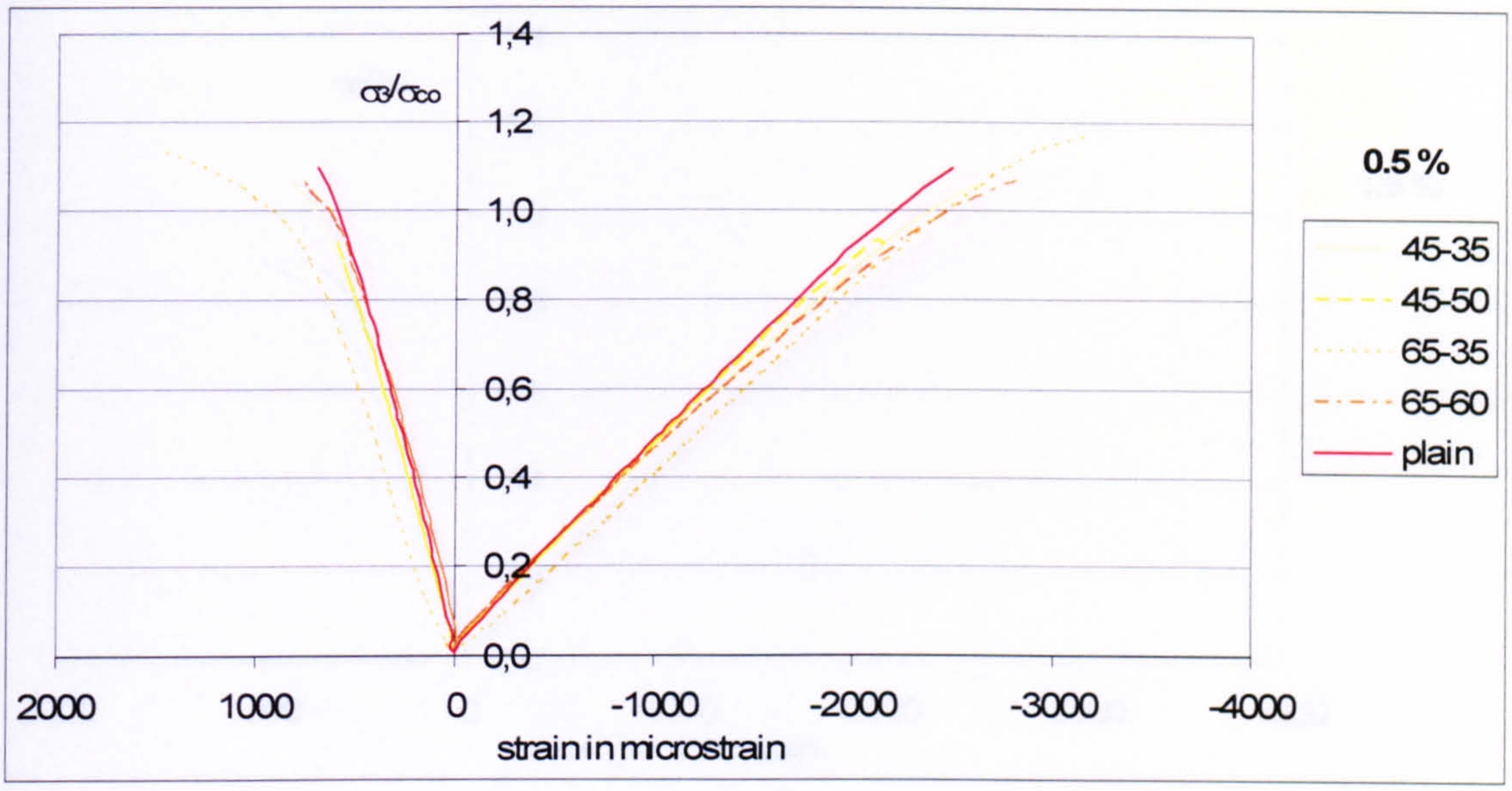

Figure 5.12 Stress-strain relationship for specimens under uniaxial compression with different fibre types of the fibre volume V_f = 0.5 % and plain HPC recorded with strain gauges and tested with solid steel blocks

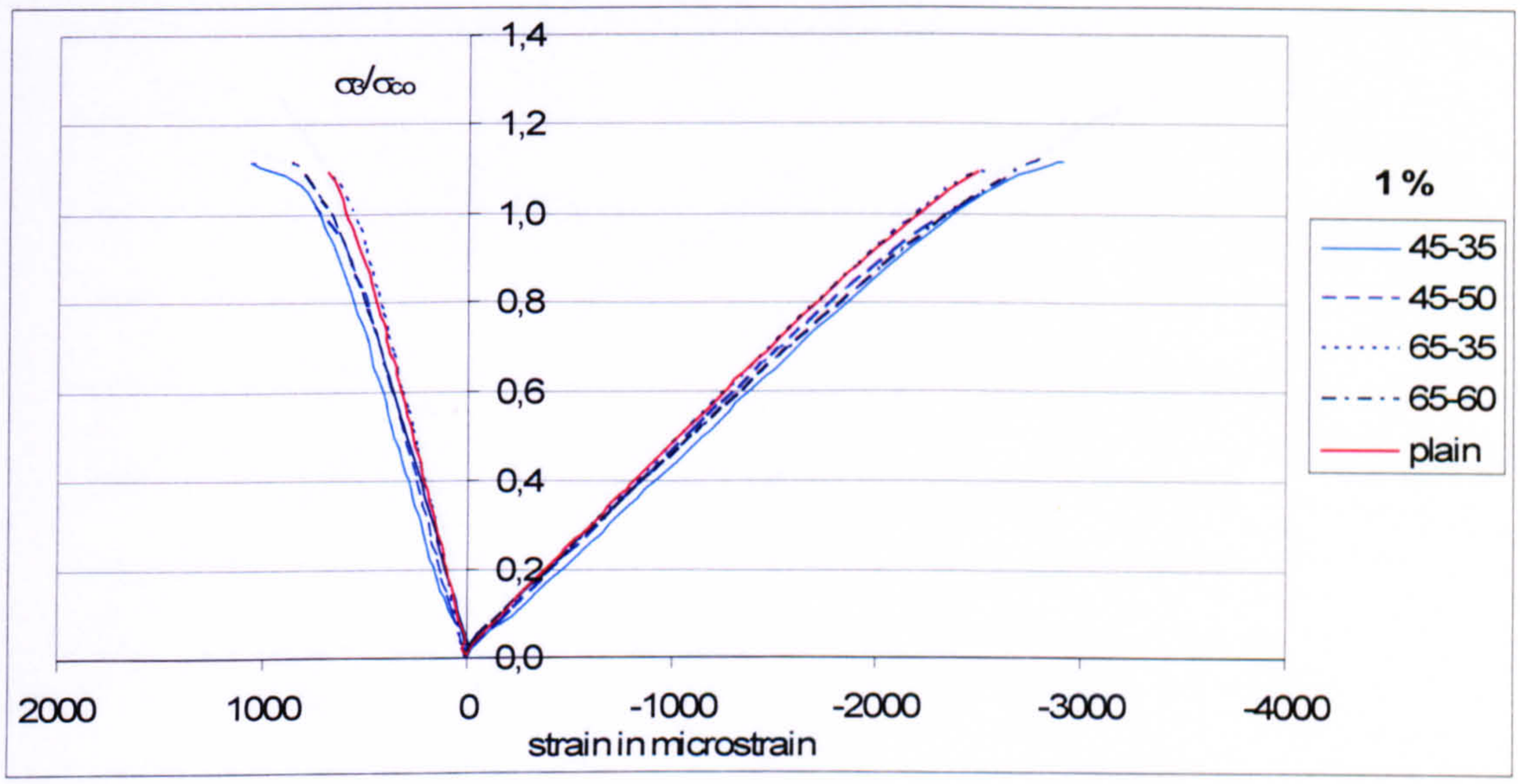

Figure 5.13 Stress-strain relationship for specimens under uniaxial compression with different fibre types of the fibre volume V_f = 1 % and plain HPC recorded with strain gauges and tested with solid steel blocks

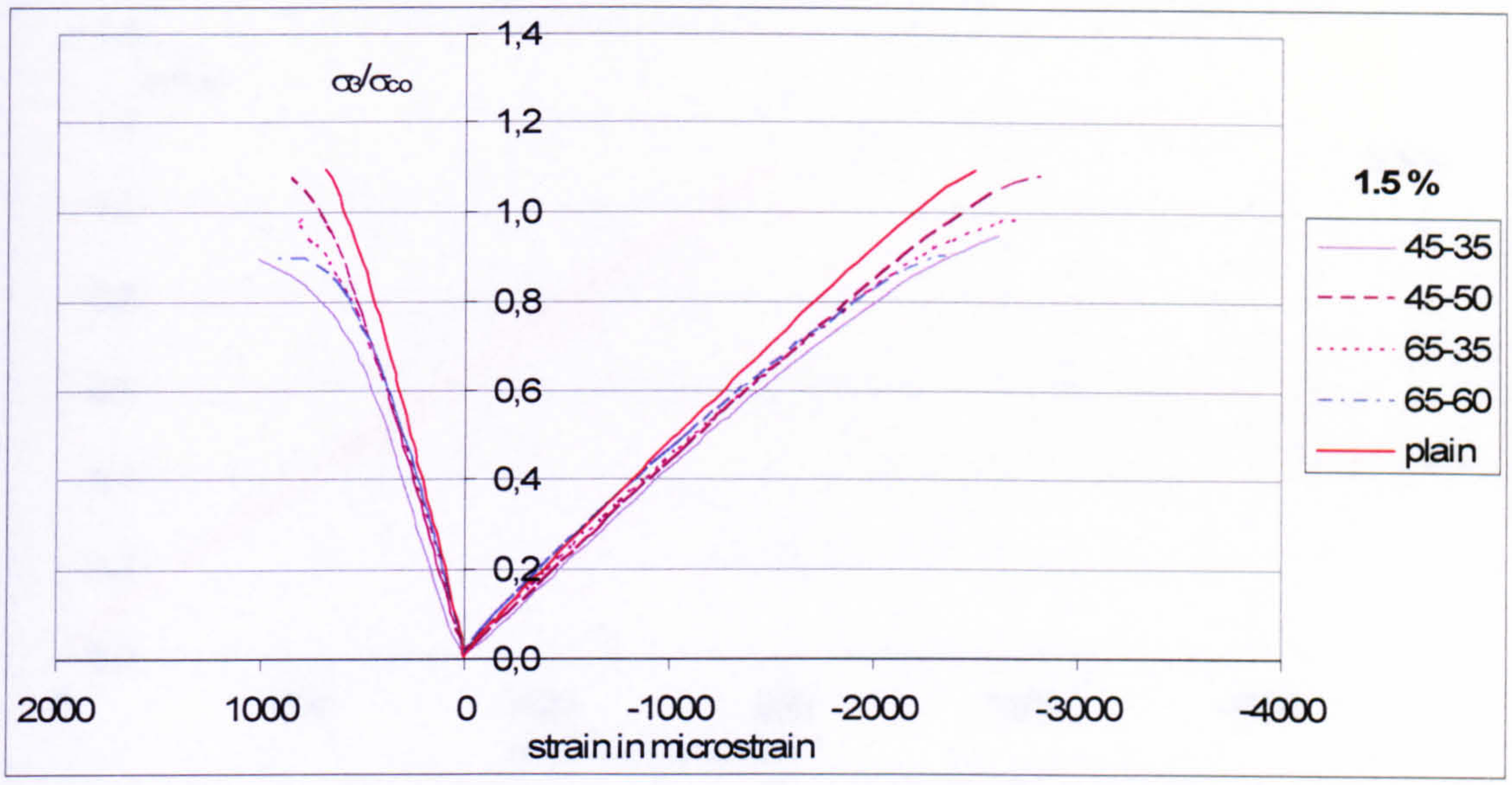

Figure 5.14 Stress-strain relationship for specimens under uniaxial compression with different fibre types of the fibre volume V_f = 1.5 % and plain HPC recorded with strain gauges and tested with solid steel blocks

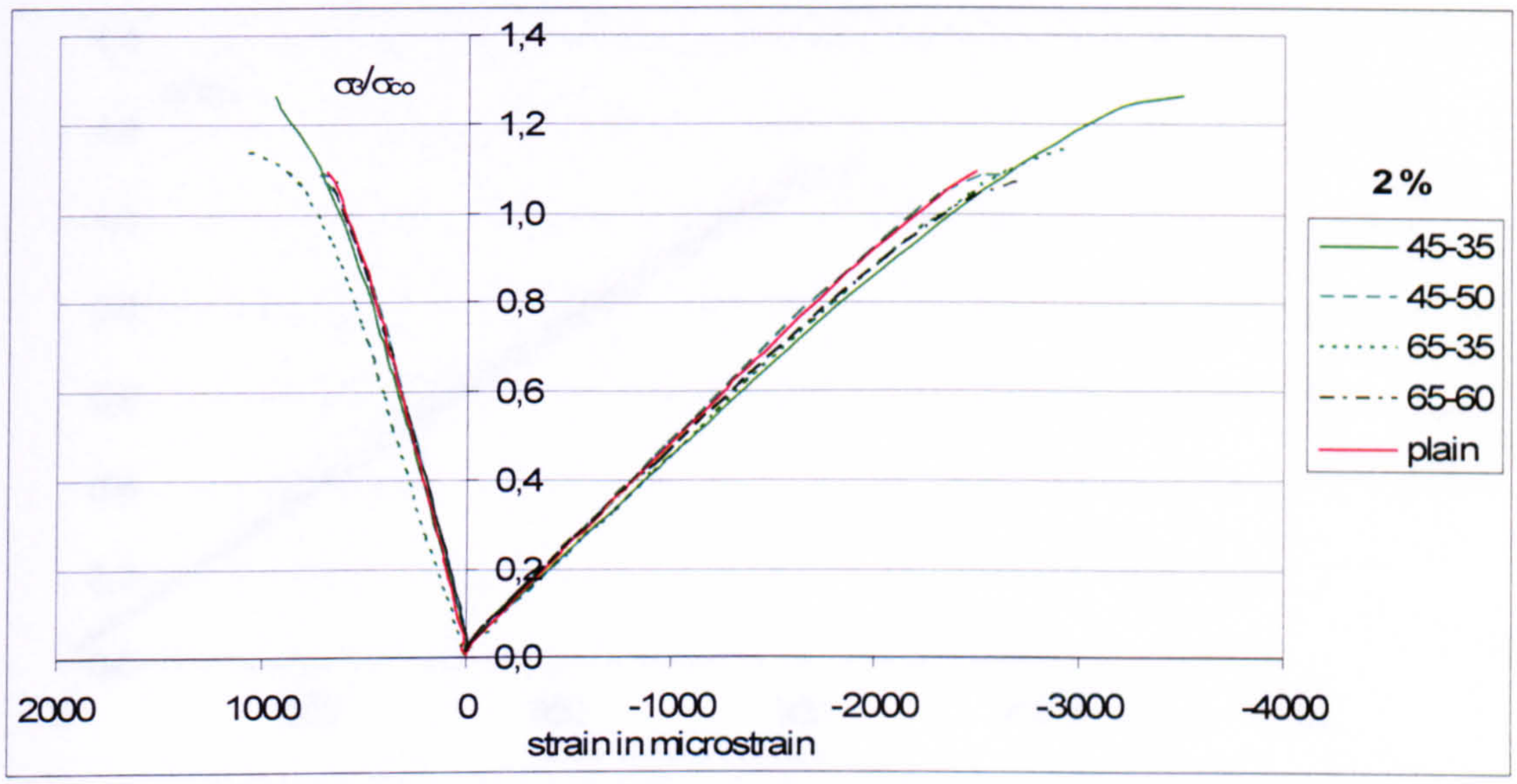

Figure 5.15 Stress-strain relationship for specimens under uniaxial compression with different fibre types of the fibre volume V_f = 2 % and plain HPC recorded with strain gauges and tested with solid steel blocks

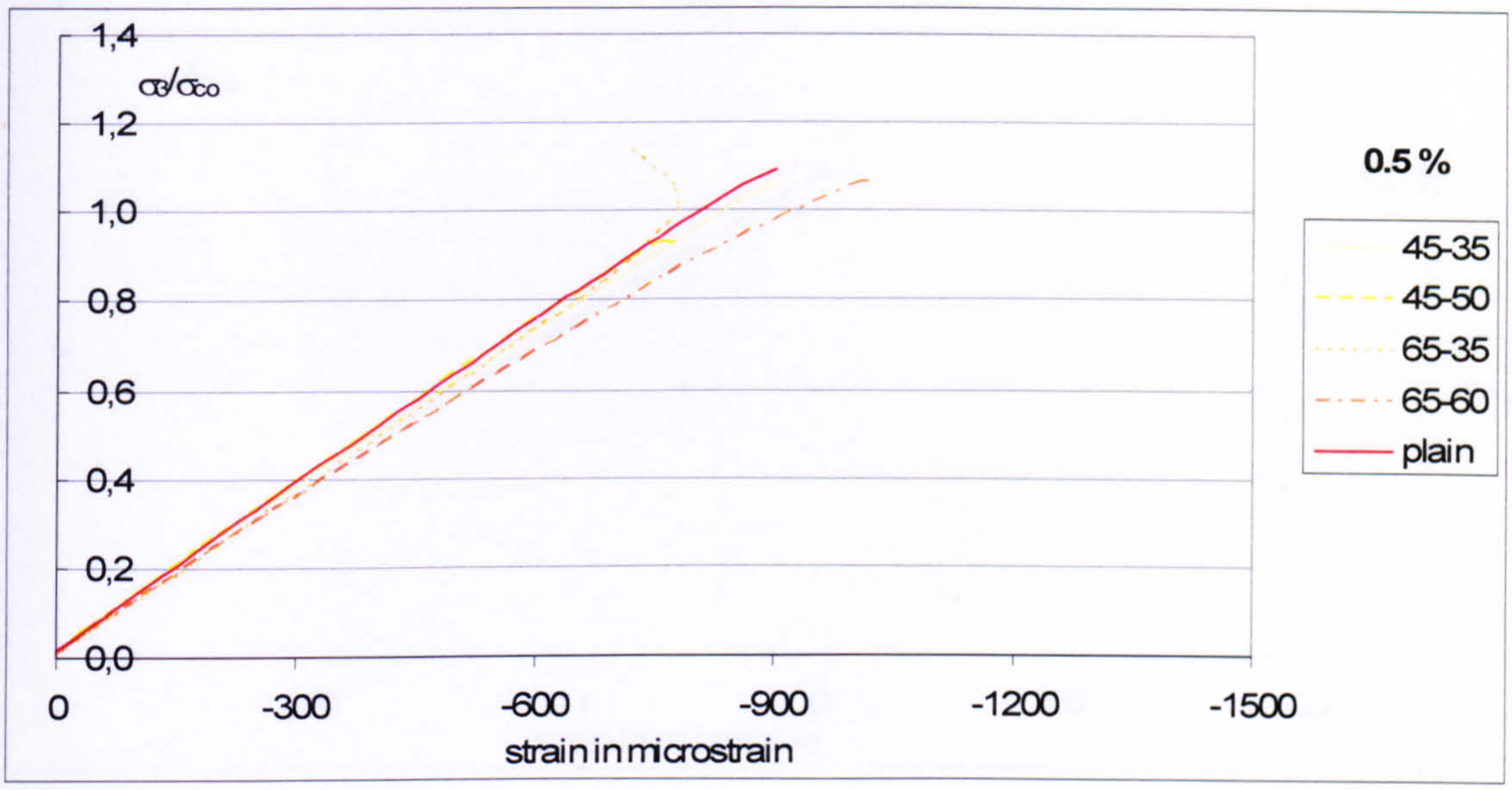

Figure 5.16 Sum of in-plane strains for specimens under uniaxial compression with different fibre types of the same fibre volume fraction V_f = 0.5 % and plain HPC recorded with strain gauges in the two in plane directions tested with solid steel blocks

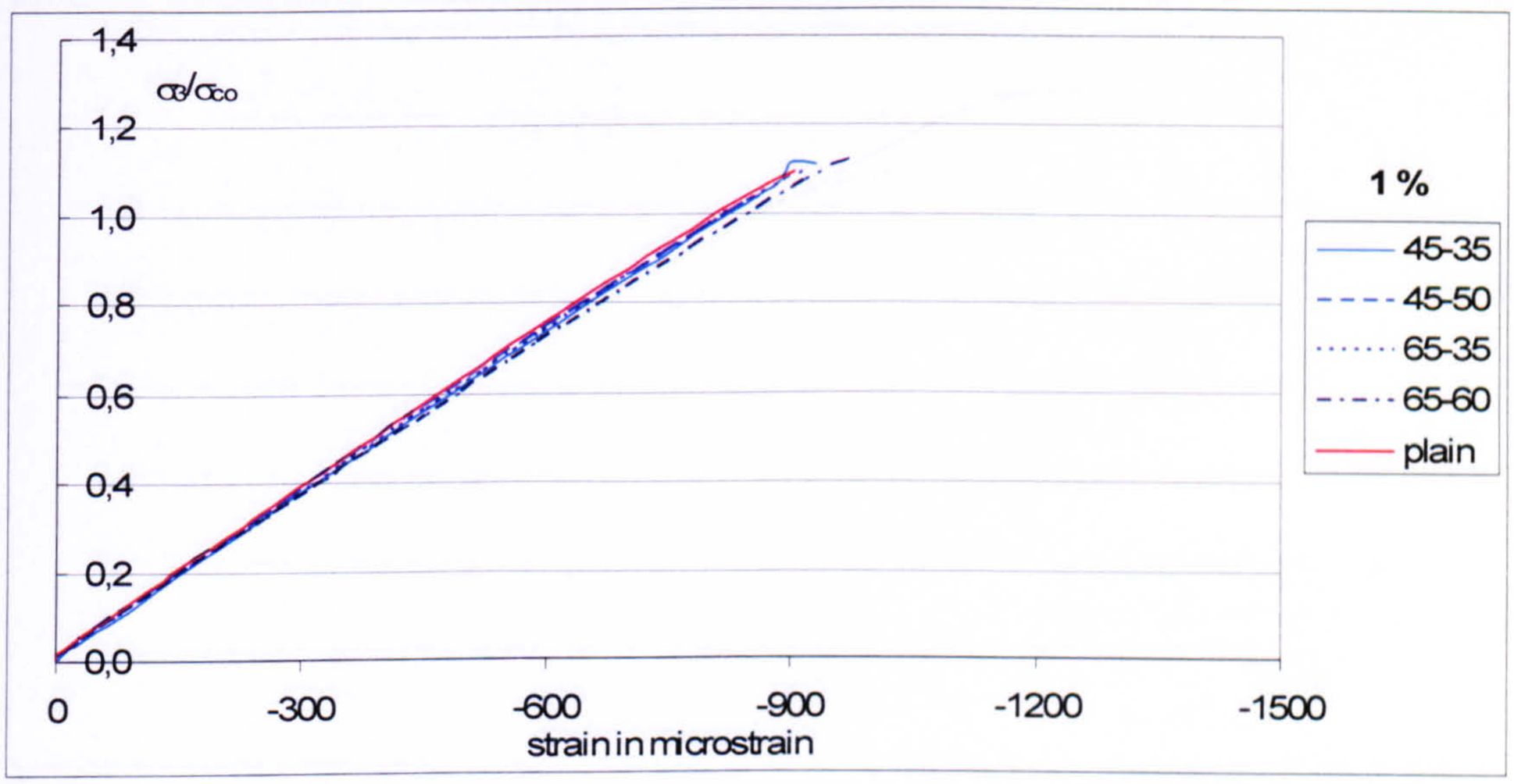

Figure 5.17 Sum of in-plane strains for specimens under uniaxial compression with different fibre types of the same fibre volume fraction V_f = 1 % and plain HPC recorded with strain gauges in the two in plane directions tested with solid steel blocks

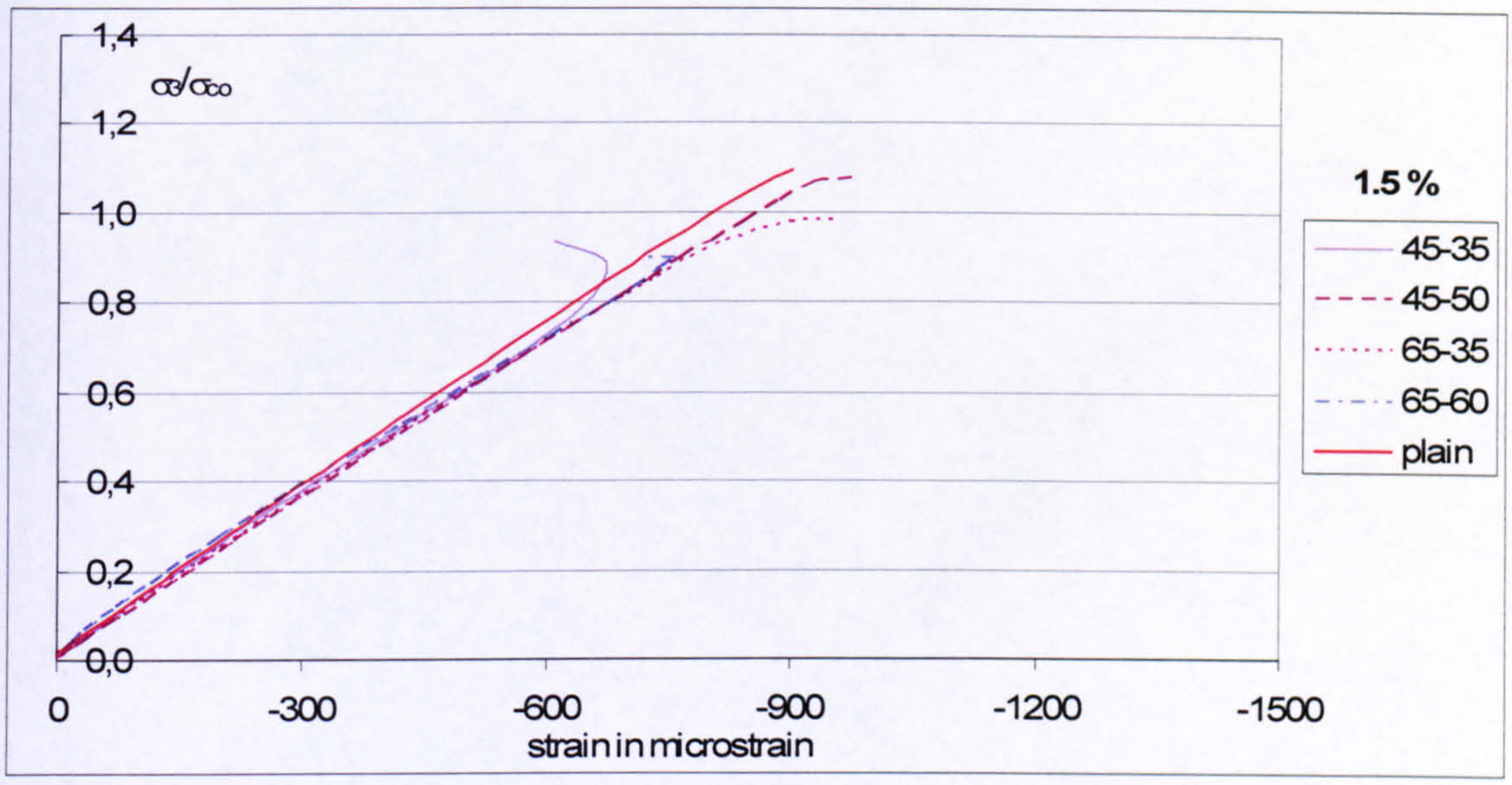

Figure 5.18 Sum of in-pane strains for specimens under uniaxial compression with different fibre types of the same fibre volume fraction V_f = 1.5 % and plain HPC recorded with strain gauges in the two in plane directions tested with solid steel blocks

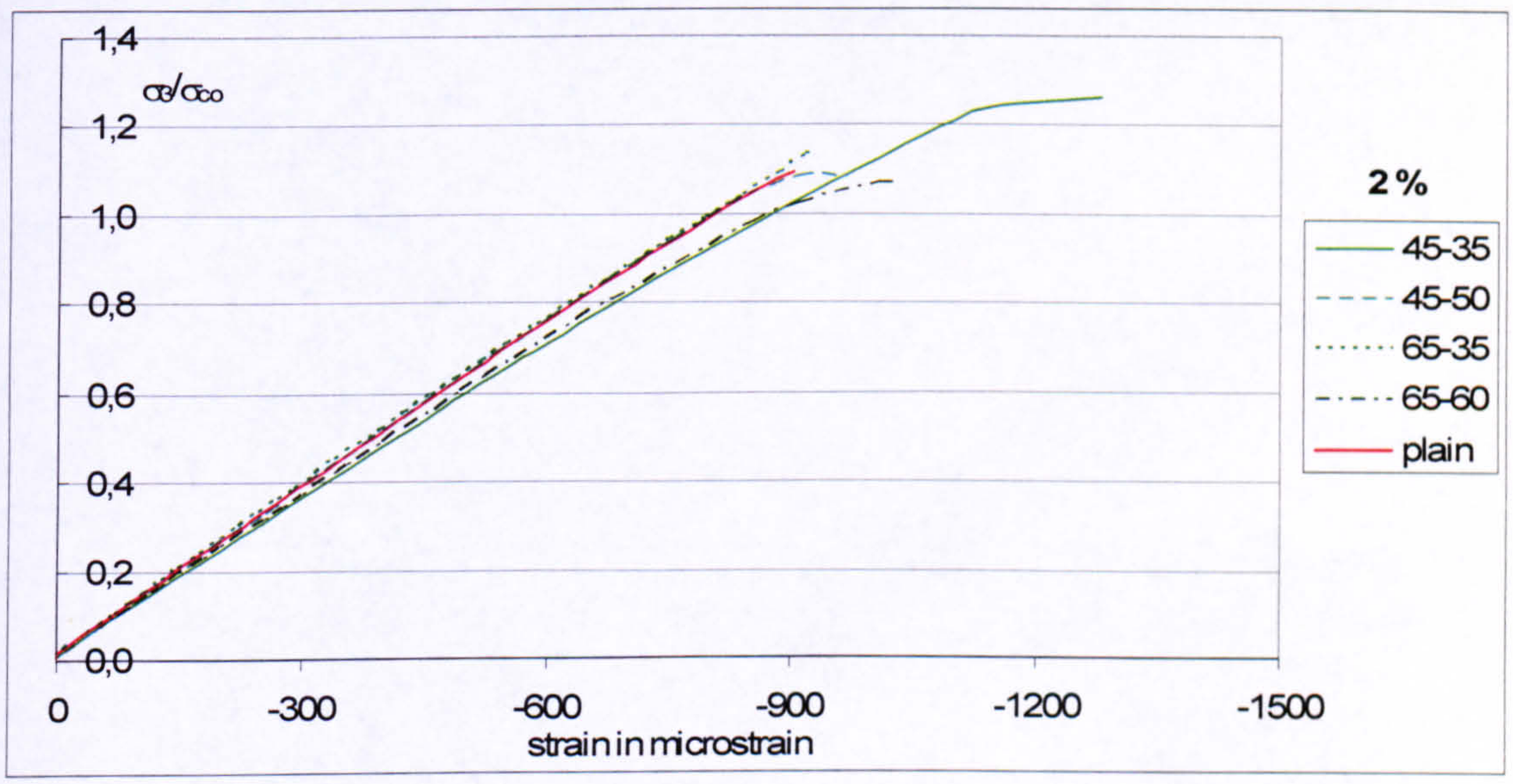

Figure 5.19 Sum of in-plane strains for specimens under uniaxial compression with different fibre types of the same fibre volume fraction V_f = 2 % and plain HPC recorded with strain gauges in the two in plane directions tested with solid steel blocks

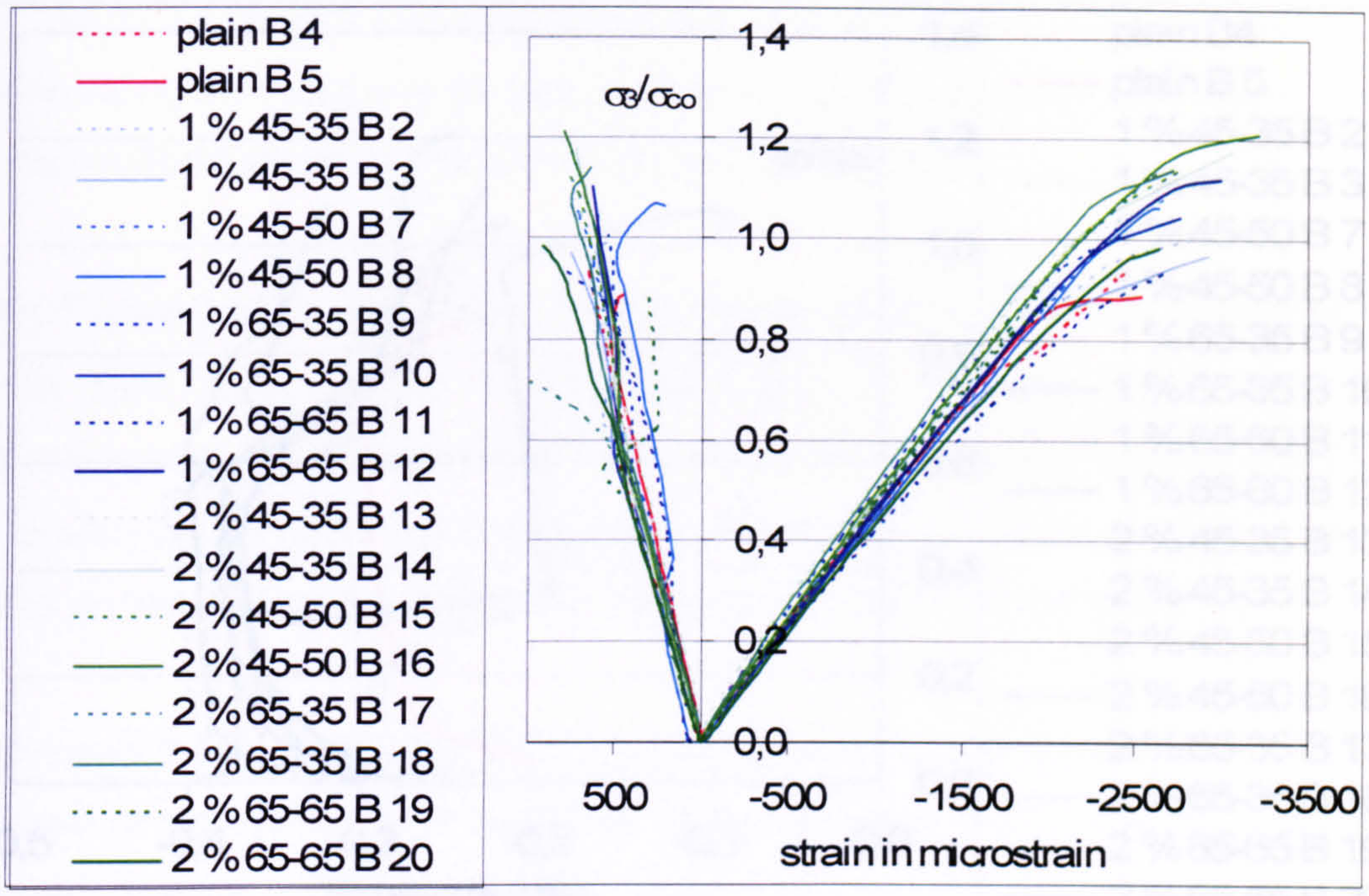

Figure 5.20 Stress-strain relationship for specimens under uniaxial compression of the compression-tension test series with different fibre types and different fibre volume V_f = 1 %, 2 % and plain HPC recorded with strain gauges and tested with solid steel blocks

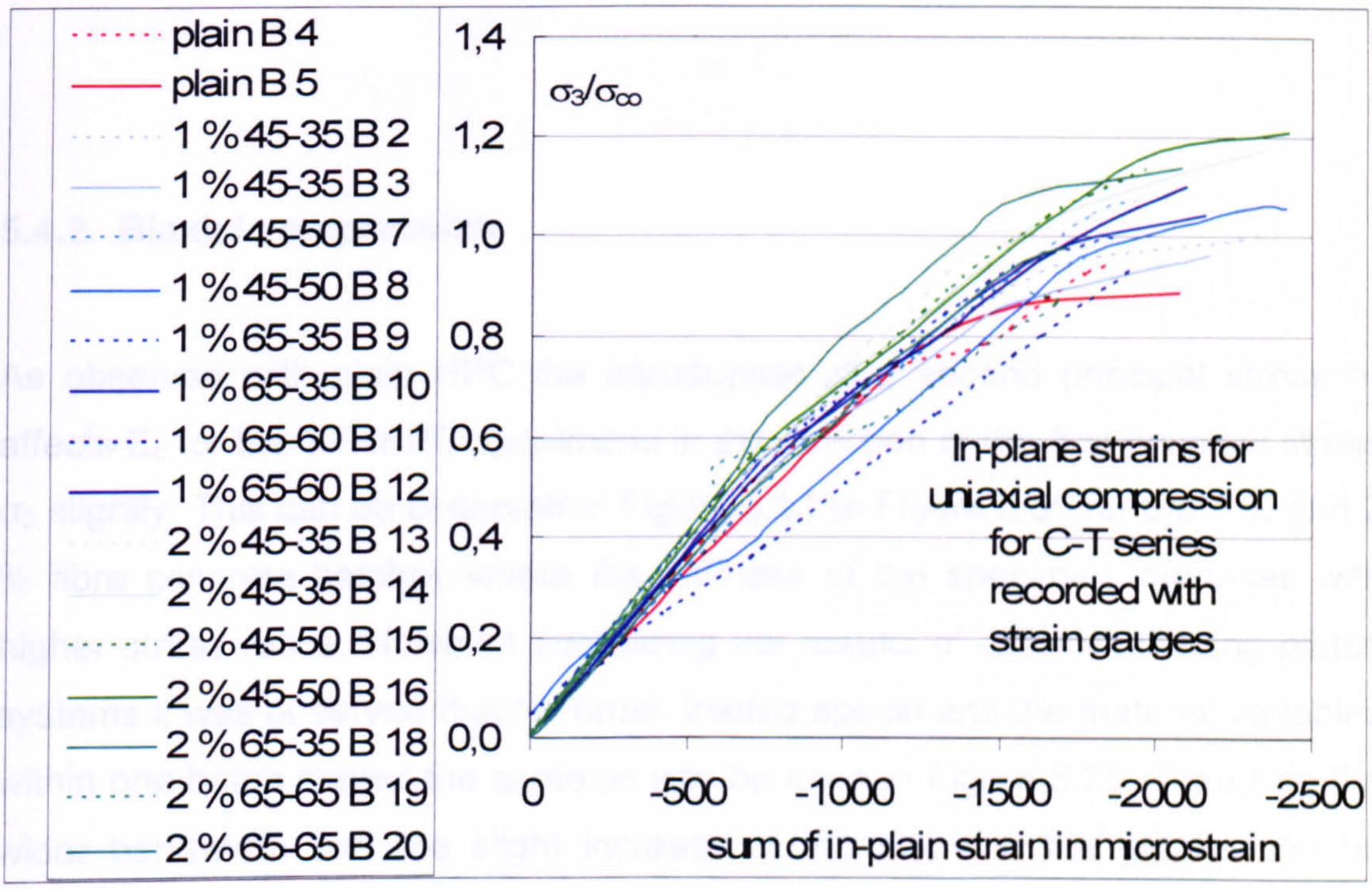

Figure 5.21 Sum of in-plain strains for specimens under uniaxial compression from the compression-tension test series with different fibre types and different fibre volume fraction V_f = 1 %, 2 % and plain HPC recorded with strain gauges in the two in plane directions tested with solid steel blocks

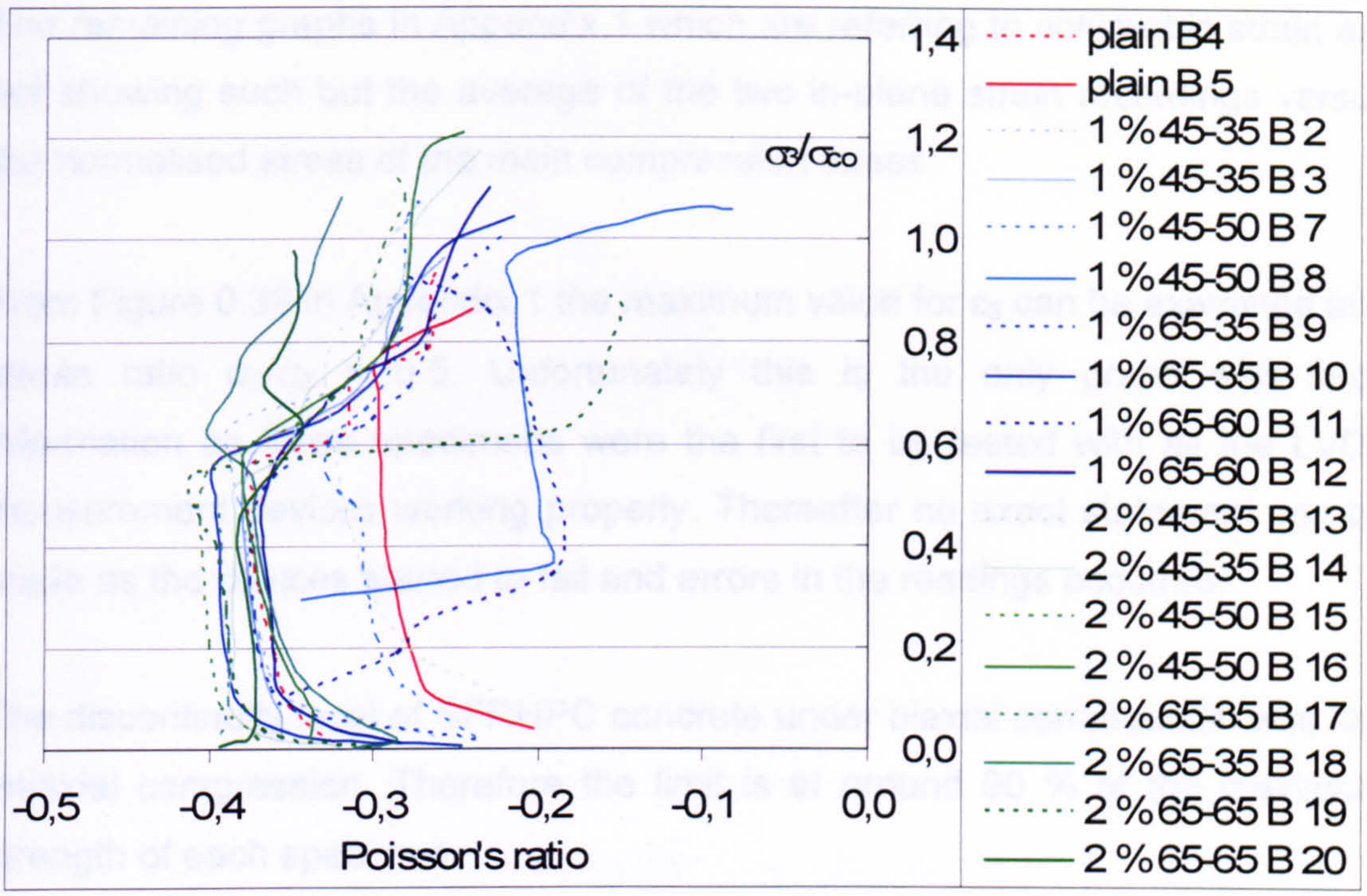

Figure 5.22 Poisson's ratio versus normalised stress in uniaxial compression recorded with strain gauges in the two in plane directions for different fibre types of the fibre volume V_f = 1 %, 2 % and plain HPC for the compression-tension test series

5.4.2. Biaxial compression

As observed with plain HPC the introduction of a second principal stress σ_2 affects E_c for the SFRHPC specimens in the direction of the first principal stress σ_3 slightly. This can be observed in Figure 5.23 to Figure 5.30 for the 1 % and 2 % fibre concrete batches where the stiffness of the specimen increases with higher stress ratios. However comparing the results of different loading platen systems it was observed that for brush loaded specimens the material variables within one batch stayed the same as can be seen in Figure 5.25. Therefore the wider bandwidth and the slight increase in the slope in the graphs can be attributed to the solid steel block platens and not to the change of material properties such as Modulus of Elasticity E_c and Poisson's ratio.

The remaining graphs in Appendix 1 which are referring to volumetric strain are not showing such but the average of the two in-plane strain recordings versus the normalised stress of the main compression stress.

From Figure 0.38 in Appendix 1 the maximum value for ε_3 can be examined at a stress ratio σ_2/σ_3 = 0.5. Unfortunately this is the only graph with such information as these specimens were the first to be tested with all the LVDT measurement devices working properly. Thereafter no exact statement can be made as the devices started to fail and errors in the readings occurred.

The discontinuity level of SFRHPC concrete under biaxial compression was like uniaxial compression. Therefore the limit is at around 90 % of the maximum strength of each specimen.

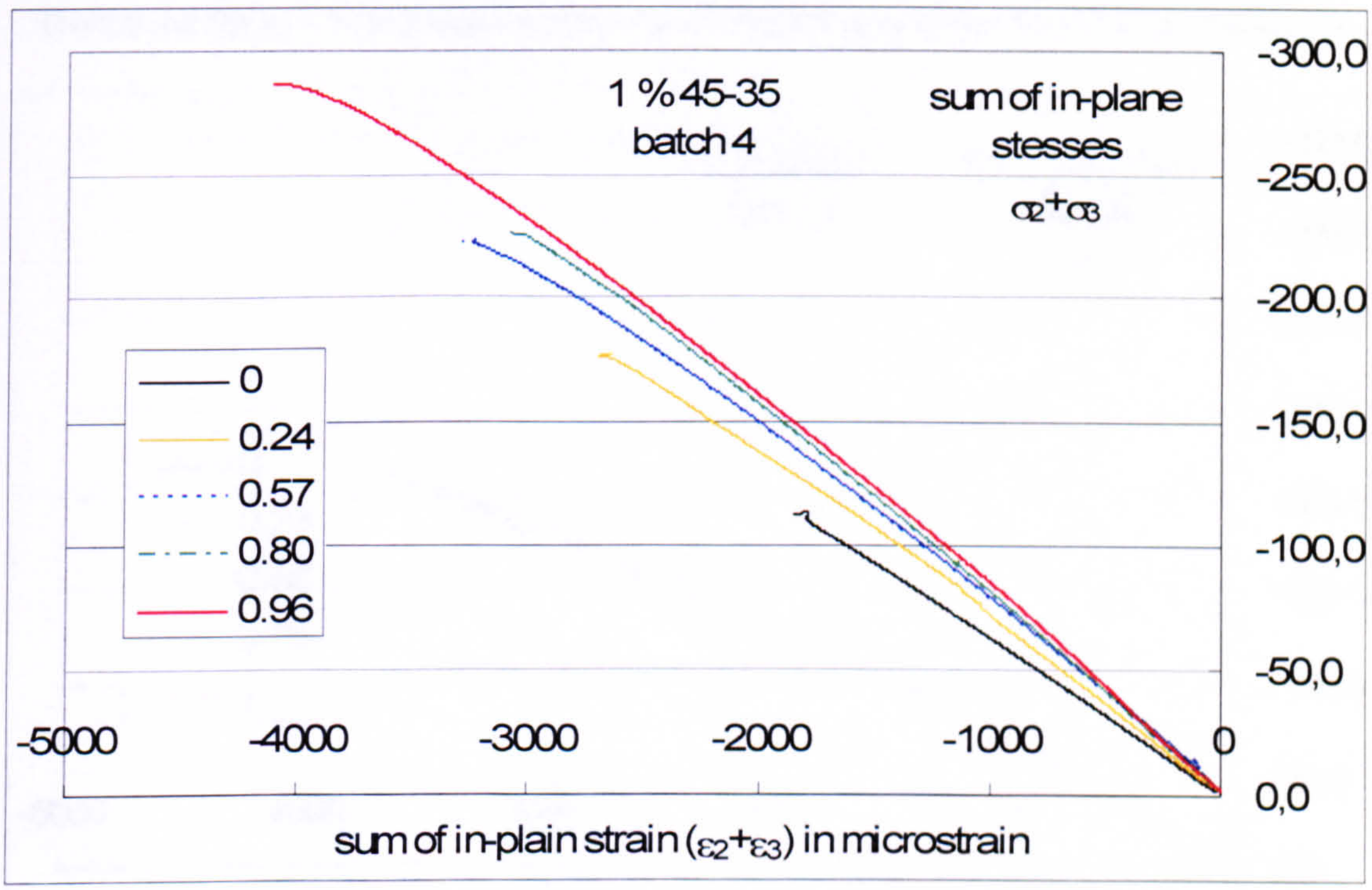

Figure 5.23 Relationship of the sum of in-plane strain and stress for different stress ratios under biaxial compression recorded with strain gauges in the two in plane directions for Vf = 1 % of the fibre type 45-35 tested with solid steel blocks (batch 04)

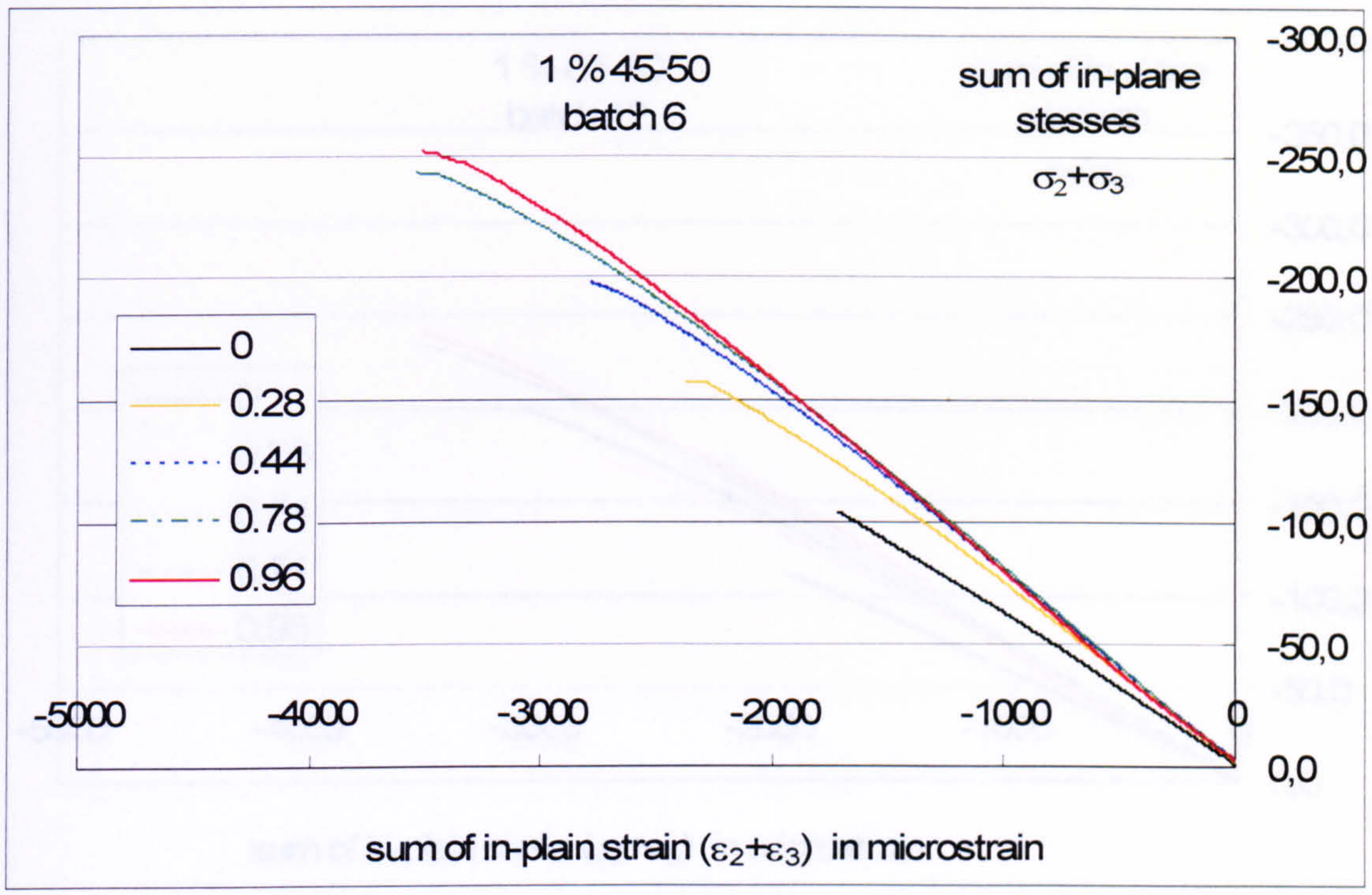

Figure 5.24 Relationship of the sum of in-plane strain and stress for different stress ratios under biaxial compression recorded with strain gauges in the two in plane directions for V_f = 1 % of the fibre type 45-50 tested with solid steel blocks (batch 06)

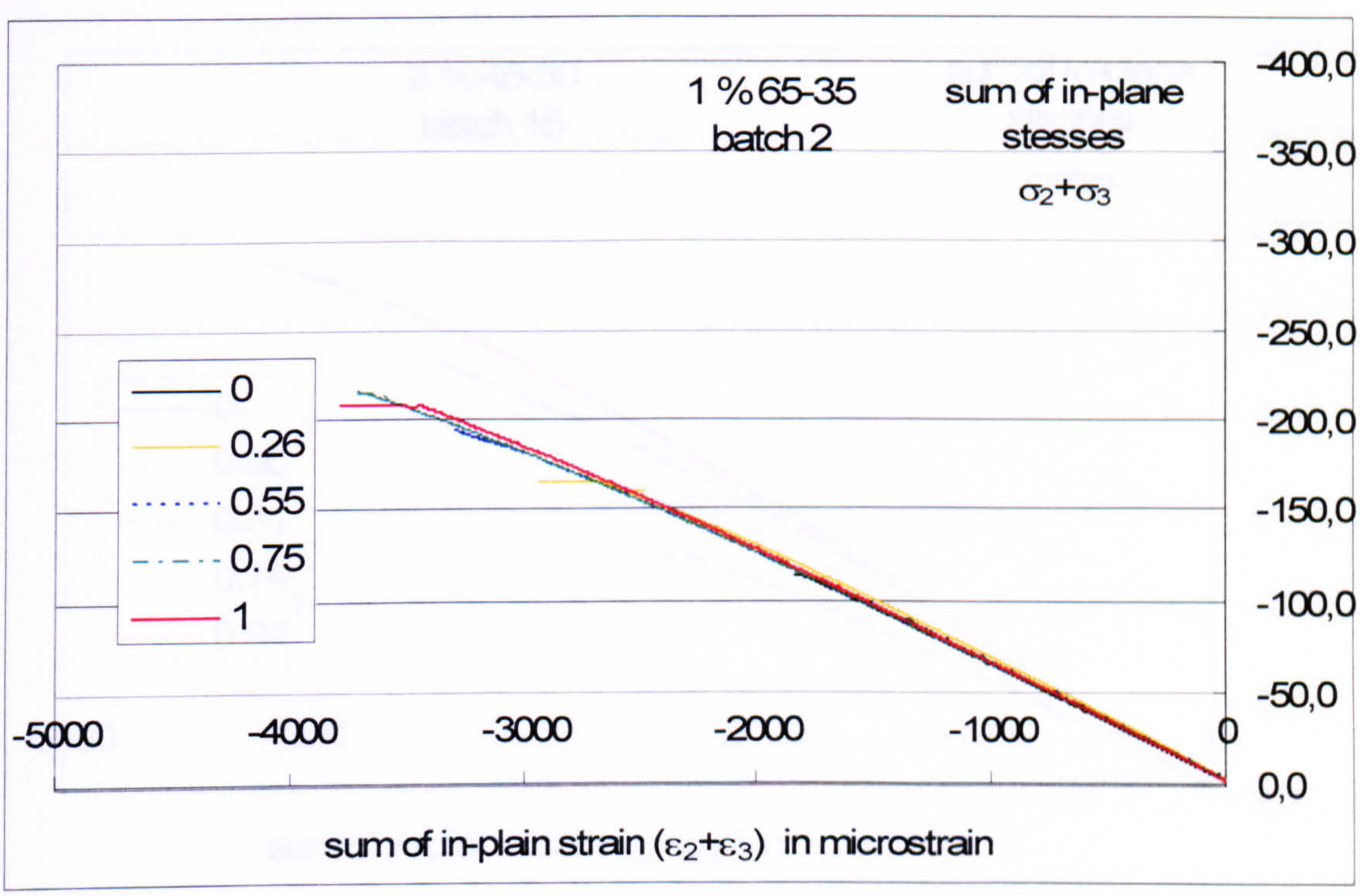

Figure 5.25 Relationship of the sum of in-plane strain and stress for different stress ratios under biaxial compression recorded with strain gauges in the two in plane directions for V_f = 1 % of the fibre type 65-35 tested with brush platen system (batch 02)

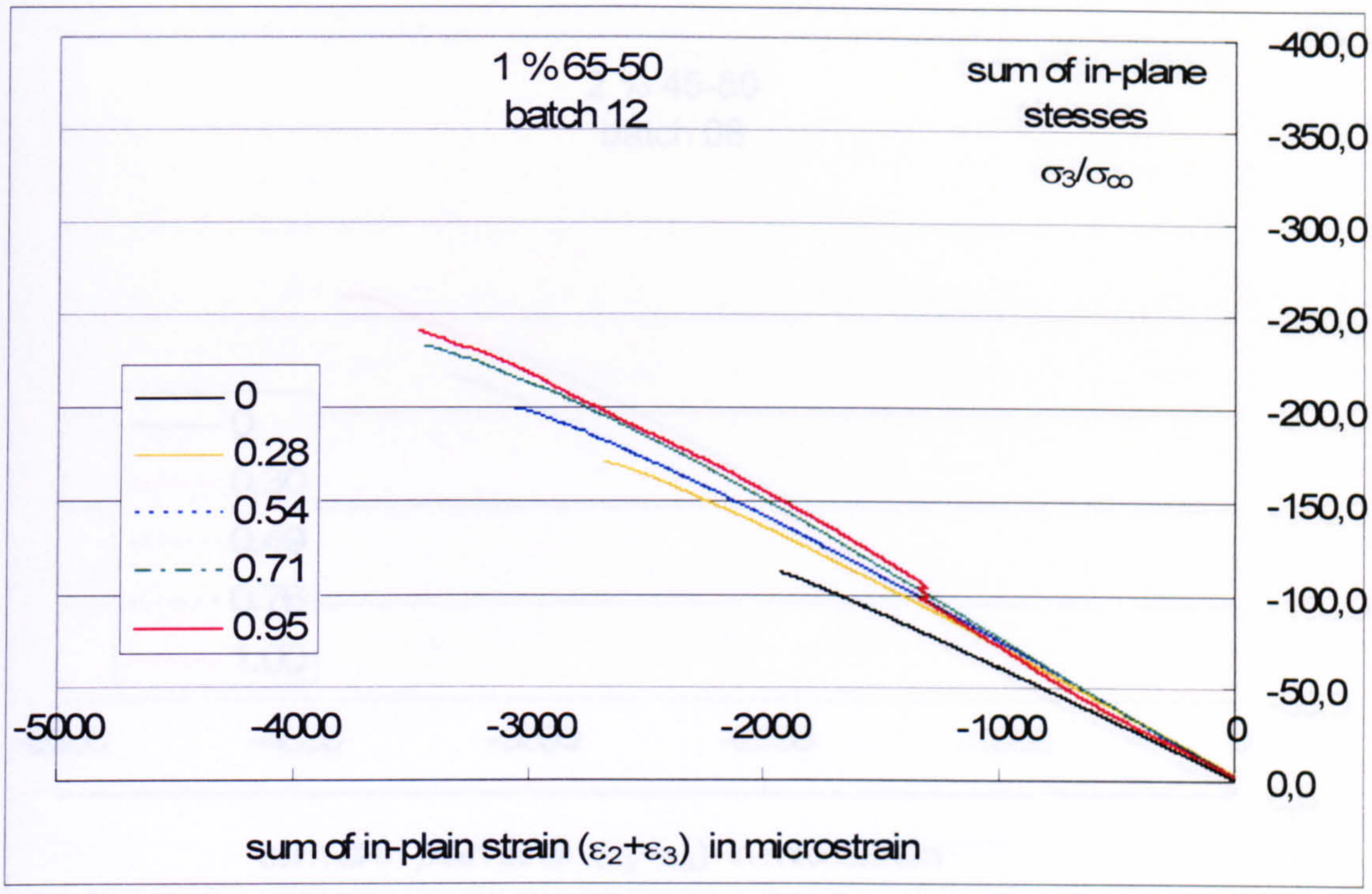

Figure 5.26 Relationship of the sum of in-plane strain and stress for different stress ratios under biaxial compression recorded with strain gauges in the two in plane directions for V_f = 1 % of the fibre type 65-60 tested with solid steel blocks (batch 12)

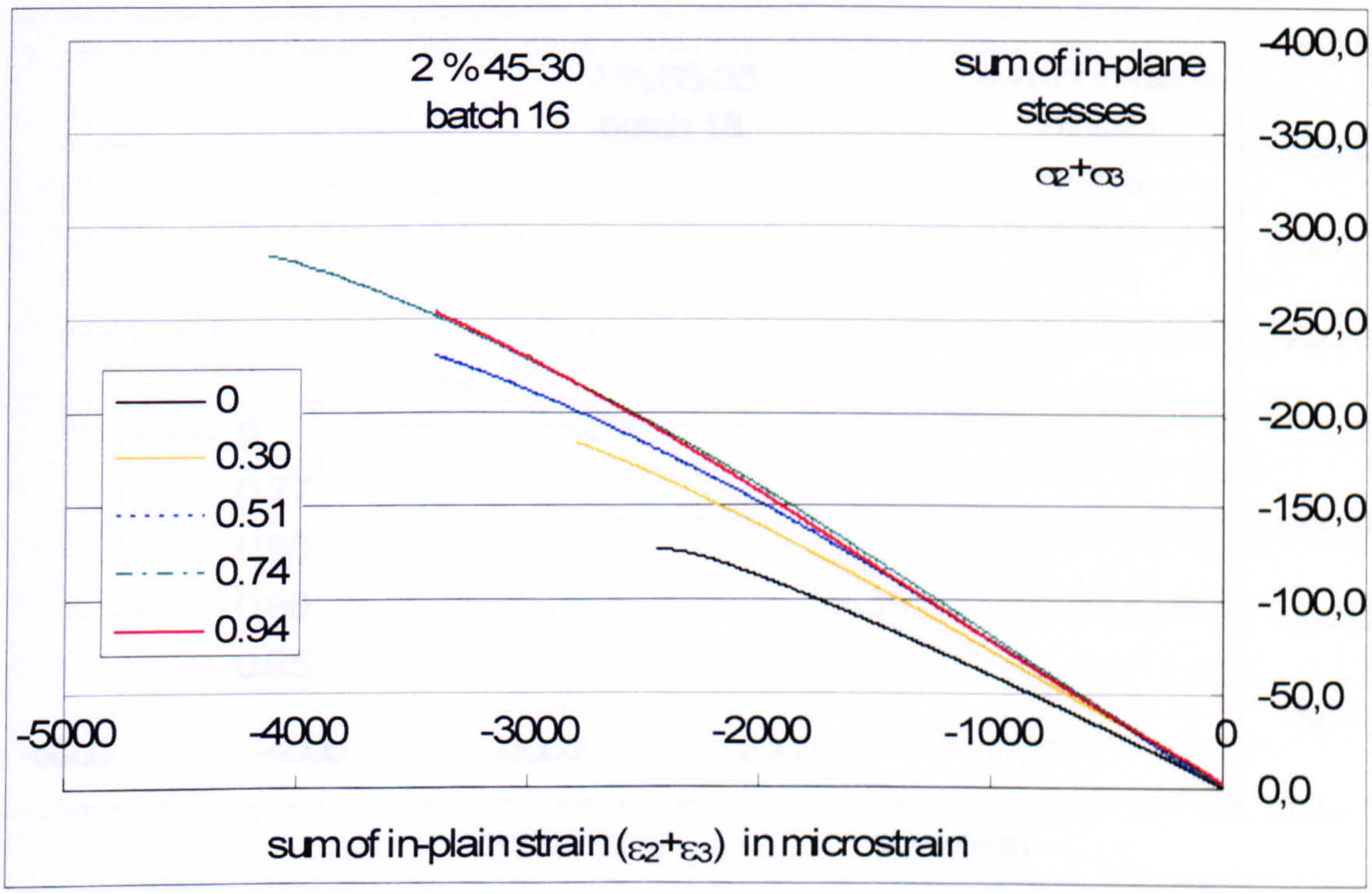

Figure 5.27 Relationship of the sum of in-plane strain and stress for different stress ratios under biaxial compression recorded with strain gauges in the two in plane directions for V_f = 2 % of the fibre type 45-35 tested with solid steel blocks (batch 16)

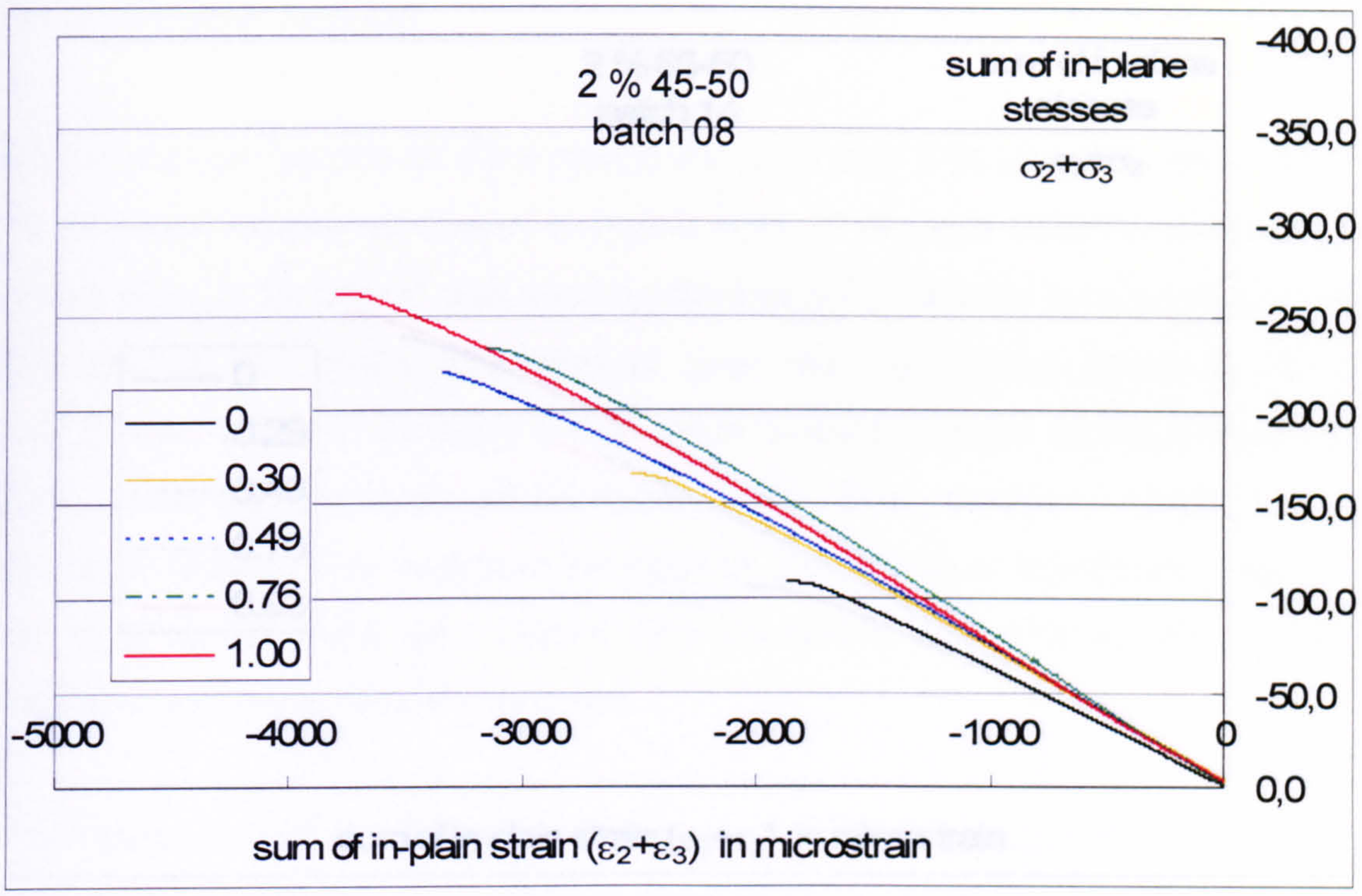

Figure 5.28 Relationship of the sum of in-plane strain and stress for different stress ratios under biaxial compression recorded with strain gauges in the two in plane directions for V_f = 2 % of the fibre type 45-50 tested with solid steel blocks (batch 08)

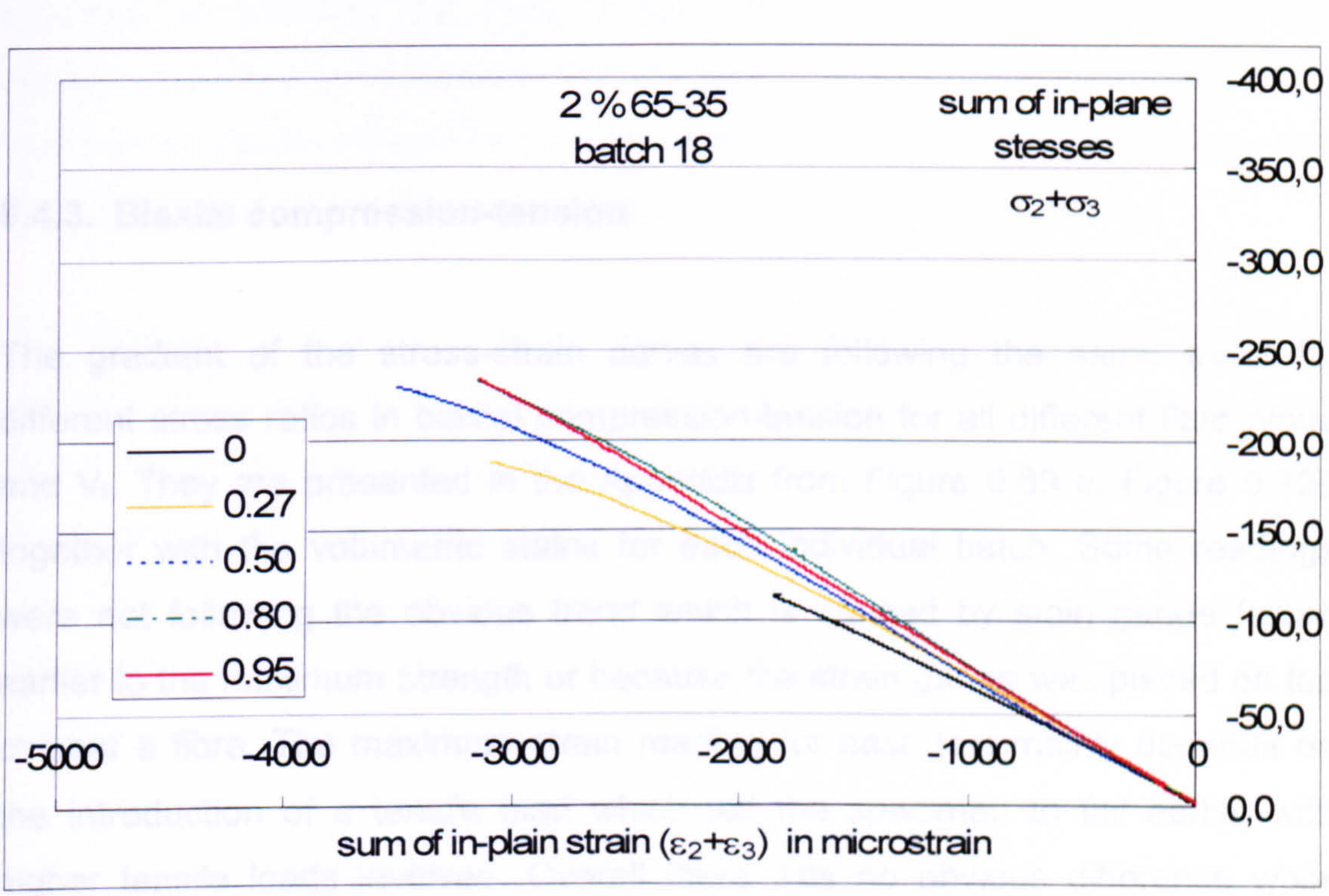

Figure 5.29 Relationship of the sum of in-plane strain and stress for different stress ratios under biaxial compression recorded with strain gauges in the two in plane directions for V_f = 2 % of the fibre type 65-35 tested with solid steel blocks (batch 18)

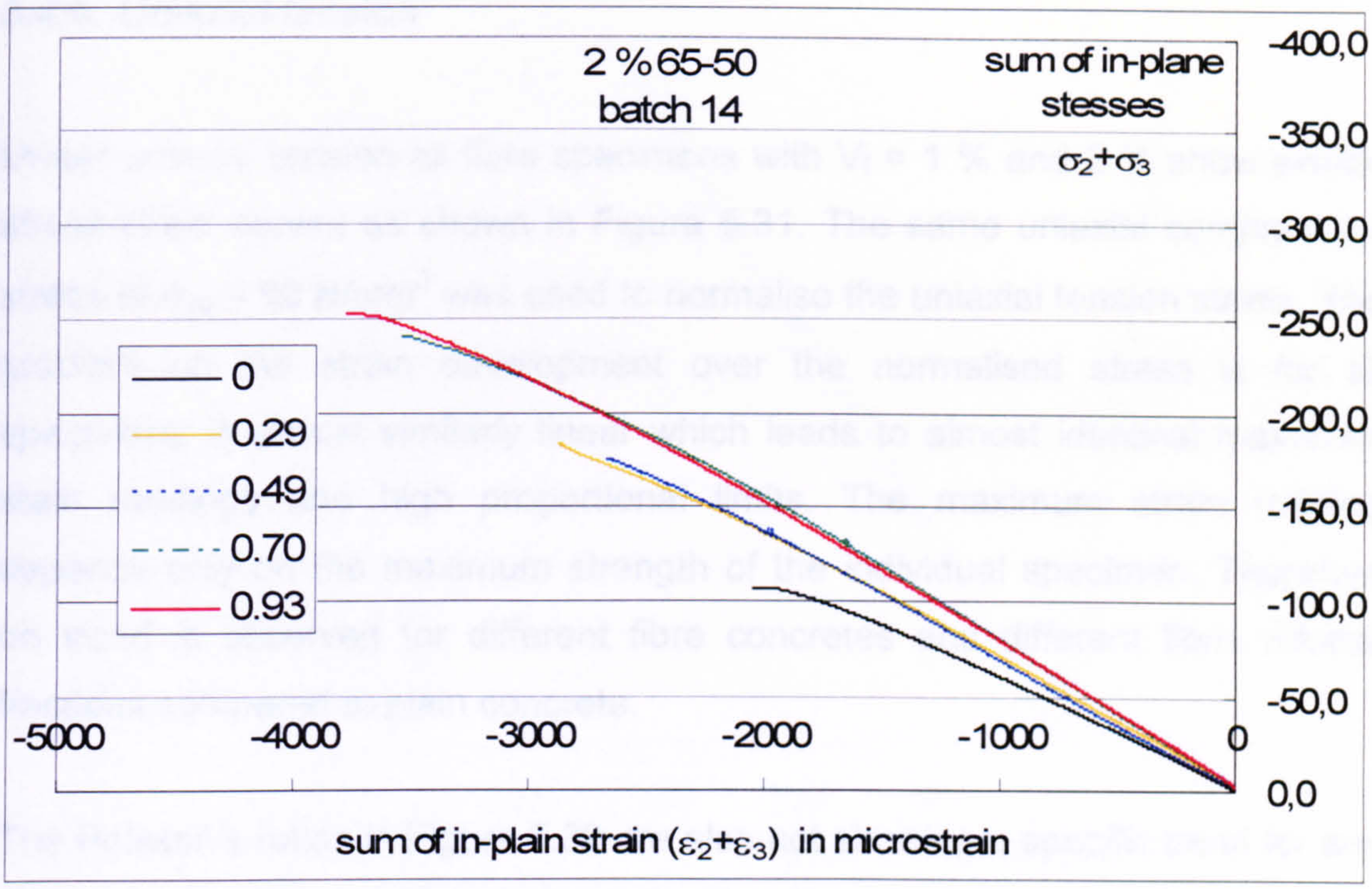

Figure 5.30 Relationship of the sum of in-plane strain and stress for different stress ratios under biaxial compression recorded with strain gauges in the two in plane directions for V_f = 2 % of the fibre type 65-60 tested with solid steel blocks (batch 14)

5.4.3. Biaxial compression-tension

The gradient of the stress-strain curves are following the same trend for different stress ratios in biaxial compression-tension for all different fibre types and V_f. They are presented in the Appendix from Figure 0.69 to Figure 0.100 together with the volumetric stains for each individual batch. Some readings were not following the obvious trend which is caused by stain gauge failure earlier to the maximum strength or because the strain gauge was placed on top or near a fibre. The maximum strain reading for each test mainly depends on the introduction of a tensile load which led the specimen to fail earlier with higher tensile loads involved. Overall there was no obvious difference while comparing the fibre graphs with the plain graphs.

5.4.4. Uniaxial tension

Under uniaxial tension all fibre specimens with V_f = 1 % and 2 % show similar stress-strain curves as shown in Figure 5.31. The same uniaxial compression stress of σ_{co} = 99 N/mm^2 was used to normalise the uniaxial tension stress. The gradient on the strain development over the normalised stress is for all specimens is almost similarly linear which leads to almost identical maximum stain readings and high proportional limits. The maximum strain reading depends only on the maximum strength of the individual specimen. Therefore no trend is observed for different fibre concretes and different fibre volume fractions compared to plain concrete.

The Poisson's ratios in Figure 5.32 are also not showing a specific trend for any fibre type or different fibre volume fraction in uniaxial tension. The average value for each tested uniaxial tension specimen varies between 0.24 and 0.31. Poisson's ratio for each batch is shown in Table 13 together with the associated Modulus of Elasticity for both uniaxial tension and compression of the compression-tension test series. Poisson's ratio for the compression specimens in the compression-tension test series varies a bit more but does not show any significant trend as can be seen in Figure 5.22 above for comparison.

The Modulus of Elasticity was in the range between 43.5 kN/mm^2 and 50.6 kN/mm^2 for uniaxial tension tests. Therefore these values were always a bit higher that the Modulus of Elasticity values for the uniaxial compression tests of the same batch. The values for plain HPC lie in the middle of the range and moreover as recorded before no obvious trend can be examined for any particular fibre type or fibre volume fraction. As with the Poisson's ratio the full information of these values are given in Table 13 above.

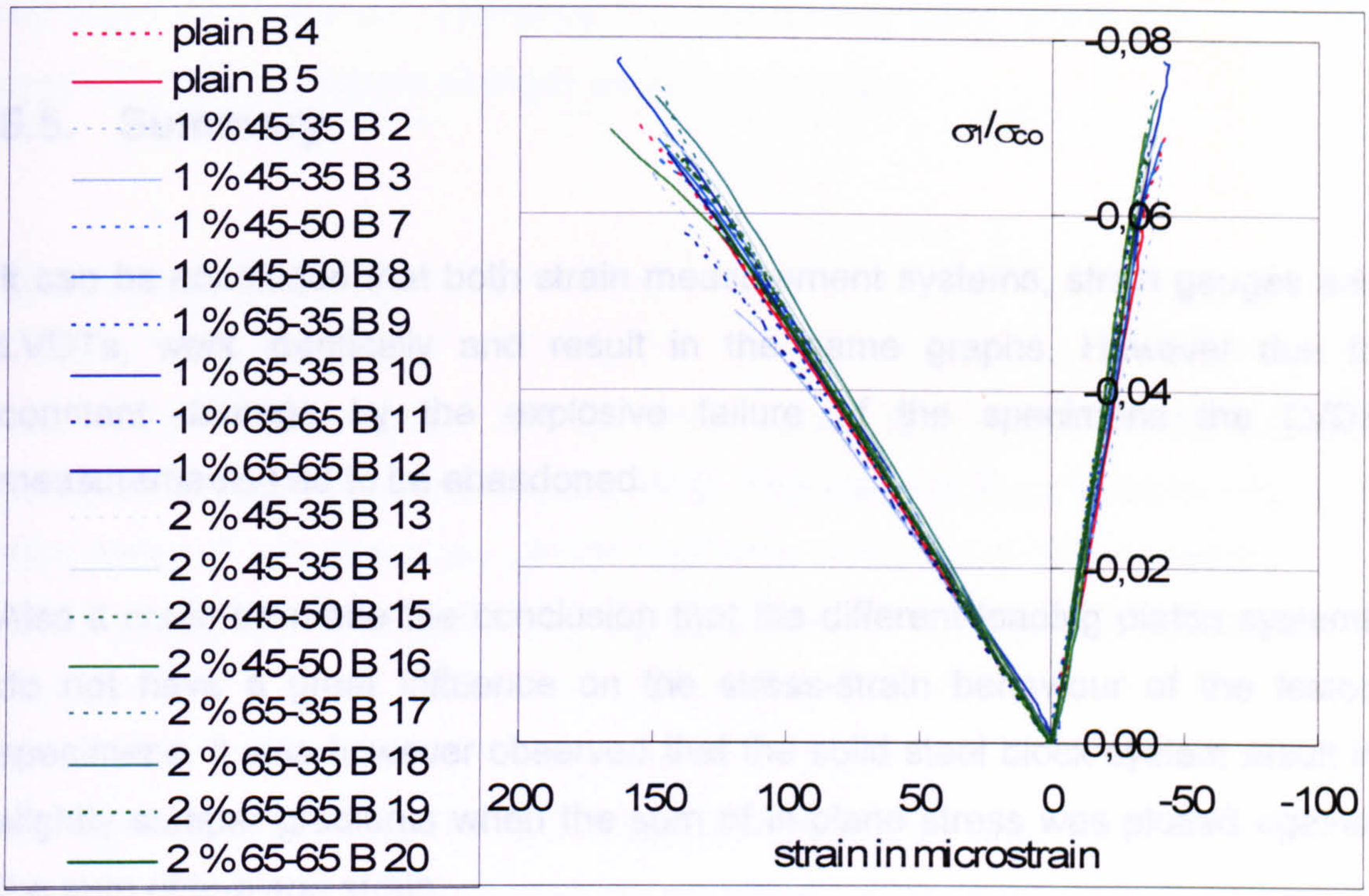

Figure 5.31 Stress-strain relationship for specimens under uniaxial tension with different fibre types of the fibre volume V_f = 1 % and 2 % and plain HPC recorded with strain gauges

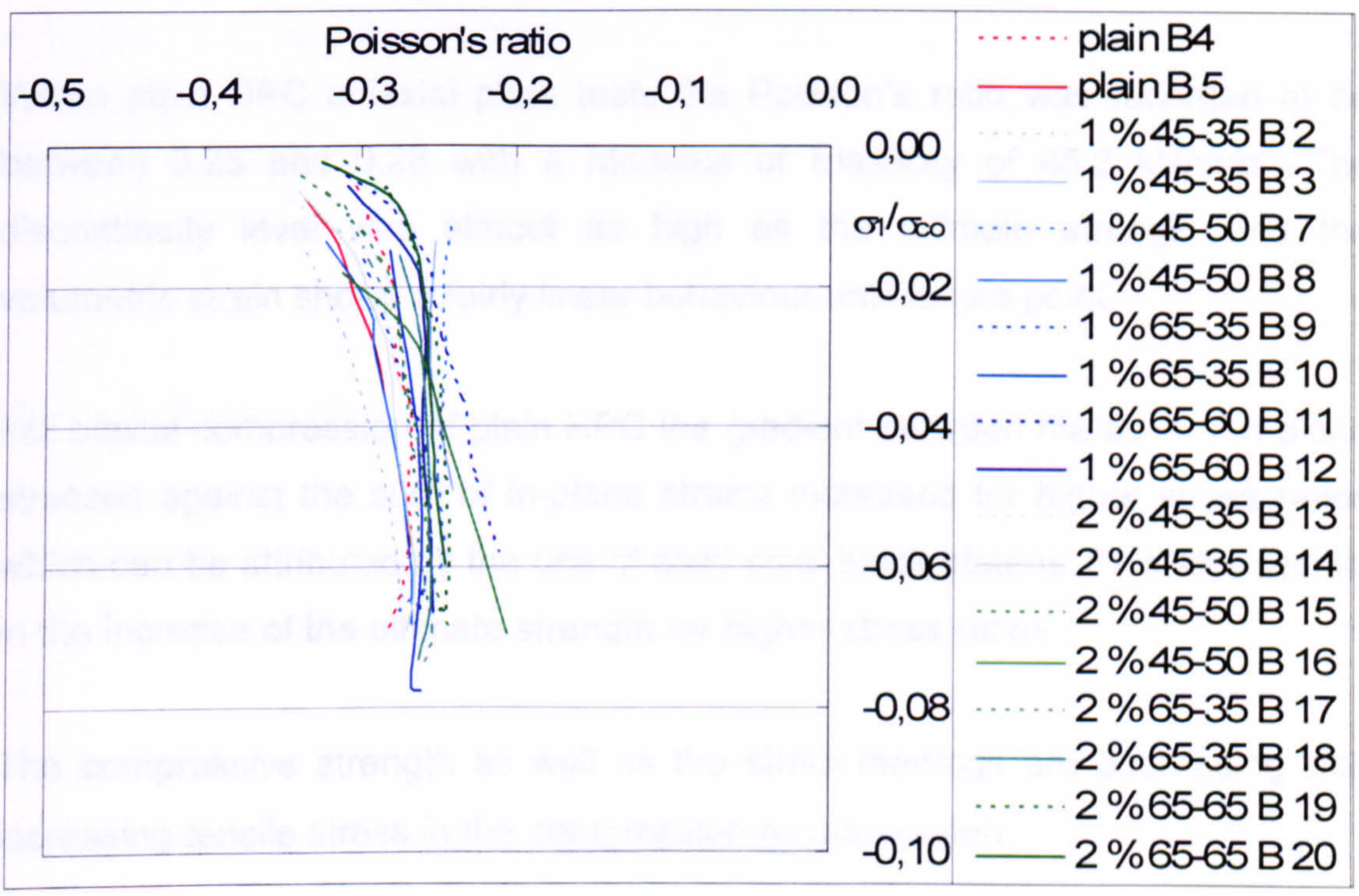

Figure 5.32 Poisson's ratio versus normalised stress in uniaxial tension recorded with strain gauges in the two in plane directions for different fibre types of the fibre volume V_f = 1 %, 2 % and plain HPC

5.5. Summary

It can be concluded that both strain measurement systems, strain gauges and LVDTs, work identically and result in the same graphs. However due to constant damage by the explosive failure of the specimens the LVDT measurements had to be abandoned.

Also it could be made the conclusion that the different loading platen systems do not have a great influence on the stress-strain behaviour of the tested specimens. It was however observed that the solid steel block system result in slightly steeper gradients when the sum of in-plane stress was plotted against the sum of in-plane strain.

Plain HPC:

Within plain HPC uniaxial plate tests the Poisson's ratio was recorded to be between 0.25 and 0.28 with a Modulus of Elasticity of 45.8 kN/mm^2. The discontinuity level was almost as high as the ultimate strength and the volumetric strain shows a fairly linear behaviour until failure point.

For biaxial compression of plain HPC the gradient between the sum of in-plane stresses against the sum of in-plane strains increased for higher stress ratios which can be attributed by the use of solid steel block platens. This also results in the increase of the ultimate strength for higher stress ratios.

The compressive strength as well as the strain readings are decreasing with increasing tensile stress in the compression-tension region.

The values in uniaxial tension tests are almost the same as in compression with a Poisson's ratio between 0.28 and 0.29 and the Modulus of Elasticity between

45.4 and 47.3 kN/mm^2. Therefore the discontinuity level, volumetric strain and proportional limit behave similarly as in compression.

Steel Fibre Reinforced HPC:

The stress-strain curves for all fibre types are similar under uniaxial compression and are close to plain HPC. The value of E_c is between 40.6 and 46.3 kN/mm^2 and therefore around the plain HPC value. The Poisson's ratio varies between 0.23 and 0.34 with no obvious trend for any fibre type or volume fraction.

No significant difference for the stress-strain readings was observed between plain and fibre HPC in the biaxial compression-compression and compression-tension region

Under uniaxial tension also no obvious difference was observed between the strain readings of plain and fibre HPC. Only the increased tensile strength lead sometimes to higher overall values but the slope of the graphs and therefore the stiffness, the proportional limit and discontinuity level are similar.

5.6. References

ASTM 2002, Standard Test Method for Static Modulus of Elasticity and Poisson's Ratio of Concrete in Compression, Designation: C 469-02.

6. Failure Mode – Test Results and Discussion

The crack patterns and failure modes were observed for all tested specimens. They were rather explosive throughout; once maximum load was reached the specimen failed instantly.

Within this chapter splitting failure describes the failure type when only one single crack occur perpendicular to the applied load. Faulting failure is also known as shear failure and describes a failure mode when the specimen breaks in several patches inclining with an angle up to 30° in the direction of loading. It should be noted that in the nature of concrete the mechanism of faulting failure also depends on the tensile capacity of the material and therefore fails under splitting effects. The specimen pieces are splitting apart in the direction of the unloaded surface.

6.1. Plain High Performance Concrete (HPC)

Under **uniaxial compression** fracture of the plain HPC specimens of the compression-compression and compression-tension series occurred by forming cracks at an angle around 25 degrees to the direction of the applied load and also to the free surface. Therefore the specimens break into a number of pieces which are plate type fractions. This failure type is caused by splitting tensile stress in a direction normal to the compressive load as mentioned by Traina and Mansour (1991). Figure 6.1 shows the failure pattern of the cracks in a plain HPC compression-compression specimen after failure under uniaxial compression whereas Figure 6.2 and Figure 6.3 show the same for a compression-tension specimen.

The failure surface of this specimen is shown in Figure 6.4 where only half the remaining pieces of the specimen is shown to illustrate the inner failure

surfaces. Cracks develop through the mortar as well as the coarse aggregates. This implies that the compressive strength of the aggregates is similar to the achieved compressive strength of the mortar and therefore the material of HPC is more homogeneous for strength and elasticity properties than normal strength concrete. In normal strength concrete hardly any cracks develop through the aggregates.

From this observation the sudden failure type of HPC can be described as there is no interlock effect as in normal strength concrete where the mortar is the weaker part and therefore cracks grow around the aggregates. The aggregates themselves behave like crack arrestors and give the concrete a more ductile behaviour in normal strength concrete whereas HPC behaves more brittle and failure is rapid (Neville, 1995).

Under **biaxial compression** failure occurred by formatting major cracks also at an angle around 25 degrees to the free surface of the specimen. This failure mode was very similar to the one observed for the uniaxial compression tests for plain concrete and the failure surfaces are similar as shown in Figure 6.5. However more diagonal cracks in the plane direction could be observed for a stress ratio of $\sigma_2/\sigma_3 = 1$.

Under **combined compression and tension** load the failure surface of plain HPC specimens behaved similar to the failure mode of either the uniaxial compression or uniaxial tension one. Between uniaxial compression and a stress ratio up to $\sigma_1/\sigma_3 = -0.06$ faulting failure types where dominant. The failure surfaces look similar to that described earlier with the uniaxial and biaxial compression. See Figure 6.6 with the specimen still in position within the test machine. The tested specimen failed at a stress ratio of $\sigma_1/\sigma_3 = -0.014$.

With a decreasing stress ratio between $\sigma_1/\sigma_3 = -0.06$ and uniaxial tension, failure occurred with one or two major cracks in the middle area (between the compression steel blocks). These were continuous cracks perpendicular to the tensile load direction and the plane of the specimen. Cracks outside the middle

area occurred when the specimen failed under tension and the machine pulled the specimen apart because of the load control system that was chosen. Therefore the middle part failed first and another crack outside this area sometimes developed when the machine went to its end position and the specimen was still held by the compression steel blocks. Figure 6.7 shows such a failure type where the stress ratio was $\sigma_1/\sigma_3 = -0.25$.

Under **uniaxial tension** the specimens of the plain HPC batches failed by formatting a single crack perpendicular to the direction of loading and the plane of the specimen as can be seen in Figure 6.8 and Figure 6.9.

The same observations can be made for the uniaxial tension fracture surface as before for the uniaxial compression one. The fracture surface of the HPC specimen progressed through the mortar and the coarse aggregates in equal proportions as can be seen in Figure 6.10. Again this implies that the strength of the mortar is as strong or even stronger than the strength of the aggregates and that the strength of the matrix is more homogeneous than for normal strength concrete where cracks develop mostly in the mortar matrix and hardly any aggregates have been cracked.

The failure mode observed for the plain HPC tests were similar to those obtained by Hussein (2000) for plain high strength concrete and plain ultra high strength concrete. The specimen in Hussein's study were of similar size and shape and were tested with a steel brush platen system rather solid steel blocks like in this study. This shows that the platen system does not affect the failure mode greatly.

Figure 6.1 Failure mode of plain HPC specimen of the compression-compression series in uniaxial compression

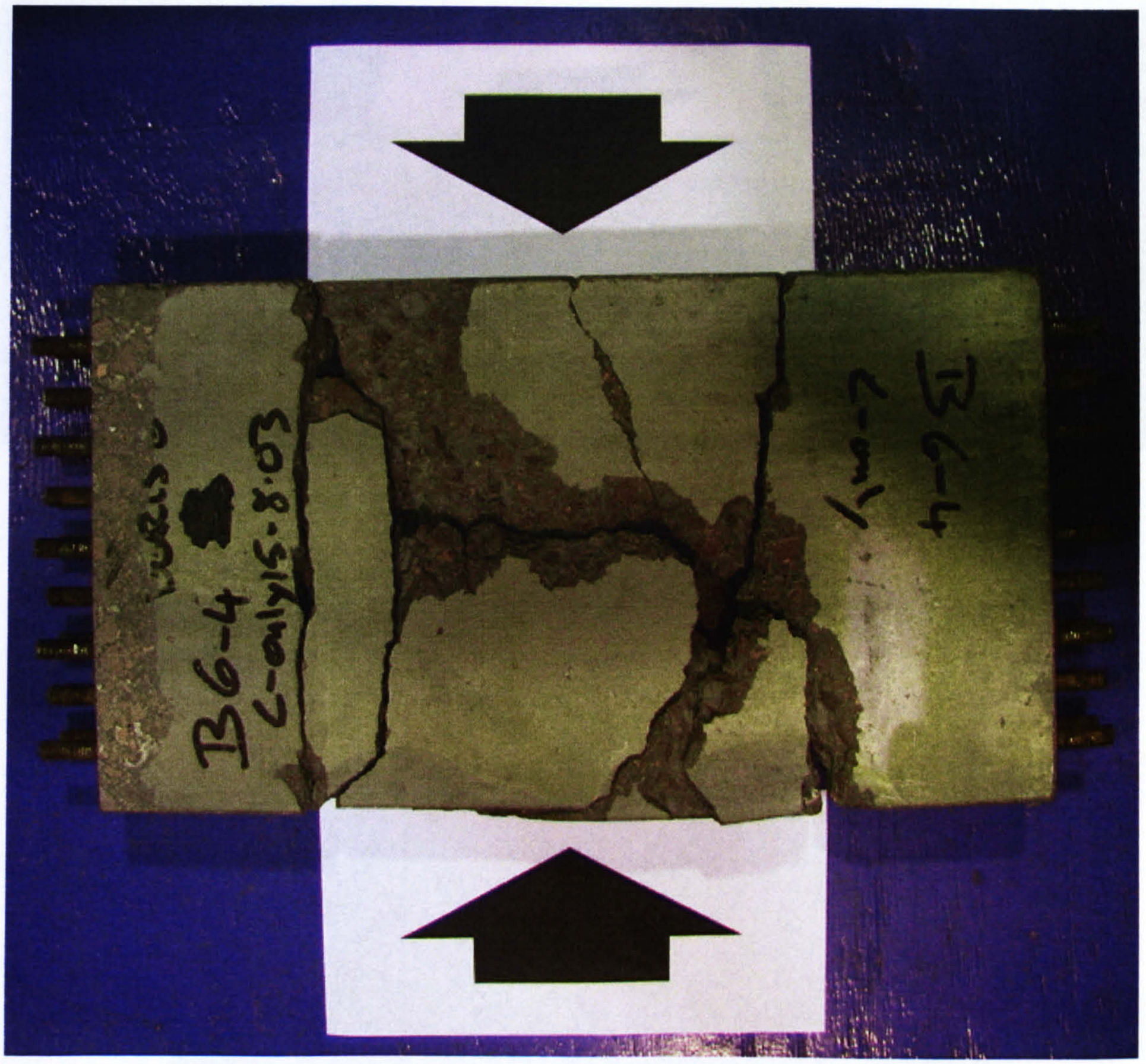

Figure 6.2 Failure mode of plain HPC specimen of the compression-tension series in uniaxial compression

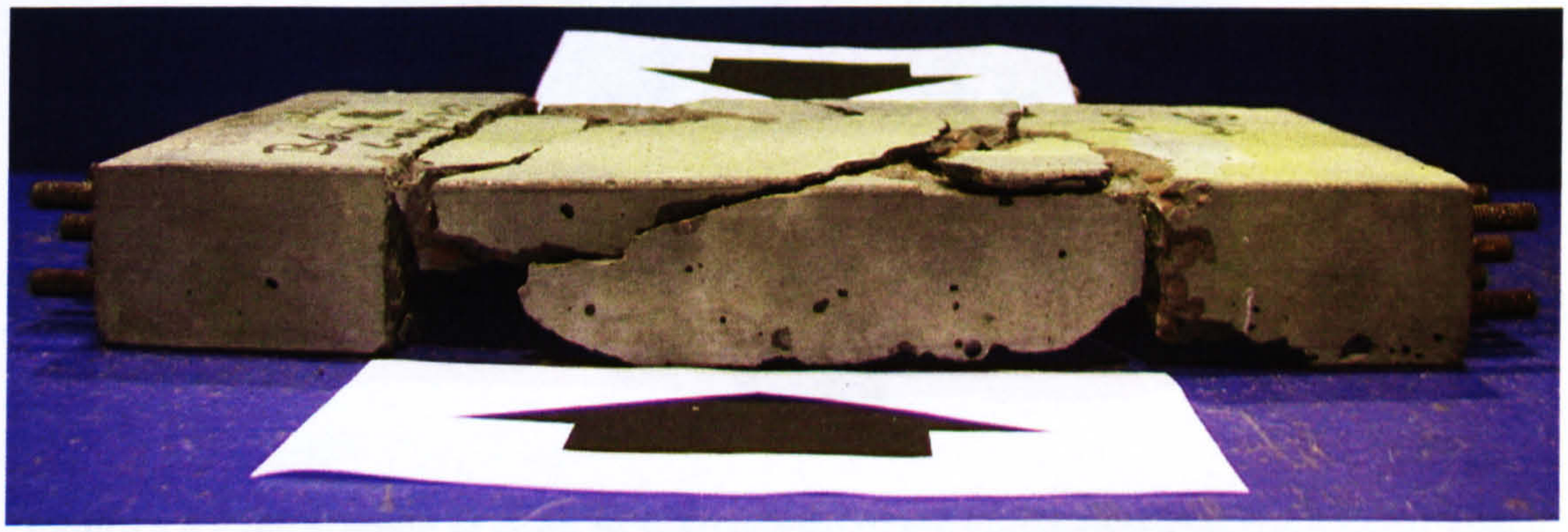

Figure 6.3 Failure mode of plain HPC specimen of the compression-tension series in uniaxial compression

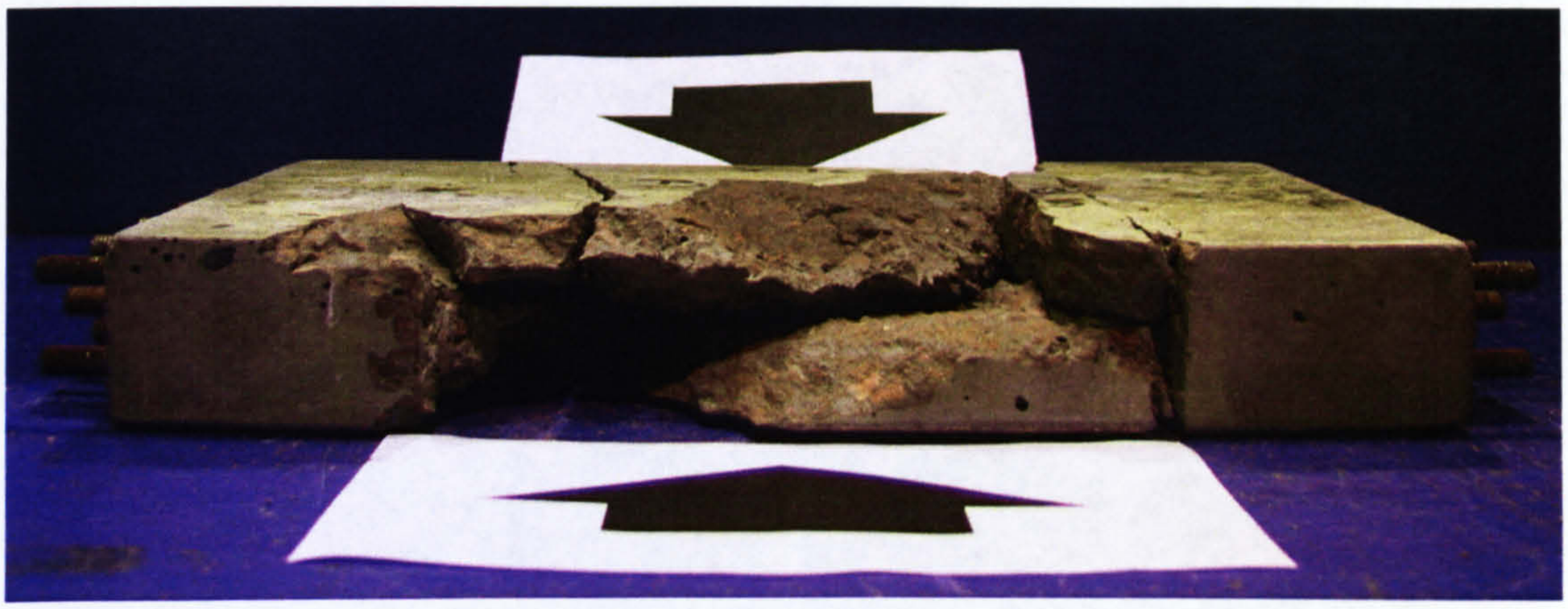

Figure 6.4 Failure surface of plain HPC specimen of the compression-tension series in uniaxial compression

Figure 6.5 Failure mode of plain HPC specimen of the compression-compression series in biaxial compression ($\sigma_2/\sigma_3 = 1$)

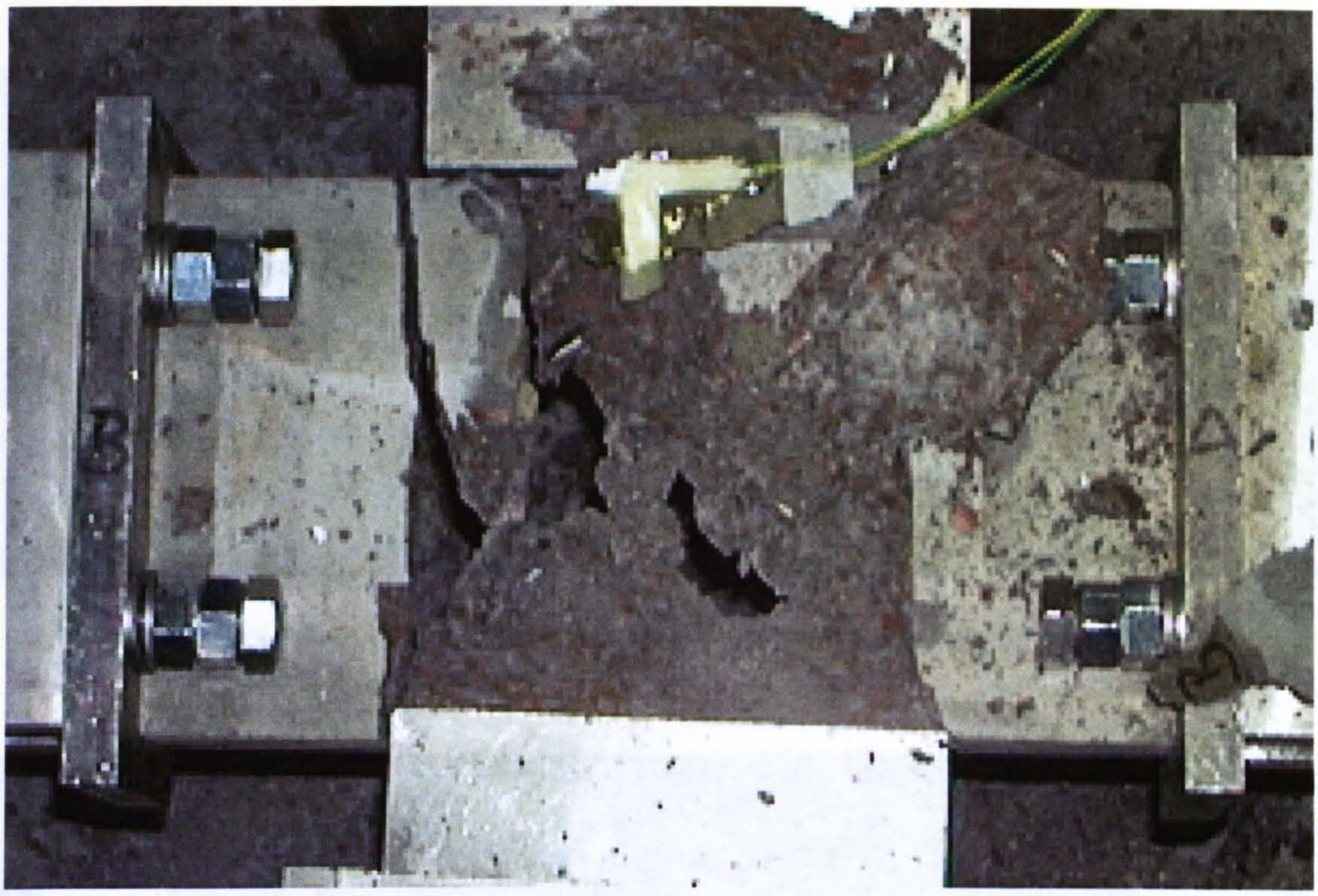

Figure 6.6 Failure mode of plain HPC specimen of the compression-tension series to combined compression and tension (σ_1/σ_3 = -0.014)

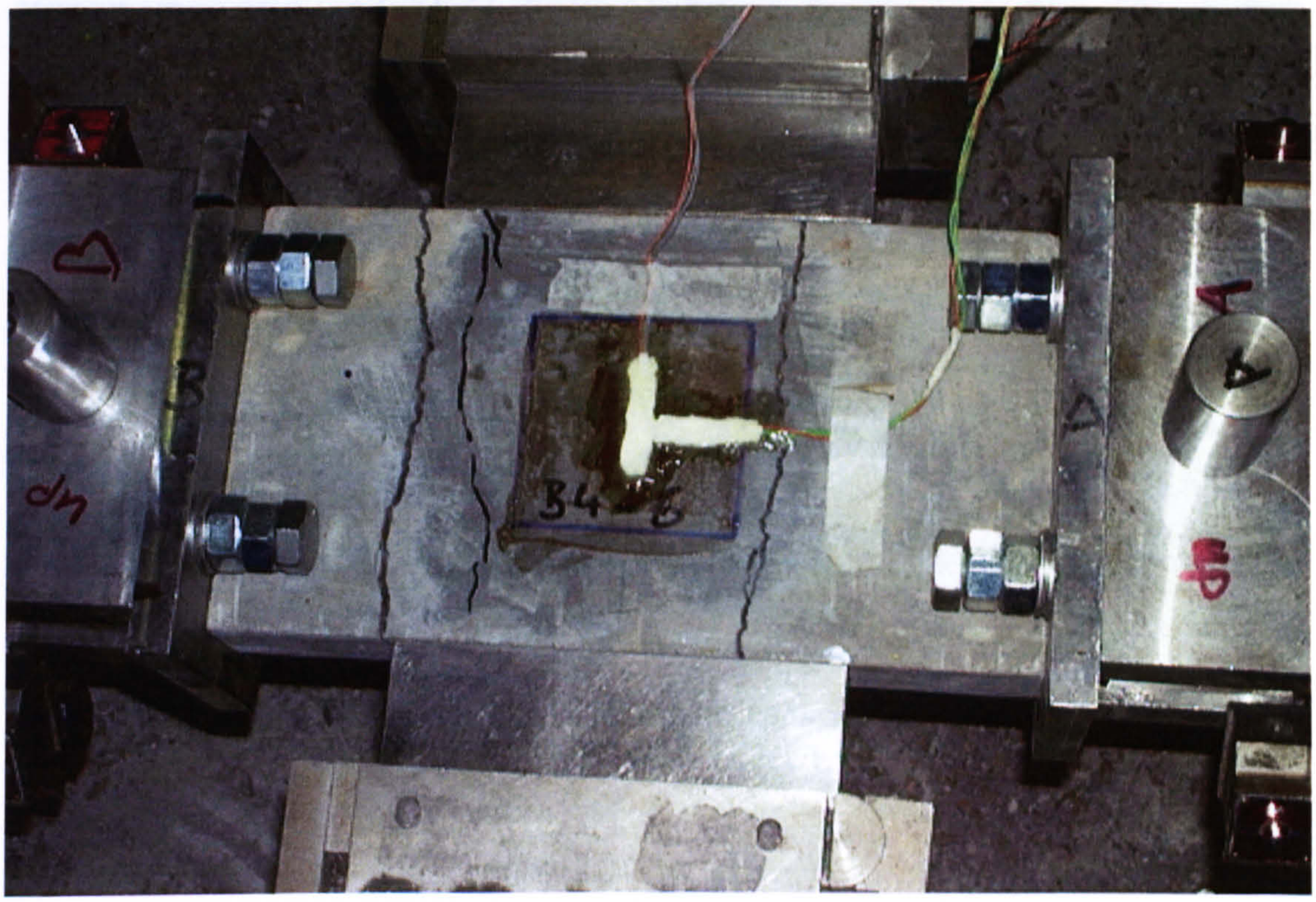

Figure 6.7 Failure mode of plain HPC specimen of the compression-tension series to combined compression and tension (σ_1/σ_3 = -0.25)

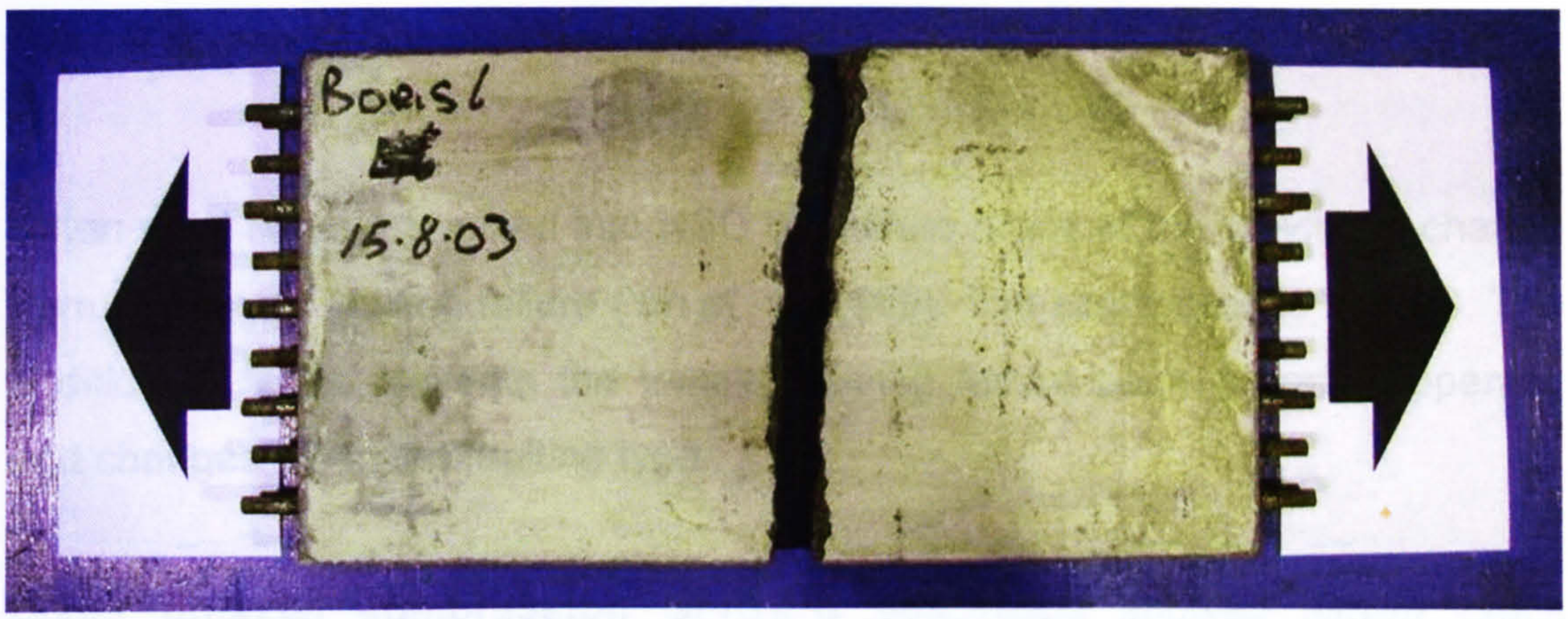

Figure 6.8 Failure mode of plain HPC specimen in uniaxial tension

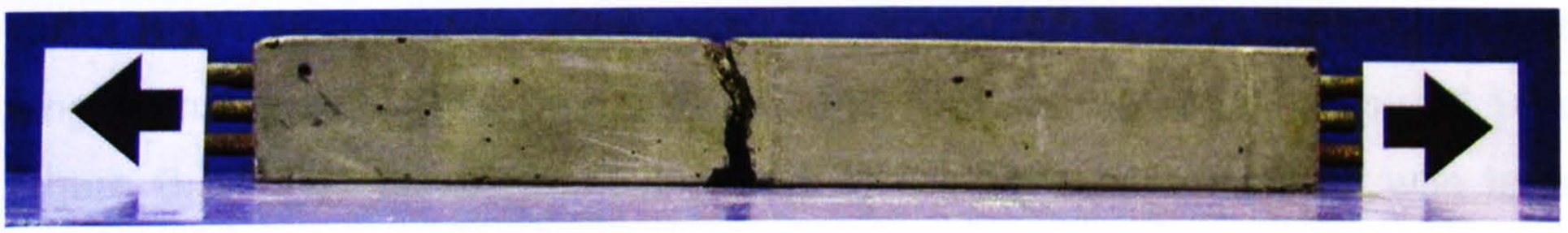

Figure 6.9 Failure mode of plain HPC specimen in uniaxial tension

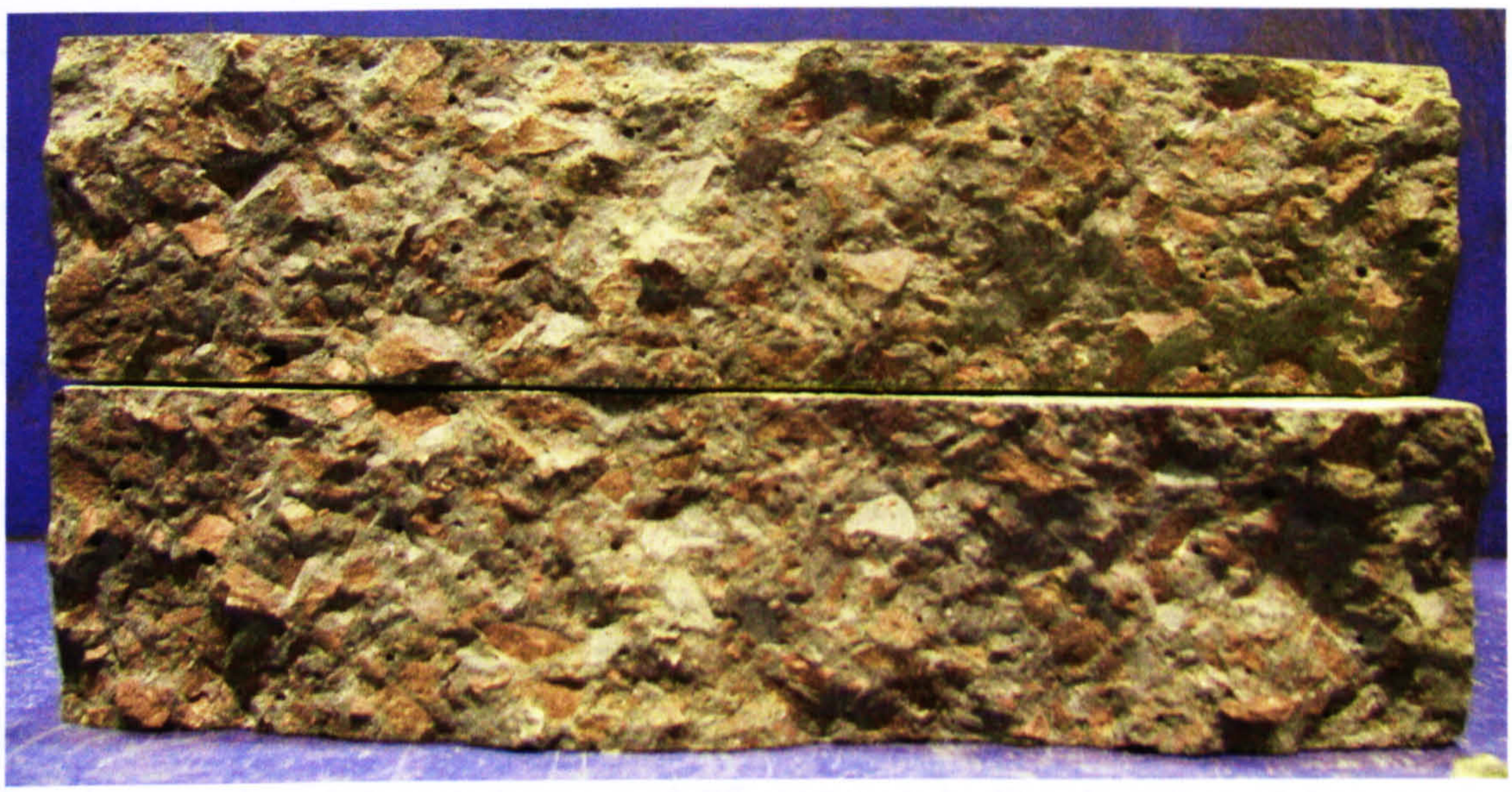

Figure 6.10 Failure surface of plain HPC specimen in uniaxial tension

6.2. Steel Fibre Reinforced High Performance Concrete (SFRHPC)

When steel fibres are mixed into NSC the failure mode of the specimen change from splitting to faulting failure (Yin et. al, 1989). The same applies in HPC. The addition of fibres prevents the tensile splitting failure pattern from happening and changes it into the faulting type.

Under **uniaxial compression** SFRHPC specimens showed similar crack patterns to plain HPC. The major difference observed was that the specimen fragments were still connected by the fibres after the specimen had been tested to the peak load and therefore could be interpreted as a faulting failure with longitudinal cracks rather than a shear band. This can be seen in Figure 6.11 to Figure 6.16. The confinement provided by the fibre reinforcement was large enough to increase the strength but not to change the failure mode which was also observed by Traina and Mansour (1991) for normal strength concrete.

The specimen tested with the steel brush platen system seems to be squeezed open by the brush on one side only as can be seen in Figure 6.12. Compared to that the solid steel block tested specimen failed more over the whole length of the unloaded sides and the main crack developed further within the specimen, see Figure 6.14. This observation could be also caused by the higher fibre content V_f of the solid steel block tested specimen which has an effect on the fibre confinement mentioned before and which also led to a higher strength.

Similar observations can be made for the specimens of the compression-tension test series tested under uniaxial compression. Failure occurred by forming cracks at an angle around 25 degrees to the direction of the applied load and also to the free surface within the middle area between the two solid steel compression block platens. The unloaded parts of the specimen to either side remained undamaged which can be seen in Figure 6.15 and Figure 6.16. Higher fibre contents V_f do not change the failure mode in this specimen type.

Under **biaxial compression** fracture occurs by the formation of micro cracks. They develop in the directions of loading which led to a few major cracks inclined at an angle of approximately 20 degrees to the direction of the major load. For a stress ratio of $\sigma_2/\sigma_3 = 1$ and the solid steel block platen system the specimen performed a diagonal crack on the surface normal to the loading direction which led also in a platen type failure as can be seen in Figure 6.19 and Figure 6.20.

The specimen shown in Figure 6.17 and Figure 6.18 were tested with the steel brush bearing system and formed more horizontally aligned cracks in the direction of loading. Other than that no difference were observed between the two load bearing systems. The increase of V_f does not change the type of failure which can be observed and compared in Figure 6.17 and Figure 6.18 for the 1 % and Figure 6.19 and Figure 6.20 for the 2 % steel fibre volume specimen.

The failure mode under **combined compression and tension** can be divided into two failure types as done with the plain HPC before. Between uniaxial compression and a stress ratio of $\sigma_1/\sigma_3 = -0.04$ a compression faulting failure type is more dominant over the splitting failure behaviour. The failure type changes into a tensile splitting failure between the stress ratio $\sigma_1/\sigma_3 = -0.04$ and -0.15 and becomes more clear as tensile failure as closer the stress ratio gets to uniaxial tension.

There was no difference in the type of failure observed between different fibre volume fractions. Typical failure patterns for the faulting failure type can be seen in Figure 6.21 and Figure 6.22 for a specimen with 1 % fibre content and tested at a stress ratio of $\sigma_1/\sigma_3 = -0.012$. Figure 6.23 and Figure 6.24 are showing a specimen with 2 % fibre content tested at a stress ratio of $\sigma_1/\sigma_3 = -0.02$. The failure type with the splitting failure being more dominant look similar to the splitting failure of the uniaxial tension specimen.

Specimens under **uniaxial tension** developed one major crack normal to the applied load and the plane surface as observed with the plain specimens. There was no change in the failure mode for higher fibre contents V_f. Figure 6.25 and Figure 6.26 show a specimen with 1 % fibre content and Figure 6.27 and Figure 6.28 present a picture with 2 % fibre content.

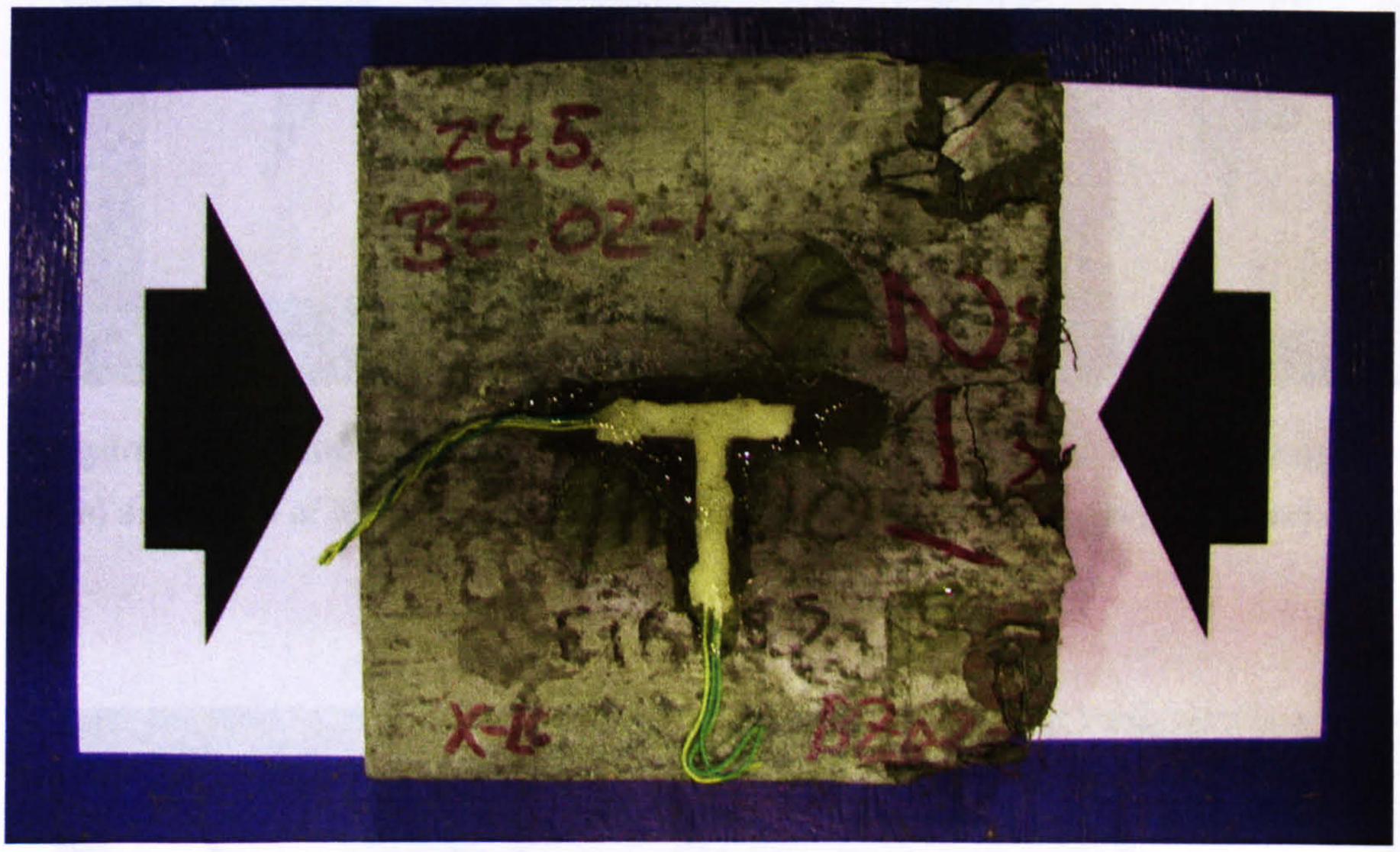

Figure 6.11 Failure mode of SFRHPC (V_f = 1 %, aspect ratio l/d = 65, fibre length l = 35 mm) specimen of the compression-compression series in uniaxial compression tested with the brush platen system

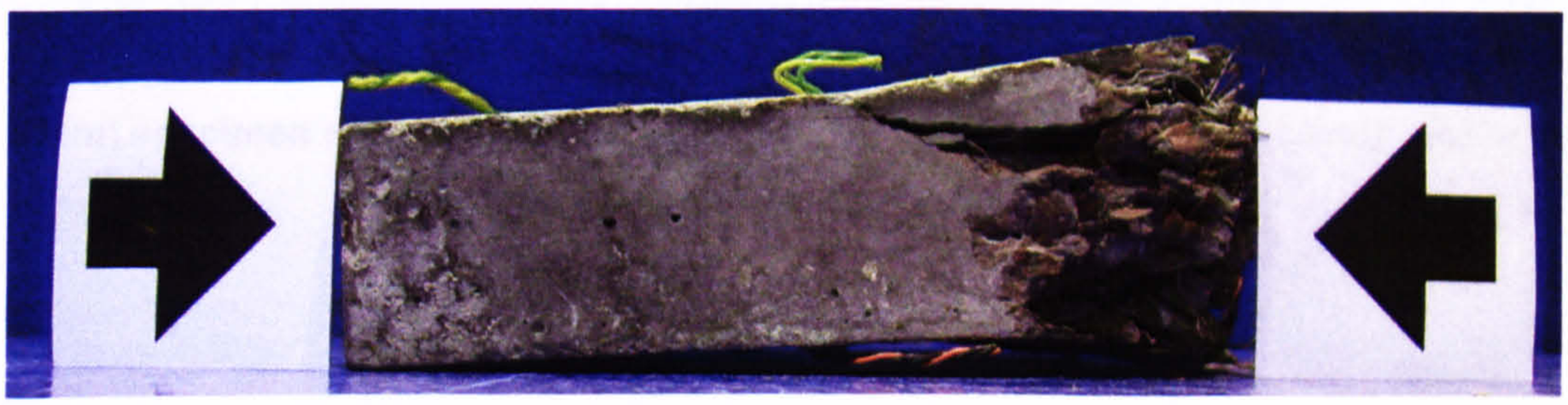

Figure 6.12 Failure mode of SFRHPC (V_f = 1 %, aspect ratio l/d = 65, fibre length l = 35 mm) specimen of the compression-compression series in uniaxial compression tested with the brush platen system

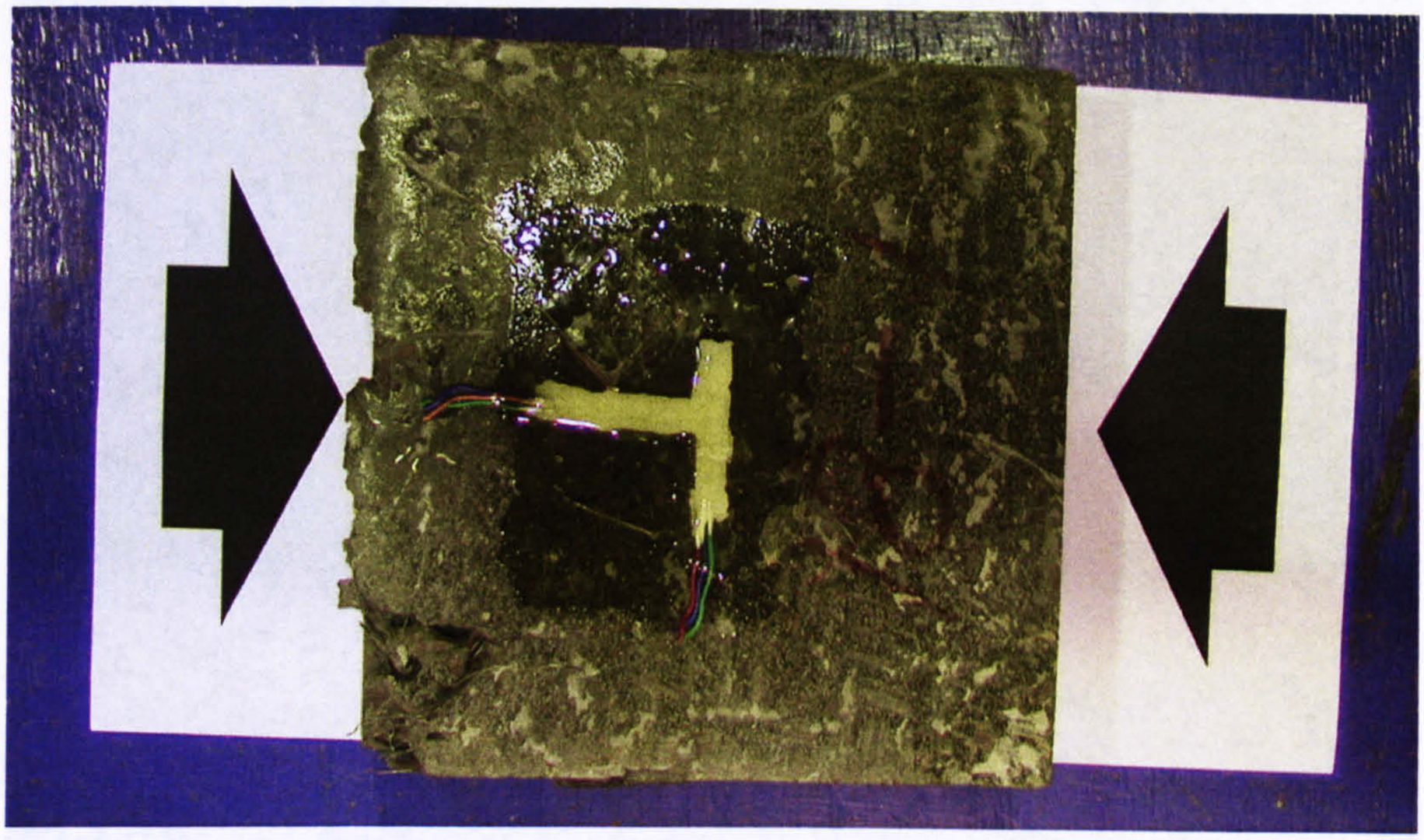

Figure 6.13 Failure mode of SFRHPC (V_f = 2 %, aspect ratio l/d = 65, fibre length l = 35 mm) specimen of the compression-compression series in uniaxial compression tested with the solid steel block platen system

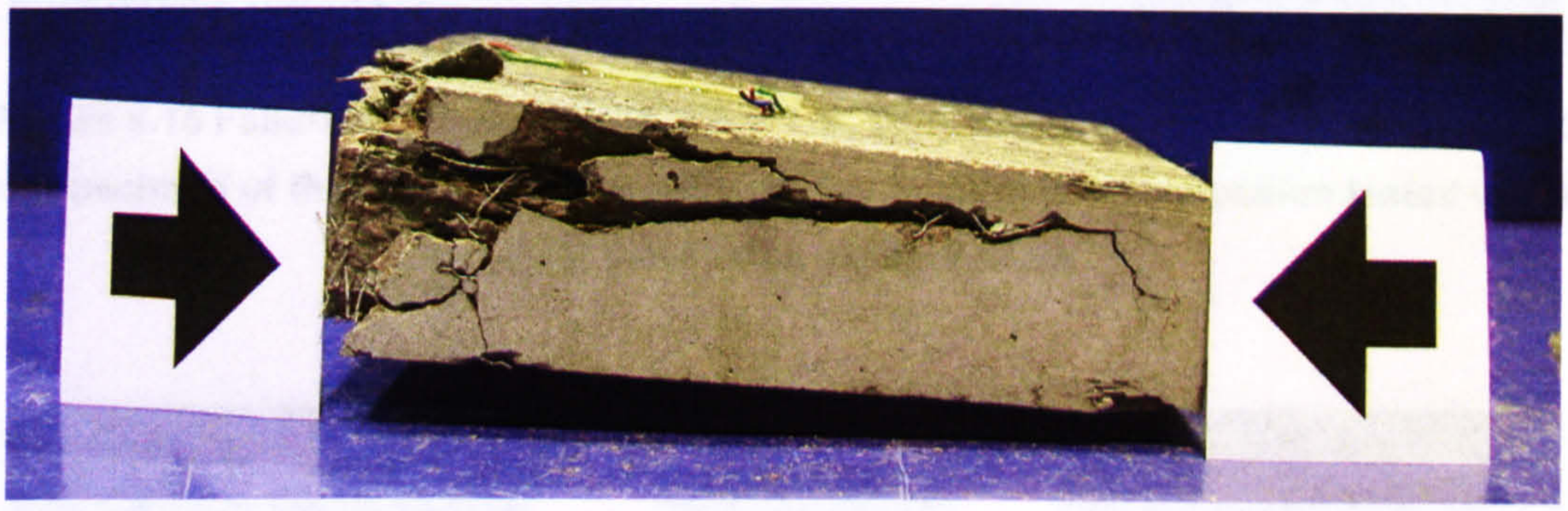

Figure 6.14 Failure mode of SFRHPC (V_f = 2 %, aspect ratio l/d = 65, fibre length l = 35 mm) specimen of the compression-compression series in uniaxial compression tested with the solid steel block platen system

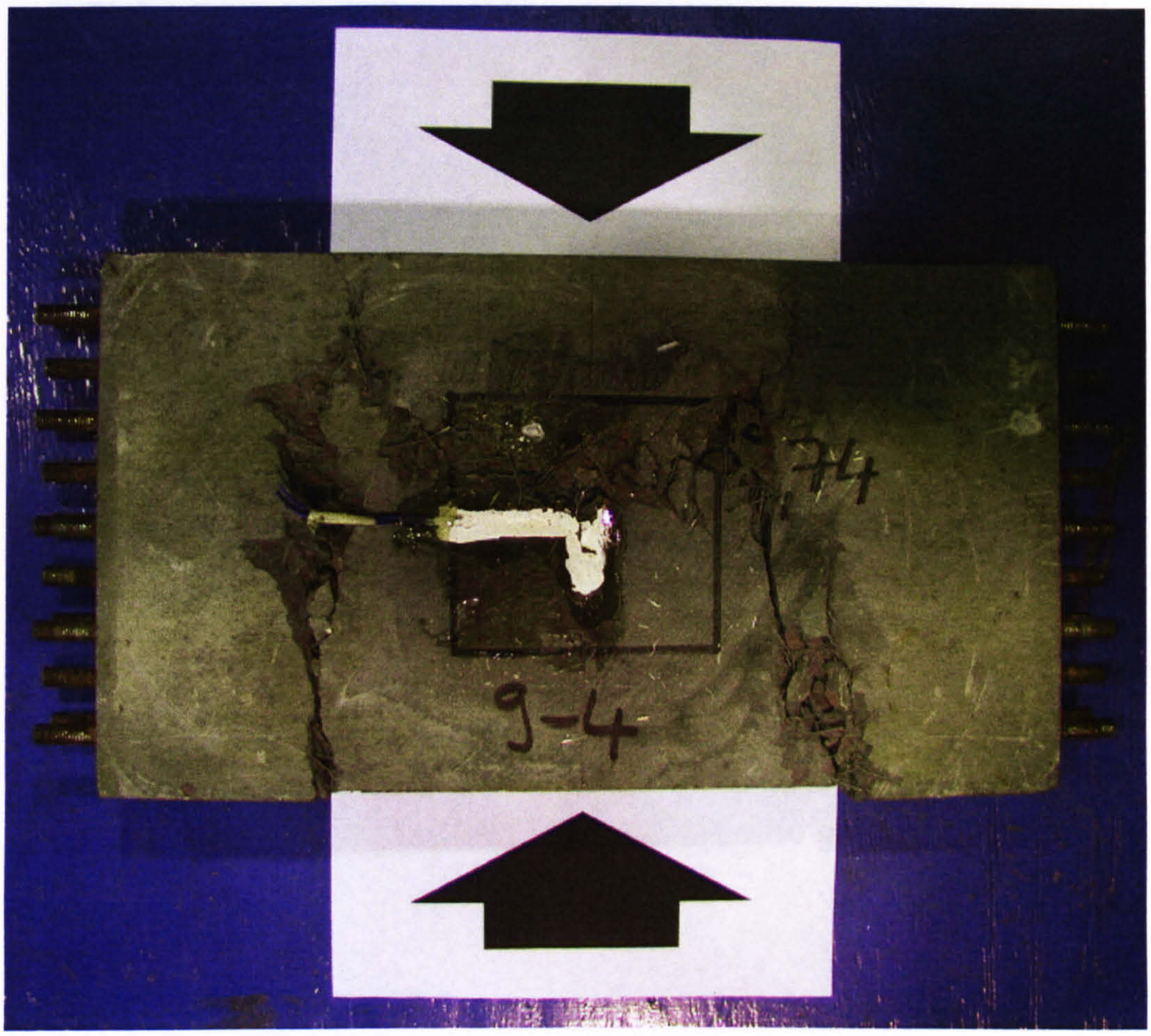

Figure 6.15 Failure mode of SFRHPC (V_f = 1 %, aspect ratio l/d = 65, fibre length l = 35 mm) specimen of the compression-tension series in uniaxial compression tested with the solid steel block platen system

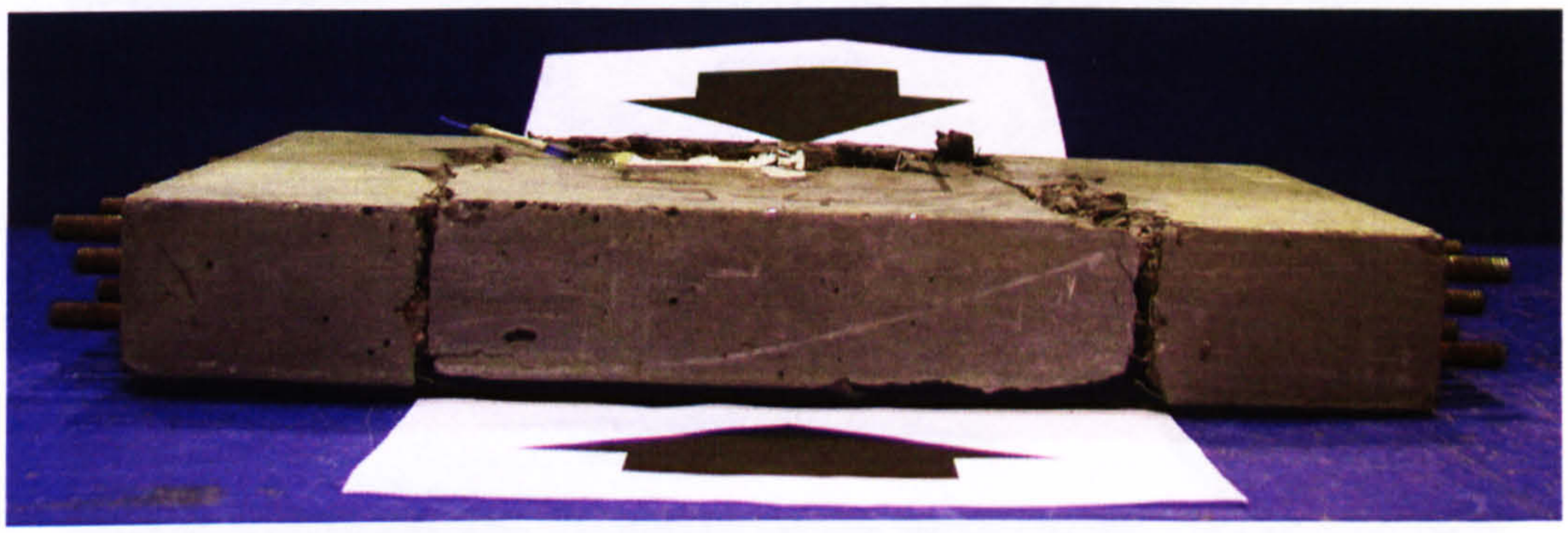

Figure 6.16 Failure mode of SFRHPC (V_f = 1 %, aspect ratio l/d = 65, fibre length l = 35 mm) specimen of the compression-tension series in uniaxial compression tested with the solid steel block platen system

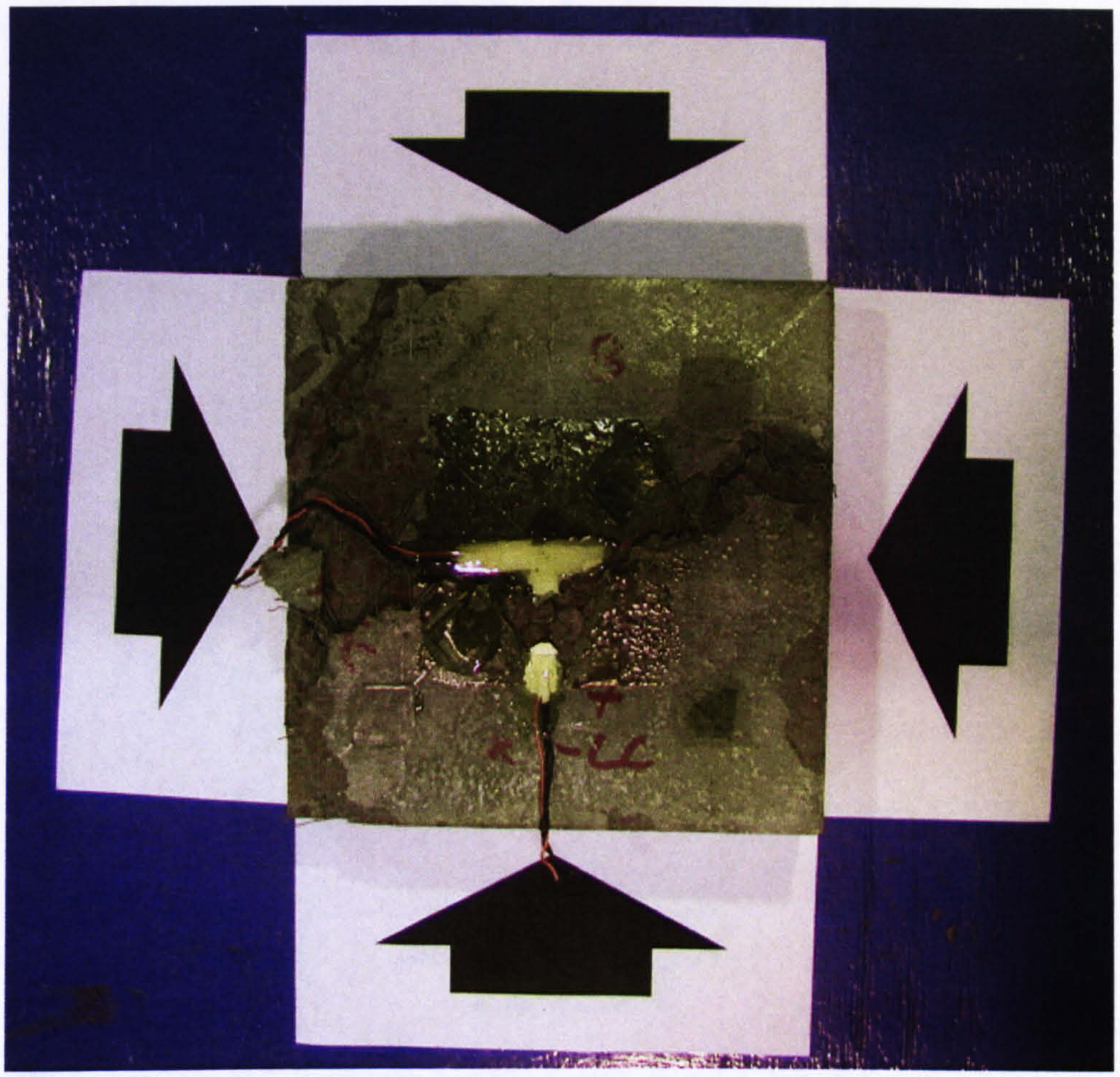

Figure 6.17 Failure mode of SFRHPC (V_f = 1 %, aspect ratio l/d = 65, fibre length l = 35 mm) specimen of the compression-compression series in biaxial compression (σ_2/σ_3 = 1) tested with the brush platen system

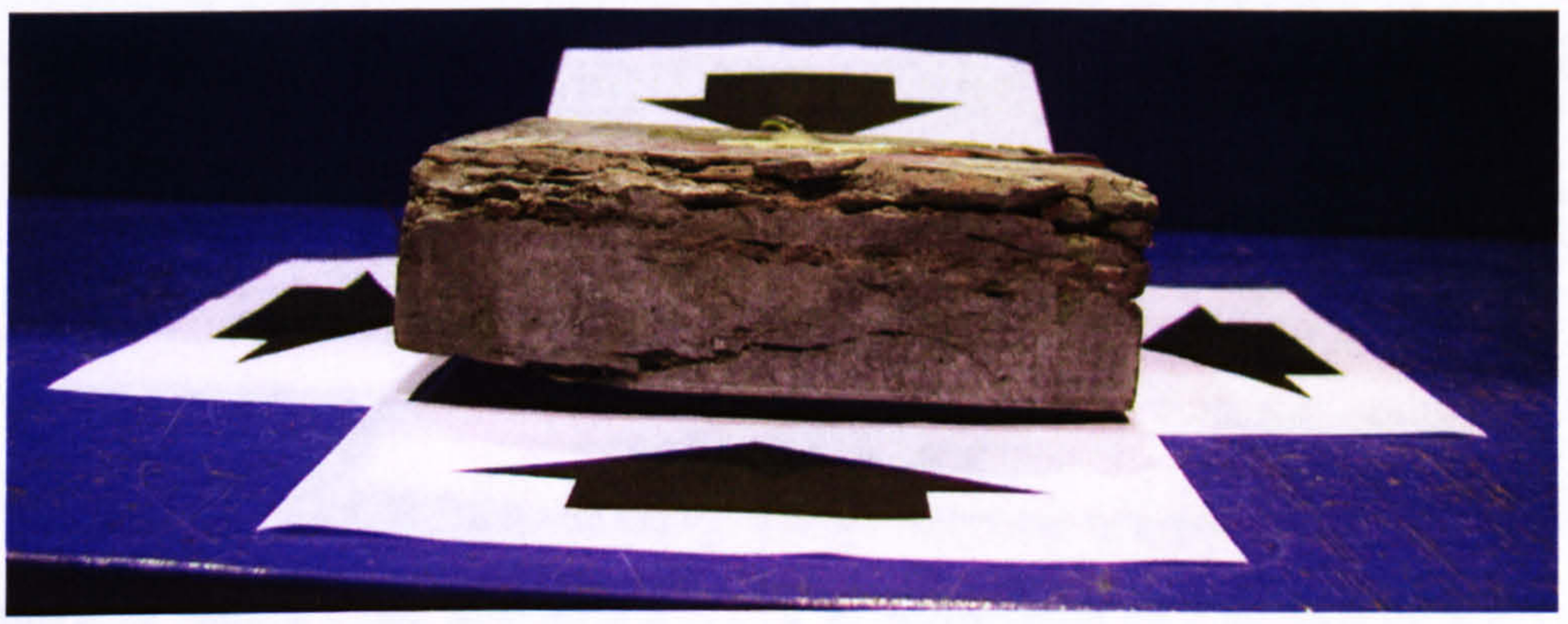

Figure 6.18 Failure mode of SFRHPC (V_f = 1 %, aspect ratio l/d = 65, fibre length l = 35 mm) specimen of the compression-compression series in biaxial compression (σ_2/σ_3 = 1) tested with the brush platen system

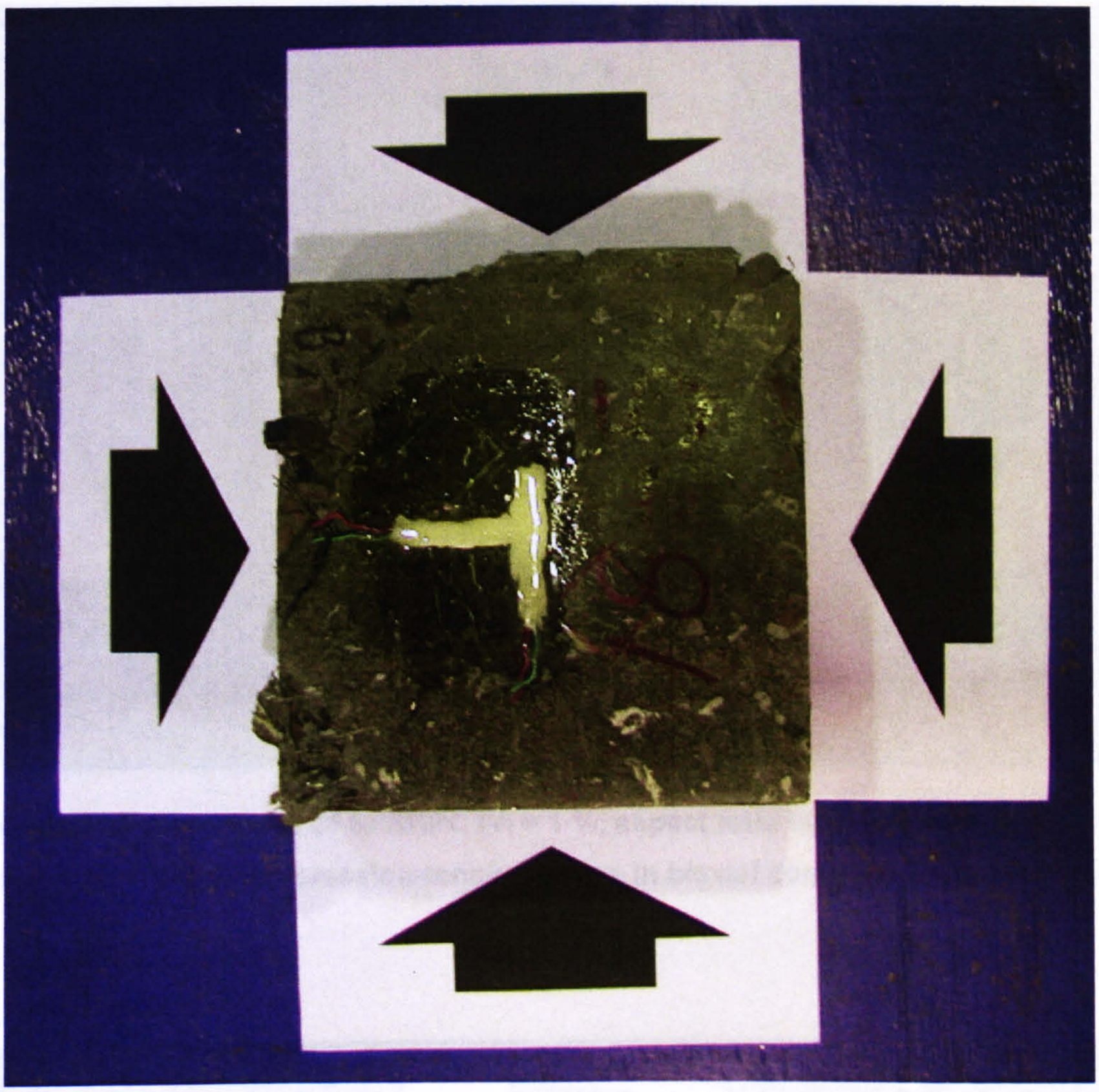

Figure 6.19 Failure mode of SFRHPC (V_f = 2 %, aspect ratio l/d = 65, fibre length l = 35 mm) specimen of the compression-compression series in biaxial compression (σ_2/σ_3 = 1) tested with the solid steel block platen system

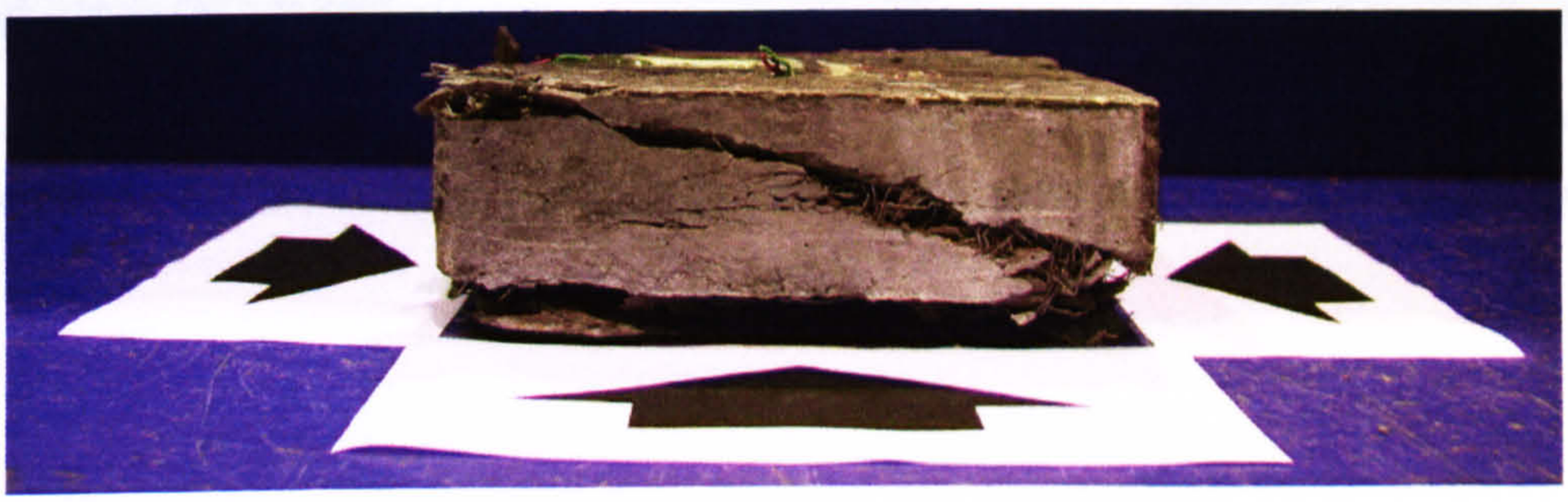

Figure 6.20 Failure mode of SFRHPC (V_f = 2 %, aspect ratio l/d = 65, fibre length l = 35 mm) specimen of the compression-compression series in biaxial compression (σ_2/σ_3 = 1) tested with the solid steel block platen system

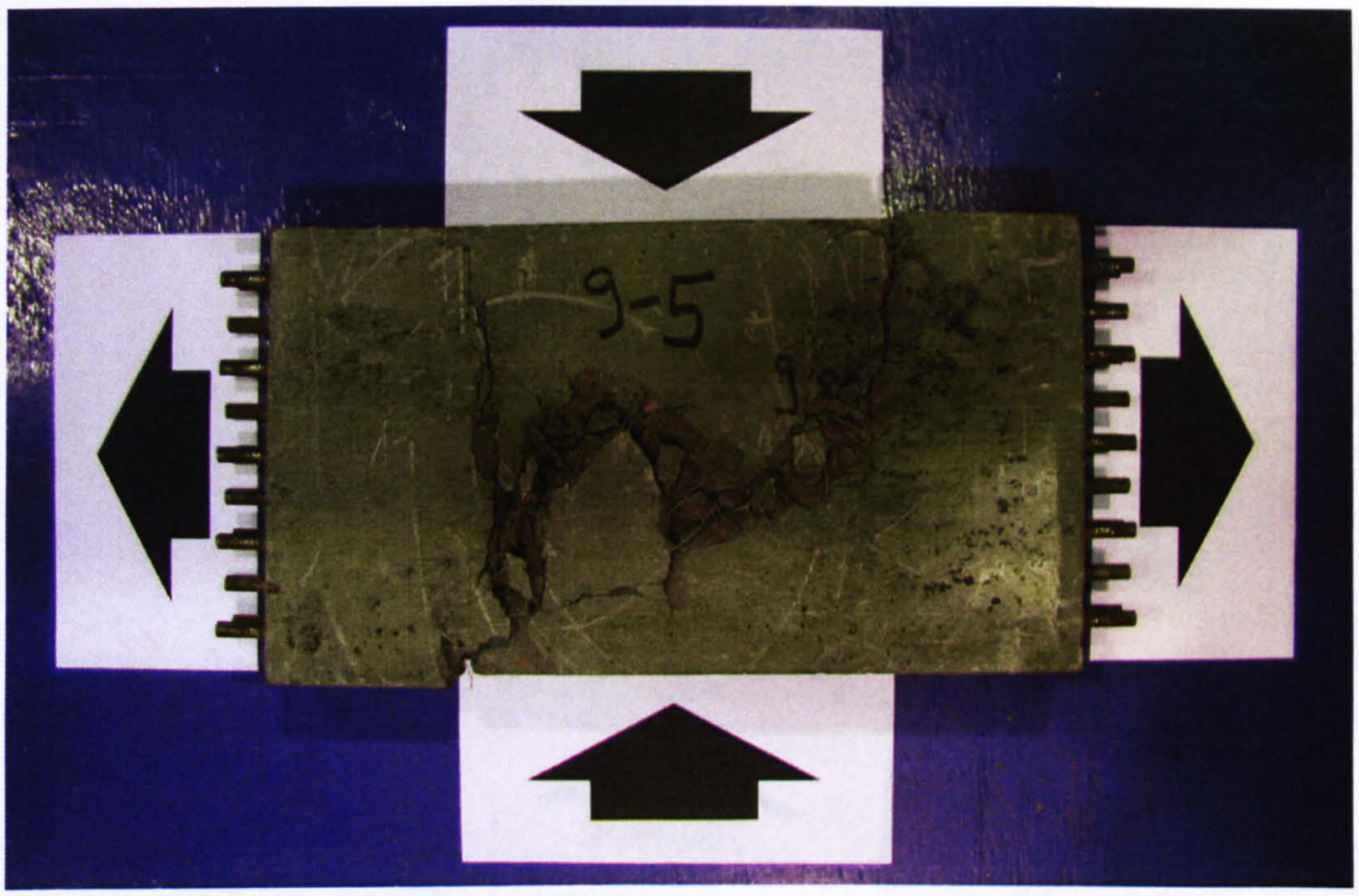

Figure 6.21 Failure mode of SFRHPC (V_f = 1 %, aspect ratio l/d = 65, fibre length l = 35 mm) specimen of the compression-tension series in biaxial compression-tension (σ_1/σ_3 = -0.012)

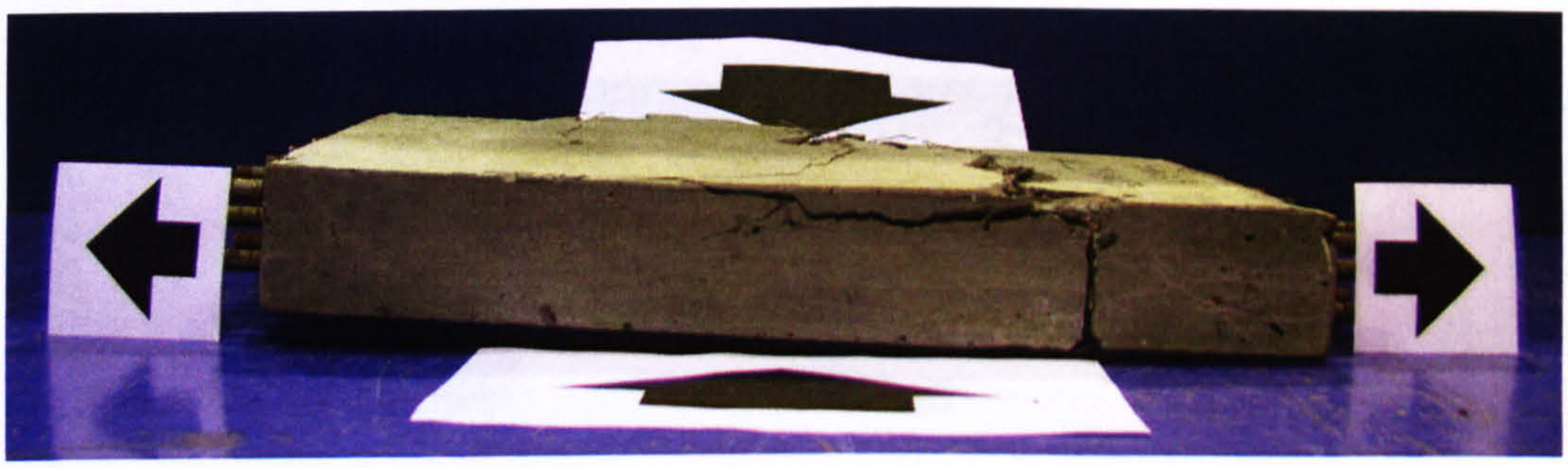

Figure 6.22 Failure mode of SFRHPC (V_f = 1 %, aspect ratio l/d = 65, fibre length l = 35 mm) specimen of the compression-tension series in biaxial compression-tension (σ_1/σ_3 = -0.012)

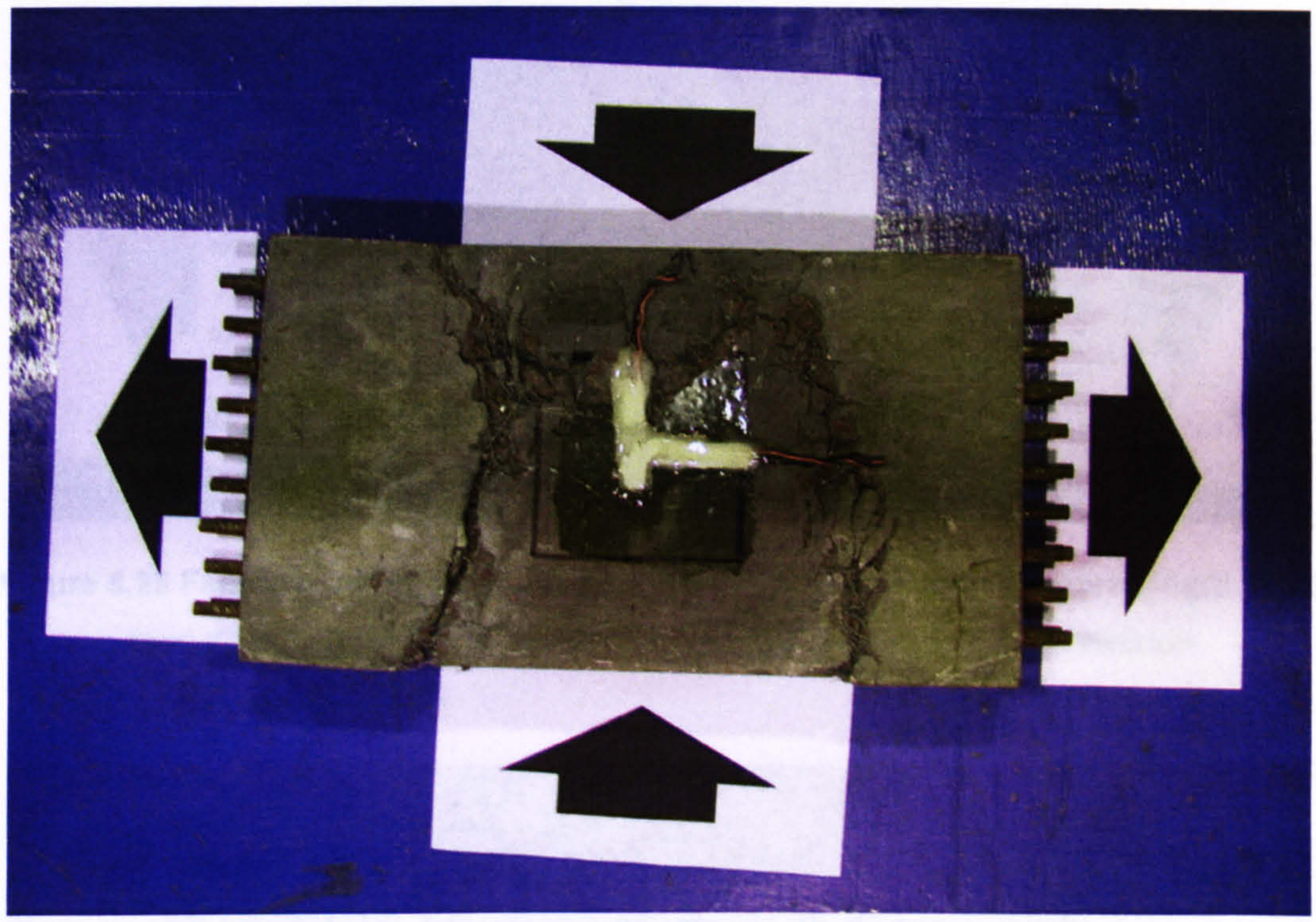

Figure 6.23 Failure mode of SFRHPC (V_f = 2 %, aspect ratio l/d = 65, fibre length l = 35 mm) specimen of the compression-tension series in biaxial compression-tension (σ_1/σ_3 = -0.02)

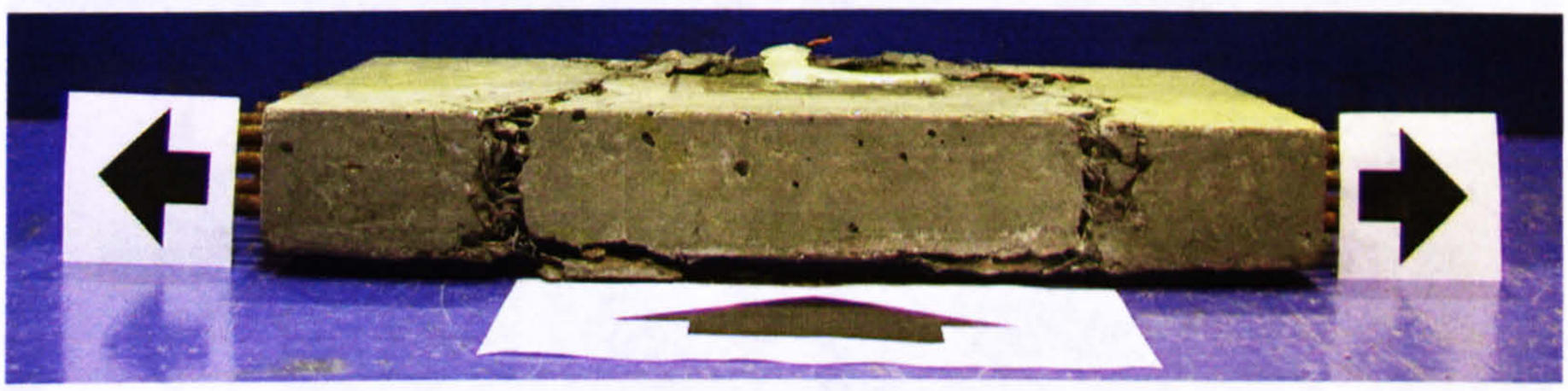

Figure 6.24 Failure mode of SFRHPC (V_f = 2 %, aspect ratio l/d = 65, fibre length l = 35 mm) specimen of the compression-tension series in biaxial compression-tension (σ_1/σ_3 = -0.02)

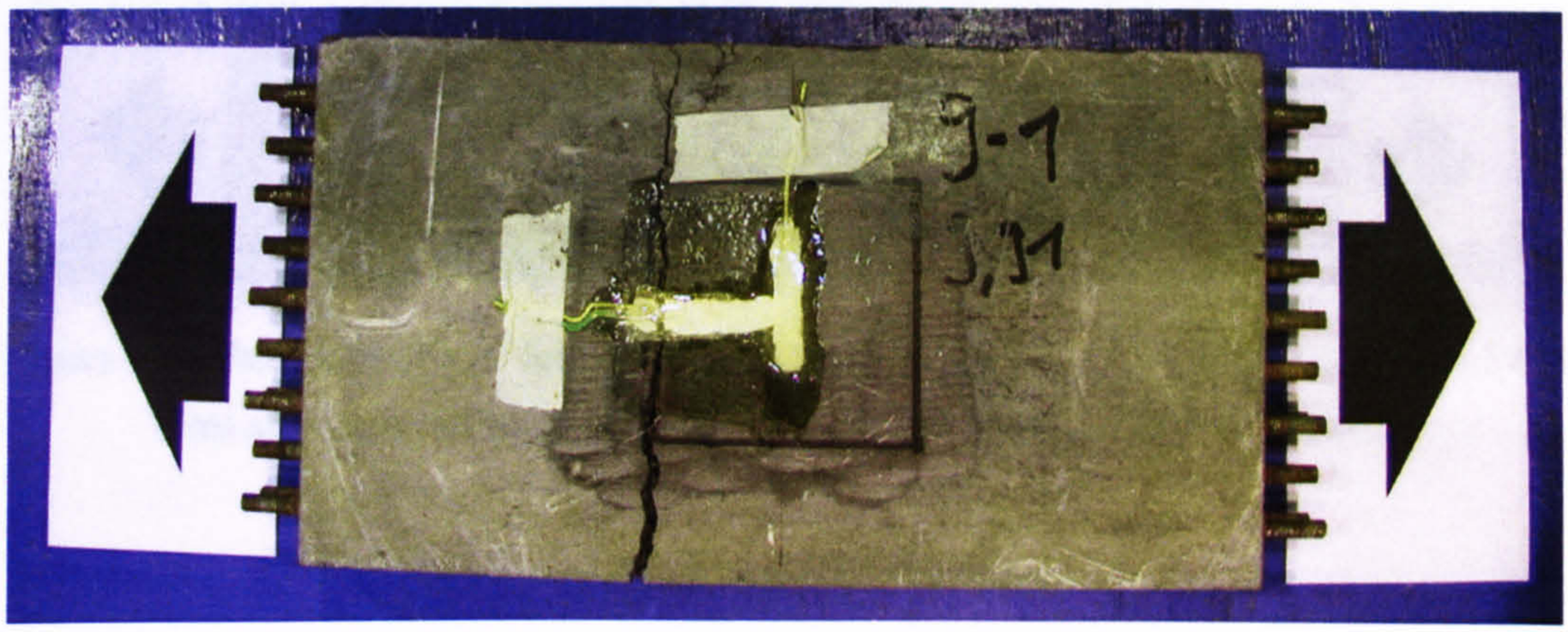

Figure 6.25 Failure mode of SFRHPC (V_f = 1 %, aspect ratio l/d = 65, fibre length l = 35 mm) specimen of the compression-tension series in uniaxial tension

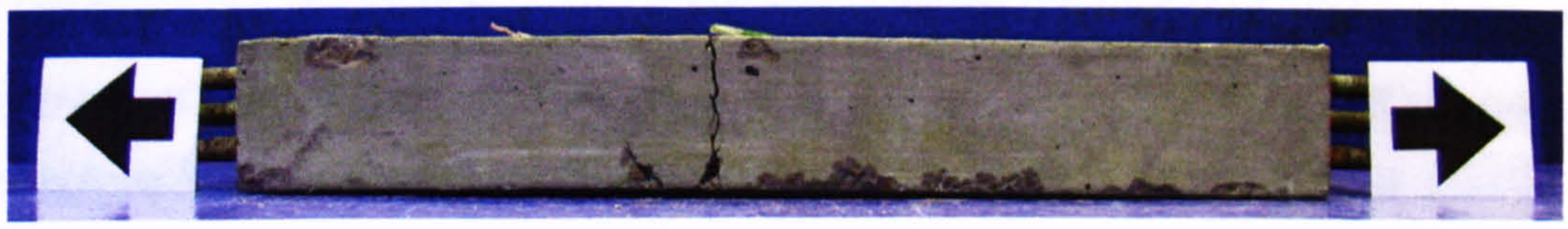

Figure 6.26 Failure mode of SFRHPC (V_f = 1 %, aspect ratio l/d = 65, fibre length l = 35 mm) specimen of the compression-tension series in uniaxial tension

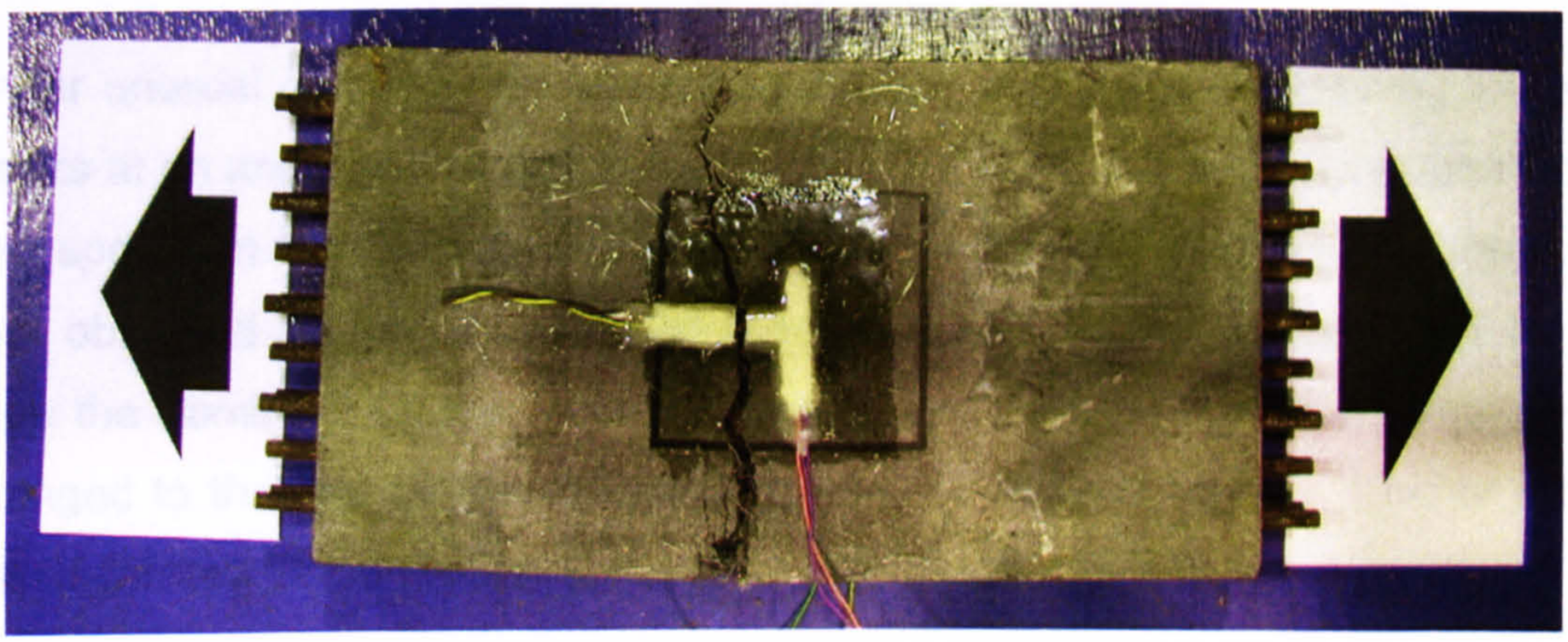

Figure 6.27 Failure mode of SFRHPC (V_f = 2 %, aspect ratio l/d = 65, fibre length l = 35 mm) specimen of the compression-tension series in uniaxial tension

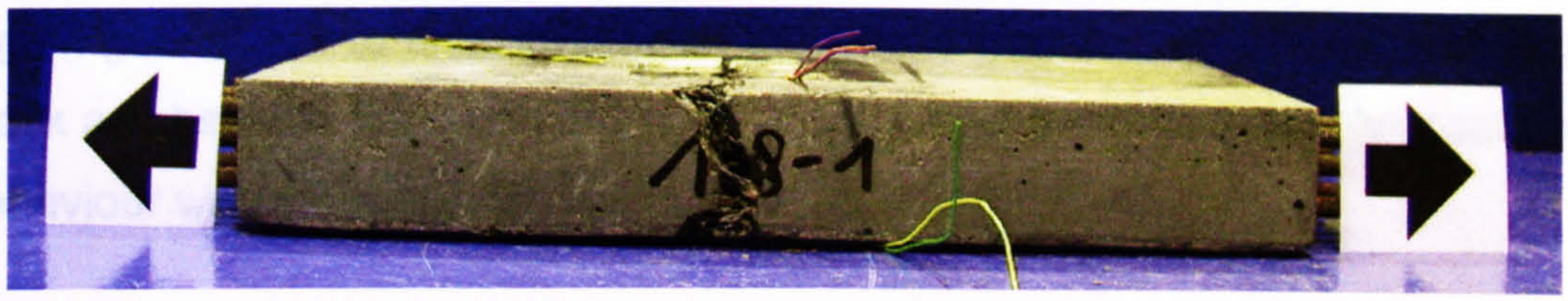

Figure 6.28 Failure mode of SFRHPC (V_f = 2 %, aspect ratio l/d = 65, fibre length l = 35 mm) specimen of the compression-tension series in uniaxial tension

6.3. Summary

In HPC cracks develop through mortar as well as aggregates. This makes the material a more homogeneous material than normal strength concrete. Therefore failure occurs more rapidly.

Plain HPC:

Under uniaxial compression and biaxial compression failure occurs by forming cracks at an angle of around 25° to the direction of the major compression load. The specimen fails into a number of plate like pieces. The same failure type was observed in the compression-tension region where compression loads were the dominant forces. After a stress ratio of σ_1/σ_3 = -0.06 the failure type changed to the one which was also observed in uniaxial tension. One or more cracks formed perpendicular to the tension force.

Steel Fibre HPC:

The addition of fibres and the increase of the fibre content do not change the failure mode significantly when compression loads are dominant. The main difference is that the specimen pieces are still connected by the fibres after the peak load was reached. When the stress ratio in the compression-tension

region gets closer to uniaxial tension the failure type changes again to a single crack as observed for plain HPC. Only the strength increases and the post peak behaviour was more ductile.

6.4. References

Hussein, A.A. 1998, *Behaviour of High-Strength Concrete under Biaxial Loading Condition,* PhD thesis, Faculty of Engineering and Applied Science, Memorial University of Newfoundland, St. John's, Canada.

Neville, A.M. 1995 *Properties of concrete.* 4th edn., Longman Group Limited, Essex, England, p. 683.

Traina, L.A. and Mansour, S.A. 1991, 'Biaxial Strength and Deformational Behavior of Plain and Steel Fibre Concrete', *ACI Material Journal*, vol. 88, no. 4, July-August, pp. 354-362.

Yin, W.S., Su, E.C.M., Mansur, M.A. and Hsu, T.T.C. 1989, 'Biaxial Tests of Plain and Fibre Concrete', *ACI Material Journal*, vol. 86, no. 3, May-June, pp. 236-243.

7. Analytical models

In the following the result of different mathematical formulations and failure criteria, introduced and described in the Literature Review, are shown and compared with experimental data from this study.

7.1. Ottosen failure criteria combined with SFRC model

The failure stresses estimated with the Ottosen failure criteria (1977) used parameters developed by the f_t/f_c ratio of 0.08. To obtain the failure envelope for SFRC using the model developed by Murugappan, (1993) and described in the Literature Review the post cracking tensile strength σ_{tu} was obtained first. The literature (Lim et al., 1987) provided the ultimate fibre bond strength τ_u = 6.72 N/mm^2 for the same fibre type as used in this study (65-35, V_f = 1%). This will be used in the following equation which was introduced in the Literature review before

$$\sigma_{tu} = \frac{\eta_l \eta_0 V_f l \tau_u}{2r} \qquad (7.1)$$

together with the values of $\eta_l = 0.5$ and $\eta_0 = 0.4$. Therefore σ_{tu} was calculated as 1.68 N/mm^2 as stated also by Murugappan et al. (1993). The value of σ_1 = -σ_{tu} was kept constant while σ_2 was increased with constant load steps and σ_3 was calculated using the failure criterion described earlier.

Typical biaxial failure envelopes for plain and SFRC with a uniaxial plate compressive strength of 99 N/mm^2 for plain concrete are shown in Figure 7.1 for different V_f and therefore different σ_{tu}. The values for σ_{tu} are 0.84, 1.68, 2.52 and 3.36 N/mm^2 for V_f = 0.5 %, 1 %, 1.5 % and 2 % respectively. The above

values are for the fibre type 65-35 as this fibre type was also used by other researchers (Traina and Mansour (1991), Lim (1987) and Murugappan et al. (1993)) and makes comparison easier in terms of the σ_{tu} values.

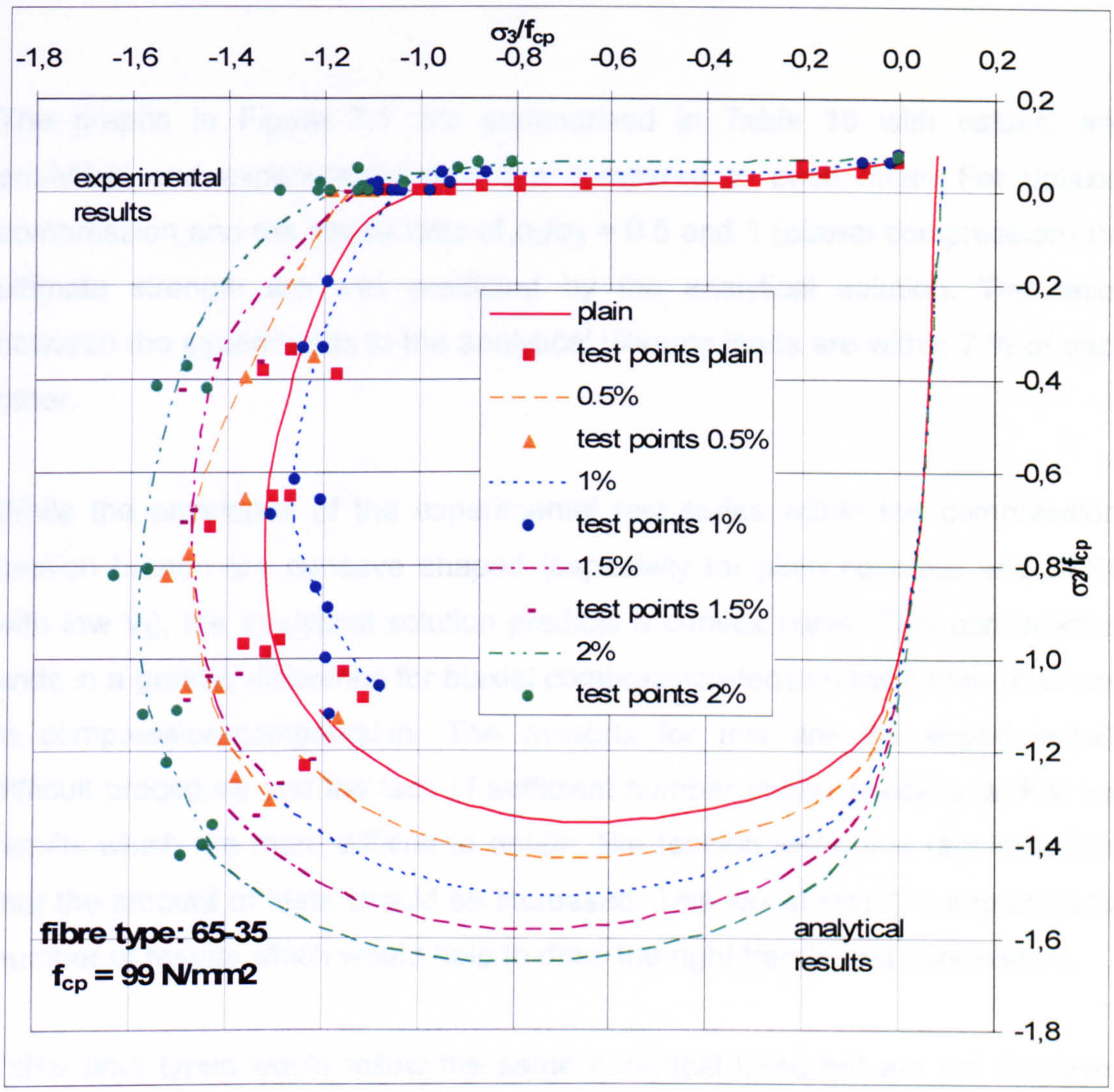

Figure 7.1 Biaxial strength envelope for plain and steel fibre concrete; test points and analytical model for fibre type 65-35

From the graph it is seen that with increasing fibre content and therefore the value of σ_{tu}, there is an increase in the biaxial strength. This trend can be observed for both, the analytical and the experimental data and was also reported by other researchers like Yin et al. (1989) and Traina and Mansour

(1991) for normal strength concrete as reported before. Note that the test points of the fibre content series V_f = 1% are not following this trend. This is because they were tested with brush loading platens at the beginning of the experimental test series before the test set-up was changed to solid steel platens which fit the analytical solution more closely.

The graphs in Figure 7.1 are summarised in Table 15 with values, and analytical and experimental data are compared to each other. For uniaxial compression and the stress ratio of σ_2/σ_3 = 0.5 and 1 (biaxial compression) the ultimate strength are well predicted by the analytical solution. The ratios between the experiments to the analytical ultimate loads are within 7 % of each other.

While the envelopes of the experimental test series within the compression-tension branch are concave shaped (especially for plain concrete and SFRC with low V_f), the analytical solution predicts a convex curve. This contradiction ends in a greater difference for biaxial compression-tension tests than observed in compression-compression. The reasons for this are the experimentally difficult procedure and the lack of sufficient number of test specimens. For test results which are more difficult to obtain, like tension tests, it is recommended that the amount of tests should be increased. This would result in a reasonable number of results which would help to draw the right trends and conclusions.

Other fibre types would follow the same analytical trend but are not displayed here because readily available values for σ_{tu} were not available at the time. The method with the constant confining pressure in the third direction caused by the presence of fibres can be also transferred to other strength criteria calculations and would show the same results.

	Stress ratio σ_2/σ_3	Test result / f_{cp}	Analytical result / f_{cp}	Ratio of test / analytical result
plain	Tension	0.065	0.077	0.84
	Compression	-1.0	-1.0	1.0
	0.5	-1.3	-1.35	0.96
	1 (biaxial comp)	-1.18	-1.16	1.02
0.5 %	Compression	-1.15	-1.03	1.11
	0.5	-1.47	-1.43	1.03
	1 (biaxial comp)	-1.31	-1.22	1.07
1 %	Tension	0.08	0.09	0.88
	Compression	-1.05	-1.06	0.99
	0.5	-1.26	-1.5	0.84
	1 (biaxial comp)	-1.08	-1.3	0.83
1.5 %	Compression	-1.13	-1.08	1.05
	0.5	-1.47	-1.58	0.93
	1 (biaxial comp)	-1.29	-1.35	0.95
2 %	Tension	0.07	0.10	0.78
	Compression	-1.18	-1.10	1.07
	0.5	-1.58	-1.66	0.95
	1 (biaxial comp)	-1.42	-1.42	1.0

Table 15 Comparison between test and analytical results (fibre type 65-35)

7.2. Willam-Warnke failure envelope

Different failure criteria are compared in a biaxial plane in Figure 7.2 with the Willam-Warnke model. The curves match the experimental data points quite well, however they overestimate them a bit, especially in the compression-tension region. Due to the large scatter of the test points the presented models are all good in representing the failure surface of HPC. Tho, Seow and Swaddiwudhipong, 2003 reported similar results for NSC. They recorded an overestimation of the ultimate stress in the analytical results due to the fact that the 3-D failure surface overestimates the two dimensional failure envelopes upon degeneration. The overestimation is more significant for biaxial load ratios around $\sigma_2/\sigma_3 = 0.5$. For load ratios close to biaxial compression $\sigma_2/\sigma_3 = 1$ the analytical curve fits the shape of the experimental curve relatively well.

For the description of the failure surface of plain HPC following five parameters were found by the calculations provided in the literature and used for this solution:

$a_0 = 0.058$ $\quad$ $b_0 = 0.045$

$a_1 = -1.571$ $\quad$ $b_1 = -1.237$

$a_2 = -1.391$ $\quad$ $b_2 = -0.834$

Also shown in Figure 7.2 is the graph developed with the formulation developed by Seow and Swaddiwudhipong, 2005 for a fibre reinforcing factor of k =1 (plain concrete). Good agreement was observed, also because the formulation was based on the Willam-Warnke failure criterion. Similar results for SFRC were obtained as shown before. The formulation for the use of fibres was assumed to be a confining stress in the third direction and therefore the envelope will look similar.

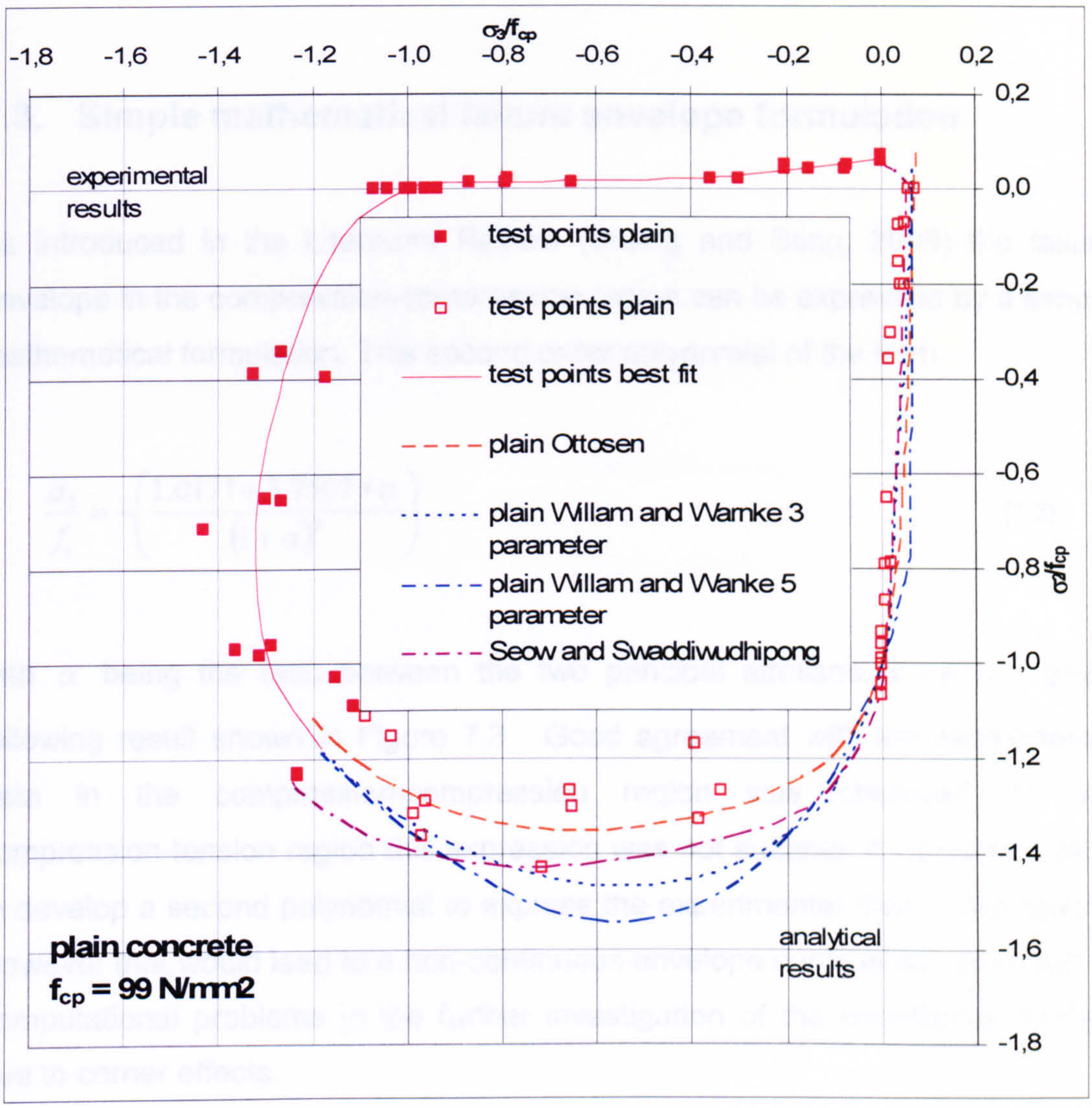

Figure 7.2 Comparison between different failure criteria with biaxial tests of plain HPC

7.3. Simple mathematical failure envelope formulation

As introduced in the Literature Review (Shang and Song, 2006) the failure envelope in the compression-compression region can be expressed by a simple mathematical formulation. This second order polynomial of the from

$$\frac{\sigma_3}{f_c} = -\left(\frac{1.0171 + 3.7507 * \alpha}{(1+\alpha)^2}\right) \tag{7.2}$$

with α being the ratio between the two principal stresses $\alpha = \sigma_2/\sigma_3$ gives following result shown in Figure 7.3. Good agreement with the experimental data in the compression-compression region was observed. In the compression-tension region this expression was not suitable. It would be useful to develop a second polynomial to express the experimental data in this region. However that would lead to a non-continuous envelope curve which will result in computational problems in the further investigation of the constitutive models due to corner effects.

Similar curves can be developed for different fibre concretes. Because the formulation takes only the compressive strength into account there are no extensive biaxial tests needed when the curve was developed once. However, the curve results in good agreement with the test data there is no formulation involved which takes the fibre variables into account. Therefore these formulations are only a curve fitting process for each individual fibre concrete.

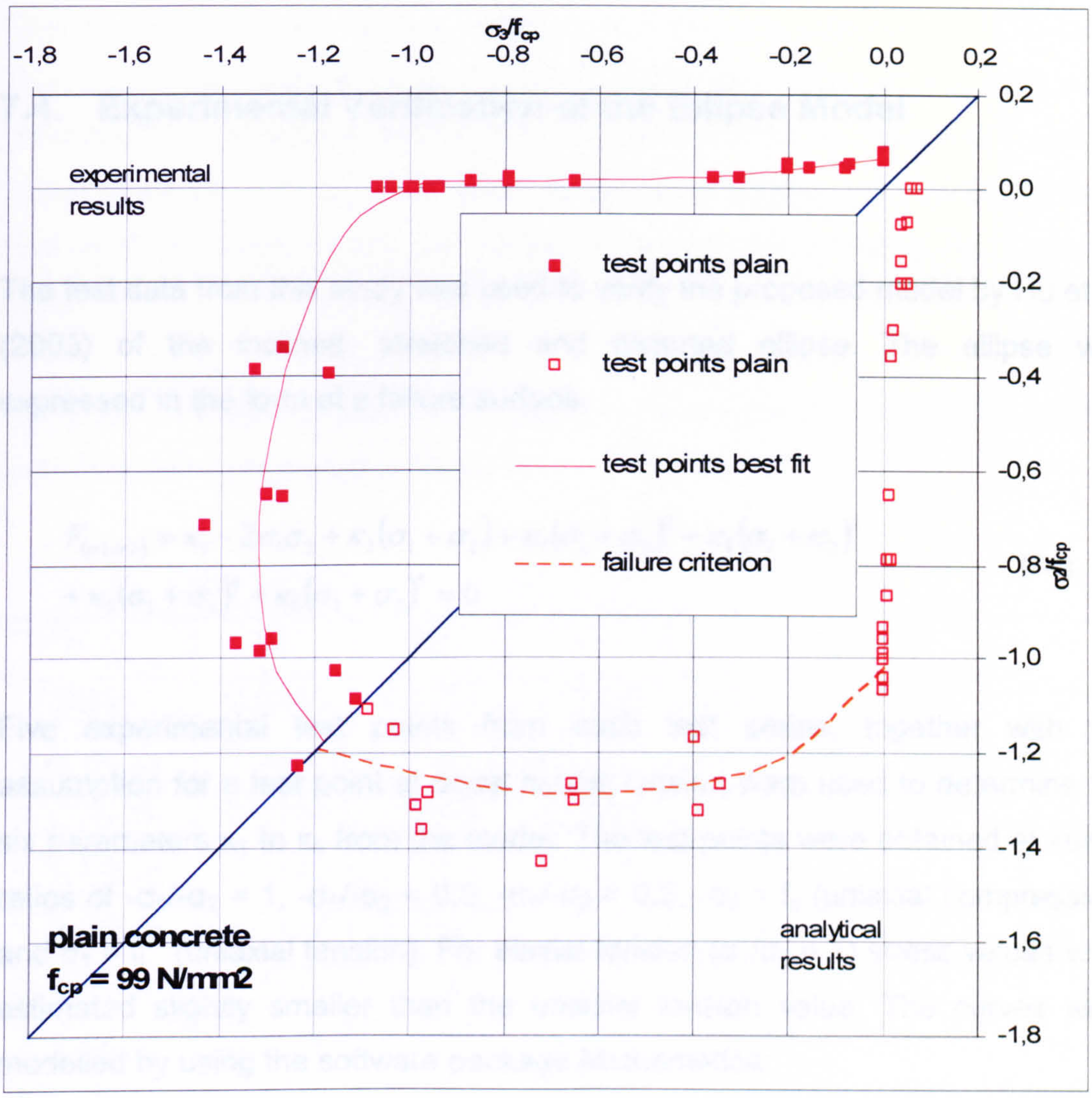

Figure 7.3 Failure envelope of plain HPC expressed by a polynomial second order in the compression-compression region

7.4. Experimental Verification of the Ellipse Model

The test data from this study was used to verify the proposed model by Hu et al. (2003) of the inclined, stretched and distorted ellipse. The ellipse was expressed in the form of a failure surface:

$$F_{(\sigma 1,\sigma 2)} = \kappa_1 - 2\sigma_1\sigma_2 + \kappa_2(\sigma_1+\sigma_2) + \kappa_3(\sigma_1+\sigma_2)^2 + \kappa_4(\sigma_1+\sigma_2)^3 + \kappa_5(\sigma_1+\sigma_2)^4 + \kappa_6(\sigma_1+\sigma_2)^5 = 0 \quad (7.3)$$

Five experimental test points from each test series, together with the assumption for a test point at equal biaxial tension were used to determine the six parameters κ_1 to κ_6 from the model. The test points were obtained at stress ratios of $-\sigma_1/-\sigma_2 = 1$, $-\sigma_1/-\sigma_2 = 0.5$, $-\sigma_1/-\sigma_2 = 0.2$, $-\sigma_2 = f_c$ (uniaxial compression) and $\sigma_1 = f_t$ (uniaxial tension). For biaxial tension ($\sigma_1/\sigma_2 = 1$) stress values were estimated slightly smaller than the uniaxial tension value. The curves were modelled by using the software package Mathematica.

Figure 7.4 to Figure 7.11 show the modelled failure envelopes together with the associated test points for each individual test series. Good agreement between test points and the modelled envelopes were observed within the compression-compression branch of the envelope. Because of the necessary continuous convexity of the curve for further computational modelling the test points in the compression-tension region for plain and lower fibre content concretes could not be easily expressed. It was possible to fit the data very well with the method described above. However the curve would not be convex anymore in the compression-tension region. In order to use these curves in a further modelling process the less accurate convex curves are displayed.

Best results for smooth failure envelopes were obtained with the values in Table 16 for the parameters κ_1 to κ_6 in the fifth order polynomial equation for each individual fibre variable. Even though some trends could be recognised with the values in the table it has to be recalled that the envelopes presented here are a best fit of the experimental test points which are also following only a vague trend.

Using the average for plain, 1 % and 2 % fibre types the values for κ_1 to κ_6 follow the trend presented in Table 17.

	κ_1	K_2	κ_3	κ_4	κ_5	κ_6
plain	-0.0084	0.1309	-0.0289	0.1456	0.4217	0.1079
1 % 45-35	Tested with brush platen system and therefore not comparable					
1 % 45-50	-0.0136	0.2398	-0.4489	-0.8347	-0.1934	-0.0103
1 % 65-30	-0.0130	0.1815	-0.1435	0.0023	0.4398	0.1310
1 % 65-50	-0.0134	0.2396	-0.4720	-0.7911	-0.1440	0.0010
2 % 45-35	-0.0112	0.1541	-0.0421	0.0599	0.2322	0.0485
2 % 45-50	-0.0109	0.1449	-0.0181	0.2123	0.3854	0.0845
2 % 65-30	-0.0109	0.1516	-0.0453	0.0802	0.2660	0.0575
2 % 65-50	-0.0108	0.1609	-0.0919	-0.0828	0.1838	0.0459

Table 16 Parameters κ1 to κ6 for the polynomial fifth order for each test series

	κ_1	K_2	κ_3	κ_4	κ_5	κ_6
plain	-0.0084	0.13	-0.029	0.146	0.422	0.108
1 %	-0.013	0.22	-0.44	-0.80	-0.15	0.01
2 %	-0.011	0.15	-0.04	0.40	0.27	0.05

Table 17 Trends for parameters κ1 to κ6

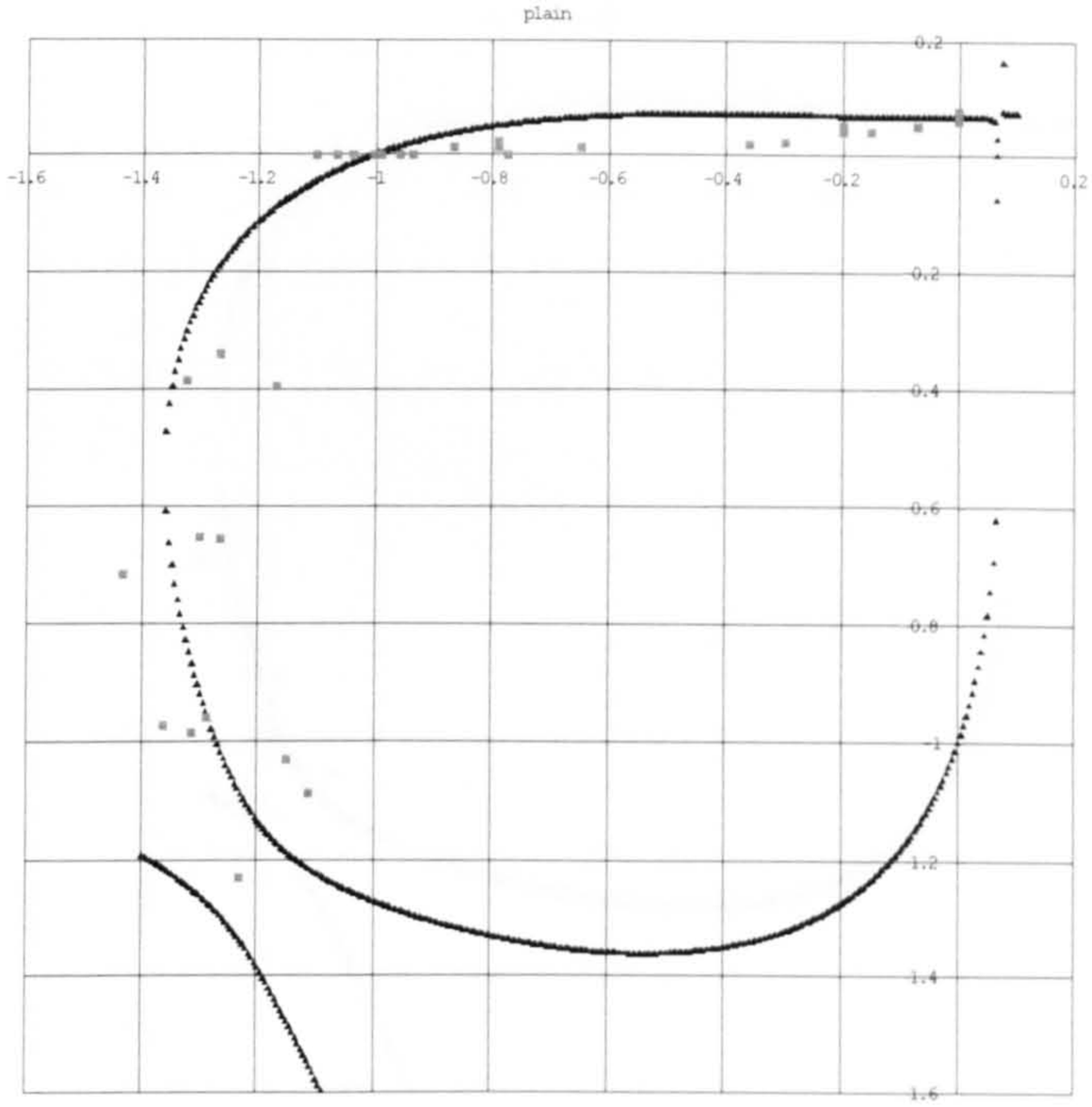

Figure 7.4 Proposed failure envelope and experimental test points for plain HPC

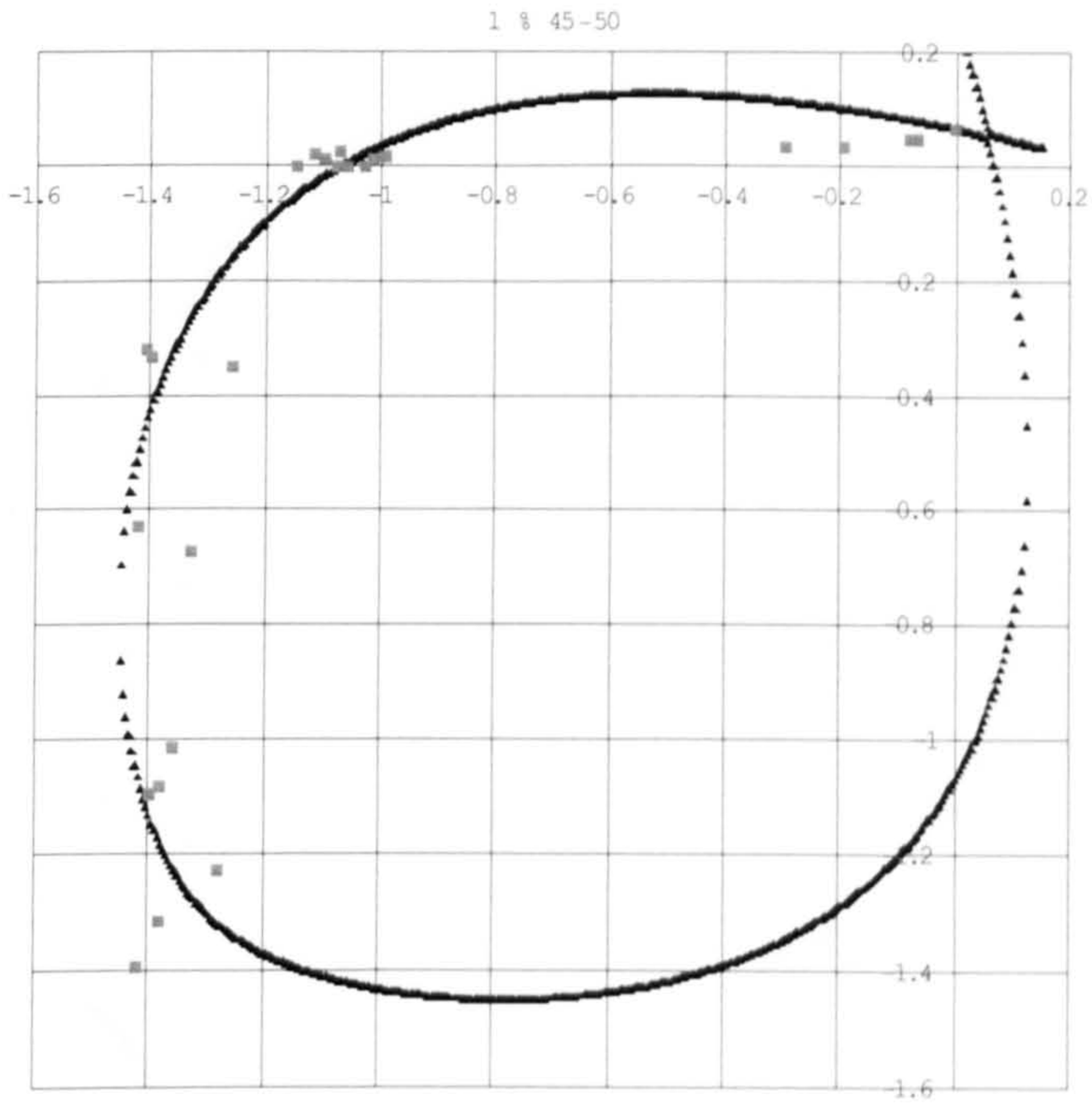

Figure 7.5 Proposed failure envelope and experimental test points for 1 % 45-50 SFHPC

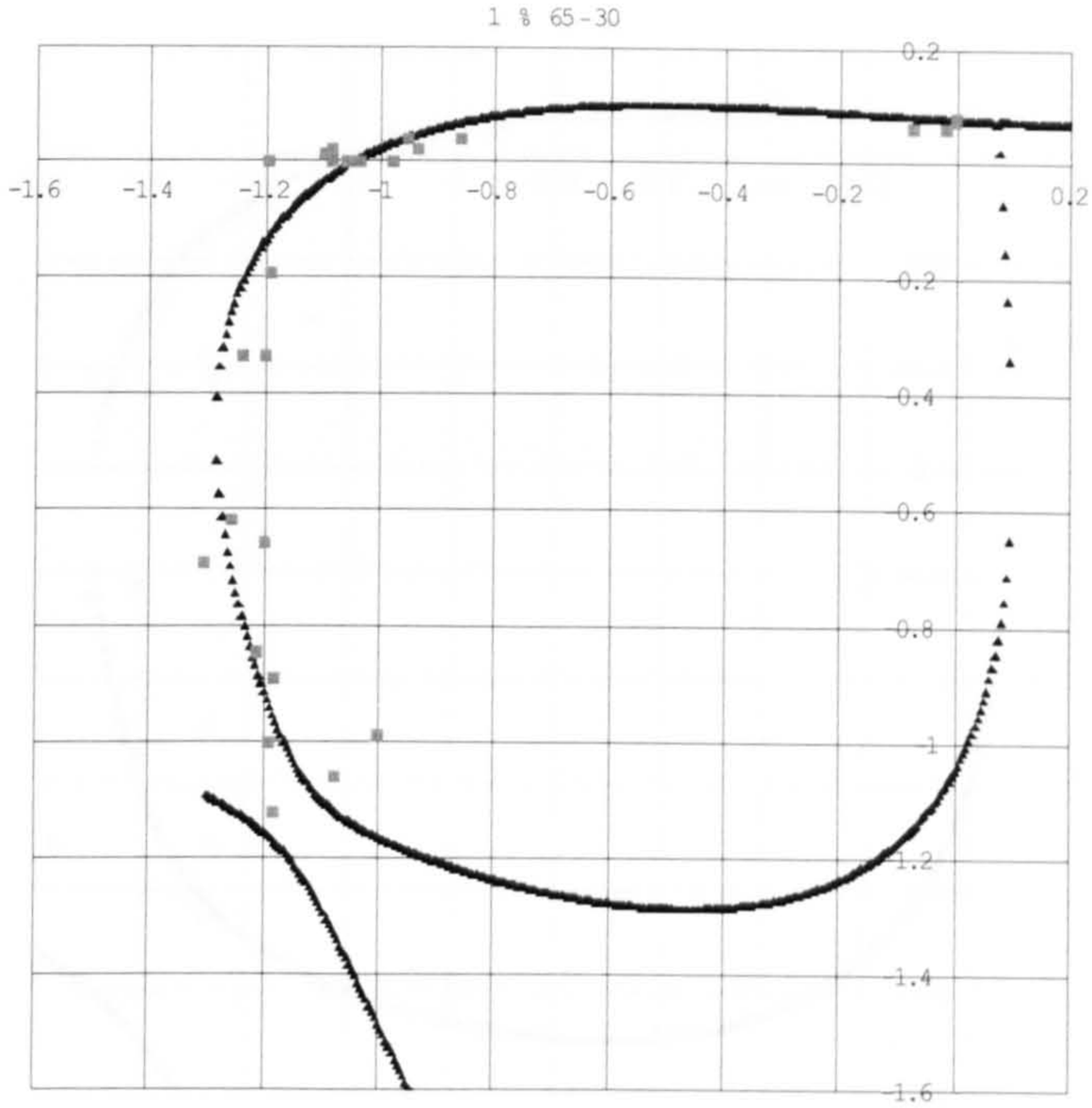

Figure 7.6 Proposed failure envelope and experimental test points for 1 % 65-30 SFHPC

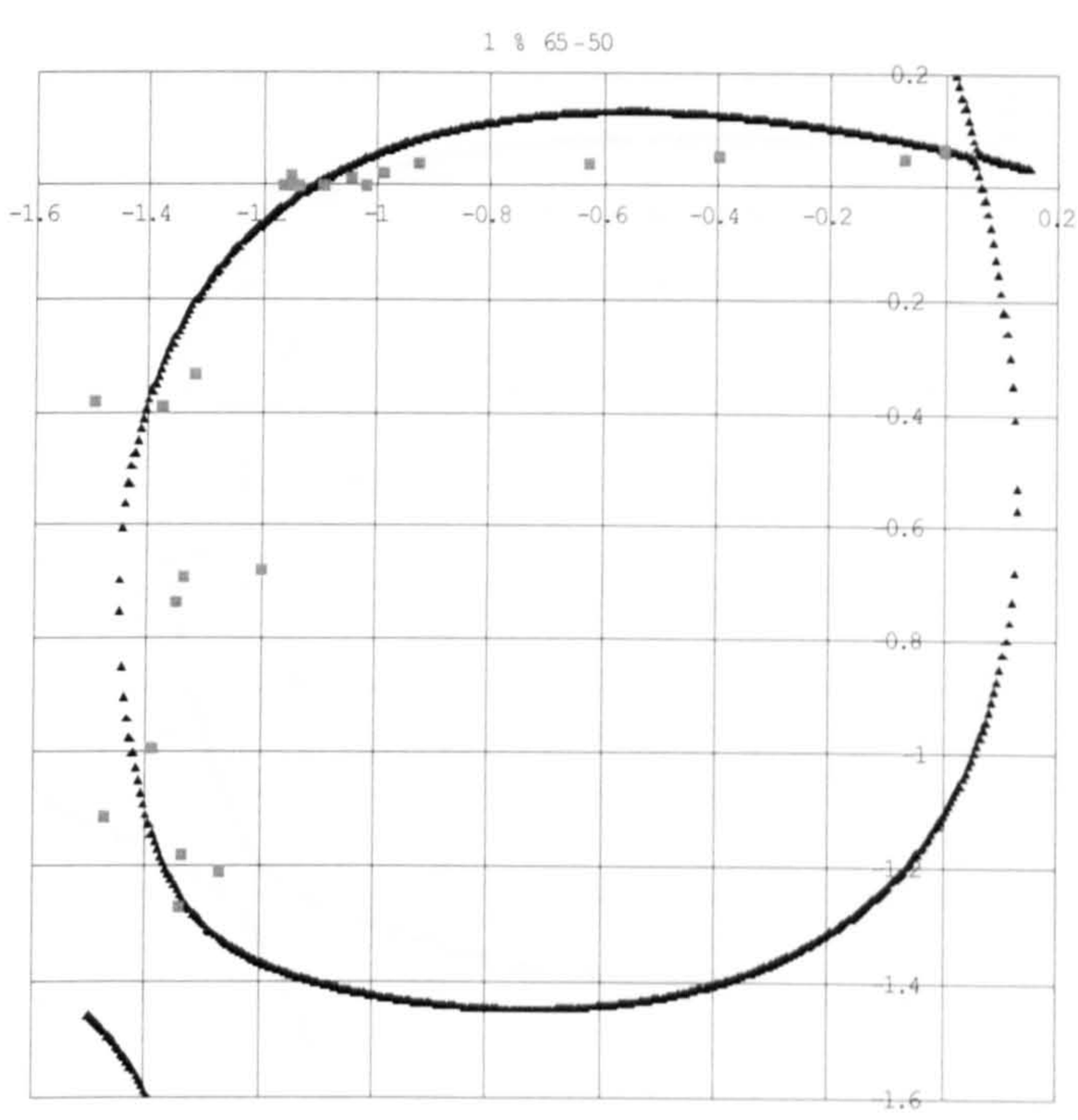

Figure 7.7 Proposed failure envelope and experimental test points for 1 % 65-50 SFHPC

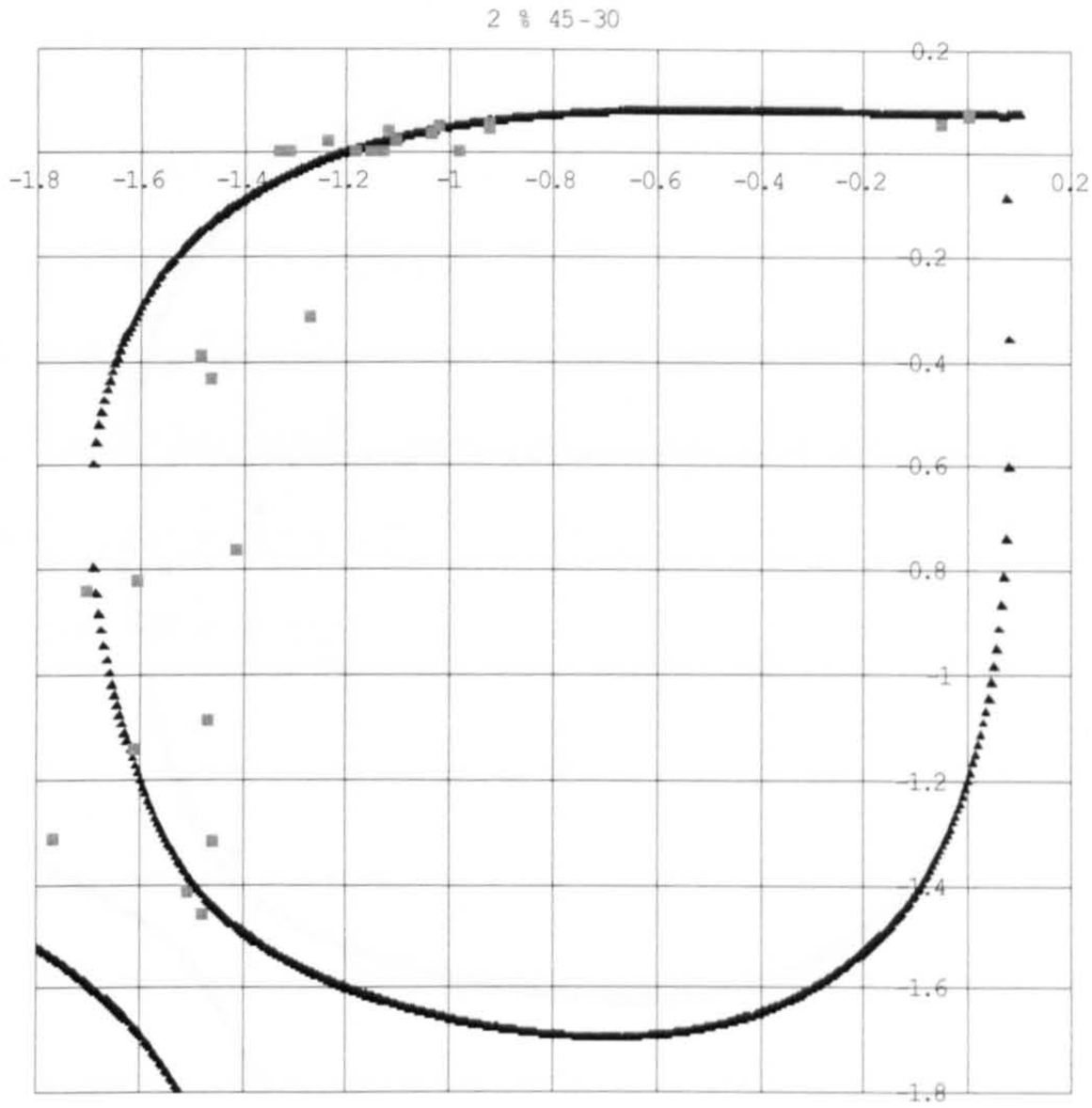

Figure 7.8 Proposed failure envelope and experimental test points for 2 % 45-30 SFHPC

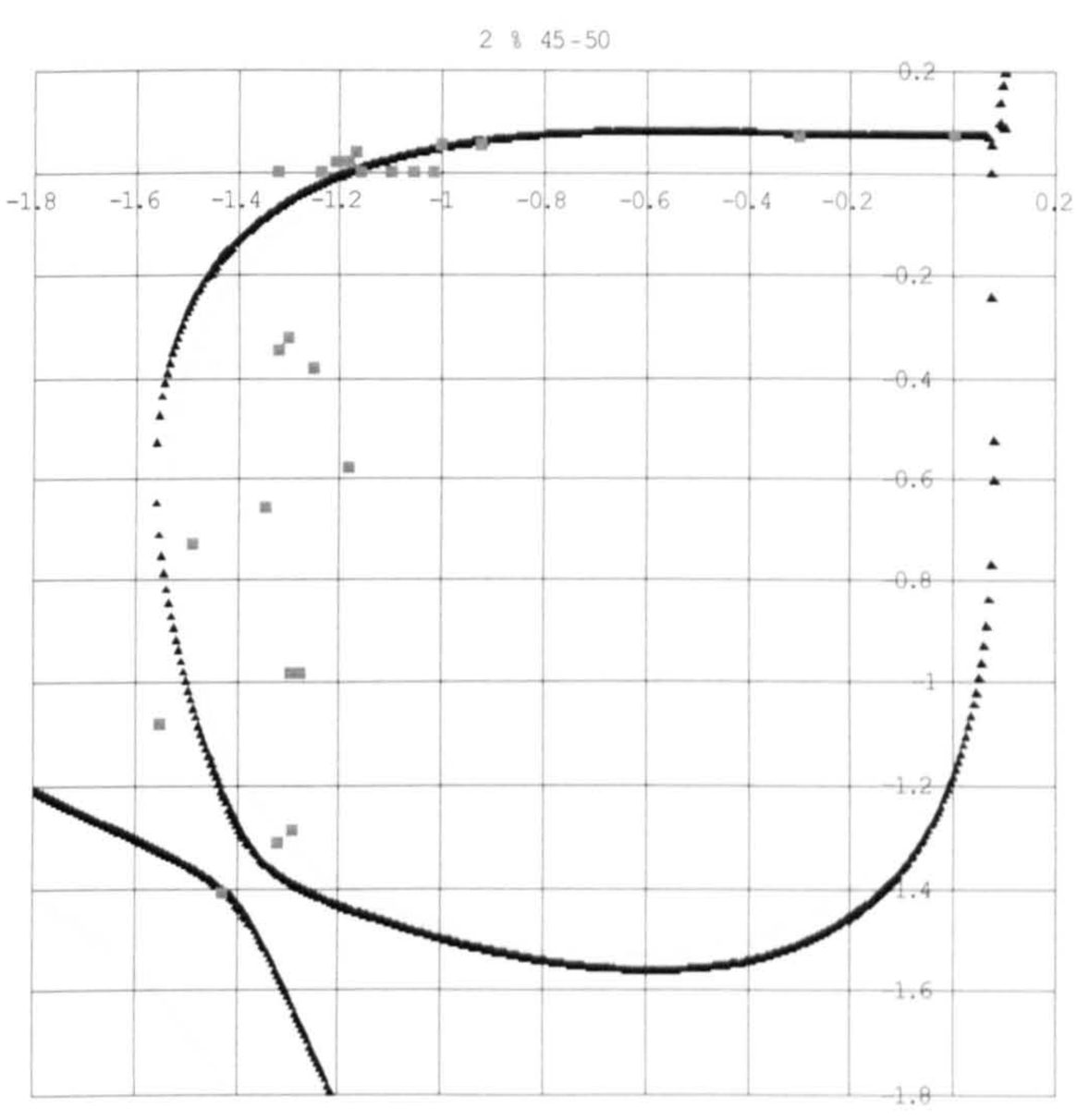

Figure 7.9 Proposed failure envelope and experimental test points for 2 % 45-50 SFHPC

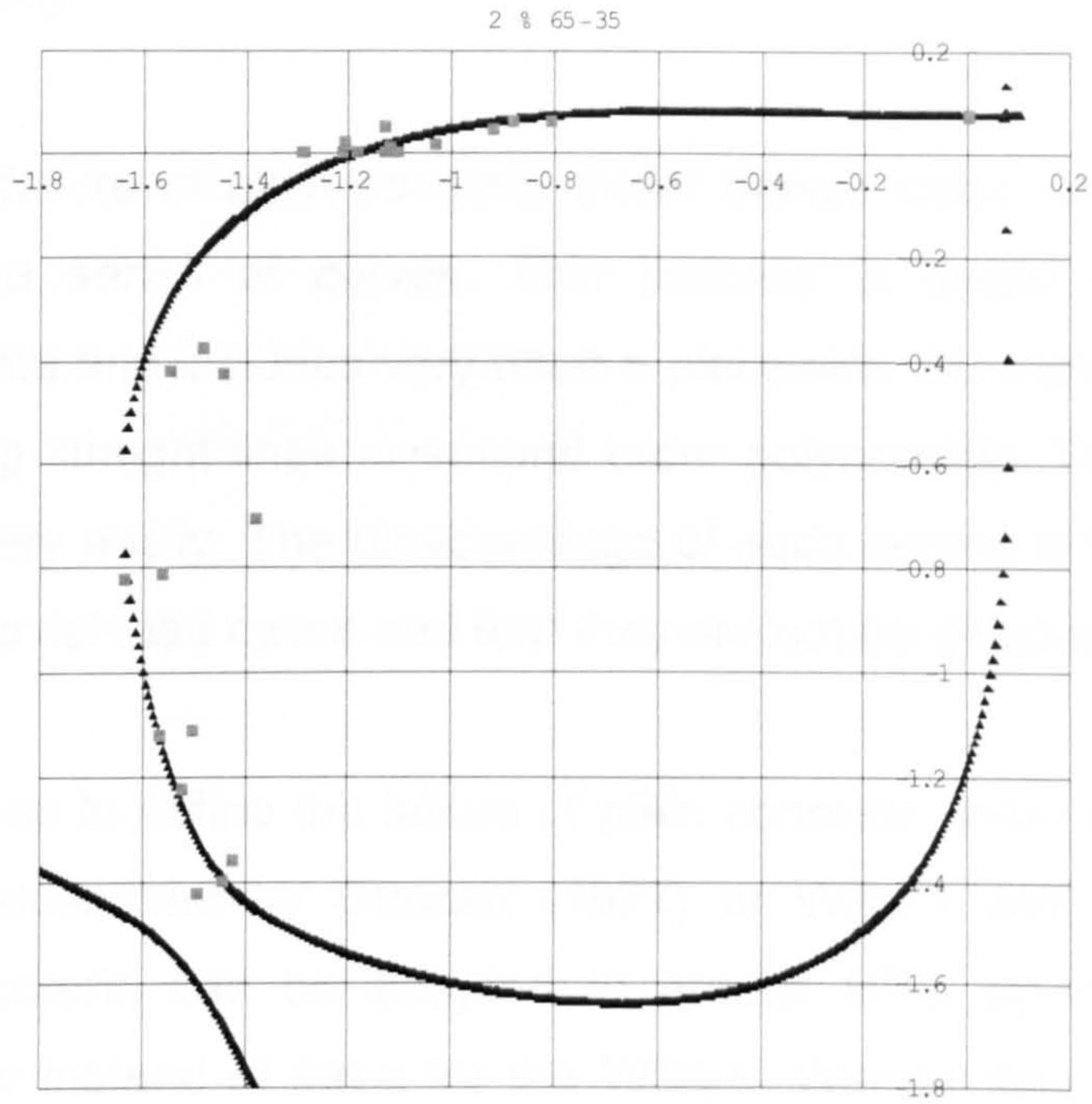

Figure 7.10 Proposed failure envelope and experimental test points for 2 % 65-35 SFHPC

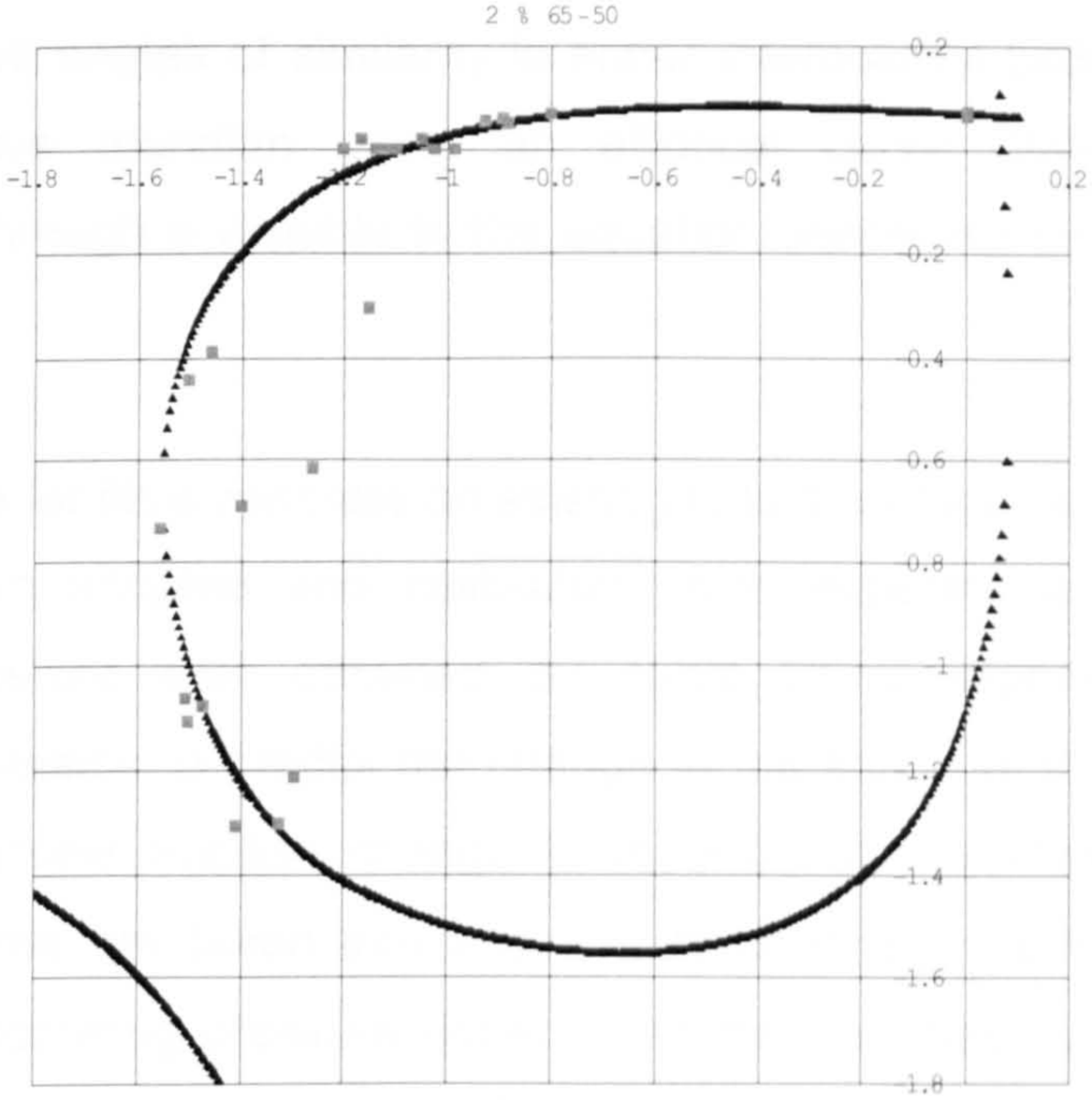

Figure 7.11 Proposed failure envelope and experimental test points for 2 % 65-50 SFHPC

7.5. Summary

To predict the failure of plain concrete under biaxial loads, envelopes can be developed as a series of curves. This process is based on curve fitting experimental data and includes very often a piecewise description of the biaxial envelopes using straight lines or second order polynomials. These curves can be computed very easily. The disadvantage of such curves is that they can be only used for biaxial load cases and that they are not continuous.

Other approaches to define the failure of plain concrete under biaxial loads are failure criteria described by Ottosen (1977) or Willam and Warnke (1974). These failure criteria can be adopted to predict HPC by introducing more parameters (five instead of three for the Willam- Warnke failure criteria). Four (Ottosen) or five parameters are required in the equations to define the entire failure surface. They are described in the three dimensional Haigh-Westergaard stress space and exist of a cone shaped failure surface described by quadratic equations along the meridians. The shape of the surface along the deviatoric plane at different angles of similarity is either interpolated between the tensile and compressive meridian using an elliptical curve (Willam-Warnke) or accounted for through a variable in the equation describing the meridian curve (Ottosen).

To obtain failure for fibre concrete an existing failure surface developed for plain concrete can be adopted and calibrated using experimental data. Such a surface is therefore also obtained by curve fitting experimental data. A systematic expression to predict the change in the shape of the failure surface as the fibre volume fraction change is introduced. Therefore under biaxial loading, the fibres are taken into account as confining pressure in the third direction. This confining pressure depends on the variables such as fibre type, fibre orientation and volume fraction. This would limit the needs for experimental data in the future once the fibre variables for each fibre type are known.

7.6. References

Hu, Xiao Dong, Day, Robert and Dux, Peter, 2003, 'Biaxial Failure Model for Fibre Reinforced Concrete', *Journal of Materials in Civil Engineering, ASCE*, Vol. 15, No. 6, pp. 609-615.

Lim, T.Y., Paramasivam, P. and Lee, S.L., 1987, 'Analytical Model for Tensile Behavior of Steel-Fibre Concrete', *American Concrete Institute Materials Journal, Proceedings*, vol. 84, no. 4, pp. 286 – 298.

Murugappan, K., Paramasivam, P. and Tan, K.H., 1993, 'Failure Envelope for Steel-Fibre Concrete under Biaxial Compression', *Journal of Materials in Civil Engineering*, vol. 5, no. 4, November 1993, pp.436 – 446.

Ottosen, N.S., 1977, 'A failure criterion for concrete', *Journal of the Engineering Mechanics Division, Proceedings*, vol. 103, EM 4, pp. 527 – 535.

Shang, H.S. and Song, Y.P., 2006, 'Experimental study of Strength and deformation of plain concrete under biaxial compression after freezing and thawing cycles', *Cement and Concrete Research*, 2006.

Tho, K.K., Seow, P.E.C and Swaddiwudhudhipong, S., 2003, 'Numerical method for analysis of concrete under multi-axial loads', *Magazine of Concrete Research*, vol. 55, no. 6, pp. 537 – 547.

Traina, Leonard A. and Mansour, Shahin A., 1991, 'Biaxial Strength and Deformational Behavior of Plain and Steel Fibre Concrete', *American Concrete Institute Materials Journal, Proceedings*, vol. 88, no. 4, pp. 354 – 362.

Willam, K.J. and Warnke, E.P., 1974, 'Constitutive models for the triaxial behavior of concrete', *International Association of the Bridge and*

Structural Engineers, Proceeding of the Seminar on Concrete Structures Subjected to Triaxial Stresses, ISMES, Bergamo, Italy, Paper no. III-I.

Yin, W.S., Su, Eric C.M., Mansur, M.A. and Hsu, Thomas T.C., 1989, 'Biaxial Tests of Plain and Fibre Concrete', *American Concrete Institute Materials Journal, Proceedings*, vol. 86, no. 3, pp. 236 – 243.

8. Conclusions

8.1. Summary

In this research the behaviour of steel fibres mixed into HPC under biaxial loading conditions were studied. A biaxial test set-up was designed and manufactured. A closed loop control system was used to control the loading process. For biaxial compression-compression an almost proportional loading was achieved whereas for the biaxial compression-tension region sequential loading was chosen. Four different steel fibres were tested, varying in length and aspect ratio. The steel fibre content varied from plain HPC to 2 % fibre content. Stress ratios were chosen in a way that the entire biaxial compression-compression and compression-tension region was covered, including the uniaxial compression and tension tests. The strength data were collected and analysed and failure envelopes were developed for each fibre concrete. The strains were also recorded in the principal directions and expressed as stress-strain graphs for different stress ratios. The failure modes and crack patterns were observed and recorded. The experimental results were then used to verify existing models by Ottosen (1977), Willam-Warnke (1974) and other mathematical expressions.

8.2. Experimental conclusions

The following conclusions can be drawn form the experimental program:

- The platen system has an influence on the strength recordings. Brush platens result in less strength increase under biaxial compression than solid dry steel platens. For the stress-strain behaviour of the tested

specimens no great difference was observed between the two different loading platens.

- Both strain measurement systems, electric resistance strain gauges and LVDTs, work identically and result in the same graphs. However due to constant damage caused by the explosive failure of the specimens the LVDT measurements had to be abandoned.

- The biaxial compressive strength of plain HPC increases compared to the uniaxial compression strength. However the increase is not as large as for NSC. The maximum biaxial strength occurs at a stress ratio of appropriately $\sigma_2/\sigma_3 = 0.5$.

- The introduction of a tension load decreases the compression capacity significantly in the compression-tension region.

- Steel fibres mixed into HPC increase the uniaxial and biaxial strength. With increasing volume fraction the strength increase in the compression-tension region is more significant than in the compression-compression region. A more beneficial behaviour of one of the tested fibre types compare to the others could not be observed.

- No significant difference for the stress-strain readings was observed between plain and fibre HPC in the biaxial compression-compression and compression-tension region and between the uniaxial compression and tension recordings. Only the increased strength for fibre concrete lead sometimes to higher overall values but the slope of the graphs and therefore the stiffness, the proportional limit and discontinuity level are similar.

- Within plain HPC uniaxial plate tests, the Poisson's ratio was recorded to be between 0.25 and 0.28 with a Modulus of Elasticity of 45.8 kN/mm^2. The discontinuity level was almost as high as the ultimate strength and

the stress-strain graphs show a fairly linear behaviour until failure point. Similar conclusions were observed for SFRHPC. The Poisson's ratio varies between 0.23 and 0.34 with no trend obvious for any fibre type or volume fraction. The value of E_c is between 40.6 and 46.3 kN/mm^2. Therefore fibres do not seem to influence these values.

- In HPC cracks develop through mortar as well as aggregates making the material a more homogeneous material than normal strength concrete. Therefore failure occurs more rapidly and the material showed a linear behaviour up to a higher stress than NSC with a higher discontinuity level.

- Under uniaxial compression and biaxial compression failure occurs by forming cracks at an angle of around 25° to the direction of the major compression load. The specimen fails into a number of plate like pieces. The same failure type was observed in the compression-tension region where compression loads were the dominant force. After a stress ratio of around σ_1/σ_3 = -0.06 the failure type changed to the one similar to that observed in uniaxial tension. One or more cracks formed perpendicular to the tension force.

- Increasing the fibre content did not change the failure mode significantly when compression loads are dominant. The main difference is that the specimen pieces were still connected by the fibres after the peak load was reached. When the stress ratio in the compression-tension region gets closer to uniaxial tension the failure type changes again to a single crack as observed for plain HPC.

8.3. Constitutive model

- Good results were obtained from the Ottosen failure criterion for plain concrete, even though the biaxial compression strength is slightly overestimated. Also good results were gained for the fibre model where the fibres are represented as a confining pressure in the third direction. However it should be noted that not all fibre types produced a continuous increase in biaxial strength with increasing fibre volume in the experimental investigation. Also noted is the great scatter of the experiments which makes it difficult to find trends. In the compression-tension branch the model overestimates the experimental results for plain and low fibre content concrete.

- The Willam-Warnke model seems to overestimate the experimental strength, especially the five parameter model. The same applies for the model introduced by Seow and Swaddiwudhipong which is based on the same idea of curved meridians of the failure surface in the Haigh-Westerguard stress space.

- Good agreement was observed for a second order polynomial mathematical description of the biaxial failure envelope. Also the use of an ellipse resulted in a close correlation with experimental data. These curves can be easily adapted to any experimental data by changing the numeral constants of the mathematical equation. These methods are more or less a curve fitting process describing the experimental results which is only as good as the experimental test points.

8.4. Recommendations for further research

Recommendations for further work are as follows:

- More tests for each stress ratio are needed to minimise scatter. Special attention should be given to a proper proportional loading device. This would make it easier to find the average experimental strength for any load ratio.

- To improve the post peak behaviour of HPC, a fibre cocktail is recommended. This would include different fibre types of different materials and shapes. Steel fibres should be amongst the used fibres as they proved to have a positive effect in arresting already developed microcracks.

- One of the major motivations of including steel fibres into HPC is to improve ductility and hence it would be desirable to examine post-peak behaviour. This was not yet possible with the test equipment used for this study. To generate such data the machine would need to be more stiffened by additional steel members. Moreover the oil pressure driven actuators could be replaced by a loading device which is based on threaded rods to generate the appropriate stresses. Alternatively the closed loop control system could be improved by a quicker response of the pressure controlling oil valve. This improvement will be limited by the pressure behaviour of the used oil and the speed of the controlling devices.

- Tests under triaxial load cases should be carried out to complete the full set of multiaxial loading conditions. Therefore a third axis needs to be placed vertically on top of the existing biaxial machine. This would include major labour and material costs.

- The development of a suitable brush platen system to minimise friction between platen system and specimen is recommended. This would give results closer to the true material behaviour. To prevent buckling and failure of the bristles it is recommended to reduce their length. Also possible are rectangular bristles rather than square shapes. This would prevent the bristles form buckling in the third out of plane direction.

- The strain measurement system should be improved, especially in the third out of plane axis. The rapid failure of the specimen tended to destroy conventional measurement devices such as LVDTs. Therefore strain gauges could be glued on a spherical metal device which is glued onto the specimen. The deformational behaviour of the metal has to be subtracted from the readings to gain information about the concrete specimen. Similar instrumentation of a reusable measurement device is also recommended for the in plane direction as this would save money spent on strain gauging. Additional tests would be necessary to find the metal behaviour under loads and to prove this method.

- Mathematical formulations of the strength envelopes together with the stress-strain behaviour should be modelled and implemented into commercial FE analyses programs and verified against full scale test data. Such data is widely available these days, for example from the classic series of beam tests conducted by Bresler and Scordelis some 40 years ago or more recently published data on the same topic. Also possible tests as a benchmark which finite element analysis models can be calibrated against are for example stud and tie or corbel column tests or simple supported concrete beams tested within undergraduate courses.

Appendix 1: Biaxial Test Results

The two tables in this appendix contain the strength result of each individual biaxial test. The first table shows the compression-compression test series where the second table shows the compression-tension series. Column three and four represent the ultimate failure strength recorded by the machine control system already normalised by using the plain cubes of every batch. Also the thickness of every individual specimen was taken into account for calculating the strength of each specimen. Column five shows the ratio between both recorded loads. The last two columns show the normalised strength where the failure strength was divided by the uniaxial plate compressive strength of plain concrete f_{cp}. For the compression-compression series this value was 103.9 N/mm^2 and for the compression-tension series 93.8 N/mm^2.

Fibre volume and type	Batch No	σ_2 N/mm^2	σ_3 N/mm^2	σ_2/σ_3	σ_2/σ_{fcp}	σ_3/σ_{fcp}
plain	9	0,00	-114,67	0,00	0,000	-1,104
	9	-40,13	-137,73	0,29	-0,386	-1,326
	9	-74,49	-148,75	0,50	-0,717	-1,432
	9	-100,87	-141,63	0,71	-0,971	-1,363
	9	-112,99	-115,54	0,98	-1,088	-1,112
	9	-40,98	-121,66	0,34	-0,394	-1,171
	9	-99,72	-133,81	0,75	-0,960	-1,288
	9	0,00	-80,19	0,00	-0,000	-0,772
	10	0,00	-108,12	0,00	0,000	-1,041
	10	-35,31	-131,66	0,27	-0,340	-1,267
	10	-68,01	-131,69	0,52	-0,655	-1,267
	10	-102,28	-136,50	0,75	-0,984	-1,314
	10	-107,15	-119,77	0,89	-1,031	-1,153
	10	0,00	-99,75	0,00	0,000	-0,960
	10	-67,69	-135,26	0,50	-0,651	-1,302
	10	-127,99	-128,05	1,00	-1,232	-1,232

Fibre volume and type	Batch No	σ_2 N/mm^2	σ_3 N/mm^2	σ_2/σ_3	σ_2/σ_{fcp}	σ_3/σ_{fcp}
0.5% 45-35	23	0,00	-120,81	0,00	0,000	-1,163
	23	-42,20	-140,33	0,30	-0,406	-1,351
	23	-82,97	-160,42	0,52	-0,799	-1,544
	23	-123,29	-146,54	0,84	-1,187	-1,410
	23	-133,94	-136,86	0,98	-1,289	-1,317
	23	-48,01	-157,99	0,30	-0,462	-1,521
	23	-111,20	-149,97	0,74	-1,070	-1,443
	23	0,00	-120,87	0,00	0,000	-1,163
	24	0,00	-116,95	0,00	0,000	-1,126
	24	-36,45	-129,45	0,28	-0,351	-1,246
	24	-49,69	-150,99	0,33	-0,478	-1,453
	24	-119,43	-154,18	0,77	-1,150	-1,484
	24	-130,67	-135,78	0,96	-1,258	-1,307
	24	0,00	-118,19	0,00	0,000	-1,138
	24	-74,32	-138,20	0,54	-0,715	-1,330
	24	-125,52	-125,91	1,00	-1,208	-1,212
0.5% 45-50	21	0,00	-97,28	0,00	0,000	-0,936
	21	-25,48	-114,37	0,22	-0,245	-1,101
	21	-83,47	-145,30	0,57	-0,803	-1,398
	21	-111,25	-134,66	0,83	-1,071	-1,296
	21	-138,17	-140,61	0,98	-1,330	-1,353
	21	-39,11	-146,28	0,27	-0,376	-1,408
	21	-100,55	-125,66	0,80	-0,968	-1,209
	21	0,00	-96,60	0,00	0,000	-0,930
	22	0,00	-102,31	0,00	0,000	-0,985
	22	-35,21	-146,44	0,24	-0,339	-1,409
	22	-69,93	-140,23	0,50	-0,673	-1,350
	22	-104,03	-146,26	0,71	-1,001	-1,408
	22	-131,25	-131,39	1,00	-1,263	-1,265
	22	0,00	-97,03	0,00	0,000	-0,934
	22	-82,80	-147,19	0,56	-0,797	-1,417
	22	-140,63	-141,06	1,00	-1,354	-1,358

Fibre volume and type	Batch No	σ_2 N/mm^2	σ_3 N/mm^2	σ_2/σ_3	σ_2/σ_{fcp}	σ_3/σ_{fcp}
0.5% 65-35	19	0,00	-114,04	0,00	0,000	-1,098
	19	-36,59	-126,71	0,29	-0,352	-1,220
	19	-68,26	-141,57	0,48	-0,657	-1,363
	19	-110,07	-153,99	0,71	-1,059	-1,482
	19	-135,89	-136,00	1,00	-1,308	-1,309
	19	-110,04	-147,29	0,75	-1,059	-1,418
	19	0,00	-122,62	0,00	0,000	-1,180
	20	0,00	-123,15	0,00	0,000	-1,185
	20	-41,43	-141,27	0,29	-0,399	-1,360
	20	-85,56	-158,36	0,54	-0,824	-1,524
	20	-121,75	-145,94	0,83	-1,172	-1,405
	20	-130,49	-143,41	0,91	-1,256	-1,380
	20	0,00	-117,38	0,00	0,000	-1,130
	20	-80,52	-153,59	0,52	-0,775	-1,478
	20	-117,32	-121,07	0,97	-1,129	-1,165
0.5% 65-60	27	0,00	-120,99	0,00	0,000	-1,164
	27	-39,76	-136,10	0,29	-0,383	-1,310
	27	-69,94	-134,41	0,52	-0,673	-1,294
	27	-96,66	-129,12	0,75	-0,930	-1,243
	27	-131,12	-133,49	0,98	-1,262	-1,285
	27	-37,04	-134,13	0,28	-0,356	-1,291
	27	-114,54	-151,07	0,76	-1,102	-1,454
	27	0,00	-103,02	0,00	0,000	-0,992
	28	0,00	-123,19	0,00	0,000	-1,186
	28	-31,48	-148,40	0,21	-0,303	-1,428
	28	-78,21	-155,91	0,50	-0,753	-1,501
	28	-110,19	-142,29	0,77	-1,061	-1,370
	28	-129,05	-133,24	0,97	1,242	-1,282
	28	0,00	-115,09	0,00	0,000	-1,108
	28	-74,27	-153,59	0,48	-0,715	-1,478
	28	-117,74	-118,13	1,00	-1,133	-1,137
1% 45-35	3	0,00	-95,06	0,00	0,000	-0,915

Fibre volume and type	Batch No	σ_2 N/mm^2	σ_3 N/mm^2	σ_2/σ_3	σ_2/σ_{fcp}	σ_3/σ_{fcp}
	3	-34,87	-125,96	0,28	-0,336	-1,212
	3	-66,80	-129,41	0,52	-0,643	-1,246
	3	-96,52	-123,07	0,78	-0,929	-1,185
	3	-94,25	-100,59	0,94	-0,907	-0,968
	3	-38,76	-136,65	0,28	-0,373	-1,315
	3	-95,64	-125,81	0,76	-0,920	-1,211
	3	0,00	-73,94	0,00	0,000	-0,712
	4	0,00	-116,76	0,00	0,000	-1,124
	4	-35,32	-150,22	0,24	-0,340	-1,446
	4	-84,18	-148,57	0,57	-0,810	-1,430
	4	-104,62	-130,07	0,80	-1,007	-1,252
	4	-144,22	-149,52	0,96	-1,388	-1,439
	4	0,00	-103,82	0,00	0,000	-0,999
	4	-81,19	-166,77	0,49	-0,781	-1,605
	4	-151,20	-156,38	0,97	-1,455	-1,505
1% 45-50	5	0,00	-119,02	0,00	0,000	-1,146
	5	-27,16	-84,73	0,32	-0,261	-0,816
	5	-70,31	-137,94	0,51	-0,677	-1,328
	5	-105,22	-141,19	0,75	-1,013	-1,359
	5	-136,87	-143,49	0,95	-1,317	-1,381
	5	-33,23	-146,16	0,23	-0,320	-1,407
	5	-112,13	-143,62	0,78	-1,079	-1,382
	5	-34,16	-145,49	0,23	0,329	-1,400
	6	0,00	-111,65	0,00	0,000	-1,075
	6	-36,41	-130,68	0,28	-0,350	-1,258
	6	-65,42	-147,64	0,44	-0,630	-1,421
	6	-113,92	-145,45	0,78	-1,096	-1,400
	6	-127,51	-133,23	0,96	-1,227	-1,282
	6	0,00	-111,22	0,00	0,000	-1,070
	6	-76,51	-147,71	0,52	-0,736	-1,422
	6	-144,70	-147,89	0,98	-1,393	-1,423
1% 65-35	1	0,00	-101,62	0,00	0,000	-0,978
	1	-20,08	-123,76	0,16	-0,193	-1,191

Fibre volume and type	Batch No	σ_2 N/mm^2	σ_3 N/mm^2	σ_2/σ_3	σ_2/σ_{fcp}	σ_3/σ_{fcp}
	1	-71,79	-135,90	0,53	-0,691	-1,308
	1	-103,99	-123,65	0,84	-1,001	-1,190
	1	-116,36	-122,76	0,95	-1,120	-1,182
	1	-34,93	-128,86	0,27	-0,336	-1,240
	1	-88,25	-125,93	0,70	-0,849	-1,212
	1	0,00	-124,08	0,00	0,000	-1,194
	2	0,00	-108,55	0,00	0,000	-1,045
	2	-34,79	-124,59	0,28	-0,335	-1,199
	2	-68,52	-124,93	0,55	-0,659	-1,202
	2	-92,52	-123,04	0,75	-0,891	-1,184
	2	-102,78	-104,16	0,99	-0,989	-1,003
	2	0,00	-107,77	0,00	0,000	-1,037
	2	-64,21	-130,83	0,49	-0,618	-1,259
	2	-110,00	-112,02	0,98	-1,059	-1,078
1% 65-60	11	0,00	-121,27	0,00	0,000	-1,167
	11	-34,57	-136,96	0,25	-0,333	-1,318
	11	-71,90	-138,90	0,52	-0,692	-1,337
	11	-115,59	-152,99	0,76	-1,113	-1,472
	11	-122,38	-139,11	0,88	-1,178	-1,339
	11	-39,26	-155,59	0,25	-0,378	-1,497
	11	-117,32	-170,69	0,69	-1,129	-1,643
	11	0,00	-113,69	0,00	0,000	-1,094
	12	0,00	-119,86	0,00	0,000	-1,154
	12	-40,48	-143,33	0,28	-0,390	-1,379
	12	-76,41	-140,26	0,54	-0,735	-1,350
	12	-103,09	-144,42	0,71	-0,992	-1,390
	12	-132,12	-139,28	0,95	-1,272	-1,341
	12	0,00	-119,16	0,00	0,000	-1,147
	12	-70,69	-124,68	0,57	-0,680	-1,200
	12	-125,31	-132,09	0,95	-1,206	-1,271
1.5% 45-35	31	0,00	-112,14	0,00	0,000	-1,079
	31	-35,31	-139,48	0,25	-0,340	-1,342

Fibre volume and type	Batch No	σ_2 N/mm^2	σ_3 N/mm^2	σ_2/σ_3	σ_2/σ_{fcp}	σ_3/σ_{fcp}
	31	-74,00	-157,15	0,47	-0,712	-1,513
	31	-117,68	-156,49	0,75	-1,133	-1,506
	31	-146,56	-149,48	0,98	-1,411	-1,439
	31	-43,41	-142,26	0,31	-0,418	-1,369
	31	-120,51	-155,85	0,77	-1,160	-1,500
	31	0,00	-114,80	0,00	0,000	-1,105
	32	0,00	-117,00	0,00	0,000	-1,126
	32	-39,45	-150,15	0,26	-0,380	-1,445
	32	-73,09	-149,19	0,49	-0,703	-1,436
	32	-110,06	-155,80	0,71	-1,059	-1,500
	32	-135,25	-146,38	0,92	-1,302	-1,409
	32	0,00	-109,37	0,00	0,000	-1,053
	32	-72,94	-153,86	0,47	-0,702	-1,481
	32	-134,19	-142,81	0,94	-1,291	-1,374
1.5% 45-50	25	0,00	-94,67	0,00	0,000	-0,911
	25	-31,44	-122,61	0,26	-0,303	-1,180
	25	-66,59	-125,63	0,53	-0,641	-1,209
	25	-105,28	-141,22	0,75	-1,013	-1,359
	25	-133,60	-140,86	0,95	-1,286	-1,356
	25	-39,41	-147,64	0,27	-0,379	-1,421
	25	-118,59	-157,24	0,75	-1,141	-1,513
	25	0,00	-117,35	0,00	0,000	-1,129
	26	0,00	-117,00	0,00	0,000	-1,126
	26	-31,41	-134,14	0,23	-0,302	-1,291
	26	-69,08	-146,47	0,47	-0,665	-1,410
	26	-94,07	-133,42	0,71	-0,905	-1,284
	26	-132,85	-133,50	1,00	-1,279	-1,285
	26	0,00	-95,72	0,00	0,000	-0,921
	26	-77,81	-144,48	0,54	-0,749	-1,391
	26	-104,62	-105,74	0,99	-1,007	-1,018
1.5% 65-35	33	0,00	-120,02	0,00	0,000	-1,155
	33	-38,03	-139,02	0,27	-0,366	-1,338
	33	-71,16	-153,02	0,46	-0,685	-1,473

Fibre volume and type	Batch No	σ_2 N/mm^2	σ_3 N/mm^2	σ_2/σ_3	σ_2/σ_{fcp}	σ_3/σ_{fcp}
	33	-107,62	-143,31	0,75	-1,036	-1,379
	33	-139,16	-139,20	1,00	-1,339	-1,340
	33	-44,43	-155,89	0,28	-0,428	-1,500
	33	-107,81	-149,90	0,72	-1,038	-1,443
	33	0,00	-116,29	0,00	0,000	-1,119
	34	0,00	-116,49	0,00	0,000	-1,121
	34	-37,54	-148,36	0,25	-0,361	-1,428
	34	-73,51	-155,24	0,47	-0,708	-1,494
	34	-113,31	-154,43	0,73	-1,091	-1,486
	34	-126,68	-127,05	1,00	-1,219	-1,223
	34	0,00	-117,59	0,00	0,000	-1,132
	34	-64,08	-131,55	0,49	-0,617	-1,266
	34	-132,12	-134,04	0,99	-1,272	-1,290
1.5% 65-60	29	0,00	-113,36	0,00	0,000	-1,091
	29	-44,89	-148,69	0,30	-0,432	-1,431
	29	-72,69	-144,13	0,50	-0,700	-1,387
	29	-110,83	-156,80	0,71	-1,067	-1,509
	29	-131,74	-134,35	0,98	-1,268	-1,293
	29	-44,17	-151,98	0,29	-0,425	-1,463
	29	-117,52	-153,45	0,77	-1,131	-1,477
	29	0,00	-117,96	0,00	0,000	-1,135
	30	0,00	-105,85	0,00	0,000	-1,019
	30	-38,18	-148,86	0,26	-0,367	-1,433
	30	-77,08	-151,54	0,51	-0,742	-1,458
	30	-104,14	-150,30	0,69	-1,002	-1,447
	30	-130,01	-131,03	0,99	-1,251	-1,261
	30	0,00	-120,68	0,00	0,000	-1,162
	30	-75,99	-147,38	0,52	-0,731	-1,419
	30	-125,30	-129,06	0,97	-1,206	-1,242
2% 45-35	15	0,00	-117,56	0,00	0,000	-1,132
	15	-33,10	-132,13	0,25	-0,319	-1,272
	15	-79,37	-146,91	0,54	-0,764	-1,414

Fibre volume and type	Batch No	σ_2 N/mm^2	σ_3 N/mm^2	σ_2/σ_3	σ_2/σ_{fcp}	σ_3/σ_{fcp}
	15	-112,88	-152,71	0,74	-1,086	-1,470
	15	-136,94	-151,77	0,90	-1,318	-1,461
	15	-40,55	-153,96	0,26	-0,390	-1,482
	15	-118,37	-167,38	0,71	-1,139	-1,611
	15	0,00	-119,82	0,00	0,000	-1,153
	16	0,00	-138,52	0,00	0,000	-1,333
	16	-45,00	-152,31	0,30	-0,433	-1,466
	16	-85,39	-166,77	0,51	-0,822	-1,605
	16	-136,17	-183,51	0,74	-1,311	-1,766
	16	-147,19	-156,85	0,94	-1,417	-1,510
	16	0,00	-102,18	0,00	0,000	-0,983
	16	-87,20	-177,25	0,49	-0,839	-1,706
	16	-151,65	-153,64	0,99	-1,460	-1,479
2% 45-50	7	0,00	-105,78	0,00	0,000	-1,018
	7	-33,61	-135,29	0,25	-0,323	-1,302
	7	-67,93	-139,70	0,49	-0,654	-1,345
	7	-102,13	-133,03	0,77	-0,983	-1,280
	7	-146,55	-148,82	0,98	-1,410	-1,432
	7	-35,82	-137,23	0,26	-0,345	-1,321
	7	-112,32	-161,24	0,70	-1,081	-1,552
	7	0,00	-120,34	0,00	0,000	-1,158
	8	0,00	-114,42	0,00	0,000	-1,101
	8	-39,46	-130,11	0,30	-0,380	-1,252
	8	-75,70	-154,61	0,49	-0,729	-1,488
	8	-102,11	-134,85	0,76	-0,983	-1,298
	8	-136,51	-137,18	1,00	-1,314	-1,320
	8	0,00	-109,75	0,00	0,000	-1,056
	8	-59,79	-122,90	0,49	-0,575	-1,183
	8	-133,52	-134,09	1,00	-1,285	-1,291
2% 65-35	17	0,00	-123,23	0,00	0,000	-1,186
	17	-44,07	-149,90	0,29	-0,424	-1,443
	17	-73,22	-143,36	0,51	-0,705	-1,380
	17	-115,44	-155,93	0,74	-1,111	-1,501

Fibre volume and type	Batch No	σ_2 N/mm^2	σ_3 N/mm^2	σ_2/σ_3	σ_2/σ_{fcp}	σ_3/σ_{fcp}
	17	-145,46	-150,03	0,97	-1,400	-1,444
	17	-38,94	-154,19	0,25	-0,375	-1,484
	17	-116,38	-162,97	0,71	-1,120	-1,569
	17	0,00	-133,93	0,00	0,000	-1,289
	18	0,00	-125,96	0,00	0,000	-1,212
	18	-43,56	-160,69	0,27	-0,419	-1,547
	18	-85,52	-169,80	0,50	-0,823	-1,634
	18	-126,98	-158,06	0,80	-1,222	-1,521
	18	-141,15	-147,96	0,95	-1,359	-1,424
	18	0,00	-134,12	0,00	0,000	-1,291
	18	-84,18	-162,35	0,52	-0,810	-1,563
	18	-147,73	-155,10	0,95	-1,422	-1,493
2% 65-60	13	0,00	-106,89	0,00	0,000	-1,029
	13	-31,90	-119,76	0,27	-0,307	-1,153
	13	-76,19	-161,81	0,47	-0,733	-1,557
	13	-111,59	-153,28	0,73	-1,074	-1,475
	13	-126,19	-134,75	0,94	-1,215	-1,297
	13	-40,77	-151,73	0,27	-0,392	-1,460
	13	-114,84	-155,92	0,74	-1,105	-1,501
	13	0,00	-125,27	0,00	0,000	-1,206
	14	0,00	-118,54	0,00	0,000	-1,141
	14	-45,90	-156,42	0,29	-0,442	-1,505
	14	-63,99	-131,13	0,49	-0,616	-1,262
	14	-110,20	-156,73	0,70	-1,061	-1,509
	14	-135,94	-146,32	0,93	-1,308	-1,408
	14	0,00	-114,63	0,00	0,000	-1,103
	14	-71,44	-145,48	0,49	-0,688	-1,400
	14	-135,27	-137,84	0,98	-1,302	-1,327

Table 18 Biaxial strength data for the compression-compression test series

Fibre volume and type	Batch No	σ_1 N/mm^2	σ_3 N/mm^2	σ_1/σ_3	σ_1/σ_{fcp}	σ_3/σ_{fcp}
plain	4	6,92	0,00		0,074	0,000
		4,79	-18,82	-0,254	0,051	-0,201
		3,86	-18,83	-0,205	0,041	-0,201
		1,93	-28,25	-0,068	0,021	-0,301
		1,02	-74,13	-0,014	0,011	-0,790
		0,00	-93,11	0,000	0,000	-0,992
	5	5,75	0,00		0,061	0,000
		4,71	-6,76	-0,697	0,050	-0,072
		3,82	-14,39	-0,266	0,041	-0,153
		1,87	-74,04	-0,025	0,020	-0,789
		1,06	-81,45	-0,013	0,011	-0,868
		0,00	-87,81	0,000	0,000	-0,936
		0,00	-100,35	0,000	0,000	-1,069
	6	5,63	0,00		0,060	0,000
		3,82	-7,27	-0,525	0,041	-0,077
		1,83	-33,66	-0,054	0,019	-0,359
		1,16	-61,00	-0,019	0,012	-0,650
		0,00	-94,07	0,000	0,000	-1,003
1% 45-35	1	4,46	0,00		0,047	0,000
		3,86	-19,22	-0,201	0,041	-0,205
		2,97	-75,80	-0,039	0,032	-0,808
		1,99	-98,01	-0,020	0,021	-1,045
		0,00	-104,98	0,000	0,000	-1,119
	2	7,50	0,00		0,080	0,000
		5,55	-10,75	-0,516	0,059	-0,115
		4,60	-31,95	-0,144	0,049	-0,341
		2,18	-105,99	-0,021	0,023	-1,130
		1,03	-108,86	-0,009	0,011	-1,160
		0,00	-113,25	0,000	0,000	-1,207
	3	5,27	0,00		0,056	0,000

Fibre volume and type	Batch No	σ_1 N/mm^2	σ_3 N/mm^2	σ_1/σ_3	σ_1/σ_{fcp}	σ_3/σ_{fcp}
		5,03	-10,23	-0,492	0,054	-0,109
		4,18	-75,97	-0,055	0,045	-0,810
		2,18	-98,41	-0,022	0,023	-1,049
		0,99	-100,32	-0,010	0,011	-1,069
		0,00	-104,44	0,000	0,000	-1,113
1% 45-50	7	6,17	0,00		0,066	0,000
		4,47	-7,60	-0,588	0,048	-0,081
		3,23	-18,30	-0,177	0,034	-0,195
		2,43	-100,52	-0,024	0,026	-1,071
		1,81	-93,09	-0,019	0,019	-0,992
		1,06	-103,33	-0,010	0,011	-1,101
		0,00	-99,58	0,000	0,000	-1,061
	8	6,23	0,00		0,066	0,000
		4,53	-6,47	-0,700	0,048	-0,069
		3,32	-27,83	-0,119	0,035	-0,297
		2,21	-104,93	-0,021	0,024	-1,118
		1,16	-95,38	-0,012	0,012	-1,016
		0,00	-96,53	0,000	0,000	-1,029
1% 65-35	9	6,80	0,00		0,073	0,000
		5,65	-7,15	-0,790	0,060	-0,076
		3,68	-89,54	-0,041	0,039	-0,954
		1,83	-87,63	-0,021	0,020	-0,934
		1,17	-103,03	-0,011	0,013	-1,098
		0,00	-99,28	0,000	0,000	-1,058
	10	7,55	0,00		0,080	0,000
		5,63	-1,78	-3,169	0,060	-0,019
		3,88	-80,63	-0,048	0,041	-0,859
		1,84	-101,73	-0,018	0,020	-1,084
		0,00	-102,03	0,000	0,000	-1,087
1% 65-60	11	5,94	0,00		0,063	0,000
		5,95	0,00		0,063	0,000
		4,81	-37,38	-0,129	0,051	-0,398
		3,81	-86,83	-0,044	0,041	-0,925

Fibre volume and type	Batch No	σ_1 N/mm^2	σ_3 N/mm^2	σ_1/σ_3	σ_1/σ_{fcp}	σ_3/σ_{fcp}
		2,04	-92,84	-0,022	0,022	-0,989
		1,00	-98,20	-0,010	0,011	-1,047
		0,00	-95,52	0,000	0,000	-1,018
	12	6,35	0,00		0,068	0,000
		4,67	-6,62	-0,706	0,050	-0,071
		3,58	-58,87	-0,061	0,038	-0,627
		1,55	-108,02	-0,014	0,017	-1,151
		0,00	-106,80	0,000	0,000	-1,138
2% 45-35	13	7,03	0,00		0,075	0,000
		5,47	-4,74	-1,156	0,058	-0,050
		4,73	-96,18	-0,049	0,050	-1,025
		3,78	-105,12	-0,036	0,040	-1,120
		1,94	-103,64	-0,019	0,021	-1,105
		0,00	-111,16	0,000	0,000	-1,185
	14	6,80	0,00		0,072	0,000
		5,48	-86,61	-0,063	0,058	-0,923
		4,54	-86,89	-0,052	0,048	-0,926
		3,61	-97,38	-0,037	0,038	-1,038
		1,95	-116,16	-0,017	0,021	-1,238
		0,00	-123,12	0,000	0,000	-1,312
2% 45-50	15	7,03	0,00		0,075	0,000
		6,44	-28,48	-0,226	0,069	-0,304
		5,14	-86,84	-0,059	0,055	-0,926
		4,00	-109,98	-0,036	0,043	-1,172
		2,05	-113,27	-0,018	0,022	-1,207
		0,00	-116,43	0,000	0,000	-1,241
	16	7,12	0,00		0,076	0,000
		5,08	-94,15	-0,054	0,054	-1,003
		2,05	-111,33	-0,018	0,022	-1,186
		0,00	-124,12	0,000	0,000	-1,323
2% 65-35	17	7,04	0,00		0,075	0,000

Fibre volume and type	Batch No	σ_1 N/mm^2	σ_3 N/mm^2	σ_1/σ_3	σ_1/σ_{fcp}	σ_3/σ_{fcp}
		5,77	-82,44	-0,070	0,062	-0,879
		4,55	-105,93	-0,043	0,049	-1,129
		1,89	-113,26	-0,017	0,020	-1,207
		0,97	-104,97	-0,009	0,010	-1,119
		0,00	-106,00	0,000	0,000	-1,130
	18	6,67	0,00		0,071	0,000
		5,76	-75,65	-0,076	0,061	-0,806
		4,41	-86,11	-0,051	0,047	-0,918
		1,79	-96,70	-0,018	0,019	-1,031
		0,00	-103,76	0,000	0,000	-1,106
2% 65-60	19	7,23	0,00		0,077	0,000
		6,52	-75,16	-0,087	0,069	-0,801
		4,84	-83,15	-0,058	0,052	-0,886
		1,90	-109,70	-0,017	0,020	-1,169
		0,00	-92,64	0,000	0,000	-0,987
	20	6,43	0,00		0,069	0,000
		6,02	0,00		0,064	0,000
		5,57	-84,07	-0,066	0,059	-0,896
		5,14	-87,40	-0,059	0,055	-0,932
		2,09	-98,55	-0,021	0,022	-1,050
		0,00	-105,82	0,000	0,000	-1,128

Table 19 Biaxial strength data for the compression-tension test series

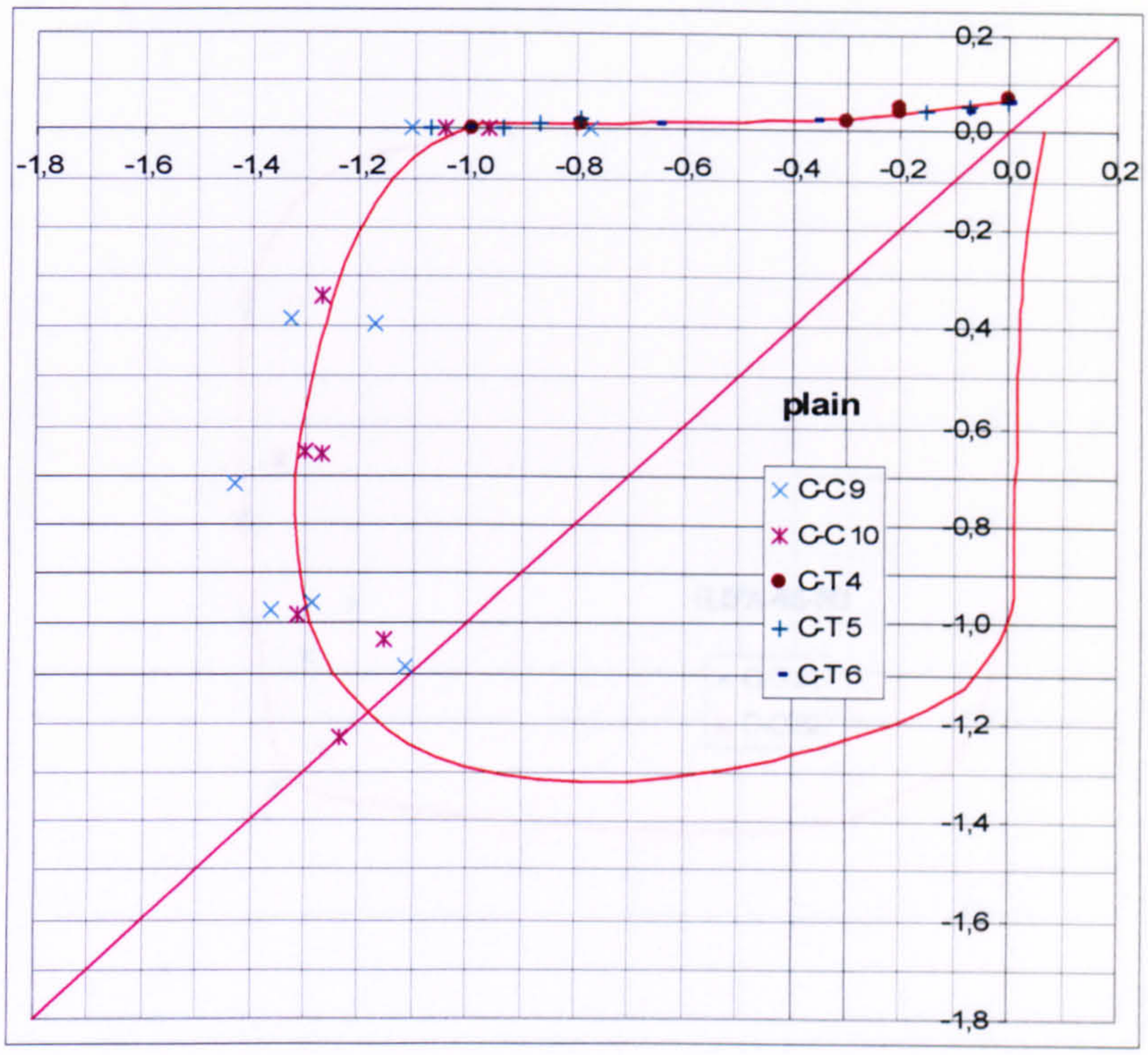

Figure 0.1 Biaxial strength envelope for plain HPC

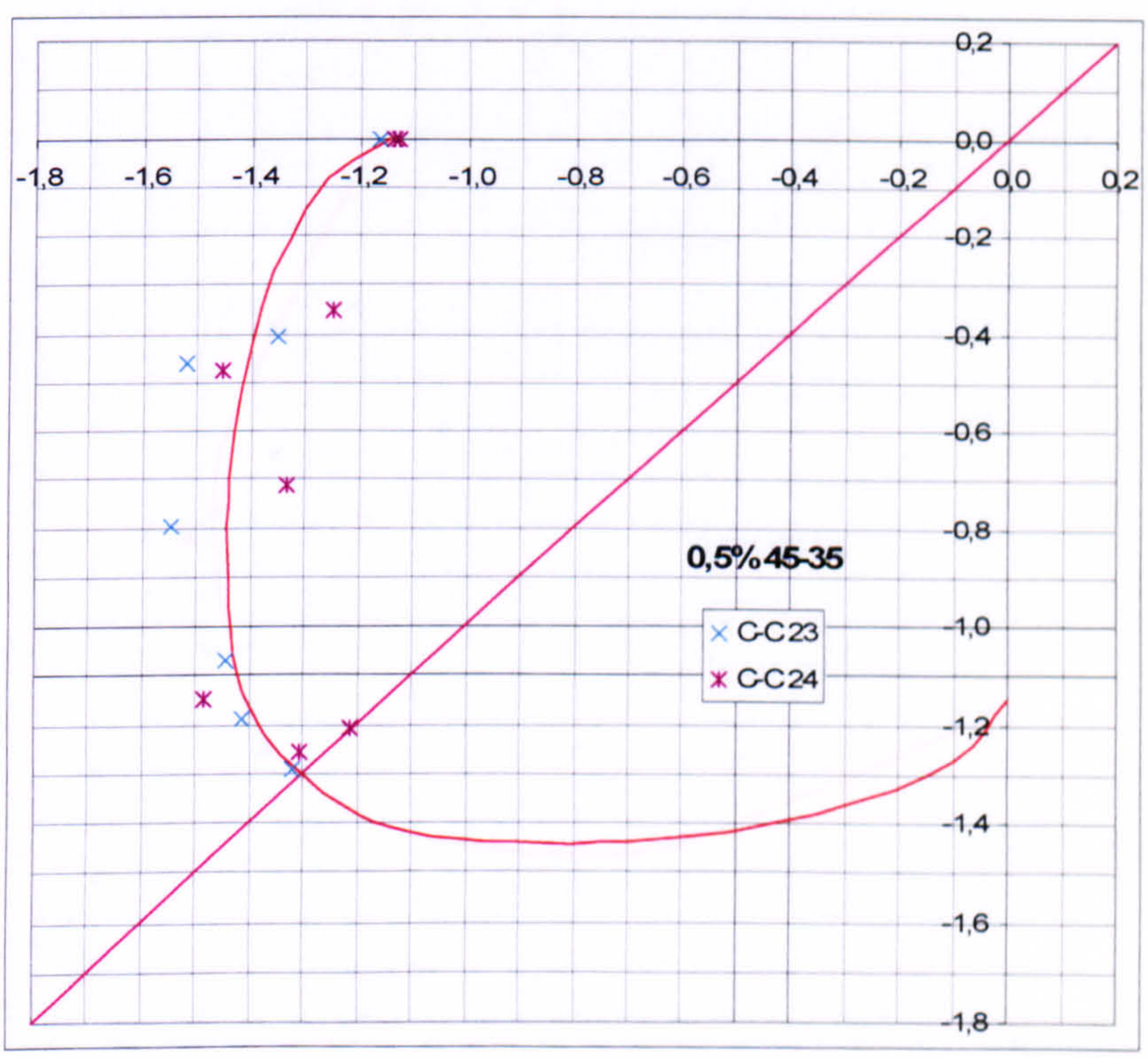

Figure 0.2 Biaxial strength envelope for fibre type 45-35 and Vf = 0.5 %

Figure 0.3 Biaxial strength envelope for fibre type 45-50 and V_f = 0.5 %

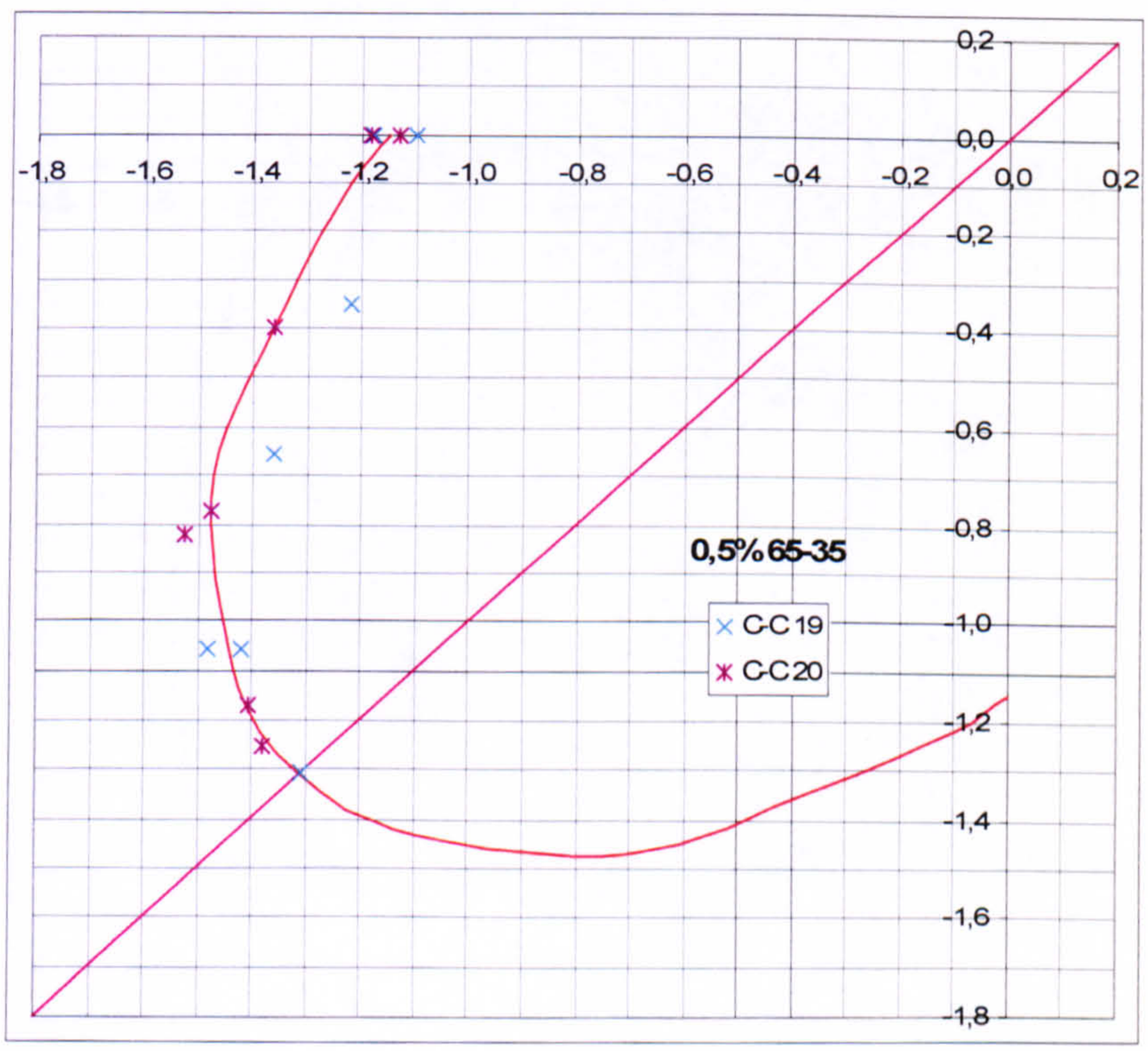

Figure 0.4 Biaxial strength envelope for fibre type 65-35 and V_f = 0.5 %

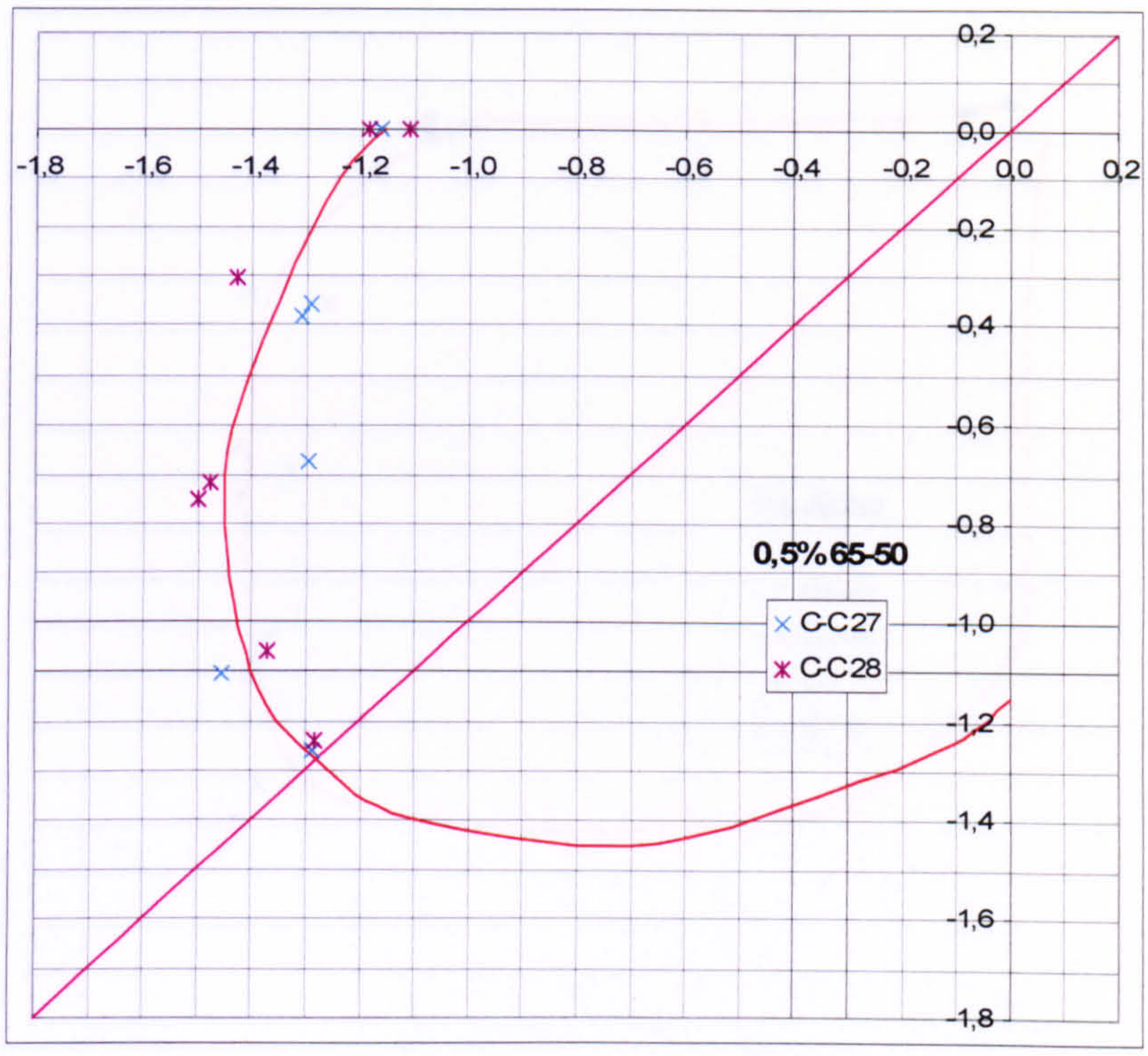

Figure 0.5 Biaxial strength envelope for fibre type 65-50 and V_f = 0.5 %

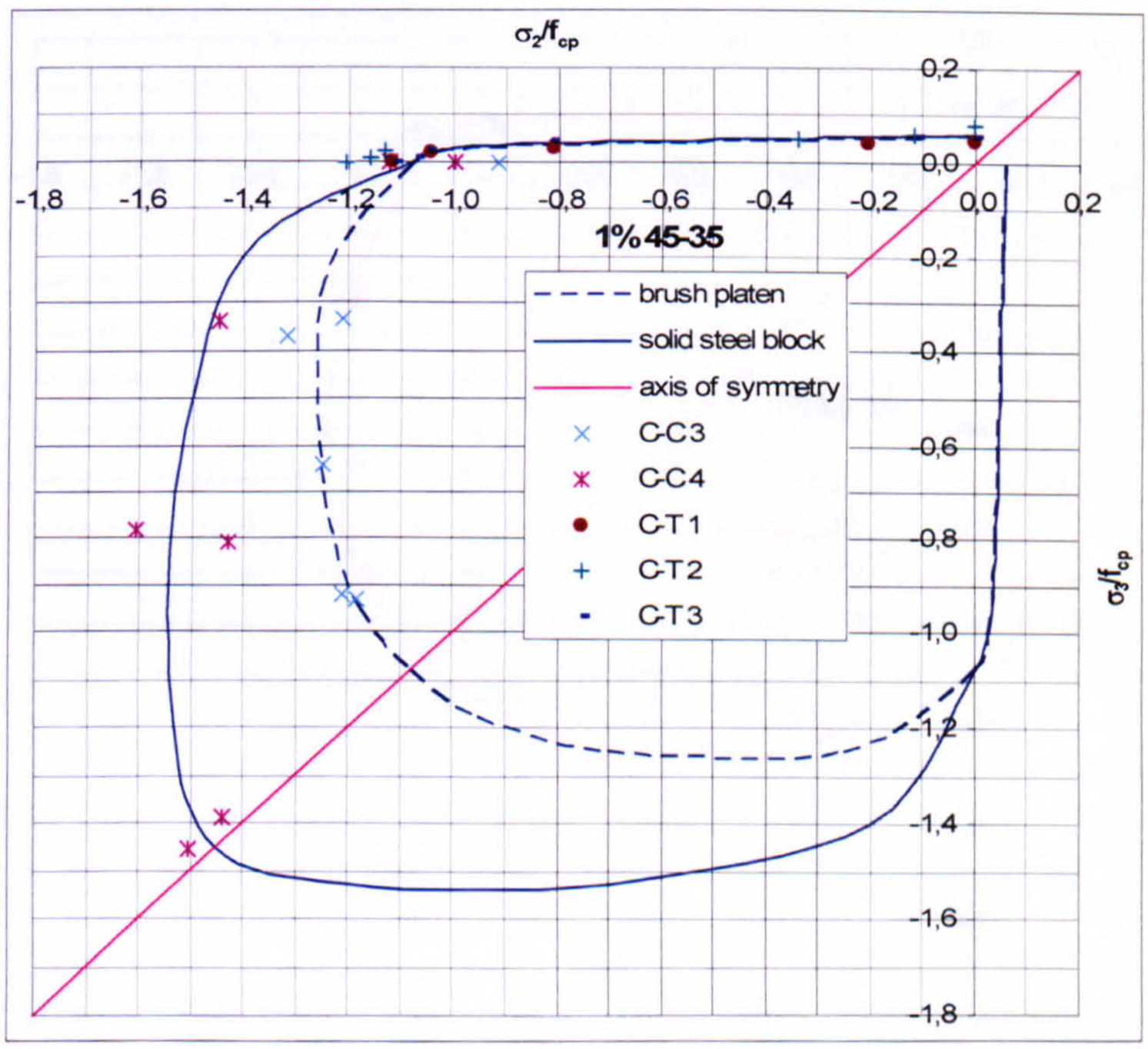

Figure 0.6 Biaxial strength envelope for fibre type 45-35 and V_f = 1 %

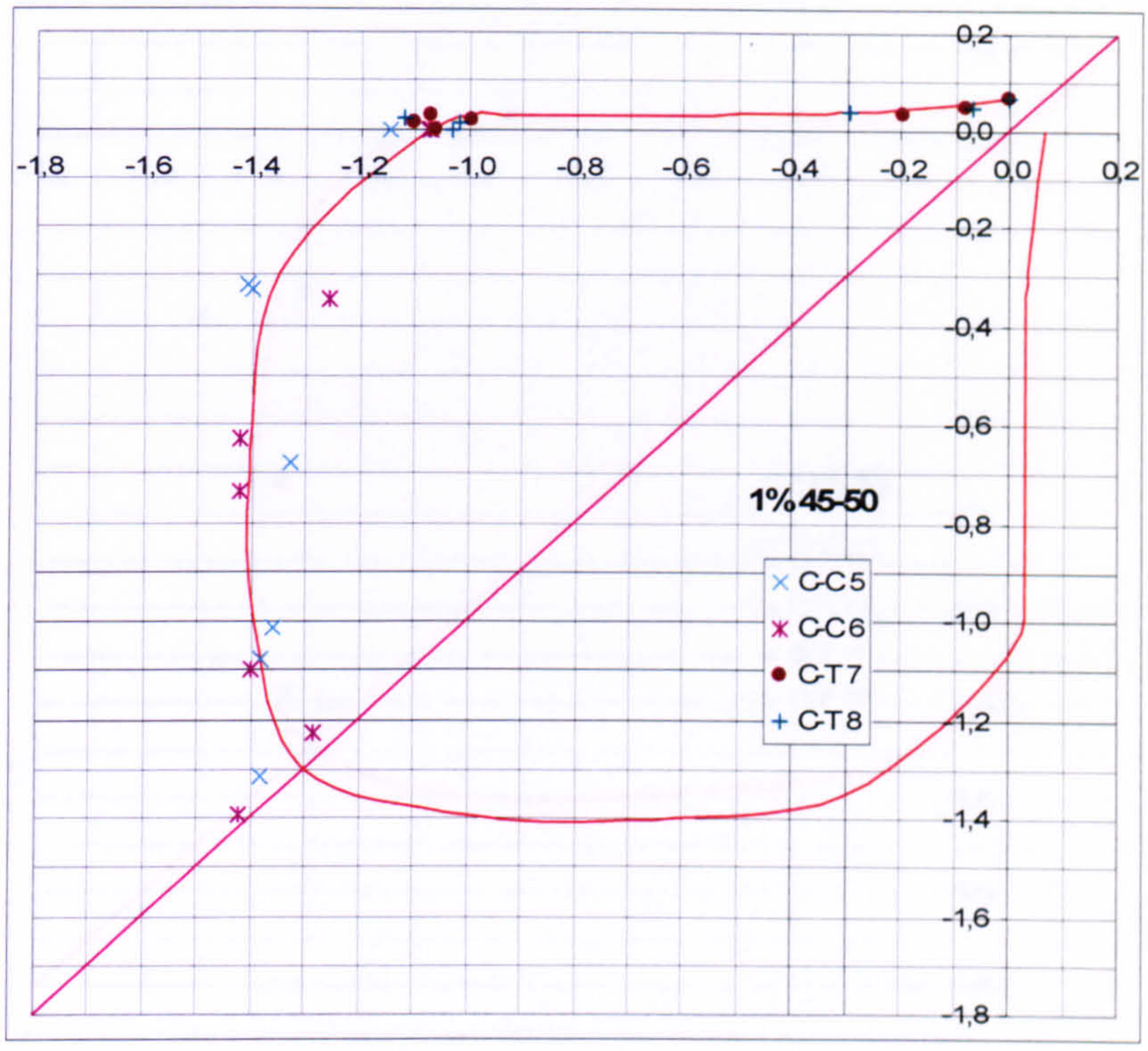

Figure 0.7 Biaxial strength envelope for fibre type 45-50 and V_f = 1 %

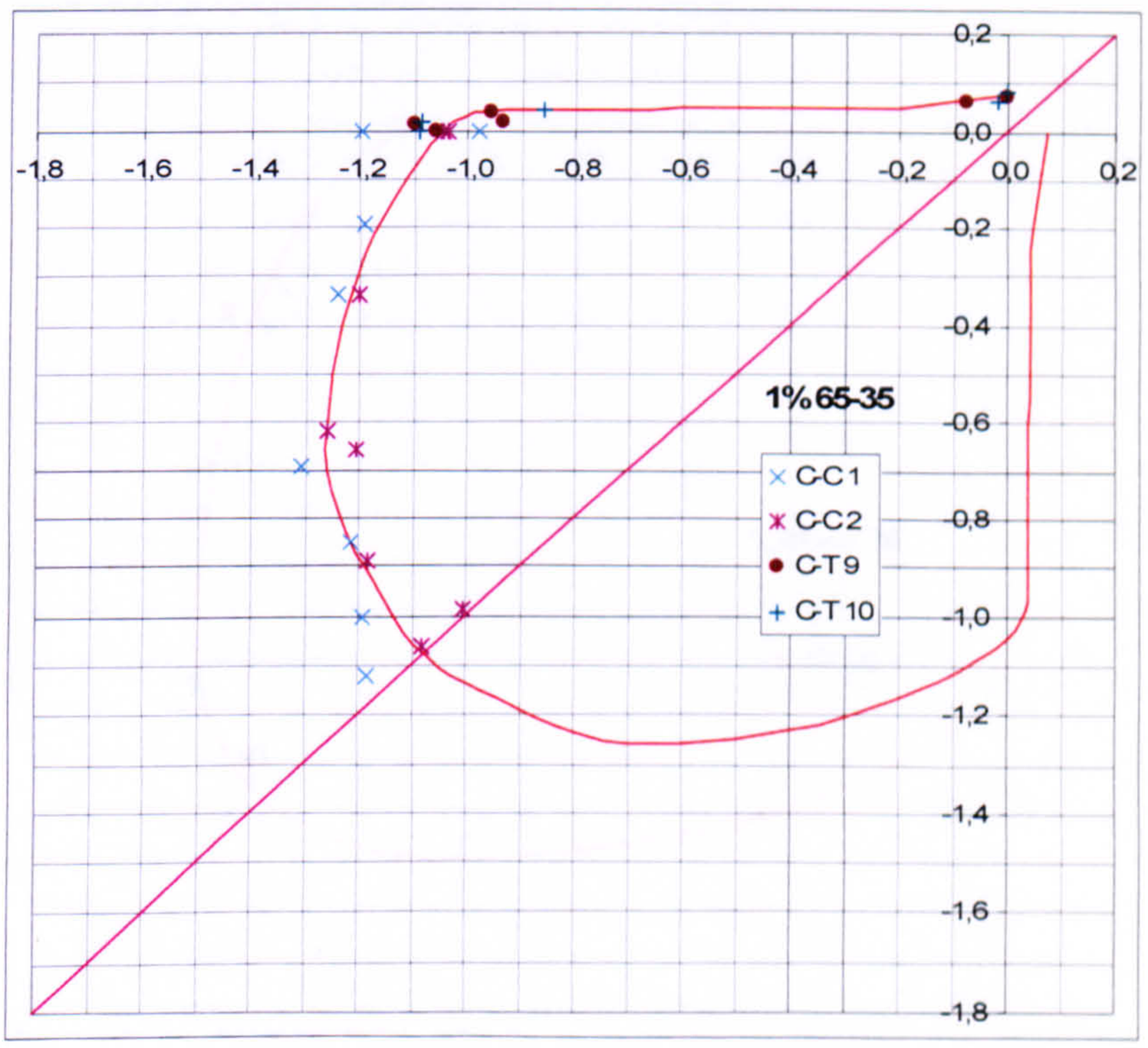

Figure 0.8 Biaxial strength envelope for fibre type 65-35 and V_f = 1 %

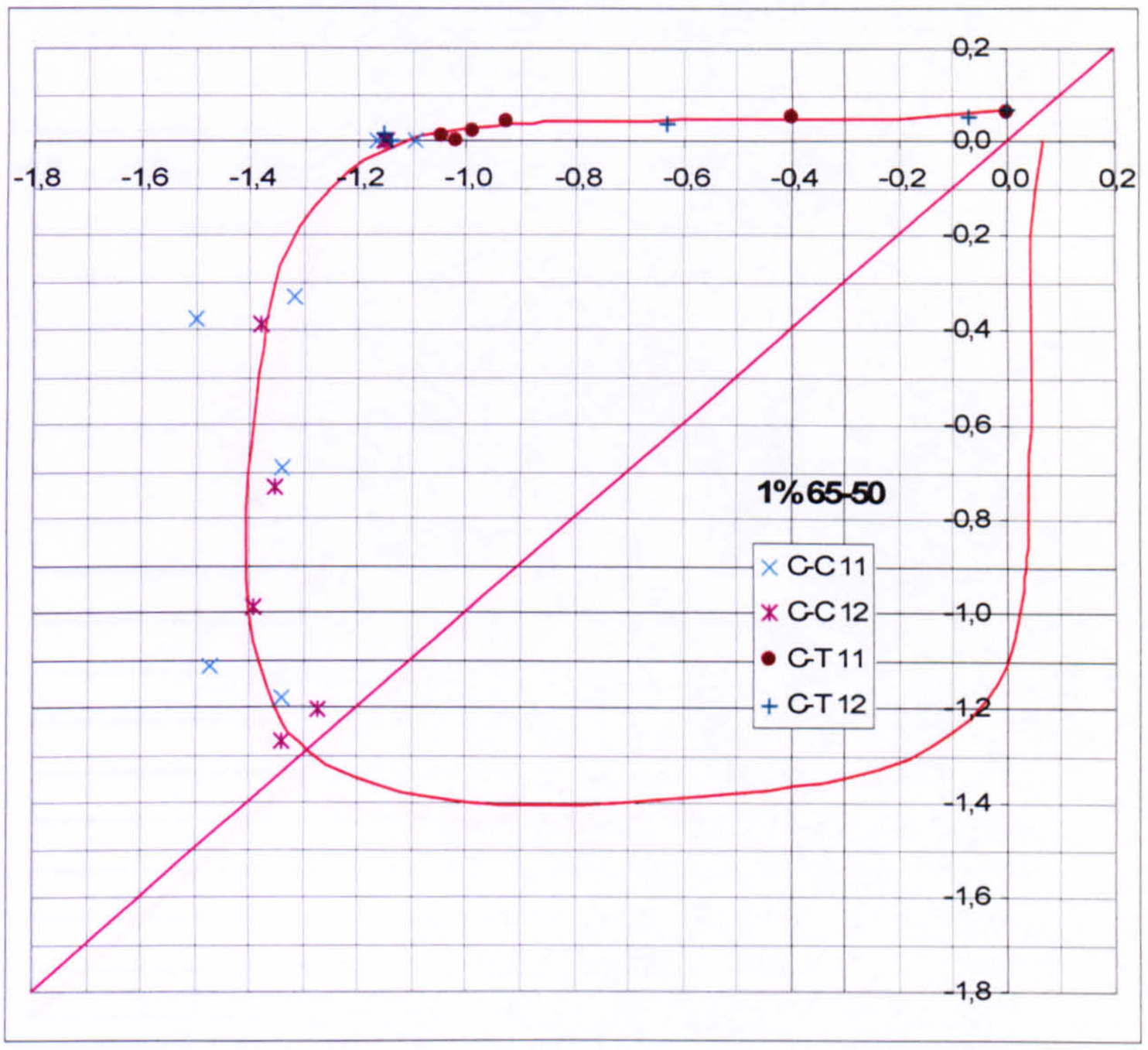

Figure 0.9 Biaxial strength envelope for fibre type 65-50 and V_f = 1 %

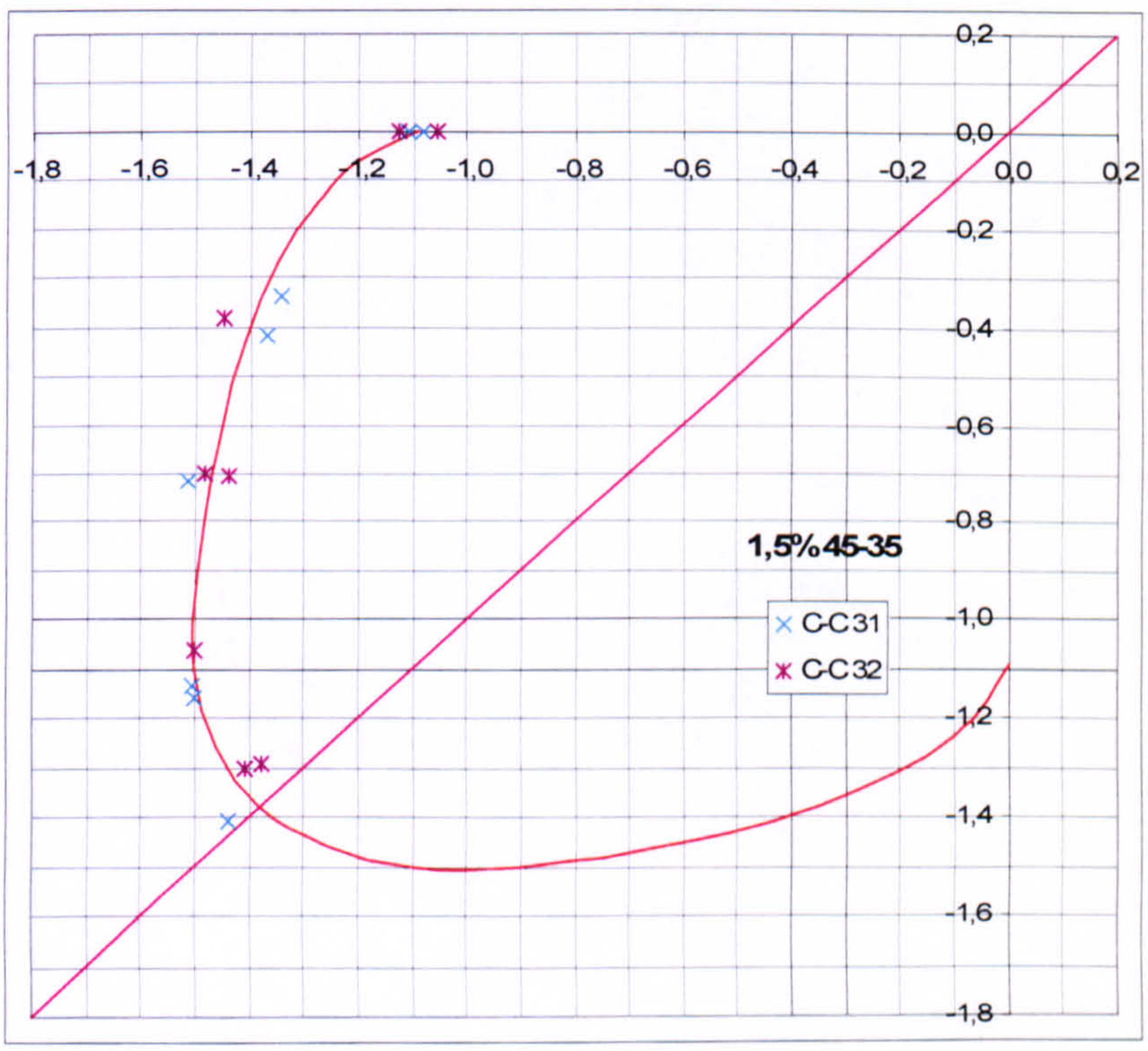

Figure 0.10 Biaxial strength envelope for fibre type 45-35 and V_f = 1.5 %

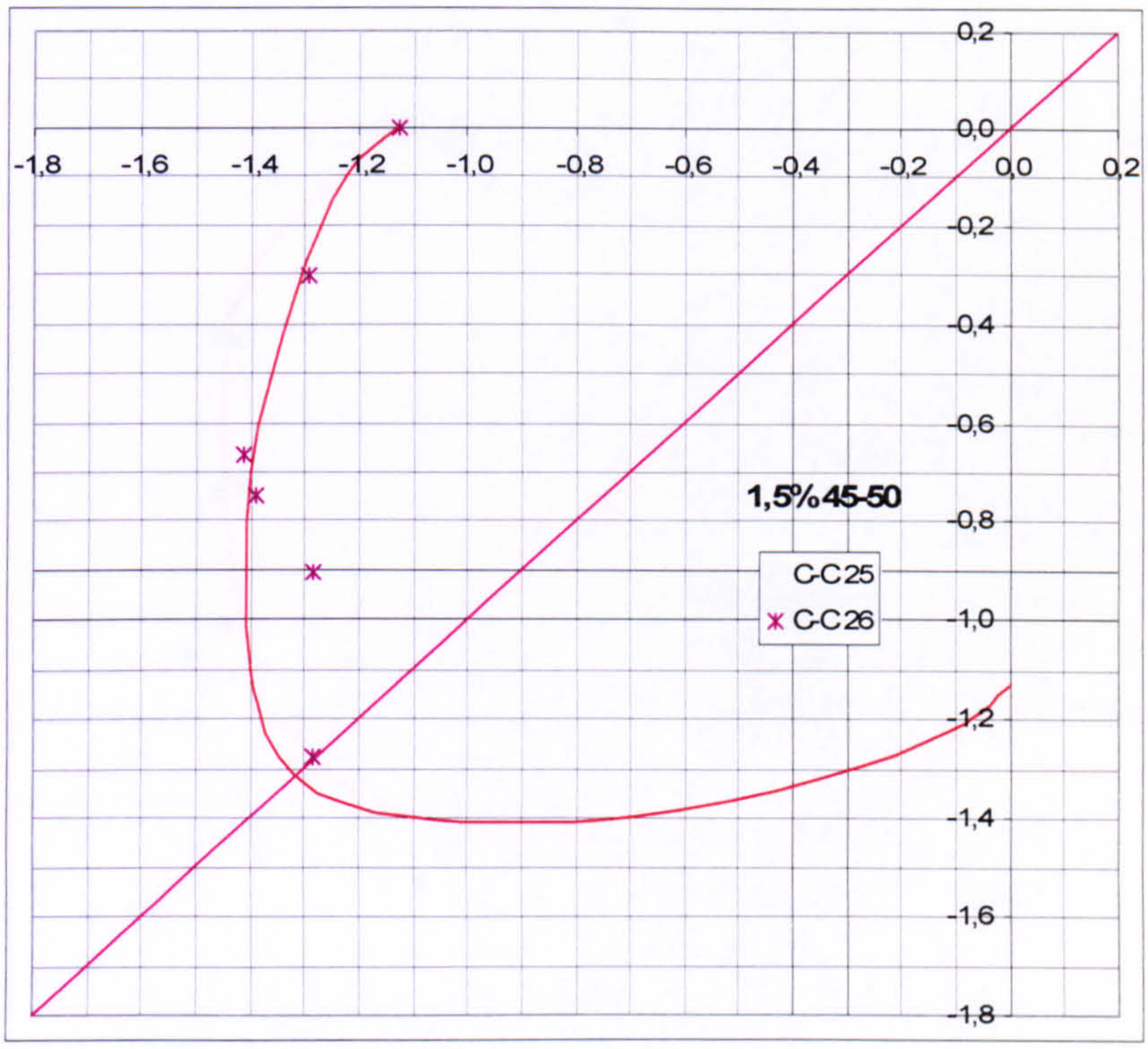

Figure 0.11 Biaxial strength envelope for fibre type 45-50 and V_f = 1.5 %

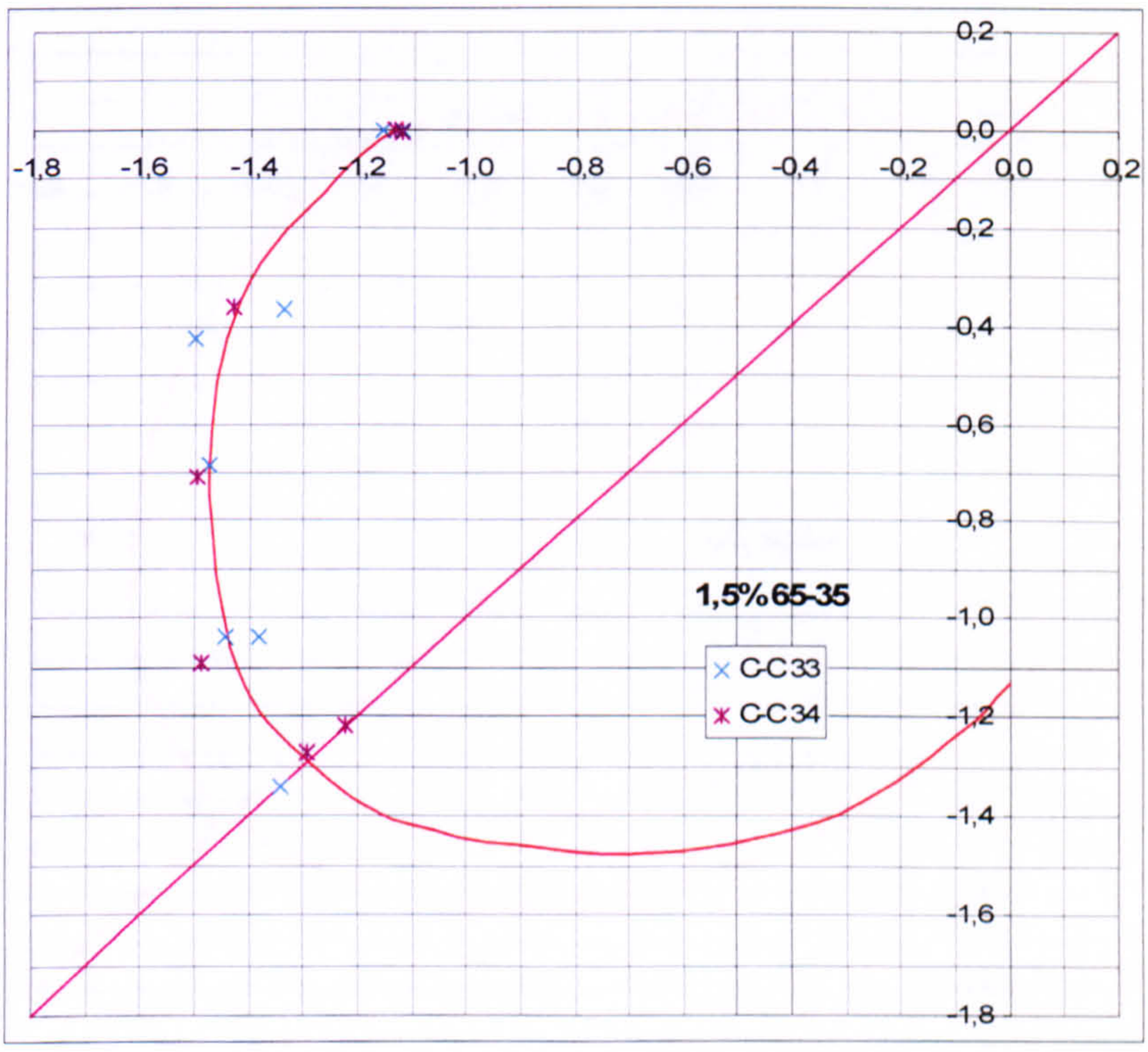

Figure 0.12 Biaxial strength envelope for fibre type 65-35 and V_f = 1.5 %

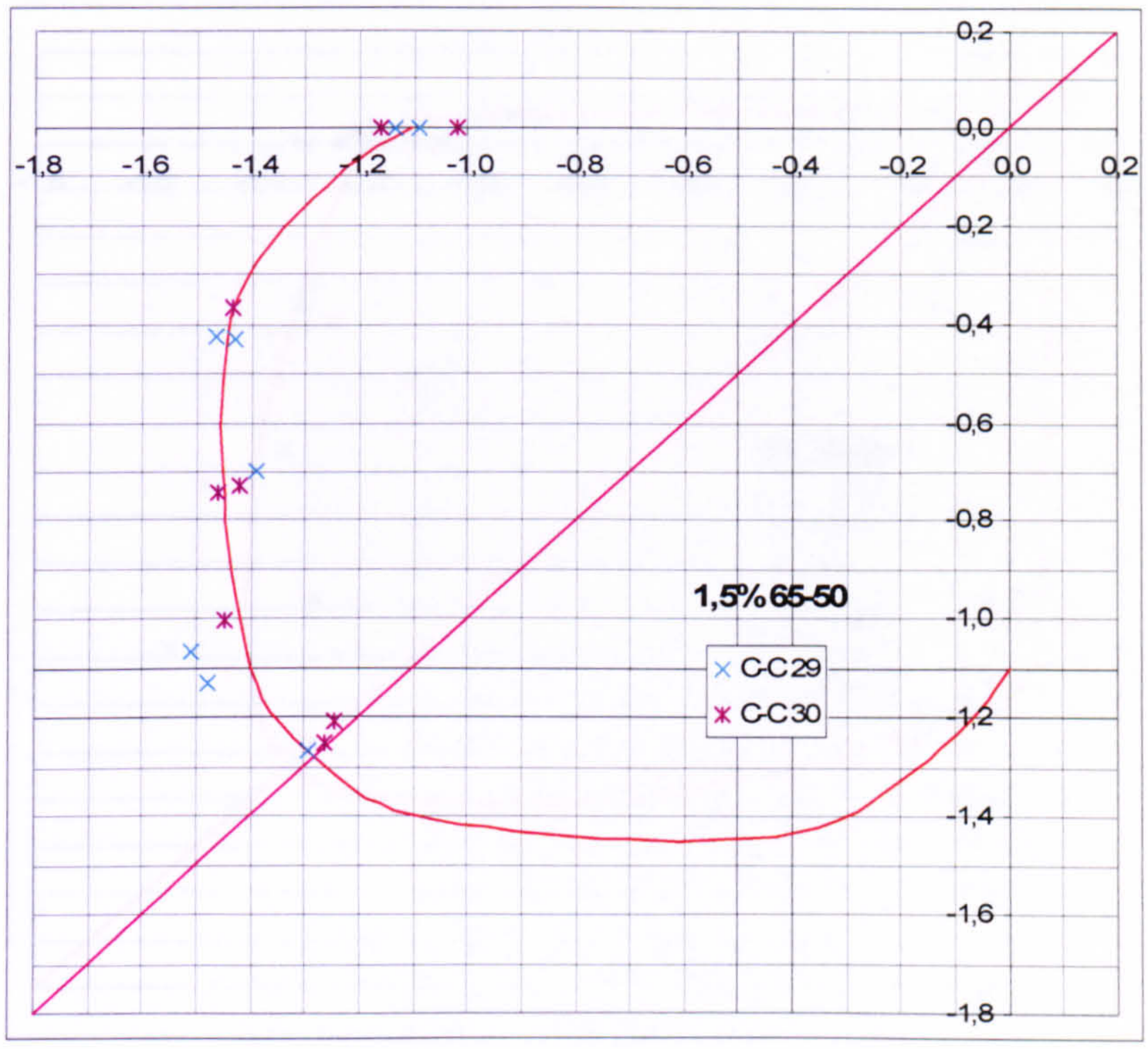

Figure 0.13 Biaxial strength envelope for fibre type 65-50 and V_f = 1.5 %

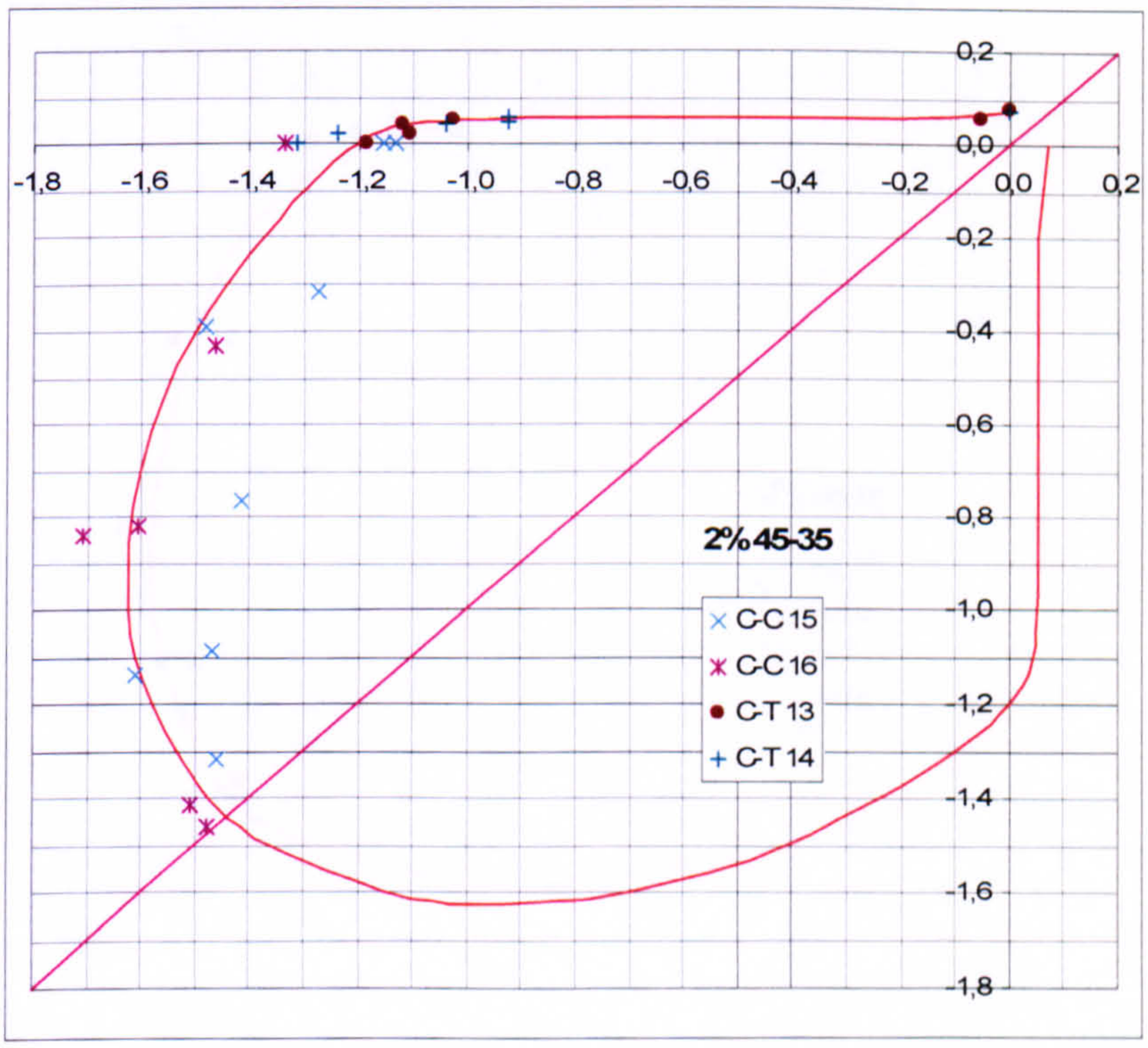

Figure 0.14 Biaxial strength envelope for fibre type 45-35 and V_f = 2 %

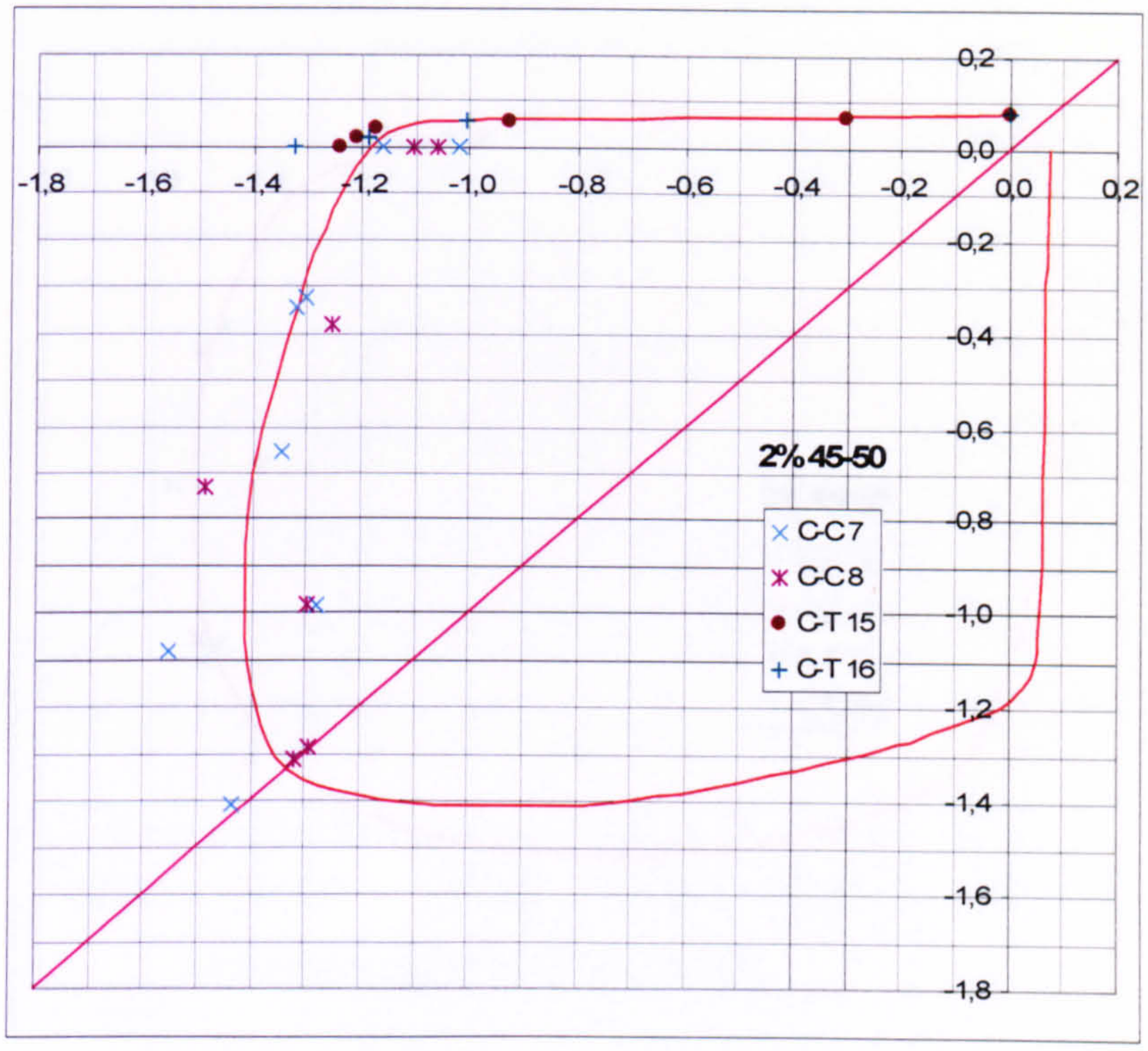

Figure 0.15 Biaxial strength envelope for fibre type 45-50 and V_f = 2 %

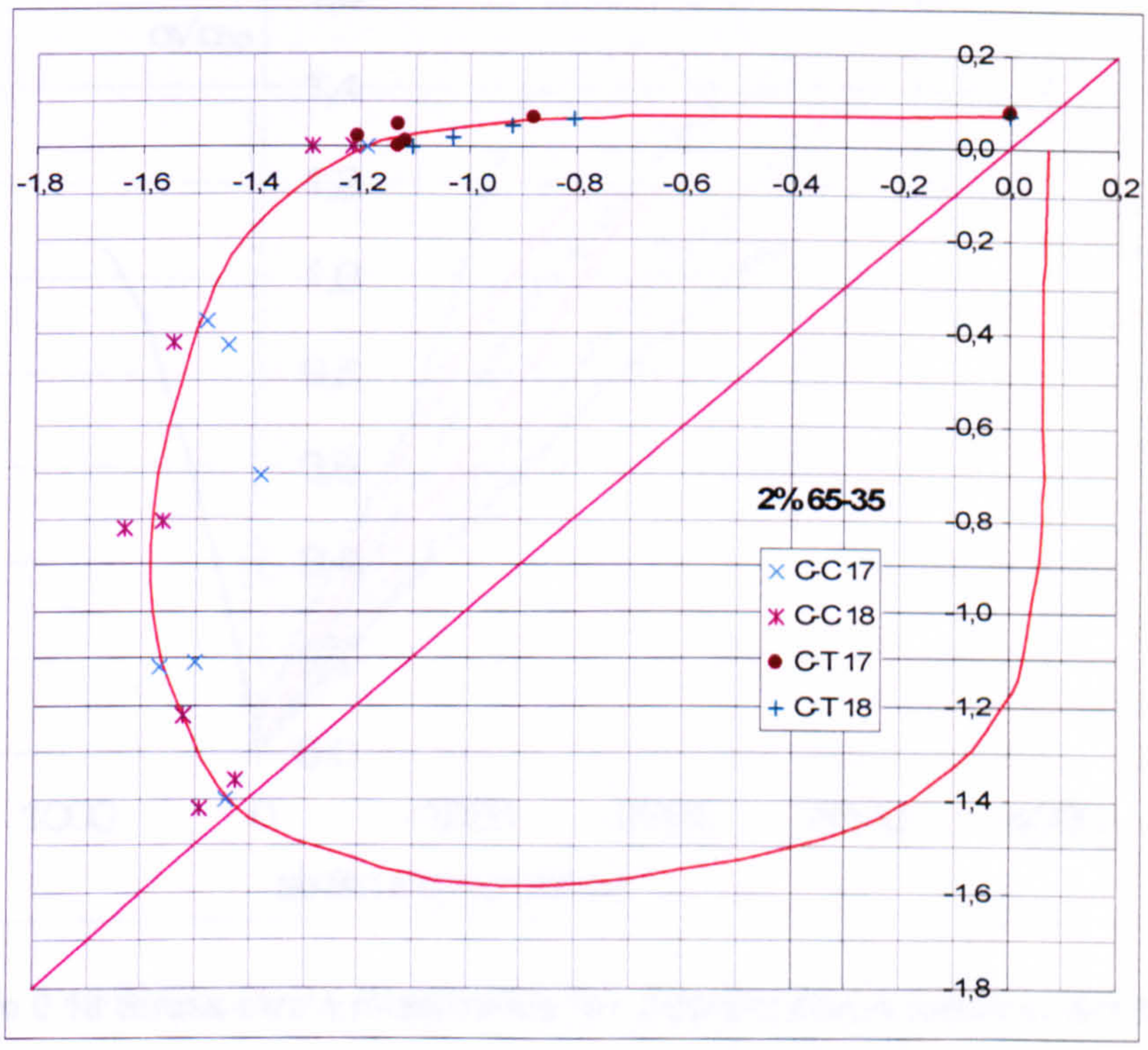

Figure 0.16 Biaxial strength envelope for fibre type 65-35 and V_f = 2 %

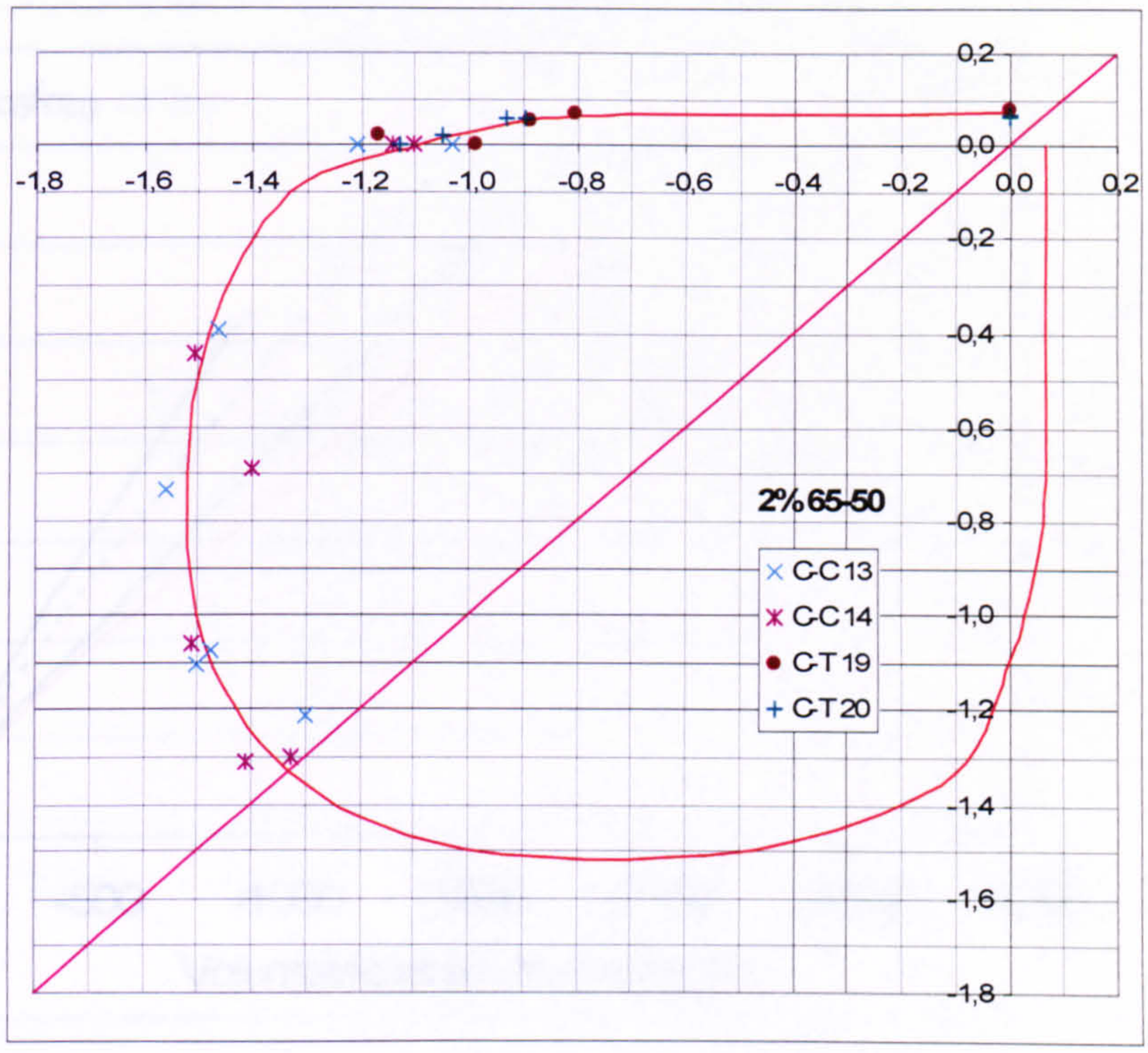

Figure 0.17 Biaxial strength envelope for fibre type 65-50 and V_f = 2 %

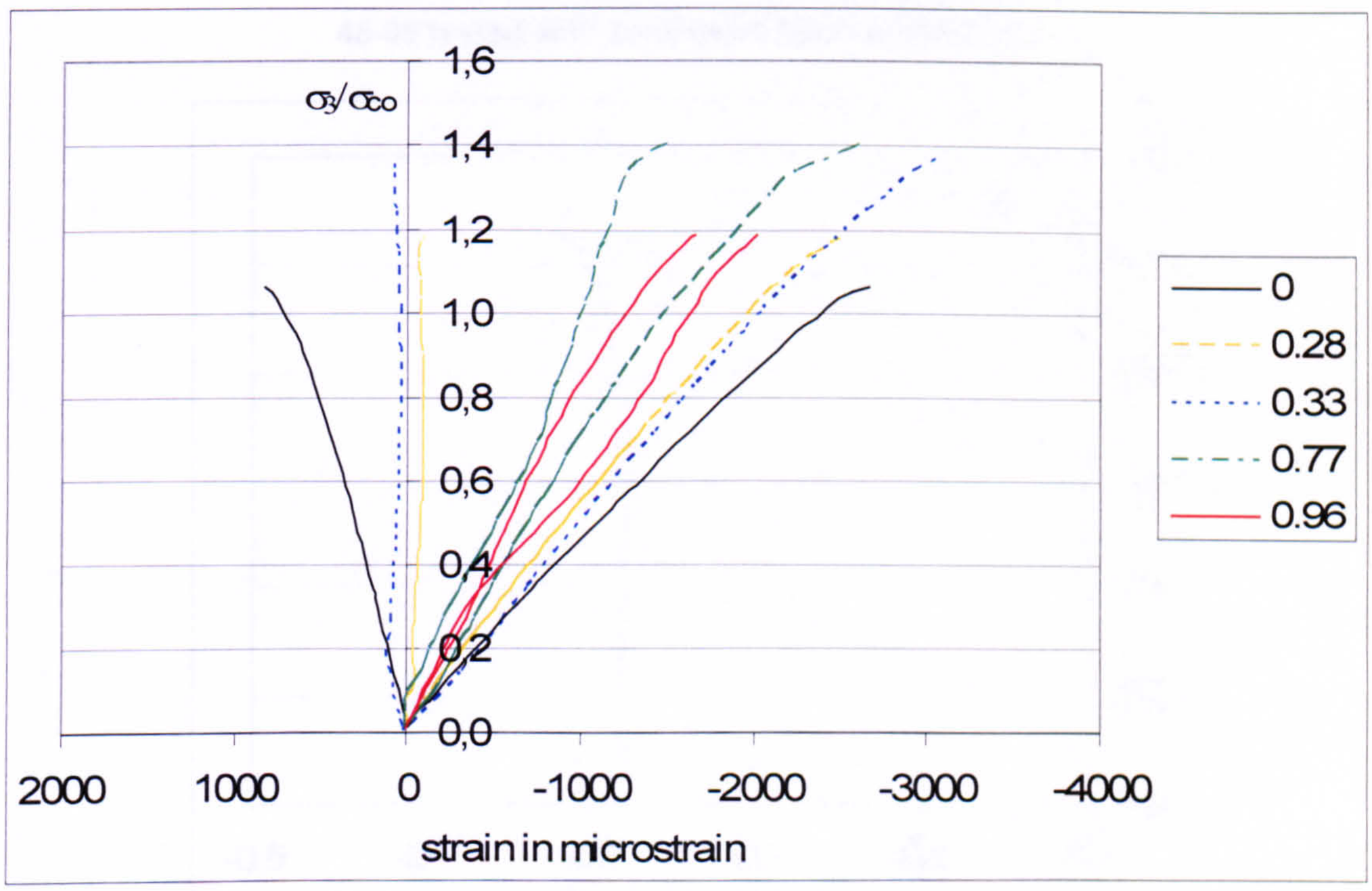

Figure 0.18 Stress-strain relationship for different stress ratios under biaxial compression recorded with strain gauges for V_f = 0.5 % of the fibre type 45-35 tested with solid steel blocks (batch 24)

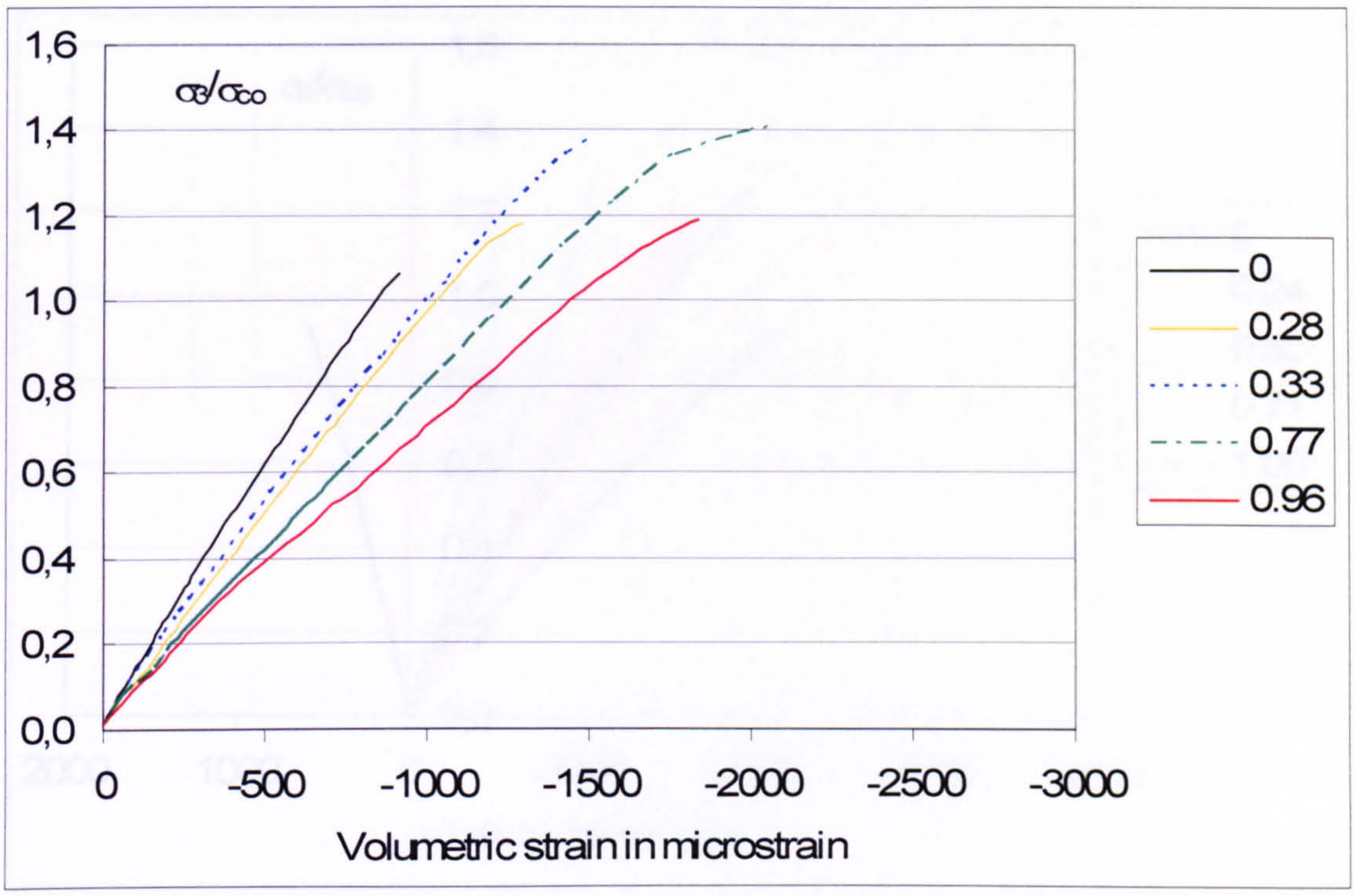

Figure 0.19 Volumetric strains for different stress ratios under biaxial compression recorded with strain gauges in the two in plane directions for V_f = 0.5 % of the fibre type 45-35 tested with solid steel blocks (batch 24)

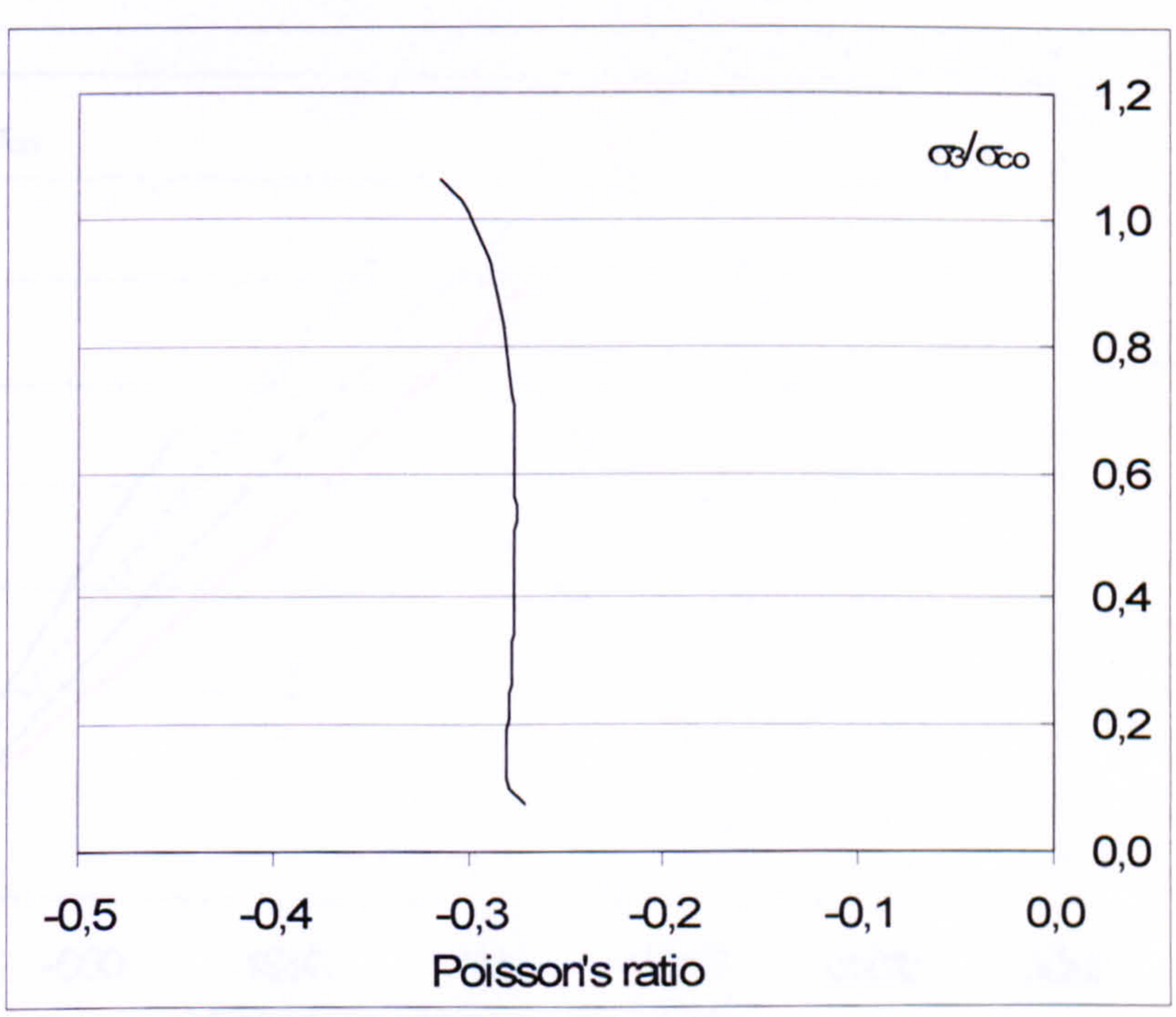

Figure 0.20 Poisson's ratio versus stress in uniaxial compression recorded with strain gauges in the two in plane directions for V_f = 0.5 % of the fibre type 45-35 tested with solid steel blocks (batch 24)

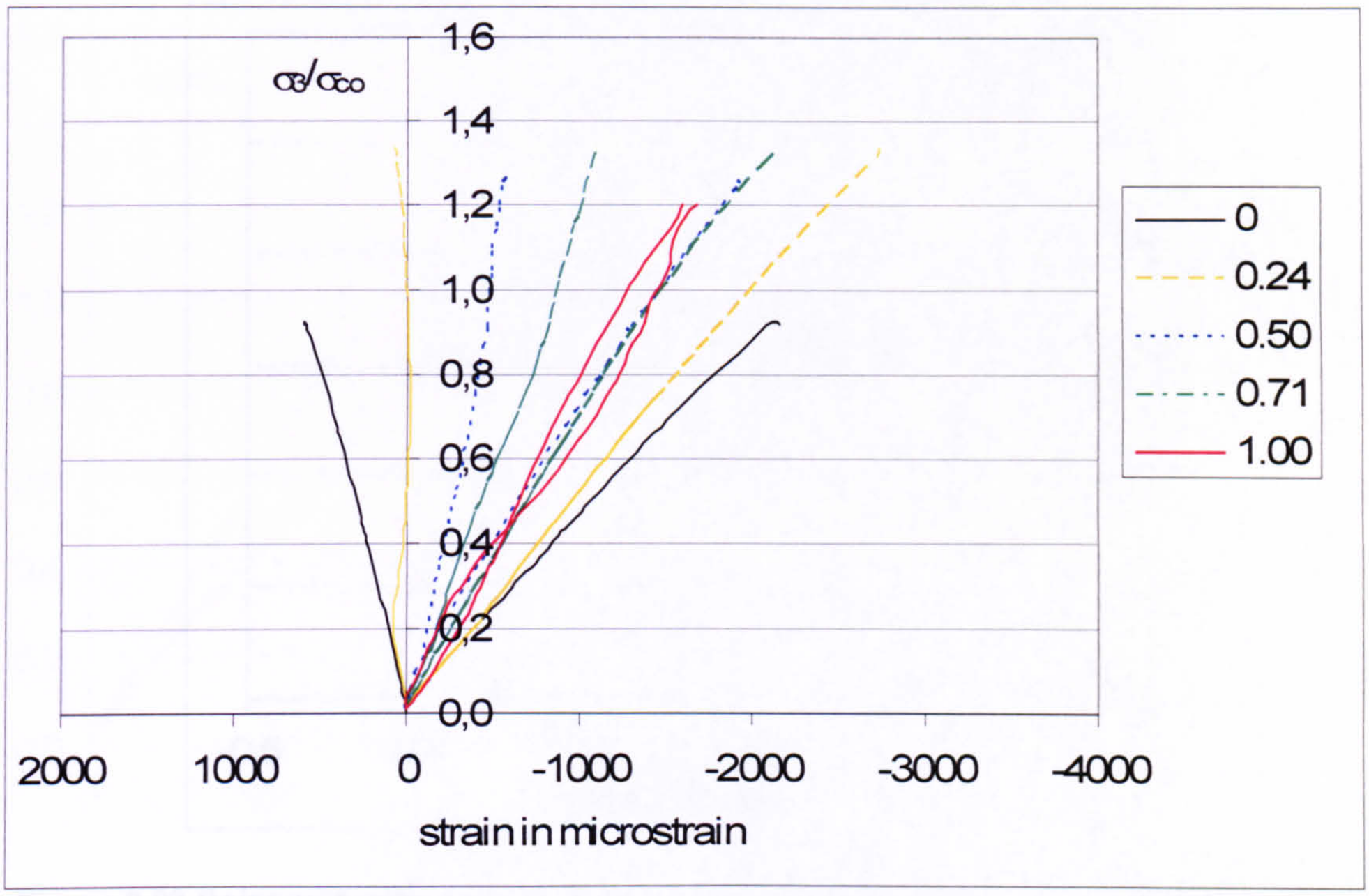

Figure 0.21 Stress-strain relationship for different stress ratios under biaxial compression recorded with strain gauges for V_f = 0.5 % of the fibre type 45-50 tested with solid steel blocks (batch 22)

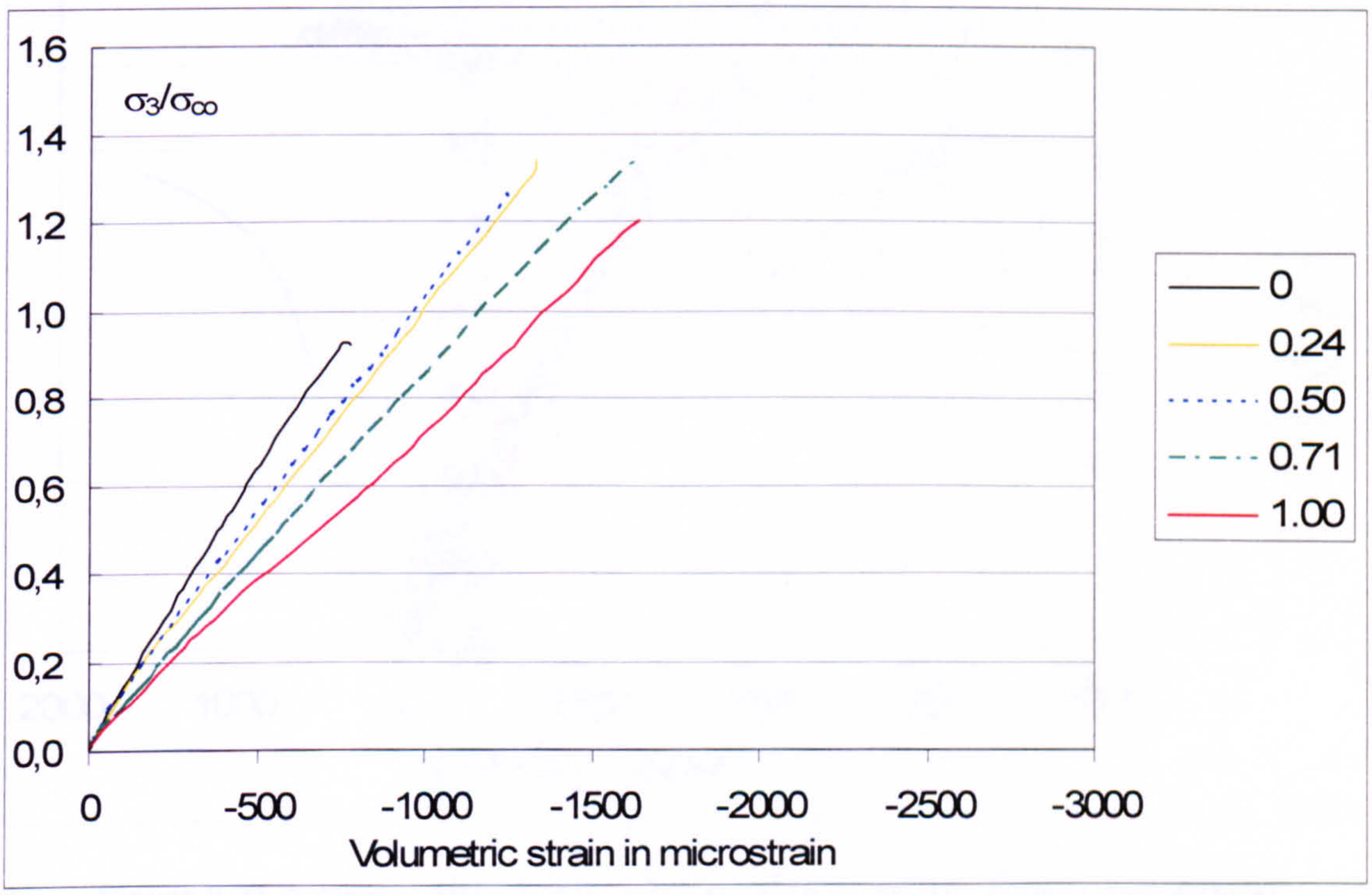

Figure 0.22 Volumetric strains for different stress ratios under biaxial compression recorded with strain gauges in the two in plane directions for V_f = 0.5 % of the fibre type 45-50 tested with solid steel blocks (batch 22)

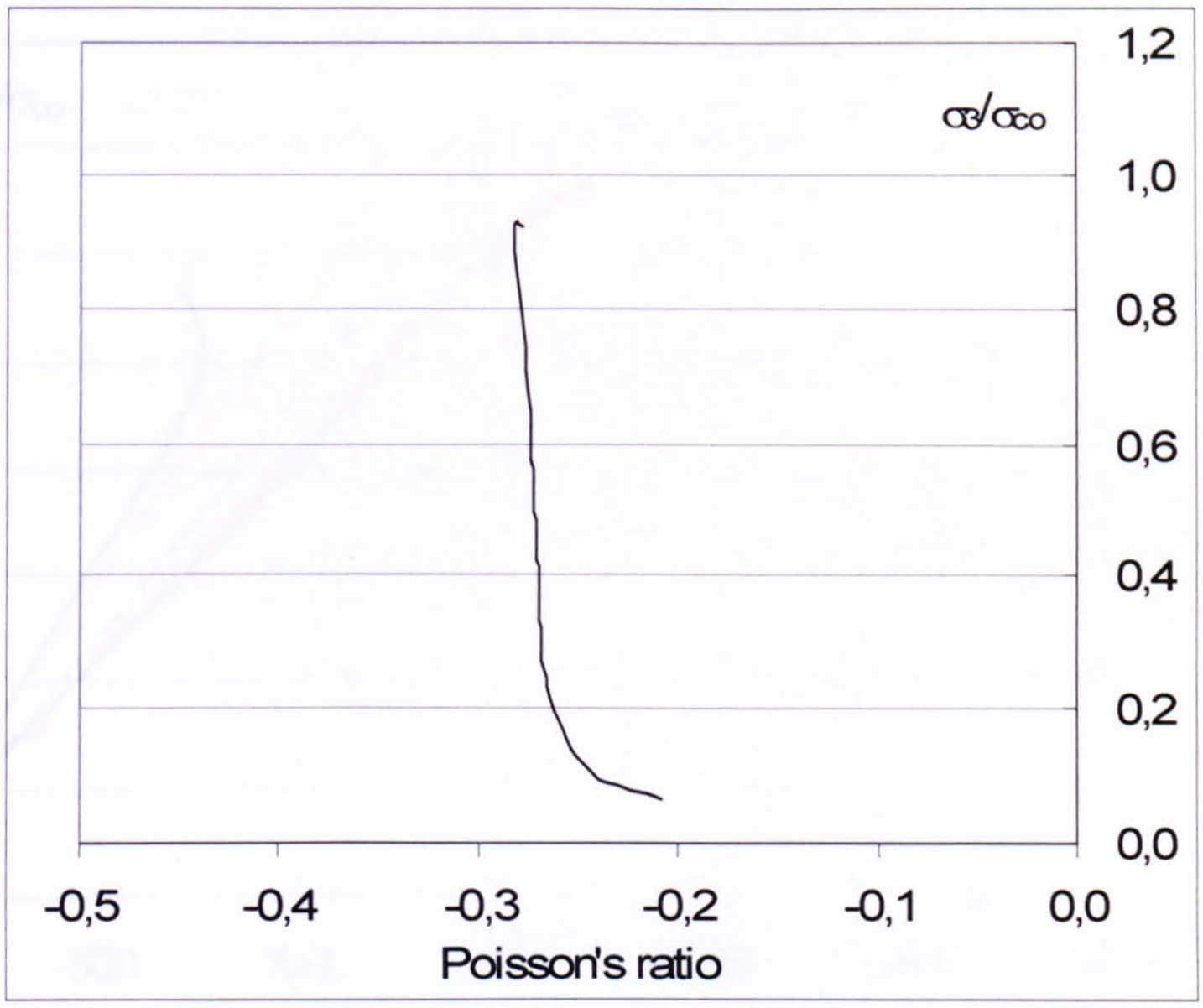

Figure 0.23 Poisson's ratio versus stress in uniaxial compression recorded with strain gauges in the two in plane directions for V_f = 0.5 % of the fibre type 45-50 tested with solid steel blocks (batch 22)

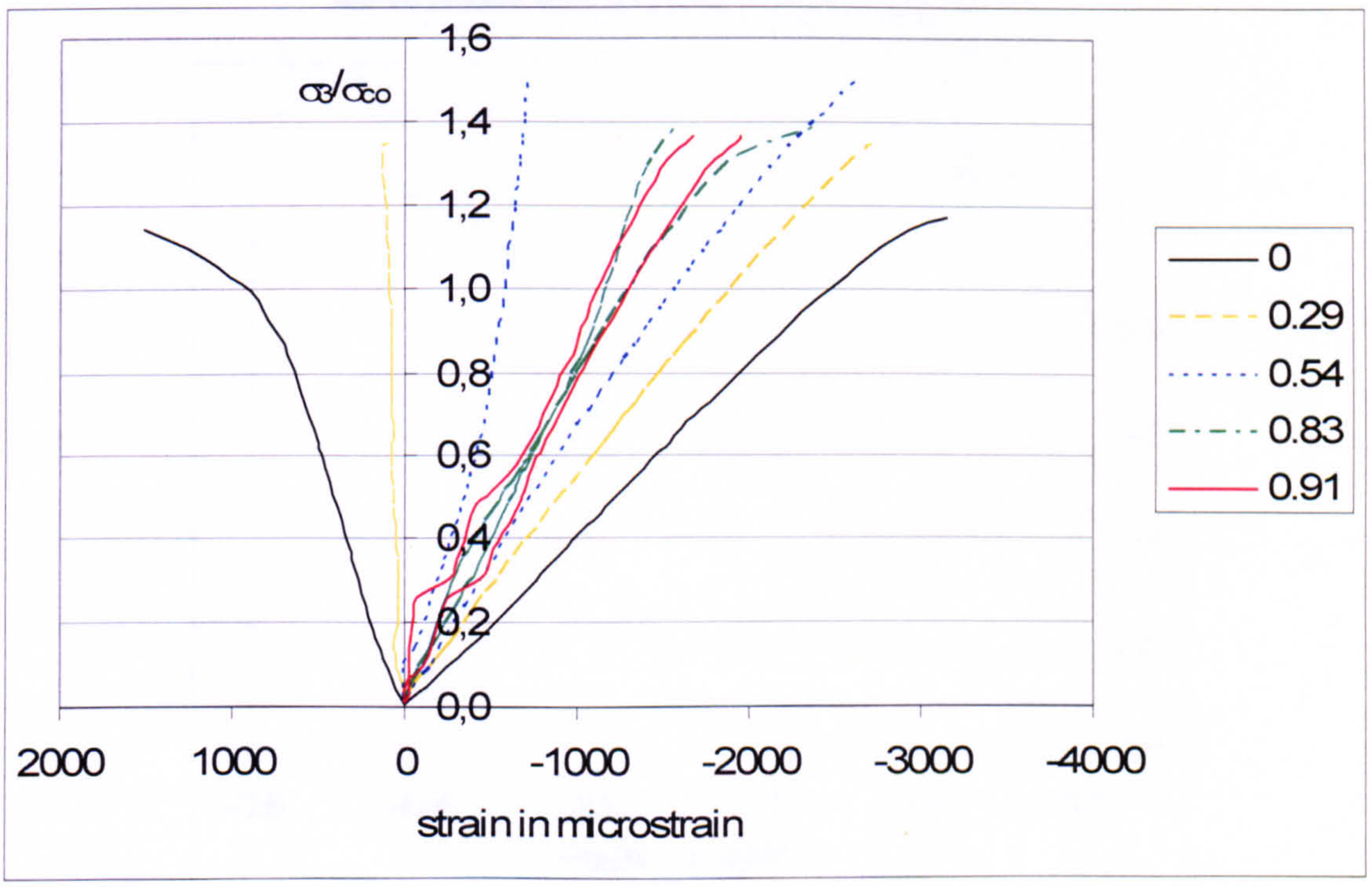

Figure 0.24 Stress-strain relationship for different stress ratios under biaxial compression recorded with strain gauges for V_f = 0.5 % of the fibre type 65-35 tested with solid steel blocks (batch 20)

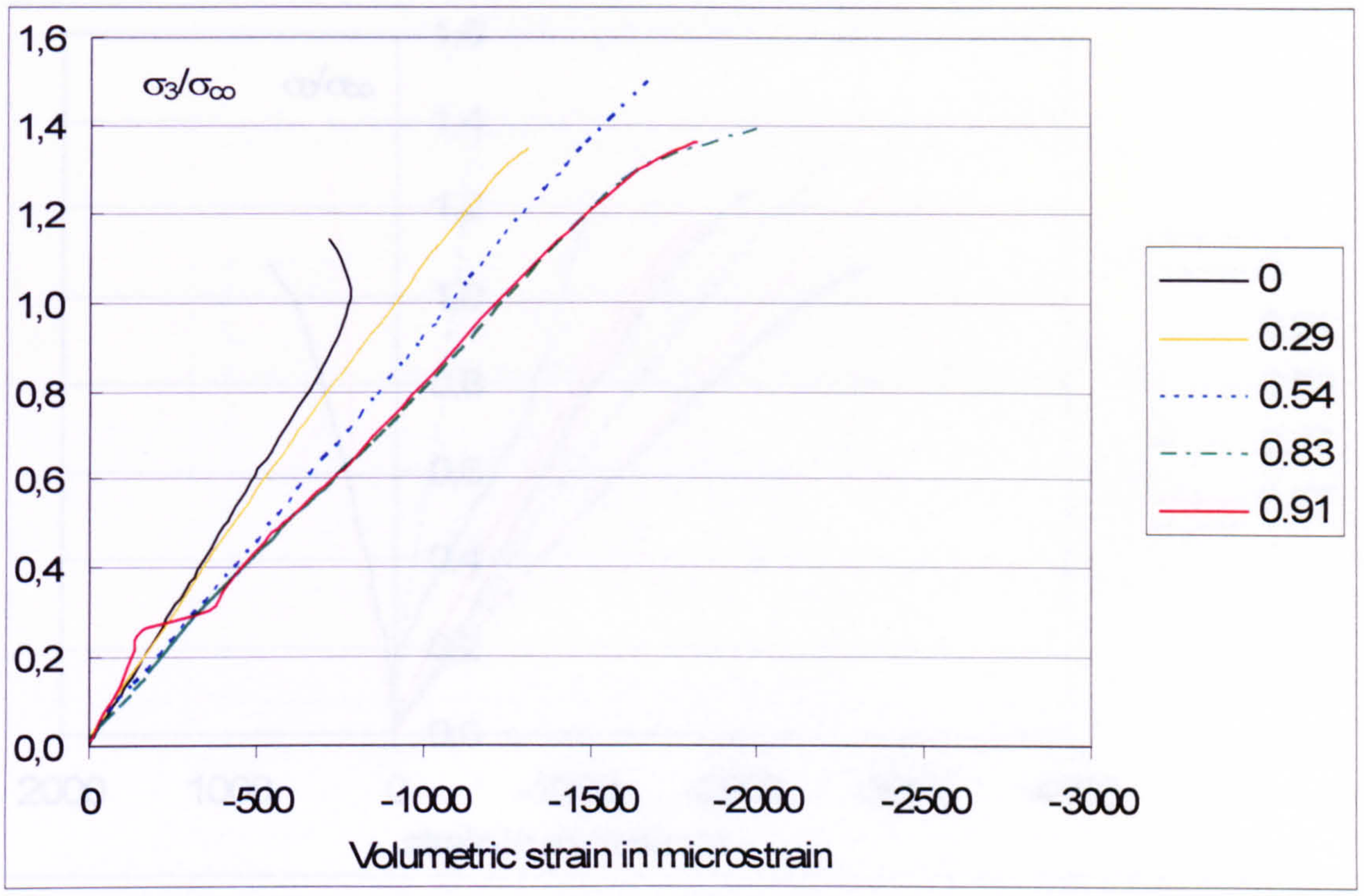

Figure 0.25 Volumetric strains for different stress ratios under biaxial compression recorded with strain gauges in the two in plane directions for V_f = 0.5 % of the fibre type 65-35 tested with solid steel blocks (batch 20)

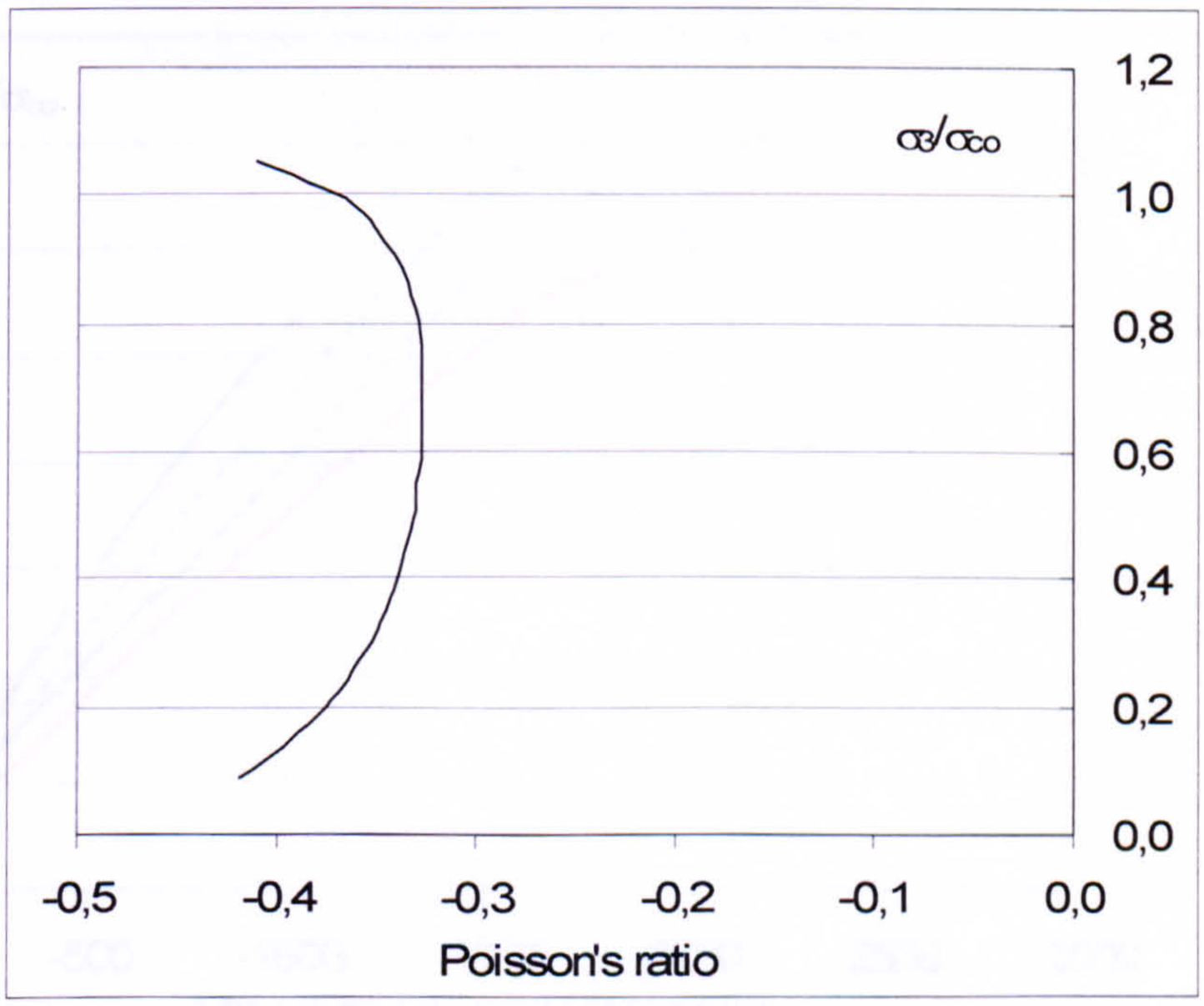

Figure 0.26 Poisson's ratio versus stress in uniaxial compression recorded with strain gauges in the two in plane directions for V_f = 0.5 % of the fibre type 65-35 tested with solid steel blocks (batch 20)

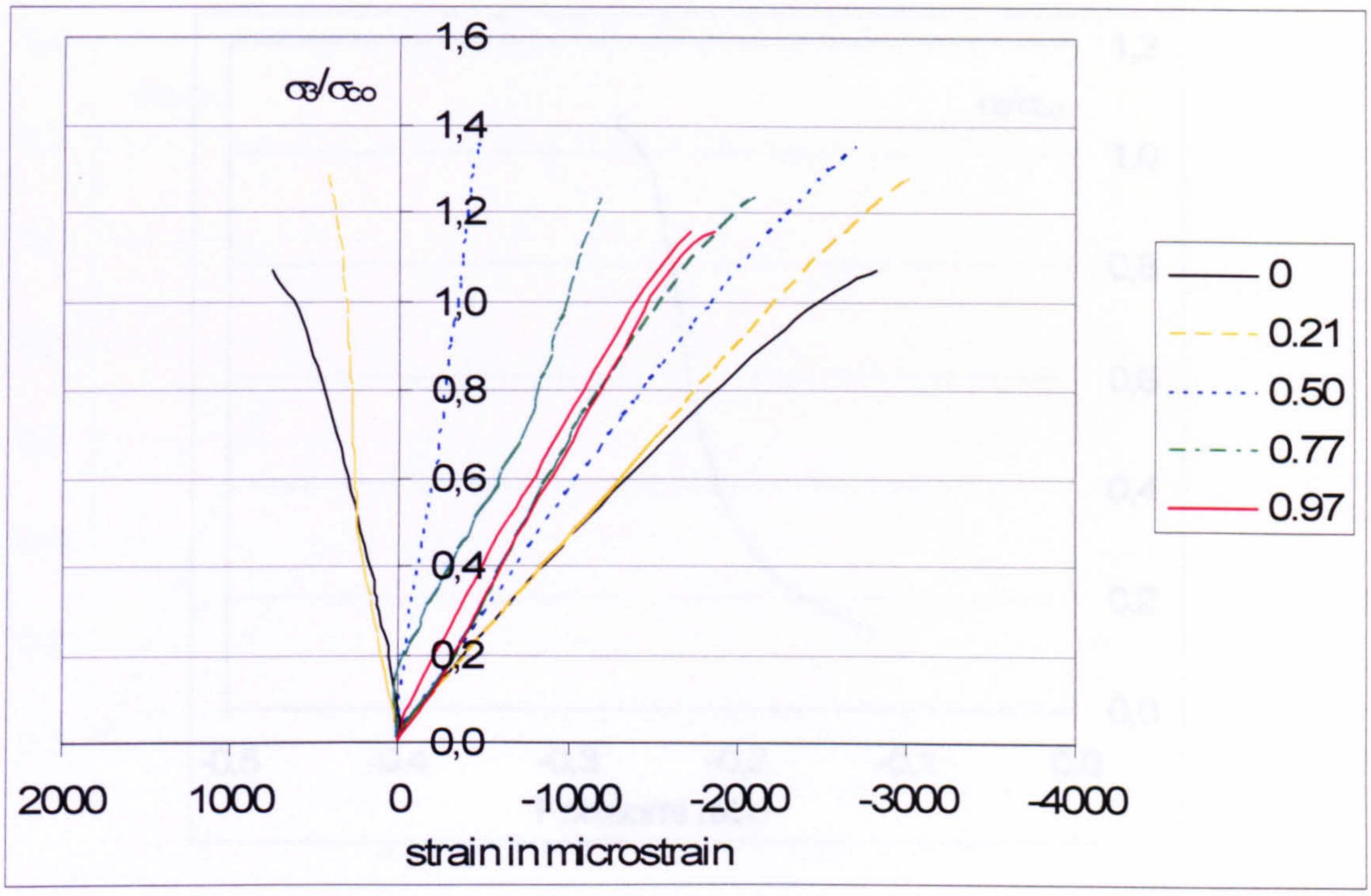

Figure 0.27 Stress-strain relationship for different stress ratios under biaxial compression recorded with strain gauges for V_f = 0.5 % of the fibre type 65-60 tested with solid steel blocks (batch 28)

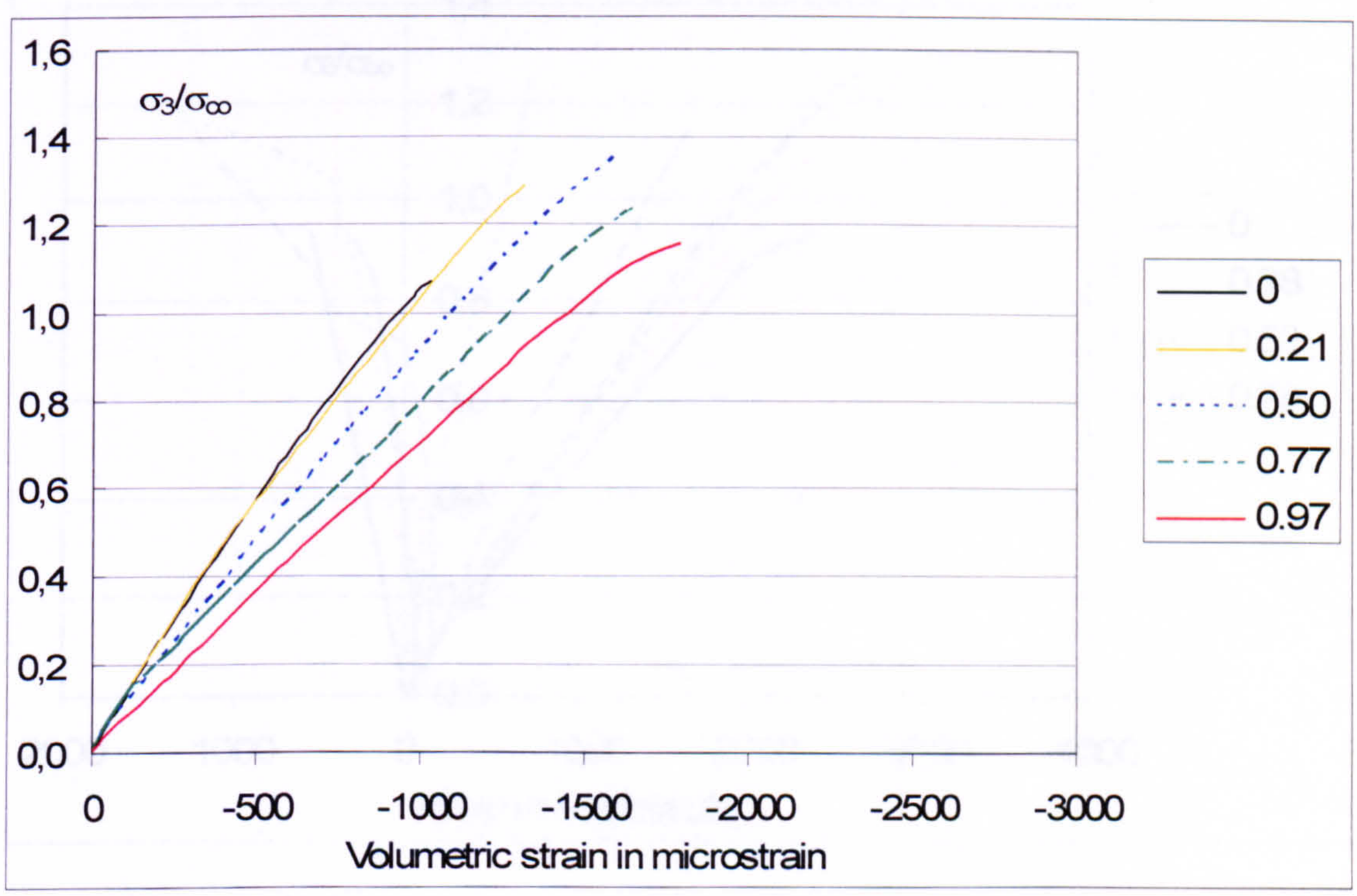

Figure 0.28 Volumetric strains for different stress ratios under biaxial compression recorded with strain gauges in the two in plane directions for V_f = 0.5 % of the fibre type 65-60 tested with solid steel blocks (batch 28)

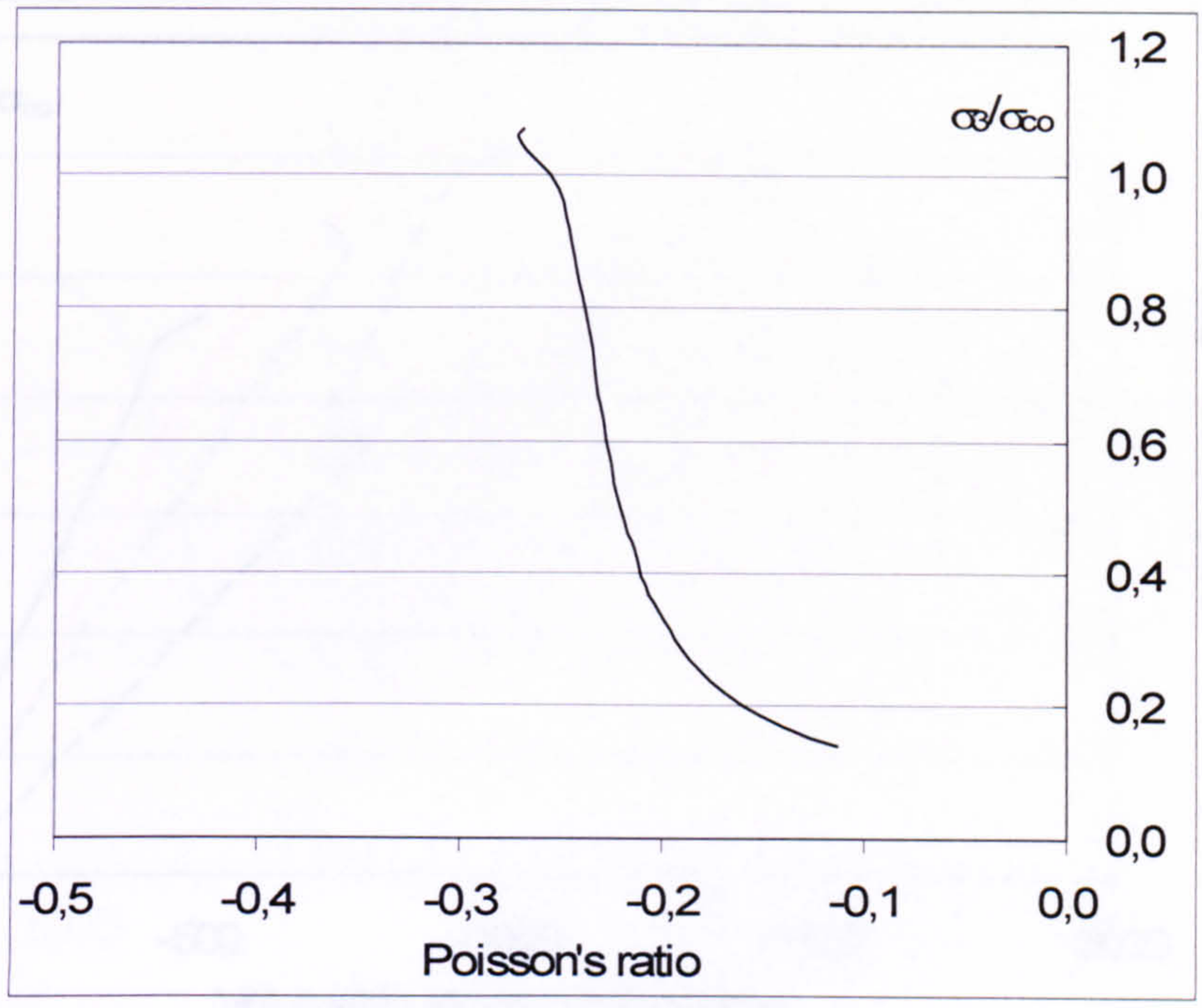

Figure 0.29 Poisson's ratio versus stress in uniaxial compression recorded with strain gauges in the two in plane directions for V_f = 0.5 % of the fibre type 65-60 tested with solid steel blocks (batch 28)

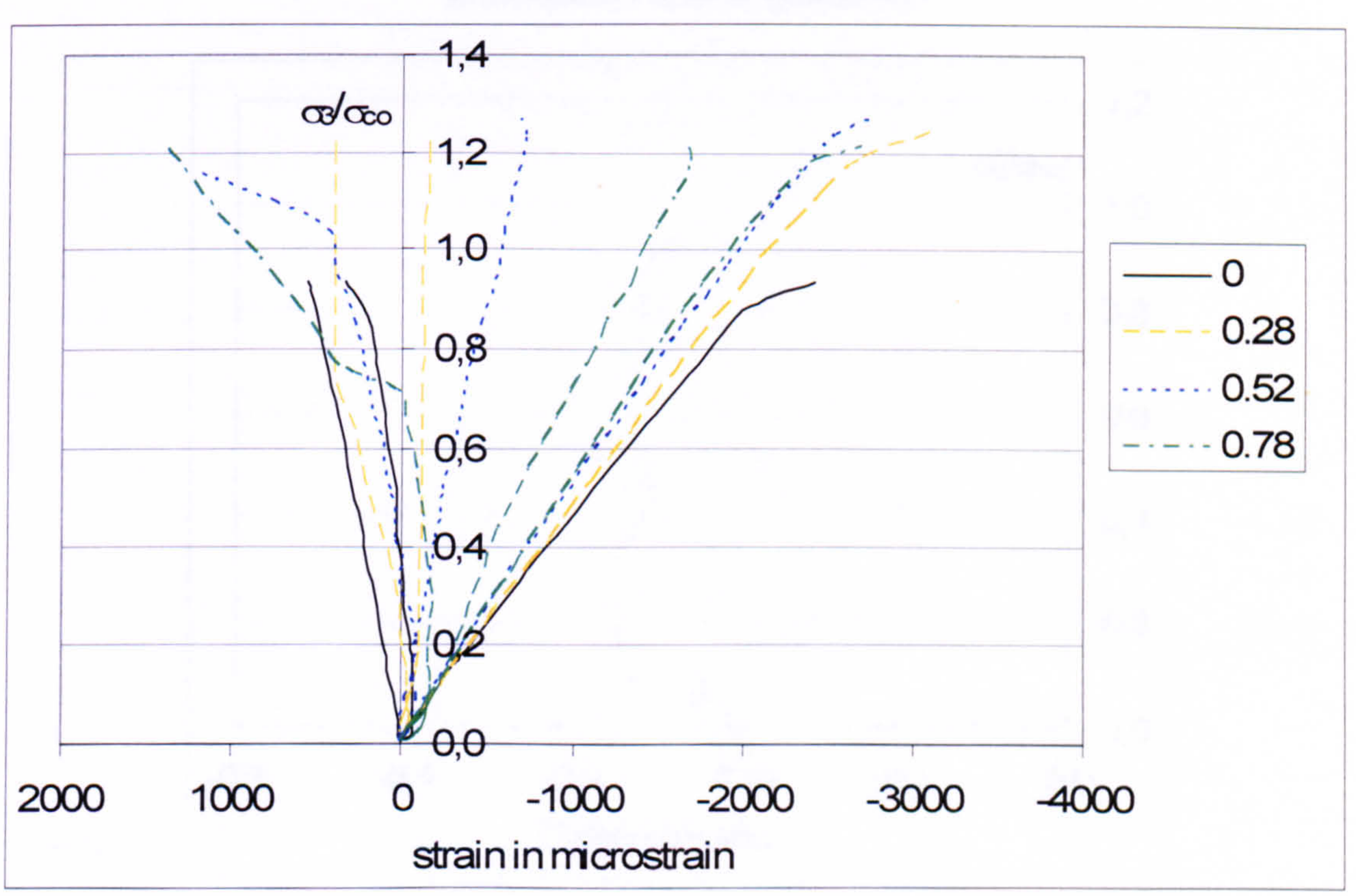

Figure 0.30 Stress-strain relationship for different stress ratios under biaxial compression recorded with LVDTs for V_f = 1 % of the fibre type 45-35 tested with brush platen system (batch 03)

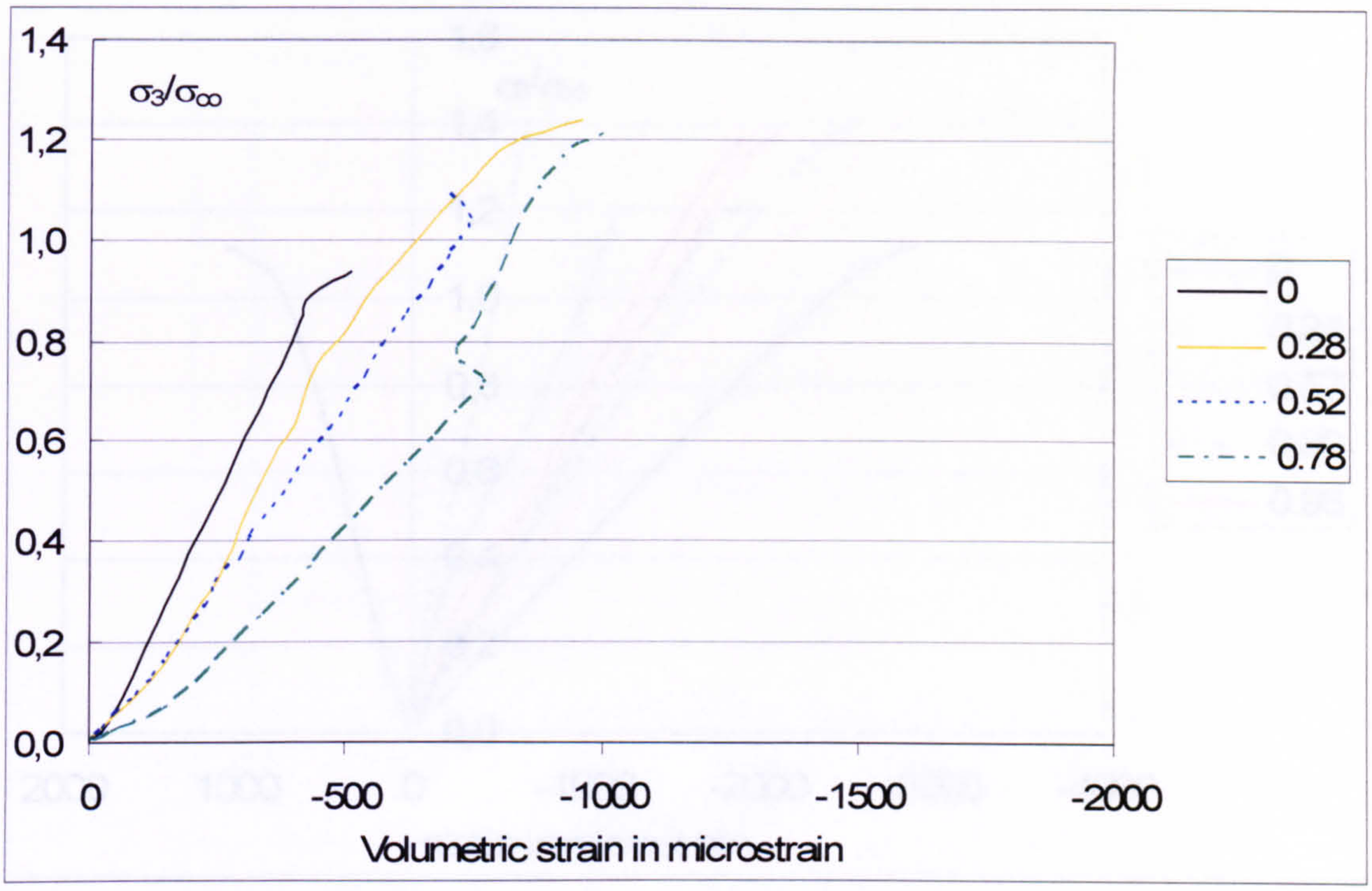

Figure 0.31 Volumetric strains for different stress ratios under biaxial compression recorded with LVDTs in three directions for V_f = 1 % of the fibre type 45-35 tested with brush platen system (batch 03)

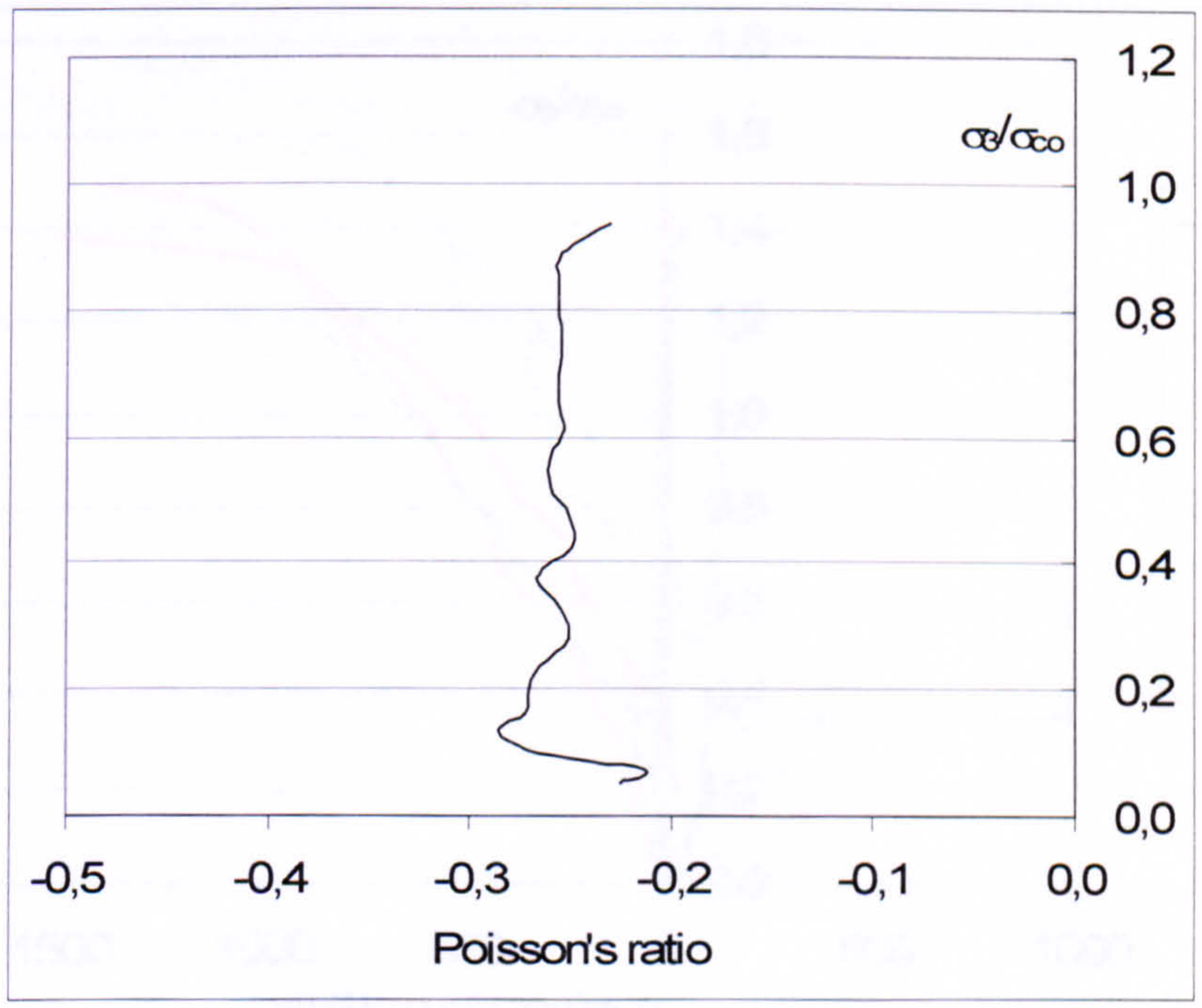

Figure 0.32 Poisson's ratio versus stress in uniaxial compression recorded with LVDTs in the two in plane directions for V_f = 1 % of the fibre type 45-35 tested with brush platen system (batch 03)

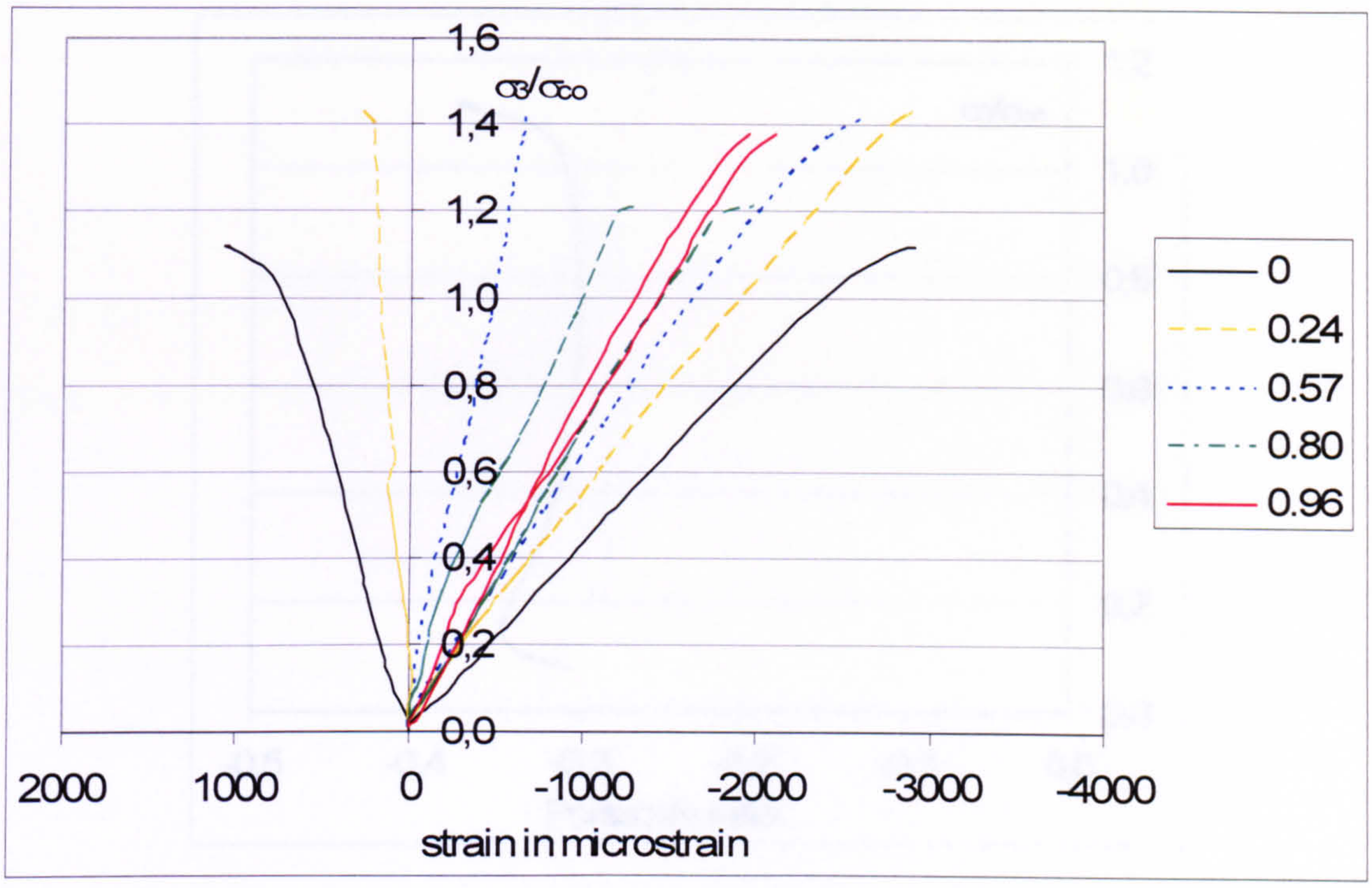

Figure 0.33 Stress-strain relationship for different stress ratios under biaxial compression recorded with strain gauges for V_f = 1 % of the fibre type 45-35 tested with solid steel blocks (batch 04)

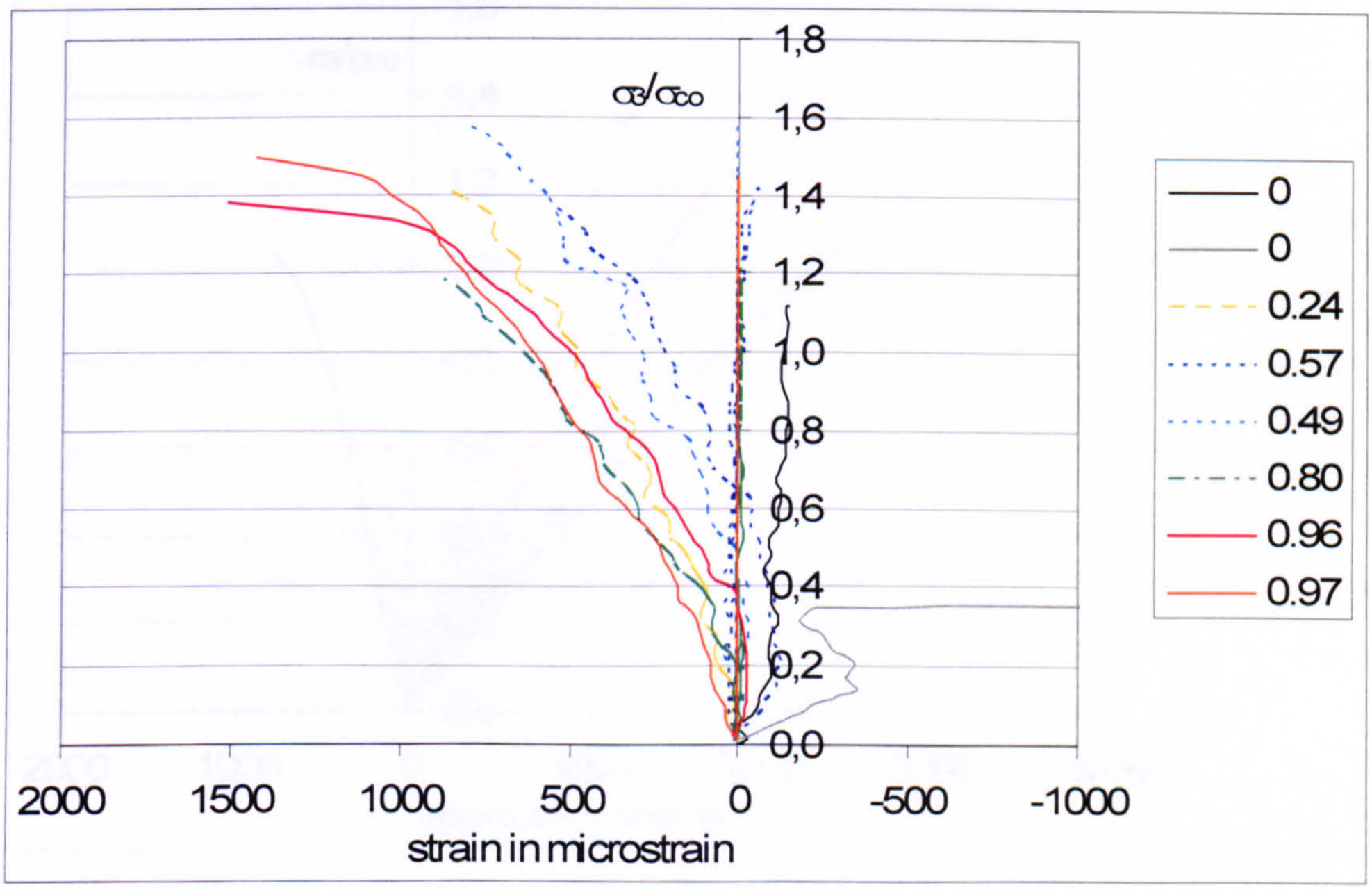

Figure 0.34 Stress-strain relationship in z direction only for different stress ratios under biaxial compression recorded with LVDTs for V_f = 1 % of the fibre type 45-35 tested with solid steel blocks (batch 04)

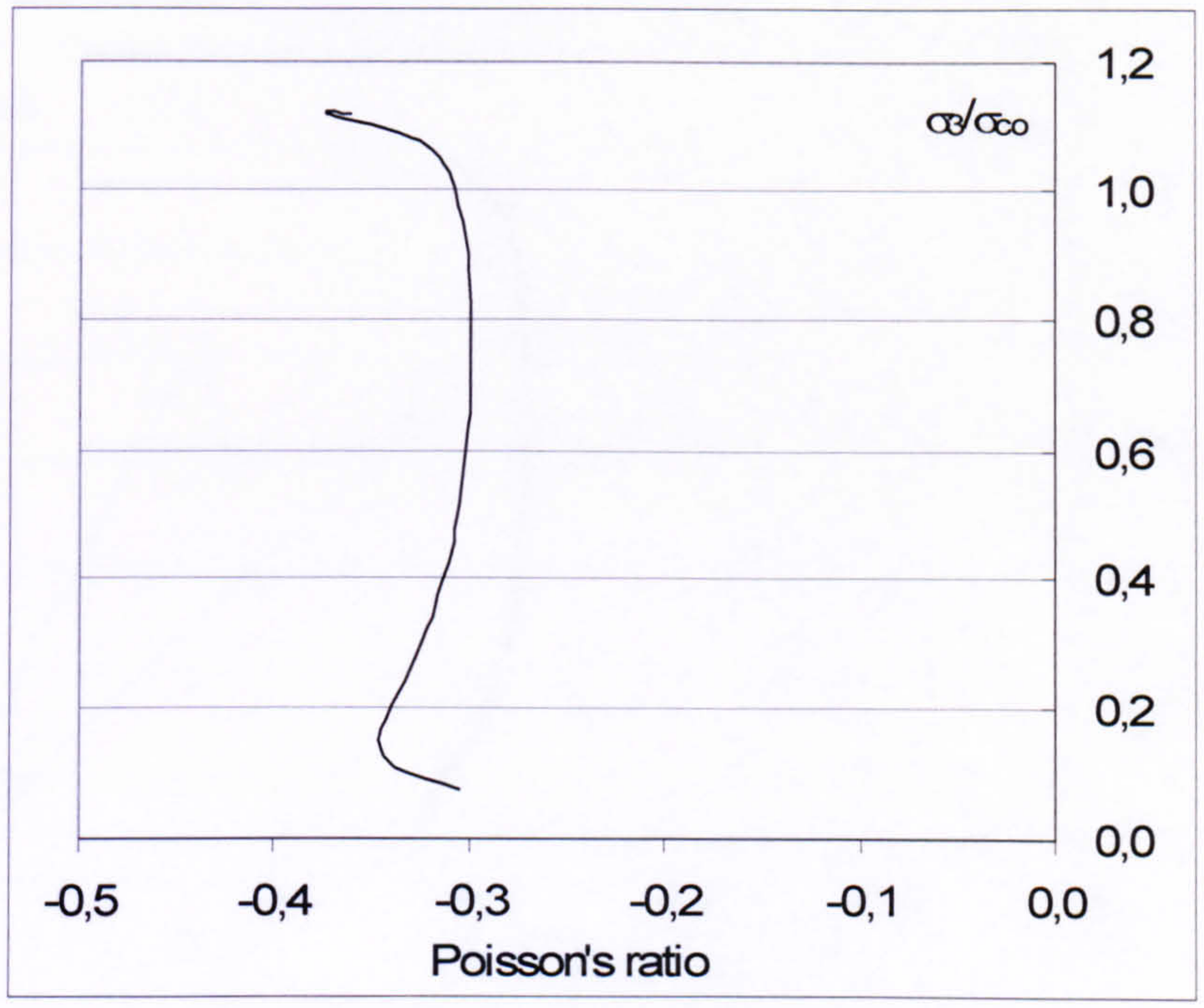

Figure 0.35 Poisson's ratio versus stress in uniaxial compression recorded with strain gauges in the two in plane directions for V_f = 1 % of the fibre type 45-35 tested with solid steel blocks (batch 04)

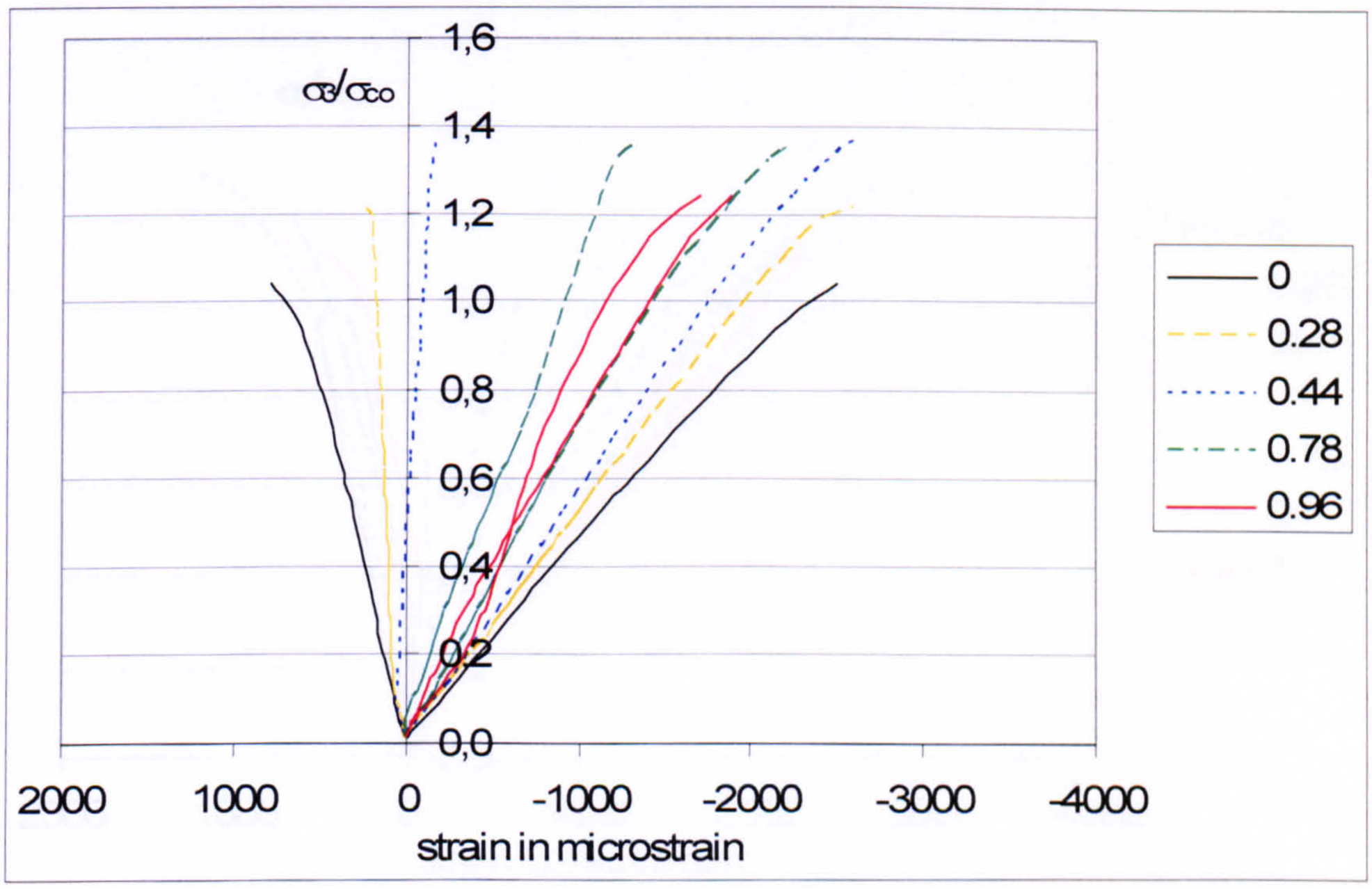

Figure 0.36 Stress-strain relationship for different stress ratios under biaxial compression recorded with strain gauges for V_f = 1 % of the fibre type 45-50 tested with solid steel blocks (batch 06)

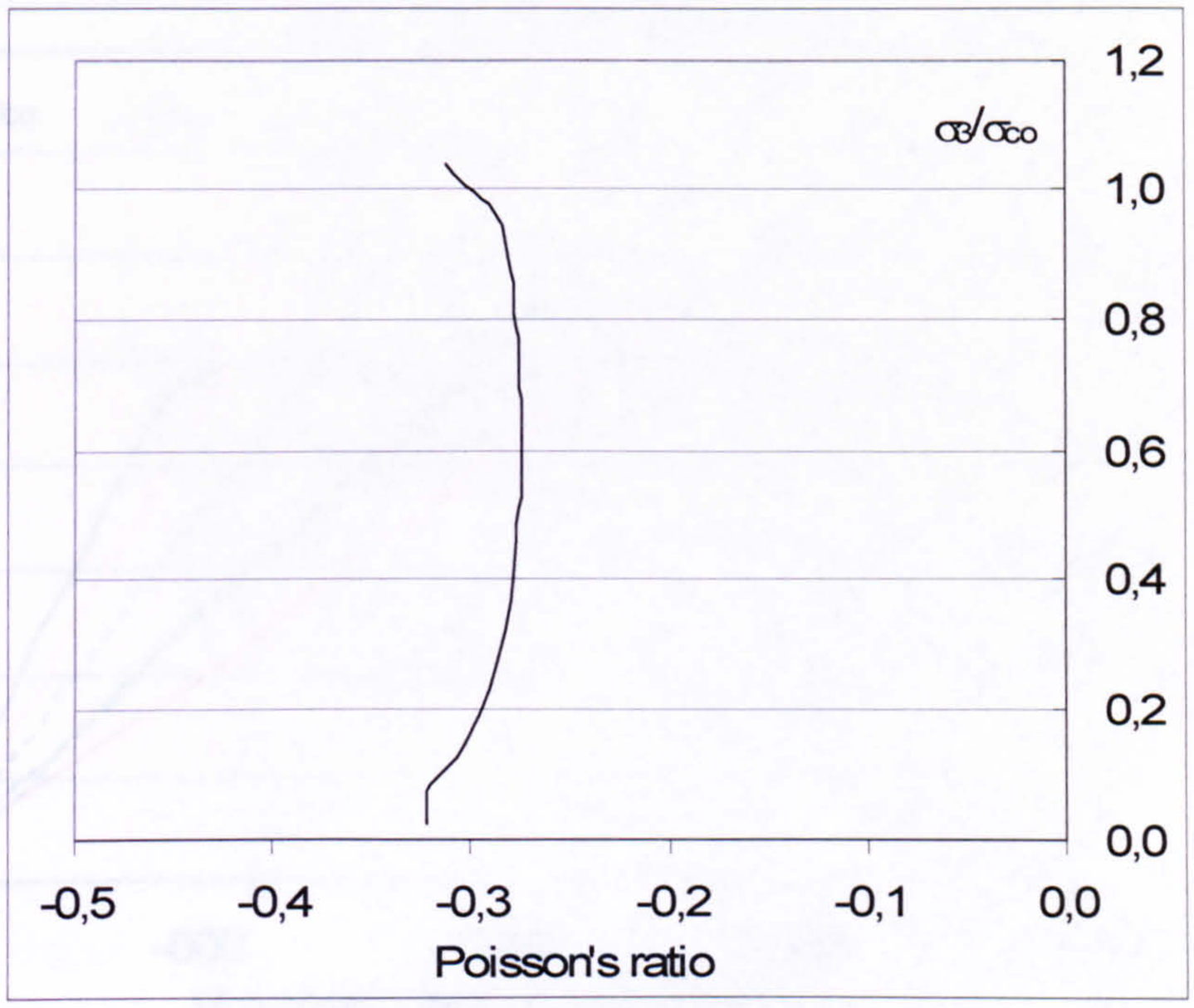

Figure 0.37 Poisson's ratio versus stress in uniaxial compression recorded with strain gauges in the two in plane directions for V_f = 1 % of the fibre type 45-50 tested with solid steel blocks (batch 06)

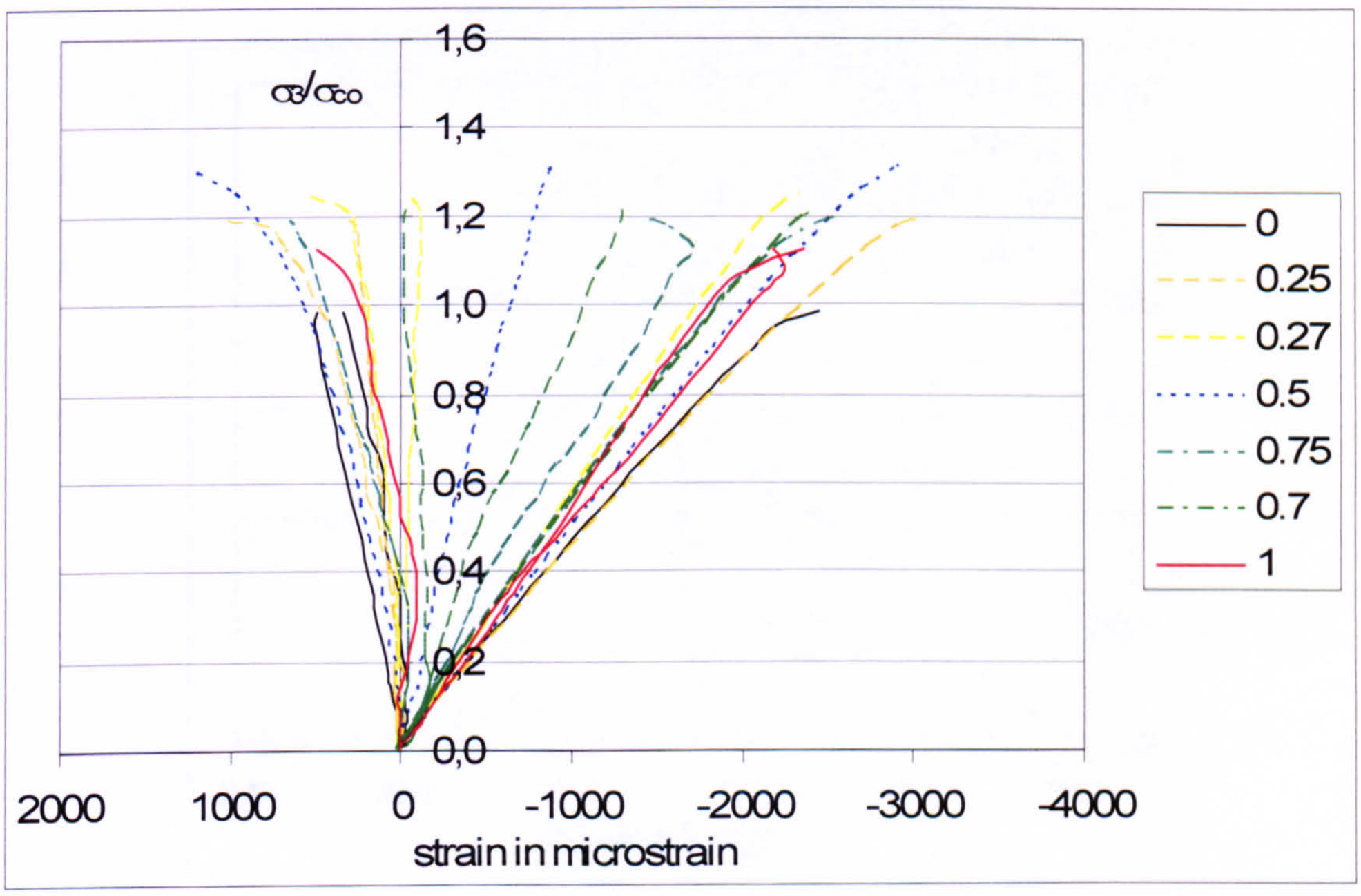

Figure 0.38 Stress-strain relationship for different stress ratios under biaxial compression recorded with LVDTs for V_f = 1 % of the fibre type 65-35 tested with brush platen system (batch 01)

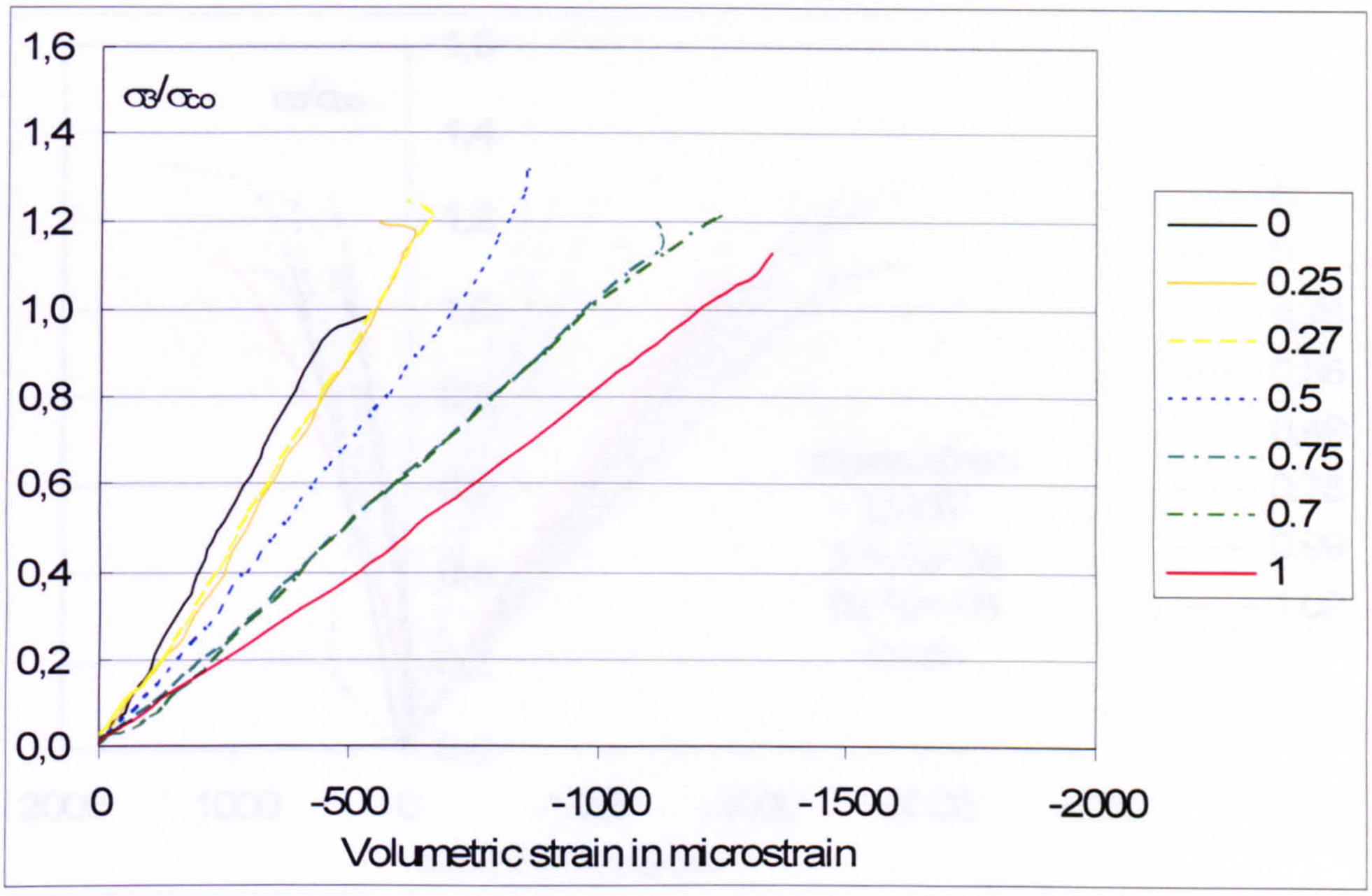

Figure 0.39 Volumetric strains for different stress ratios under biaxial compression recorded with LVDTs in three directions for V_f = 1 % of the fibre type 65-35 tested with brush platen system (batch 01)

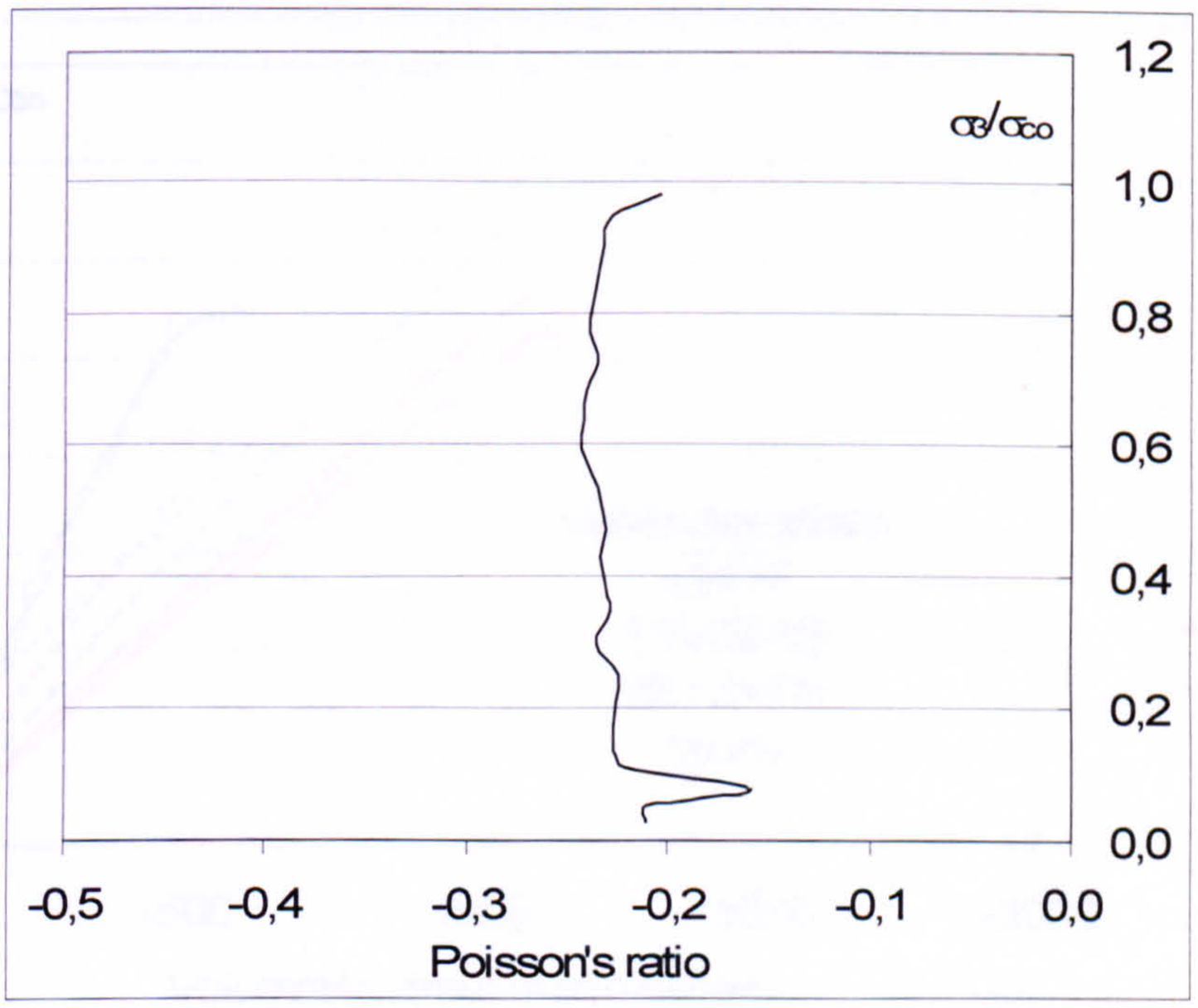

Figure 0.40 Poisson's ratio versus stress in uniaxial compression recorded with LVDTs in the two in plane directions for V_f = 1 % of the fibre type 65-35 tested with brush platen system (batch 01)

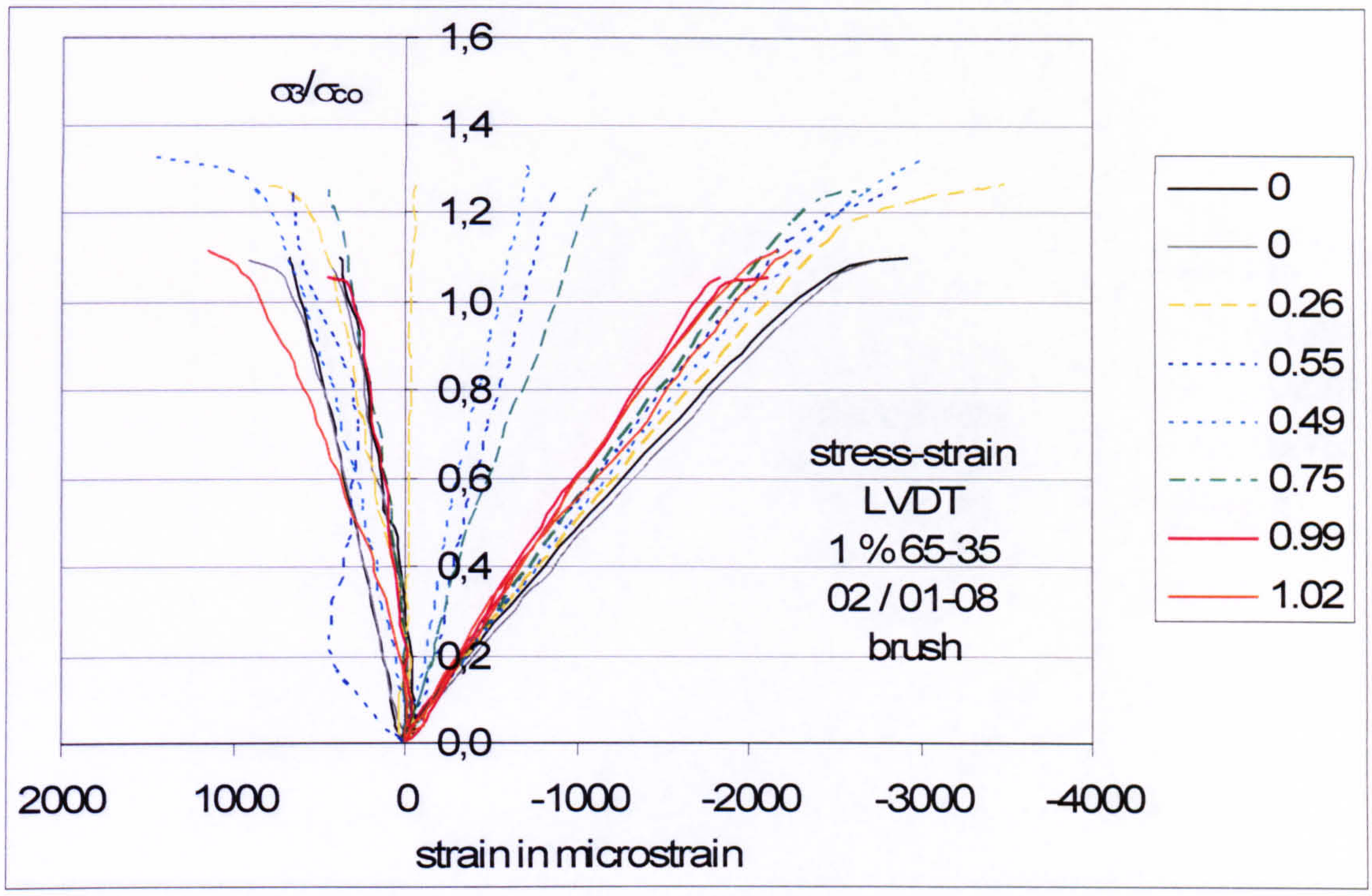

Figure 0.41 Stress-strain relationship for different stress ratios under biaxial compression recorded with LVDTs for V_f = 1 % of the fibre type 65-35 tested with brush platen system (batch 02)

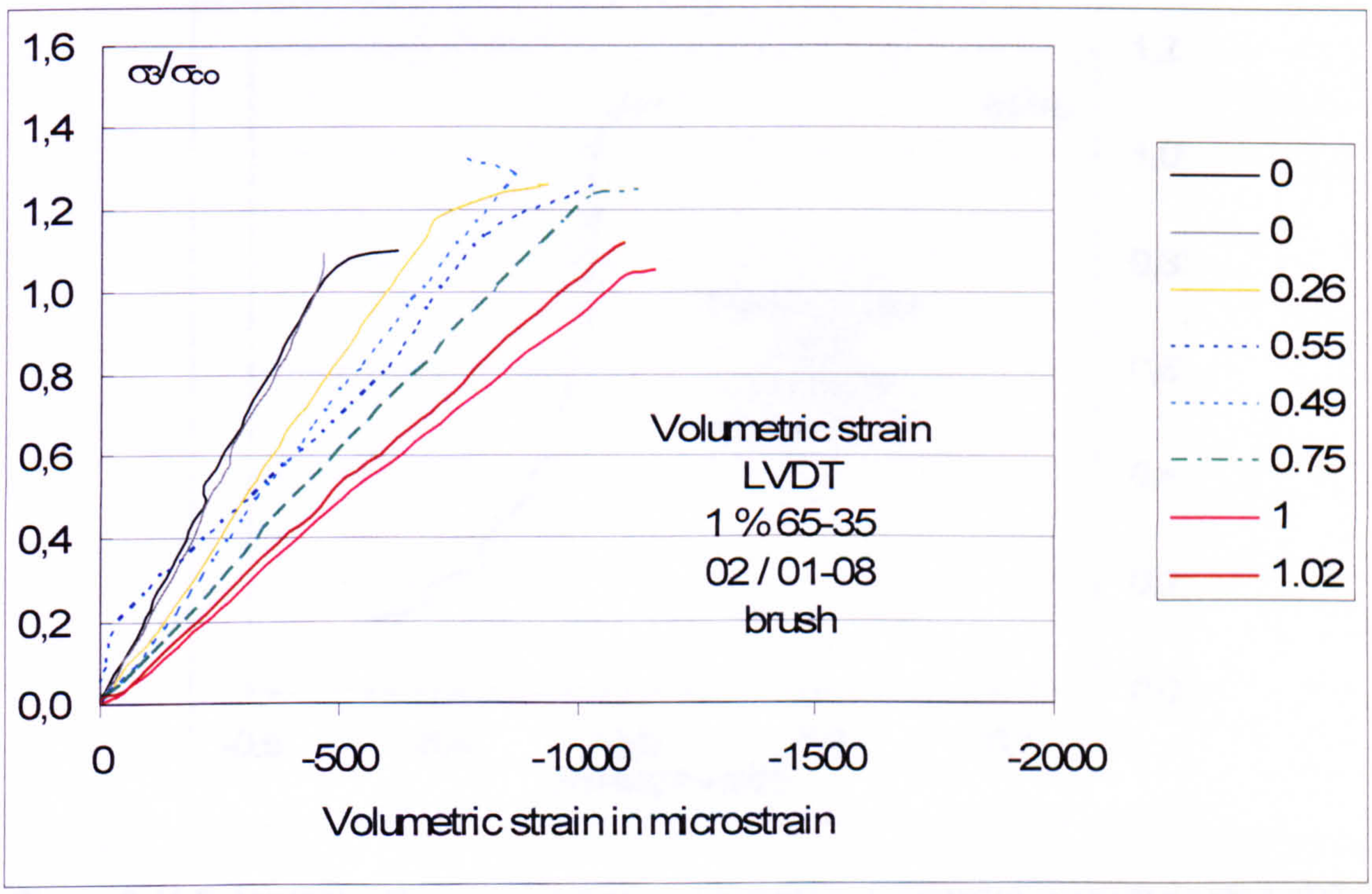

Figure 0.42 Volumetric strains for different stress ratios under biaxial compression recorded with LVDTs in three directions for V_f = 1 % of the fibre type 65-35 tested with brush platen system (batch 02)

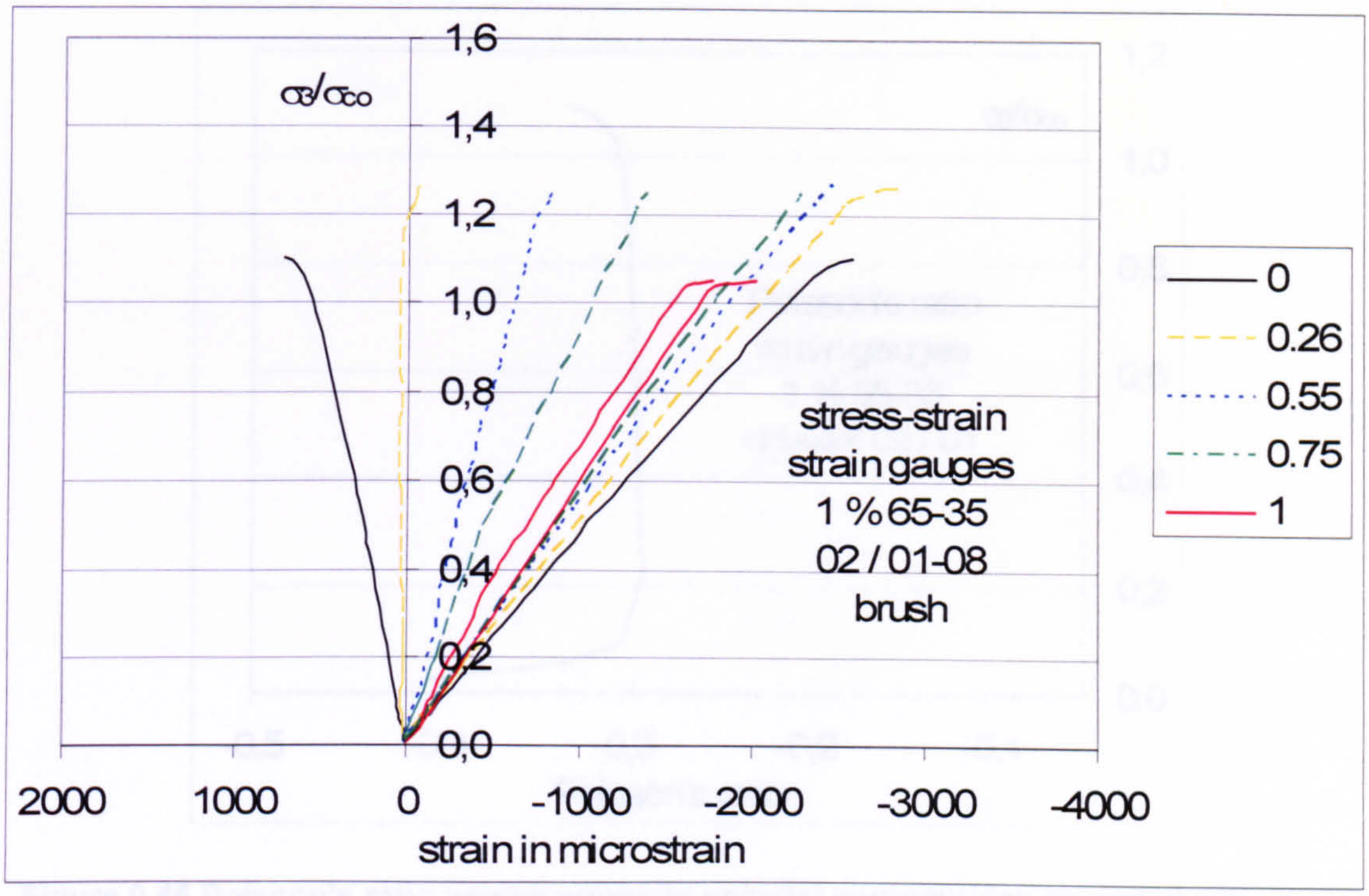

Figure 0.43 Stress-strain relationship for different stress ratios under biaxial compression recorded with strain gauges for V_f = 1 % of the fibre type 65-35 tested with brush platen system (batch 02)

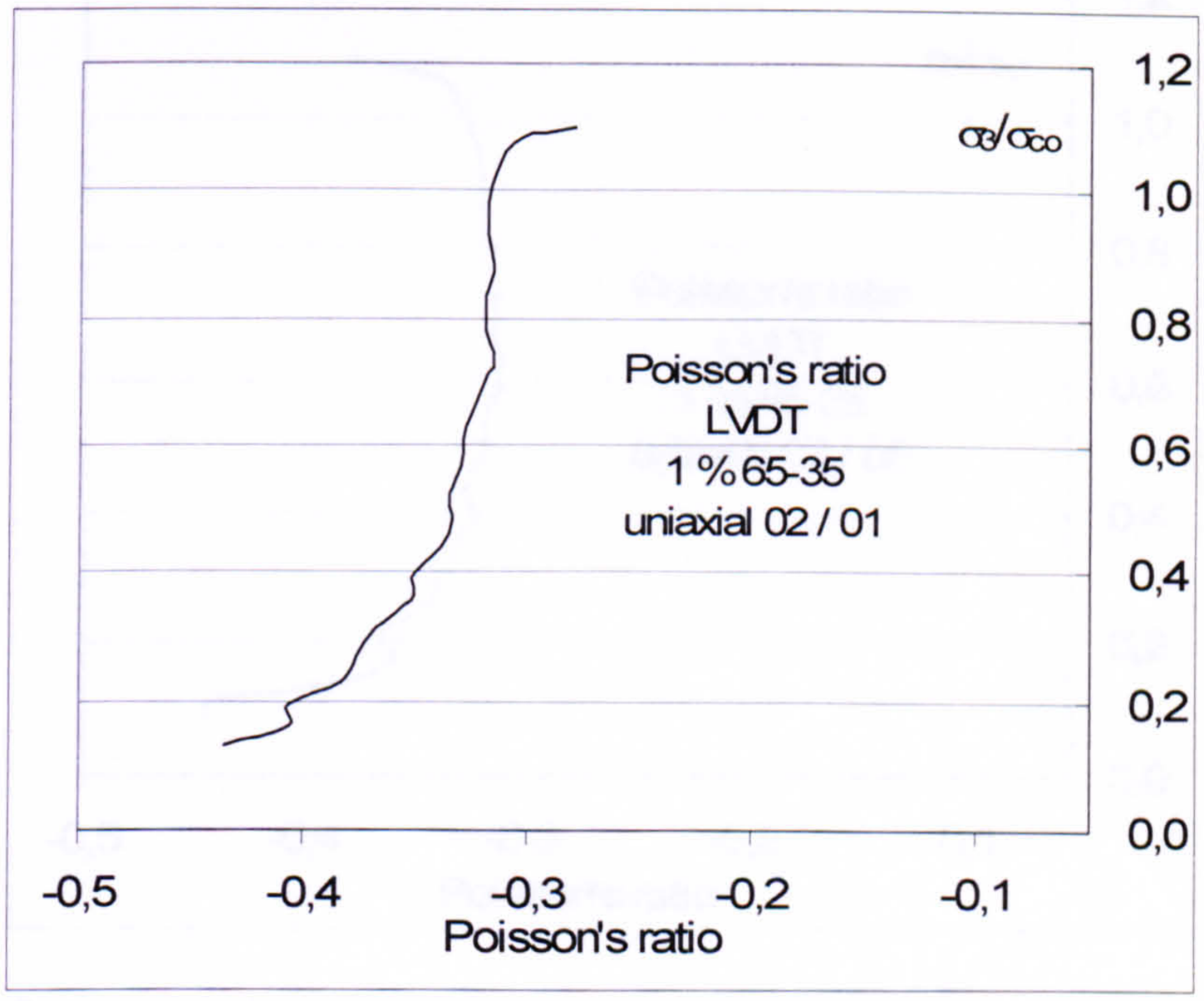

Figure 0.44 Poisson's ratio versus stress in uniaxial compression recorded with LVDTs in the two in plane directions for V_f = 1 % of the fibre type 65-35 tested with brush platen system (batch 02, specimen 01)

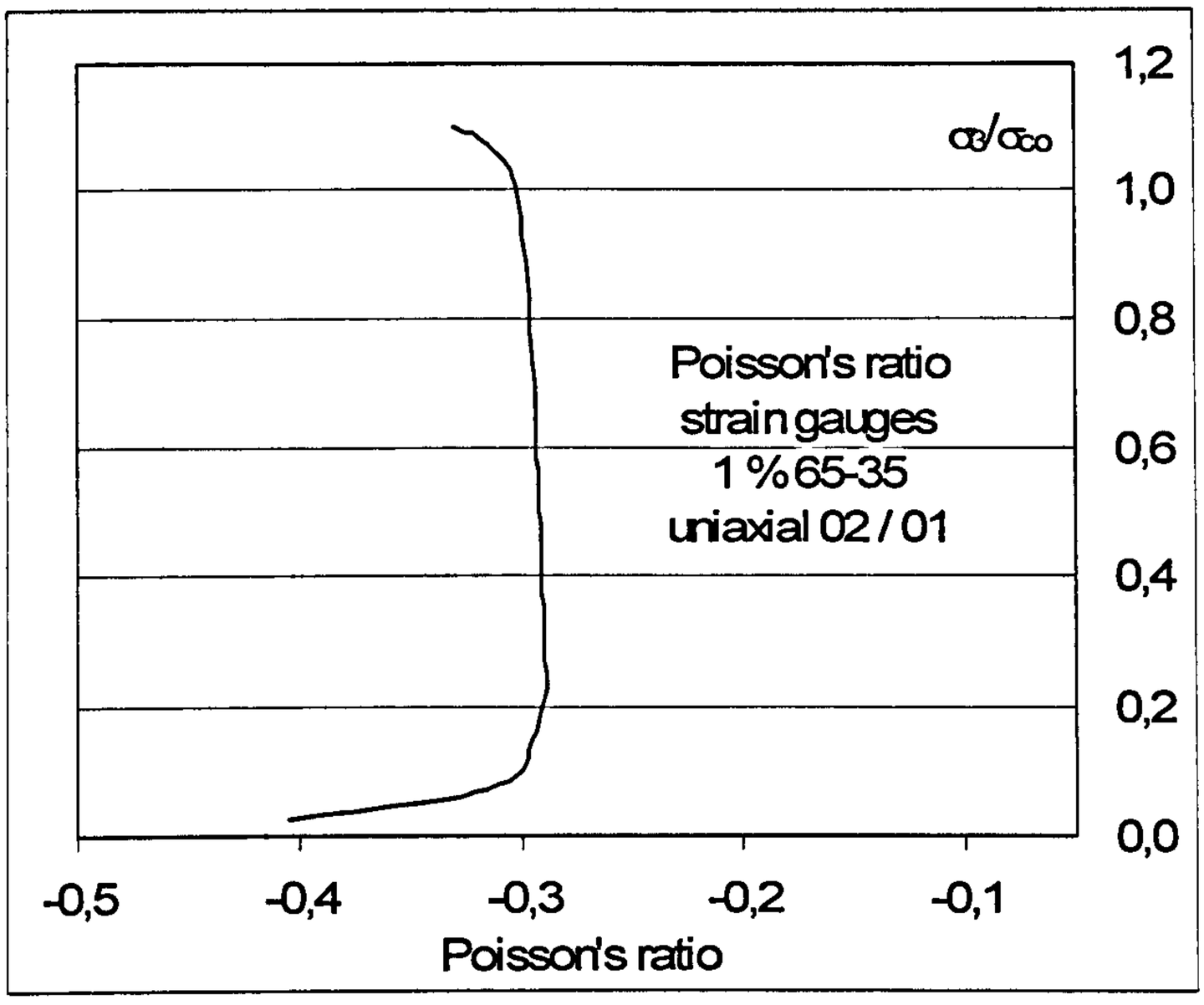

Figure 0.45 Poisson's ratio versus stress in uniaxial compression recorded with strain gauges in the two in plane directions for V_f = 1 % of the fibre type 65-35 tested with brush platen system (batch 02, specimen 01)

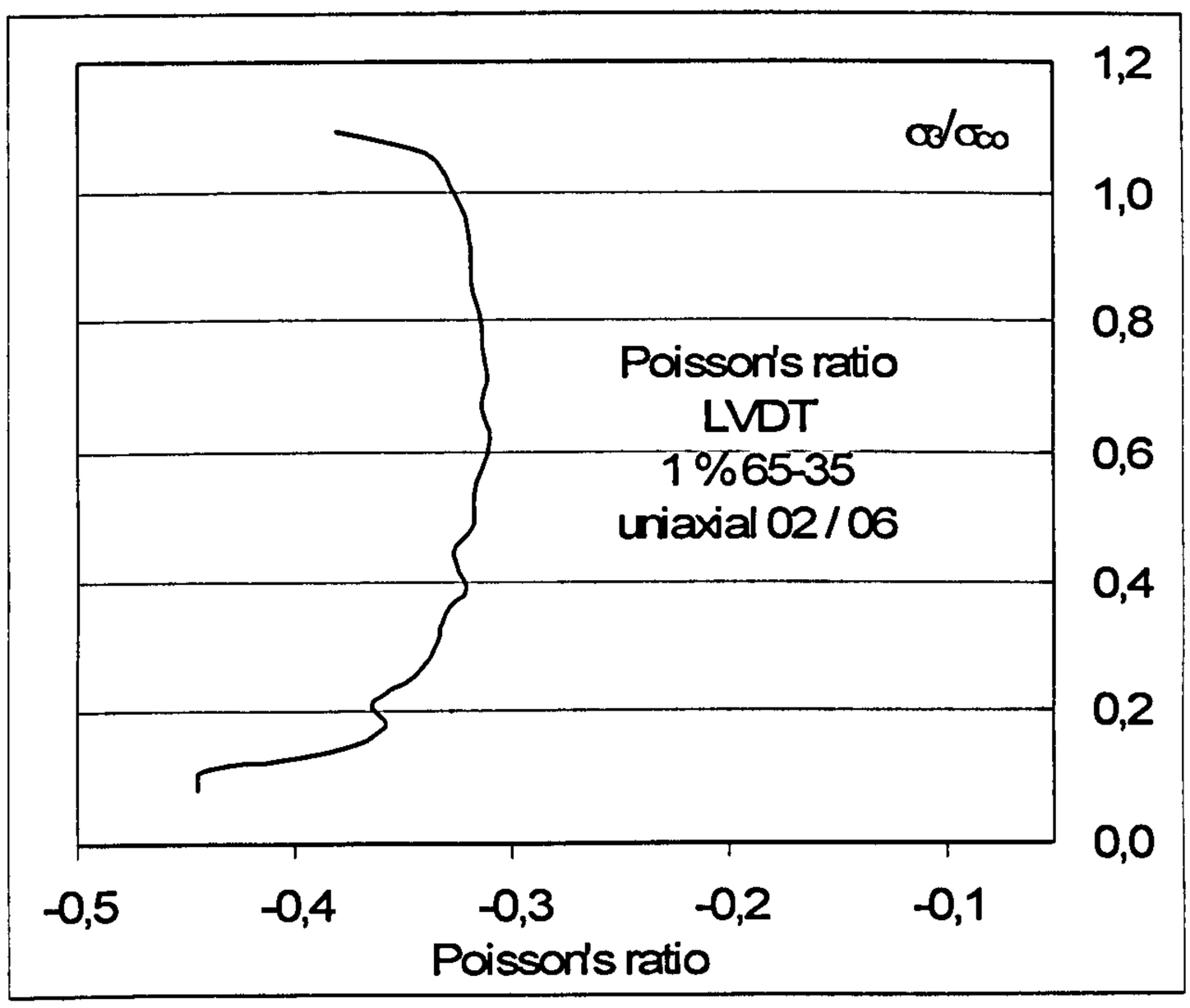

Figure 0.46 Poisson's ratio versus stress in uniaxial compression recorded with LVDTs in the two in plane directions for V_f = 1 % of the fibre type 65-35 tested with brush platen system (batch 02, specimen 06)

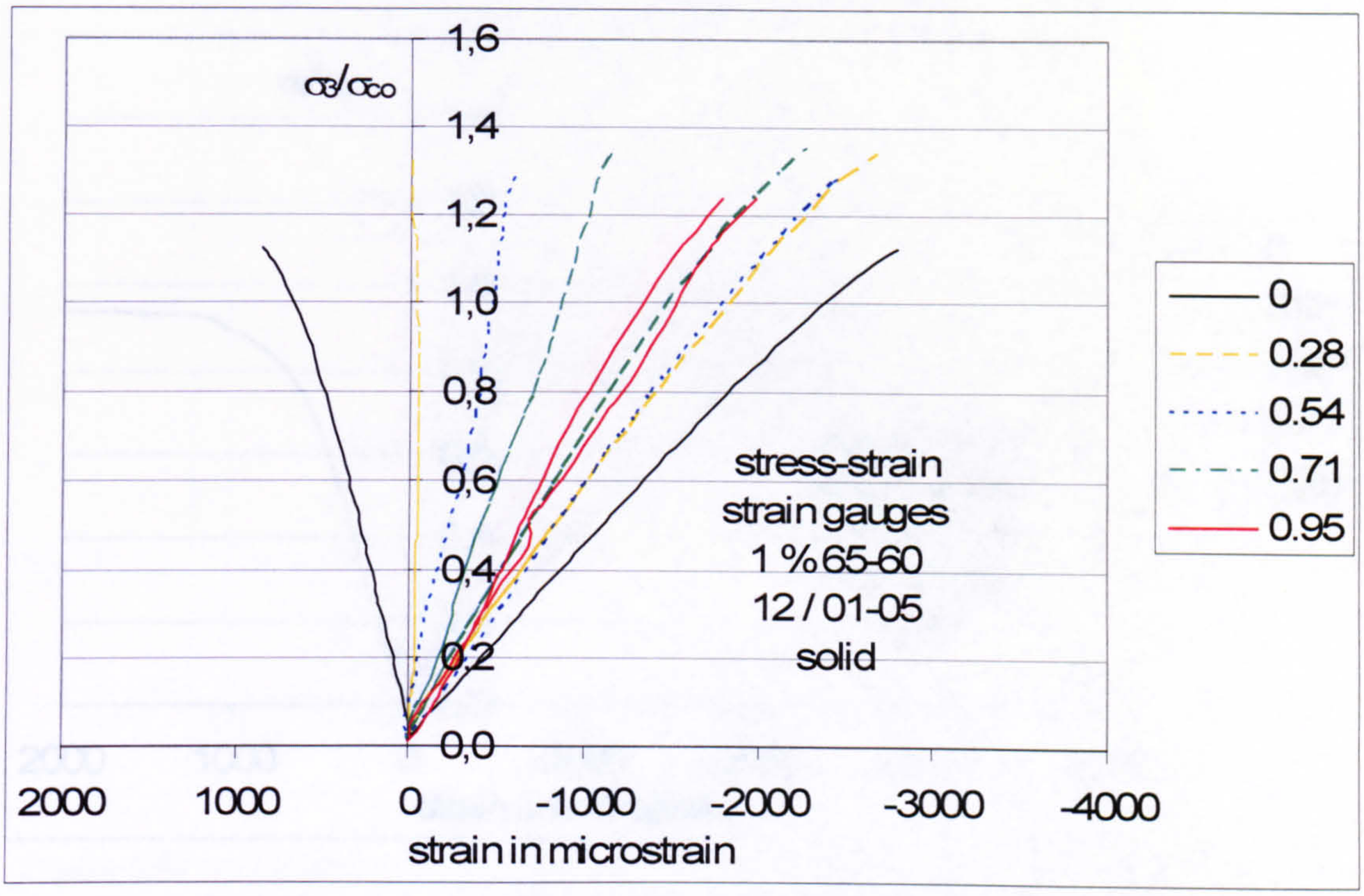

Figure 0.47 Stress-strain relationship for different stress ratios under biaxial compression recorded with strain gauges for V_f = 1 % of the fibre type 65-60 tested with solid steel blocks (batch 12)

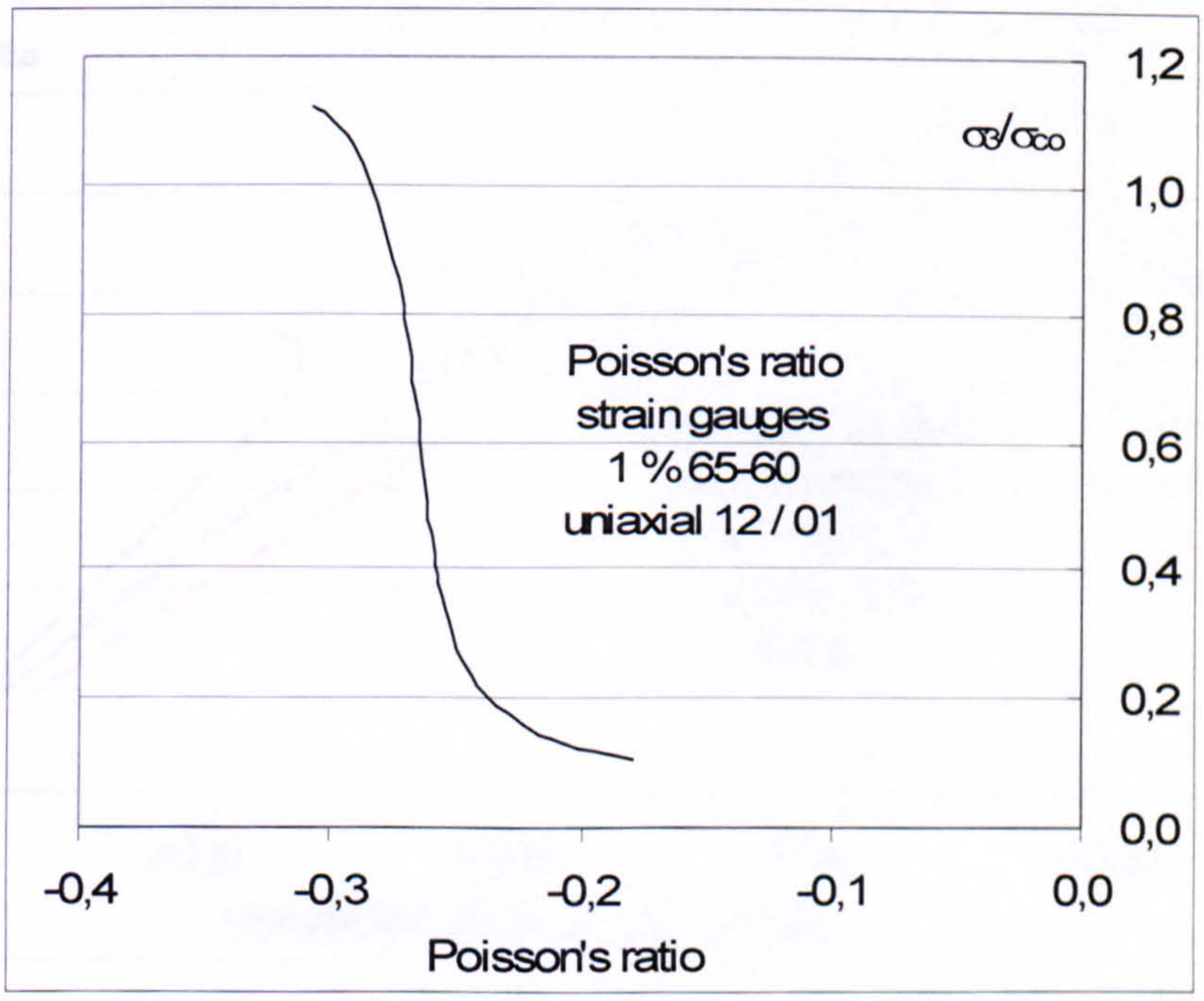

Figure 0.48 Poisson's ratio versus stress in uniaxial compression recorded with strain gauges in the two in plane directions for V_f = 1 % of the fibre type 65-60 tested with solid steel blocks (batch 12)

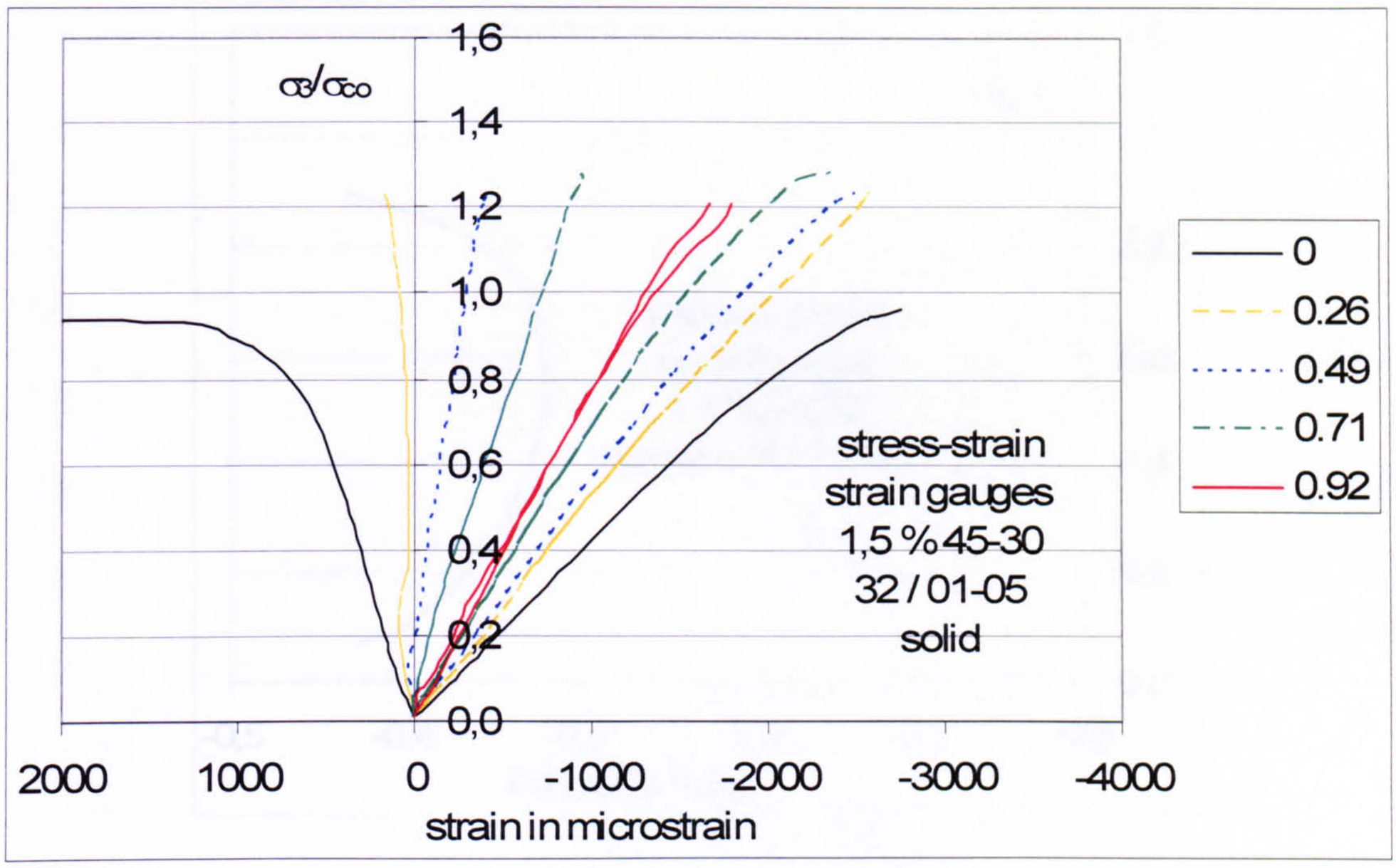

Figure 0.49 Stress-strain relationship for different stress ratios under biaxial compression recorded with strain gauges for V_f = 1.5 % of the fibre type 45-35 tested with solid steel blocks (batch 32)

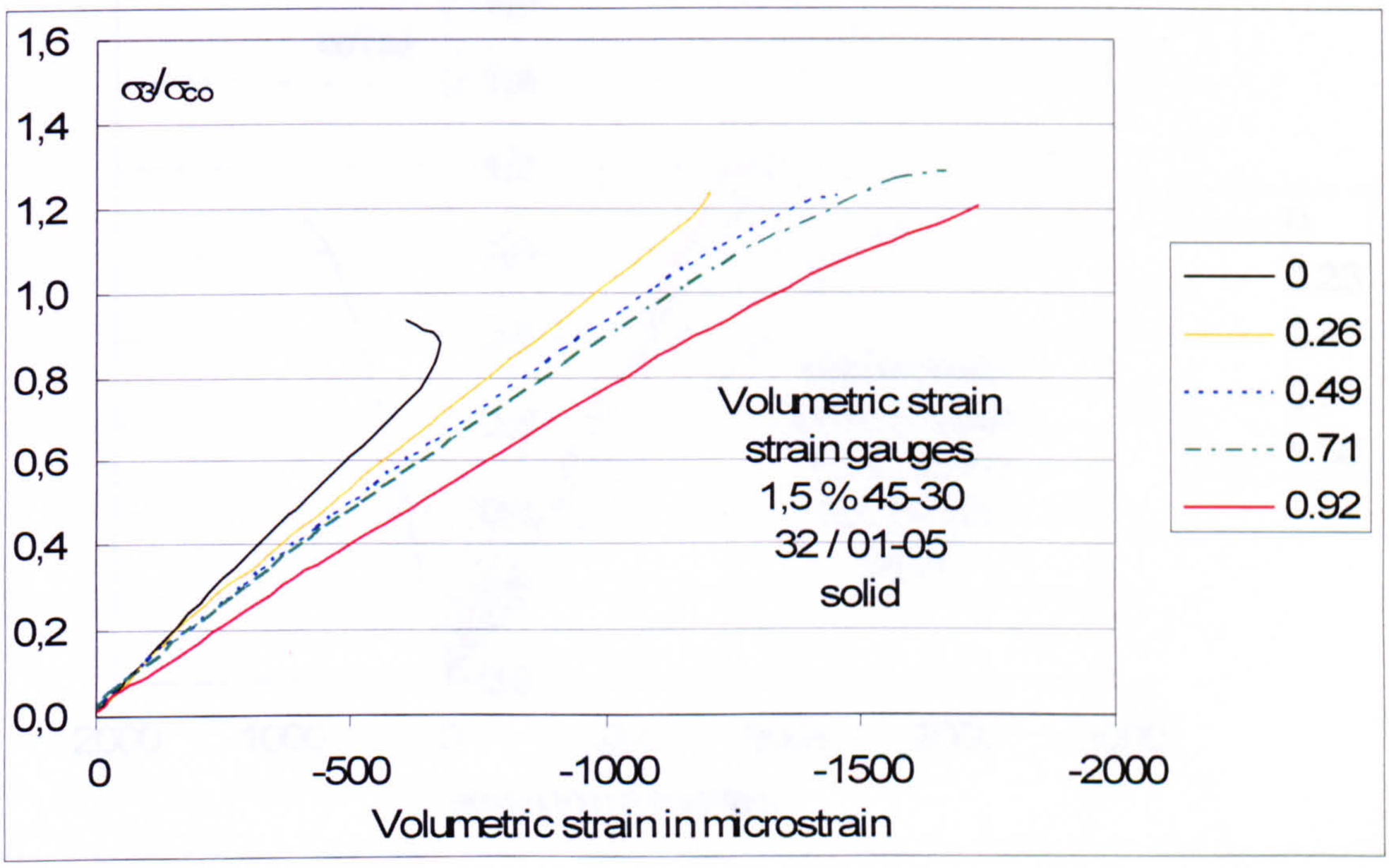

Figure 0.50 Volumetric strains for different stress ratios under biaxial compression recorded with strain gauges in the two in plane directions for V_f = 1.5 % of the fibre type 45-35 tested with solid steel blocks (batch 32)

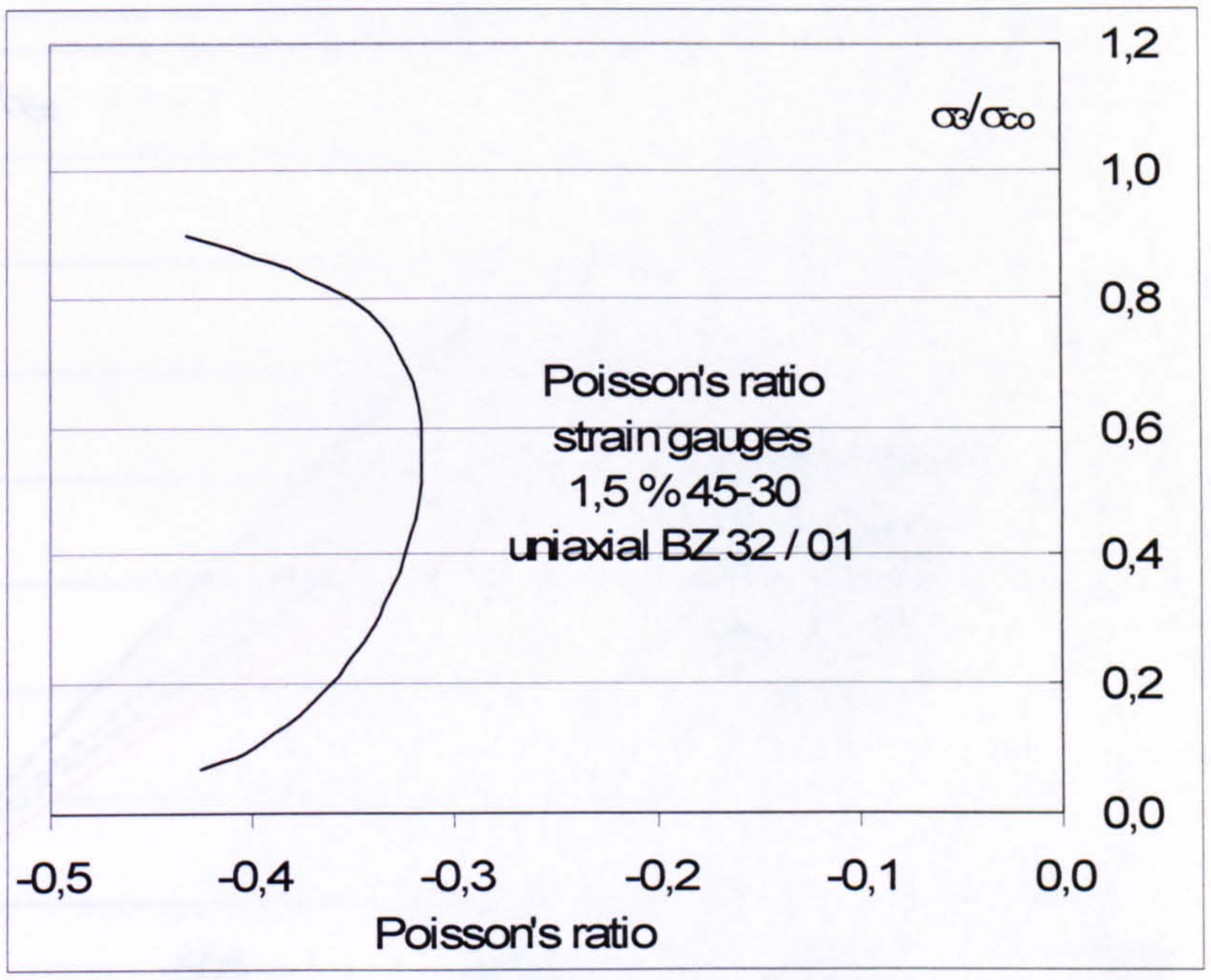

Figure 0.51 Poisson's ratio versus stress in uniaxial compression recorded with strain gauges in the two in plane directions for V_f = 1.5 % of the fibre type 45-35 tested with solid steel blocks (batch 32)

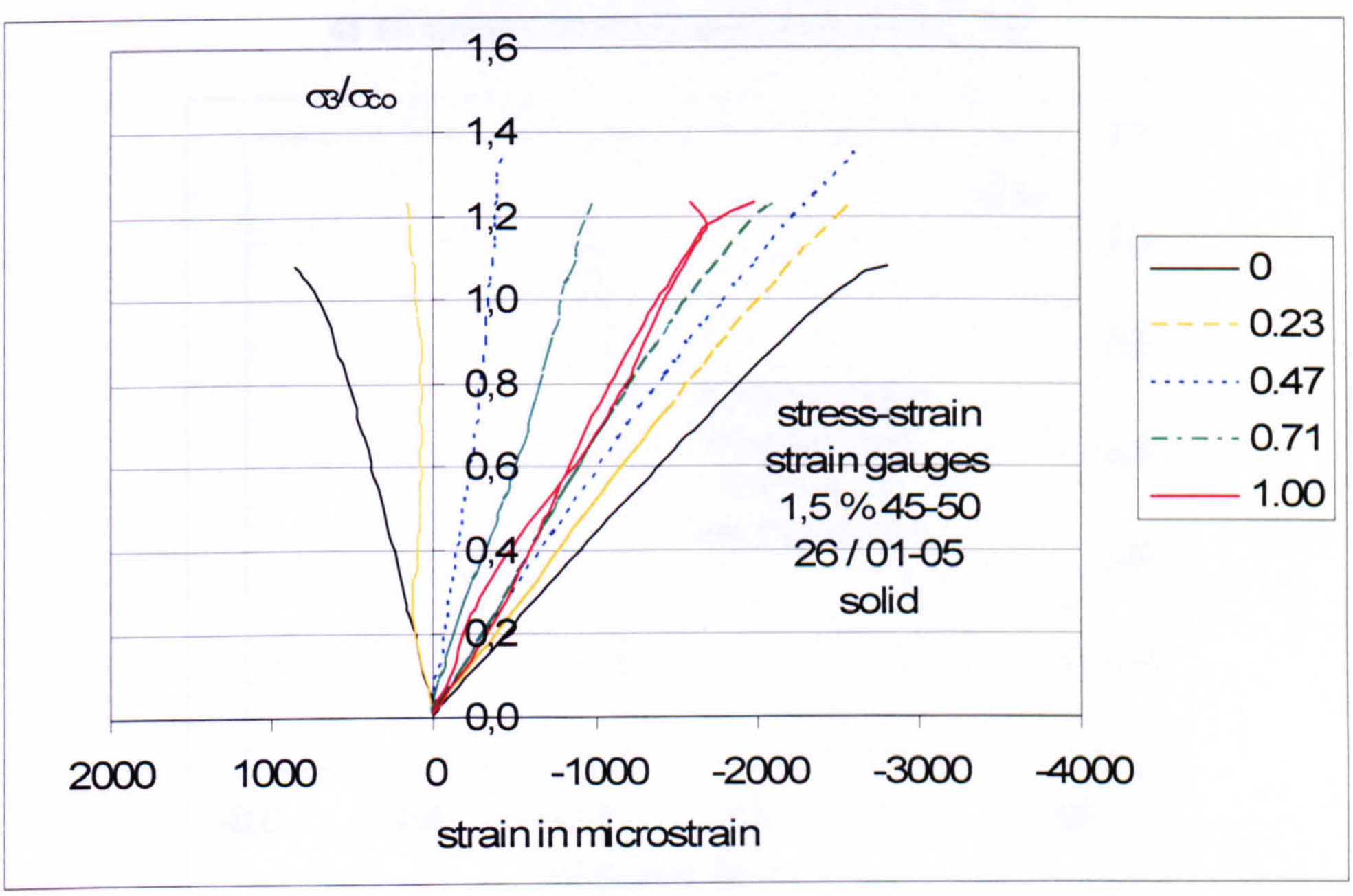

Figure 0.52 Stress-strain relationship for different stress ratios under biaxial compression recorded with strain gauges for V_f = 1.5 % of the fibre type 45-50 tested with solid steel blocks (batch 26)

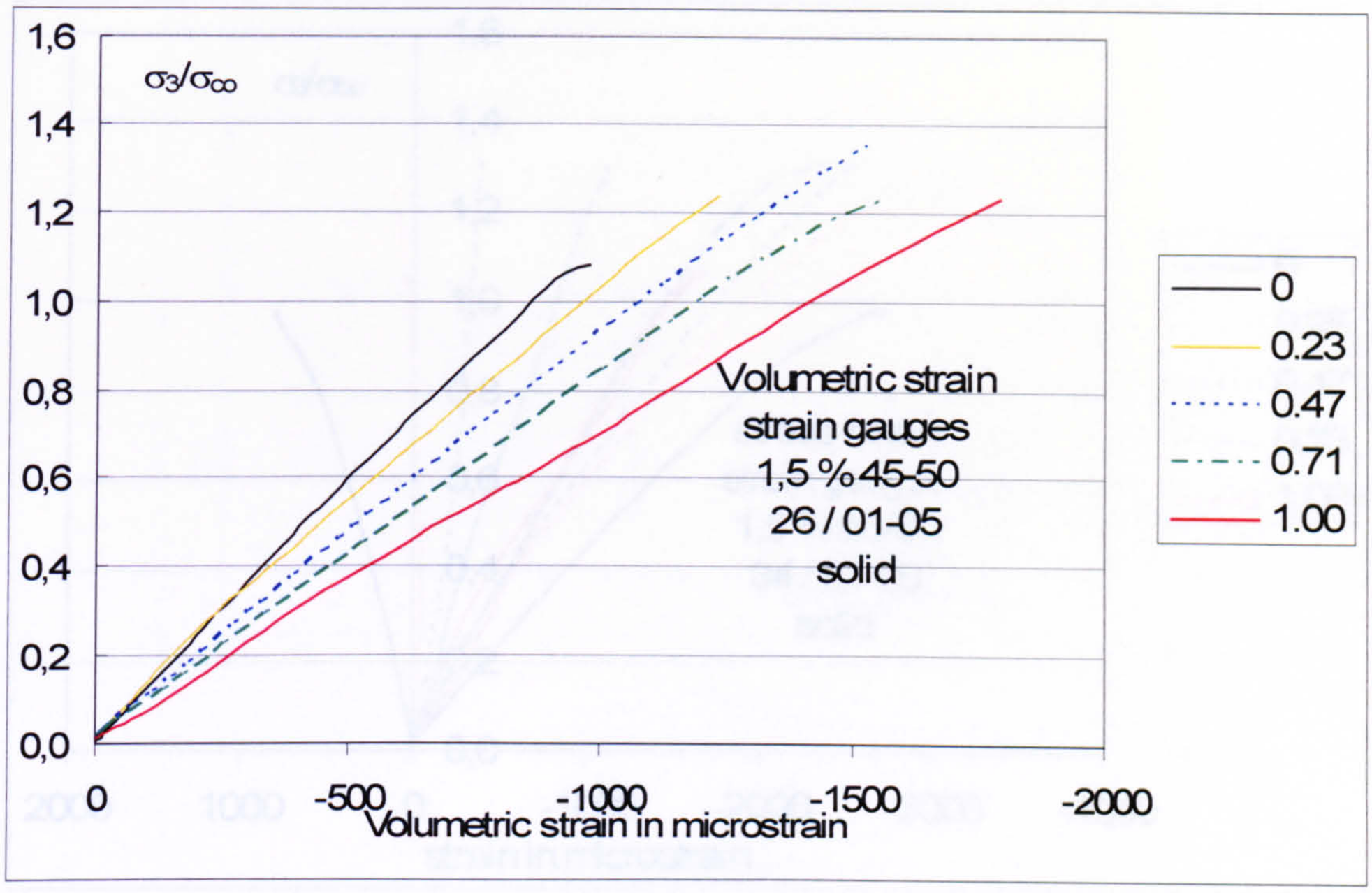

Figure 0.53 Volumetric strains for different stress ratios under biaxial compression recorded with strain gauges in the two in plane directions for V_f = 1.5 % of the fibre type 45-50 tested with solid steel blocks (batch 26)

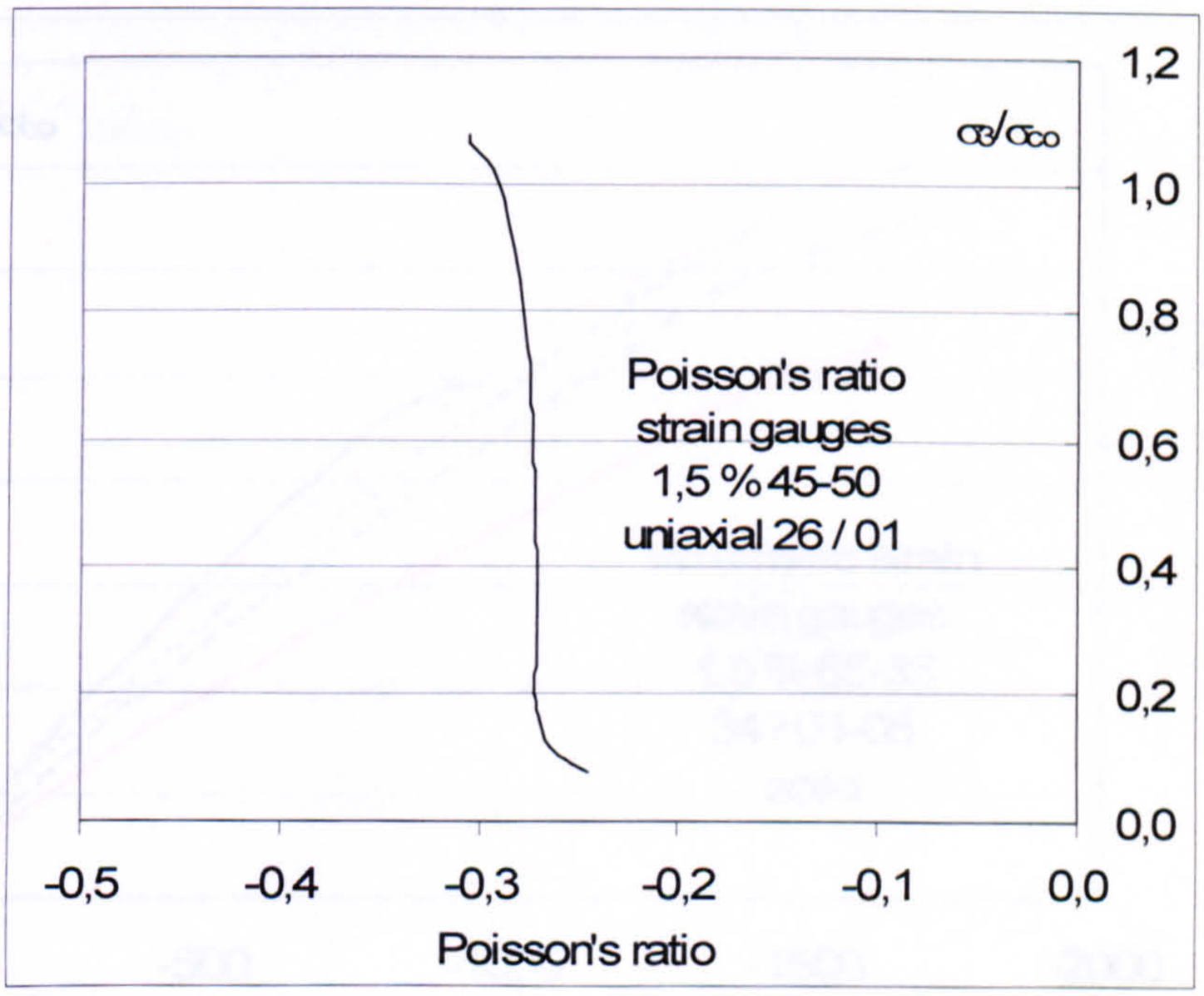

Figure 0.54 Poisson's ratio versus stress in uniaxial compression recorded with strain gauges in the two in plane directions for V_f = 1.5 % of the fibre type 45-50 tested with solid steel blocks (batch 26)

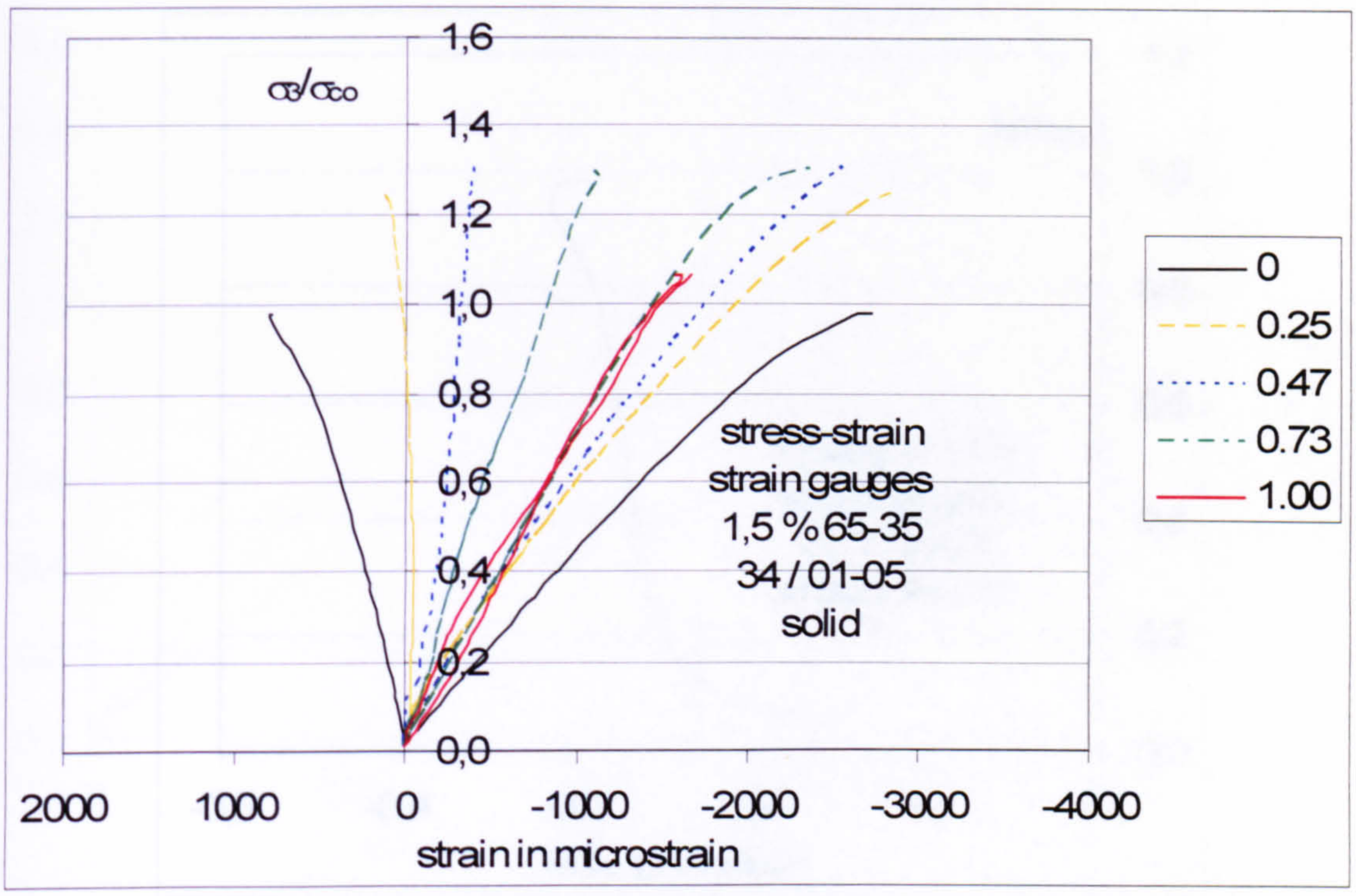

Figure 0.55 Stress-strain relationship for different stress ratios under biaxial compression recorded with strain gauges for V_f = 1.5 % of the fibre type 65-35 tested with solid steel blocks (batch 34)

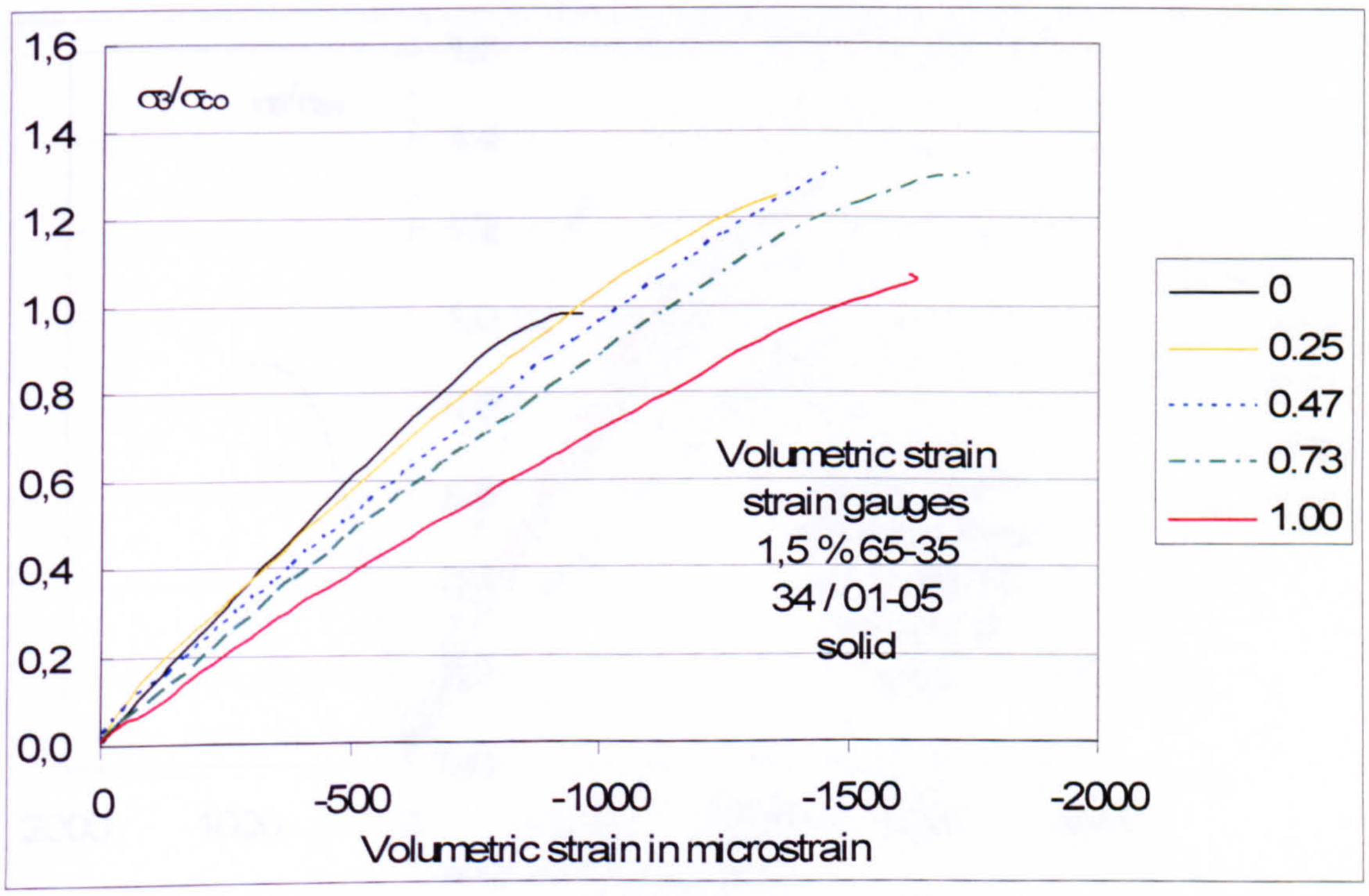

Figure 0.56 Volumetric strains for different stress ratios under biaxial compression recorded with strain gauges in the two in plane directions for V_f = 1.5 % of the fibre type 65-35 tested with solid steel blocks (batch 34)

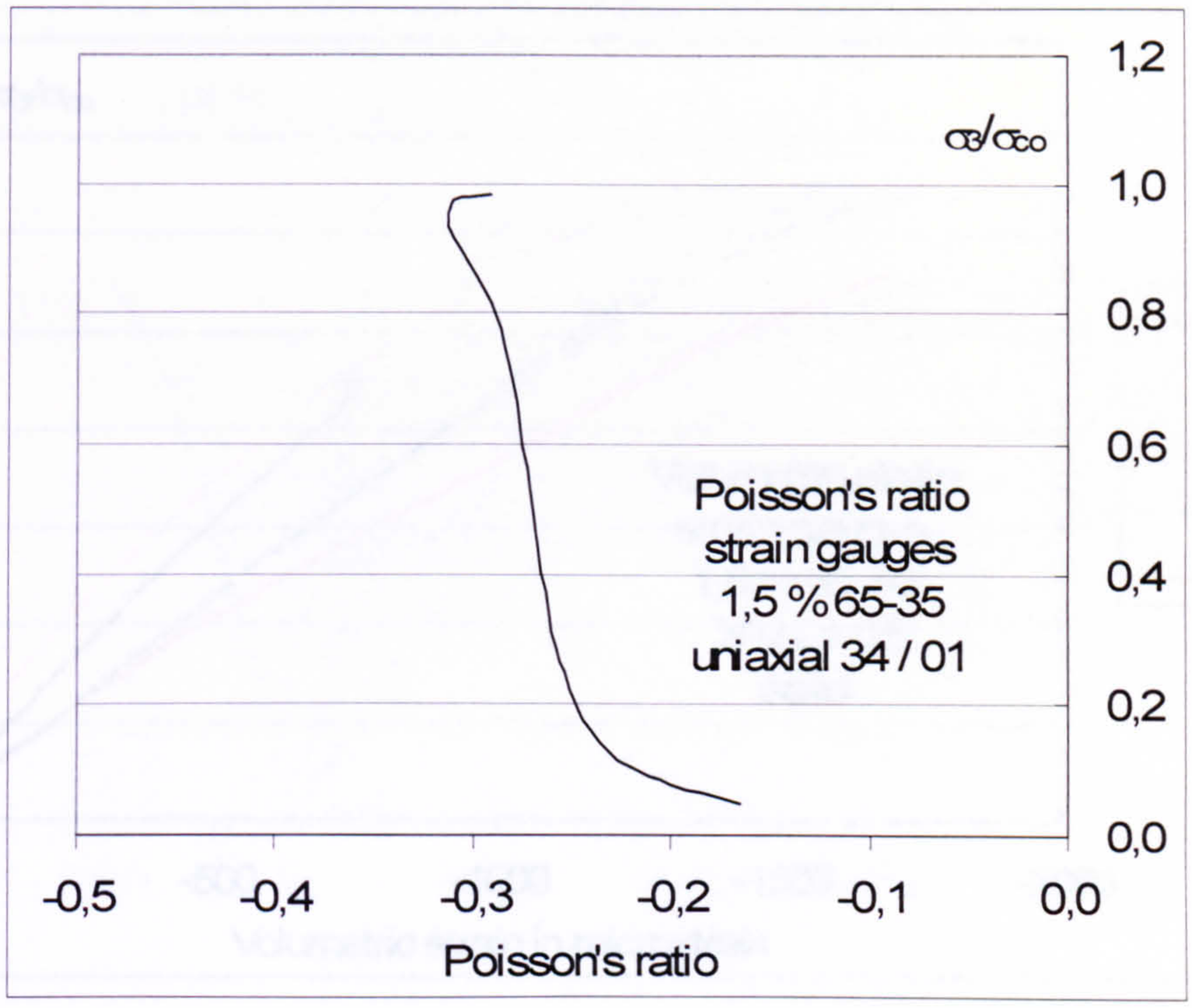

Figure 0.57 Poisson's ratio versus stress in uniaxial compression recorded with strain gauges in the two in plane directions for V_f = 1.5 % of the fibre type 65-35 tested with solid steel blocks (batch 34)

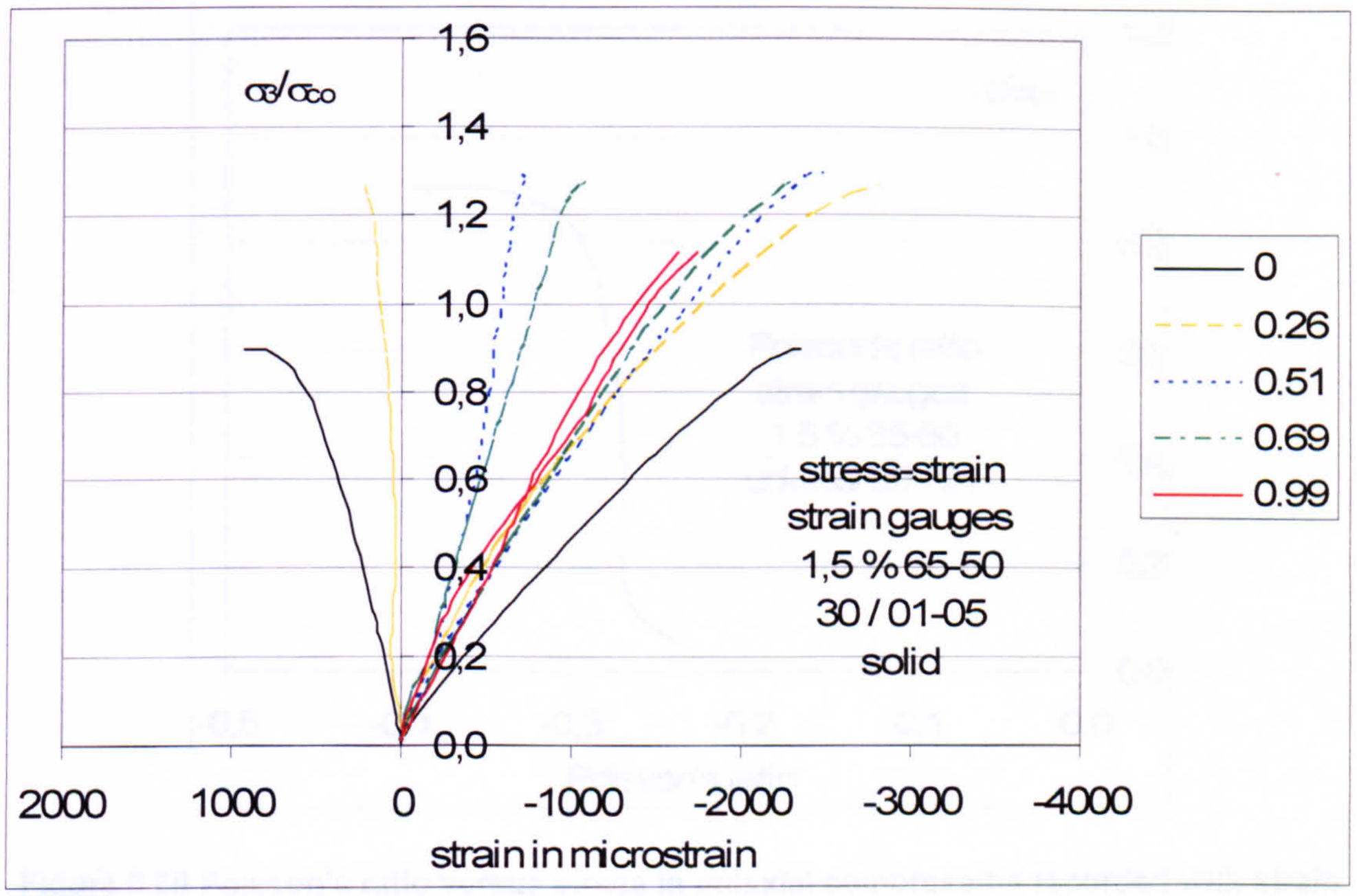

Figure 0.58 Stress-strain relationship for different stress ratios under biaxial compression recorded with strain gauges for V_f = 1.5 % of the fibre type 65-60 tested with solid steel blocks (batch 30)

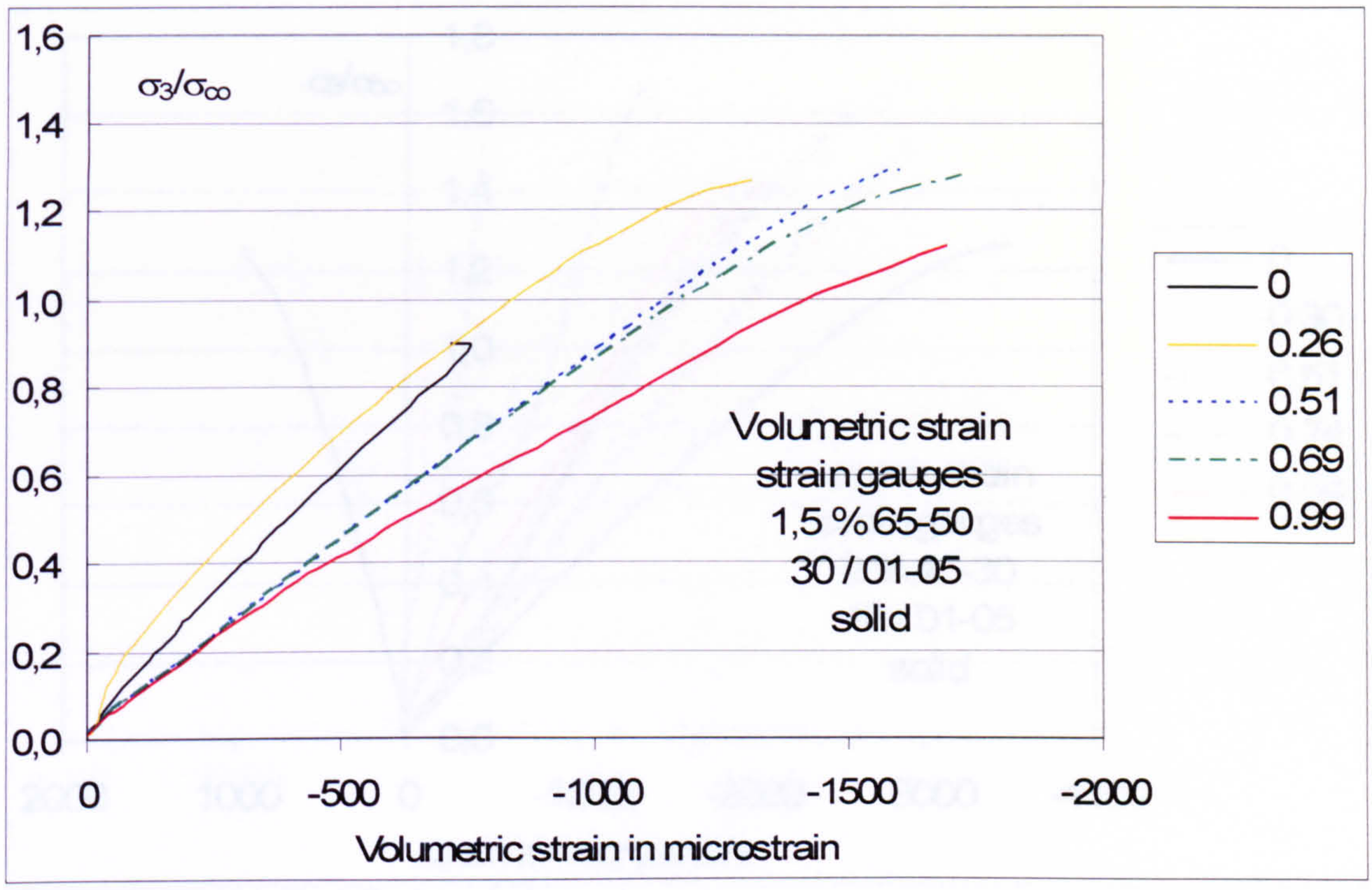

Figure 0.59 Volumetric strains for different stress ratios under biaxial compression recorded with strain gauges in the two in plane directions for V_f = 1.5 % of the fibre type 65-60 tested with solid steel blocks (batch 30)

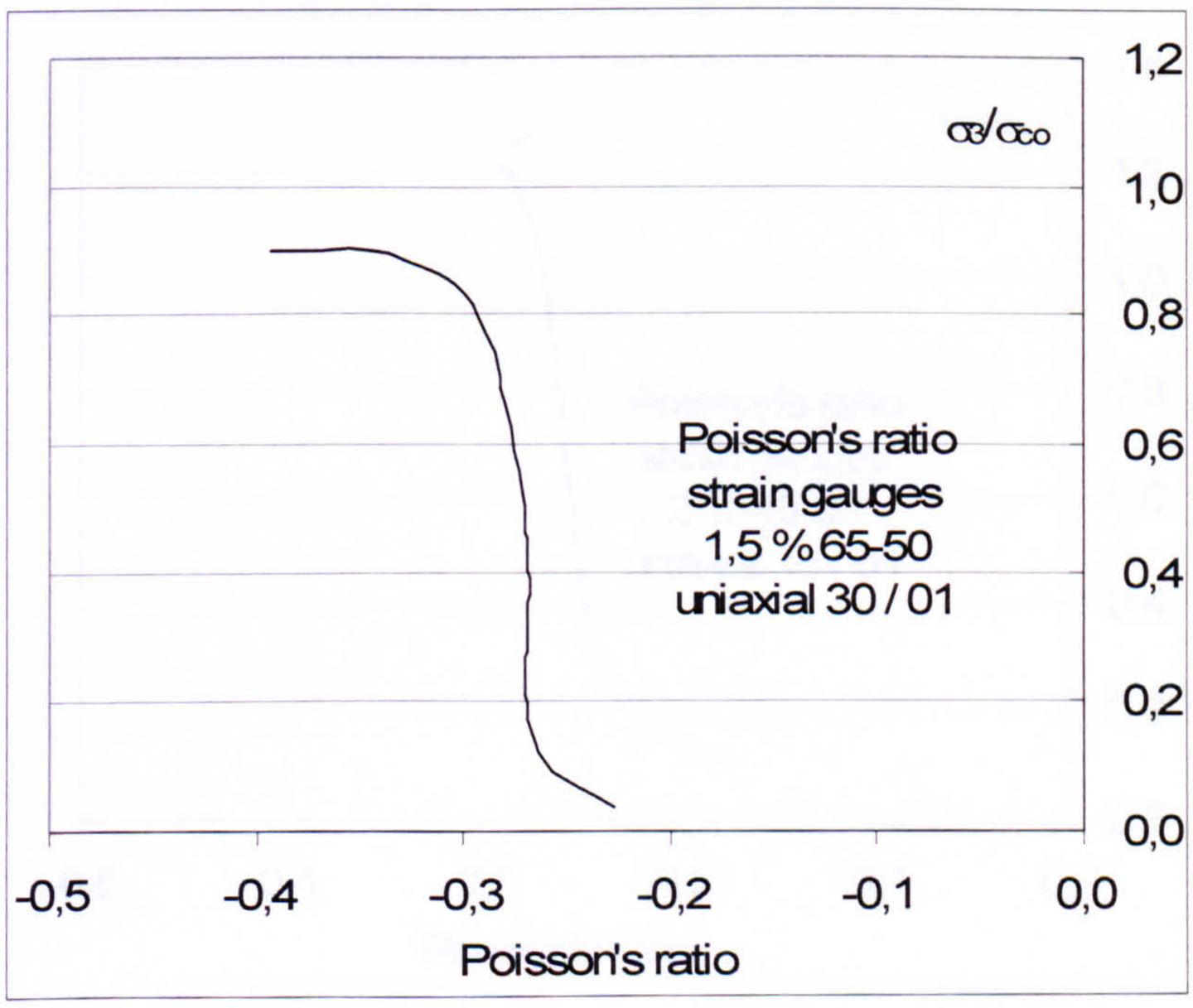

Figure 0.60 Poisson's ratio versus stress in uniaxial compression recorded with strain gauges in the two in plane directions for V_f = 1.5 % of the fibre type 65-60 tested with solid steel blocks (batch 30)

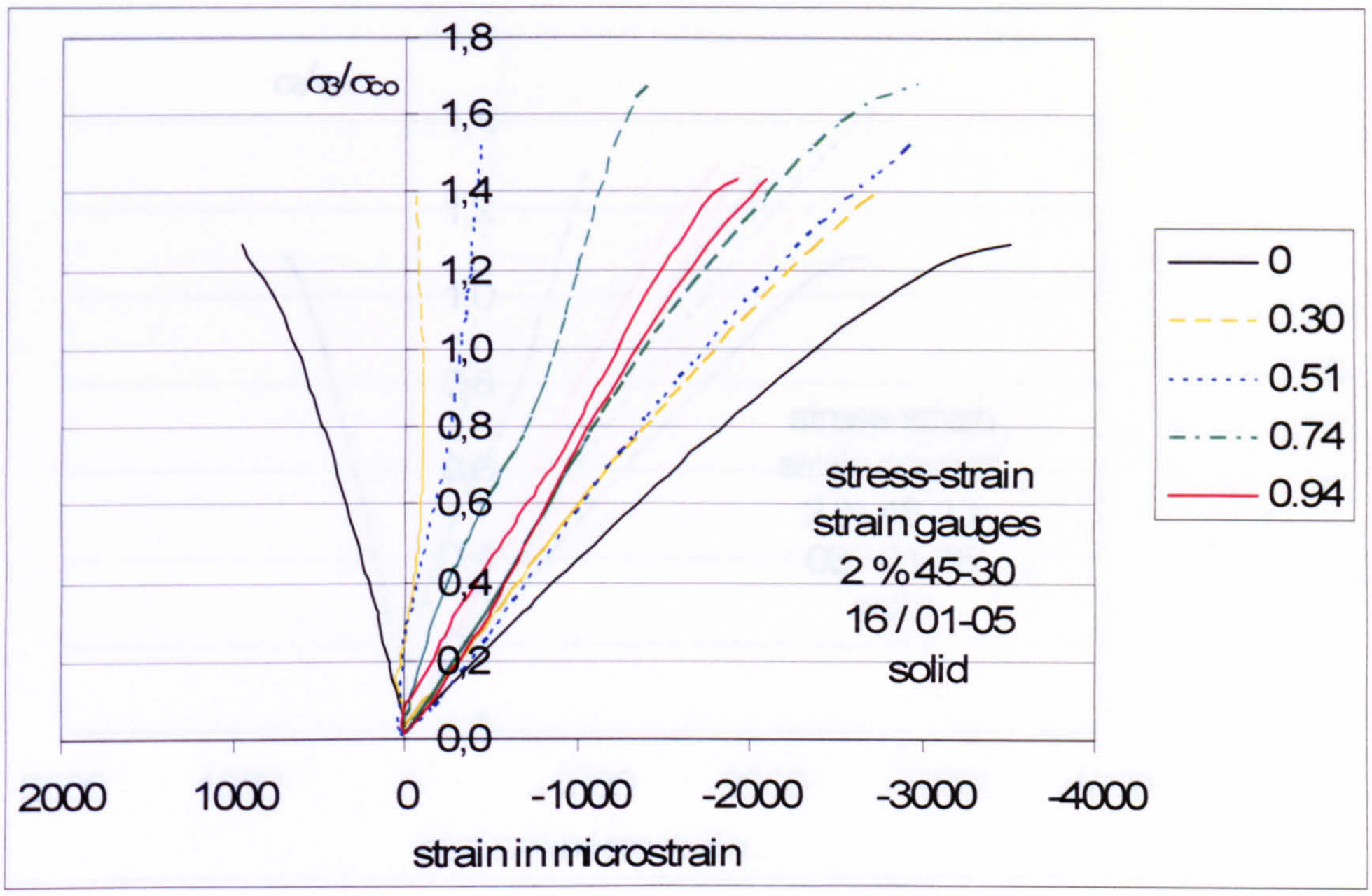

Figure 0.61 Stress-strain relationship for different stress ratios under biaxial compression recorded with strain gauges for V_f = 2 % of the fibre type 45-35 tested with solid steel blocks (batch 16)

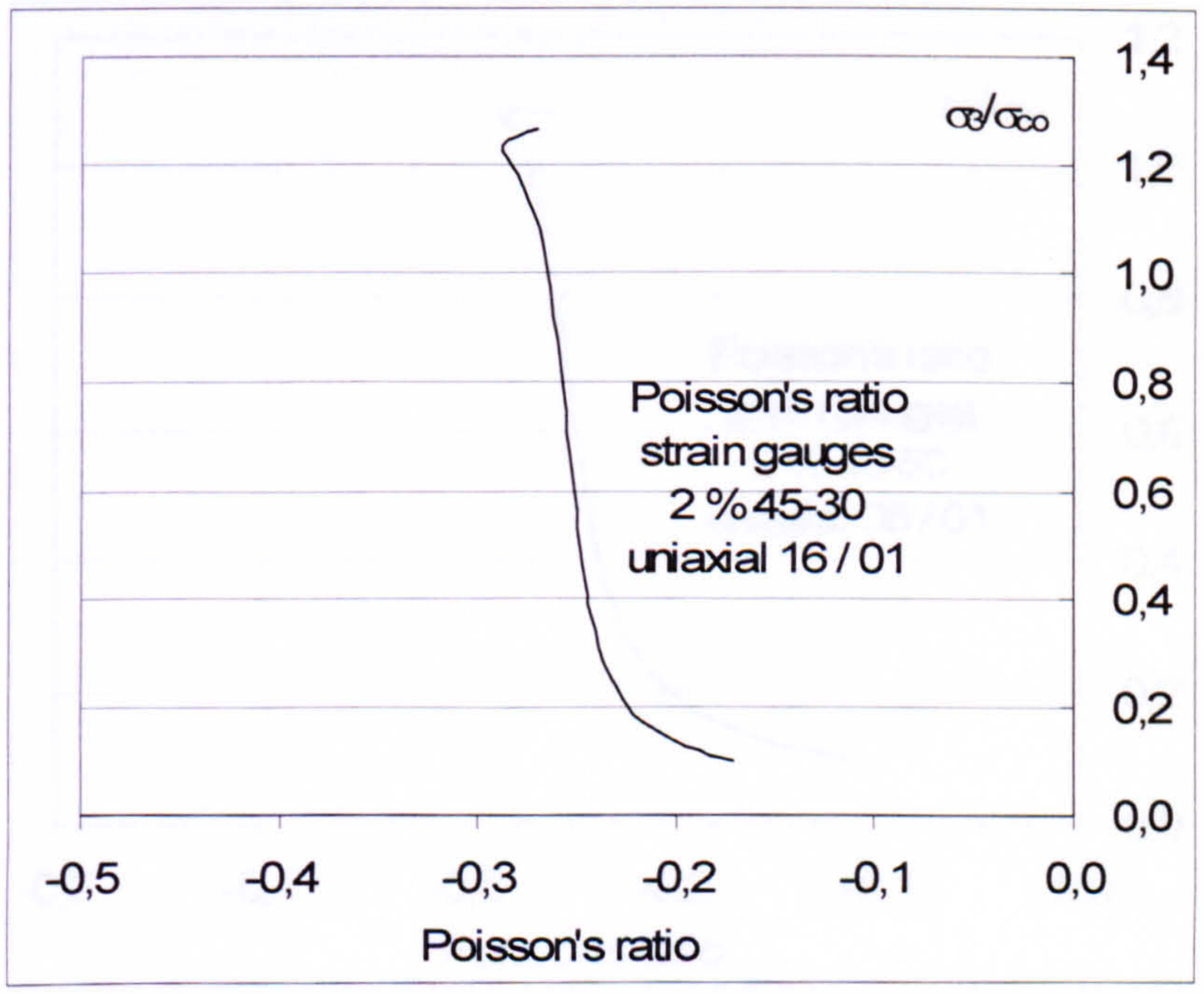

Figure 0.62 Poisson's ratio versus stress in uniaxial compression recorded with strain gauges in the two in plane directions for V_f = 2 % of the fibre type 45-35 tested with solid steel blocks (batch 16)

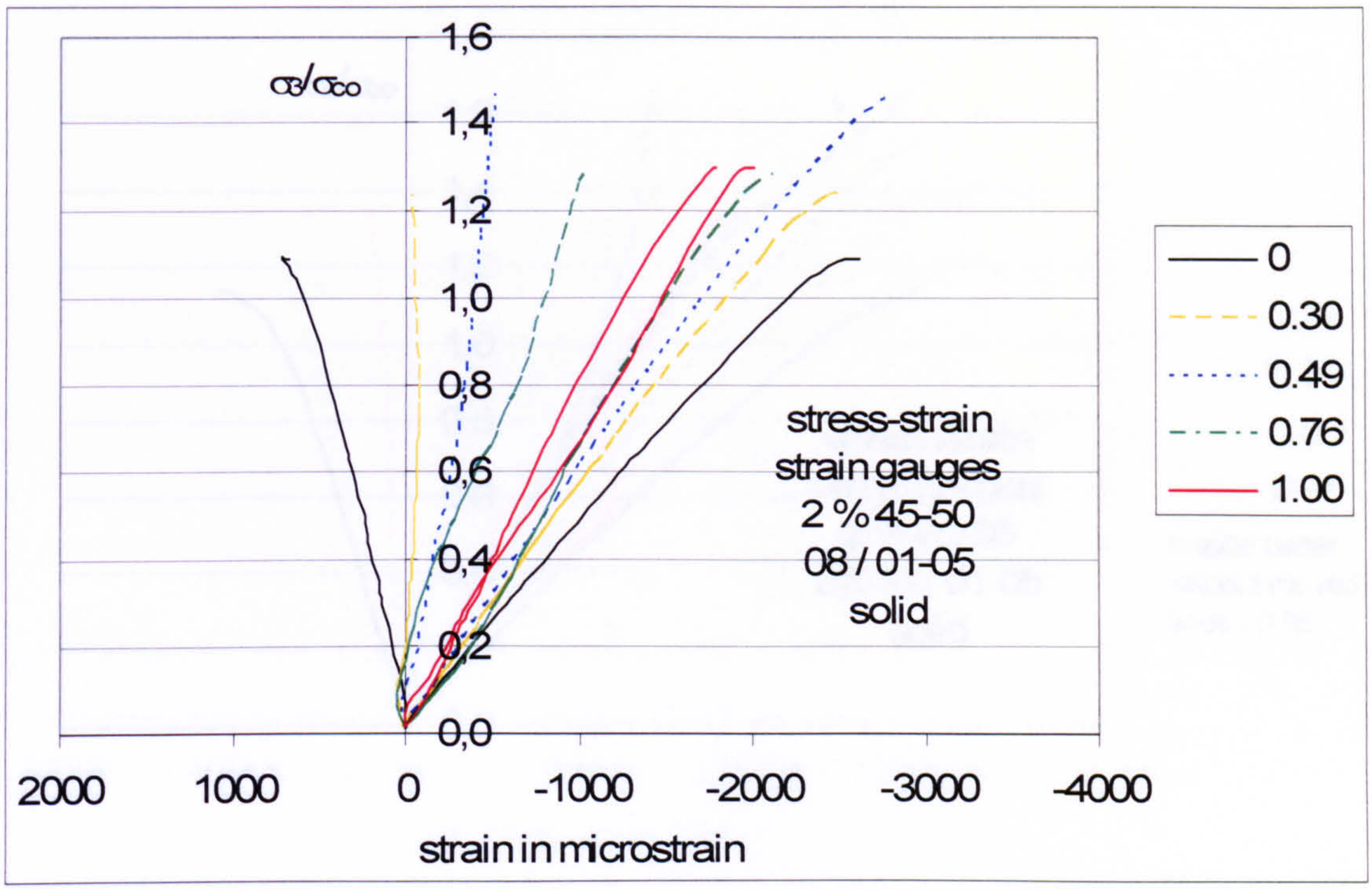

Figure 0.63 Stress-strain relationship for different stress ratios under biaxial compression recorded with strain gauges for V_f = 2 % of the fibre type 45-50 tested with solid steel blocks (batch 08)

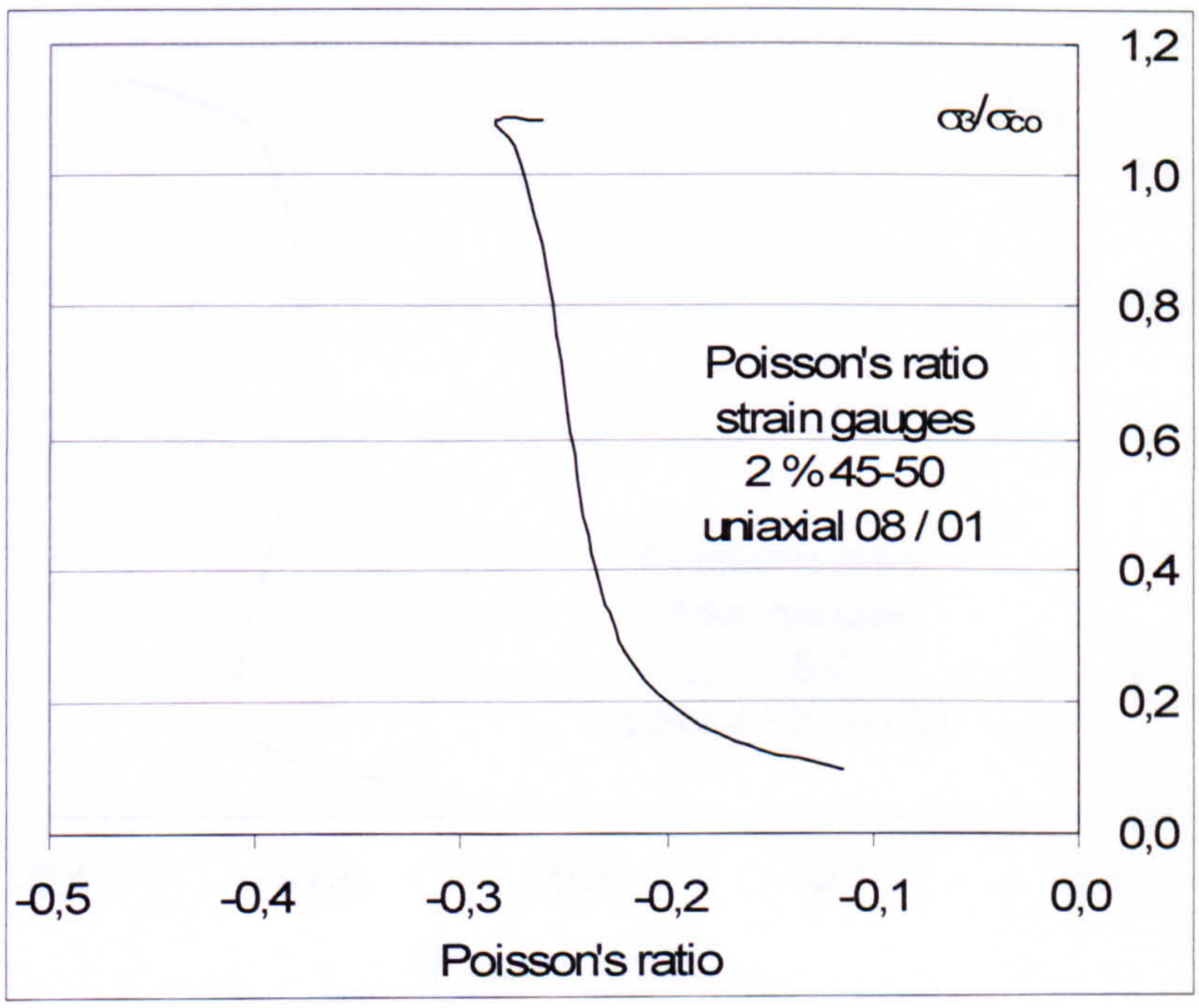

Figure 0.64 Poisson's ratio versus stress in uniaxial compression recorded with strain gauges in the two in plane directions for V_f = 2 % of the fibre type 45-50 tested with solid steel blocks (batch 08)

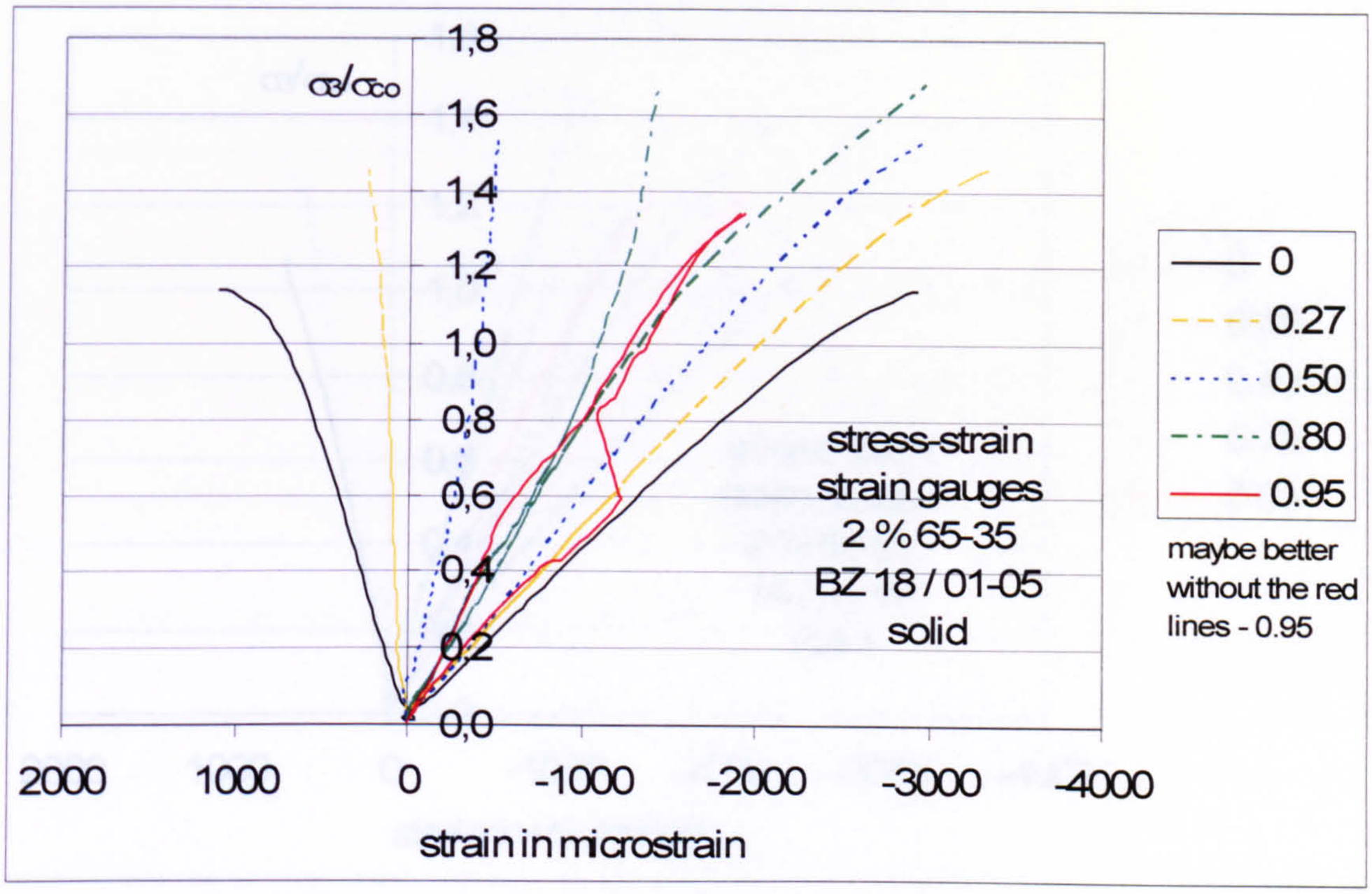

Figure 0.65 Stress-strain relationship for different stress ratios under biaxial compression recorded with strain gauges for V_f = 2 % of the fibre type 65-35 tested with solid steel blocks (batch 18)

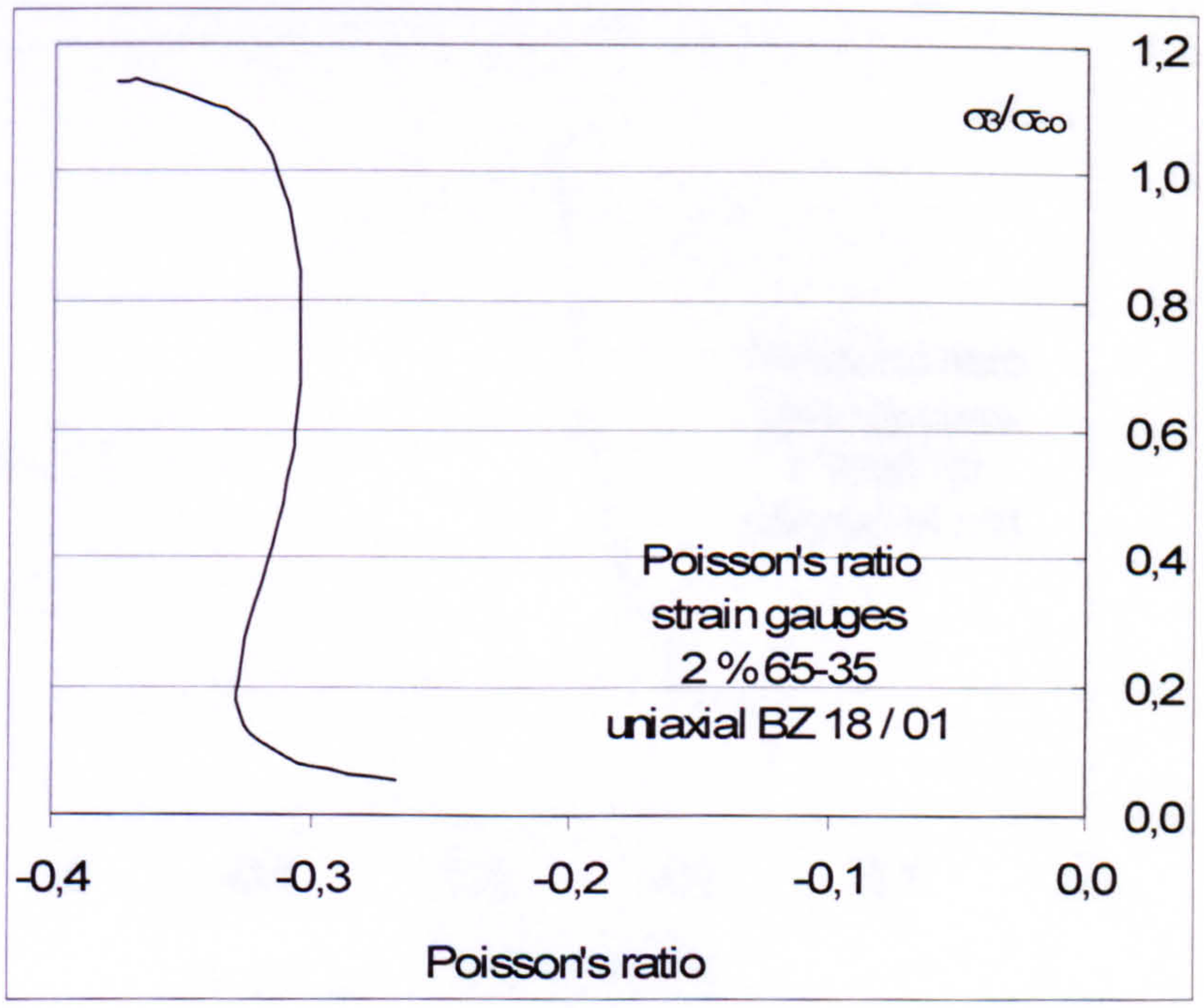

Figure 0.66 Poisson's ratio versus stress in uniaxial compression recorded with strain gauges in the two in plane directions for V_f = 2 % of the fibre type 65-35 tested with solid steel blocks (batch 18)

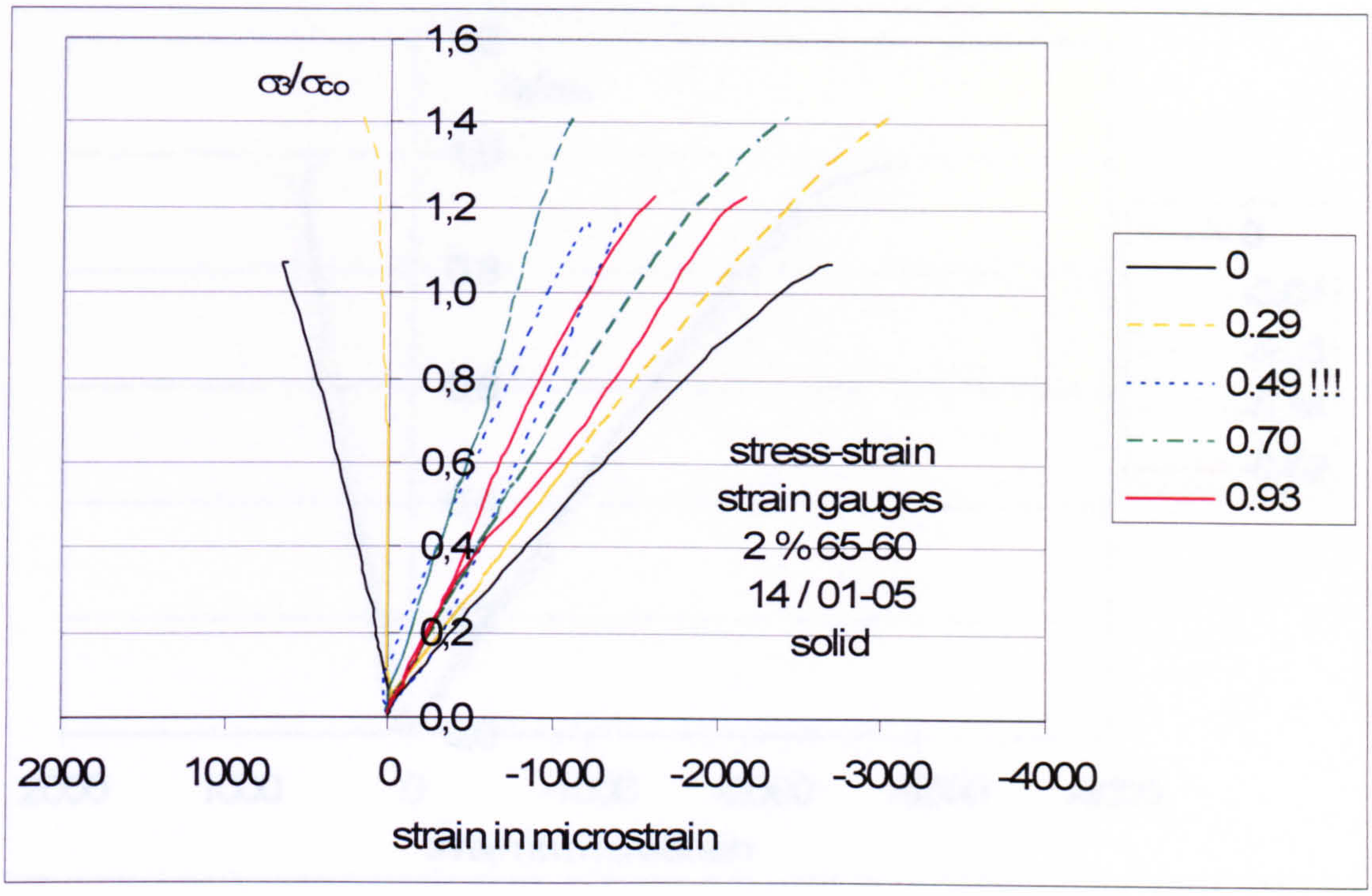

Figure 0.67 Stress-strain relationship for different stress ratios under biaxial compression recorded with strain gauges for V_f = 2 % of the fibre type 65-60 tested with solid steel blocks (batch 14)

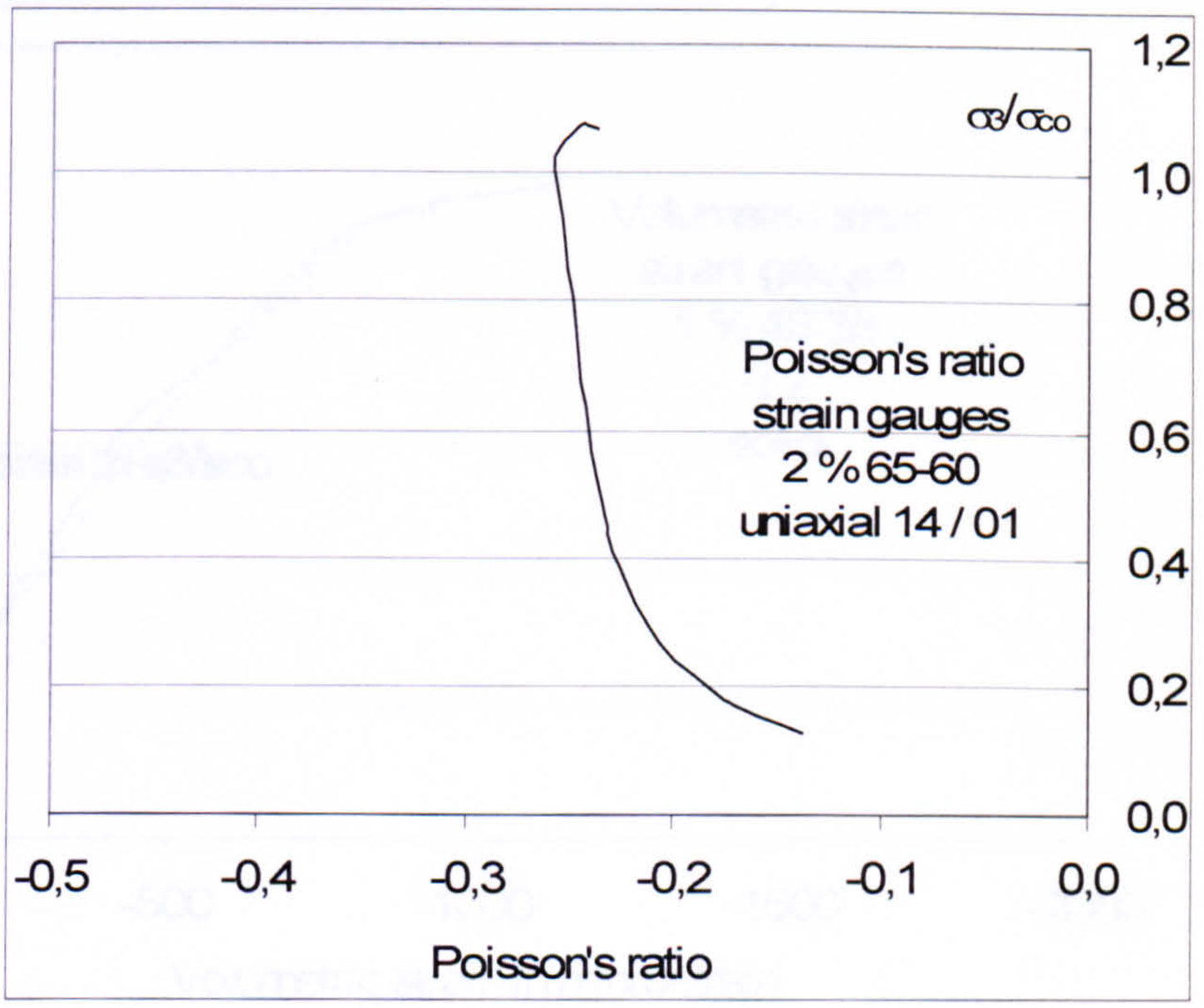

Figure 0.68 Poisson's ratio versus stress in uniaxial compression recorded with strain gauges in the two in plane directions for V_f = 2 % of the fibre type 65-60 tested with solid steel blocks (batch 14)

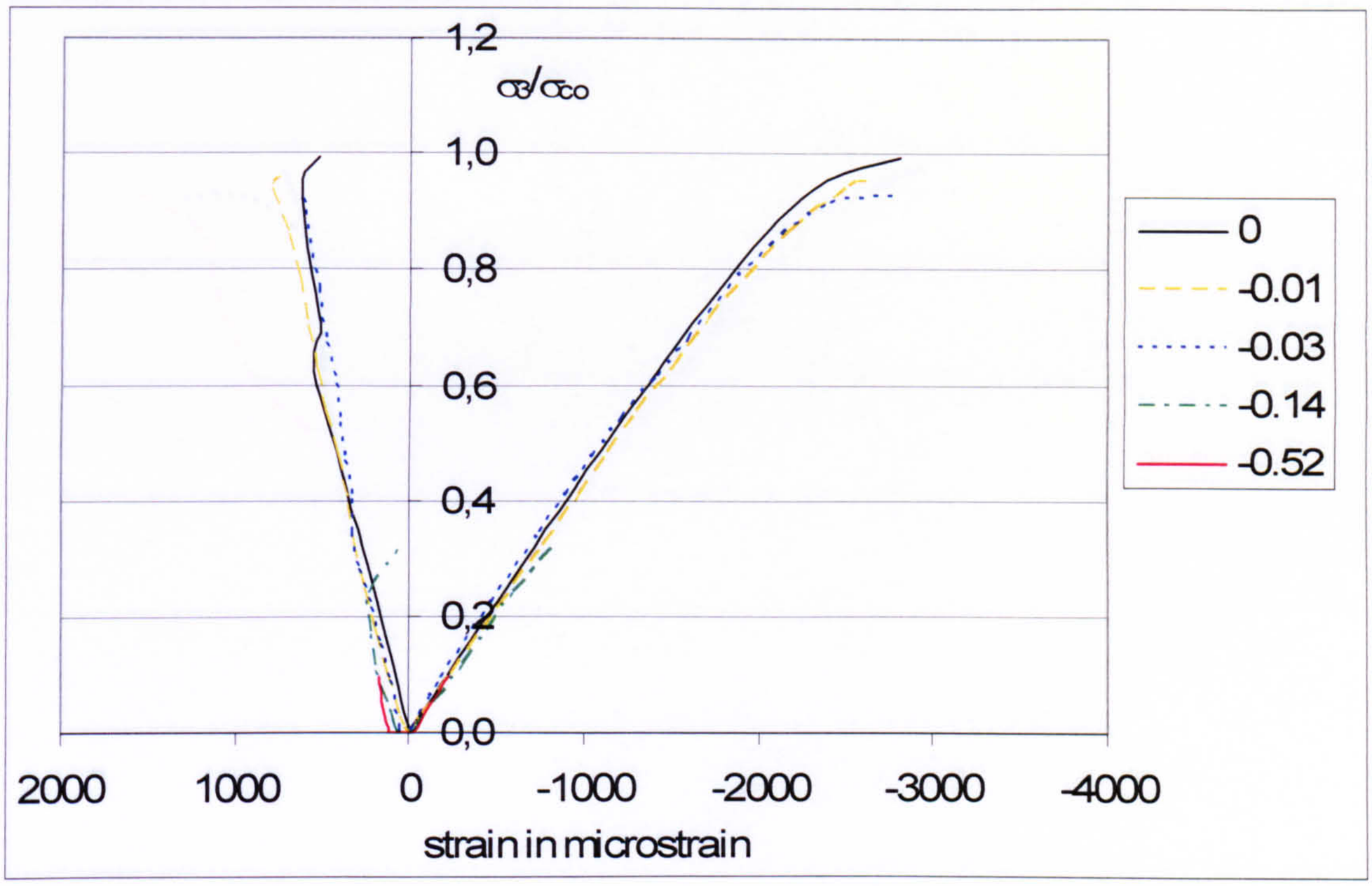

Figure 0.69 Stress-strain relationship for different stress ratios under biaxial compression-tension recorded with strain gauges for V_f = 1 % of the fibre type 45-35 tested with solid steel compression blocks (batch c-t 2)

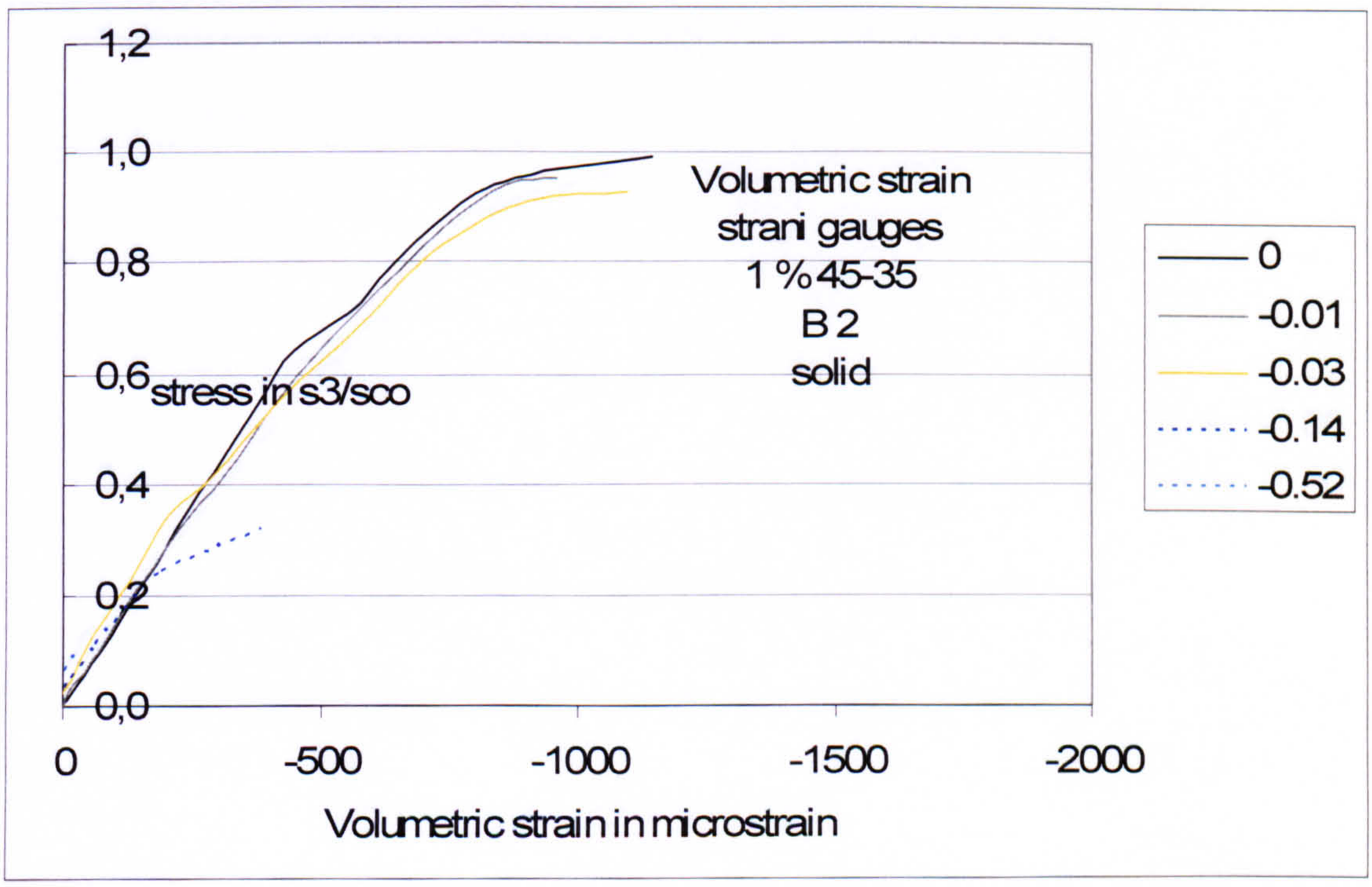

Figure 0.70 Volumetric strains for different stress ratios under biaxial compression-tension recorded with strain gauges in the two in plane directions for V_f = 1 % of the fibre type 45-35 tested with solid steel compression blocks (batch c-t 2)

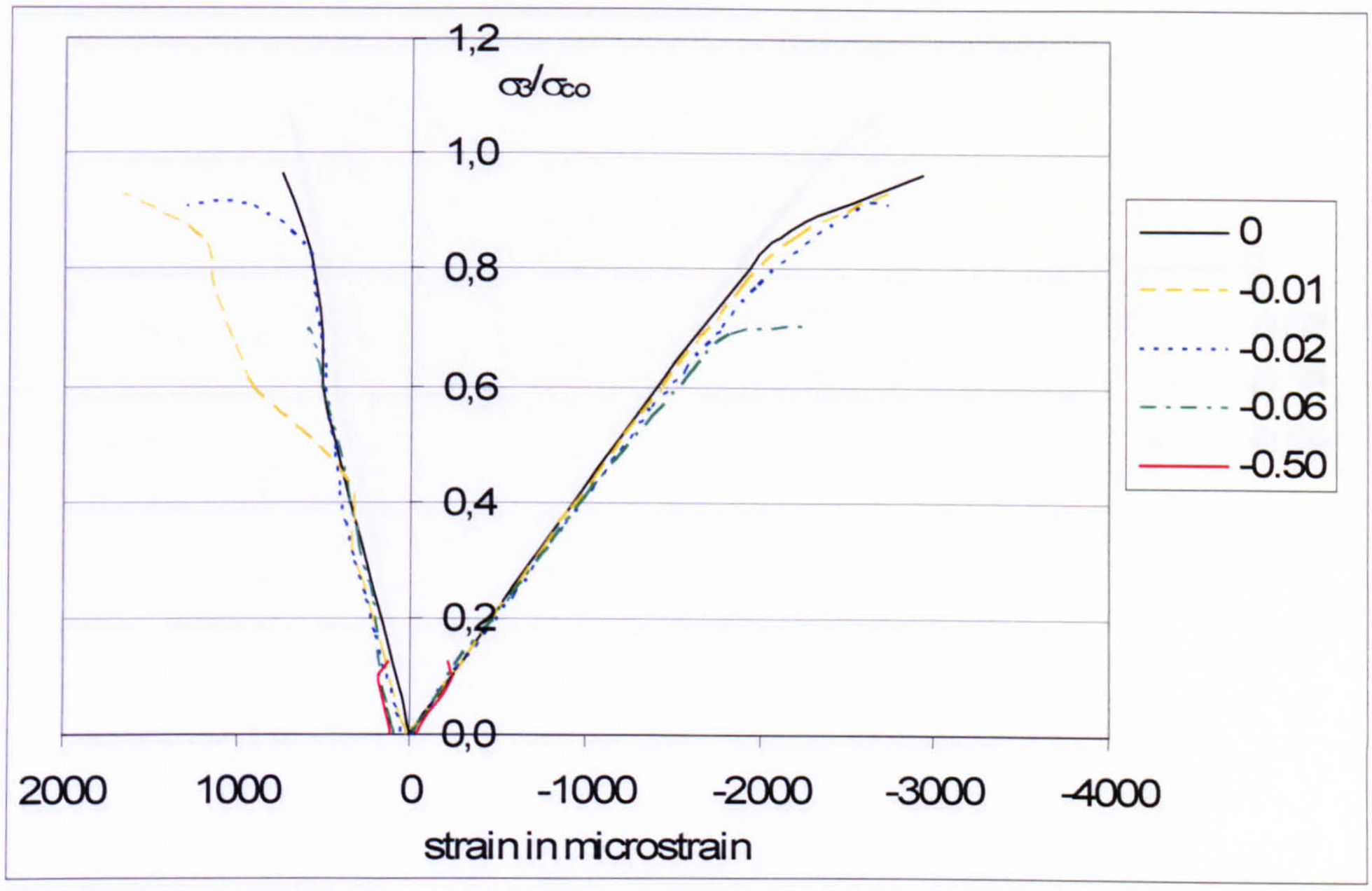

Figure 0.71 Stress-strain relationship for different stress ratios under biaxial compression-tension recorded with strain gauges for V_f = 1 % of the fibre type 45-35 tested with solid steel compression blocks (batch c-t 3)

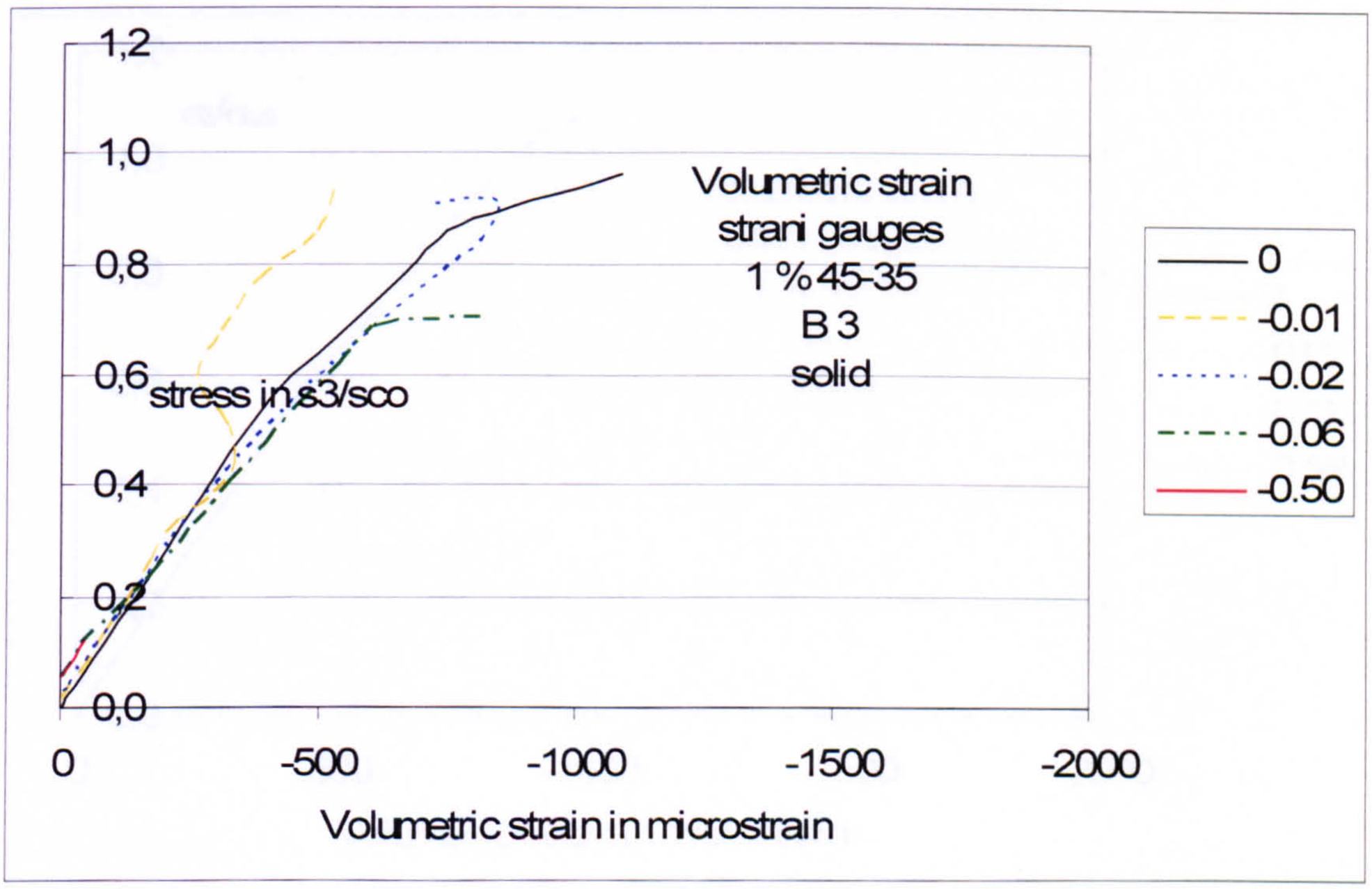

Figure 0.72 Volumetric strains for different stress ratios under biaxial compression-tension recorded with strain gauges in the two in plane directions for V_f = 1 % of the fibre type 45-35 tested with solid steel compression blocks (batch c-t 3)

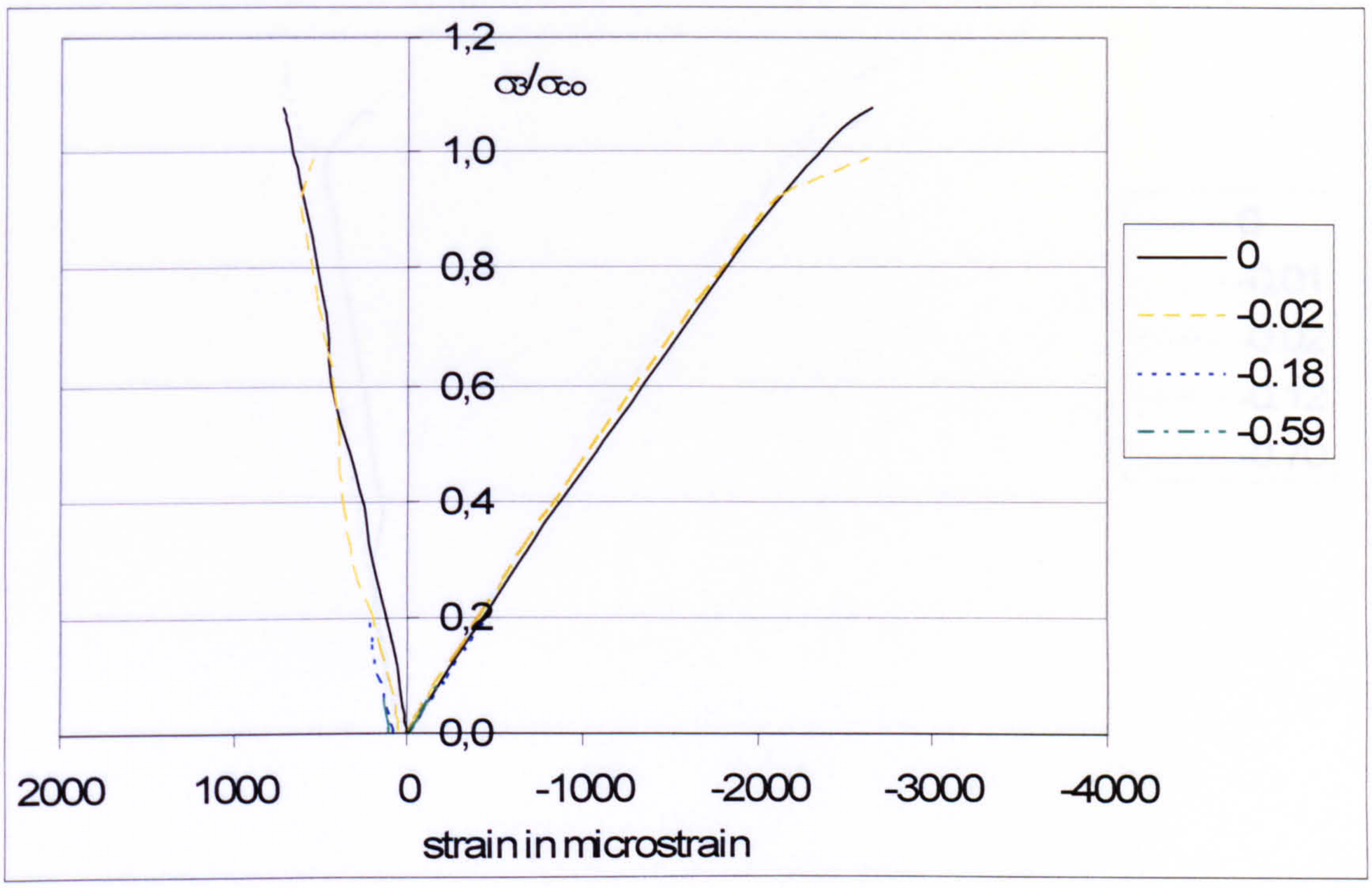

Figure 0.73 Stress-strain relationship for different stress ratios under biaxial compression-tension recorded with strain gauges for V_f = 1 % of the fibre type 45-50 tested with solid steel compression blocks (batch c-t 7)

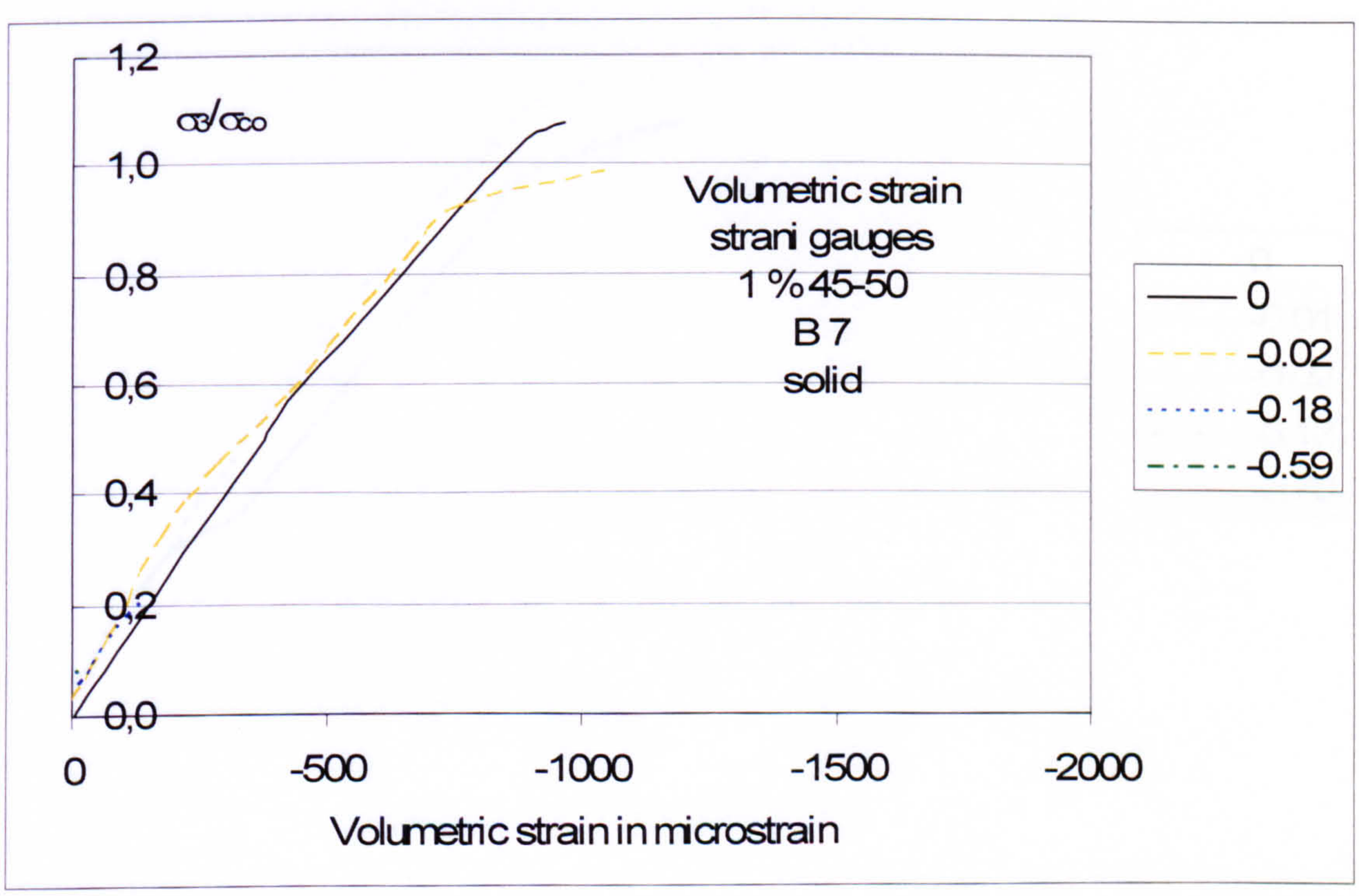

Figure 0.74 Volumetric strains for different stress ratios under biaxial compression-tension recorded with strain gauges in the two in plane directions for V_f = 1 % of the fibre type 45-50 tested with solid steel compression blocks (batch c-t 7)

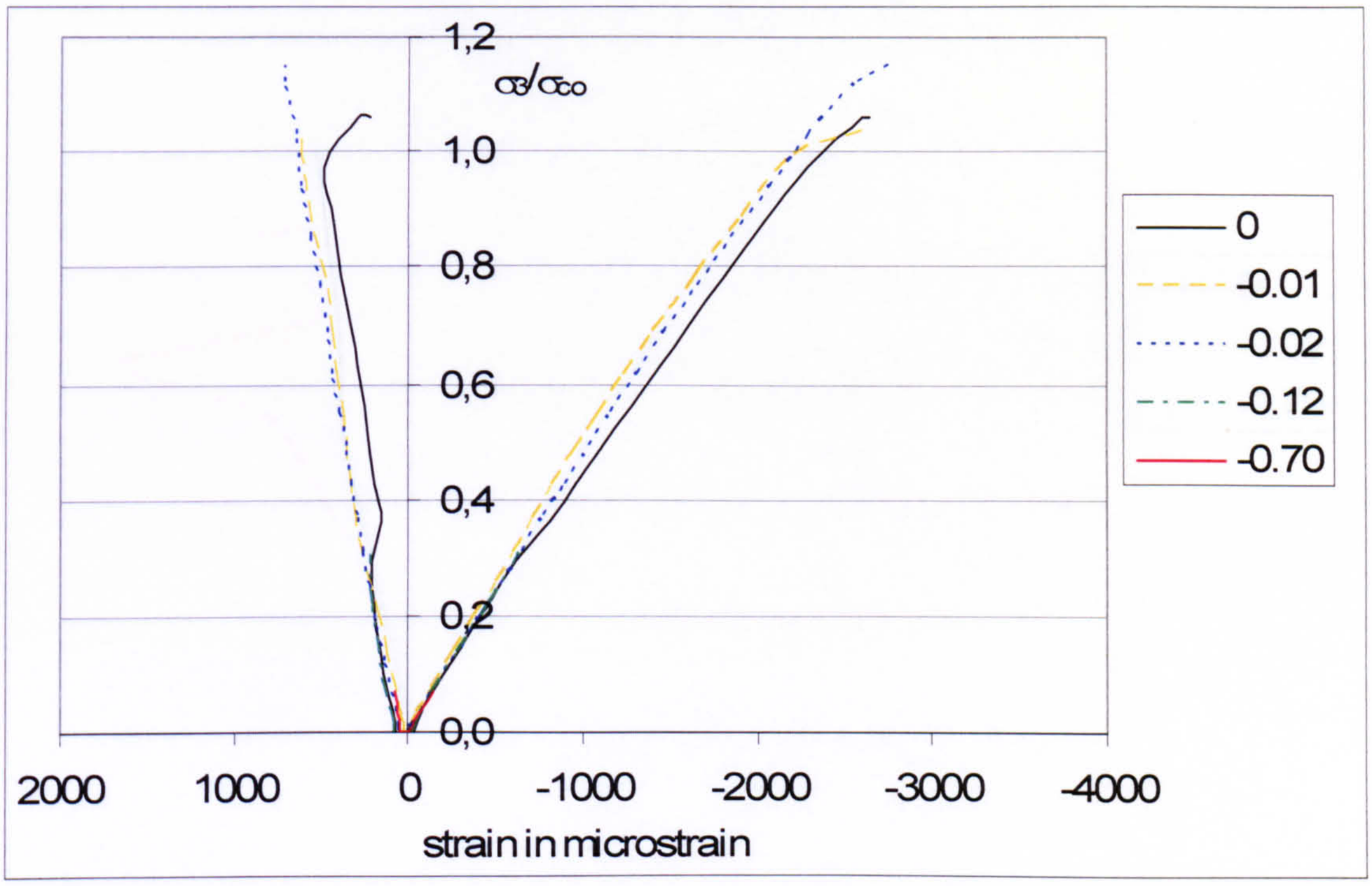

Figure 0.75 Stress-strain relationship for different stress ratios under biaxial compression-tension recorded with strain gauges for V_f = 1 % of the fibre type 45-50 tested with solid steel compression blocks (batch c-t 8)

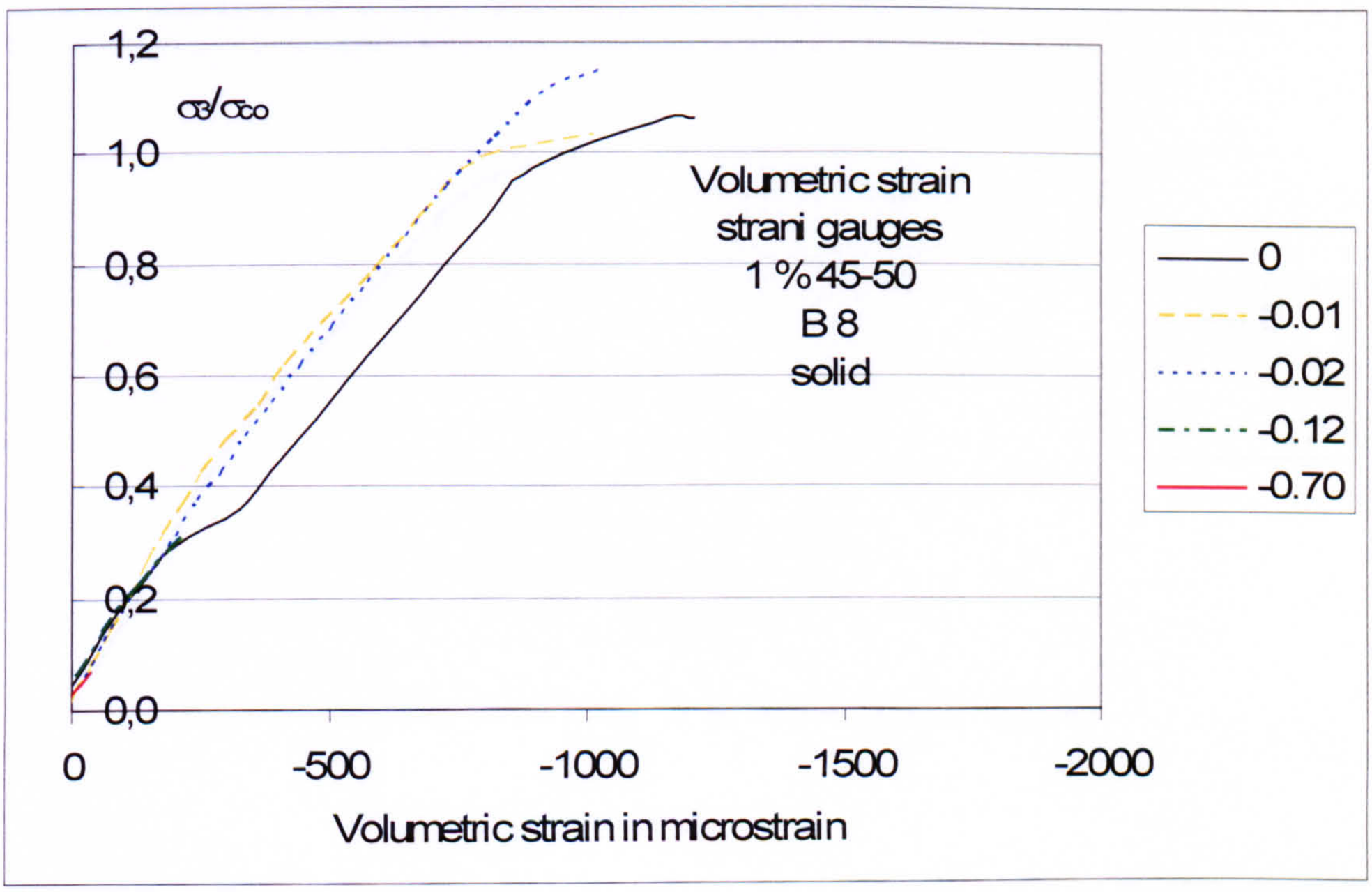

Figure 0.76 Volumetric strains for different stress ratios under biaxial compression-tension recorded with strain gauges in the two in plane directions for V_f = 1 % of the fibre type 45-50 tested with solid steel compression blocks (batch c-t 8)

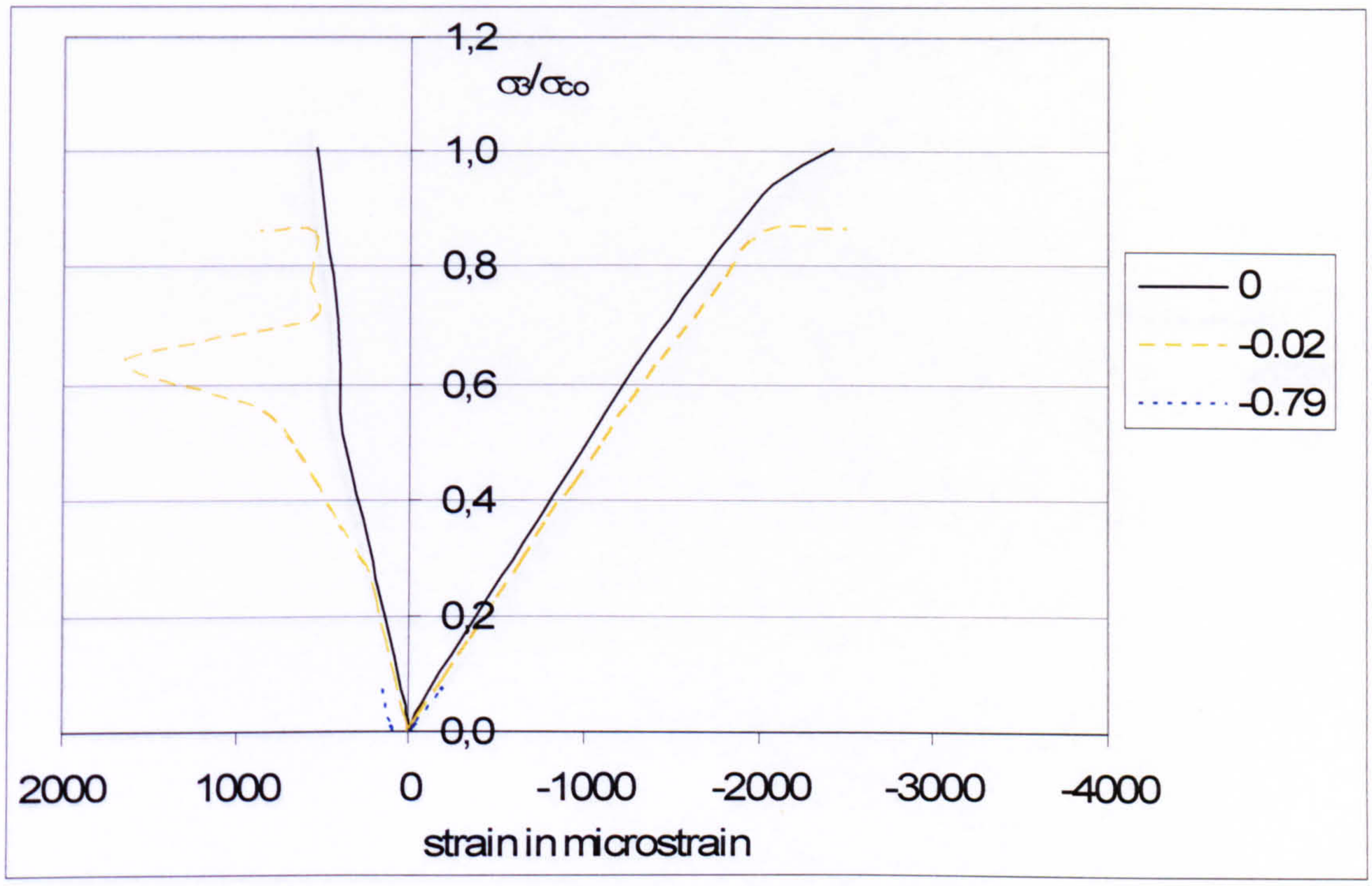

Figure 0.77 Stress-strain relationship for different stress ratios under biaxial compression-tension recorded with strain gauges for V_f = 1 % of the fibre type 65-35 tested with solid steel compression blocks (batch c-t 9)

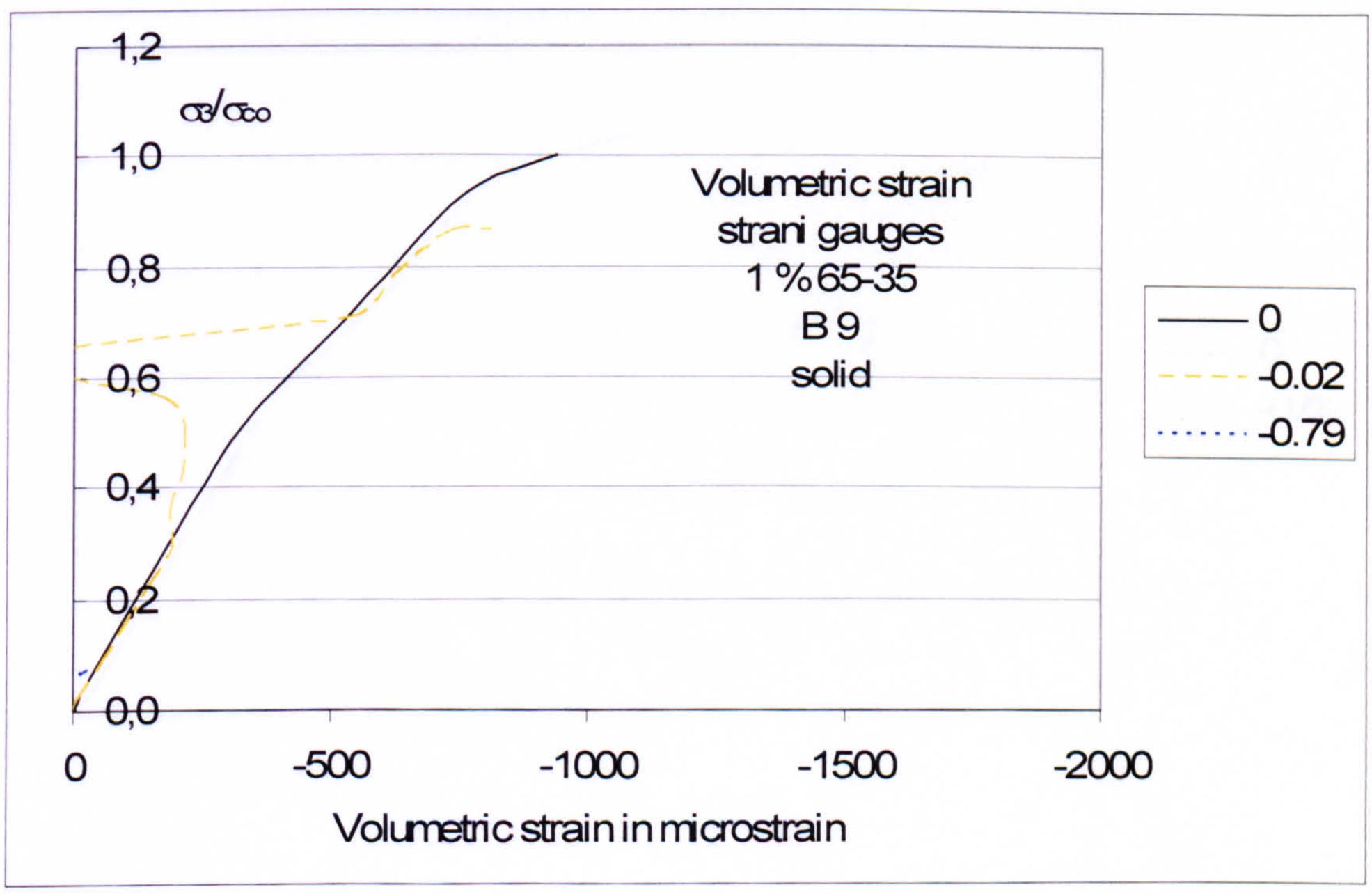

Figure 0.78 Volumetric strains for different stress ratios under biaxial compression-tension recorded with strain gauges in the two in plane directions for V_f = 1 % of the fibre type 65-35 tested with solid steel compression blocks (batch c-t 9)

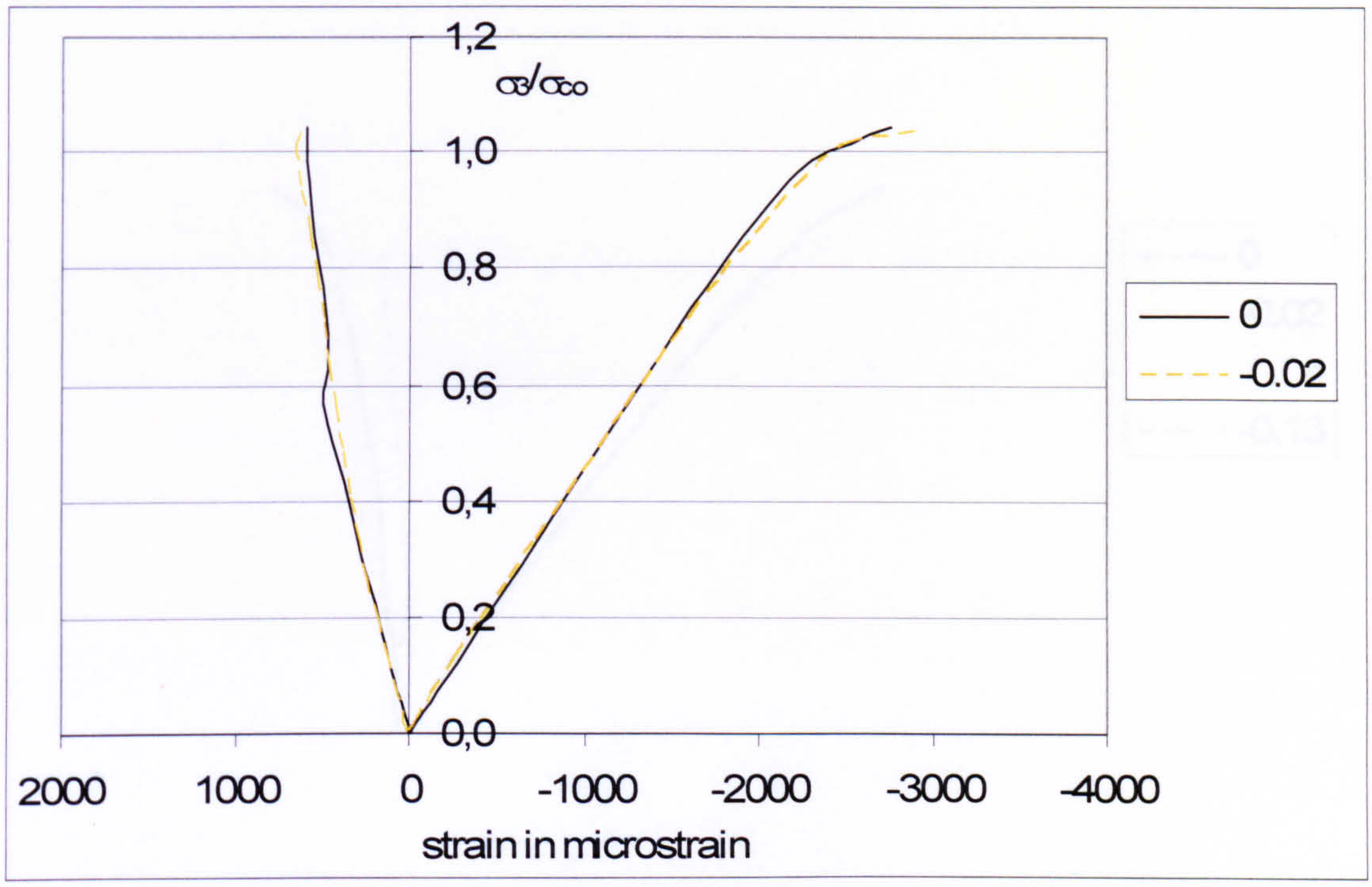

Figure 0.79 Stress-strain relationship for different stress ratios under biaxial compression-tension recorded with strain gauges for V_f = 1 % of the fibre type 65-35 tested with solid steel compression blocks (batch c-t 10)

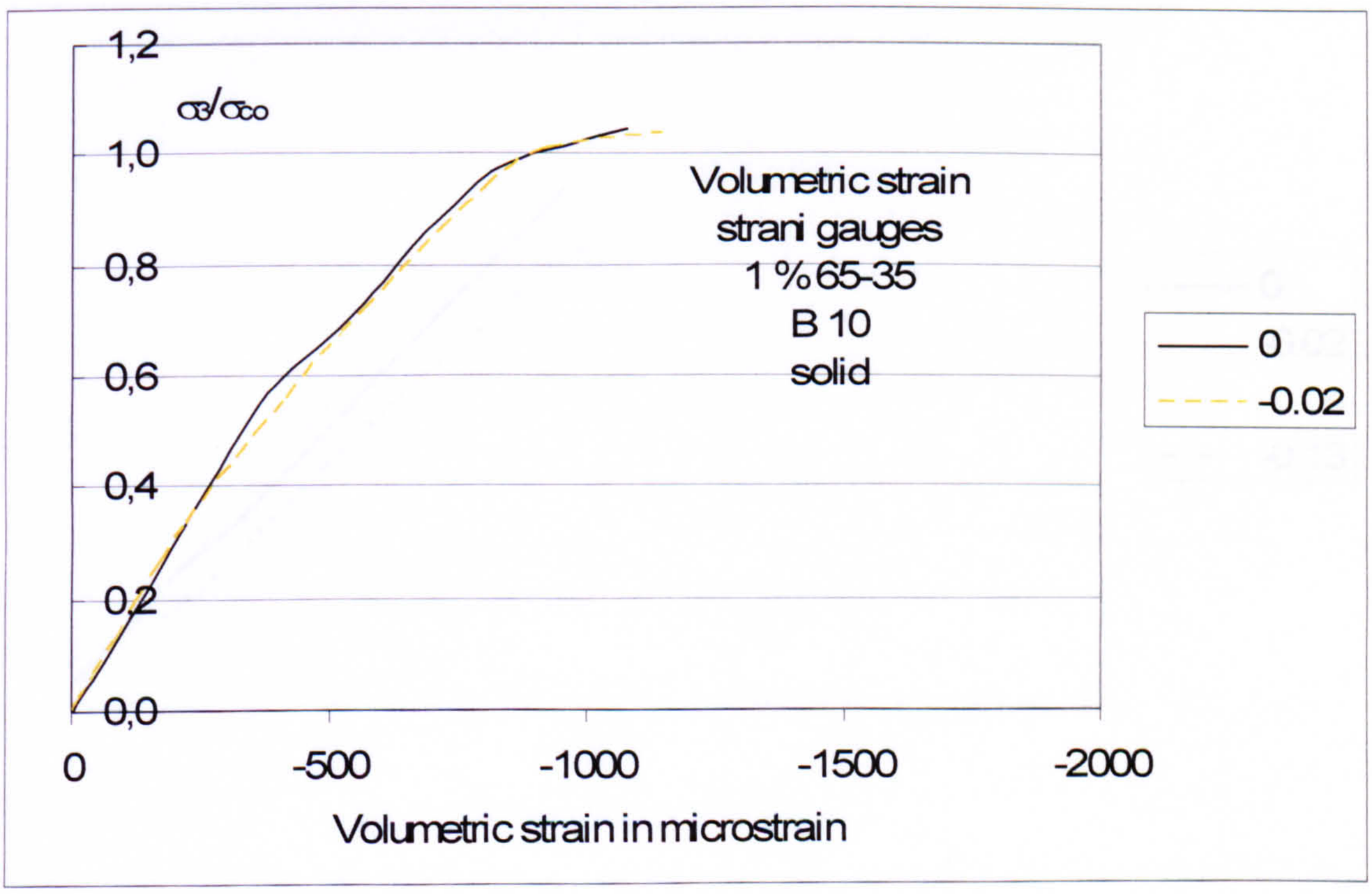

Figure 0.80 Volumetric strains for different stress ratios under biaxial compression-tension recorded with strain gauges in the two in plane directions for V_f = 1 % of the fibre type 65-35 tested with solid steel compression blocks (batch c-t 10)

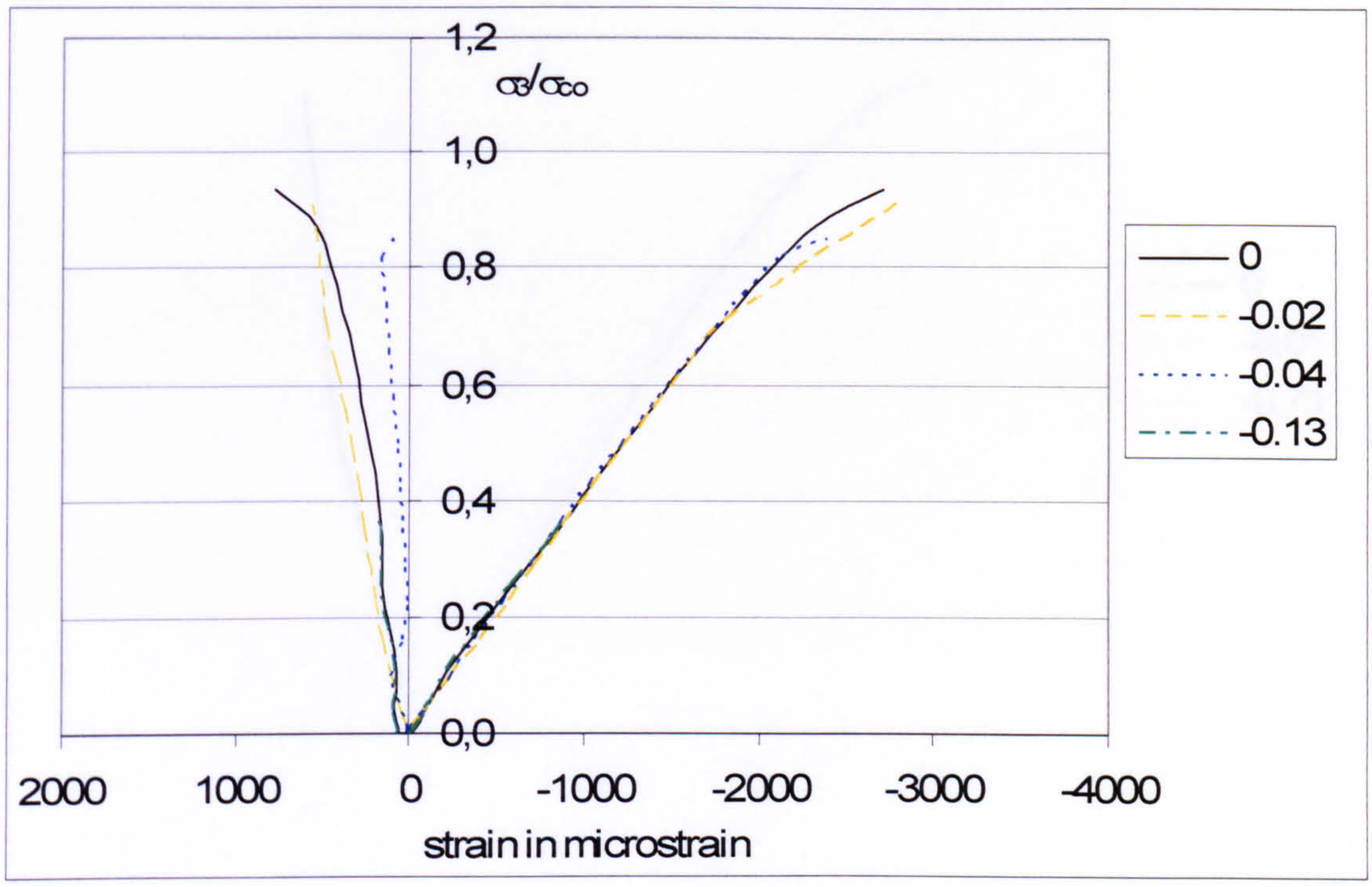

Figure 0.81 Stress-strain relationship for different stress ratios under biaxial compression-tension recorded with strain gauges for V_f = 1 % of the fibre type 65-60 tested with solid steel compression blocks (batch c-t 11)

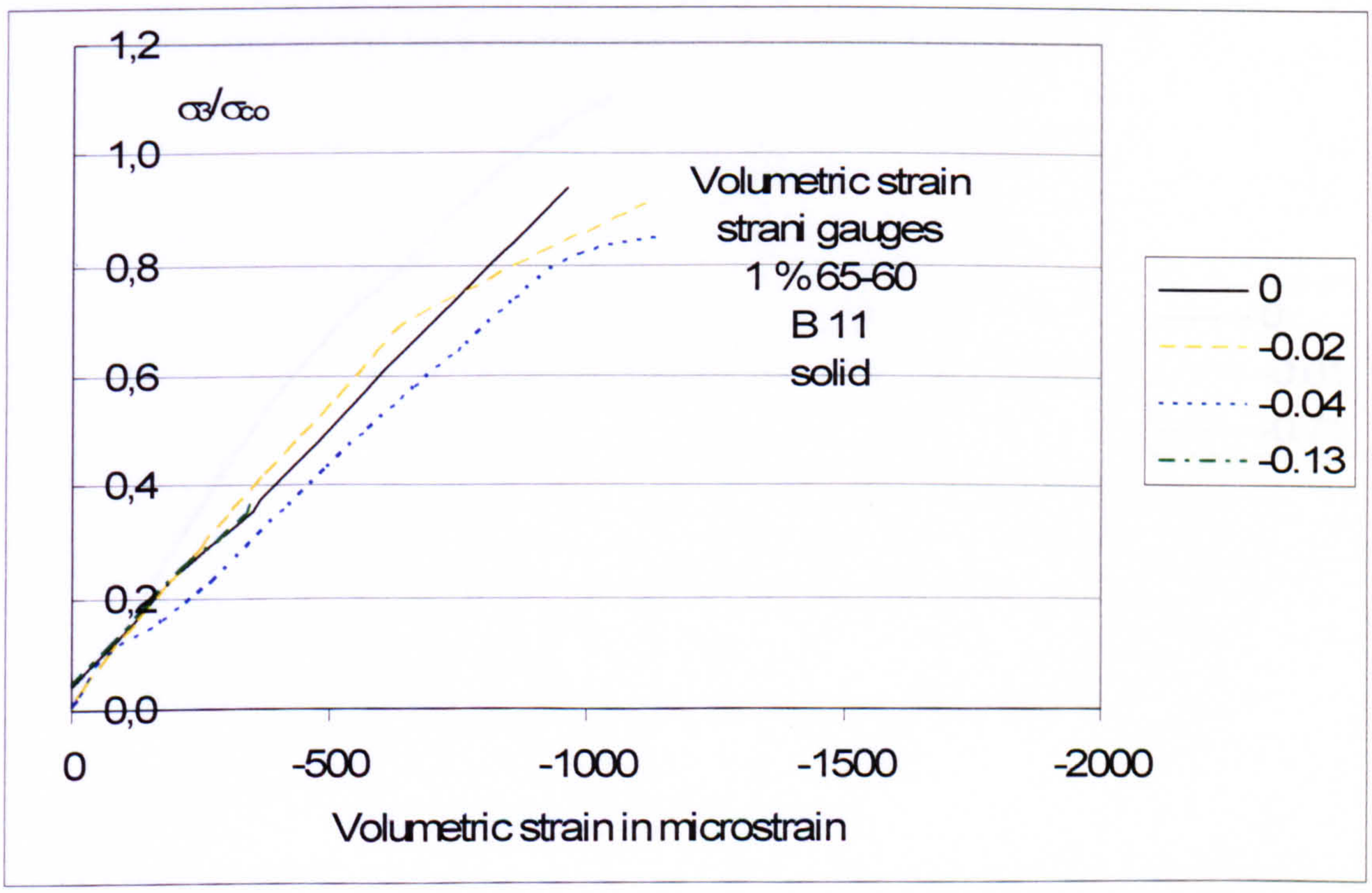

Figure 0.82 Volumetric strains for different stress ratios under biaxial compression-tension recorded with strain gauges in the two in plane directions for V_f = 1 % of the fibre type 65-60 tested with solid steel compression blocks (batch c-t 11)

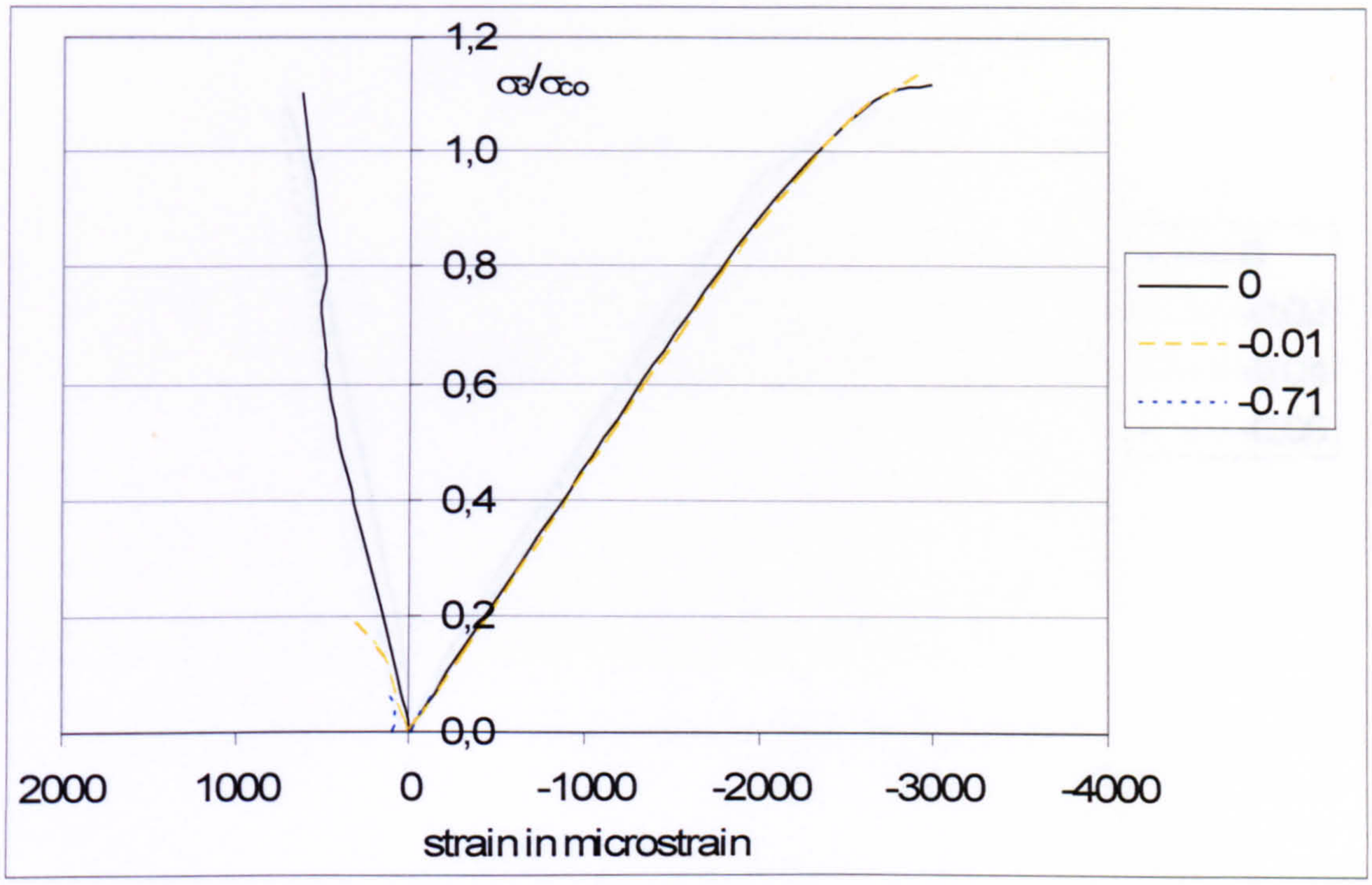

Figure 0.83 Stress-strain relationship for different stress ratios under biaxial compression-tension recorded with strain gauges for V_f = 1 % of the fibre type 65-60 tested with solid steel compression blocks (batch c-t 12)

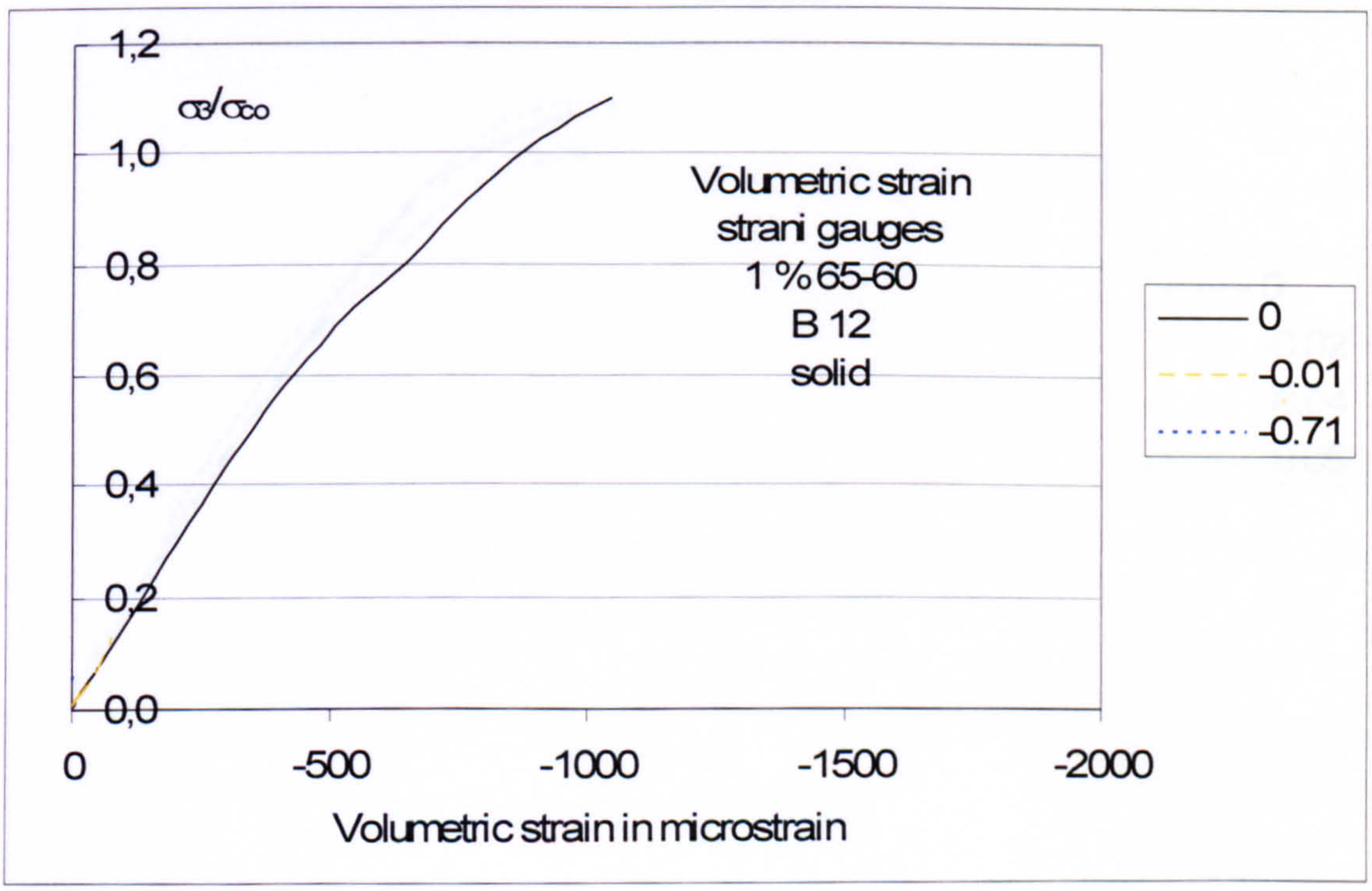

Figure 0.84 Volumetric strains for different stress ratios under biaxial compression-tension recorded with strain gauges in the two in plane directions for V_f = 1 % of the fibre type 65-60 tested with solid steel compression blocks (batch c-t 12)

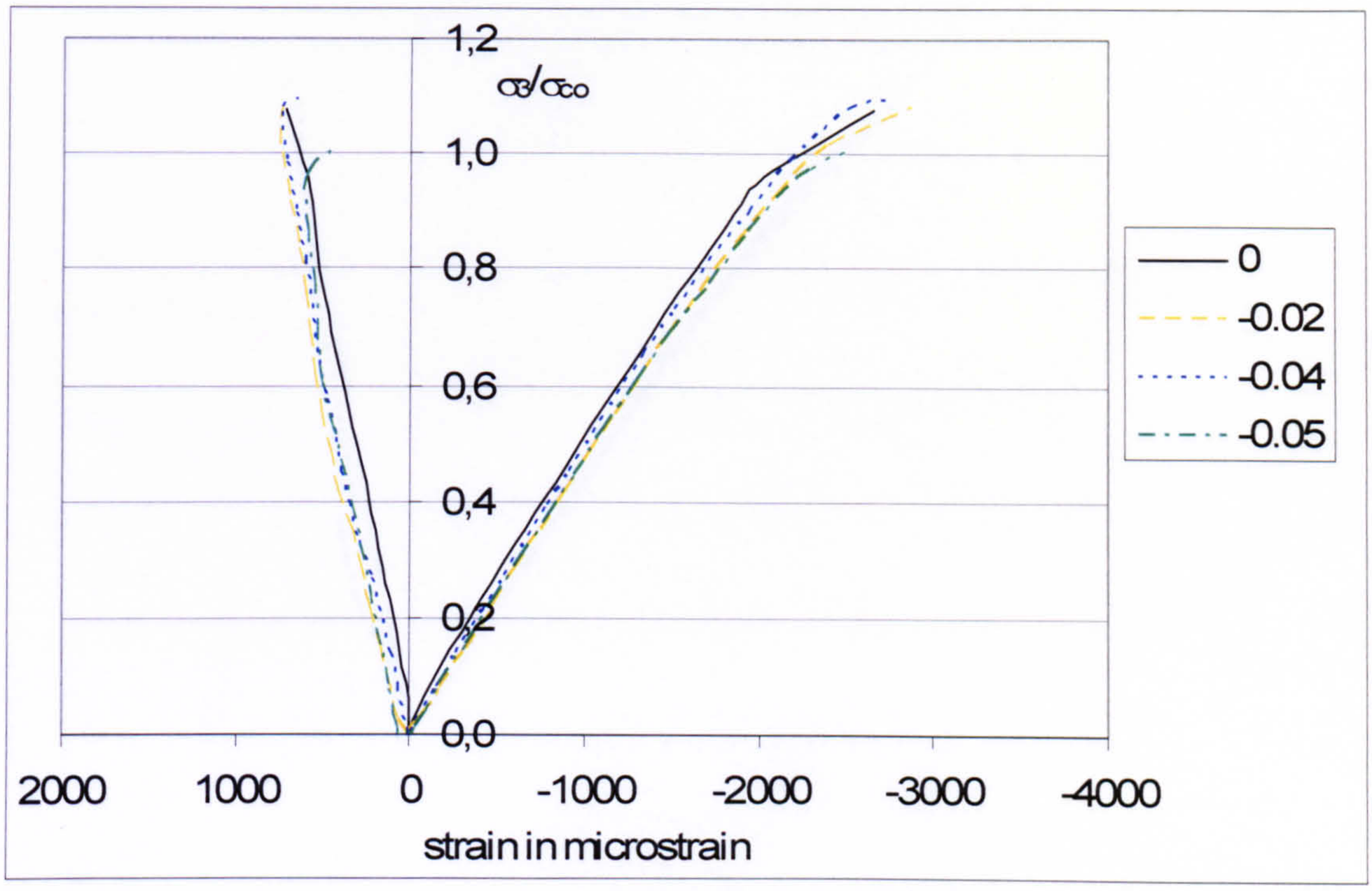

Figure 0.85 Stress-strain relationship for different stress ratios under biaxial compression-tension recorded with strain gauges for V_f = 2 % of the fibre type 45-35 tested with solid steel compression blocks (batch c-t 13)

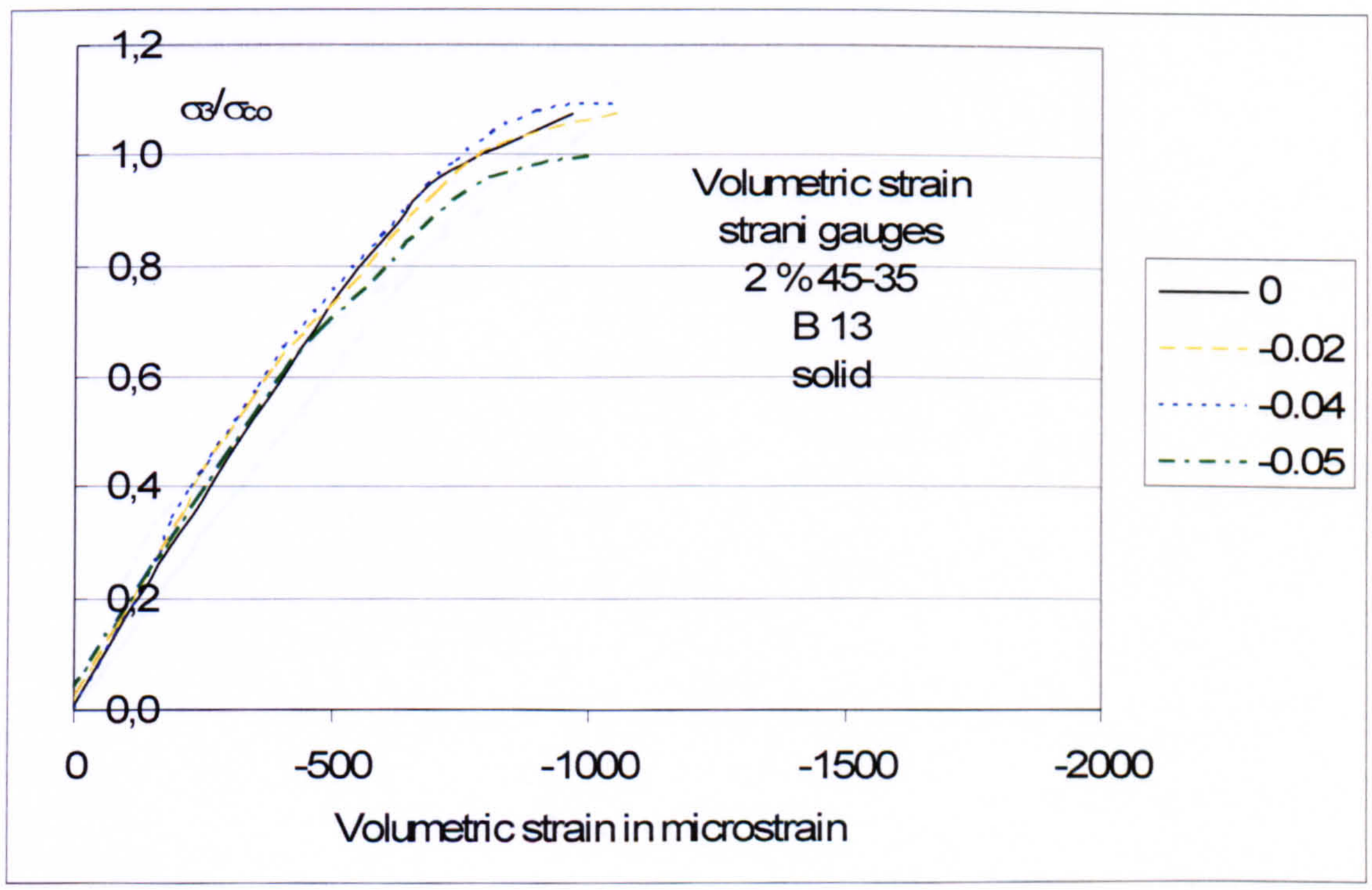

Figure 0.86 Volumetric strains for different stress ratios under biaxial compression-tension recorded with strain gauges in the two in plane directions for V_f = 2 % of the fibre type 45-35 tested with solid steel compression blocks (batch c-t 13)

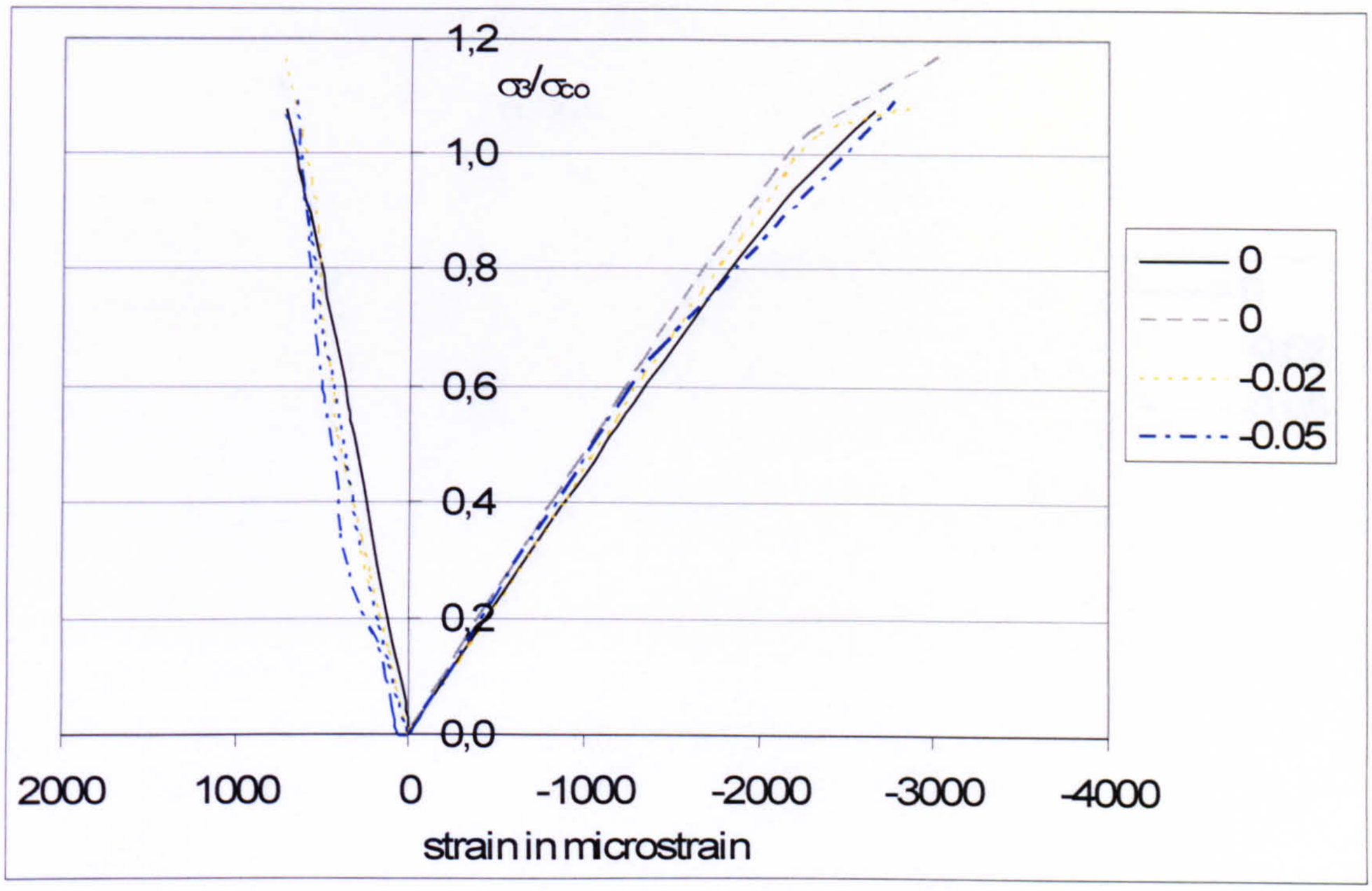

Figure 0.87 Stress-strain relationship for different stress ratios under biaxial compression-tension recorded with strain gauges for V_f = 2 % of the fibre type 45-35 tested with solid steel compression blocks (batch c-t 14)

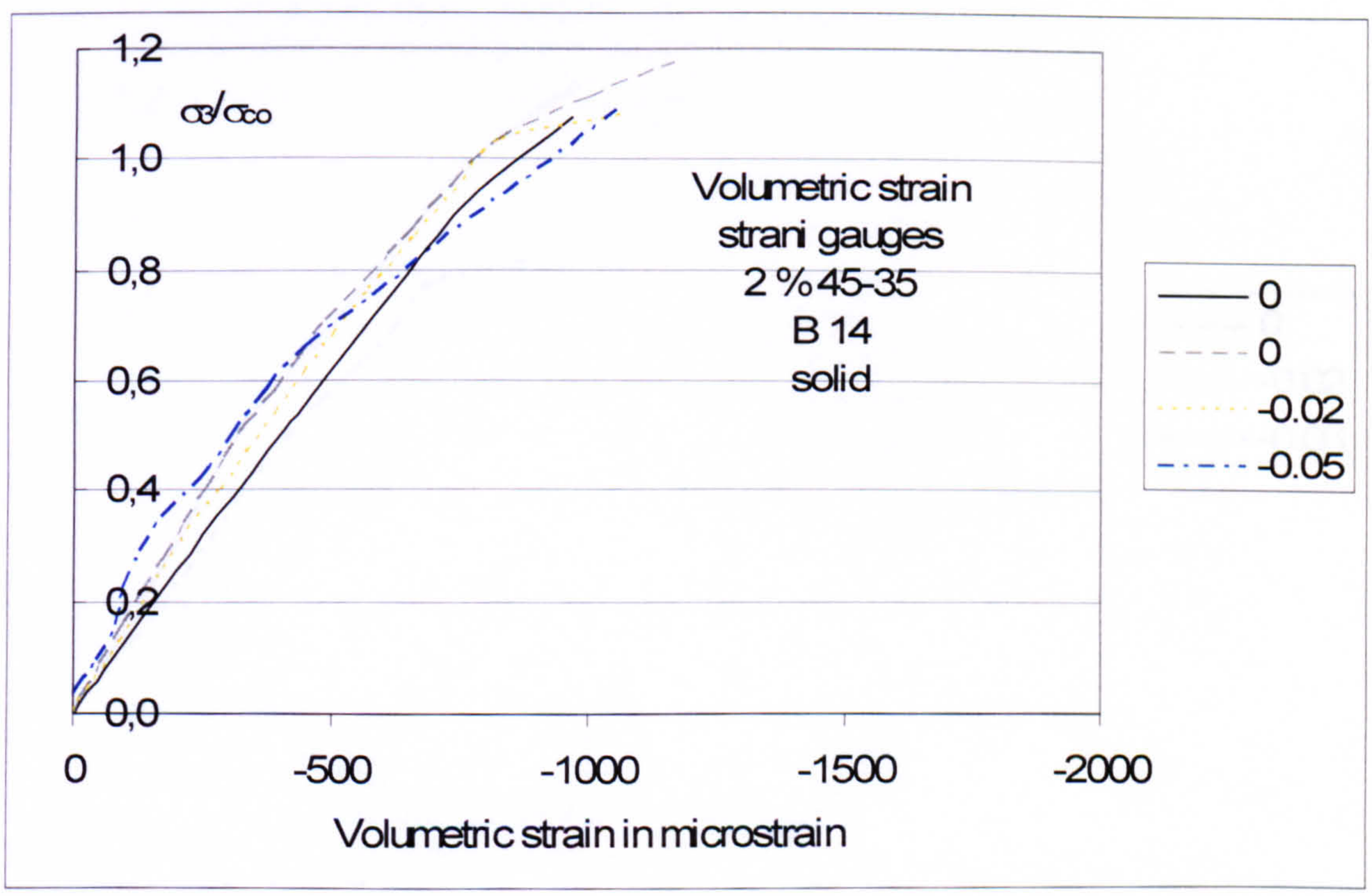

Figure 0.88 Volumetric strains for different stress ratios under biaxial compression-tension recorded with strain gauges in the two in plane directions for V_f = 2 % of the fibre type 45-35 tested with solid steel compression blocks (batch c-t 14)

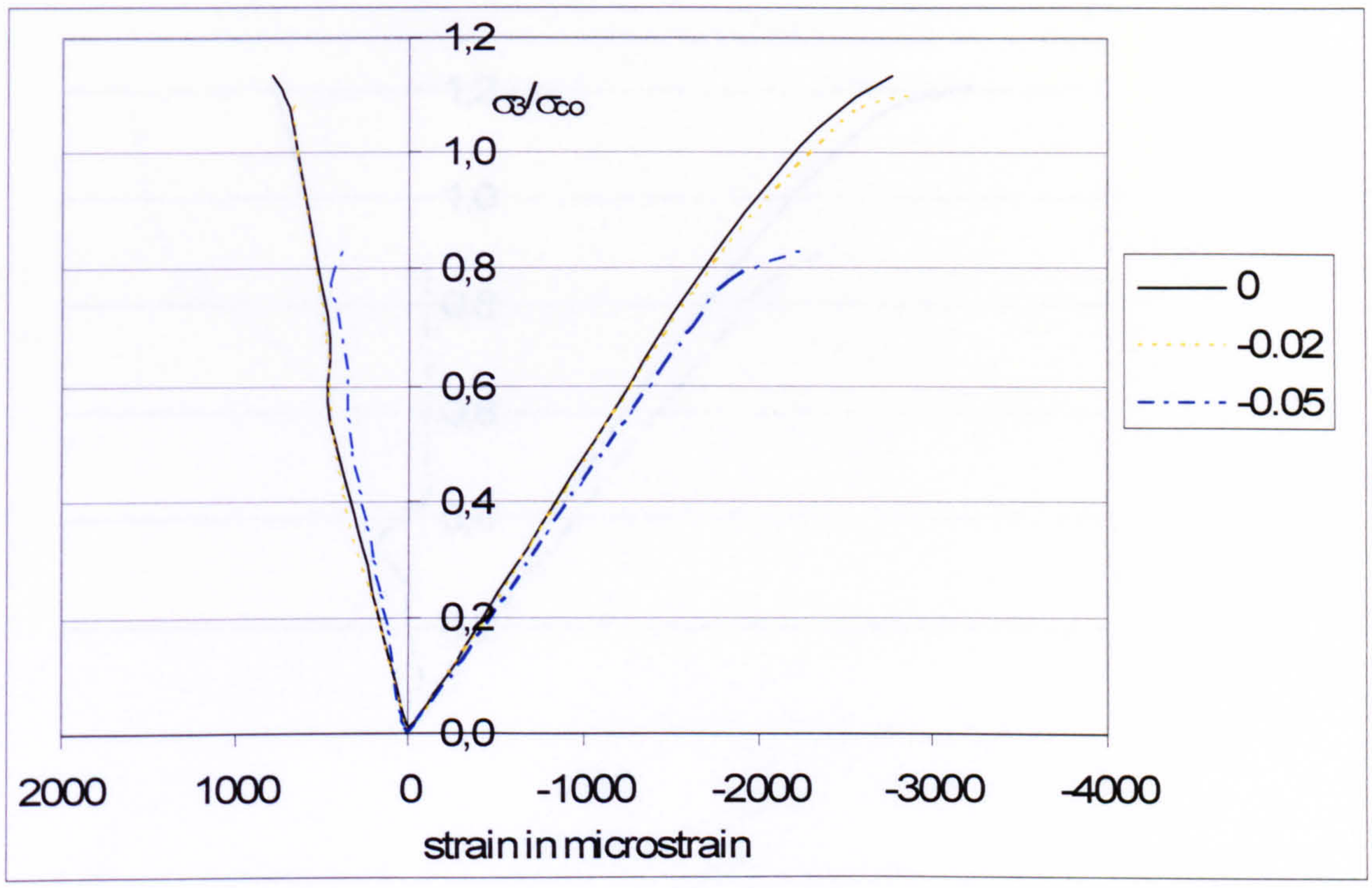

Figure 0.89 Stress-strain relationship for different stress ratios under biaxial compression-tension recorded with strain gauges for V_f = 2 % of the fibre type 45-50 tested with solid steel compression blocks (batch c-t 15)

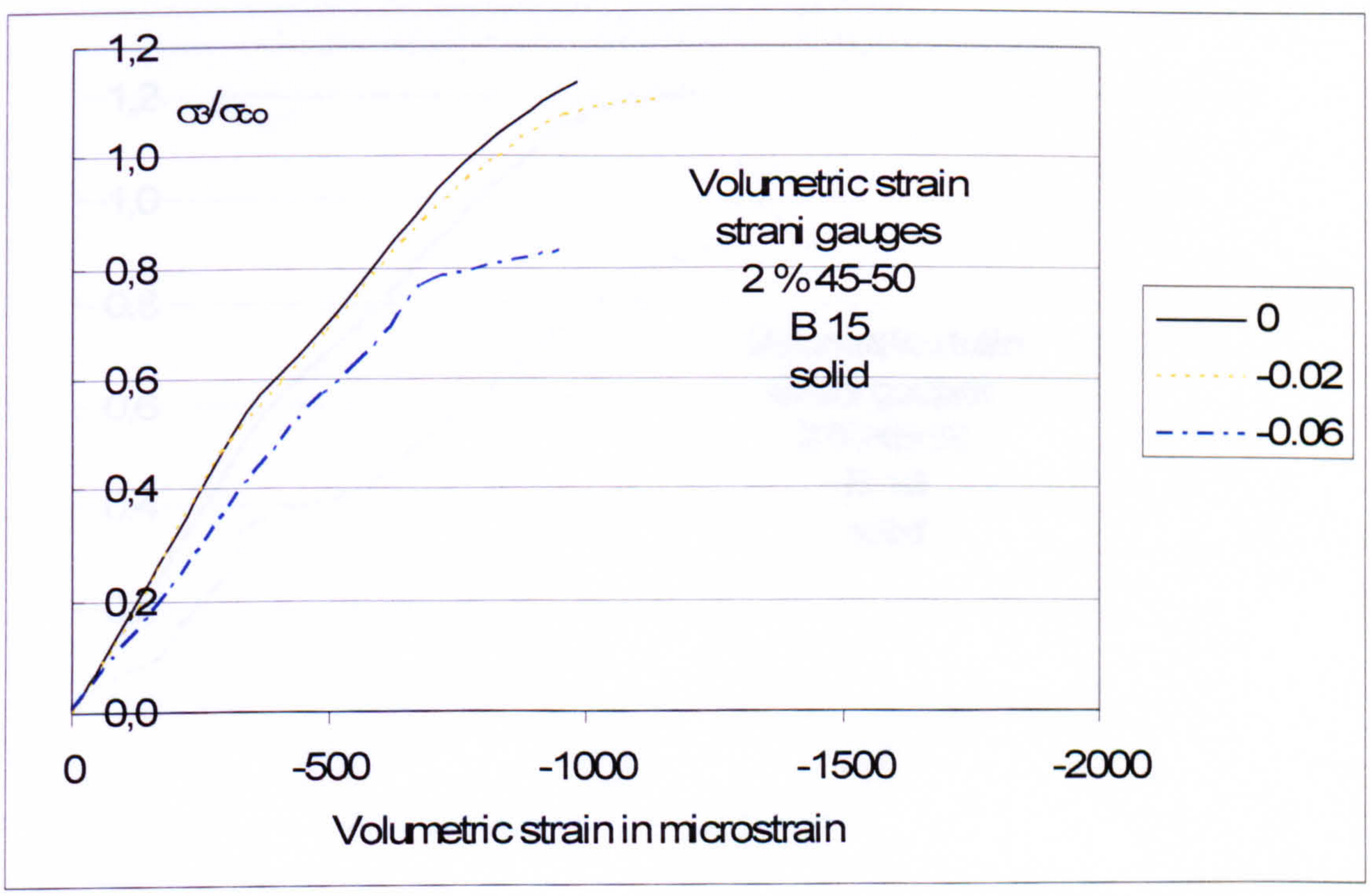

Figure 0.90 Volumetric strains for different stress ratios under biaxial compression-tension recorded with strain gauges in the two in plane directions for V_f = 2 % of the fibre type 45-50 tested with solid steel compression blocks (batch c-t 15)

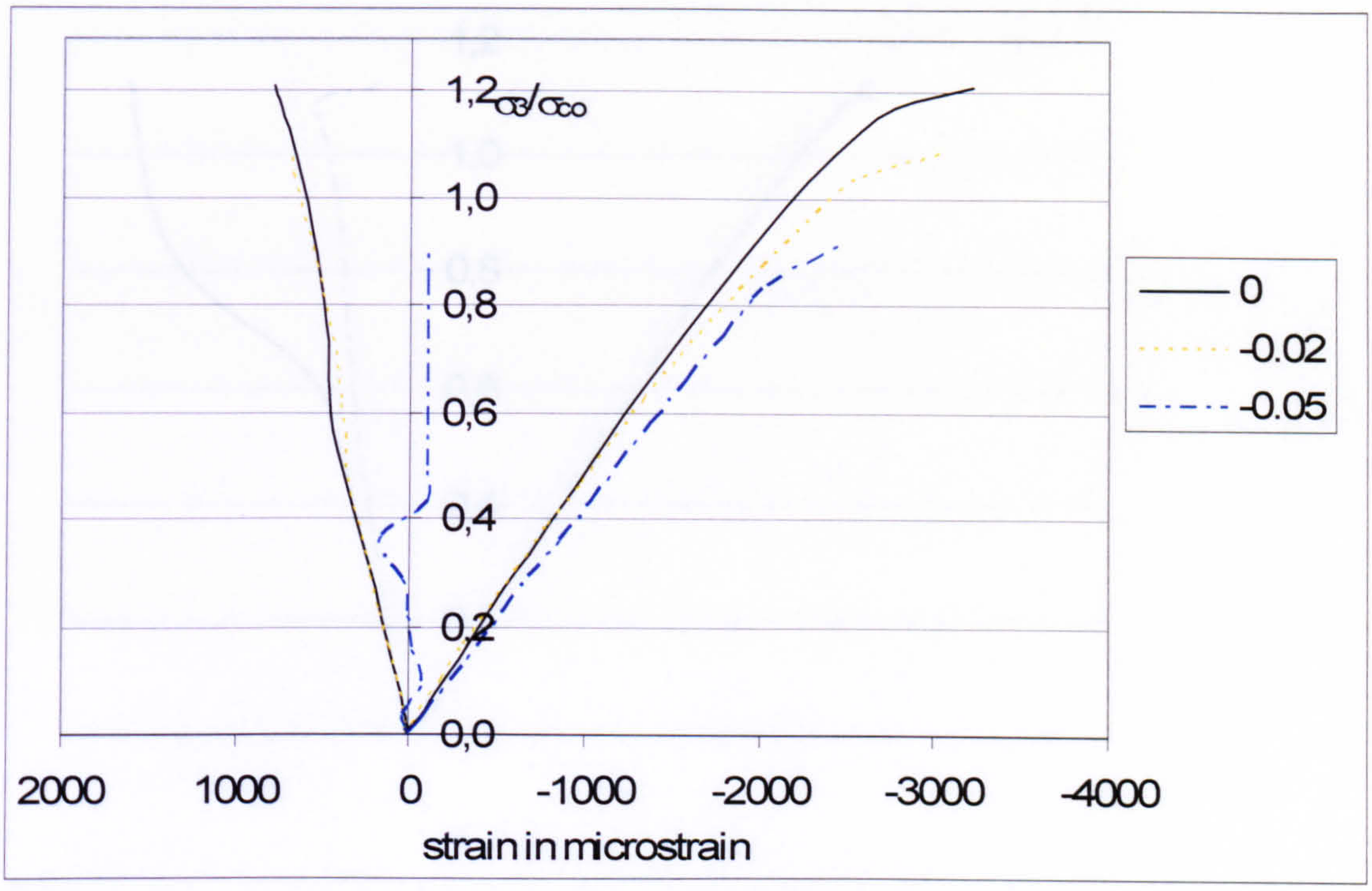

Figure 0.91 Stress-strain relationship for different stress ratios under biaxial compression-tension recorded with strain gauges for V_f = 2 % of the fibre type 45-50 tested with solid steel compression blocks (batch c-t 16)

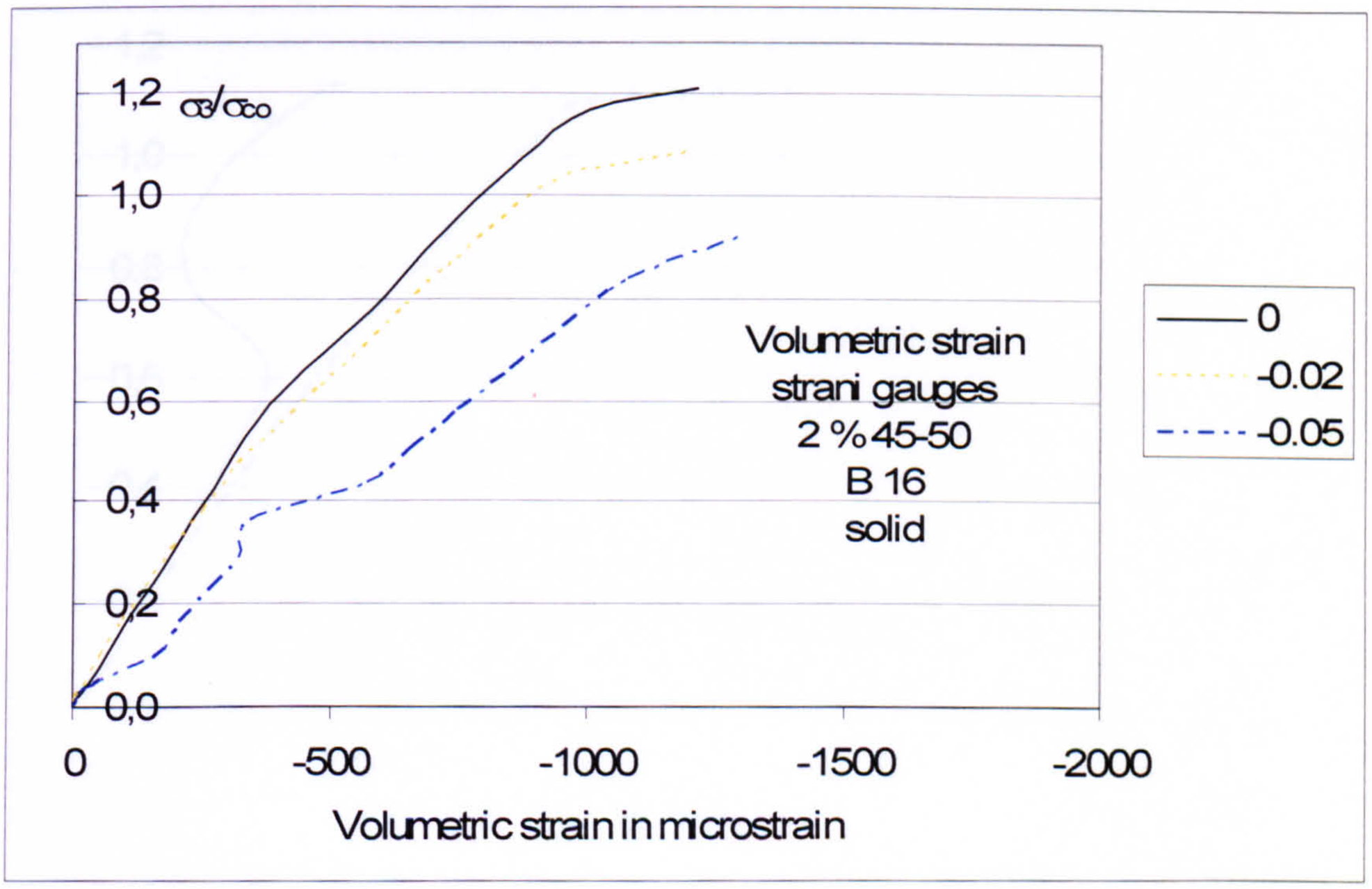

Figure 0.92 Volumetric strains for different stress ratios under biaxial compression-tension recorded with strain gauges in the two in plane directions for V_f = 2 % of the fibre type 45-50 tested with solid steel compression blocks (batch c-t 16)

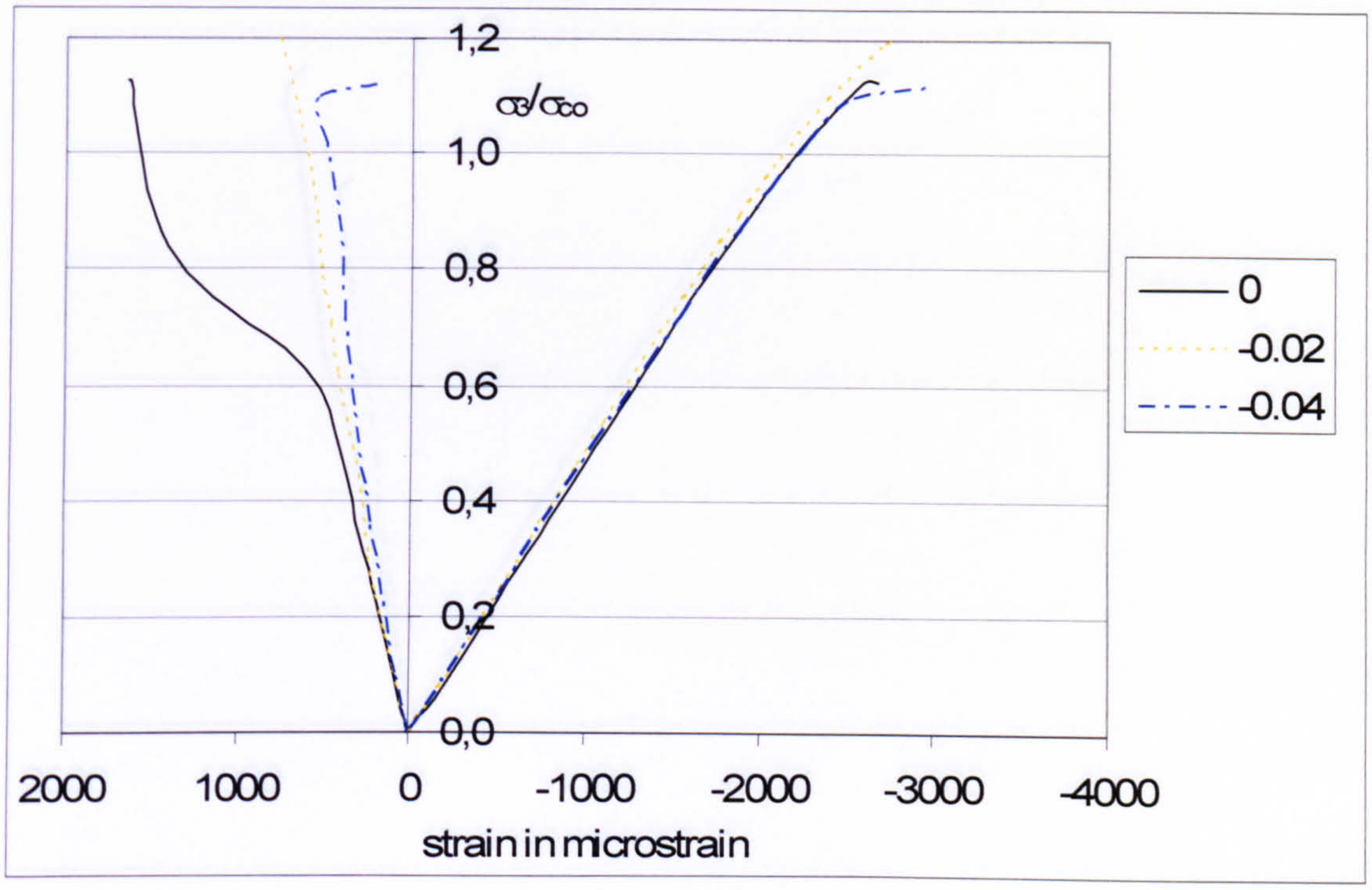

Figure 0.93 Stress-strain relationship for different stress ratios under biaxial compression-tension recorded with strain gauges for V_f = 2 % of the fibre type 65-35 tested with solid steel compression blocks (batch c-t 17)

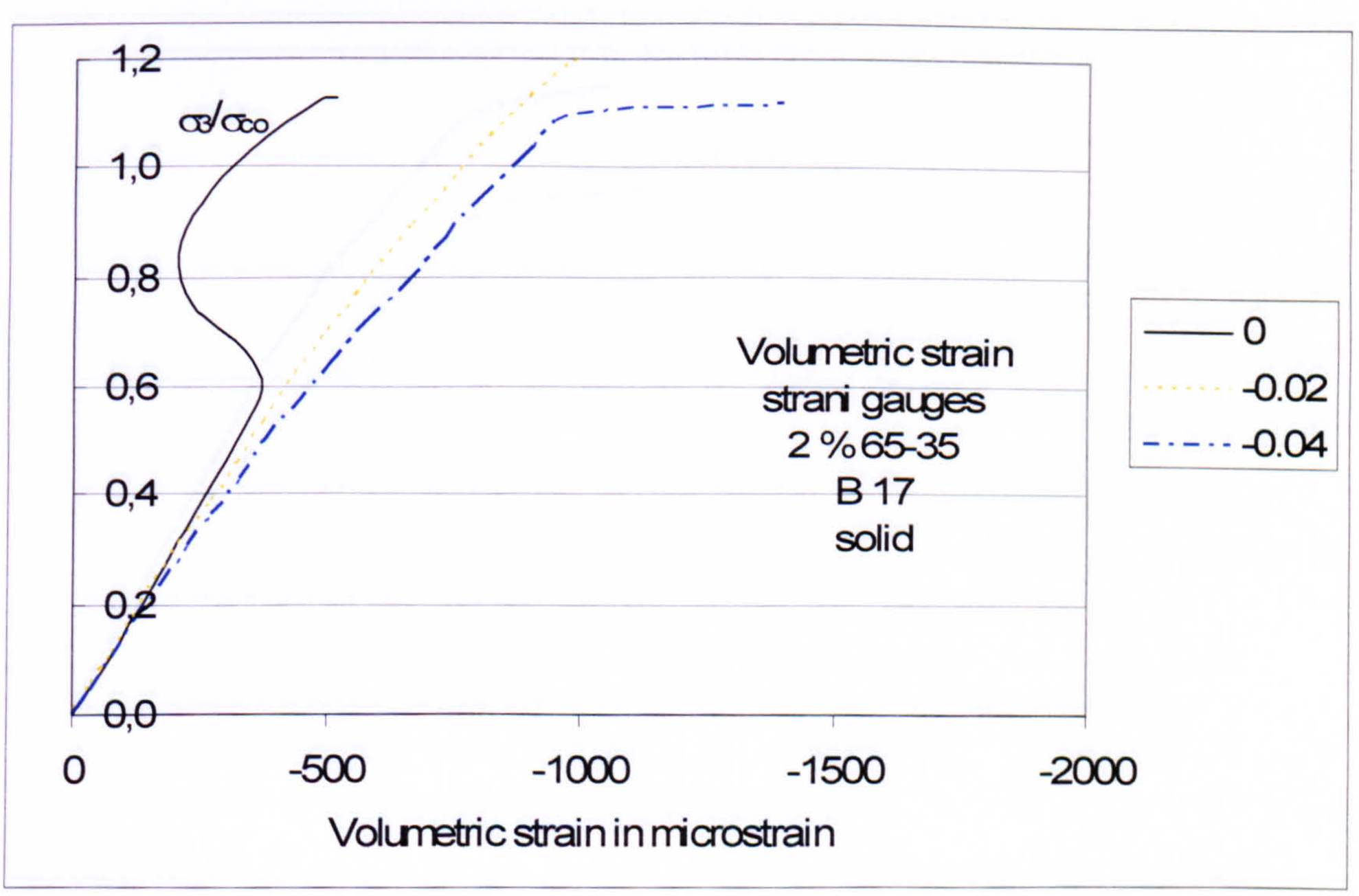

Figure 0.94 Volumetric strains for different stress ratios under biaxial compression-tension recorded with strain gauges in the two in plane directions for V_f = 2 % of the fibre type 65-35 tested with solid steel compression blocks (batch c-t 17)

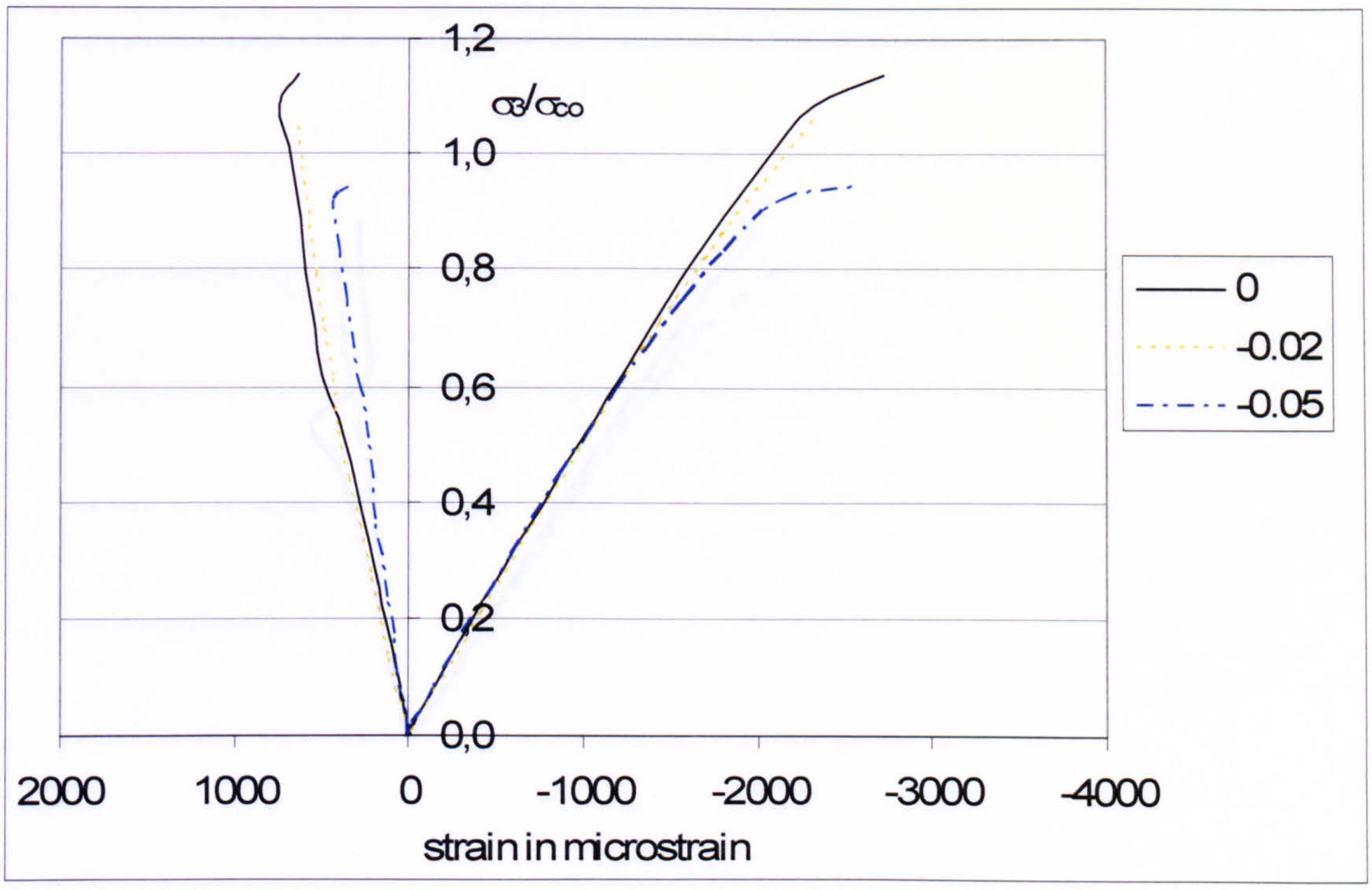

Figure 0.95 Stress-strain relationship for different stress ratios under biaxial compression-tension recorded with strain gauges for V_f = 2 % of the fibre type 65-35 tested with solid steel compression blocks (batch c-t 18)

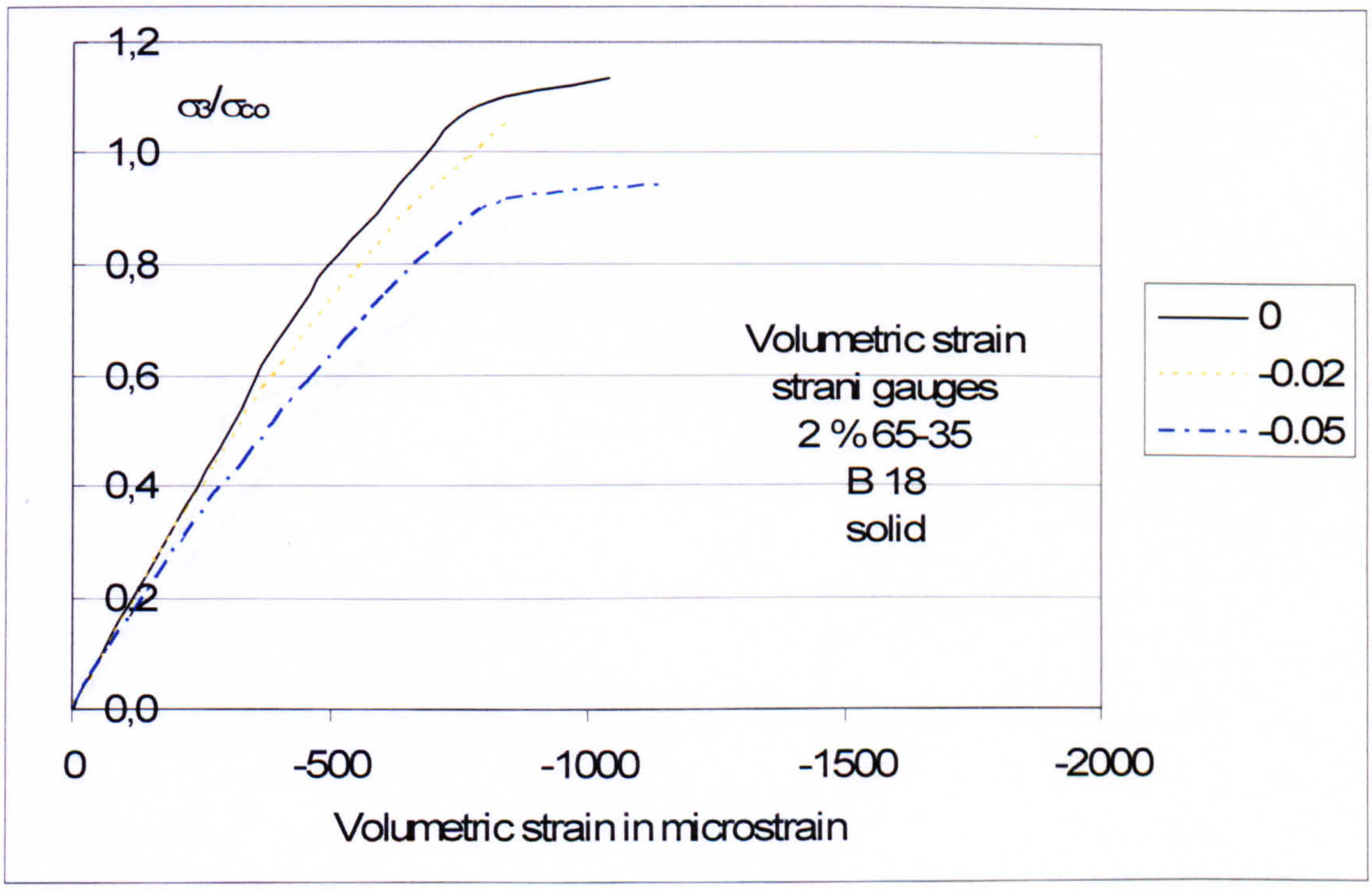

Figure 0.96 Volumetric strains for different stress ratios under biaxial compression-tension recorded with strain gauges in the two in plane directions for V_f = 2 % of the fibre type 65-35 tested with solid steel compression blocks (batch c-t 18)

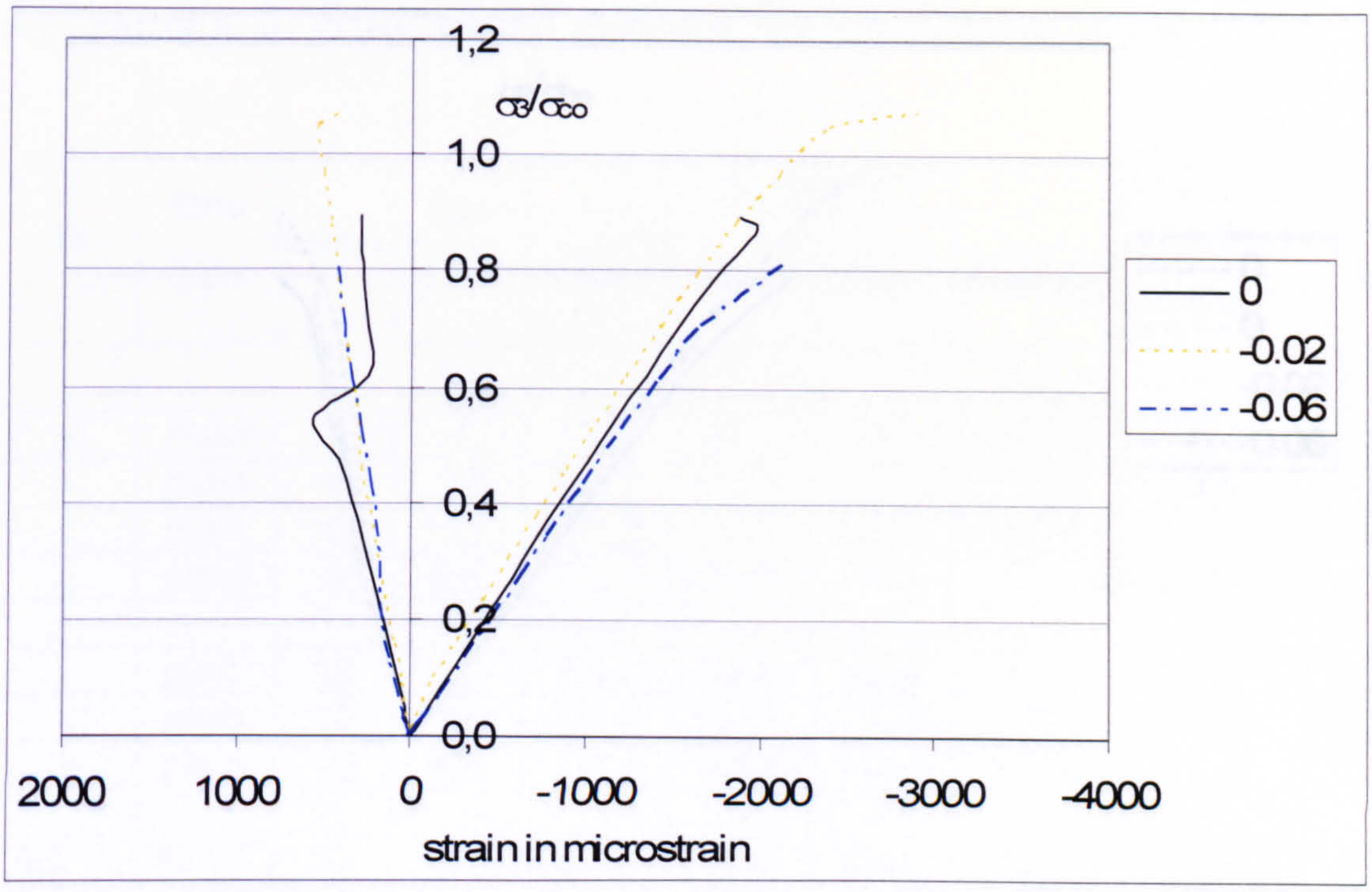

Figure 0.97 Stress-strain relationship for different stress ratios under biaxial compression-tension recorded with strain gauges for V_f = 2 % of the fibre type 65-60 tested with solid steel compression blocks (batch c-t 19)

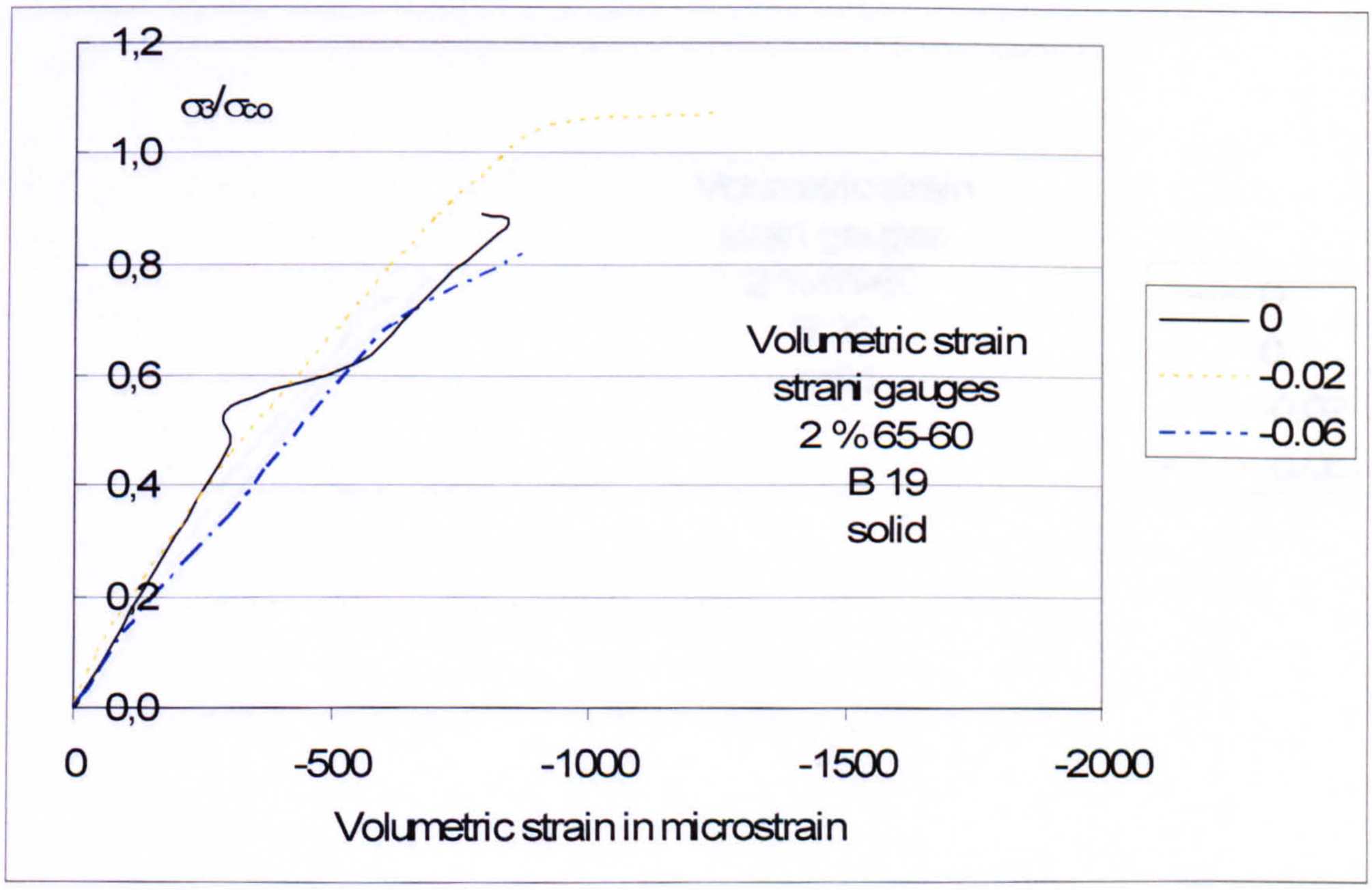

Figure 0.98 Volumetric strains for different stress ratios under biaxial compression-tension recorded with strain gauges in the two in plane directions for V_f = 2 % of the fibre type 65-60 tested with solid steel compression blocks (batch c-t 19)

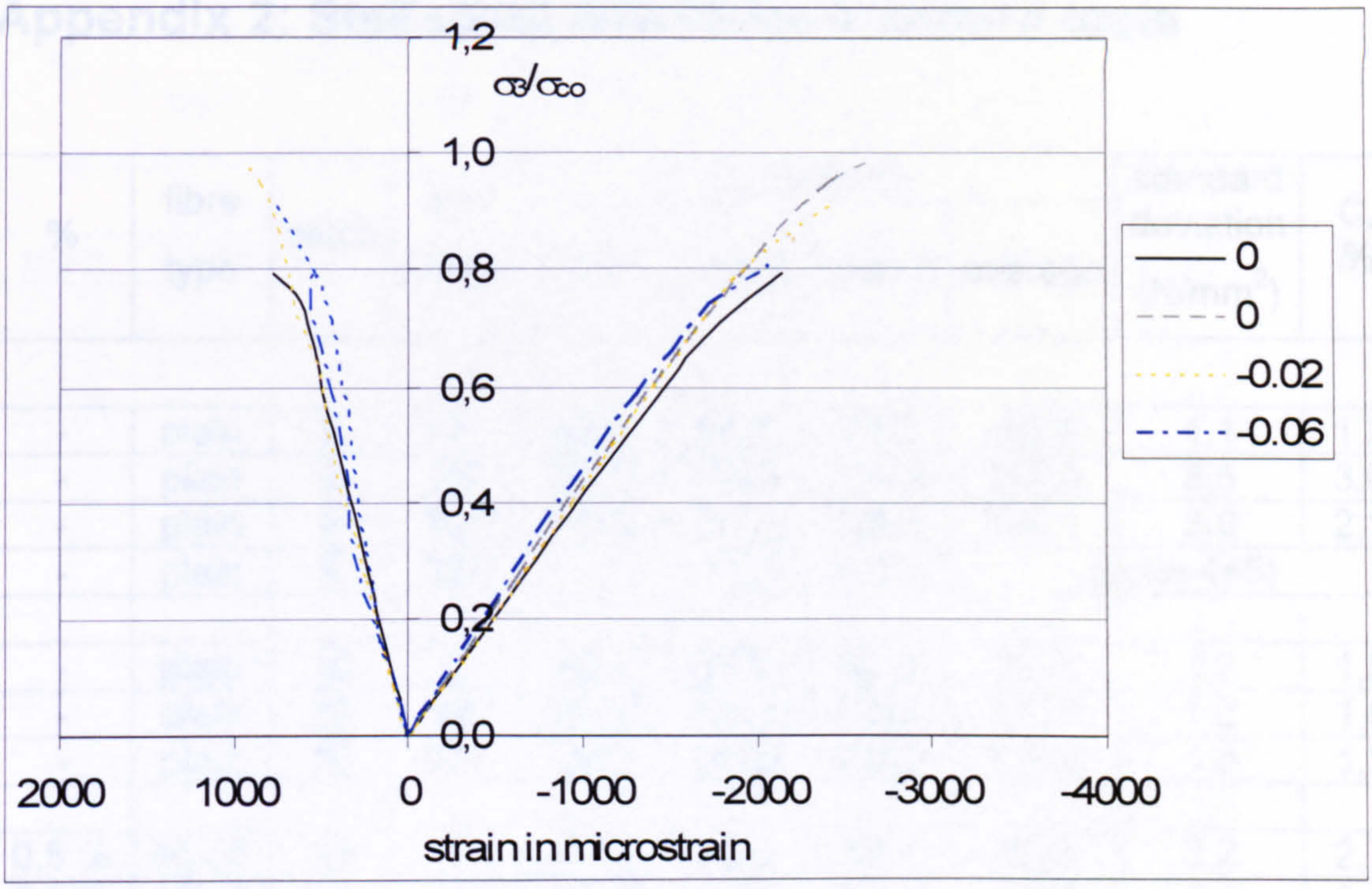

Figure 0.99 Stress-strain relationship for different stress ratios under biaxial compression-tension recorded with strain gauges for V_f = 2 % of the fibre type 65-60 tested with solid steel compression blocks (batch c-t 20)

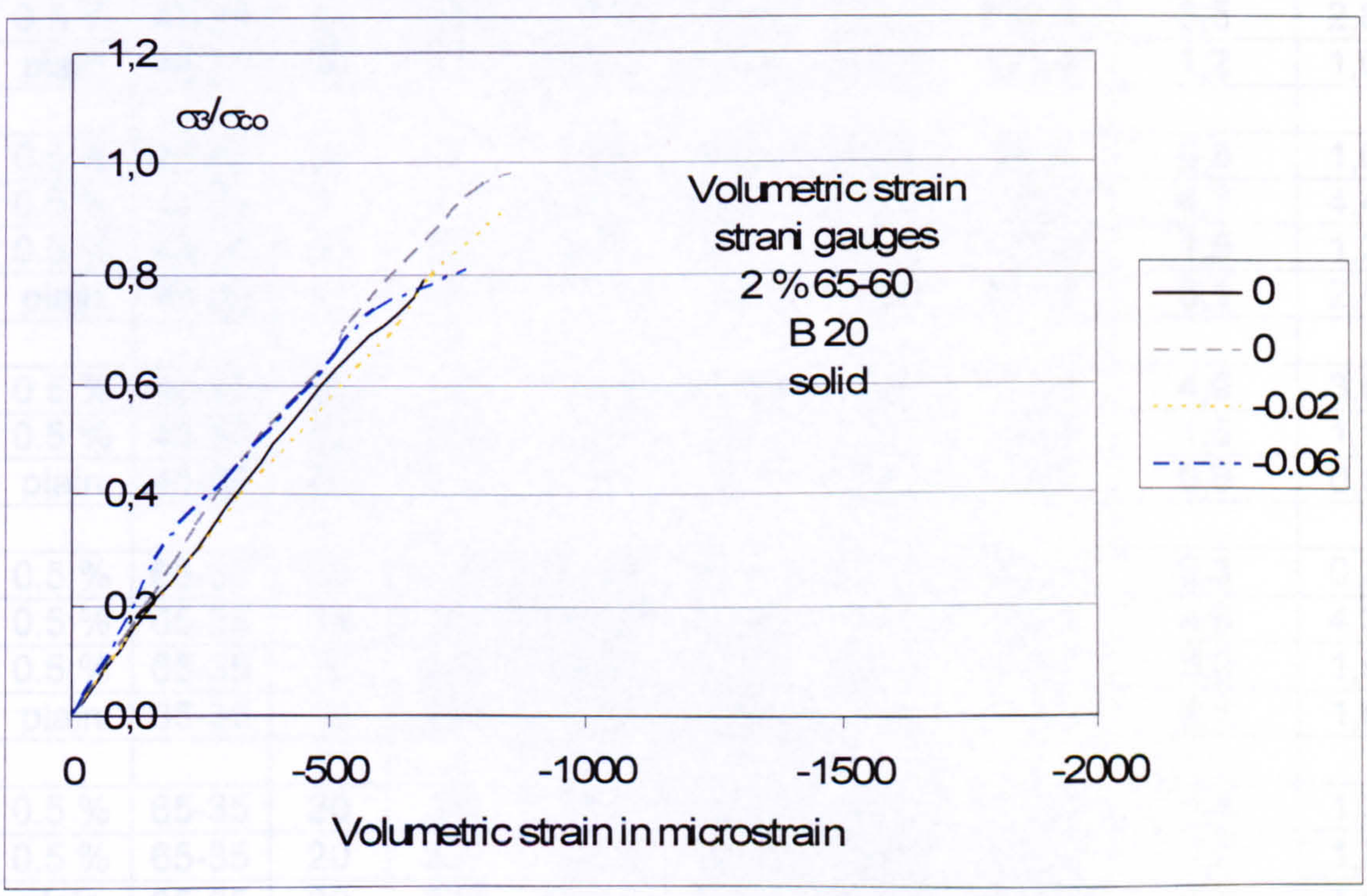

Figure 0.100 Volumetric strains for different stress ratios under biaxial compression-tension recorded with strain gauges in the two in plane directions for V_f = 2 % of the fibre type 65-60 tested with solid steel compression blocks (batch c-t 20)

Appendix 2: Statistical details for standard tests

%	fibre type	batch	age (days)	f_{cu} (N/mm^2)				standard deviation (N/mm^2)	C_v %
				cube 1	cube 2	cube 3	average		
-	plain	9	7	92,4	91,1	93,3	92,3	1,1	1,2
-	plain	9	28	120,5	117,1	113,5	117,0	3,5	3,0
-	plain	9	325	135,0	141,9	139,9	140,1	3,0	2,1
-	plain	9	325		142,1	141,5	(cube 4+5)		
-	plain	10	7	90,4	90,6	92,8	91,3	1,3	1,5
-	plain	10	28	122,0	121,0	119,6	120,9	1,2	1,0
-	plain	10	324	139,1	141,6	138,2	139,6	1,8	1,3
0.5 %	45-35	23	7	81,7	80,3	84,6	82,2	2,2	2,7
0.5 %	45-35	23	28	101,7	107,3	102,0	103,7	3,2	3,0
0.5 %	45-35	23	248	121,2	123,3	121,3	121,9	1,2	1,0
plain	45-35	23	248	122,3	118,8	127,5	122,9	4,4	3,6
0.5 %	45-35	24	28	104,5	107,3	105,1	105,6	1,5	1,4
0.5 %	45-35	24	321	121,8	119,6	126,4	122,6	3,5	2,8
plain	45-35	24	321	126,7	124,5	126,5	125,9	1,2	1,0
0.5 %	45-50	21	7	86,5	86,9	85,3	86,2	0,8	1,0
0.5 %	45-50	21	28	104,3	108,1	113,7	108,7	4,7	4,4
0.5 %	45-50	21	262	126	128,7	126,3	127,0	1,5	1,2
plain	45-50	21	262	128,1	134	132,7	131,6	3,1	2,4
0.5 %	45-50	22	28	107,4	113,3	115	111,9	4,0	3,6
0.5 %	45-50	22	330	131,5	131,2	128,8	130,5	1,5	1,1
plain	45-50	22	330	126,1	125,8	126,9	126,3	0,6	0,5
0.5 %	65-35	19	7	88,10	87,60	88,10	87,9	0,3	0,3
0.5 %	65-35	19	28	109,6	119,3	115,5	114,8	4,9	4,3
0.5 %	65-35	19	269	136,5	137,2	140,3	138,0	2,0	1,5
plain	65-35	19	269	134	132,2	129,8	132,0	2,1	1,6
0.5 %	65-35	20	28	113	115,7	114,1	114,3	1,4	1,2
0.5 %	65-35	20	337	135,1	131,8	134,2	133,7	1,7	1,3
plain	65-35	20	337	129,1	131,3	134,3	132,8	2,1	1,6
0.5 %	65-50	27	7	76,2	80,1	79,6	78,6	2,1	2,7
0.5 %	65-50	27	28	106,9	106,4	106,2	106,5	0,4	0,3
0.5 %	65-50	27	233	120,8	125,6	124,1	123,5	2,5	2,0

%	fibre type	batch	age (days)	f_{cu} (N/mm^2)				standard deviation (N/mm^2)	C_v %
				cube 1	cube 2	cube 3	average		
plain	65-50	27	233	127,6	132,7	128,5	129,6	2,7	2,1
0.5 %	65-50	28	28	97,1	100,9	99,5	99,2	1,9	1,9
0.5 %	65-50	28	306	116	119	125	120,0	4,6	3,8
plain	65-50	28	306	120,5	118,1	121,6	120,1	1,8	1,5
1%	45-35	3	7	92,4	93,1	96	93,8	1,9	2,0
1%	45-35	3	28	118,8	120,8	116,6	118,7	2,1	1,8
1%	45-35	3	194	129,9	134	137,8	133,9	4,0	3,0
plain	45-35	3	194	136,4	134,2	138,6	136,4	2,2	1,6
1%	45-35	4	28	97,80	96,80	96,80	97,1	0,6	0,6
1%	45-35	4	190	140,4	141,3	135,2	139,0	3,3	2,4
plain	45-35	4	190	131,8	133,4	132,7	135,3	1,6	1,1
1%	45-50	5	7	92,1	88,4	91,3	90,6	1,9	2,1
1%	45-50	5	29	119,4	119,8	117,5	118,9	1,2	1,0
1%	45-50	5	318	136,9	134	136,9	135,9	1,7	1,2
plain	45-50	5	318	134,7	121,7	129,6	128,7	6,6	5,1
1%	45-50	6	28	113,60	114,70	115,70	114,7	1,1	0,9
1%	45-50	6	316	131,8	135,5	133,9	133,7	1,9	1,4
plain	45-50	6	316	132	126,4	128,1	128,8	2,9	2,2
1%	65-35	1	7	95,3	97,1	95,7	96,0	0,9	1,0
1%	65-35	1	28	126,8	125,5	123,7	125,3	1,6	1,2
1%	65-35	1	183	131,2	146,1	138,5	138,6	7,5	5,4
plain	65-35	1	183	134,1	134,9	132,7	133,9	1,1	0,8
1%	65-35	2	28	121,8	120,2	118,9	120,3	1,5	1,2
1%	65-35	2	182	135,90	137,00	130,30	134,4	3,6	2,7
plain	65-35	2	182	140,3	137,9	142,6	140,3	2,4	1,7
1%	65-50	11	7	96,9	97,7	97,9	97,5	0,5	0,5
1%	65-50	11	28	125,6	124,1	121,3	123,7	2,2	1,8
1%	65-50	11	281	125,7	145,6	142,9	138,1	10,8	7,8
plain	65-50	11	281	136,8	125,5	129,4	130,6	5,7	4,4
1%	65-50	12	28	116,2	116,5	115	115,9	0,8	0,7
1%	65-50	12	280	131,5	130	130,8	130,8	0,8	0,6
plain	65-50	12	280	124,5	130,3	133,6	129,5	4,6	3,6

%	fibre type	batch	age (days)	f_{cu} (N/mm^2)				standard deviation (N/mm^2)	C_v %
				cube 1	cube 2	cube 3	average		
1.5 %	45-35	31	8	88,3	88,9	90,4	89,2	1,1	1,2
1.5 %	45-35	31	28	110,5	111,2	113,8	111,8	1,7	1,6
1.5 %	45-35	31	220	125,9	127,5	127,8	127,1	1,0	0,8
plain	45-35	31	220	119,4	124,3	128	123,9	4,3	3,5
1.5 %	45-35	32	28	102,9	101,8	101,2	102,0	0,9	0,8
1.5 %	45-35	32	293	123,1	118,2	117	119,4	3,2	2,7
plain	45-35	32	293	114,3	115,7	111,9	114,0	1,9	1,7
1.5 %	45-50	25	8	85,1	84,3	87,1	85,5	1,4	1,7
1.5 %	45-50	25	29	110,7	99,4	105,5	105,2	5,7	5,4
1.5 %	45-50	25	241	121,4	120,3	123,2	121,6	1,5	1,2
plain	45-50	25	241	128,6	129	113,6	123,7	8,8	7,1
1.5 %	45-50	26	28	109,9	107,4	109,7	109,0	1,4	1,3
1.5 %	45-50	26	314	126,9	125,4	124,9	125,7	1,0	0,8
plain	45-50	26	314	125,2	130	128	127,7	2,4	1,9
1.5 %	65-35	33	7	81,3	81	81,8	81,4	0,4	0,5
1.5 %	65-35	33	28	103,7	106,5	105,1	105,1	1,4	1,3
1.5 %	65-35	33	213	118,1	115,6	118,7	117,5	1,6	1,4
plain	65-35	33	213	117,7	116,3	116	116,7	0,9	0,8
1.5 %	65-35	34	28	101,5	102,9	102,6	102,3	0,7	0,7
1.5 %	65-35	34	285	114,2	117,2	115,3	115,6	1,5	1,3
plain	65-35	34	285	115,8	116,4	117,9	116,7	1,1	0,9
1.5 %	65-50	29	7	83,2	80,4	81	81,5	1,5	1,8
1.5 %	65-50	29	28	107,1	108	104,6	106,6	1,8	1,7
1.5 %	65-50	29	227	122,2	119,4	125,6	122,4	3,1	2,5
plain	65-50	29	227	119,3	120,9	116,7	119,0	2,1	1,8
1.5 %	65-50	30	28	101,5	99,3	96,4	99,1	2,6	2,6
1.5 %	65-50	30	300	111,5	116,2	118	115,2	3,4	2,9
plain	65-50	30	300	116,9	119,6	118,1	118,2	1,4	1,1
2%	45-35	15	7	93,2	93,8	93,4	93,5	0,3	0,3
2%	45-35	15	28	122,4	125,5	120,8	122,9	2,4	1,9
2%	45-35	15	268	147,3	145	147,3	146,5	1,3	0,9
plain	45-35	15	268	135,9	136,2	136,4	136,2	0,3	0,2
2%	45-35	16	28	118,3	115,6	115,4	116,4	1,6	1,4

%	fibre type	batch	age (days)	f_{cu} (N/mm^2)				standard deviation (N/mm^2)	C_v %
				cube 1	cube 2	cube 3	average		
2%	45-35	16	267	138,6	135,1	136,4	136,7	1,8	1,3
plain	45-35	16	267	127,6	127,7	124,3	126,5	1,9	1,5
2%	45-50	7	7	95,4	97,7	96,7	96,6	1,2	1,2
2%	45-50	7	28	107,4	108,9	120,7	112,3	7,3	6,5
2%	45-50	7	315	129,2	137,8	138,2	135,1	5,1	3,8
plain	45-50	7	315	134,1	126,7	133,9	131,6	4,2	3,2
2%	45-50	8	28	114,7	116,8	114,6	115,4	1,2	1,1
2%	45-50	8	314	134,1	134,1	130,1	132,8	2,3	1,7
plain	45-50	8	314	132,6	130,6	131	131,4	1,1	0,8
2%	65-35	17	7	90,9	89,4	90,2	90,2	0,8	0,8
2%	65-35	17	28	118,9	117,1	120,3	118,8	1,6	1,4
2%	65-35	17	261	147,8	141	139,9	142,9	4,3	3,0
plain	65-35	17	261	128,9	134,2	132,6	131,9	2,7	2,1
2%	65-35	18	28	115,4	117,2	114,8	115,8	1,2	1,1
2%	65-35	18	260	139,2	140,8	136	138,7	2,4	1,8
plain	65-35	18	260	121	130,1	125	125,4	4,6	3,6
2%	65-50	13	7	100,1	98	99,7	99,3	1,1	1,1
2%	65-50	13	28	125,7	120,8	120	122,2	3,1	2,5
2%	65-50	13	274	140,7	140,8	141,9	141,1	0,7	0,5
plain	65-50	13	274	140,9	127,6	136,5	135,0	6,8	5,0
2%	65-50	14	28	112,3	113,2	110,7	112,1	1,3	1,1
2%	65-50	14	273	127,8	123,7	120,3	123,9	3,8	3,0
plain	65-50	14	273	128,6	126	120,6	125,1	4,1	3,3

Table 20 Statistical details for plain and fibre cube tests of the compression-compression test series

%	fibre type	batch	age (days)	f_{cu} (N/mm^2)				standard deviation (N/mm^2)	C_v %
				cube 1	cube 2	cube 3	average		
	plain	4	7	99,9	96,5	98,3	98,2	1,7	1,7
	plain	4	28	113,7	118,3	109,3	113,8	4,5	4,0
	plain	4	255	124,8	128,3	131	128,0	3,1	2,4
	plain	5	7	93,3	94,5	97,2	95,0	2,0	2,1
	plain	5	27	112,2	112,2	116,4	113,6	2,4	2,1
	plain	5	263	131	125,3	130,1	128,8	3,1	2,4
	plain	6	7	99,9	92,6	100,3	97,6	4,3	4,4
	plain	6	28	116,8	115,6	119,4	117,3	1,9	1,7
	plain	6	251	119,6	132,9	129	127,2	6,8	5,4
	plain	6	252	129,5	129,3	126,7	128,5	1,6	1,2
1%	45-35	1	7	97,7	98,5	95,4	97,2	1,6	1,7
1%	45-35	1	28	114	111,8	113,4	113,1	1,1	1,0
1%	45-35	1	265	130	129,6	124,6	128,1	3,0	2,3
plain	45-35	1	28	103,7	105,8	100,4	103,3	2,7	2,6
plain	45-35	1	265	124,3	120,7	122,9	122,6	1,8	1,5
1%	45-35	2	7	87,9	87,1	88,5	87,8	0,7	0,8
1%	45-35	2	28	108	106,2	104,7	106,3	1,7	1,6
1%	45-35	2	258	127,4	124,2	124,5	125,4	1,8	1,4
plain	45-35	2	28	96,7	101,7	100,1	100,9	1,1	1,1
plain	45-35	2	258	112,5	110,7	110,1	111,1	1,2	1,1
1%	45-35	3	7	83,7	79,8	81,1	81,5	2,0	2,4
1%	45-35	3	28	98,7	100,5	103,6	100,9	2,5	2,5
1%	45-35	3	260	113,1	114	109,4	112,2	2,4	2,2
plain	45-35	3	28	87,5	98,7	92,5	92,9	5,6	6,0
plain	45-35	3	260	118,8	114	120,1	117,6	3,2	2,7
1%	45-50	7	7	103,1	103,7	105,1	104,0	1,0	1,0
1%	45-50	7	28	126,8	121,5	117,3	121,9	4,8	3,9
1%	45-50	7	281	142,7	140	136,7	139,8	3,0	2,1
plain	45-50	7	7	103,3	99,5	101,3	101,4	1,9	1,9
plain	45-50	7	281	134	134,6	141,1	136,6	3,9	2,9
1%	45-50	8	7	109	106	109,4	108,1	1,9	1,7
1%	45-50	8	26	128,8	124,7	126,9	126,8	2,1	1,6
1%	45-50	8	285	142	139,2	142	141,1	1,6	1,1
plain	45-50	8	26	129,4	122,9	122,1	124,8	4,0	3,2

%	fibre type	batch	age (days)	f_{cu} (N/mm^2)				standard deviation (N/mm^2)	C_v %
				cube 1	cube 2	cube 3	average		
plain	45-50	8	285	143,2	133,9	139,4	138,8	4,7	3,4
1%	65-35	9	6	96,5	94	91,9	94,1	2,3	2,4
1%	65-35	9	32	112,8	124,4	121,4	119,5	6,0	5,0
1%	65-35	9	285	138,2	129,4	129,4	132,3	5,1	3,8
plain	65-35	9	32	122	120,8	124,2	122,3	1,7	1,4
plain	65-35	9	285	134,4	125,3	124,1	127,9	5,6	4,4
1%	65-35	10	7	102,1	102	99,7	101,3	1,4	1,3
1%	65-35	10	28	125,4	121,1	124,7	123,7	2,3	1,9
1%	65-35	10	288	136,7	131,9	136,5	135,0	2,7	2,0
plain	65-35	10	28	110	124,7	124,8	119,8	8,5	7,1
plain	65-35	10	288	121,8	128,4	140,4	130,2	9,4	7,2
1%	65-60	11	7	85,9	85,1	89,1	86,7	2,1	2,4
1%	65-60	11	28	110,6	107,2	107,5	108,4	1,9	1,7
1%	65-60	11	307	123,7	123,3	113,4	120,1	5,8	4,9
plain	65-60	11	28	109,4	110,3	111,3	110,3	1,0	0,9
plain	65-60	11	307	124,4	126,5	121	124,0	2,8	2,2
1%	65-60	12	7	104,1	102,2	104,2	103,5	1,1	1,1
1%	65-60	12	28	121,9	123,9	125,6	123,8	1,9	1,5
1%	65-60	12	303	140,3	136,4	135,7	137,5	2,5	1,8
plain	65-60	12	28	119,6	119,1	119	119,2	0,3	0,3
plain	65-60	12	303	134,9	135,4	127,9	132,7	4,2	3,2
2%	45-35	13	7	108,7	106,9	104,4	106,7	2,2	2,0
2%	45-35	13	28	123,5	125,5	124,9	124,6	1,0	0,8
2%	45-35	13	306	138,7	142,6	138,2	139,8	2,4	1,7
plain	45-35	13	28	110,3	112,2	116,1	112,9	3,0	2,6
plain	45-35	13	306	128,4	135,4	132,1	133,8	2,3	1,7
2%	45-35	14	7	104,5	104,8	106,3	105,2	1,0	0,9
2%	45-35	14	28	127,2	125,9	127,8	127,0	1,0	0,8
2%	45-35	14	288	132	137	138,1	135,7	3,3	2,4
plain	45-35	14	28	110,8	114,9	120,9	115,5	5,1	4,4
plain	45-35	14	288	131,2	130	131,2	130,8	0,7	0,5
2%	45-50	15	7	99,4	99,9	100,3	99,9	0,5	0,5
2%	45-50	15	28	121,6	122	123,4	122,3	0,9	0,8
2%	45-50	15	287	133,7	136,8	137	135,8	1,9	1,4
plain	45-50	15	28	114,5	118,4	112,6	115,2	3,0	2,6
plain	45-50	15	287	121,9	116,1	131,8	123,3	7,9	6,4

%	fibre type	batch	age (days)	f_{cu} (N/mm^2)				standard deviation (N/mm^2)	C_v %
				cube 1	cube 2	cube 3	average		
2%	45-50	16	7	99,7	101	99,4	100,0	0,9	0,9
2%	45-50	16	28	119,6	120	119,4	119,7	0,3	0,3
2%	45-50	16	286	134,2	132,6	136,1	134,3	1,8	1,3
plain	45-50	16	28	108,1	112,5	115,7	112,1	3,8	3,4
plain	45-50	16	286	126,4	122	122,2	123,5	2,5	2,0
2%	65-35	17	7	106,8	108	105,9	106,9	1,1	1,0
2%	65-35	17	28	130,9	130,9	133,2	131,7	1,3	1,0
2%	65-35	17	281	143,5	144,7	150	146,1	3,5	2,4
plain	65-35	17	28	107,1	112,5	115,5	111,7	4,3	3,8
plain	65-35	17	281	133,3	138,2	132,1	134,5	3,2	2,4
2%	65-35	18	7	108,3	107,8	105,9	107,3	1,3	1,2
2%	65-35	18	28	133,6	132,2	130,8	132,2	1,4	1,1
2%	65-35	18	280	146,6	147,8	146,8	147,1	0,6	0,4
plain	65-35	18	28	118,8	123,4	121,5	121,2	2,3	1,9
plain	65-35	18	280	138,9	137,6	140,8	139,1	1,6	1,2
2%	65-60	19	7	102,9	102,5	101,6	102,3	0,7	0,7
2%	65-60	19	28	129,3	128,3	125,1	127,6	2,2	1,7
2%	65-60	19	275	138	126,8	141	135,3	7,5	5,5
plain	65-60	19	28	110,1	113,7	115,2	113,0	2,6	2,3
plain	65-60	19	275	119	130,9	122,8	124,2	6,1	4,9
2%	65-60	20	7	97,7	92,1	93,4	94,4	2,9	3,1
2%	65-60	20	28	113,3	116,2	115,8	115,1	1,6	1,4
2%	65-60	20	273	130,9	126,6	126,1	127,9	2,6	2,1
plain	65-60	20	28	109,1	101,9	105,2	105,4	3,6	3,4
plain	65-60	20	273	107,9	125,7	117,7	117,1	8,9	7,6

Table 21 Statistical details for plain and fibre cube tests of the compression-tension test series

fibre type	batch	age (days)	f_c' (N/mm^2)				standard deviation (N/mm^2)	C_v %
			cylinder 1	cylinder 2	cylinder 3	average		
plain	9	336	81,5	74,9	73,2	76,5	4,36	5,7
0.5 % 45-35	23	275	90,7	87,9	82,2	86,9	4,36	5,0
0.5 % 45-50	21	289	97,6	95,5	89,1	94,0	4,39	4,7
0.5 % 65-35	19	296	96,6	94,1	91,6	94,1	2,49	2,7
0.5 % 65-50	27	261	93,7	89,1	91,3	91,3	2,29	2,5
1 % 45-35	3	272	108,6	101,9	96,4	102,3	6,09	6,0
1 % 45-50	5	180	90,1	93,5	96,7	93,4	3,28	3,5
1 % 65-35	1	273	99,8	87,6	103,9	97,1	8,47	8,7
1 % 65-50	11	276	96,3	103,0	92,3	97,2	5,41	5,6
1.5 % 45-35	31	249	95,6	97,1	95,0	95,9	1,08	1,1
1.5 % 45-50	25	269	101,9	96,9	101,9	100,3	2,88	2,9
1.5 % 65-35	33	244	98,0	101,7	99,5	99,7	1,85	1,9
1.5 % 65-50	29	256	97,5	97,9	98,4	97,9	0,45	0,5
2 % 45-35	15	263	108,6	113,7	109,1	110,5	2,79	2,5
2 % 45-50	7	315	108,6	111,4	111,4	110,4	1,60	1,5
2 % 65-35	17	259	116,0	110,0	108,0	111,3	4,19	3,8
2 % 65-50	13	270	107,3	105,6	110,4	107,8	2,44	2,3

Table 22 Statistical details for cylinder compression tests of the compression-compression test series

fibre type	batch	age (days)	f_c' (N/mm^2)				standard Deviation (N/mm^2)	C_v %
			cylinder 1	cylinder 2	cylinder 3	average		
plain	4	255	90,1	82,0	77,7	83,3	6,3	7,6
plain	5	265	83,32	77,83	71,04	77,4	6,2	7,9
plain	6	252	76,98	82,64	81,11	80,2	2,9	3,6
1 % 45-30	1	268	72,68	80,04	74,61	75,8	3,8	5,0
1 % 45-30	2	266	94,29	84,67	84,79	87,9	5,5	6,3
1 % 45-30	3	260	76,92	77,04	85,64	79,9	5,0	6,3
1 % 45-50	7	281	96,21	94,52	102,7	97,8	4,3	4,4
1 % 45-50	8	285	84,9	95,76	86,03	88,9	6,0	6,7
1 % 65-35	9	285	101,9	105,1	96,21	101,1	4,5	4,5
1 % 65-35	10	288	82,24	96,67	97,12	92,0	8,5	9,2
1 % 65-60	11	307	82,64	94,18	88,86	88,6	5,8	6,5
1 % 65-60	12	303	89,43	102,9	101,5	97,9	7,4	7,6
2 % 45-35	13	306	103,4	105,6	103,9	104,3	1,2	1,1
2 % 45-35	14	288	102,3	107,3	109,8	106,5	3,8	3,6
2 % 45-50	15	287	101	102,6	106,5	103,4	2,8	2,7
2 % 45-50	16	286	102,1	109,3	101,1	104,2	4,5	4,3
2 % 65-35	17	281	104,3	112	115,5	110,6	5,7	5,2
2 % 65-35	18	280	117,7	123	116,6	119,1	3,4	2,9
2 % 65-60	19	275	no data available					
2 % 65-60	20	273	99,49	100,1	98,48	99,4	0,8	0,8

Table 23 Statistical details for cylinder compression tests of the compression-tension test series

fibre type	batch	age (days)	f_t' (N/mm^2)				standard deviation (N/mm^2)	C_v %
			cylinder 1	cylinder 2	cylinder 3	average		
plain	9	336	5,4	5,7	5,0	5,4	0,32	5,9
0.5 % 45-30	23	252	7,0	6,8	7,0	7,0	0,12	1,8
0.5 % 45-50	21	263	6,9	8,6	7,2	7,6	0,90	11,9
0.5 % 65-35	19	270	7,6	7,1	7,3	7,3	0,22	3,0
0.5 % 65-50	27	237	7,7	7,6	8,7	8,0	0,63	7,9
1 % 45-35	3	194	9,4	8,1	10,4	9,3	1,15	12,4
1 % 45-50	5	180	10,4	10,5	9,7	10,2	0,45	4,34
1 % 65-35	1	183	10,4	9,7	11,1	10,4	0,70	6,8
1 % 65-50	11	280	9,6	9,2	10,9	9,9	0,85	8,6
1.5 % 45-35	31	224	10,1	11,2	11,1	10,8	0,56	5,2
1.5 % 45-50	25	145	9,1	11,1	10,3	10,1	1,02	10,1
1.5 % 65-35	33	216	11,6	10,4	12,4	11,5	1,04	9,0
1.5 % 65-50	29	231	11,0	11,0	11,1	11,0	0,10	0,9
2 % 45-35	15	267	13,0	10,2	13,0	12,1	1,59	13,1
2 % 45-50	7	315	12,1	12,0	12,9	12,3	0,48	3,9
2 % 65-35	17	260	15,0	13,8	13,4	14,1	0,82	5,9
2 % 65-50	13	272	12,5	12,5	13,1	12,8	0,36	2,8

Table 24 Statistical details for cylinder splitting tests of the compression-compression test series

fibre type	batch	age (days)	f_t' (N/mm^2)				standard deviation (N/mm^2)	C_v %
			cylinder 1	cylinder 2	cylinder 3	average		
plain	4	255	5,15	5,97	6,97	6,0	0,9	15,1
plain	5	264	6,48	5,29	5,73	5,8	0,6	10,3
plain	6	252	5,41	5,74	6,49	5,9	0,6	9,4
1 % 45-30	1	266	10,47	9,76	10,01	10,1	0,4	3,6
1 % 45-30	2	259	9,85	8,09	10,46	9,5	1,2	13,0
1 % 45-30	3	260	9,33	8,71	8,77	8,9	0,3	3,8
1 % 45-50	7	281	9,97	10,44	10,41	10,3	0,3	2,6
1 % 45-50	8	285	10,14	10,37	11,21	10,6	0,6	5,3
1 % 65-35	9	285	9,99	10,2	-	10,1	0,1	1,5
1 % 65-35	10	288	10,02	9,77	9,48	9,8	0,3	2,8
1 % 65-60	11	307	9,9	8,1	9,37	9,1	0,9	10,1
1 % 65-60	12	303	8,13	10,57	9,56	9,4	1,2	13,0
2 % 45-35	13	306	12,99	11,77	12,28	12,3	0,6	5,0
2 % 45-35	14	288	13,56	14,39	13,54	13,8	0,5	3,5
2 % 45-50	15	287	13,67	13,19	11,83	12,9	1,0	7,4
2 % 45-50	16	286	11,48	10,97	12,6	11,7	0,8	7,1
2 % 65-35	17	281	16,06	14,82	15,95	15,6	0,7	4,4
2 % 65-35	18	280	14,86	13,29	15,71	14,6	1,2	8,4
2 % 65-60	19	275	no data available					
2 % 65-60	20	273	13,32	13,51	11,58	12,8	1,1	8,3

Table 25 Statistical details for cylinder splitting tests of the compression-tension test series

Appendix 3: Mix Design

Concrete mix design form

Job title C 100 FRC

Stage	Item		*Reference* or calculation	Values
1	1.1	Characteristic strength	Specified	70 N/mm² at 28 days
				Proportion defective ____ %
	1.2	Standard deviation	Fig 3	____ N/mm² or no data ____ N/mm²
	1.3	Margin	C1 or Specified	(k = ____) ____ × ____ = ____ N/mm²
				____ N/mm²
	1.4	Target mean strength	C2	70 + 5 = 75 N/mm²
	1.5	Cement type	Specified	OPC/SRPC/RHPC
	1.6	Aggregate type: coarse Aggregate type: fine	granite	Crushed/uncrushed Crushed/uncrushed
	1.7	Free-water/cement ratio	Table 2, Fig 4	0,33
	1.8	*Maximum free-water/cement ratio*	*Specified*	____ Use the lower value: 0,33
2	2.1	Slump or Vebe time	Specified	Slump 30-60 (120) mm or Vebe time 3-6 s
	2.2	Maximum aggregate size	Specified	10 mm
	2.3	Free-water content	Table 3	230 kg/m³
3	3.1	Cement content	C3	230 ÷ 0,33 = 697 kg/m³
	3.2	*Maximum cement content*	*Specified*	550 kg/m³
	3.3	*Minimum cement content*	*Specified*	500 kg/m³ water 175 kg/m³
				use 3.1 if ⩽ 3.2 use 3.3 if > 3.1 — 525 kg/m³
	3.4	Modified free-water/cement ratio		0,44
4	4.1	Relative density of aggregate (SSD)		2,7 known/assumed
	4.2	Concrete density	Fig 5	2450 kg/m³
	4.3	Total aggregate content	C4	2450 − 175 − 525 = 1750 kg/m³
5	5.1	Grading of fine aggregate	Percentage passing 600 μm sieve	38,9 %
	5.2	Proportion of fine aggregate	Fig 6	46 %
	5.3	Fine aggregate content	C5	1750 × 0,46 = 805 kg/m³
	5.4	Coarse aggregate content		1750 − 805 = 945 kg/m³

Quantities	Cement (kg)	Water (kg or *L*)	Fine aggregate (kg)	Coarse aggregate (kg) 10 mm	20 mm ~~57~~	40 mm ~~SP~~
per m³ (to nearest 5 kg)	525	175	805	945	52	3675 mL
per trial mix of 0,0075 m³	39,4	13,1	58,5	69,0	3,9	276 mL

Items in italics are optional limiting values that may be specified (see Section 7)

10% of Cement

1 N/mm² = 1 MN/m² = 1 MPa (see footnote to Section 3).
OPC = ordinary Portland cement; SRPC = sulphate-resisting Portland cement; RHPC = rapid-hardening Portland cement.
Relative density = specific gravity (see footnote to Para 5.4). SSD = based on a saturated surface-dry basis.

Appendix 4: Publications

This Appendix contains the title of a conference paper produced from the work carried out and published during the course of this research.

B. Kölle, D.V. Phillips, B. Zhang, P. Bhatt, C.J. Pearce, 2004, 'Experimental investigation of the biaxial properties of high performance steel fibre reinforced concrete', in RILEM Proceedings PRO 39, Fibre-Reinforced Concretes, BEFIB 2004, Proceeding of the Sixth International RILEM Symposium, edited by M. di Prisco, R. Felicetti and D.A. Plizzari, 20-22 September 2004, Varenna, Italy, ISBN: 2-912143-49-7, volume 1, pp. 369 – 378.

Furthermore this project was presented by following poster presentations:

D.V. Phillips, P. Bhatt, C.J Pearce, B. Zhang, B. Kölle, 2002, 'High strength fibre reinforced concrete under biaxial compression', International Congress 'Challenges of Concrete Construction – Composite materials in Concrete Construction', Dundee, UK, September 2002.

B. Kölle, D.V. Phillips, P. Bhatt, B. Zhang, C.J Pearce, 2002, 'Biaxial Properties of Fibre Reinforced High Performance Concrete', Presentations by Britain's Younger Engineers at the House of Commons, London, December 2002.